

Midwestern Regional Carbon Sequestration
Partnership (MRCSP) Phase III (Development Phase)



Enhanced Recovery Opportunities in the Appalachian Basin

Prepared by:

Battelle
505 King Avenue
Columbus, Ohio 43201

Principal Investigator: Dr. Neeraj Gupta

Authors: Kristin M. Carter, Jessica P. Moore, J. Eric Lewis, Brandon C. Nuttall, Philip Dinterman, Gary W. Daft, Jr., Robin V. Anthony, Katherine W. Schmid, Brian J. Dunst, Thomas N. Sparks, Stephen F. Greb, Michael P. Solis, James McDonald and Richard A. Ortt

Submitted to:

The U.S. Department of Energy, National Energy Technology Laboratory
Program Manager: Andrea McNemar

DOE MRCSP Project #DE-FC26-05NT42589

September 2020

Notice

This report was prepared by Battelle as an account of work sponsored by an agency of the United States Government and other project sponsors, including Core Energy, LLC and The Ohio Development Services Agency. Neither the United States Government, nor any agency thereof, nor any of their employees, nor Battelle and other cosponsors, makes any warranty, express or implied, or assumes any liability or responsibility for the accuracy, completeness, or usefulness of any information, apparatus, product, or process disclosed, or represents that its use would not infringe privately owned rights. Reference herein to any specific commercial product, process, or service by trade name, trademark, manufacturer, or otherwise does not necessarily constitute or imply its endorsement, recommendations, or favoring by the United States Government or any agency thereof. The views and the opinions of authors expressed herein do not necessarily state or reflect those of the United States Government or any agency thereof.

Battelle does not engage in research for advertising, sales promotion, or endorsement of our clients' interests including raising investment capital or recommending investments decisions, or other publicity purposes, or for any use in litigation.

Battelle endeavors at all times to produce work of the highest quality, consistent with our contract commitments. However, because of the research and/or experimental nature of this work the client undertakes the sole responsibility for the consequence of any use or misuse of, or inability to use, any information, apparatus, process or result obtained from Battelle, and Battelle, its employees, officers, or Trustees have no legal liability for the accuracy, adequacy, or efficacy thereof.

Acknowledgements

Sponsorships - This report is part of a series of reports prepared under the Midwestern Regional Carbon Sequestration Partnership (MRCSP) Phase III (Development Phase). These reports summarize and detail the findings of the work conducted under the Phase III project. The primary funding for the MRCSP program is from the US Department of Energy's National Energy Technology Laboratory (NETL) under DOE project number DE-FC26-05NT42589 with Ms. Andrea McNemar as the DOE project manager. The past DOE project managers for MRCSP include Dawn Deel, Lynn Brickett, and Traci Rodosta. Many others in the DOE leadership supported, encouraged, and enabled the MRCSP work including but not limited to Kanwal Mahajan, John Litynski, Darin Damiani, and Sean Plasynski.

The Michigan Basin large-scale test received significant in-kind cost share from Core Energy, LLC, who also provided essential access to the field test site and related data. This contribution by Core Energy CEO Robert Mannes, VP Operations Rick Pardini, and Allan Modroo, VP Exploration, and the entire Core Energy staff is gratefully acknowledged. MRCSP work in Ohio has been supported by the Ohio Coal Development Office in the Ohio Development Services Agency under various grants (CDO D-10-7, CDO-D-13-22, CDO-D-D-13-24, and CDO-D-15-08) with Mr. Greg Payne as the OCDO project manager. Finally, several industry sponsors and numerous technical team members from State Geological Surveys, universities, and field service providers have supported MRCSP through cash and in-kind contributions over the years as listed in the individual reports.

Program Leadership – During the MRCSP Phase III project period, several Battelle staff and external collaborators contributed to the successful completion of the program through their efforts in field work, geological data analysis and interpretation, and/or reporting. The primary project managers over the MRCSP performance period have included Rebecca Wessinger, Neeraj Gupta, Jared Walker, Rod Osborne, Darrell Paul, David Ball. Additional project management support has been provided by Andrew Burchwell, Christa Duffy, Caitlin McNeil, and Jacqueline Gerst over the years.

Principal Investigator: Neeraj Gupta (614-424-3820/ gupta@battelle.org)

Report Authors and Principal Technical Contributors – Kristin M. Carter, Jessica P. Moore, J. Eric Lewis, Brandon C. Nuttall, Philip Dinterman, Gary W. Daft, Jr., Robin V. Anthony, Katherine W. Schmid, Brian J. Dunst, Thomas N. Sparks, Stephen F. Greb, Michael P. Solis, James McDonald and Richard A. Ort.

Table of Contents

	Page
List of Acronyms	xxv
Units of Measure.....	xxvii
Section 1. Introduction	1
Section 2. Appalachian Basin Research Efforts	2
2.1 Purpose	2
2.2 Project Team.....	2
2.3 Overview of Major Tasks.....	2
2.3.1 Assessment of Storage and Enhanced Recovery for Oil and Gas Fields	2
2.3.2 Assessment of Storage and Enhanced Recovery for Organic-Rich Shale.....	3
2.3.3 Evaluation of CCUS Opportunities	3
Section 3. Appalachian Basin.....	5
3.1 CO ₂ Point-Sources	5
3.2 Geology	7
3.3 Stratigraphy.....	8
Section 4. Oil and Gas Field Storage and Enhanced Recovery Assessment	9
4.1 Introduction	9
4.2 Methods	9
4.2.1 Digital Data Compilation and Regional Mapping.....	9
4.2.2 Storage Resource Estimates for Oil and Gas Fields.....	17
4.3 Storage Resource Estimates for the Appalachian Basin.....	18
4.4 Evaluating Oil Field Opportunities	23
Section 5. Organic-Rich Shale Storage and Enhanced Recovery Assessment	25
5.1 Introduction	25
5.2 Models and Methods.....	26
5.3 Middle Devonian Marcellus Shale	28
5.3.1 Geologic Setting.....	28
5.3.2 Data	33
5.3.3 Methods	36
5.3.4 Results and Discussion	41
5.4 Upper Ordovician Utica Shale/Point Pleasant Formation Interval	50
5.4.1 Geologic Setting.....	50

5.4.2	Data	55
5.4.3	Data Review and Management	57
5.4.4	Methods	60
5.4.5	Results and Discussion	64
5.5	Carbon Storage Potential	76
5.5.1	Middle Devonian Marcellus Shale	76
5.5.2	Upper Ordovician Utica Shale/Point Pleasant Formation Interval	78
5.6	Enhanced Recovery	80
5.7	Conclusions	81
Section 6.	Evaluation of CCUS Opportunities	82
6.1	Overview	82
6.2	Subsurface Geology of the Tri-State Area	83
6.3	Rating Enhanced Recovery Reservoirs	85
6.4	Ohio Case Studies	91
6.4.1	Overview	91
6.4.2	Lithostratigraphy	93
6.4.3	East Canton Consolidated Field	96
6.4.4	Clayton and Philo Consolidated Fields	122
6.4.5	Stacked Opportunities	138
6.4.6	Summary	153
6.5	Pennsylvania Case Studies	154
6.5.1	Overview	154
6.5.2	Venango Group Lithostratigraphy	155
6.5.3	Area Cross Sections	166
6.5.4	Washington-Taylorstown Field	173
6.5.5	Linden Field	180
6.5.6	New Freeport Field	187
6.5.7	History of EOR in Southwestern Pennsylvania	189
6.5.8	Stacked CCUS Potential	194
6.5.9	Summary	205
6.6	West Virginia Case Studies	206
6.6.1	Overview and Area Geology	206
6.6.2	Jacksonburg-Stringtown Field	210
6.6.3	Mannington Field	231
6.6.4	Salem-Wallace Field	242
6.6.5	Wolf Summit-Big Isaac Field	249

6.6.6	Summary of EOR Operations in West Virginia Case Study Fields.....	256
6.6.7	Legacy Wells.....	262
6.6.8	Stacked CCUS Potential	262
6.6.9	Summary.....	271
Section 7.	Discussion.....	273
7.1	Summary of Findings	273
7.1.1	Prospective Reservoirs	273
7.1.2	Storage Resource Estimates.....	275
7.1.3	Challenges	276
7.1.4	Opportunities.....	278
7.2	Recommendations	279
Section 8.	References Cited.....	281

List of Appendices

	Page
Appendix A. Pennsylvania Databook of Devonian Marcellus Shale Information	
Appendix B. Supplemental Data for Statistical Treatments	
Appendix C. Ordovician Utica Shale Databook	
Appendix D. Tri-state Area Oil Field Rating Results	
Appendix E. Tri-state Area Gas Field Rating Results	
Appendix F. Tri-state Area Regional Cross Sections	
Appendix G. Geologic Cross Sections Used to Correlate Lithostratigraphy for Pennsylvania Case Studies	
Appendix H. Kanavy (2018): Mineralogy and Porosity Report, #1 Harry Hatfield and #3299 Hamilton Wells, Linden Field, Washington County, PA	
Appendix I. Remis (2018): Reservoir Characterization of the Gantz and Gordon Sandstones, Linden Field, North Strabane Township, Washington County, Pennsylvania	
Appendix J. Opsitnick (2015): Reservoir Quality of the Marcellus Shale Play in the Hill Unit 2H and 3H Wells: Determining Mineralogical and Lithological Properties	
Appendix K. Cooney (2016): Vitrinite Reflectance Report: Antero Hill Unit 2H and Antero Hill Unit 3H Wells, Washington County, Pennsylvania	
Appendix L. Carter (2017): Shale Gas Case Study Report, Starvaggi No. 1 (API# 3712522278), Washington County, Pennsylvania	

List of Tables

	Page
Table 3-1. Cross section plates reported in Dinterman et al. (2019).....	8
Table 4-1. Oil and gas field efficiency factors for the MRCSP Region.....	18
Table 5-1. Calculated volumes of net organic-rich Marcellus Shale in the study area.....	49
Table 5-2. Descriptive statistics of TOC data in the Utica Shale databook grouped by stratigraphic categories. Samples were grouped as Logana Member if they were an organic-rich shale in the Lower Trenton (Lexington) Limestone. All Upper Ordovician non-Point Pleasant and Utica samples above the Trenton were placed in the Kope and other formations grouping.....	59
Table 5-3. Correlation coefficients (R) between TOC, RHOB and GR for 1356 observations from 124 wells (using data from Patchen and Carter, 2015).....	61
Table 5-4. Fit statistics for the eight models investigated to calculate TOC from geophysical log data in order by the coefficient of determination (r^2) and minimum RMSE. Highlighted values emphasize models with better predictive power.....	64
Table 5-5. Generalized CO ₂ density values for calculating free gas in pore space.....	68
Table 5-6. Volumetrics using net thickness of the Utica Shale and Point Pleasant intervals separately with median (P50) TOC greater than or equal to 1.5 percent.....	75
Table 5-7. Volumetrics using net thickness in ft, illustrating potential CO ₂ storage resource of the combined Utica Shale-Point Pleasant intervals with (P50) TOC greater than or equal to 1.5 percent with reference to the area shown in Figure 5-42.....	75
Table 5-8. Estimated CO ₂ storage by state for the Middle Devonian Marcellus Shale interval.....	78
Table 5-9. Estimated CO ₂ storage by state as adsorbed gas and free gas in matrix porosity for the Utica Shale/Point Pleasant interval in millions of tons at 3 and 10 percent efficiencies.....	79
Table 6-1. Rating criteria used to assess CCUS opportunities for oil fields in the tri-state area.....	86
Table 6-2. Rating criteria used to assess CCUS opportunities for gas fields in the tri-state area.....	87
Table 6-3. Oil fields selected for case study assessment in the tri-state area.....	91
Table 6-4. Unit-specific reservoir characteristics of the Venango Group, Washington and Greene counties, Pennsylvania.....	157
Table 6-5. Unit-specific reservoir characteristics for the Venango Group in Washington-Taylorstown Field.....	176
Table 6-6. Gordon stray and Gordon sandstone core test results for the James McMannis No. 9 (API No. 3712501189).....	177
Table 6-7. Gordon sandstone core test results for the Lemon Carson No. 10 (API No. 3712501137).....	178
Table 6-8. Gordon sandstone core test results for the James Hodgins No. 13 (API No. 3712501175).....	179

Table 6-9.	Unit-specific reservoir characteristics for the Venango Group in Linden Field.....	181
Table 6-10.	Gordon sandstone core test results for the J.L. Kenamond No. 1 (API No. 3712592783).....	182
Table 6-11.	Unit-specific reservoir characteristics for the Venango Group in New Freeport Field.....	188
Table 6-12.	EOR activity in Southwestern Pennsylvania oil fields.	191
Table 6-13.	Storage resource estimates for case study fields.	197
Table 6-14.	Average mineralogy and vitrinite reflectance data for the Marcellus Shale in two Washington County wells (modified from Cooney, 2016).	202
Table 6-15.	Starvaggi No. 1 TOC results (modified from Patchen and Carter, 2015).	204
Table 6-16.	Core Analysis of the Gordon sandstone in Jacksonburg-Stringtown well F.R. Ball 18. Zone of highest porosity and permeability ranges from ~2992 to 3002 ft (WVGES Pipeline Plus).	221
Table 6-17.	Core Analysis of the Gordon sandstone in Jacksonburg-Stringtown well Irene Reilly 13. Note relatively low porosity and permeability values, as compared to the Ball 18 well (WVGES Pipeline Plus).	224
Table 6-18.	Field-level reservoir data for the Gordon sandstone in Jacksonburg-Stringtown Field.	225
Table 6-19.	Unit-specific reservoir characteristics for the Mannington Field.	233
Table 6-20.	Field-level reservoir data for the Gordon sandstone in Salem-Wallace Field.	243
Table 6-21.	Unit-specific reservoir characteristics for the Wolf Summit-Big Isaac Field.....	249
Table 6-22.	Wells per acre in the study area. Well counts current as of mid-2018 (WVGES).	262
Table 6-23.	Storage resource estimates for case study fields.	264
Table 6-24.	Storage resource estimates for gas-producing fields near the case study areas.....	265
Table 6-25.	Storage resource estimates for area Huntersville Chert/Oriskany Sandstone gas fields.....	268

List of Figures

	Page
Figure 3-1. Major structural features in the MRCSP Region (Dinterman et al., 2019).....	5
Figure 3-2. Average yearly power plant CO ₂ emissions by state and fuel source (2005 – 2015).....	6
Figure 3-3. Comparison of previously used point-source data (black circles) to those used in the current study (yellow triangles).	7
Figure 4-1. Power plant distribution and emissions relative to regional infrastructure.	10
Figure 4-2. Power plants and petroleum fields in the MRCSP region.	11
Figure 4-3. Surface temperature and geothermal gradient map used to determine temperature at depth.....	13
Figure 4-4. Distribution of Appalachian Basin oil fields where oil gravities were calculated (yellow) versus reported (green).....	14
Figure 4-5. Comparison of miscibility via depth (A) and miscibility via MMP (B) for Appalachian Basin oil fields. Red arrows indicate variations in miscible/immiscible determinations using the two methods.	17
Figure 4-6. Total carbon storage resource estimate of Appalachian Basin oil fields by state.....	18
Figure 4-7. Mode storage resource values for (A) all fields (combined), (B) oil fields and (C) gas fields in the Appalachian Basin – Phase II vs. Phase III results.	20
Figure 4-8. Stacked reservoirs are more common east of the dashed line. This may at least partially account for the larger storage resource estimates in West Virginia and Pennsylvania relative to other basin states.	22
Figure 4-9. Oil reservoir data gathered for the current study, reported as a percentage available on a field-level basis for each of five states in the Appalachian Basin.....	23
Figure 4-10. Mode storage resource in Appalachian Basin oil fields.....	24
Figure 5-1. Typical GR-RHOB crossplot showing effect of increasing TOC in organic-rich Devonian black shales (black dots), inorganic gray shales (gray diamonds) and clastic units (yellow diamonds) with model parameters: minimum GR cutoff for organic richness (GRmin), maximum RHOB of inorganic gray shale (Rhomax), and the slope of a linear least squares fit (Schmoker's A parameter).	27
Figure 5-2. Structure contour map (500-ft contour interval) of the top of the Middle Devonian Marcellus Shale in the Appalachian Basin. Bold black lines represent generalized major fault zones.....	29
Figure 5-3. Gross thickness map (20-ft contour interval) of the Middle Devonian Marcellus Shale in the Appalachian Basin. Bold black lines represent generalized major fault zones.	30
Figure 5-4. GR and RHOB type log for the Devonian Marcellus Shale, Susquehanna County, Pennsylvania. GR is colored from high (red) to moderate (yellow, green) to low (blue, purple) API values.....	31

Figure 5-5.	Generalized cross section along strike showing stratigraphic and lithofacies variations for the Marcellus Shale interval. Well spacing is not to scale. See Figure 5-6 for section location.....	32
Figure 5-6.	Distribution of 1870 well locations with LAS data in the Marcellus Shale project area (magenta). The blue line with numbered wells is the location of the cross section in Figure 5-5. The red well, although not within the assessment area, is discussed later in the report.	34
Figure 5-7.	Marcellus reference well counts with digital GR and RHOB data in LAS format by state.	35
Figure 5-8.	Standard OLS linear regression model of TOC as a function of laboratory-determined RHOB using data compiled from the Pennsylvania databook.	36
Figure 5-9.	Examples of problems in log curves and crossplots illustrating problems identified in some LAS files during quality-control review: A) same curve digitized for both GR and RHOB resulting in a perfect correlation; B) GR clipped at edge of right track, resulting in lower (and the same) API readings for the interval clipped; C) Narrow, RHOB low-density spikes, which may be likely related to an enlarged wellbore “washouts” rather than true low-density rock. Each of these types of problems had to be identified and addressed in the dataset. Depth, GR and RHOB scales vary.....	38
Figure 5-10.	Histogram and probability density of observed RHOB for the Hamilton Group/Marcellus interval with GR \geq 180 API, from 528 wells. Kernel density is explained in Appendix B.	40
Figure 5-11.	Example GR-RHOB crossplot for API No. 3709720002 showing the calculated slope of the linear regression (the Schmoker A value) to calculate TOC.	42
Figure 5-12.	Distributions of TOC data calculated for each of four models and the P50 model for API No. 3709720002. The box and whisker plot (top) shows the range of the laboratory-derived TOC values for sampled intervals in the well. Schmoker: results from Equation 8, Schmoker (mod): results from Equation 9, Marcellus (OLS): results from Equation 10, Schmoker (GR): results from Equation 11.	43
Figure 5-13.	GR and RHOB logs with the modeled TOC curves and laboratory TOC data for the Marcellus interval (API No. 3709720002). Note the P50 curve overlies the green Marcellus (Equation 10) and orange Schmoker (Equation 9) curves in some places.	44
Figure 5-14.	Spatial distribution of average TOC in the Marcellus Shale interval from calculated P50 well log curve data. The blue outline is the Marcellus assessment area.....	45
Figure 5-15.	Estimated vertical drilling depth to the top of the Marcellus interval (500-ft contour interval) used to establish the updip limit of the area selected for storage resource estimates. The blue outline is the Marcellus Shale assessment area.....	46
Figure 5-16.	Net thickness map (10-ft contour interval) of organic-rich shale (>180 API units) in the Hamilton Group/Marcellus Shale interval. The blue outline is the Marcellus Shale assessment area.....	47
Figure 5-17.	Maps of net thickness of organic-rich Marcellus Shale (10-ft contour interval) with TOC from the P50 curve greater than or equal to A) 2	

percent (shale source rock potential), and B) 4 percent (greater shale gas/liquids potential)48

Figure 5-18. General stratigraphic nomenclature employed by the Utica Shale Appalachian Basin Exploration Consortium. TOC and digital geophysical data were grouped by the formation names highlighted in the “This Study” column (Patchen and Carter, 2015).50

Figure 5-19. Type geophysical log for the units included in the Utica study area (modified from Patchen and Carter, 2015).51

Figure 5-20. Generalized cross section along strike showing stratigraphic and lithofacies variations for the Utica Shale and Point Pleasant Formation. See Figure 5-25 for cross section location.52

Figure 5-21. Areal extent and structure map (400-ft contour interval) on top of the Point Pleasant Formation (modified from Patchen and Carter, 2015). Major basement faults are indicated by red lines.53

Figure 5-22. Areal extent and structure map (500-ft contour interval) on top of the Utica Shale (modified from Patchen and Carter, 2015). Major basement faults are indicated by red lines.53

Figure 5-23. Gross thickness map (20-ft contour interval) of the Point Pleasant Formation (modified from Patchen and Carter, 2015). Major basement faults are indicated by red lines.54

Figure 5-24. Gross thickness map (20-ft contour interval) of the Utica Shale (modified from Patchen and Carter, 2015). Major basement faults are indicated by red lines.54

Figure 5-25. Well coverage utilized by the Utica Shale Play Book Study (modified from Patchen and Carter, 2015). The approximate extents of the Utica and Point Pleasant formations are shown by the blue and red outlines, respectively. The green outline represents the Utica/Point Pleasant play area. The red well and API number is the location of an example well used in the report. Light gray shaded polygons represent Ordovician outcrop areas.....56

Figure 5-26. 1125 wells associated with the Utica Shale databook. Yellow circles (1020) are wells with digital geophysical log data files (LAS); non-digital well locations used in the study lack circles; red=gas show or production; green=oil show or production, black=dry hole, blue=salt-water disposal well. Gray shaded polygons represent Ordovician outcrop areas.57

Figure 5-27. Measured TOC observations associated with RHOB data by state for Point Pleasant Formation, Utica Shale and Kope and other formations.....60

Figure 5-28. Distributions of TOC for selected Upper Ordovician units by stratigraphic group showing fiftieth percentile TOC values. See Table 5-2 for number of samples from each interval. Data from the Lexington (Trenton) Limestone, and Logana Member (and equivalents) of the lower Lexington (Trenton) Limestone, were not used for additional regional analyses.....60

Figure 5-29. Crossplots of Kope and other (green), Utica (red) and Point Pleasant (blue) geophysical and TOC data: A) GR and RHOB; B) TOC and GR; and C) TOC and RHOB. Panel C includes R values for each of the grouped stratigraphic units.....61

Figure 5-30. The distribution of the difference between measured and modeled TOC (residuals) in the Utica and Point Pleasant formations as determined using TOC estimated from RHOB using four models.62

Figure 5-31. Distributions of residuals generated by multiple train-test-split iterations to determine multivariate regression parameters for modeling TOC in the Utica and Point Pleasant formation groups.64

Figure 5-32. Distribution of residuals between measured and predicted TOC for four proposed models for the Utica/Point Pleasant interval.65

Figure 5-33. Example model performance for the CNG Shepard No. 1 well (Madison County, New York), showing the distribution of measured TOC values (box and whisker chart, top) and TOC calculated from geophysical log data (kernel distribution plots, bottom).65

Figure 5-34. GR and RHOB logs for the CNG Shepard No. 1 well (Madison County, New York), with measured TOC data and calculated TOC curves. Note the Multivariate (blue) and Wang (mod) (green) TOC curves plot close together, so appear as only a green line.66

Figure 5-35. Map of Utica Shale and Point Pleasant Formation TOC from the Utica Shale databook. Contours represent mean measured TOC values for 264 wells. TOC values range from 0.05 percent (dark blue) to more than 2.95 percent (red).67

Figure 5-36. Distribution of RHOB and calculated DPHI from geophysical logs processed to remove outliers and observations with calculated DPHI <0: (A) raw RHOB values; (B) calculated DPHI (decimal fraction).68

Figure 5-37. Distributions of TOC calculated from RHOB log data by formation (with outliers removed and TOC greater than zero). The overall distribution for both formations is shown by the box and whisker plot at the top.69

Figure 5-38. Distribution of calculated theoretical maximum CO₂ storage quantities in tons per acre foot for adsorbed gas (A) and free gas in matrix porosity (B) for the Utica Shale and Point Pleasant Formation.70

Figure 5-39. Map of TOC (P50) calculated from geophysical logs for the Utica Shale and Point Pleasant Formations to top of the Trenton/Lexington Formation interval for data with either or both Utica and Point Pleasant tops (368 wells). Color values range from 2.0 (red) to 0 (dark blue). Black lines are basement faults.71

Figure 5-40. Subset maps of TOC (P50) calculated from geophysical logs for the Utica and Point Pleasant formations to top of the Trenton/Lexington Formation interval. (A) Point Pleasant TOC only, no Utica present or mapped (254 wells); (B) Utica TOC only, no Point Pleasant present or mapped (276 wells); (C) Utica TOC where both Utica and Point Pleasant intervals present (162 wells). Black lines are basement faults.72

Figure 5-41. Isopach maps of net thickness with TOC greater than 1.5 percent by unit: (A) Utica Shale map interval (169 wells); (B) Point Pleasant Formation map interval (181 wells); Color values range from 0 (dark blue) to 120 ft (red) in both maps. Black lines are basement faults.74

Figure 5-42. Net isopach map of the combined Utica Shale and Point Pleasant Formation with TOC greater than 1.5 percent. Blue outline illustrates the Utica Shale area of investigation. Red outline illustrates Point Pleasant

	Formation area of investigation. Color values range from 0 (dark blue) to 185 ft (red). Black lines are basement faults.....	75
Figure 5-43.	Regional distribution of carbon storage potential for the Middle Devonian Hamilton Group/Marcellus Shale interval at efficiency factors of (A) 3 percent and (B) 10 percent. Estimated storage potential ranges from 0 (purple) to more than 700,000 short tons (red). (One short ton equals 0.907185 tonnes). Black lines represent basement faults.....	77
Figure 5-44.	Regional distribution of estimated CO ₂ storage (short tons) in the combined Utica Shale/Point Pleasant interval at efficiency factors of (A) 3 percent and (B) 10 percent. (One short ton equals 0.907185 tonnes).	78
Figure 6-1.	Tri-state study area, showing historical and active oil, gas and storage fields.	82
Figure 6-2.	Generalized correlation chart for subsurface geologic units in the tri-state area using Pennsylvania terminology.	84
Figure 6-3.	Oil fields selected for case study assessment.	90
Figure 6-4.	Structure map (200-ft contour intervals highlighted) on top of the Medina group showing field location (green) evaluated for CO ₂ -EOR potential. The structure in eastern Ohio forms a monocline dipping eastward into the Appalachian Basin, with pre-existing basement and Ordovician faults (red) mostly cutting across the regional dip (modified from Solis and Bloxson, 2019).....	92
Figure 6-5.	Regional correlation chart with Medina group type log (modified from Mishra, 2015), illustrating triple-combo curves [GR, RHOB and NPHI], along with a PE curve.	93
Figure 6-6.	Gross thickness map (50-ft contour intervals highlighted) of the Medina group clastic wedge relative to case study fields (green) and influence on deposition from the pre-existing fault systems (modified from Solis and Bloxson, 2019).	94
Figure 6-7.	Measured depth to the top of the “Clinton” sandstone (200-ft contour interval).	95
Figure 6-8.	Medina group outcrop at the Niagara escarpment in western New York State. The photograph illustrates the contact of the Grimsby Sandstone with overlying dolomite and underlying shale, using equivalent drillers’ terms from eastern Ohio.....	96
Figure 6-9.	East Canton Consolidated Field production decline curve (Mishra, 2014).	97
Figure 6-10.	Diagram delineating facies relationship of the “Clinton” sandstone (CLNN) as it intertongues with the Cabot Head Shale in eastern Ohio, with relation to the East Canton Consolidated Field (modified from Riley et al., 2011).	98
Figure 6-11.	“Red Clinton” core photographs and geophysical log for the Smith and Evans well (API No. 3401920256). A) Vertically oriented core of the CLNN 4 and associated red beds. B) Vertically oriented core sample of basal section of CLNN 4 and associated dark-colored flooding surface separating CLNN 4 and CLNN 3. Arrow points to core sampling interval. Flooding surface between CLNN 4 and CLNN 3 is shown with dark gray shading (modified from Mishra, 2015).	99
Figure 6-12.	“White Clinton” core photographs and geophysical log for the McCabe No. 1 well (API No. 3415124758) Photos of the oriented core show A) the	

contact at the base of the CLNN 3 with underlying shale, B) an open fracture, and C) a mineralized fracture. Red arrow points to core sampling interval (modified from Riley et al., 2011). 100

Figure 6-13. Lithologic analysis of the Medina group using the GR log from a well in Osnaburg Township, Stark County, Ohio. This traditional method works well in older fields where the standardized triple-combo log suite is not available for analysis (modified from Knight, 1969). 101

Figure 6-14. Net (75 percent) clean sandstone thickness map (modified from Riley et al., 2011), illustrating the regional depositional setting for the “Clinton” sandstone in East Canton Consolidated Field. Three distributary systems intersect the field, and its western margin bounded by the limits of the paleo-shoreline. 102

Figure 6-15. Measured depth to the top of the “Clinton” sandstone. 103

Figure 6-16. Structure map on the base of the Dayton Dolomite (i.e., “Packer Shell”) compared to cumulative production (modified from Riley et al., 2011). Yellow arrows point toward lineaments (fracture trends) in this interval that appear to be associated with the highest oil production (red bubbles). Mapped study area is outlined in Figure 6-4 and Figure 6-15. 105

Figure 6-17. Yellow arrow points to the high cumulative oil production near two CSDs and one east-west fault, which intersect the thickest local accumulation of net sandstone in the CLNN 4 (“Red Clinton”) reservoir (modified from Riley et al., 2011). 106

Figure 6-18. Yellow arrow points to the high cumulative oil production near two CSDs that intersect a thick local accumulation of net sandstone in the CLNN 3 (“White Clinton”) reservoir (modified from Riley et al., 2011). 107

Figure 6-19. RHOB maps for the CLNN 4 and CLNN 3 intervals, compared to cumulative oil production (modified from Riley et al., 2011). 108

Figure 6-20. Water saturation in the CLNN 4 and CLNN 3 intervals. Yellow arrows point to areas of higher water saturation bounded by two CSDs (modified from Riley et al., 2011). 110

Figure 6-21. Surface lineament locations and cumulative oil production plotted on a structure map of the Dayton Dolomite base (modified from Riley et al., 2011). 111

Figure 6-22. Development of the thickest sandstones occurred along the paleo-shoreline edge (N-S strike section). Heterogeneity is somewhat more pronounced in the W-E dip section, where a combination of distributary sandstones and tidal flat shales are present. Sandstone tends to be most developed where the distributary system intersected the paleo-shoreline. Shading is based upon GR API units, with lower values (yellow) representing cleaner sandstones in the clastic lithologies and dolomites in carbonate lithologies, higher values (green) representing increasing shale content. Formation and lithological divisions follow those of Mishra (2015) based on Riley et al. (2011). 113

Figure 6-23. N-S strike and W-E dip sections using geophysical log control (shading as described in Figure 6-22). The log character displayed in these sections illustrate the complexity of facies distribution encountered by Riley et al. (2011) in their detailed study of the west-central portion of East Canton Consolidated Field. 114

Figure 6-24. Cross sections in the south-central portion of East Canton Consolidated Field, as modified from Mishra (2015). SW-NE section in the south-central quadrant of the field (see inset map, top right) follows basin strike and is subparallel to the north-south trend of the paleo-shoreline. Both the upper CLNN 4 (“Red Clinton”) and the lower CLNN 3 (“White Clinton”) intervals (highlighted in yellow) show gradual thickening and thinning along the shoreline trend. Thicker shoreline sandstones occur where fed by the distributary channels illustrated in the NW-SE dip section, which intersects the general east-west trend of tidal channels (see Figure 6-14) as they weave through the delta plain to the shoreline. Thick sandstone in the middle of the distributary (tidal channel) facies in one well differs from that of delta plain siltstones encountered in an offset well at the same stratigraphic interval. This creates a “zig-zag” effect, enhanced by Mishra’s color scheme, where the solid yellow delineating the reservoir makes “Clinton” heterogeneity more apparent. The index map (top right) shows GR log signatures for the 30 control wells having standardized triple combo logs for the two major producing intervals (CLNN 4 and CLNN 3), separated by the flooding surface identified by Riley et al. (2011). Modern log control in this portion of the field and a smaller area to the north allows for detailed mapping and assessment of production controls. These findings may allow for extrapolation of reservoir parameters thought to influence production to areas where modern log suites are less abundant, or not available at all.115

Figure 6-25. N-S strike and W-E dip sections over the same area as Figure 6-24, using geophysical log control to emphasize the clean sandstone to shale aspect within “Clinton” reservoirs.116

Figure 6-26. N-S strike section shows that clean CLNN 4 and CLNN 3 intervals thin and become more shaley at the southern terminus of the field. Dry holes separate the thin reservoir unit from thicker sandstones downdip to the east, suggesting the presence of good lateral stratigraphic seals. The sandstone character does not change in the updip direction, but legacy wells (see Figure 6-30C) transition from mostly oil producers to gas producers moving updip.117

Figure 6-27. Legacy wells in the north area of East Canton Consolidated Field. A) Producing formation – Most wells produce from the “Clinton” sandstone (orange). Rose Run producers (purple) at top right of map indicate a stacked opportunity (see Section 6.5.5). B) Plugged wells and dry holes – Several dry holes at right edge of field may indicate increasing water saturation and decreasing permeability in the “Clinton” downdip area, forming a lateral seal. C) Well type – Water injection wells (blue) indicate beginning of secondary recovery operations in this field. Gas-oil contact in the “Clinton” sandstone is visible at the western edge of the field.118

Figure 6-28. Legacy wells in the north-central area of East Canton Consolidated Field. A) Producing formation – A majority of wells produce from “Clinton sandstone” (orange). A handful of deep wells (purple) to the east are Rose Run/Beekmantown producers, representing stacked potential (see Section 6.5.5). A deep well (purple) in the heart of the “Clinton” oil field is producing from the Point Pleasant Formation. B) Plugged wells and dry holes - Forty percent of wells have been plugged. Dry holes mark the

eastern field boundary. C) Well type – Note the gas contact to the west and pilot waterflood operations (blue) in the center of the oil field. 119

Figure 6-29. Legacy wells in the south-central area of East Canton Consolidated Field. This area was studied by Mishra (2015). A) Producing formation – A majority of wells produce from “Clinton” sandstone (orange). Point Pleasant organic-rich shale wells (purple) produce to the east just outside of the field footprint, and maps (see Section 6.5.5) indicate this deeper formation may exist as stacked potential within the field itself. Immiscible shallow Berea oil wells (yellow) inside and outside of the field (gray/green) boundaries exist, although most of these have been plugged. B) Plugged wells and dry holes –Approximately 40 to 50 percent of formerly producing wells have been plugged. Dry holes mark the eastern field boundary, indicating a good lateral seal in the form of porosity, permeability, lithology and structural barriers. C) Well type – Note the gas contact to the west. McCormac et al. (1996) noted poor communication between East Canton and Canton Consolidated (west) portions of the field. Note the oil wells and limited waterflood operations in the center of the field footprint. 120

Figure 6-30. Legacy wells in the south area of East Canton Consolidated Field. A) Producing formation – A large, immiscible shallow Berea Sandstone oil field has been mostly plugged to the south. Most wells within the field are producing or have produced from “Clinton” sandstone (orange). Organic-rich shale wells targeting the Point Pleasant Formation (purple) produce to the east of the field footprint. B) Plugged wells and dry holes – Dry holes mark the eastern boundary, as in the other areas of the field, but also wrap around to the south and partially to the west, marking the field terminus. C) Well type – Most oil producers occur in the eastern half of the field, with combination oil and gas wells grading into the gas contact (Canton Consolidated Field) updip to the west..... 121

Figure 6-31. Production decline curve for the Philo Consolidated Field, from Mishra (2014) indicates secondary recovery operations starting in the mid-1960s..... 122

Figure 6-32. IP and MMP for the case study fields in Ohio. Linear and exponential IPs and MMPs are graphed. Calculated IPs from Lewis et al. (2019) correlate well with the upper bound IP of Mishra (2014)..... 123

Figure 6-33. Measured depth to the top of the “Clinton” sandstone in Clayton and Philo Consolidated fields (MRCSP database). Cumulative oil production bubble map indicates possible structural influence along the Cambridge CSD (dark red line)..... 124

Figure 6-34. Net clean sandstone thickness map of the “Clinton” sandstone in Clayton and Philo Consolidated fields (MRCSP database). Cumulative oil production bubble map may be indicative of thicker, cleaner and/or more permeable sandstones. Note that some of the higher cumulative production occurs in gas-prone areas (purple). 125

Figure 6-35. Cross section from southwest to northeast over the northern edge of Clayton Consolidated and Philo Consolidated fields, illustrating the “Clinton” sandstone pinchout to the west..... 127

Figure 6-36. Cross section from southwest to northeast through the central field area, illustrating generally thin sandstone lenses with discontinuous, locally thick accumulations of sandstone in some places. 128

Figure 6-37. Individual “Clinton” sandstone units can be traced as they thicken and thin (and become increasingly sandy or more shaley), using denser well control in this particular cross section.....129

Figure 6-38. Disconnected sandstone bodies, in addition to the structural position and pressure drop during production, may influence the division between oil- and gas-producing areas of the field.130

Figure 6-39. Permeability barriers due to structural and diagenetic controls may have influenced field footprints as much as sandstone development (indicated by the GR log signatures).....131

Figure 6-40. The most significant feature of this producing formation legacy well map is relatively large number of wells targeting the Rose Run Formation (purple) both inside and outside the field footprint (Clayton Consolidated Field straddles the Cambro-Ordovician Rose Run subcrop). “Clinton” producing wells are shown with orange dots. Yellow dots represent shallow, immiscible Berea Sandstone producers, and only one injection well (blue) is present.132

Figure 6-41. From this well type legacy map, the geographic separation between oil producing wells and other types of hydrocarbon production is evident, suggesting that Clayton Consolidated Field may have the trapping mechanisms necessary for CO₂-EOR. Multiple water injection wells (blue) are visible. Shallow, immiscible Berea oil wells are represented by dense masses of green dots.....133

Figure 6-42. Several dry holes exist in the Clayton Consolidated Field, indicative of either the age of these wells (i.e., pre-modern-day stimulation techniques) and/or areas of thin sandstone between thicker, discontinuous lenses. The number of plugged wells relative to producing wells is quite high, especially in some of the oil producing areas. Nearly all shallow Berea Sandstone wells have been plugged.....134

Figure 6-43. The producing formation legacy well map shows several wells targeting the Rose Run or Beekmantown formations along a west/north-east to east/southeast trend that also corresponds to some Oriskany Sandstone wells and to the divisions between oil and gas footprints in the “Clinton” sandstone. This strongly suggests the presence of a major structural feature (possibly a wrench fault because of the lack of visible throw; see Figure 6-33). There are also several wells targeting the Oriskany along the Cambridge CSD. Shallow, immiscible Berea Sandstone wells are present in thin, well-defined bands.....135

Figure 6-44. This well type legacy map shows most of the current “Clinton” oil producers to be in the southern portion of Philo Consolidated Field. Gas-prone areas have many gas wells, but oil, gas and combination oil and gas wells are present in both the oil and gas field footprints. The shallow Berea wells are primarily oil wells. A few, isolated injection wells are visible.....136

Figure 6-45. This map of plugged wells and dry holes illustrates that dry holes occur with greater frequency around the margins of Philo Consolidated Field. However, there are also several producing “Clinton” wells of the same well type (mostly combination oil and gas wells) connecting this field to adjacent fields, such that trap integrity would have to be carefully evaluated. The highest cumulative oil producers in the gas footprint, which all occur in a narrow west-east trend, have been plugged. It is unclear

	whether oil production in this case was entirely associated with fracture permeability or whether matrix permeability also exists. Most oil wells in the oil footprints of this field have also been plugged, which may require additional drilling or possibly horizontal drilling access to the “Clinton” sandstone for CO ₂ -EOR.....	137
Figure 6-46.	Stacked opportunities for CCUS occur above and below the “Clinton” sandstone (orange) from Cambro-Ordovician carbonates and sandstones through organic-rich Devonian shales. Southwest-northeast cross section runs from Clayton and Philo Consolidated fields to East Canton Field.	138
Figure 6-47.	Cross section through the center of the Clayton and Philo Consolidated fields, illustrating stacked formations with CO ₂ -EOR and CCUS potential in this area.....	139
Figure 6-48.	Cross section along the northern edge of the Clayton and Philo Consolidated fields area, illustrating the updip pinchout of the “Clinton” sandstone and subcrop of the Rose Run Formation.....	140
Figure 6-49.	Gross thickness map (50-ft contour interval) of the Rose Run sandstone where it subcrops at the Knox unconformity in the case study area. Depleted hydrocarbon reservoirs with CCUS potential occur in the horizontally and vertically sealed erosional remnants (modified from Riley et al., 1993).....	142
Figure 6-50.	Structure map (100-ft contour interval) on top of the Rose Run Formation in eastern Ohio.....	143
Figure 6-51.	Rose Run type section (Flood, 2011).....	144
Figure 6-52.	Structure map (100-ft contour interval) on the top of the Point Pleasant Formation in eastern Ohio. Inset map outlined in red adjacent to the East Canton Consolidated Field is derived from seismic time data, showing near-basement structure over an area producing from the Utica/Point Pleasant (modified from Torry, 2014).....	146
Figure 6-53.	Horizontal Utica-Point Pleasant activity (ODNR, 2019) shows producing wells in and near case study field locations in eastern Ohio.....	147
Figure 6-54.	Utica-Point Pleasant play area in Ohio (modified from Wickstrom et al., 2012) showing case study fields relative to S1 data. To date, development of the shale play has occurred mainly east of the case study fields.....	148
Figure 6-55.	A) Type section for the Utica/Point Pleasant interval from Tuscarawas County (modified from Riley et al., 2010) located midway between case study fields. B) Comparison to type log from the Utica Play Book (modified from Patchen and Carter, 2015).....	149
Figure 6-56.	NPHI thickness (Bloxxon, 2017) overlain with “Newburg” gas fields (pink, from Noger et al., 1996). Clayton Consolidated Field appears to be on trend, although lack of gas development suggests it may be more brine saturated than gas depleted.....	150
Figure 6-57.	Isochore Contours of the Lockport Dolomite (Solis and Bloxxon, 2019), overlain with “Newburg” gas fields (pink, from Noger et al., 1996), shows the location of patch reef bioherms (darkest turquoise, indicating greatest thickness, in the north-central portion of map) in the Lockport to “Newburg” gas fields.....	151
Figure 6-58.	Although in the oil window in Ohio, most of the Upper Devonian shales are too shallow to support miscible storage of CO ₂ . Of those that are, the	

	Marcellus is absent to very thin throughout the case study area (B), which lies 1500 to 3000 ft below sea level where present (A).....	152
Figure 6-59.	Current development of the Marcellus is restricted to the extreme southeastern edge of Ohio in Jefferson, Belmont and Monroe counties, where the formation thickens rapidly, as seen in this 3D model (The Energy Consulting Group-accessed online 5/2019).....	153
Figure 6-60.	Pennsylvania case study locations.....	154
Figure 6-61.	Generalized subsurface stratigraphic chart, highlighting Venango Group lithostratigraphy as used in southwestern Pennsylvania.....	156
Figure 6-62.	Structure map (100-ft contour interval) on top of the Venango Group in southwestern Pennsylvania.....	159
Figure 6-63.	Gross thickness map (5-ft contour interval) of the Gantz sandstone in Greene and Washington counties.	161
Figure 6-64.	Gross thickness map (10-ft contour interval) of the Fifty-Foot sandstone in Greene and Washington counties.	163
Figure 6-65.	Gross thickness map (10-ft contour interval) of the Gordon sandstone in Greene and Washington counties.	165
Figure 6-66.	Location of well control and geologic cross sections prepared for the Venango Group interval in Greene and Washington counties.	166
Figure 6-67.	Dip cross section A-A', western Washington County through eastern Greene County.....	169
Figure 6-68.	Strike cross section B-B', including the western portion of Washington-Taylorstown Field and points farther north.	170
Figure 6-69.	Strike cross section D-D', New Freeport Field to Linden Field.....	171
Figure 6-70.	Strike cross section F-F', eastern Greene County.	172
Figure 6-71.	Washington-Taylorstown Field and its prominent discovery wells.	174
Figure 6-72.	The Washington-Taylorstown Field has produced oil, gas and shale gas from more than 1500 wells (EDWIN, 2019).	175
Figure 6-73.	The Linden Field has produced shallow oil and gas from more than 200 wells (EDWIN, 2019).	181
Figure 6-74.	SEM images (secondary electron imaging) of the Gantz sandstone at 2420-2424 ft (left) and Gordon sandstone at 2672-2680 ft (right). Platy clay minerals are visible in both samples.	184
Figure 6-75.	SEM images of porosity (dark spots with dimension) in the Gordon sandstone at 2690-2700 ft (backscatter electron composition, left; secondary electron imaging, right).	184
Figure 6-76.	Porosity-permeability crossplot, using Gordon sandstone core data from Washington County wells (Hodgins No. 13, API No. 3712501175; Kenamond No. 1, 3712592783; PA DCNR, 2009).....	185
Figure 6-77.	Hamilton No. 3299 (API No. 3712520107) GR and sample logs.	186
Figure 6-78.	The New Freeport Field has produced shallow oil and gas (including some CBM) from approximately 400 wells (EDWIN, 2019).	188
Figure 6-79.	EOR activities in southwestern Pennsylvania (modified from Riley et al., 2010).....	190
Figure 6-80.	Oil production and EOR activities in Washington-Taylorstown Field.....	192

Figure 6-81. Modern EOR operations in Washington-Taylorstown Field.	193
Figure 6-82. Stratigraphic representation of stacked CCUS potential in southwestern Pennsylvania.....	195
Figure 6-83. Southwestern Pennsylvania’s stacked storage potential is defined by the lithology, structure and hydrocarbon trapping mechanisms of its subsurface rocks, as well as the geologic history of the area (inset structure contour map from Figure 6-63).....	196
Figure 6-84. Oriskany Sandstone structure and plays in southwestern Pennsylvania (modified from Kostelnik and Carter, 2009).	198
Figure 6-85. Marcellus Shale structure contour map for southwestern Pennsylvania (modified from Harper et al., 2017).....	199
Figure 6-86. Mineralogy analysis of the vertical section of Hill Unit 2H, API No. 3712523880, Washington County, PA (modified from Opsitnick, 2015).....	200
Figure 6-87. Mineralogy analysis of the vertical section of Hill Unit 3H, API No. 3712523879, Washington County, PA (modified from Opsitnick, 2015).....	201
Figure 6-88. Utica Shale structure contour map for southwestern Pennsylvania (modified from Patchen and Carter, 2015).	203
Figure 6-89. Mineralogy versus sample depth for the Starvaggi No. 1 (modified from Patchen and Carter, 2015).	204
Figure 6-90. Regional Stratigraphic chart with local stratigraphic column with drillers’ names on the right. Red arrows highlight potential CCUS horizons.....	207
Figure 6-91. Four case study fields mapped with regional anticlines and synclines (modified from Moore et al., 2013).	208
Figure 6-92. Case study fields with regional anticlines and synclines and structure map (100-ft contour interval) on the base of the Gordon sandstone (modified from Moore et al., 2013).	209
Figure 6-93. Stacked sandstones of the Venango, Bradford and Elk groups in northern West Virginia (modified from Boswell et al., 1996).....	211
Figure 6-94. Oil and gas wells in the Jacksonburg-Stringtown Field.	213
Figure 6-95. Structure map (20-ft contour interval) on the top of the Gordon sandstone (modified from Matchen, 2001, and Moore et al., 2013).	214
Figure 6-96. Status of wells associated with waterflood operations in the Jacksonburg-Stringtown Field, currently operated by Ascent Resources.....	215
Figure 6-97. Well log submitted as part of the geologic review for Ascent Resources UIC Area Permit. Note the recognition of three individual parasequences in the Gordon Stray interval, each with a low GR signature and crossover of DPHI and NPHI logs, suggesting presence of hydrocarbons (WVDEP).	217
Figure 6-98. Full-core photograph of the Ball 18 well (McBride, 2004).	219
Figure 6-99. Core log of the Gordon Stray sandstone from the Ball 18 well, Jacksonburg-Stringtown Field (McBride, 2004).....	220
Figure 6-100. Core log of the Gordon Stray sandstone from the Reilly 13 well, Jacksonburg-Stringtown Field (McBride, 2004).	222
Figure 6-101. Full-core photograph of the Irene Reilly 13 well (McBride, 2004).....	223
Figure 6-102. Gross thickness map (10-ft contour interval) of the Gordon sandstone in Wetzel, Tyler and Doddridge counties (Moore et al., 2013).....	226

Figure 6-103. West to east Gordon cross section through Jacksonburg-Stringtown Field (Moore et al., 2013).....	227
Figure 6-104. North to south Gordon cross section through Jacksonburg-Stringtown Field (Moore et al., 2013).	228
Figure 6-105. Petrophysical analysis of the Gordon Stray (GRSR) and lower Gordon sandstones (GRDN-GRDN_B) in Wetzels 568 (Moore et al., 2013).....	229
Figure 6-106. Waterflood wells in the Jacksonburg-Stringtown Field.....	230
Figure 6-107. Annual oil production (DDS5, 2018) and waterflood well completions in Jacksonburg-Stringtown Field.	231
Figure 6-108. Oil and gas wells in the Mannington Field.	232
Figure 6-109. Oil wells of the Mannington Field.....	233
Figure 6-110. Gross thickness map (25-ft contour interval) of the “Big Injun” sandstone in northern West Virginia (modified from Vargo and Matchen, 1996). The Mannington Field shown in the rectangular box.	234
Figure 6-111. Gross thickness (10-ft contour interval) of the Gordon sandstone in Marion County (Moore et al., 2013).....	235
Figure 6-112. Southwest to northeast stratigraphic cross section of the Gordon sandstone in Marion County, flattened on the base of the Gordon sandstone interval (Moore et al., 2013).	236
Figure 6-113. Northwest to southeast stratigraphic cross section of the Gordon sandstone in Marion County, flattened on the base of the Gordon sandstone interval (Moore et al., 2013).	237
Figure 6-114. Petrophysical analysis of Venango Group sandstones in Marion 1077 (Moore et al., 2013).....	238
Figure 6-115. Waterflood wells in Mannington Field. The different colors represent total depth formations as reported by drillers.	240
Figure 6-116. Annual oil production (DDS5, 2018) and waterflood well completions in the Mannington Field (1979-2011).	241
Figure 6-117. Map of wells in Salem-Wallace (green) and Wolf Summit-Big Isaac (blue) fields.	242
Figure 6-118. Gross thickness map (10-ft contour interval) of the Gordon interval in the Salem-Wallace Field (Moore et al., 2013).	244
Figure 6-119. South to north Gordon stratigraphic cross section through the Salem-Wallace Field. Note the stacked sandstone layers of the Gordon in this area (Moore et al., 2013).....	245
Figure 6-120. Petrophysical analysis of Venango Group sandstones in Harrison 2195 (Moore et al., 2013).....	246
Figure 6-121. Salem-Wallace cumulative and decline curves on historical production with modern production data (from Ober and Eckert, 2014). *Data obtained from Rietz Tucker, Assistant State Geologist of West Virginia.....	248
Figure 6-122. Oil wells in the Wolf Summit-Big Isaac Field.....	250
Figure 6-123. Gross thickness map (10-ft contour interval) of the Gordon interval in the Wolf Summit-Big Isaac Field (Moore et al., 2013).	252
Figure 6-124. South to north cross section through the Wolf Summit-Big Isaac Field (Moore et al., 2013).....	253

Figure 6-125. Petrophysical analysis of Venango Group sandstones in Harrison 1156 (Moore et al., 2013).....254

Figure 6-126. Secondary recovery waterflood well locations in the northern portion of Wolf Summit-Big Isaac Field.255

Figure 6-127. Annual oil production (DDS5, 2018) and waterflood well completions in the Wolf Summit-Big Isaac Field.256

Figure 6-128. Secondary oil recovery operations via waterflooding (red). Recovery operations in Mannington Field have been discontinued (Moore et al., 2013).....257

Figure 6-129. Annual oil production and waterflood wells drilled in Jacksonburg-Stringtown, Wolf Summit and Mannington fields.259

Figure 6-130. Normalized annual oil production and number of waterflood wells drilled in Jacksonburg-Stringtown, Wolf Summit and Mannington fields.261

Figure 6-131. Stratigraphic column illustrating stacked CCUS potential in north-central West Virginia.....263

Figure 6-132. Case study fields with Brown Lumberport (gray) and Jarvisville (tan) fields producing gas from the Bradford and Elk groups.265

Figure 6-133. Huntersville Chert/Oriskany Sandstone fields (yellow) in the case study area.266

Figure 6-134. Structure map (100-ft contour interval) on top of the Oriskany Sandstone in northern West Virginia.....267

Figure 6-135. Structure map (100-ft contour interval) on the base of the Marcellus Shale in northern West Virginia.268

Figure 6-136. Bubble map of Marcellus Shale gas production in relation to the study area (modified from Dinterman, 2018).....269

Figure 6-137. Deviated well paths (permitted, completed and cancelled) in the case study area. The Wolf Summit waterflood wells are circled.....270

Figure 6-138. Utica Shale structure contour map for northern West Virginia (modified from Patchen and Carter, 2015).....271

List of Acronyms

API	American Petroleum Institute
BHT	Bottom hole temperature
CBM	Coalbed methane
CCS	Carbon capture and storage
CCUS	Carbon capture, utilization and storage
CLNN	“Clinton” sandstone
CO ₂	Carbon dioxide
CSD	Cross-structural discontinuity
DOE	U.S. Department of Energy
DPHI	Density porosity
EDWIN	Exploration and Development Well Information Network
EGR	Enhanced gas recovery
EOR	Enhanced oil recovery
GR	Gamma ray
IDE	Interactive development environment
IQT	Inter-quartile distance
IP	Initial pressure
KDE	Kernel density estimate
KGS	Kentucky Geological Survey
KU	University of Kansas
LAS	Los Ascii Standard format
MMP	Minimum miscibility pressure
MRCSP	Midwest Regional Carbon Sequestration Partnership
MSL	Mean sea level
NETL	National Energy Technology Laboratory
NGL	Natural gas liquids
NPHI	Neutron porosity
ODGS	Ohio Division of Geological Survey
OLS	Ordinary Least Squares
OOIP	Original oil in place

List of Acronyms

PAGS	Pennsylvania Geological Survey
PE	Photoelectric effect
Pi	Lithostatic pressure
RHOB	Bulk density
RMSE	Root mean square error
SEM	Scanning electron microscopy
SGR	Spectral gamma ray
SMU	Southern Methodist University
SON	Sonic
TOC	Total organic carbon
TORIS	Tertiary Oil Recovery Information System
UIC	Underground Injection Control
UND	University of North Dakota
XRD	X-ray Diffraction
WVDEP	West Virginia Department of Environmental Protection
WVGES	West Virginia Geological and Economic Survey

Units of Measure

ac	acres
ac-ft	acre-feet
BBL	barrel
BBL/ac-ft	barrels per acre-foot
BCF	billion cubic feet
BOPD	barrels of oil per day
°F	degrees Fahrenheit
ft	feet
g/cm ³	grams per cubic centimeter
m	meters
mi	miles
mD	milliDarcy
mD-ft	milliDarcy-feet
MCF	million cubic feet
MMBLS	million barrels
MMBO	million barrels of oil
ppm	parts per million
psi	pounds per square inch
TCF	trillion cubic feet

1.0 Introduction

The Midwest Regional Carbon Sequestration Partnership (MRCSP) has incorporated the work of geologic research teams (Geoteams) in its regional characterization, project planning and carbon dioxide (CO₂) injection implementation work since the partnership was established by the U.S. Department of Energy (DOE) in 2003. Over this 16-year period, the cohort of Geoteams has grown from five to ten states and has contributed to the characterization of geologic sequestration opportunities, refinement of reservoir and seal data, and supported injection efforts through both predictive and post-injection assessments.

The regional characterization work conducted by the Geoteams during the MRCSP Phase III project period (2010 – 2019) focused on the following tasks: (1) refinement of geologic seals/reservoir systems; (2) assessment of Atlantic Coastal Plain and offshore opportunities; (3) expanded assessments of oil and gas fields, particularly as they relate to enhanced recovery opportunities; (4) regional support for implementation of carbon capture utilization and storage (CCUS) in the partnership area; and (5) communication and data sharing. The findings of this work are summarized in the final report entitled *Final Report of Geologic Carbon Capture Utilization and Storage Opportunities* in the form of a state-by-state presentation for the MRCSP Region.

In addition to the capstone deliverable mentioned above, the Geoteams have also prepared a series of topical reports to elaborate on specific geologic intervals and/or geographic areas of study completed during the Phase III project period. Specifically, these topical reports address: (1) the Atlantic Coastal Plain and adjacent offshore; (2) Cambro-Ordovician reservoirs/seals in the region; (3) enhanced oil and gas recovery opportunities in the Appalachian Basin; and (4) enhanced oil recovery (EOR) in the Michigan Basin. The remainder of this topical report presents our findings relative to enhanced recovery opportunities in the Appalachian Basin.

2.0 Appalachian Basin Research Efforts

Regional-scale geologic characterization efforts have been vital to understanding the breadth and extent of carbon storage and enhanced recovery opportunities in the Appalachian Basin geologic structure. During the Phase III project period, Geoteam members added to the knowledge acquired from previous work in Phases I and II by developing and applying data transforms to make the most of publicly available data; augmenting existing datasets to refine geological, petrophysical and reservoir characteristics of the many target intervals in the basin; and establishing a series of metrics to assess CCUS prospects, with particular consideration given to stacked potential. This information has been used to map subsurface geologic units, refine potential storage resource volumes and identify new potential CCUS opportunities.

2.1 Purpose

In many places across the MRCSP Region, oil and gas fields are considered to be the best near-term candidates for implementing CCUS because of opportunities for the enhanced recovery of petroleum hydrocarbons. This is particularly true in the Appalachian Basin portion of the region, where the petroleum industry was born more than 150 years ago. This CCUS potential is notable because many CO₂ point-sources exist here; the area is home to both shallow and deep oil and gas fields that are still actively produced, as well as fields considered to be depleted and/or have been converted to gas storage; and unconventional oil and gas development is particularly prominent in this area. In other words, both legacy and modern-day oil and gas activity in the Appalachian Basin offer opportunities for miscible and/or immiscible enhanced recovery operations in an area whose populace is familiar with industry operations and has existing (or pending) infrastructure that may facilitate CCUS.

2.2 Project Team

The Appalachian Basin Geoteam consists of geologists from the state geological surveys of Kentucky, Maryland, New York, Ohio, Pennsylvania and West Virginia. Pennsylvania and West Virginia led the research related to enhanced recovery opportunities in oil and gas fields, while Kentucky led the work associated with enhanced gas recovery (EGR) opportunities in organic-rich shales.

Research team members include Stephen Greb, David Harris, Brandon Nuttall and Thomas Sparks (Kentucky); Rebecca Adams, David Andreasen, David Brezinski, William Junkin, Richard Ortt, Jr. and Andrew Staley (Maryland); Brian Slater (New York); Michael Angle, James McDonald, Michael Solis, Paul Spahr and Christopher Waid (Ohio); Robin Anthony, Kristin Carter, Michele Cooney, Brian Dunst, John Harper (ret.), Katherine Schmid and Ion Simonides (Pennsylvania); and Mitch Blake, Gary Daft, Philip Dinterman, J. Eric Lewis, Jessica Moore and Susan Pool (West Virginia).

2.3 Overview of Major Tasks

2.3.1 Assessment of Storage and Enhanced Recovery for Oil and Gas Fields

The Appalachian Basin Geoteam evaluated reservoirs amenable to CO₂-EOR and EGR using a combination of data sources and technical approaches. The team supplemented pre-existing MRCSP EOR reservoir data (Wickstrom et al., 2005; Riley et al., 2010) with additional information from other sources, including the Tertiary Oil Recovery Information System (TORIS) (PTTC, 2005; Patchen, 1996), Takacs et al. (2011) and Carter et al. (2015). The research team also reviewed publicly available (post-2012) drilling, completion and production data to vet

existing EOR opportunities, and to identify potential new enhanced recovery opportunities in the basin.

MRCSP's earlier analyses (Riley et al., 2010) assessed oil fields at depths of ≥ 2500 feet (ft). This criterion was established because CO₂ remains supercritical and suitable for miscible EOR flooding at this minimum depth. The current analysis included all oil fields so as to characterize those located at depths shallower than 2500 ft, and therefore potentially suitable for a near-miscible CO₂ flood.

Although oil fields were the primary focus of the current reservoir characterization work, the current effort provided additional field-level reservoir data compilation and assessment for natural gas reservoirs as well.

2.3.2 Assessment of Storage and Enhanced Recovery for Organic-Rich Shale

Exploration and development of relatively shallow oil and gas resources in the Appalachian Basin over the past 150+ years has led to the identification of several organic-rich source rock intervals including the Ohio, Marcellus and Utica shales. Since 2006, the introduction of horizontal wells and multi-stage fracture stimulations has served to unlock these source rocks to become prolific producing reservoirs. These stacked reservoirs are a world-class resource and present an opportunity to address growing energy demands both domestically and abroad. Continued use of petroleum-based fuels also encompasses the challenge to minimize the environmental impact of associated CO₂ emissions. Previous work has suggested one possibility is to use CO₂ injected into organic-rich shales yielding both enhanced production and storage of the CO₂ in an immobile state, adsorbed onto organic matter and clays. Research has found that intraparticulate porosity in organic matter increases as it matures during hydrocarbon generation (Mastalerz et al., 2013). This effect influences both gas storage volumes and production rates or injection rates during EGR.

The Appalachian Basin Geoteam investigated the potential for carbon storage and EGR within organic-rich shales, including the Middle Devonian Marcellus and Upper Ordovician Utica/Point Pleasant formations. This work was built on past research of the Huron shale in Kentucky, which documented a relationship between total organic carbon (TOC) and bulk density (RHOB) in downhole geophysical log profiles (Nuttall et al., 2006; Schmoker, 1981, 1993). The team utilized these same types of data to assess the distribution of organic matter, CO₂ storage estimates and potential for enhanced recovery of petroleum hydrocarbons.

2.3.3 Evaluation of CCUS Opportunities

Reservoir characterization efforts were used to inform an additional component of this scope of work – evaluation of CCUS opportunities for the tri-state area of Ohio, Pennsylvania and West Virginia. The Geoteam identified more than 4800 oil, gas and gas storage fields in this area, which encompass about 17,000 square miles (sq mi) and approximately 40 counties.

The intent of this work was to consider prospective reservoirs regardless of depth (i.e., both miscible and immiscible CCUS were considered), including horizons that are being produced for the first time, are considered depleted or depleting or are associated with natural gas storage (active or abandoned). In this manner, we improve the likelihood of identifying localities where an industrial source of CO₂ is proximal to: (1) reservoirs that would benefit from enhanced recovery operations and/or could be used to permanently store CO₂; and (2) the infrastructure necessary to make injection feasible (e.g., access to pipeline rights-of-way, temporary storage of CO₂ to be injected using abandoned gas storage fields, etc.).

The Geoteam characterized the subsurface geology of the area in stepwise fashion, starting with existing geologic maps and fields/pools data generated as part of previous MRCSP regional characterization research. With these data in hand, the Geoteam correlated stratigraphy and generated cross sections to delineate the extent, depths and thicknesses of those formations that may serve as reservoirs for either miscible or immiscible enhanced recovery projects. In addition, the team prepared structure and isopach maps for prospective formations, as well as assessments of gross and net porosity of these units. Once prospective localities were identified, the Geoteam selected a short list of oil fields in each of the three states for assessment by way of case study preparation.

3.0 Appalachian Basin

The MRCSP Region encompasses nine major physiographic provinces that span both onshore and offshore environments. The Appalachian Basin geologic structure is situated in the center of the region, with the Michigan Basin and Kankakee, Cincinnati and Findlay arches to west and the Fold and Thrust Belt, Coastal Plain and Continental Shelf to the east (Figure 3-1).

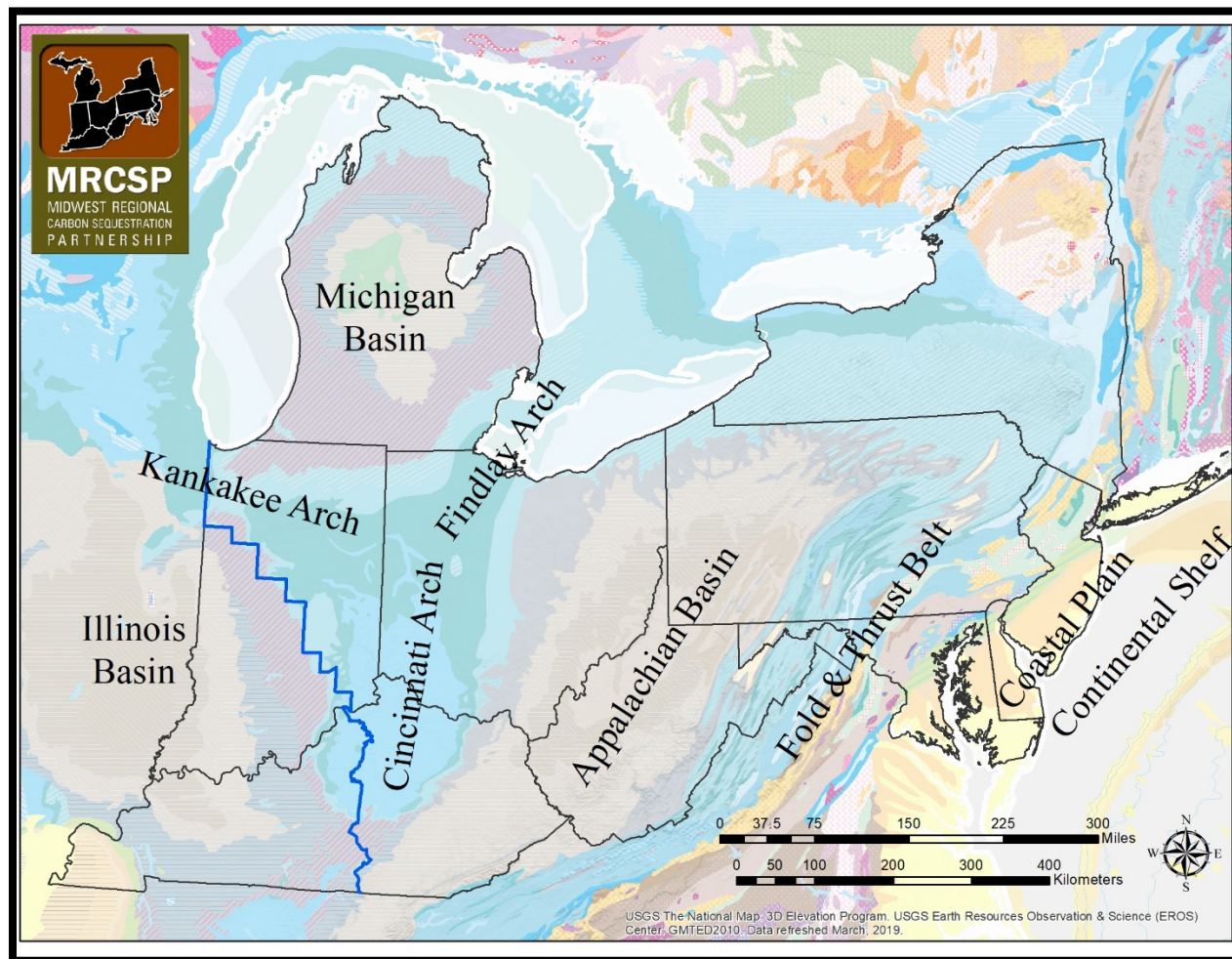


Figure 3-1. Major structural features in the MRCSP Region (Dinterman et al., 2019).

The Findlay Arch (northern Ohio) separates the Michigan Basin from the Appalachian Basin to the southeast, and the Cincinnati Arch (Kentucky, Indiana and Ohio) separates the Illinois Basin from the Appalachian Basin to the east. The western boundary of the MRCSP Region (jagged blue line in Figure 3-1) approximates the boundary between the Illinois Basin and the Cincinnati Arch.

3.1 CO₂ Point-Sources

Figure 3-2 illustrates the relative magnitude and source of CO₂ emissions from power plants throughout the MRCSP Region over a ten-year period (2005 – 2015). During this timeframe, total emissions averaged 750,754,783 tonnes per year. While a majority of these emissions are derived from coal, natural gas sources play a notable role in coastal states.

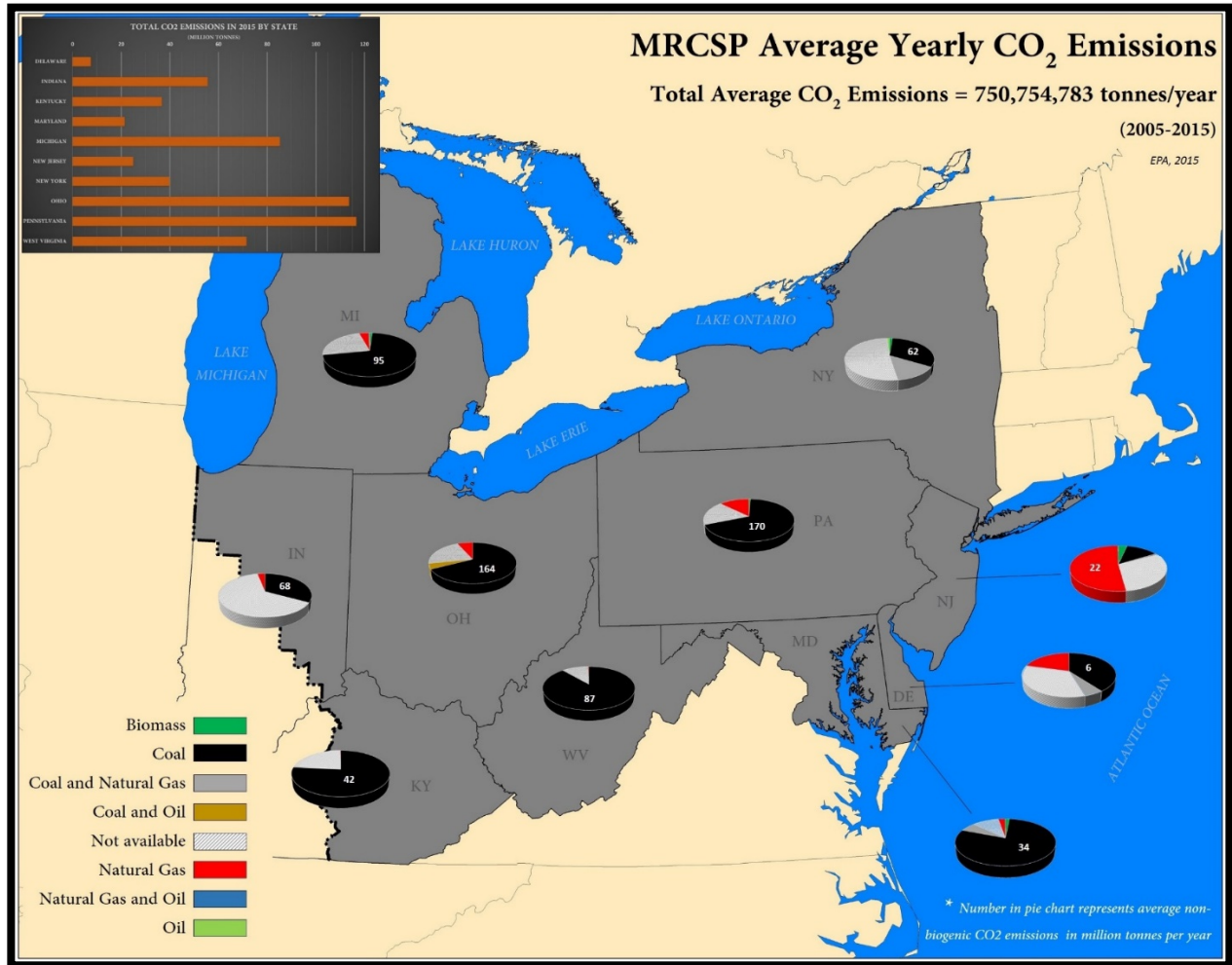


Figure 3-2. Average yearly power plant CO₂ emissions by state and fuel source (2005 – 2015).

Previous MRCSP assessments targeted deep saline formations exclusively for permanent storage and considered CO₂ point-sources with emissions greater than 100,000 tonnes/year (NATCARB, 2014). Evaluating the MRCSP Region for both permanent storage and enhanced recovery opportunities, which is the focus of the current work, necessitates the inclusion of sources with a wider range of CO₂ emissions. Accordingly, this study has incorporated emission statistics from the Environmental Protection Agency (EPA) for sources emitting more than 25,000 tonnes in 2017. As illustrated in Figure 3-3, this augments previously used point-source data from 2014 (black circles) with those reporting a wider range of CO₂ emissions in 2017 (yellow triangles).

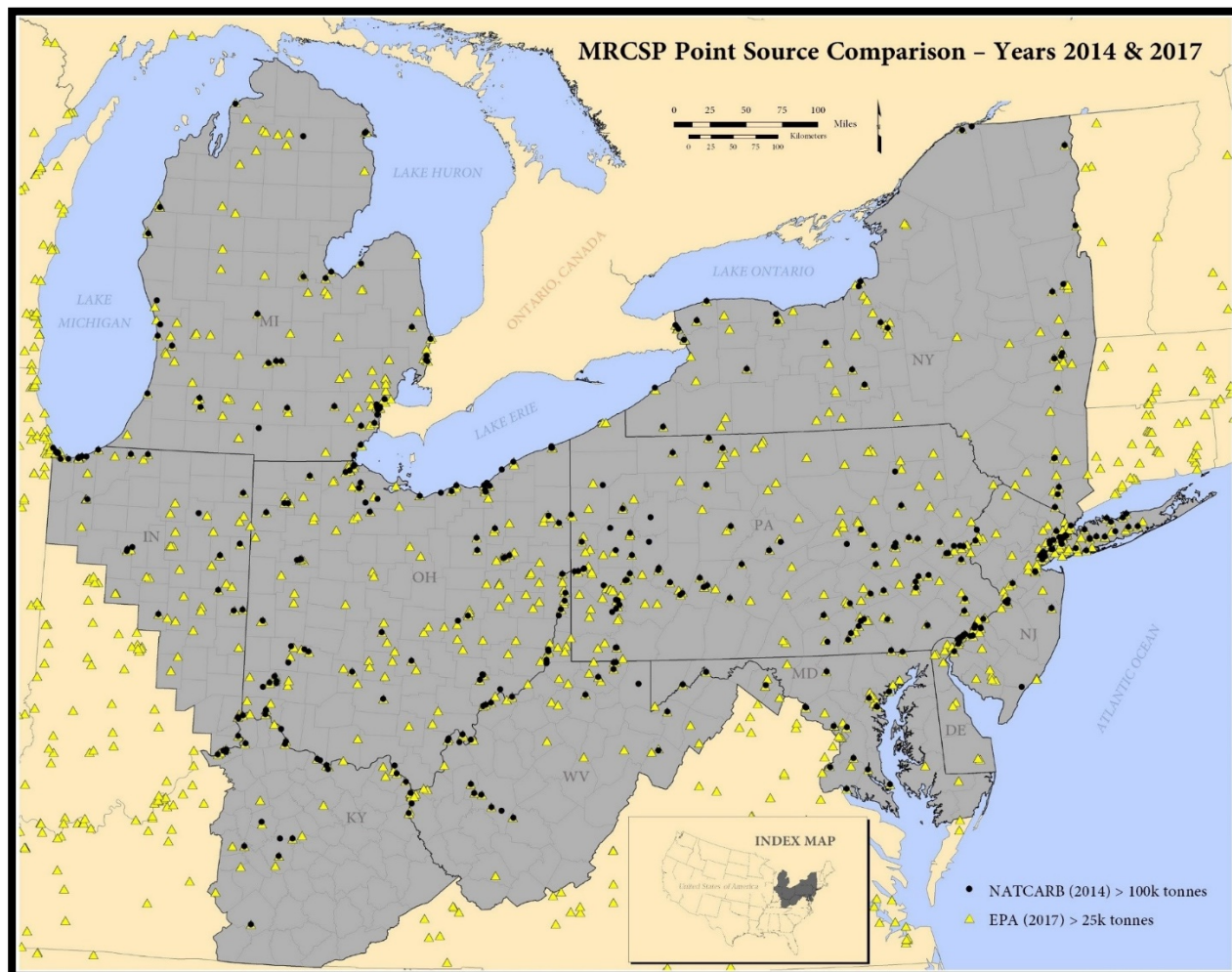


Figure 3-3. Comparison of previously used point-source data (black circles) to those used in the current study (yellow triangles).

3.2 Geology

The Appalachian Basin is northeast-southwest-trending asymmetric foreland sedimentary basin that extends from Quebec (Canada) to northern Alabama (United States) and contains preserved sediments derived from multiple tectonic events that span a period of several hundred million years. Within the MRCSP Region, the Appalachian Basin encompasses portions of Kentucky, Maryland, New York, Ohio, Pennsylvania and West Virginia. The basin's eastern margin is obscured by the Fold and Thrust Belt of central Pennsylvania, Maryland, West Virginia and Virginia, and the western margin extends to central Ohio and east-central Kentucky (Figure 3-1).

Wickstrom et al. (2005) described the geologic evolution of the Appalachian Basin, particularly as it relates to the observed depth, thickness and extent of sedimentary strata that may offer carbon storage potential in the region. In summary, the basin began to form in Cambrian time above the Rome Trough, a tectonically induced basement structure that extends from Kentucky through West Virginia, and northeastward into western Pennsylvania and possibly to parts of the northern Appalachian Basin. Over geologic time, the basin was enlarged by periodic reactivation of faults that developed in response to collisional mountain building events and provided

accommodation space for the deposition of sediments shed from the highlands. These include the Taconic Orogeny of Late Ordovician time; the Acadian Orogeny of Middle to Early Mississippian time; and the Alleghanian Orogeny of Pennsylvanian-Permian time.

As a consequence of this extensive geologic history, sedimentary rocks in the Appalachian Basin range from Neoproterozoic (540+ million years) to Permian (~300 million years) in age (USGS, 2010). The basin holds a relatively continuous stratigraphic succession of sediments that are thickest within and adjacent to the area of the Rome Trough in eastern Kentucky, West Virginia and Pennsylvania. In fact, more than 45,000 ft of sedimentary strata exist in the deepest reaches of the basin (i.e., central Pennsylvania). The reader is referred to Appendix A of Wickstrom et al. (2005) for a focused presentation of regional geologic units that may serve as either carbon storage reservoirs or seals; these formations range from Cambrian to Pennsylvanian in age.

3.3 Stratigraphy

The lithostratigraphy of the MRCSP Region is presented in Dinterman et al. (2019), using both stratigraphic correlation charts and geologic cross sections that canvas the ten-state region. These graphical representations have been prepared to: (1) depict and correlate subsurface stratigraphy from state to state; and (2) illustrate lateral and vertical relationships among potential carbon storage targets (whether local or regional) and confining units. The stratigraphic correlations provided in Dinterman et al. (2019) represent a revision of Wickstrom et al. (2005)'s Figure 5, having incorporated the states added to MRCSP since 2005, as well as refinements in lithostratigraphic nomenclature and categorization of reservoirs (targets) and seals (confining units).

Table 3-1 lists the naming convention, orientation and geographic location of each of Dinterman et al. (2019)'s cross section plates. The locations of these cross sections were selected not only to incorporate the region's major structural features but also to pass through areas of dense CO₂ point-source emissions (where carbon storage will be needed) and modern deep well control (to provide the most thorough illustration of subsurface geology possible).

Table 3-1. Cross section plates reported in Dinterman et al. (2019).

Cross Section	Orientation	Physiographic Province(s)	States
A-A'	north-south	Michigan Basin, Arches, Appalachian Basin	Michigan, Indiana, Ohio, Kentucky
B-B'	west-east	Michigan Basin, Arches, Appalachian Basin	Indiana, Ohio, Pennsylvania
C-C'	northwest-southeast	Michigan Basin, Arches, Appalachian Basin	Michigan, Indiana, Ohio, West Virginia
D-D'	west-east	Illinois Basin, Cincinnati Arch, Appalachian Basin	Indiana, Kentucky, Ohio, West Virginia
E-E'	southwest-northeast	Illinois Basin, Appalachian Basin	Kentucky, Illinois, Ohio, West Virginia, Pennsylvania
F-F'	west-east	Coastal Plain, Continental Shelf	New Jersey, Mid-Atlantic U.S. Offshore

Of these, Cross Section E-E' is most pertinent to the Appalachian Basin, as it runs along the Ohio River Valley corridor and roughly parallel to basin strike through West Virginia and western Pennsylvania. This section illustrates the thick accumulations of sedimentary rocks in this part of the basin and multiple options for local and regional carbon storage.

4.0 Oil and Gas Field Storage and Enhanced Recovery Assessment

4.1 Introduction

The Appalachian Basin contains conventional siliciclastic reservoirs of various ages (Mississippian through Cambrian) and at various depths (less than 1000 ft to more than 10,000 ft). A large majority of the proven oil producers are typically shallow (less than ~3000 ft), with many also producing gas. Natural gas has been developed throughout the region from numerous units, both shallow and deep.

The variety of existing opportunities for petroleum hydrocarbon production in the Appalachian Basin, as well as the attractiveness of repurposing reservoirs for storage post-production, necessitate a thoughtful, measured approach for developing regional CCUS implementation strategies that make the most of the basin's subsurface geologic resources. In this chapter, the West Virginia Geological and Economic Survey (WVGES) has compiled petroleum hydrocarbon reservoir data at the field level; used this information to estimate the CO₂ storage potential in the basin's depleted/depleting oil and gas fields; and prepared an assessment of these data to rank the most favorable areas for CO₂-EOR in the Appalachian Basin. These data and findings are intended to provide the geospatial and technical context for support of CCUS in the MRCSP Region into the future.

4.2 Methods

4.2.1 Digital Data Compilation and Regional Mapping

Geoteam members compiled pertinent well, core, geologic and field/pool data for each of the states in the MRCSP Region and provided the information to WVGES using PETRA[®], ArcGIS[®] and Excel[®] formats. WVGES reviewed and incorporated these data into a master geodatabase of petroleum fields (Lewis et al., 2019), from which field-level reservoir assessments and regional maps could be prepared.

Proximity to CO₂ point-sources is a major factor when assessing reservoirs and their ability to utilize and store carbon. Figure 4-1 and Figure 4-2 illustrate the geospatial distribution of power plants (EPA, 2017) in relation to infrastructure and petroleum fields within the region, respectively.

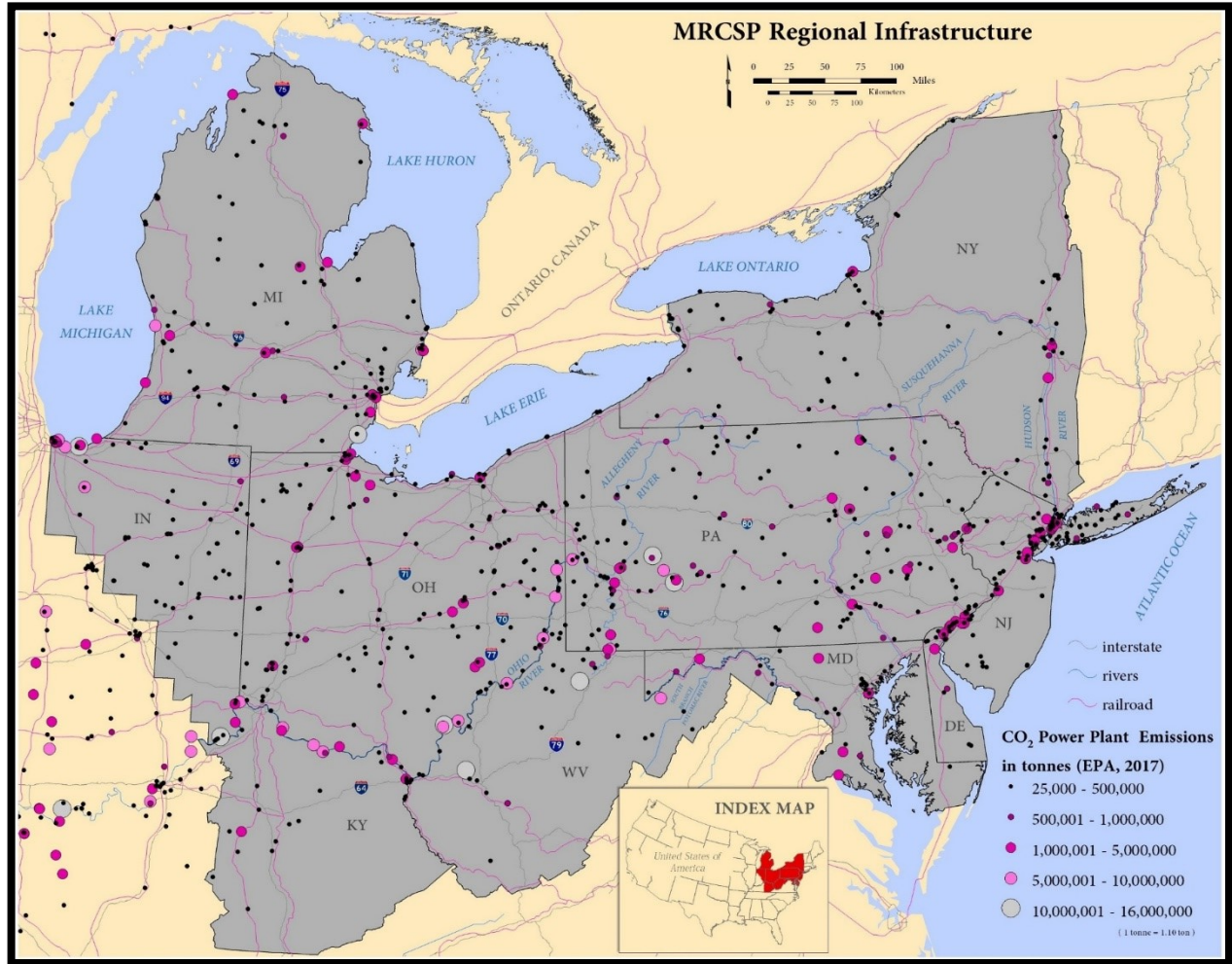


Figure 4-1. Power plant distribution and emissions relative to regional infrastructure.

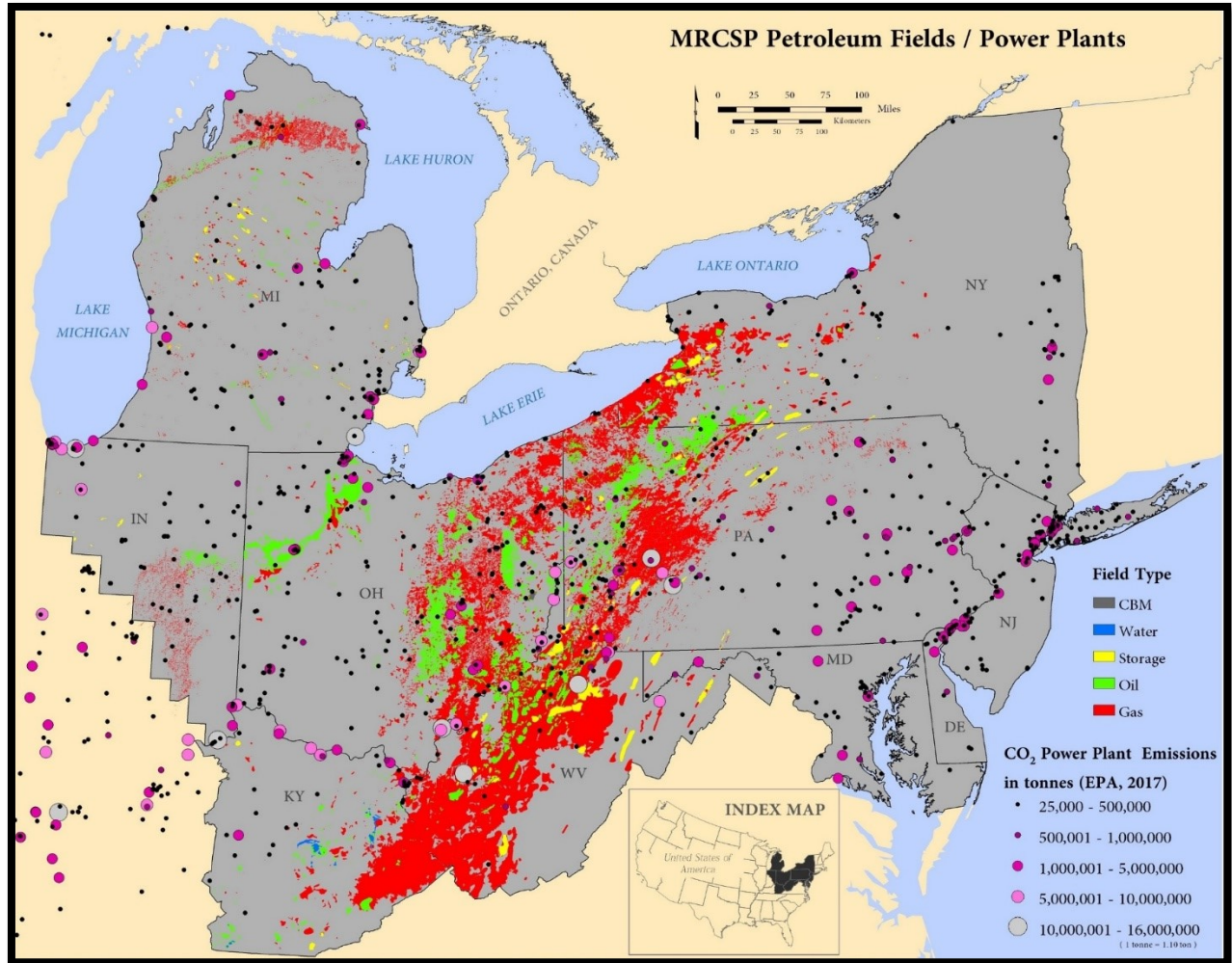


Figure 4-2. Power plants and petroleum fields in the MRCSP region.

4.2.1.1 Temperature Determination

Temperature at depth, used to calculate minimum miscibility pressure (MMP) and oil gravity, varies with geographic location and is dependent on the geothermal gradient and surface temperature (Equation 1; Dutta, 2016). Surface temperatures were digitized from Gass (1982), and thermal data for the MRCSP Region consists almost exclusively of bottom hole temperatures (BHTs) taken from borehole measurements and geophysical logs of area wells. The majority of these do not have information on the time after end of circulation before temperatures were measured and, thus, their BHT values are most certainly not equilibrium values – they are rough estimates at best.

$$T_z = T_0 + (\nabla \times Z) \quad \text{[Equation 1]}$$

where: T_z = temperature at depth, in units of degrees Fahrenheit (°F); T_0 = average surface temperature; ∇ = geothermal gradient; and Z = depth.

Several methods have been proposed to correct BHT values to equilibrium including one by researchers at Southern Methodist University (SMU), the University of Kansas (KU) and the University of North Dakota (UND). Each of these correction methods have been developed for

specific basins elsewhere in the United States. After examining the example maps constructed using the various proposed BHT correction models, WVGES chose SMU's method of correction (Frone et al., 2015; Equations 2, 3 and 4) as most appropriate for the Appalachian and Michigan basins. All wells with a BHT and a depth measurement were corrected (T_z) using this method. A gradient for each well was then calculated using Equation 5 (modified from Equation 1).

If shallower than 1000 meters (m), $T_z = BHT$ [Equation 2]

If >1000 m and shallower than 3900 m,

$T_z = -16.5 + 0.018 \times Z - 0.00000234 \times Z^2$ [Equation 3]

If >3900 m,

$T_z = BHT + 19.1^\circ F$ [Equation 4]

$\nabla = (T_z - T_0) \div Z$ [Equation 5]

To further prepare data for mapping, wells with depths less than 1000 ft (305 m) and wells with negative gradients were omitted. To create the maps, gradient values were modeled spatially using distance-weighted gridding (weight = $1/d^6$) with a relatively coarse, square grid (10,000 m x 10,000 m) (Figure 4-3).

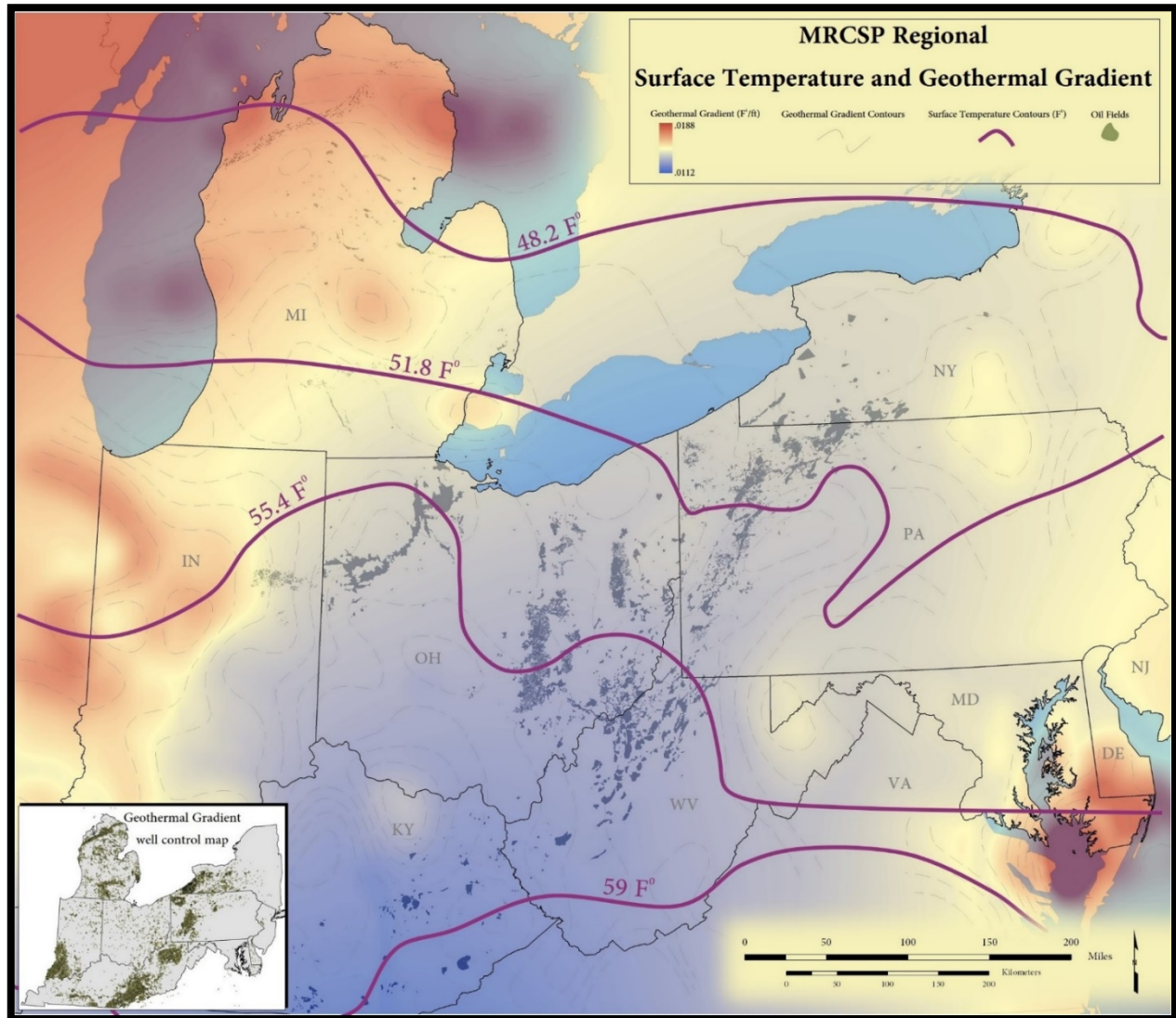


Figure 4-3. Surface temperature and geothermal gradient map used to determine temperature at depth.

4.2.1.2 Oil Gravity Determination

One of the most critically essential (and often nominally available) datasets for estimation of reservoir suitability is oil gravity. Oil gravity is important because it is used to calculate MMP, an attribute that is useful for determining if a field is suitable for miscible EOR. Reported oil gravity data were limited in most states' datasets. To increase data density, WVGES used linear regression analysis to predict missing oil gravities as a function of depth for petroleum fields in the region (Carter et al., 2015; Whieldon and Eckard, 1963) (Figure 4-4). Because the regression did not show high correlations, these values were tabulated separately from reported oil gravity values and were used in calculations only where reported values were lacking.

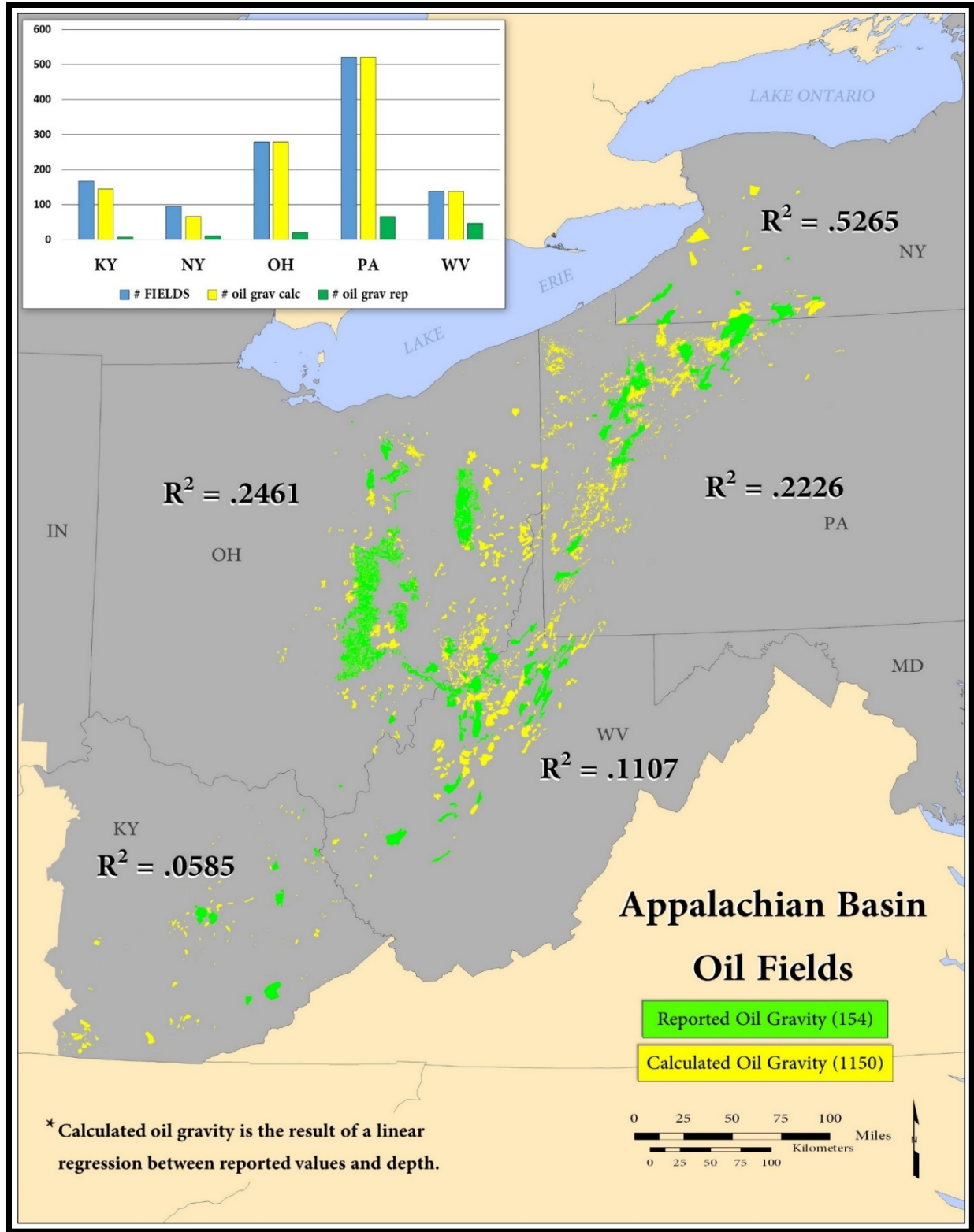


Figure 4-4. Distribution of Appalachian Basin oil fields where oil gravities were calculated (yellow) versus reported (green).

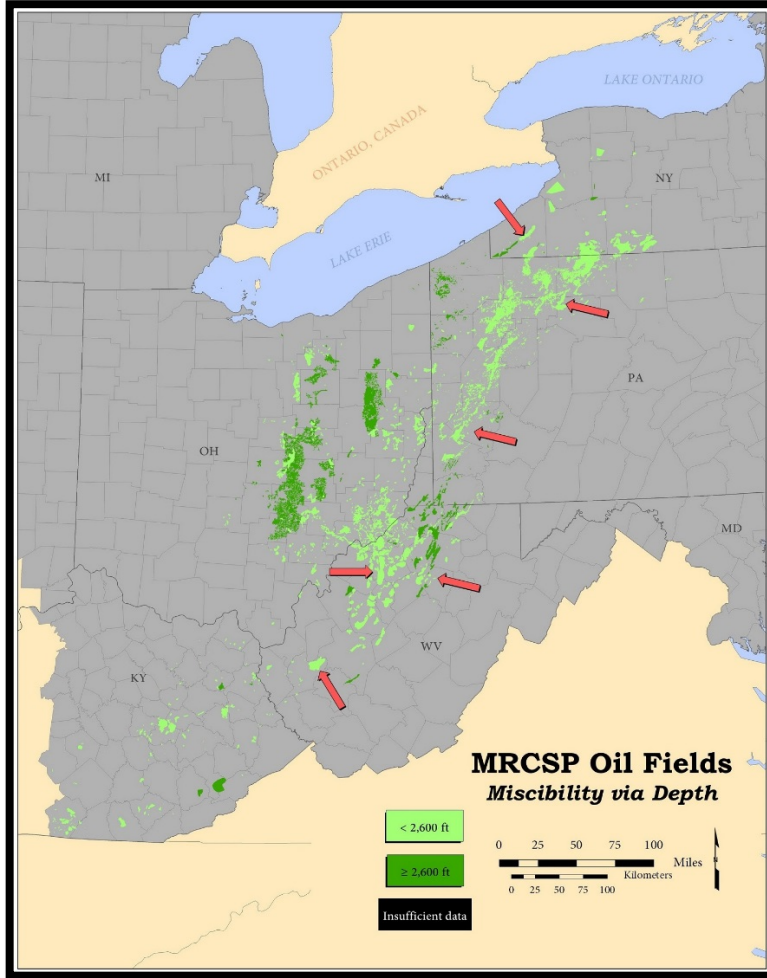
4.2.1.3 Minimum Miscibility Pressure Determination

Enhanced recovery using CO₂ as a catalyst has proven beneficial in immiscible oil fields by repressurization, and in miscible fields by interacting with the remaining oil (Riley et al., 2010). Two methods for determining an oil field's potential for miscibility includes using depth of the reservoir (i.e., *miscibility via depth*) or, examining the reservoir's MMP (i.e., *miscibility via MMP*). Earlier phases of MRCSP regional characterization work have defined miscible fields as those deeper than 2500 – 2600 ft. The current work determined MMP values using the approach of Takacs et al. (2011), as shown in Equation 6, which requires both reservoir temperature and oil gravity data.

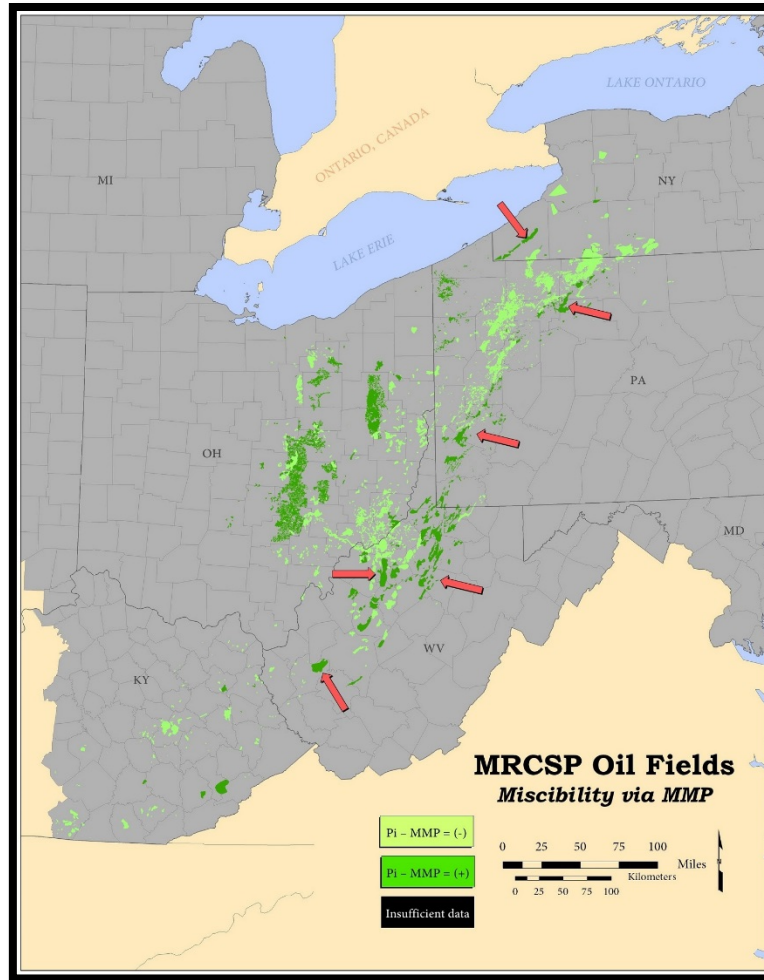
$$MMP = 15.988 \times T_z^{(0.744206+0.0011038 \times MW_{C5+})} \quad [\text{Equation 6}]$$

Where T_z = temperature at depth; and the molecular weight of hydrocarbons containing at least five carbon atoms in a single chain (MW_{C5+}) = $4247.98641 \times \text{oil gravity}^{(-0.87022)}$.

While assessing *miscibility via depth* is acceptable for regional assessments and in those situations where reservoir-specific data are lacking, evaluating *miscibility via MMP* provides more precise results specific to an individual reservoir or oil field. For the current study, MMP values greater than the calculated hydrostatic pressure (P_i) are identified as immiscible [$P_i - MMP = (-)$] (Takacs et al., 2011). Figure 4-5 illustrates the difference in miscible/immiscible determinations using the two methods. Where oil gravity data have been predicted in Pennsylvania and West Virginia oil fields, additional potential miscible EOR opportunities have been identified (red arrows).



A.



B.

Figure 4-5. Comparison of *miscibility via depth* (A) and *miscibility via MMP* (B) for Appalachian Basin oil fields. Red arrows indicate variations in miscible/immiscible determinations using the two methods.

The identification of an oil field as a miscible opportunity is not the only requirement for a successful CO₂-EOR operation. In addition to the relationship between a reservoir's thickness and permeability, oil saturation can also influence the success of an EOR operation. In addition, the presence of lighter oils (i.e., lower specific gravities) will interact more favorably with injected CO₂, improving oil production (Takacs et al., 2011).

4.2.2 Storage Resource Estimates for Oil and Gas Fields

The storage resources of Appalachian Basin conventional oil and gas reservoirs were estimated using Equation 7:

$$\text{Storage Resource} = A \times h \times \Phi \times (1 - S_w) \times \frac{\rho}{(2200 \times E_f)} \quad [\text{Equation 7}]$$

where A = field area (ft²); h = field thickness (ft); ϕ = field porosity; S_w = water saturation; ρ = CO₂ density (lb/ft³); and E_f = efficiency factor.

Carbon dioxide density, a critical variable in determining the storage resource, was calculated using MegaWatSoft® (<http://www.megawatsoft.com/excel-add-in-libraries/carbon-dioxide-properties-excel.aspx#.VfLwQCZRfF>).

Three variations of efficiency factors (E_f) have been used in this assessment to indicate a best case (Min), most likely (Mode) and worst case (Max) scenario for each field. These values, calculated for the Appalachian, Michigan and Illinois basins, are based on oil reservoir simulations and reservoir parameters loosely based on Goodman et al. (2011) and provided in Table 4-1 (Sminchak, pers. comm., 2014). Please note that these efficiency factors were applied to storage resource estimates prepared for all conventional reservoirs in the MRCSP Region, not just oil reservoirs.

Table 4-1. Oil and gas field efficiency factors for the MRCSP Region.

Region	States	Efficiency Factor (E_f)		
		Min	Min	Min
Appalachian Basin	OH, eastern KY, PA, WV, NY	0.177	0.294	0.539
Michigan and Illinois basins	MI, IN, western KY	0.372	0.557	0.680

4.3 Storage Resource Estimates for the Appalachian Basin

Storage resource estimates were calculated for conventional oil and gas fields in the MRCSP Region where the necessary parameters (Equation 7) were available. Figure 4-6 graphs the total Min, Mode and Max carbon storage resource estimates determined for individual oil fields by state. Ohio, Pennsylvania and West Virginia offer the large majority of potential oil field storage in the Appalachian Basin, with mode storage resource estimates ranging from ~100,000,000 to 400,000,000 tonnes in individual fields. Other states reported total mode storage estimates less than 100,000,000 tonnes.

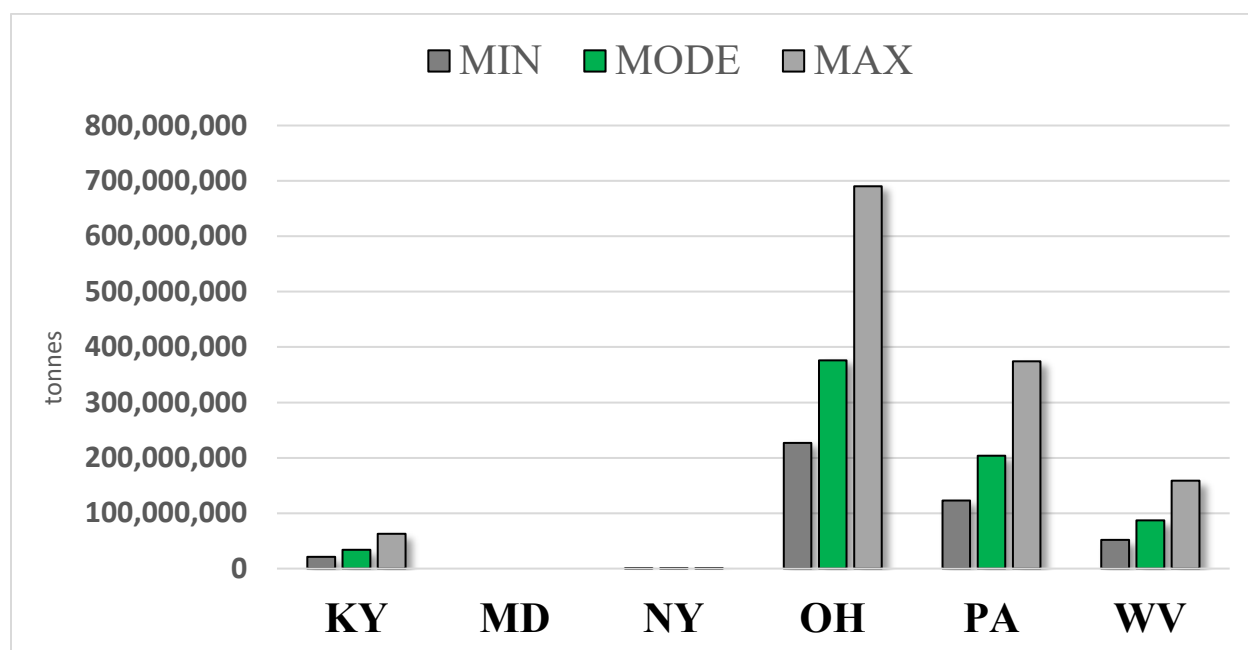


Figure 4-6. Total carbon storage resource estimate of Appalachian Basin oil fields by state.

The mode carbon storage resource estimates, totaled by state for all types of fields (i.e., oil, gas, gas storage, water and coalbed methane [CBM]), are graphed in Figure 4-7A. This bar chart shows the results from MRCSP's previous reporting period (gold bars) next to those of the current study (blue bars). Based on these data, most of the storage resource for the Appalachian Basin is likely to be found in West Virginia, Pennsylvania and Ohio, with lesser amounts in Kentucky, New York and Maryland. Specific to oil fields assessed as part of the current study (green bars; Figure 4-7B), Ohio and Pennsylvania have the largest mode resource estimate totals. With respect to gas fields (red bars; Figure 4-7C), West Virginia and Pennsylvania have the largest estimate totals.

Figure 4-7 shows how the results of the current study are more conservative than those reported in MRCSP's Phase II assessment (Battelle, 2010). There are several reasons for this: (1) Geoteam members reviewed and revised field sizes (i.e., boundaries), as part of the current study; this has led to an overall reduction in the carbon storage footprint for the region; (2) redundant oil field data have been eliminated from the geodatabase; and (3) shale gas fields have been exempted from storage resource calculations. Shale gas fields are considered unconventional resources for many reasons, although perhaps the most important relative to carbon storage potential has to do with pore space. TOC content is an important factor when determining the porosity of shale gas formations, as the pore space in these reservoirs is principally associated with organic matter. The premise here is that a greater abundance of organic pores offers a larger carbon storage potential. Although an ongoing part of MRCSP research activities, the compilation of field-level TOC data for organic-rich shales is not yet complete. For this reason, the storage resources for shale gas fields have not been determined as part of the current work.

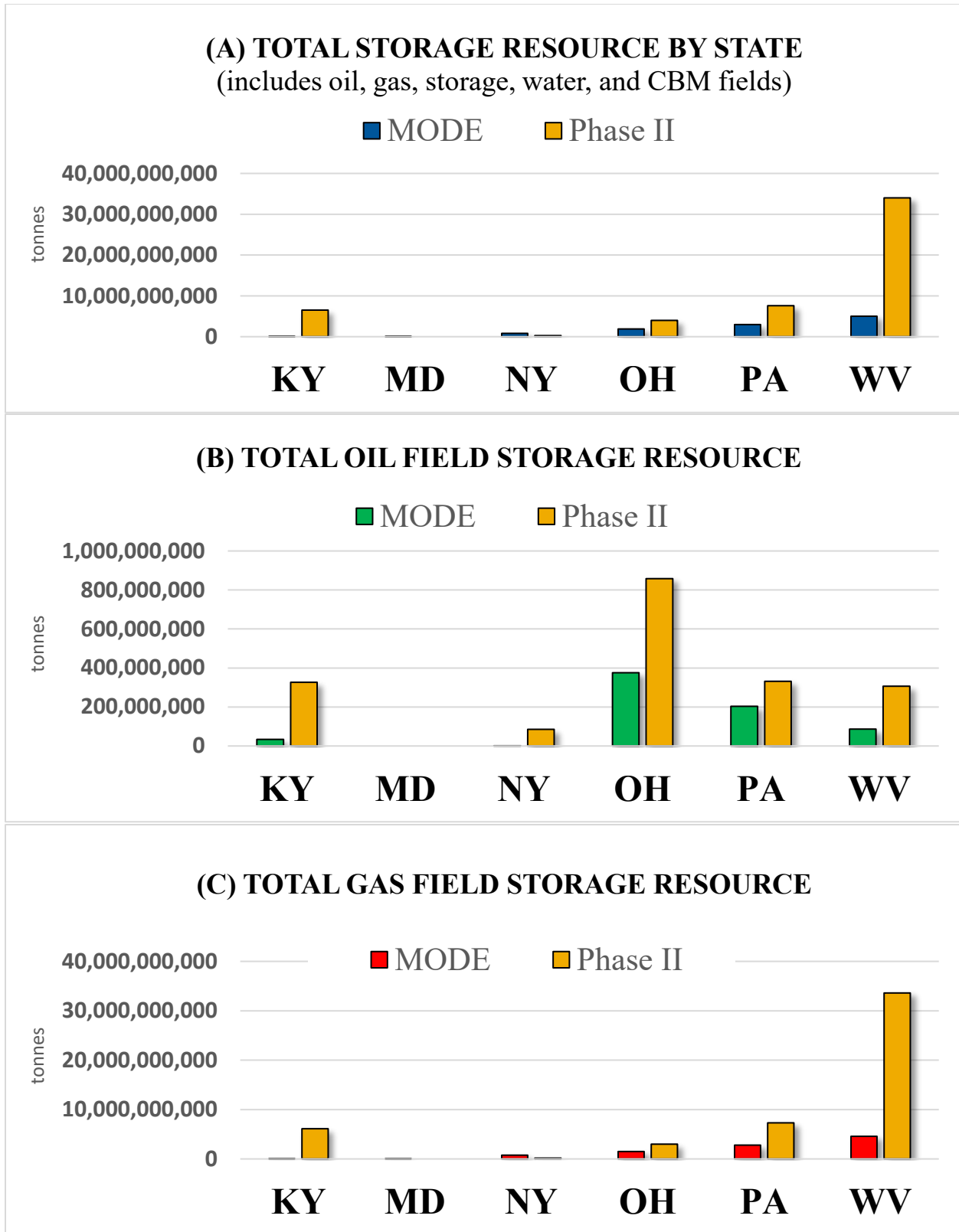


Figure 4-7. Mode storage resource values for (A) all fields (combined), (B) oil fields and (C) gas fields in the Appalachian Basin – Phase II vs. Phase III results.

The size of an oil or gas field is not the sole determining factor of its capability to store CO₂. As an example, the total carbon storage resource estimated for West Virginia and Pennsylvania is higher than other Appalachian Basin states, whether looking at Phase II or Phase III mode resource values (Figure 4-7A). The relatively large area over which oil and gas extraction activities have occurred in these states is part of the reason for the large estimates, but not the only one. Pennsylvania and West Virginia have an abundance of stacked reservoirs (i.e., different oil and gas reservoirs producing at variable depths; Figure 4-8). In addition, in some areas of the basin, field-level reservoir parameters were lacking, which precluded WVGES from preparing carbon storage estimates. When conducting a regional desktop assessment such as this, the amount of oil and gas activity in an area and the degree to which it has been documented seem to be most influential in locating areas that may serve as potential carbon storage reservoirs.

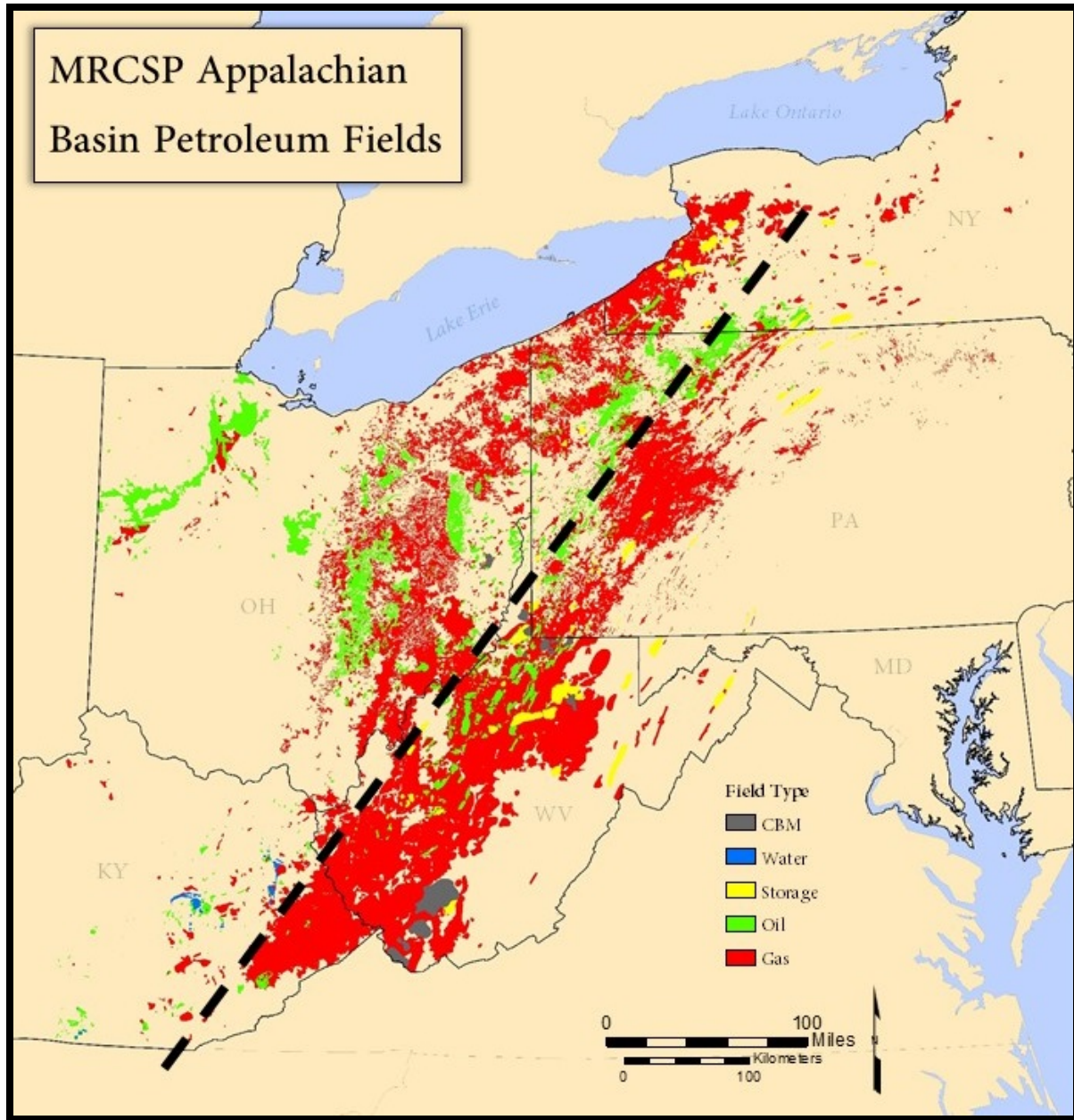


Figure 4-8. Stacked reservoirs are more common east of the dashed line. This may at least partially account for the larger storage resource estimates in West Virginia and Pennsylvania relative to other basin states.

4.4 Evaluating Oil Field Opportunities

Data availability is critical to successful evaluation of a region's carbon storage potential. Previous MRCSP efforts focused on storage in deep saline formations and required basic reservoir data including thickness, porosity, depth and water saturation (Wickstrom et al., 2005). Due to the current focus on CO₂-EOR with associated storage, the current study added reservoir permeability, oil gravity and oil saturation to data compilation efforts, to the extent this information was available. As an example, Figure 4-9 shows the relative availability of oil reservoir data for states in the Appalachian Basin portion of the MRCSP Region.

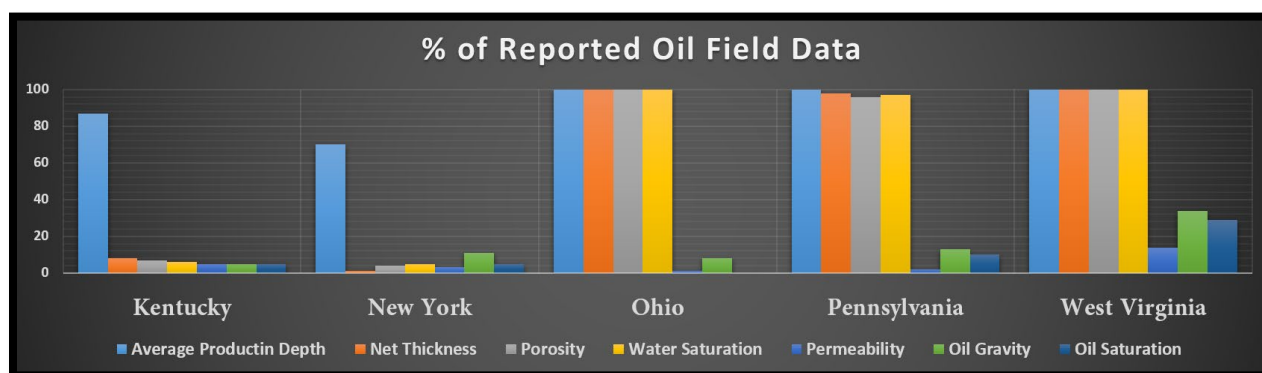


Figure 4-9. Oil reservoir data gathered for the current study, reported as a percentage available on a field-level basis for each of five states in the Appalachian Basin.

There are 993 individual oil fields in the Appalachian Basin represented by more than 1200 polygons of variable size and reservoir attribute content (Figure 4-10). Minimum, mode and maximum storage resource estimates were calculated for these fields. The “mode” storage resource is the preferred estimate of the storage resource for a given field, pool or reservoir, as it represents the most likely outcome when compared to “minimum” and “maximum” values, which are conservative and generous, respectively (Kuuskraa et al., 2011). Approximately 25 percent of the oil fields do not have the required attributes to calculate storage resource (black shading in Figure 4-10). The remaining field report mode storage estimates of up to 50,419,261 tonnes of CO₂ (green, yellow and orange shading). East Canton oil field (red shading) dwarfs all other fields in the basin with an estimated mode storage resource of 104,522,399 tonnes.

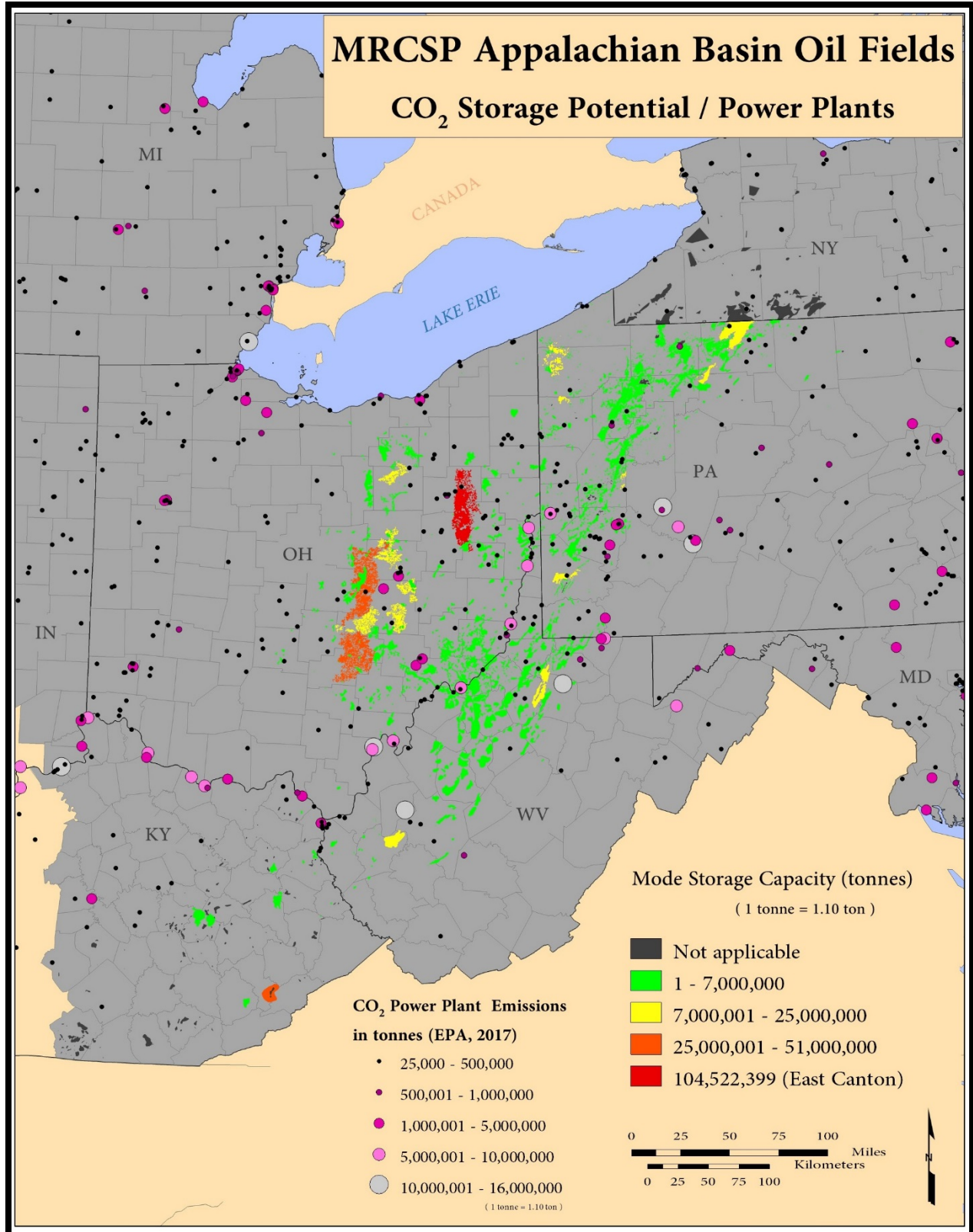


Figure 4-10. Mode storage resource in Appalachian Basin oil fields.

5.0 Organic-Rich Shale Storage and Enhanced Recovery Assessment

5.1 Introduction

Many organic-rich shales occur in Upper Ordovician, Middle Devonian and Upper Devonian strata of the Appalachian Basin. These shales are source rocks for conventional oil and gas in the basin, and several are important unconventional oil and gas plays. These shales may also have potential for future carbon storage with enhanced oil and gas production. Understanding the distribution of organic matter in organic-rich, unconventional resource plays is key to developing estimates for their CO₂ storage potential. In this chapter, the Kentucky Geological Survey (KGS) has adapted previous methods for estimating the CO₂ storage potential of the Upper Devonian Ohio Shale to:

1. model the TOC of the Middle Devonian Marcellus Shale and the Upper Ordovician Utica Shale and Point Pleasant formations;
2. develop maps to refine the understanding of organic matter distribution in these units; and
3. estimate the CO₂ storage resource.

Geologic carbon storage is most commonly examined in deep saline formations, and in combination with enhanced oil and gas production in conventional reservoirs. It may also be possible, however, to CO₂ in organic-rich shales. In organic-rich shales, CO₂ preferentially adsorbs with respect to methane (Nuttall et al., 2006, 2009). Investigators have suggested that this preferential adsorption could be exploited to produce additional methane with CO₂ (Bachu and Gunter, 1998; Reznik et al., 1984). Karmis et al. (2018) conducted a pilot study to inject CO₂ into low-permeability organic-rich shale and demonstrated both sequestration and enhanced natural gas and liquids recovery. Also, Yost et al. (1993) studied fracture stimulation methods and found that CO₂ (cryogenic) fracs performed better in organic-rich shale than either conventional hydraulic or nitrogen fracs. Although CO₂ is not currently used for enhanced oil and gas recovery in shales, the regional distribution of organic-rich shales and increasing production of shale gas from several plays in the basin warrant investigation and estimation of carbon storage potential in these shales, especially if CO₂ costs decrease in the future or there are incentives for using CO₂ for enhanced recovery.

The TOC content of geologic formations has long been an integral part of understanding source rocks (Dow, 1977; Jacobson, 1991; Jarvie, 1991). Carbon dioxide has a preferential affinity for organic molecules and will adsorb onto the organic matrix of black shale, while displacing methane molecules (Bachu and Gunter, 1998; Core Laboratories, 2008; Nuttall et al., 2009; Reznik et al., 1984). Some CO₂ can also be stored in free space within matrix porosity and fractures similar to those of conventional reservoirs. Previous research has shown that the amount of CO₂ adsorbed is related to the TOC of the shale (Godec, 2013a; Karmis et al., 2018). Hence, TOC data from shales is critical for estimation of carbon storage potential. Laboratory-measured TOC data from rock material acquired from wellbores (cuttings or core) are relatively sparse. Simple trend surface analysis can be used to map available laboratory-derived TOC, but such maps are hindered by uneven spatial distribution of data and provide minimal information about the three-dimensional (3D) variations of TOC within the units of interest at a basin-wide scale. This is especially difficult when multiple analyses are available for multiple target intervals in the same well. What single number would best characterize that specific spatial data point: mean, median or value range? How should these data be gridded and contoured to best characterize vertical and lateral variability?

Because of the constraints in using lab-derived core data alone for regional shale analyses, petrophysical methods have been developed to infer TOC from available geophysical log data. There are many more wells with geophysical logs than with core data, so spatially significant datasets can be assembled to examine meaningful regional trends. Most of these log-derived methods were developed using laboratory data to constrain a model based on selected well-log curves. Curves that have been used in modeling TOC include gamma ray (GR), spectral gamma ray (SGR), density (RHOB), neutron porosity (NPHI), photoelectric effect (PE), sonic (SON) and resistivity (RT) logs (Godec, 2013b; Herron, 1991; Meyer and Nederlof, 1984; Passey et al., 1990; Schmoker, 1979, 1981, 1993). Although many log types can be used for analyses using different models, the regional availability of different log types and quality of log data is not the same. Many of the curves (e.g., SGR, PE and other measurements) are not available for historical wells. Either data for a specific petrophysical property was not acquired or the data are not available in a digital format. Some data, like RT (including conductivity and induction) often depend on drilling fluids to provide electrical conductivity with the rock material. Most well logs in digital format available today are derived from scanned images of paper logs. Some curves are difficult to reliably digitize. Hence, for reasons of availability and practicality, models used for this study were based on GR and density logs. While it is expected that including other log data related to lithology (PE or NPHI) would improve the predictive power of the models, these data were not widely available.

5.2 Models and Methods

Petrophysical models for TOC estimation assume a lithology model that when combined with porosity and pore fluid information are statistically related to organic matter content. Organic matter tends to concentrate and preserve uranium, potassium and thorium, which results in higher GR values in organic-rich zones (Herron, 1991). Organic matter also has a low density with respect to other matrix components, approximately 1 gram per cubic centimeter (g/cm^3), so that for a given lithology model, an increase in organic matter tends to lower the observed density (Schmoker, 1979, 1993), as illustrated in Figure 5-1.

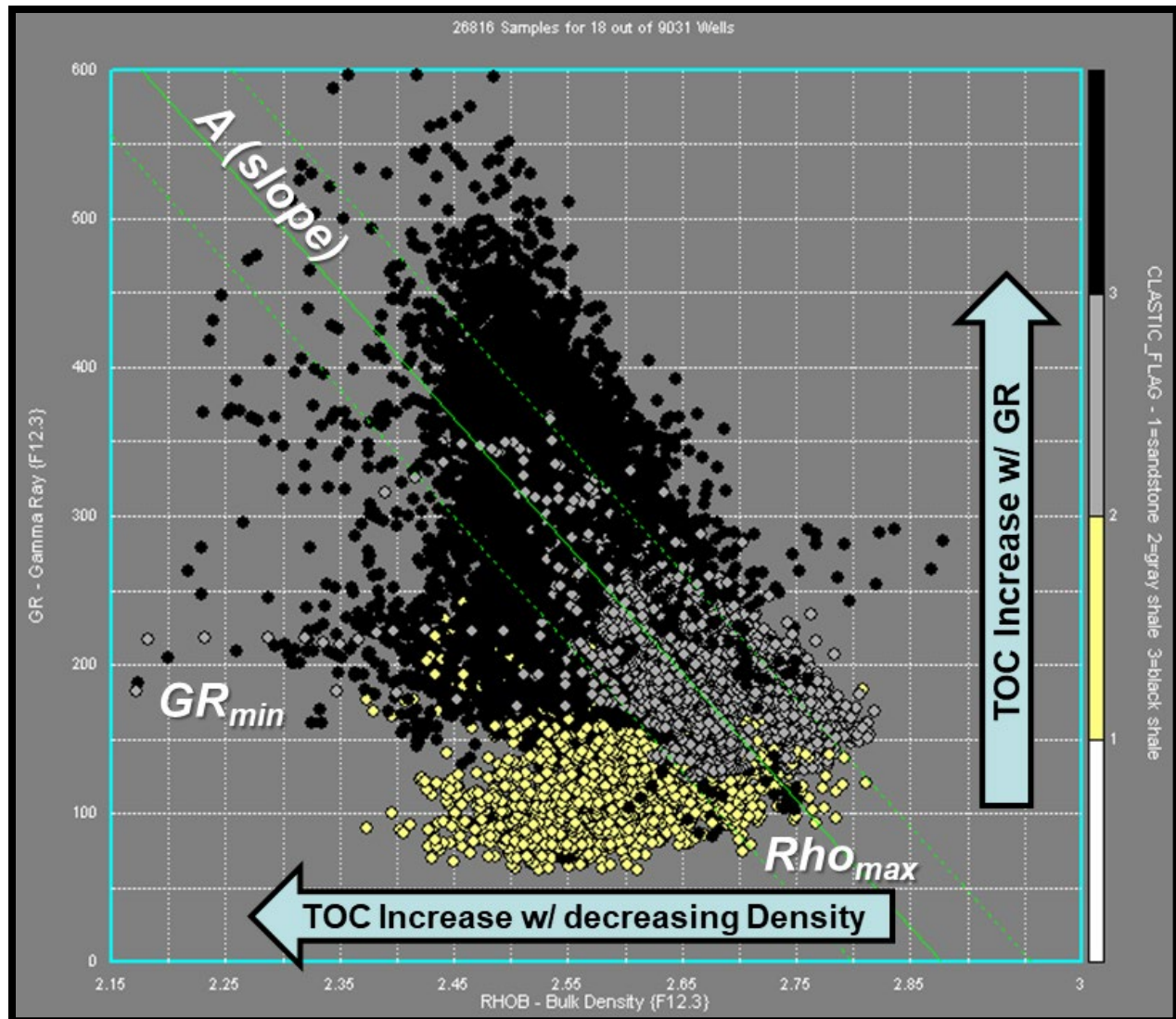


Figure 5-1. Typical GR-RHOB crossplot showing effect of increasing TOC in organic-rich Devonian black shales (black dots), inorganic gray shales (gray diamonds) and clastic units (yellow diamonds) with model parameters: minimum GR cutoff for organic richness (GR_{min}), maximum RHOB of inorganic gray shale (Rho_{max}), and the slope of a linear least squares fit (Schmoker's A parameter).

Schmoker (1993) published a commonly used model that assumes shale density is a function of four primary components: (1) the mineralogy of the matrix; (2) porosity; (3) pyrite content; and (4) organic matter. The effect of TOC on density in the density-based models is illustrated by a GR and RHOB crossplot of data for the Devonian Ohio Shale in Kentucky (Nuttall et al., 2006). As illustrated, measured GR intensity increases and RHOB decreases with increasing TOC, with some natural variability. Several model parameters used in the Schmoker equations, and discussed later in this chapter, can be determined from such crossplots:

- GR_{min} is the minimum GR intensity in API units of gray shale with no organic matter. For this study, in general, a cutoff value of 180 API was selected for distinguishing a shale lithology from other clastic lithologies (Figure 5-1).

- Rho_{max} is the maximum density of those gray shales (2.758 g/cm³ – estimated from the figure). Note that this is a subjective value selected as regionally “typical.”
- A is the slope of the GR vs RHOB crossplot. This is established by least squares linear regression methods.

These parameters are somewhat subjective and are expected to vary between wells and across regions. Schmoker (1981) includes a map (p. 1292) showing the regional variability of the A parameter across the shale region of the Appalachian Basin. This model is used as the basis for interpreting TOC from well logs in the Marcellus Shale, and then the Utica Shale/Point Pleasant Formation interval (with several variations discussed in the text).

All code and scripts used for data compilation, analysis and some visualizations were made using environments and modules provided with the open-source Anaconda distribution of Python 3.7 (<https://www.anaconda.com>). The two main environments used were the Spyder Interactive Development Environment (IDE) and Jupyter notebooks. Spyder (<https://www.spyder-ide.org>) is a classic editor that provides for composition, testing, debugging and introspection of code. Jupyter notebooks (<https://jupyter.org>) provide interactive tools for creating descriptive documents containing imbedded code and output. The LASIO module was used for Log ASCII Standard (LAS) digital well log file input and output. The source code and documentation are available from <https://github.com/kinverarity1/lasio>.

To optimize the predictive power of a particular model, either the coefficient of determination (r^2) can be maximized or the root mean square error (RMSE) between the measured and calculated values can be minimized. The coefficient of determination represents the proportion of the variance in the dependent variable explained by any independent variables. An r^2 value of one indicates a perfect prediction. It bears noting that for ordinary least-squares (OLS) linear regression, the correlation coefficient (R) ranges from -1.0 to +1.0 and is the square root of r^2 (James et al., 2013; Wilcox, 2010). Calculating r^2 can yield a negative number, whereas calculations for R provide a positive value. Given either fitness statistic, the difference between the measured and calculated values (the residuals) should cluster near zero and should also exhibit a relatively narrow spread, that is, low variance. The distribution of residuals is examined using plots of the kernel density estimate (KDE). The KDE is a non-parametric representation of the probability density distribution function of a random variable and is equivalent to a smoothed histogram.

5.3 Middle Devonian Marcellus Shale

5.3.1 Geologic Setting

The Middle Devonian Marcellus Shale is a regionally extensive, fissile, thin-bedded, gray to black, fractured, organic-rich shale (e.g., De Witt et al., 1993). It is dominated by quartz and illite, with lesser chlorite, pyrite and carbonates (Hosterman and Whitlow, 1981; Wang and Carr, 2013; Wilson et al., 2016). The Marcellus is the oldest of a succession of Devonian and Mississippian black shales in the Appalachian Basin (e.g., Etensohn et al., 1988; Roen and De Witt, 1984). It extends from New York south to West Virginia and east to Ohio. It is deepest in Pennsylvania and West Virginia west of the Allegheny Front (Figure 5-2), with elevations from approximately 1000 ft Mean Sea Level (MSL) (red) to -8000 ft MSL (purple). The Marcellus is thickest in the northeast portion of the Appalachian Basin (red) (Figure 5-3). The shale thins or is truncated by overlying units (sub-Genesee unconformity) southward and westward (green) (Boswell, 1996; Etensohn et al., 1988; Roen et al., 1978a, 1978b).

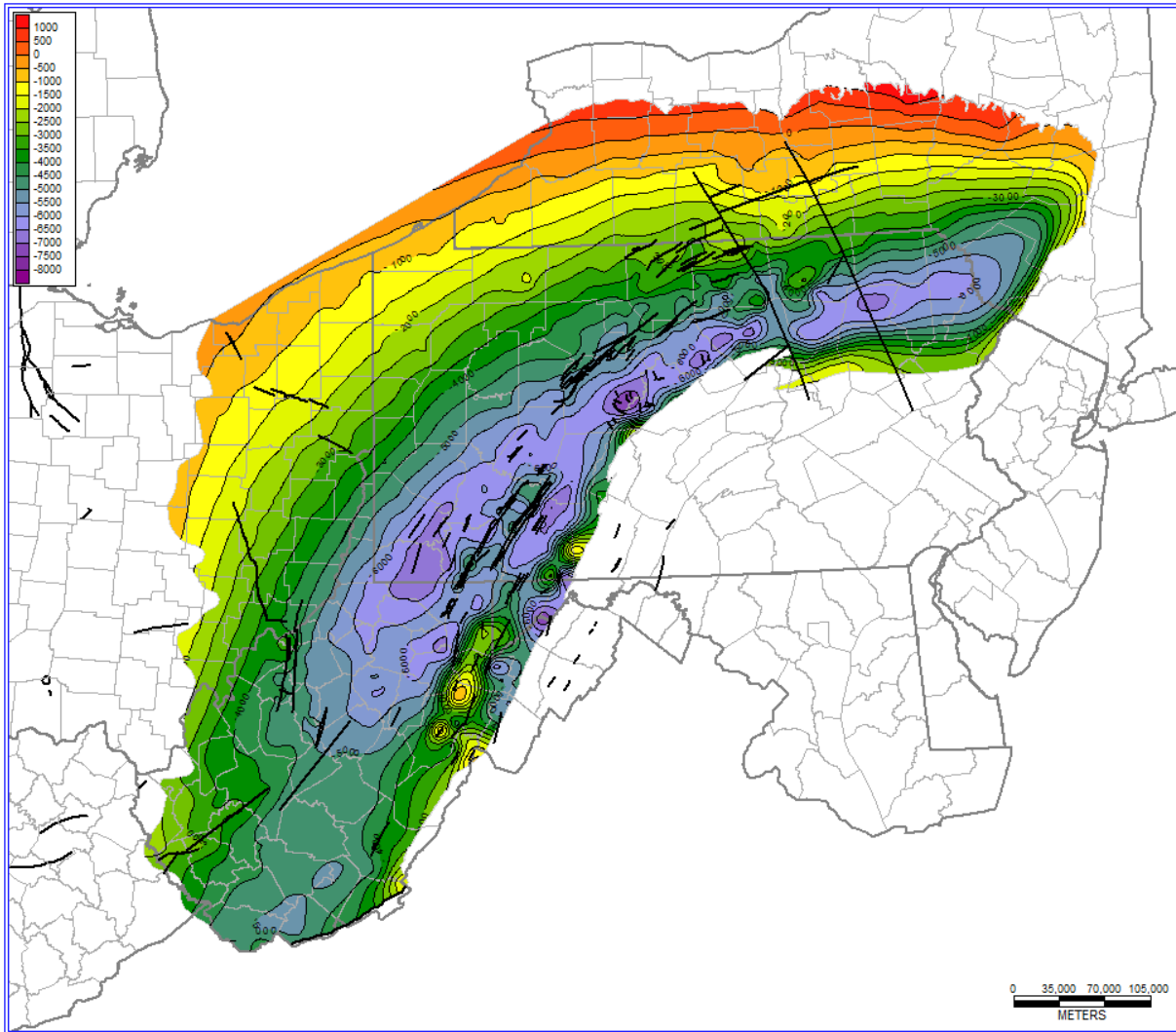


Figure 5-2. Structure contour map (500-ft contour interval) of the top of the Middle Devonian Marcellus Shale in the Appalachian Basin. Bold black lines represent generalized major fault zones.

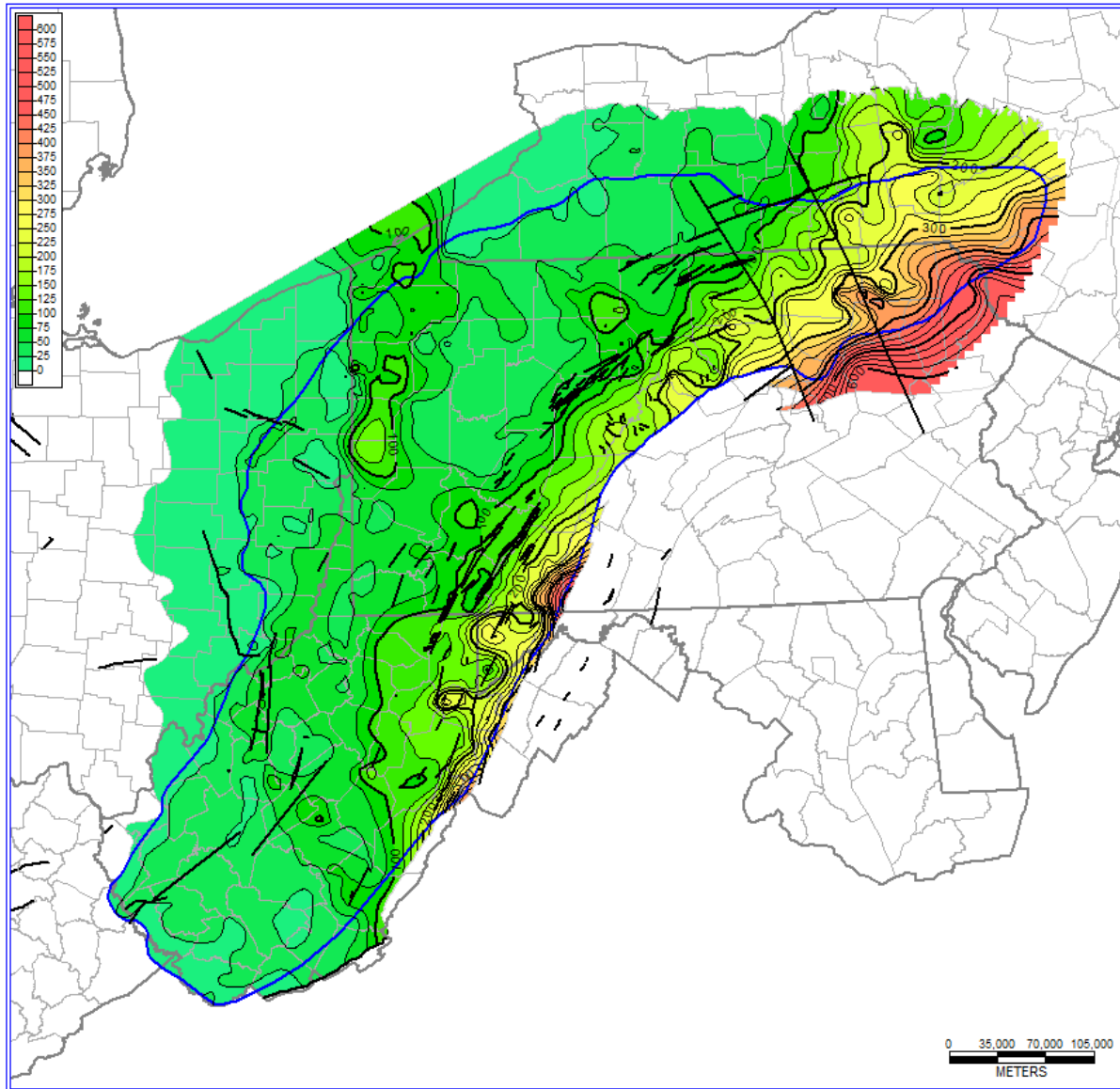


Figure 5-3. Gross thickness map (20-ft contour interval) of the Middle Devonian Marcellus Shale in the Appalachian Basin. Bold black lines represent generalized major fault zones.

The Marcellus play boundary used for this assessment includes the area west of the Allegheny Front to a drilling depth to the top of the shale of 2500 ft or a shale thickness less than 25 ft.

In Pennsylvania, the Marcellus occurs at the base of the Hamilton Group and overlies the Onondaga Limestone (Figure 5-4). The shale is overlain by a succession of different formations in the Hamilton Group and younger strata westward (Figure 5-5). A typical log for the shale where it is thick in Pennsylvania, shows the GR-RHOB profiles for the Marcellus Shale and internal stratigraphy of the unit (Figure 5-4). In much of the play area, the Marcellus is composed of three members; the Union Springs Shale Member, Cherry Valley Limestone Member and Oatka Creek Shale Member. The two shale members contain both organic-rich black shales and less organic-rich gray shales. In much of the area, the Oatka Creek Shale Member is overlain by the Stafford Limestone Member of the Skaneateles Formation (Figure 5-4 and Figure 5-5). In parts of northern Pennsylvania and New York, however, the Stafford Limestone Member is included in the Marcellus Formation, and dark shales above the Stafford are included in an upper Oatka Creek Shale Member (Figure 5-5).

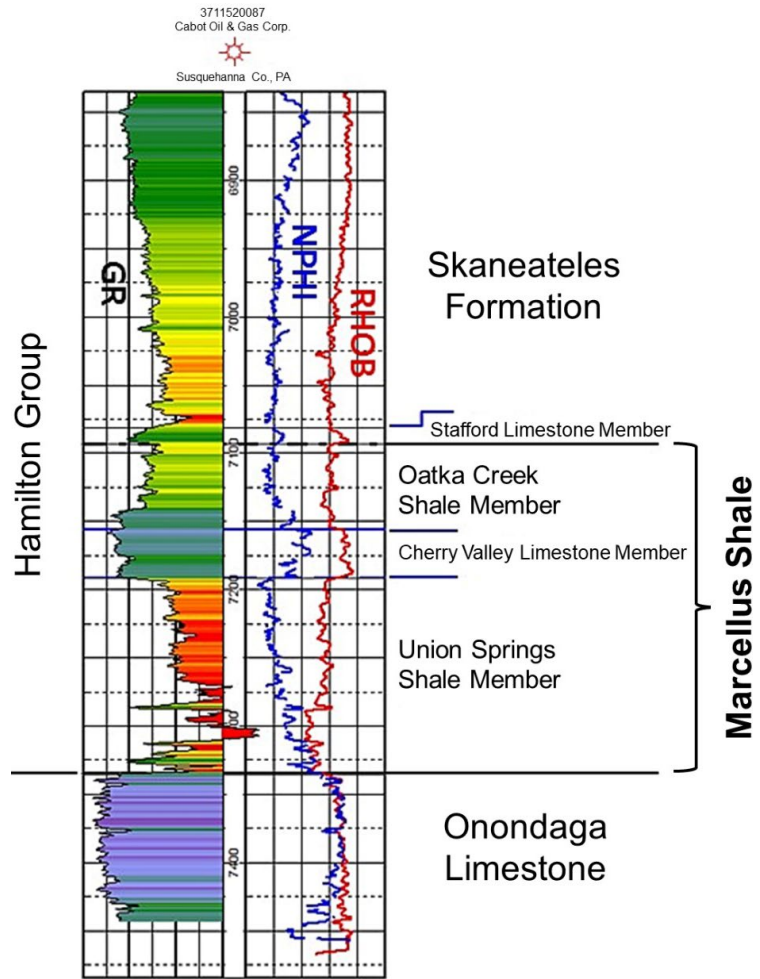


Figure 5-4. GR and RHOB type log for the Devonian Marcellus Shale, Susquehanna County, Pennsylvania. GR is colored from high (red) to moderate (yellow, green) to low (blue, purple) API values.

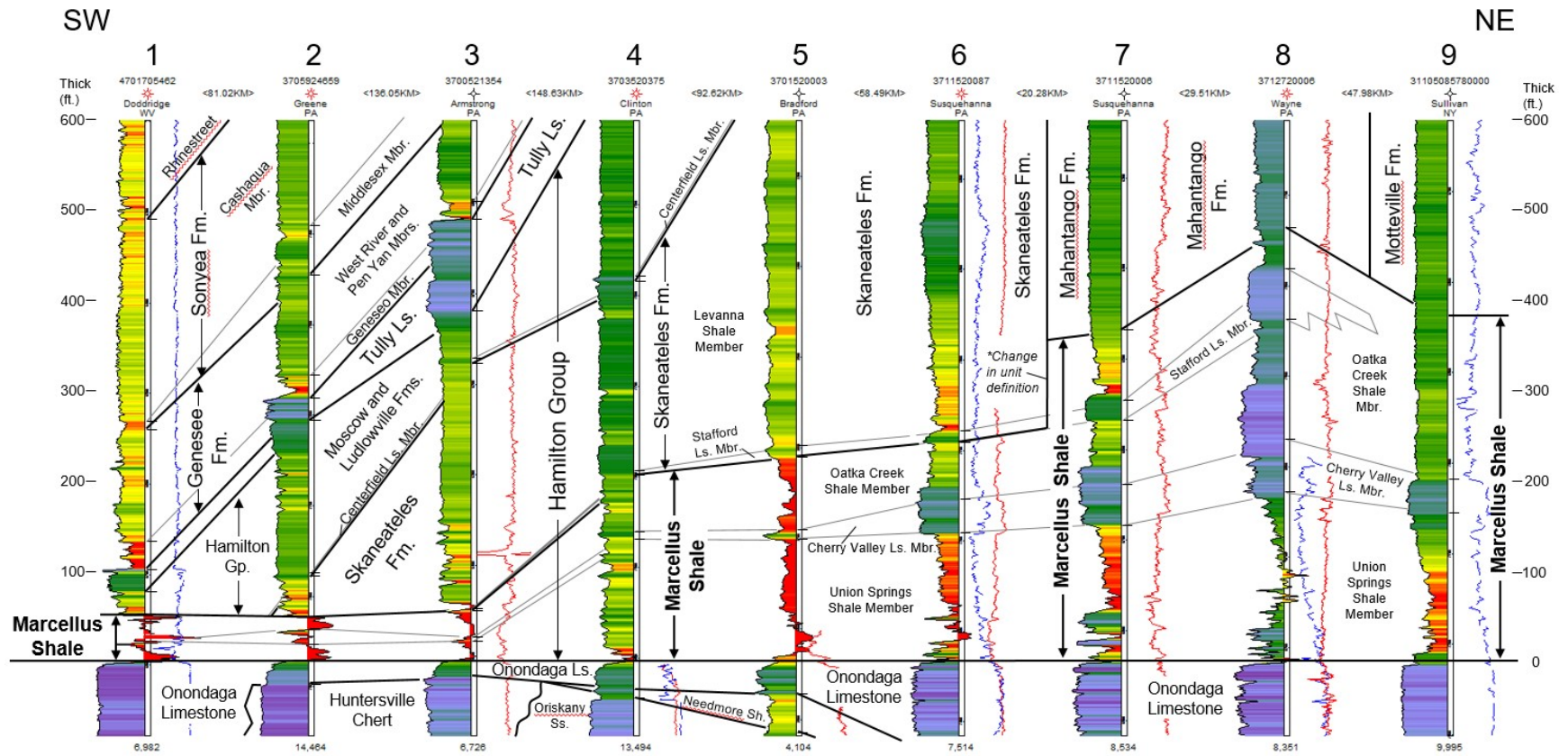


Figure 5-5. Generalized cross section along strike showing stratigraphic and lithofacies variations for the Marcellus Shale interval. Well spacing is not to scale. See Figure 5-6 for section location.

Devonian black shales of the Appalachian Basin are interpreted to have accumulated in a succession of restricted basins related to migration of forebulges from the Acadian Orogeny (Ettensohn and Barron, 1981; Ettensohn, 1985; Ettensohn et al., 1988). Preservation of organic matter within these basins has been attributed to development of a pycnocline, stagnation of the water column and bottom anoxia as the basin deepened (Byers, 1977; De Witt et al., 1993; Ettensohn, 1985; Ettensohn et al., 1988; Ettensohn, 1992). More recent geochemical work, however, indicates a range of oxic to anoxic conditions during deposition of the Marcellus Shale, so more variable stagnation of the water column (Sageman et al., 2003; Werne et al., 2002), and perhaps shallower water conditions (Bruner et al., 2015), than previously thought. Other factors that have been attributed to organic matter preservation in Devonian black shales include: (1) high primary production resulting from major changes in earth's biochemical cycles during the evolution of land plants, which caused changes to sedimentation rates and terrestrially-derived nutrients into the Devonian seas (Algeo et al., 1995; Algeo and Sheckler, 1998; Tuite and Macko, 2013); (2) sea-level changes and deposition of black shales in condensed sections (Lash and Blood, 2014; Slatt and Rodriguez, 2012; Werne et al., 2002); and (3) episodic mixing of nutrient-rich waters causing a productivity-anoxia feedback mechanism (Chen and Sharma, 2016; Ingall and Jahnke, 1997) or eutrophication pump (Sageman et al., 2003), possibly with more efficient recycling of phosphorus (Murphy et al., 2000). Although terrestrial nutrient flux may have led to increased organic productivity (phytoplankton and algal blooms), the oil-prone organic material that accumulated was dominantly marine algae (e.g., *Leiosphaerida*, *Tasmanites*) and yields Type 2 kerogens (Obermajer et al., 1999; Sageman et al., 2003).

5.3.2 Data

KGS prepared a PETRA[®] project database containing location and header information for more than 10,000 wells for this study. Stratigraphic tops data were compiled for wells with digital geophysical log data supplied by Geoteam members in LAS format. Only wells with both LAS files and stratigraphic tops data were utilized for log-based correlations and calculations.

5.3.2.1 Pennsylvania Databook

The Pennsylvania Geological Survey (PAGS) supplied an Excel workbook consisting of X-ray Diffraction (XRD), RockEval pyrolysis and shale rock analyses for 129 wells arranged as one well per workbook table. These data were compiled from multiple laboratory sources with varying data heading values, depth intervals and analyses. A Python script was developed for interrogation of each tab in the workbook to compile a data dictionary of the included information. The data dictionary was used to configure mapping the spreadsheet data to an output data base for further analysis. A Python script was then developed to extract data from each tab and create the database, which is provided as Appendix A in this report.

5.3.2.2 LAS Files and Stratigraphic Tops

LAS data files were provided for 1870 wells penetrating the Marcellus interval across the six-state study area of Kentucky, Ohio, Maryland, New York, Pennsylvania and West Virginia (Figure 5-6). Of these, only 813 wells included stratigraphic tops for the Marcellus Shale interval. The GR and RHOB curve data for the Marcellus interval in these wells were exported to LAS files for calculations and analysis. Thirty-one of these LAS files had no data for the Marcellus interval, leaving 782 wells with full digital log coverage over the entire shale interval. Most these wells are in New York and Pennsylvania (Figure 5-7).

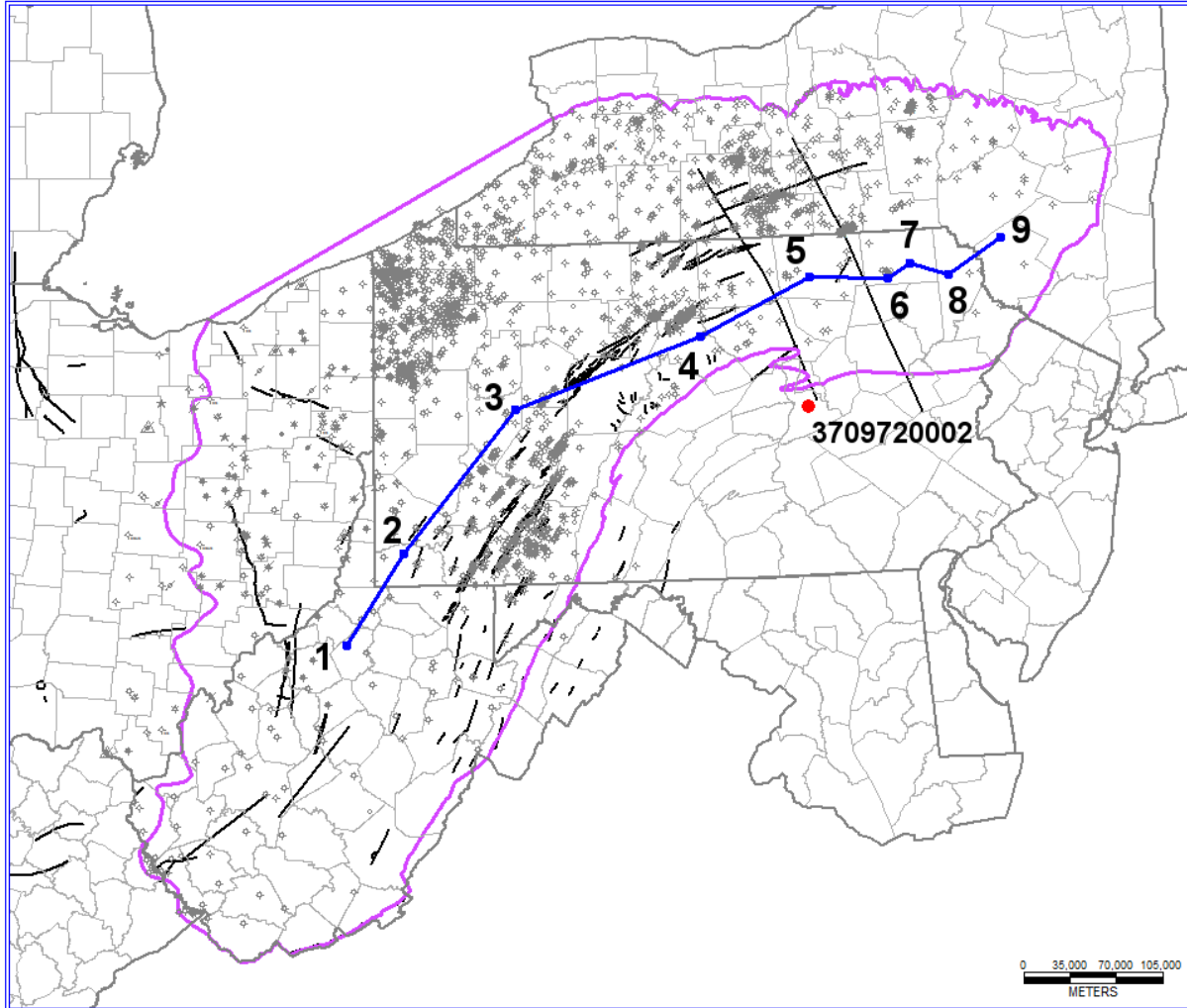


Figure 5-6. Distribution of 1870 well locations with LAS data in the Marcellus Shale project area (magenta). The blue line with numbered wells is the location of the cross section in Figure 5-5. The red well, although not within the assessment area, is discussed later in the report.

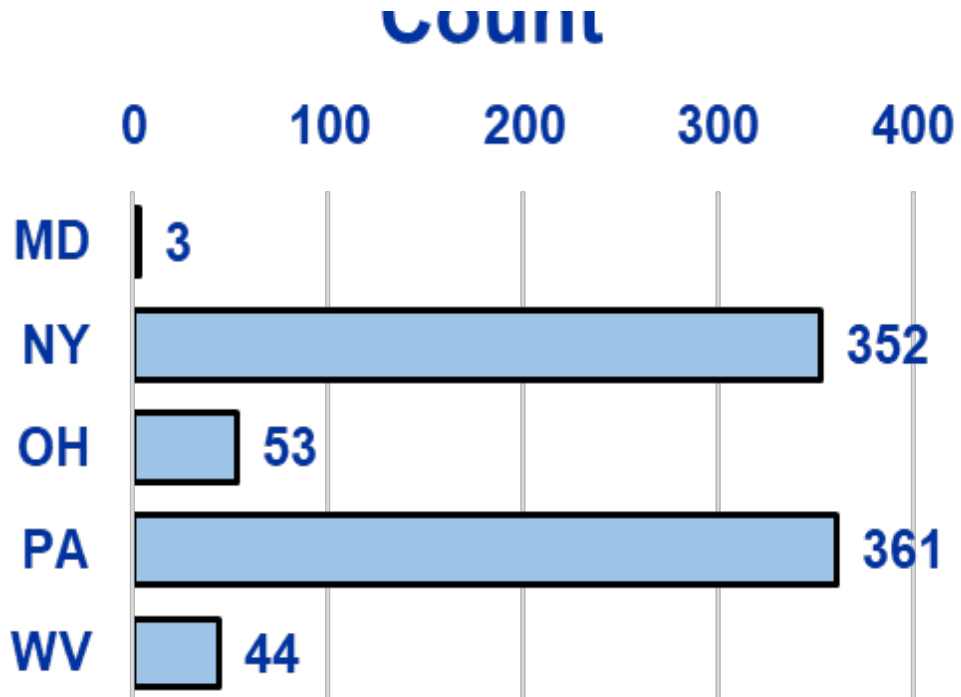


Figure 5-7. Marcellus reference well counts with digital GR and RHOB data in LAS format by state.

5.3.3 Methods

As part of this study, KGS extended well-log-based stratigraphic interpretations for the Marcellus Shale from tops information provided by Geoteam members. Well tops information included not only the Marcellus Shale but also the Hamilton Group, Skaneateles Formation, Stafford Limestone, Oatka Creek Shale, Cherry Valley Limestone, Union Springs Shale and Onondaga Limestone. To simplify and facilitate analysis, stratigraphic zones were generalized and grouped to focus on TOC calculations for the Hamilton Group/Marcellus Shale interval.

One of the most straightforward ways to model TOC using geophysical data is with an OLS regression of available data. Information from the Pennsylvania databook were queried to identify observations related to organic-rich shales that had both laboratory-measured TOC and calculated RHOB values. A standard OLS linear regression was fit to these 219 data points (Figure 5-8) with a resulting R^2 value of 0.88, indicating a significant correlation. This relationship was selected as one of the models used to calculate TOC from digital geophysical data.

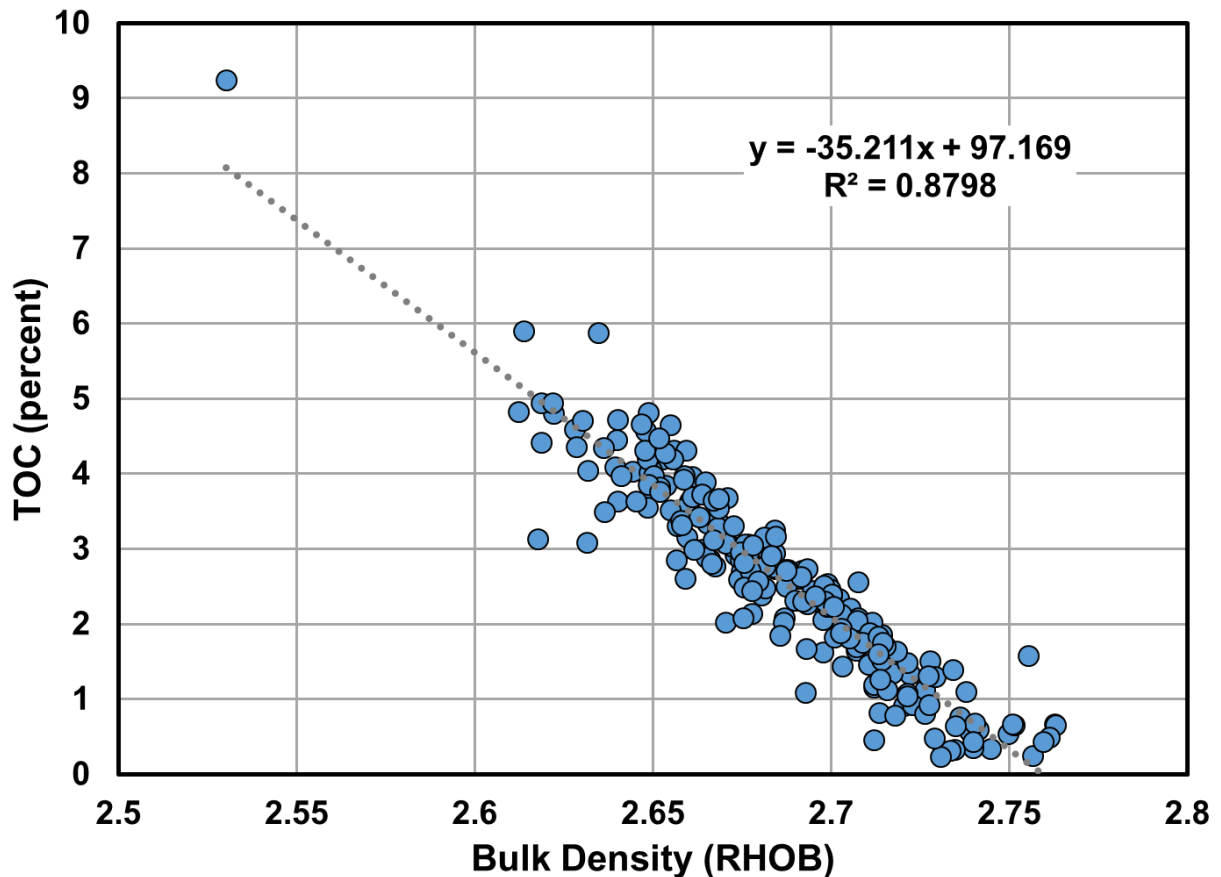


Figure 5-8. Standard OLS linear regression model of TOC as a function of laboratory-determined RHOB using data compiled from the Pennsylvania databook.

Wells with valid GR and RHOB log traces across the Marcellus interval were selected for an additional quality control review. Digitized curve traces may be misidentified, or the scale range values set incorrectly (Figure 5-9A). Off-scale curves can be mishandled. The curve can be clipped at the track edges (Figure 5-9B), curve wrapping can be incorrectly identified, or the off-scale interval can be set to a missing value (preferred in the case of an error). Even when a curve is scaled and digitized correctly, the data may be suspect because of downhole conditions such as washouts (an enlarged section of the borehole that particularly affects density log traces; Figure 5-9C). Scripts for reading, plotting and processing the available digital logs were developed to identify as many problematic intervals as possible and drop those data from consideration. Clipping problems were determined primarily by identifying consecutive data points that occur within a small range of typical track boundary values (commonly 150, 300 or 400 API units on the GR curve). Incorrectly scaled traces were found by comparing the range of the observed curve to the expected and typical value range for that curve. Outlier selection was employed to assist with computational identification of washouts. The outliers were identified using the method discussed by Wilcox (2010) and values were dropped from the data set if less than the lower bound or greater than the upper bound with the bound defined by:

- Interquartile distance (IQT) = $Q75 - Q25$
- Lower bound = $Q25 - 1.5 \cdot IQT$
- Upper bound = $Q75 + 1.5 \cdot IQT$

where Q25 is the 25th percentile value and Q75 is the 75th percentile value. Of the 782 wells subjected to quality control review, 574 were selected for modeling.

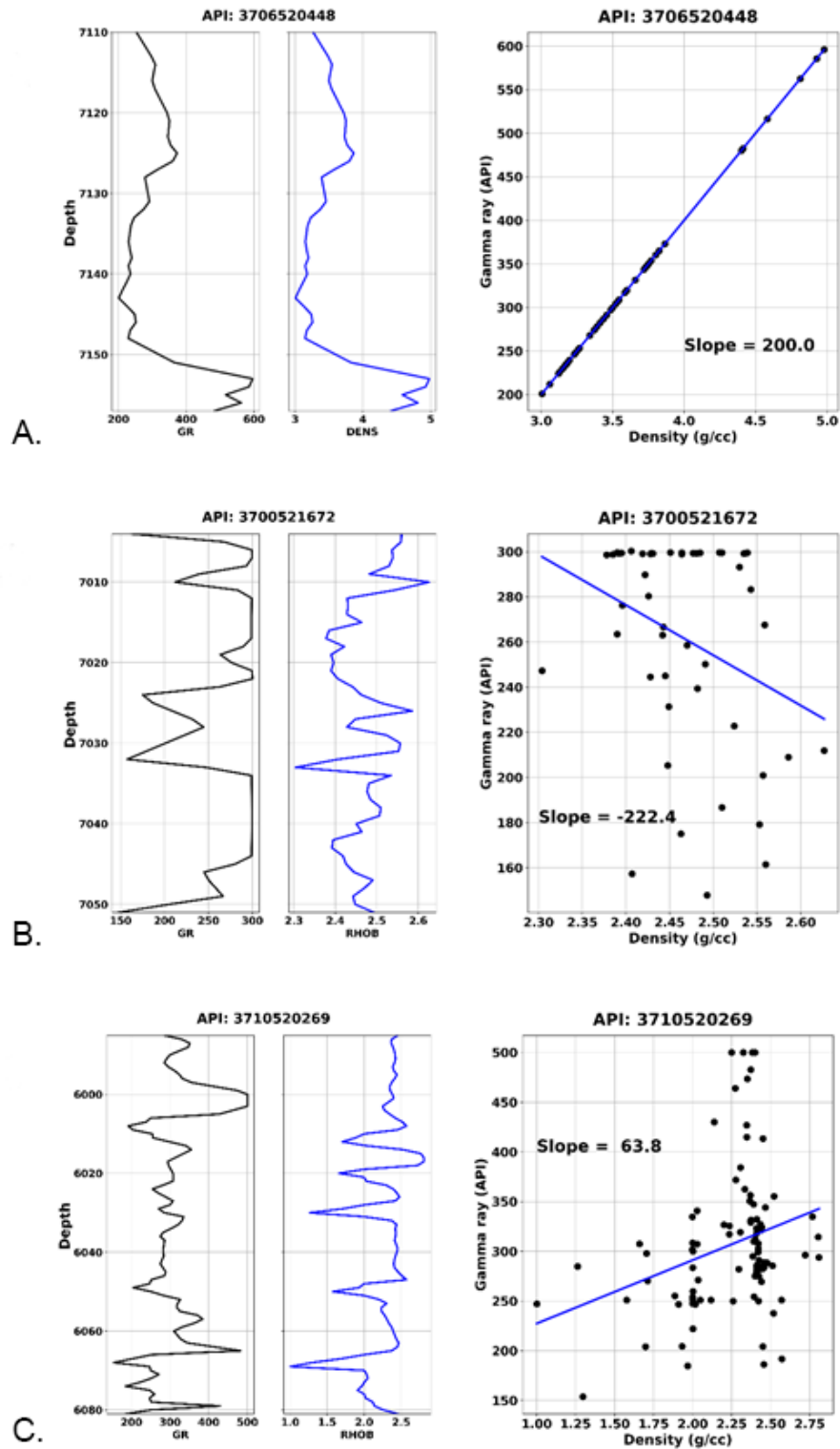


Figure 5-9. Examples of problems in log curves and crossplots illustrating problems identified in some LAS files during quality-control review: A) same curve digitized for both GR and RHOB resulting in a perfect correlation; B) GR clipped at edge of right track, resulting in lower (and the same) API readings for the interval clipped; C) Narrow, RHOB low-density spikes, which may be likely related to an enlarged wellbore “washouts” rather than true low-density rock. Each of these types of problems had to be identified and addressed in the dataset. Depth, GR and RHOB scales vary.

5.3.3.1 TOC Estimate Models

TOC can be estimated from available GR and RHOB geophysical logs. Four models were chosen for comparison of calculated TOC values:

- The Schmoker model (Schmoker, 1979, 1993) was developed using primarily the Devonian Ohio Shale in the Appalachian Basin. The calculated log trace is identified as “TOCSH.”

$$TOC_{Schmoker} = 55.822 \times \left(\frac{Rho_{max}}{RHOB} - 1 \right) \quad \text{[Equation 8]}$$

- TOC_{Mod} is a modified Schmoker model, the result of applying the Excel linear solver to minimize the RMSE between actual and calculated TOC values using Marcellus Shale RHOB data from the Pennsylvania data workbook. The calculated log trace is identified as “TOCMD.”

$$TOC_{Mod} = 88.55 \times \left(\frac{Rho_{max}}{RHOB} - 1 \right) \quad \text{[Equation 9]}$$

- TOC_{linreg} is an OLS linear regression model based on the laboratory TOC and density data from the Pennsylvania databook with an R^2 of 0.88 (Figure 5-8).

$$TOC_{Linreg} = -35.21 \times RHOB + 97.17 \quad \text{[Equation 10]}$$

- TOC_{GR} , is Schmoker’s GR model (Schmoker, 1981), where A is slope of GR-RHOB crossplot (e.g., Figure 5-1). The calculated log trace is identified as “TOCGR.”

$$TOC_{GR} = \left(\frac{GR_{min} - GR}{1.378 \times A} \right) \quad \text{[Equation 11]}$$

5.3.3.2 Selection of RHOB Values

Bulk density data are required for three of the models used in this study. Available data from digital geophysical logs for the Hamilton Group/Marcellus interval were filtered to identify more organic-rich zones by selecting those with observed GR values greater than or equal to 180 API units (based on shale cutoff value in Figure 5-1). In addition, data were also filtered to select RHOB values ranging from 2.0 to 3.0 g/cm³ to minimize the potential influence of washouts and digitizing errors. The resulting distribution of observed RHOB data for the 528 wells that met these criteria is illustrated in Figure 5-10. The average RHOB value is 2.53 g/cm³, which was used in subsequent calculations.

In applying Equations 8 and 9 to calculate TOC, the maximum bulk density (Rho_{max}) was set to the maximum RHOB observed in each well for the Hamilton Group/Marcellus interval.

Observed Bulk Density of the Hamilton Group/Marcellus Interval

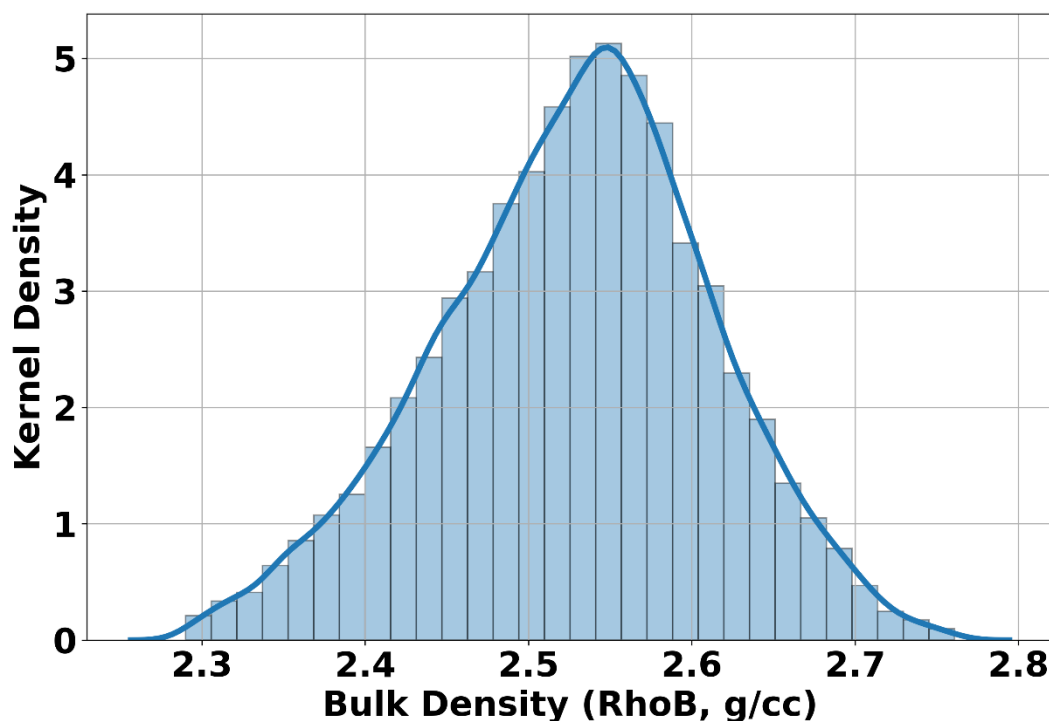


Figure 5-10. Histogram and probability density of observed RHOB for the Hamilton Group/Marcellus interval with GR \geq 180 API, from 528 wells. Kernel density is explained in Appendix B.

5.3.3.3 Selection of the Schmoker A Value

Schmoker's GR-based model (Equation 11) requires the determination of the slope of the GR and RHOB crossplot, termed the A value. Schmoker (1981) provides a generalized map showing the variability of this parameter across the basin, suggesting it varies by well. The availability of digital well log data provides a strategy for determining the A value on a case-by-case basis. Where both GR and RHOB logs were available (528 wells), the slope was determined using OLS linear regression estimators. Figure 5-11 shows a GR-RHOB crossplot for an example well (API No. 3709720002; see location in Figure 5-6), with the calculated A value of -343.51 ($R = -0.741$).

Tests of the significance of the regression were not conducted on an individual well basis. The correlation between GR and RHOB was considered significant if the absolute value of the correlation coefficient (R) exceeded 0.4 (alpha is 0.5 percent, two variables, 20 or more observations) as determined from tables provided by Crow et al. (1960). For wells with a poor (i.e., not statistically significant) relationship between GR and RHOB or wells with only a GR curve (231 wells), an average slope was determined from the wells with significant correlations. The default Schmoker A value in these situations was -796.71.

5.3.3.4 TOC Calculations

For each LAS file, TOC curves were generated using each of the four equations based on available GR and RHOB curves. In the absence of a GR curve, three TOC curves were calculated using the density-based equations (Equations 8, 9 and 10). In the absence of density curve data, only the GR method (Equation 11) was used. Lastly, a TOC curve was calculated for the modeled curves data at each depth point in the LAS file to determine a fiftieth percentile value (median or P50) curve. To obtain a better probabilistic determination of these variable TOC curves, the mean, median, mode, tenth percentile (P10) and the ninetieth percentile (P90) values were calculated for the Marcellus Shale interval in 574 wells and employed in mapping.

5.3.4 Results and Discussion

An example well – the BP Wilhour No. 1 well (API No, 3709720002, Northumberland County, Pennsylvania) – was selected to illustrate how TOC assessments were prepared for each of the wells with available digital geophysical data. Although the well is shallower than 2500 ft and outside of the assessment area, it has a good analytical dataset for illustrating the comparison between modeled results and analytical data. The selected models yielded up to five TOC curves depending on the availability of both GR and RHOB curve data and including the P50 curve. The Schmoker *A* value was determined using the slope of the GR-RHOB crossplot (Figure 5-11). Figure 5-12 shows the distributions of the Leco TOC data (top: box and whisker plot) and the calculated TOC for each model (bottom: density plots). For this well, all calculated TOC curves exceeded the range observed for the laboratory-derived data. The standard Schmoker model (Equation 8) appears to be a better match to TOC data derived from laboratory measurements. The GR model (Equation 11) consistently overestimates the laboratory TOC, a finding also reported by Godec (2013b). The modified Schmoker (Equation 9) and Marcellus OLS linear regression (Equation 10) models bracket the fiftieth percentile curve (P50). Note that the trend of the P50 curve mitigates the overall influence of the TOC curve calculated from GR data. A plot of the GR and RHOB logs for the example well (Figure 5-13), along with the calculated TOC curves and observed laboratory TOC data, illustrates the vertical variations between calculated and measured TOC data. These findings suggest that for wells with multiple TOC values over the interval of interest, it might be prudent to use a linear solver to optimize the model on a well-by-well basis. Descriptive statistics were calculated for the P50 TOC curve using PETRA[®] software. The mean of the P50 curve data was gridded and mapped to show general trends in the distribution of TOC, and for ultimate use in determining carbon storage resource estimates.

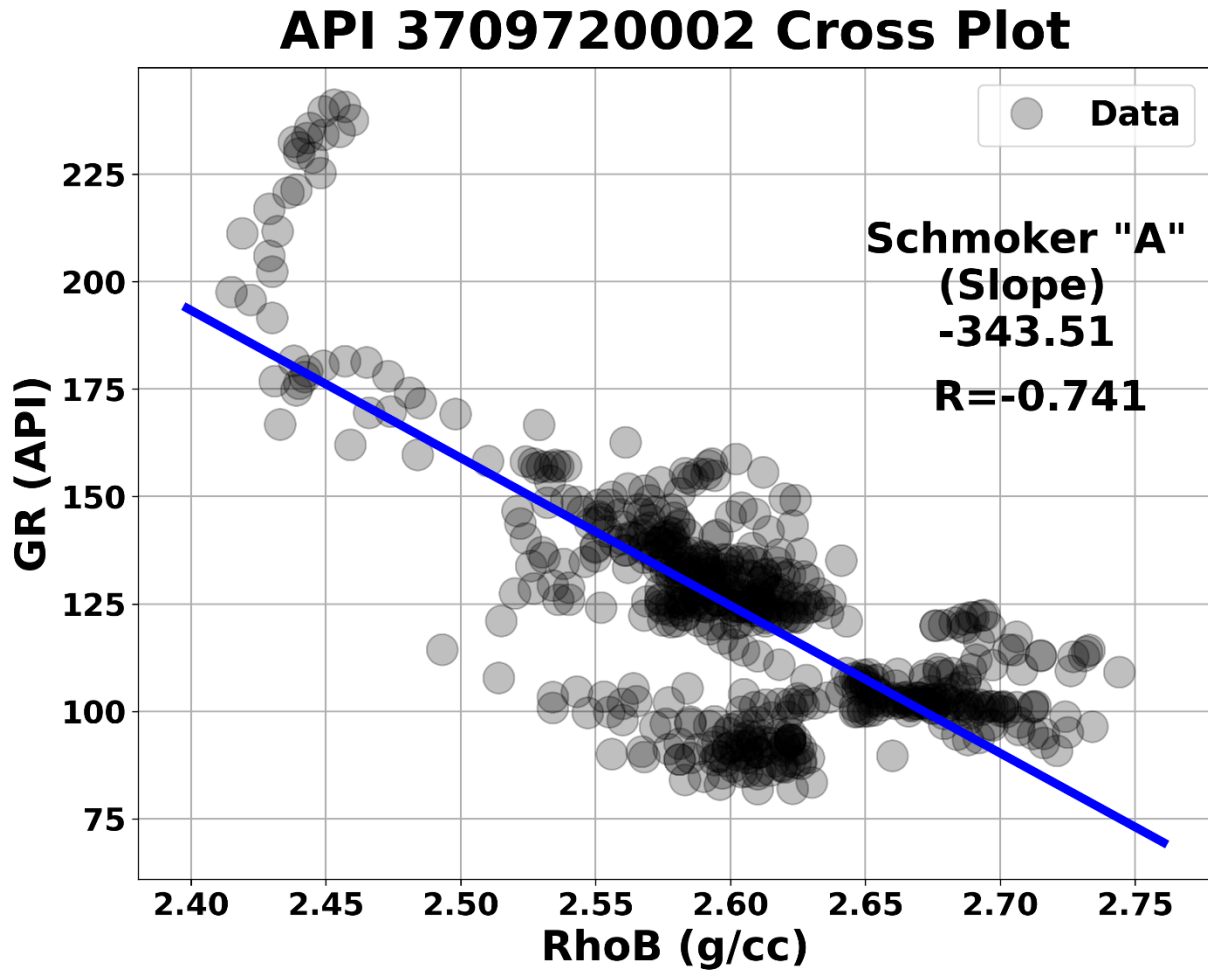


Figure 5-11. Example GR-RHOB crossplot for API No. 3709720002 showing the calculated slope of the linear regression (the Schmoker A value) to calculate TOC.

API 3709720002

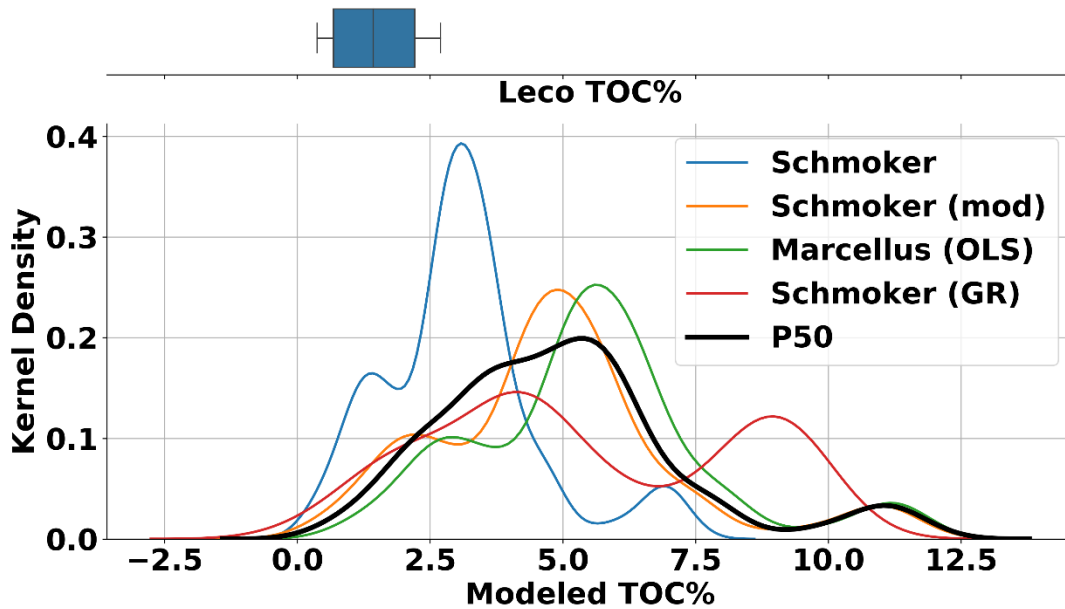


Figure 5-12. Distributions of TOC data calculated for each of four models and the P50 model for API No. 3709720002. The box and whisker plot (top) shows the range of the laboratory-derived TOC values for sampled intervals in the well. Schmoker: results from Equation 8, Schmoker (mod): results from Equation 9, Marcellus (OLS): results from Equation 10, Schmoker (GR): results from Equation 11.

API: 3709720002

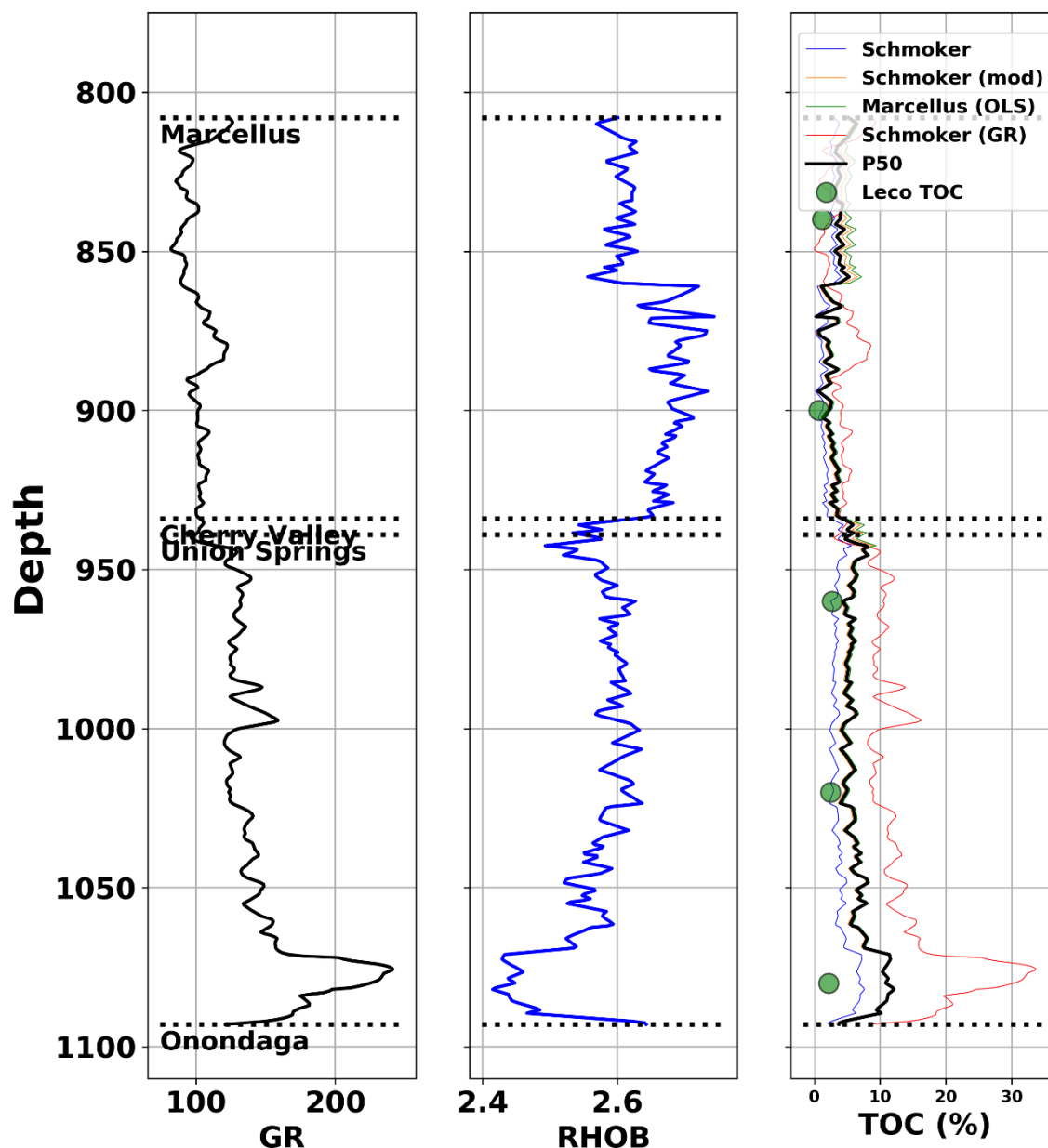


Figure 5-13. GR and RHOB logs with the modeled TOC curves and laboratory TOC data for the Marcellus interval (API No. 3709720002). Note the P50 curve overlies the green Marcellus (Equation 10) and orange Schmoker (Equation 9) curves in some places.

Several maps were generated to determine the areal and thickness limits for volumetric assessment of the Marcellus Shale storage resource. Figure 5-14 summarizes the spatial distribution of estimated average TOC in the Marcellus interval using the calculated P50 well log curve data, which ranged from less than 2 percent (purple) to more than 11 percent (red). An isopleth map (Figure 5-15) shows estimated vertical drilling depth to the top of the Marcellus Shale. Depth values range from 0 (red) to greater than 9500 ft (purple). The map was constructed by subtracting the top of Marcellus structure map grid from a digital elevation model of surface elevations and was used to set a northern updip limit to the estimated storage area.

That limit was established at the 2500-ft measured depth contour, the presumption being that no storage would be attempted at shallower depths. The Hamilton Group/Marcellus Shale net thickness ranges from 0 (purple) to more than 200 ft (red) (Figure 5-16). This isopach map was used to establish a western limit to the storage resource area where the total interval thickness exceeds 25 ft. It was presumed that no storage would be attempted where the total thickness was less than 25 ft.

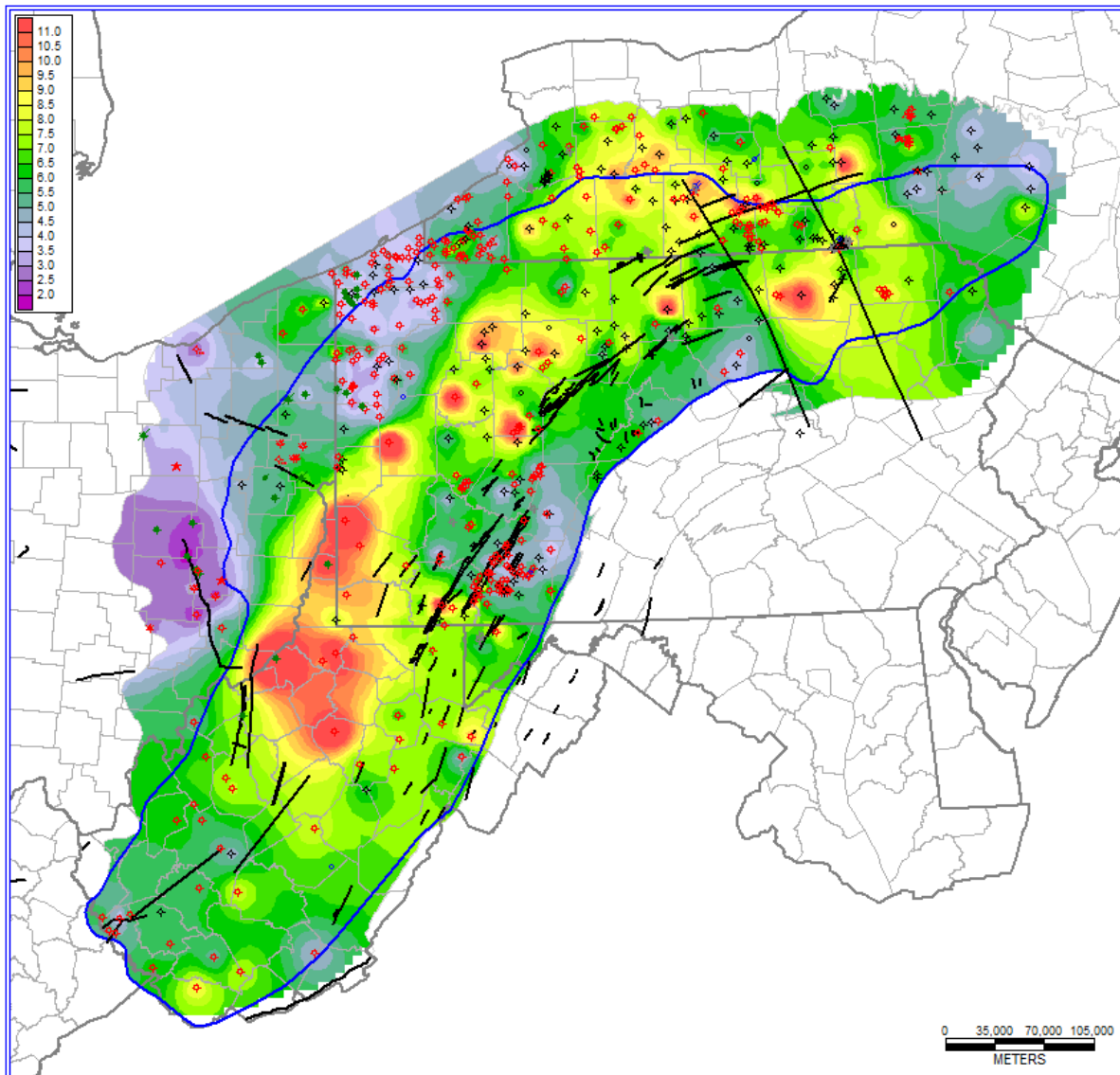


Figure 5-14. Spatial distribution of average TOC in the Marcellus Shale interval from calculated P50 well log curve data. The blue outline is the Marcellus assessment area.

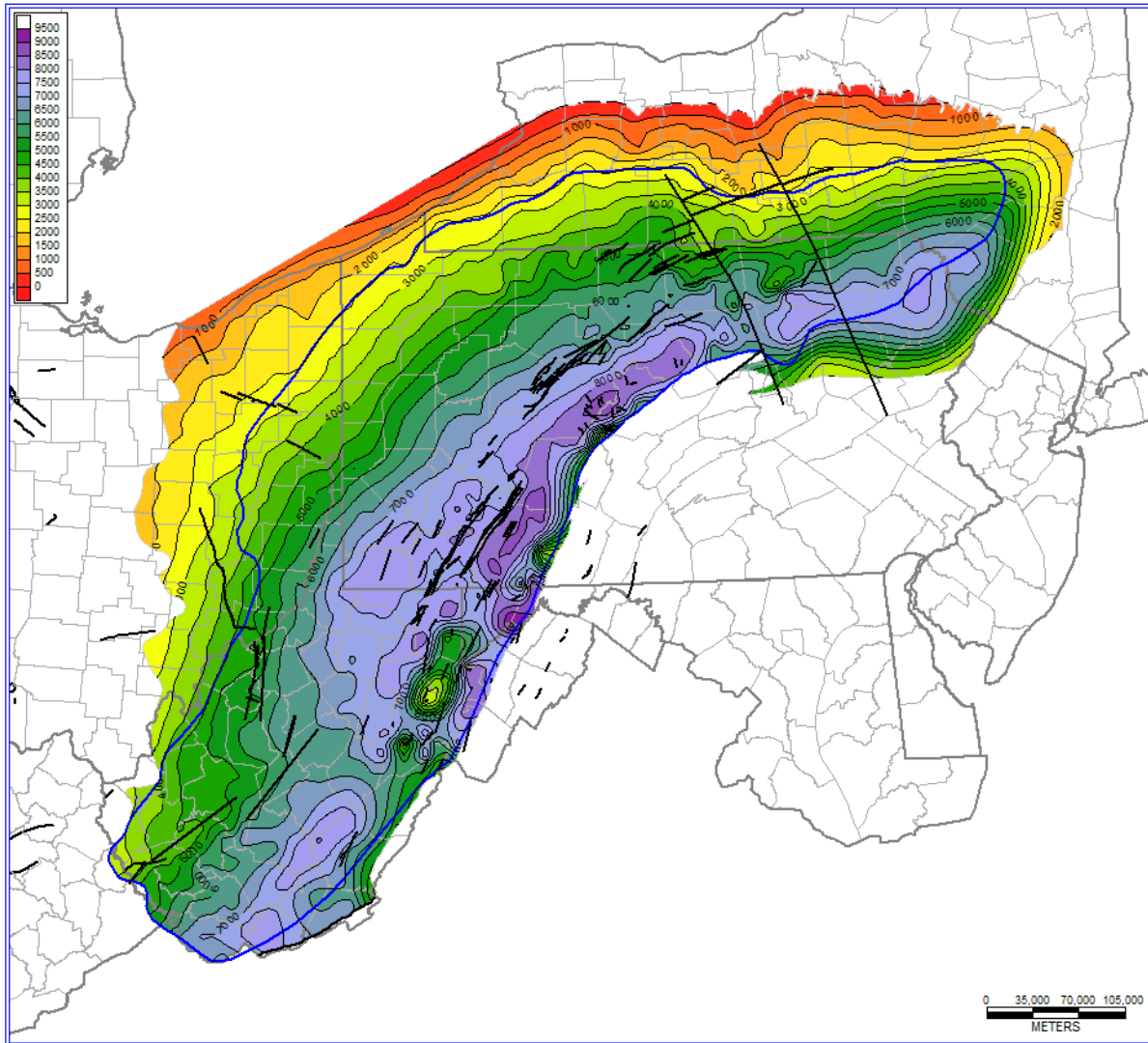


Figure 5-15. Estimated vertical drilling depth to the top of the Marcellus interval (500-ft contour interval) used to establish the updip limit of the area selected for storage resource estimates. The blue outline is the Marcellus Shale assessment area.

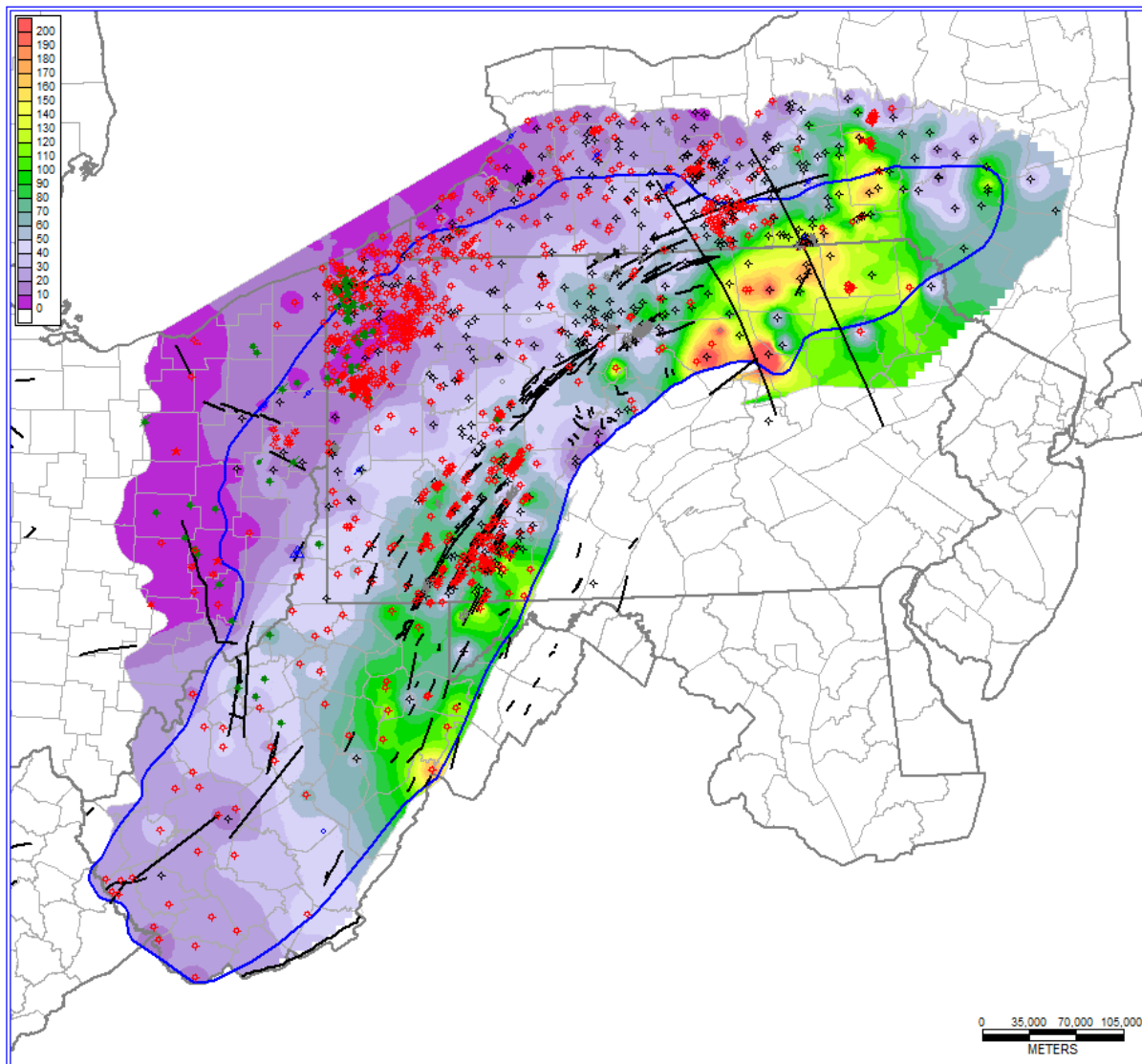


Figure 5-16. Net thickness map (10-ft contour interval) of organic-rich shale (>180 API units) in the Hamilton Group/Marcellus Shale interval. The blue outline is the Marcellus Shale assessment area.

Carbon storage resource estimates were performed using volumetrics tools available in the PETRA[®] software. A net thickness of organic-rich Marcellus Shale (i.e., GR >180 API units) was mapped from a potential database of 1558 wells (Figure 5-16). Having eliminated anomalous data points (e.g., expanded or repeated Marcellus Shale, incomplete logged section or abnormal log scales), the final mapped dataset totaled 1495 wells (Figure 5-17). The raw estimated total shale volume is approximately two billion acre-ft, with an average thickness of 55 ft. With TOC data from the calculated P50 digital log data, the net thickness of organic-rich Marcellus Shale with TOC greater than or equal to a 2 percent cutoff (common shale source rock potential) and with a greater than or equal to 4 percent cutoff (common cutoff for a greater shale gas and liquids potential) were investigated using 574 well points (Figure 5-17). Thickness values range from 0 (purple) to more than 300 ft thick (red) on both maps. The assessment volumes determined by applying these limiting parameters are provided in Table 5-1.

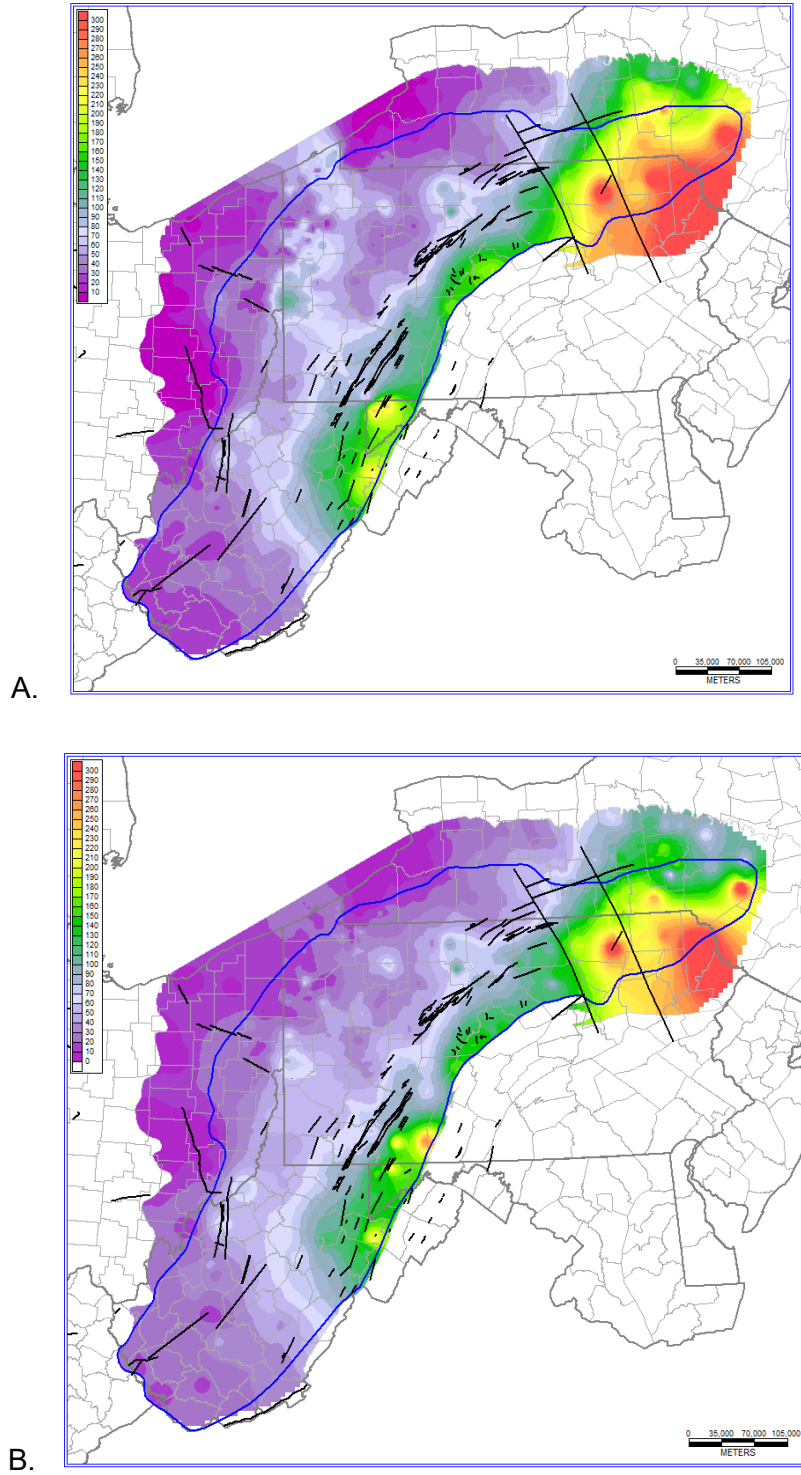


Figure 5-17. Maps of net thickness of organic-rich Marcellus Shale (10-ft contour interval) with TOC from the P50 curve greater than or equal to A) 2 percent (shale source rock potential), and B) 4 percent (greater shale gas/liquids potential)

Table 5-1. Calculated volumes of net organic-rich Marcellus Shale in the study area.

Assessment Parameters	Total Area (Million ac)	Assessment Area (Million ac)	Average Thickness (ft)	Volume (Million ac-ft)
TOC ≥ 2 percent Shale Source Rock Potential	36.45	36.41	90.44	3,292.9
TOC ≥ 4 percent Shale Gas/Liquids Potential	36.45	36.41	75.99	2,766.9

For this assessment, calculations were made using gridded data with a grid size of 8895.8 ac per grid cell (6000 m x 6000 m). Carbon storage volumes were estimated by first determining the tons of CO₂ stored per short ton of shale modified from the relationship developed by Nuttall et al. (2009) (Equation 12).

$$\frac{CO_2 \text{ tons}}{\text{ton of shale}} = \frac{(7.9 \times TOC_{P50} + 20.7)}{17800} \quad \text{[Equation 12]}$$

where TOC_{P50} is the mean TOC (P50) per grid cell (see Figure 5-14); and 17,800 is the conversion factor for standard cubic ft of CO₂ to tons of CO₂.

With an average density of 3440 tons per ac-ft (equals 2.53 g/cm³) and 8895.8 ac per grid cell, there are 30,601,492 short tons of shale per ft in each grid cell. Multiplying the net thickness of the Hamilton Group/Marcellus interval (Figure 5-16) by this conversion factor yields an estimate of the short tons of shale per grid cell. CO₂ storage in short tons per grid cell is derived by multiplying together the two grids of short tons of CO₂ per ton of shale and short tons of shale per grid cell. Final storage volumes were estimated by applying storage efficiencies of 3 and 10 percent and summing the grid values represented by the mapped areas in Figure 5-17.

5.4 Upper Ordovician Utica Shale/Point Pleasant Formation Interval

5.4.1 Geologic Setting

Dark, organic-rich shales are common in several Upper Ordovician units of the Appalachian Basin. The Utica and Point Pleasant formations (and their correlative equivalents) straddle the boundary of the Cincinnati/Mohawkian stages and regional Edenian/Chatfieldian (Shermanian) substages (Brett et al., 2004; Mitchell et al., 1992) (Figure 5-18). The Upper Ordovician Utica Shale/Point Pleasant Formation interval contains organic-rich shales, considered source rocks for conventional Trenton (and other) fields in the Appalachian Basin (Ryder et al., 1998; Ryder, 2008), and more recently are targets for oil and gas production (Kirschbaum et al., 2012; Patchen and Carter, 2015; Ryder et al., 1998).

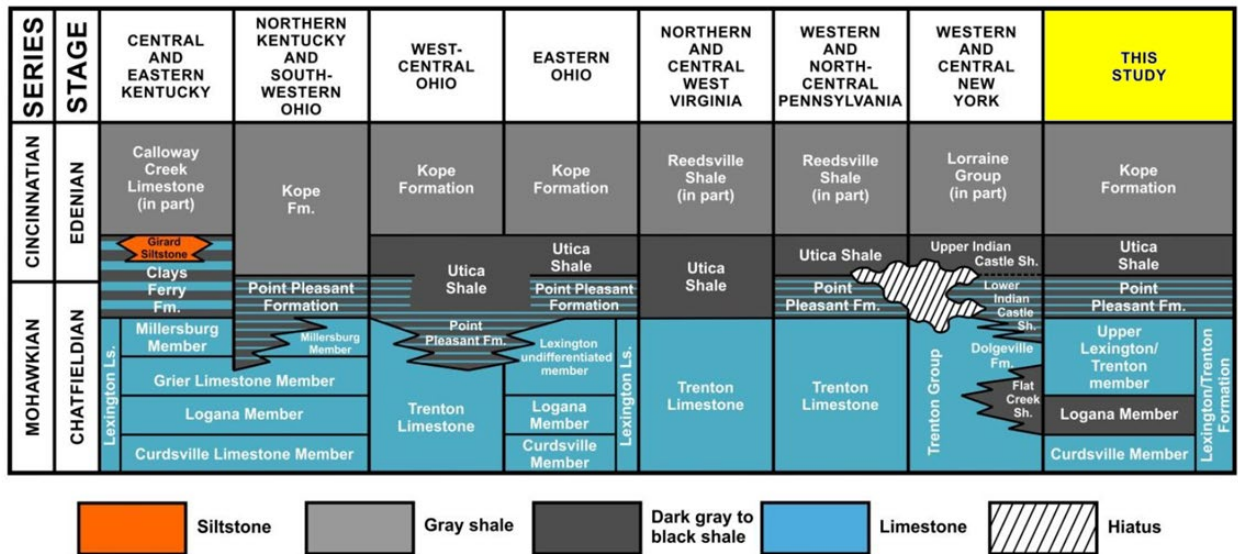


Figure 5-18. General stratigraphic nomenclature employed by the Utica Shale Appalachian Basin Exploration Consortium. TOC and digital geophysical data were grouped by the formation names highlighted in the “This Study” column (Patchen and Carter, 2015).

Figure 5-19 is a typical well log from the study area, showing the general “shaling-up” profile of the Trenton through Utica interval. A cross section (Figure 5-20) illustrates the general trend of thick Trenton (Lexington) Limestone carbonates, overlain by interbedded carbonates and shales (mudstones) of the Point Pleasant Formation, which are overlain by shales (mudstones) and carbonates of the Utica Shale. Thin black shales occur locally in the Trenton Limestone, but are more common in the Point Pleasant and Utica intervals. The Utica is overlain by calcareous gray shales of the Kope Formation and equivalents.

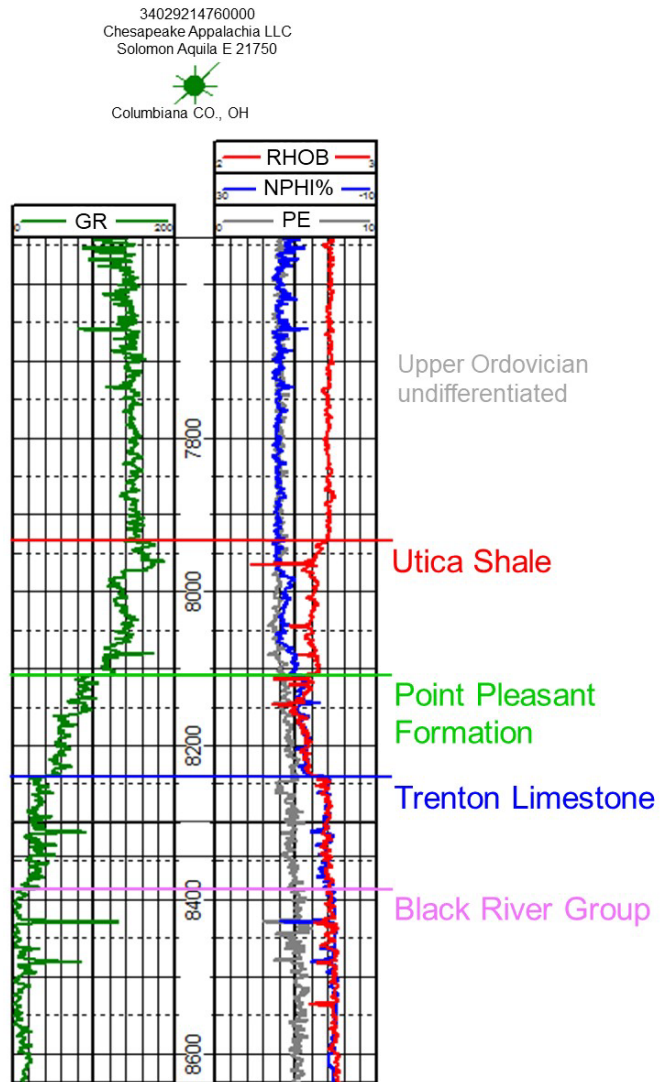


Figure 5-19. Type geophysical log for the units included in the Utica study area (modified from Patchen and Carter, 2015).

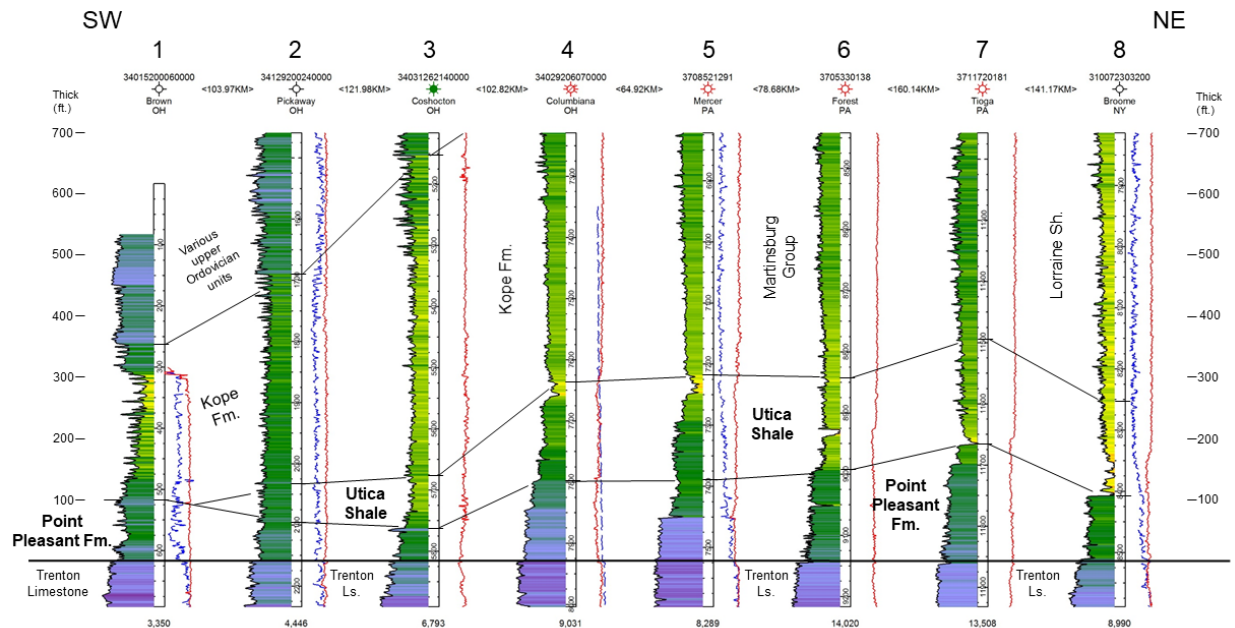


Figure 5-20. Generalized cross section along strike showing stratigraphic and lithofacies variations for the Utica Shale and Point Pleasant Formation. See Figure 5-25 for cross section location.

The Point Pleasant Formation and Utica Shale are shallowest on the arches along the north and west sides of the MRCSP Region and deepen eastward into the Appalachian Basin (Figure 5-21 and Figure 5-22, respectively). The Allegheny Front serves as the eastern margin of these structure maps. Utica shale elevations range from about 800 ft (red) to more than -16,000 ft MSL (dark blue). Point Pleasant elevations range from approximately 1500 ft (red) to more than -16,000 ft MSL (dark blue).

The Point Pleasant Formation thickens eastward into the Appalachian Basin and is more than 200 ft thick in north-central Pennsylvania (Figure 5-23). The Utica Shale is thick in an irregular belt in southern New York, northern Pennsylvania and northern Ohio (Figure 5-24). It is more than 400 ft thick in New York and thins to both the north and south, pinching out in Kentucky, southern Ohio and southern West Virginia. Several pods of thick shale appear to correspond to basement faulting (Figure 5-24).

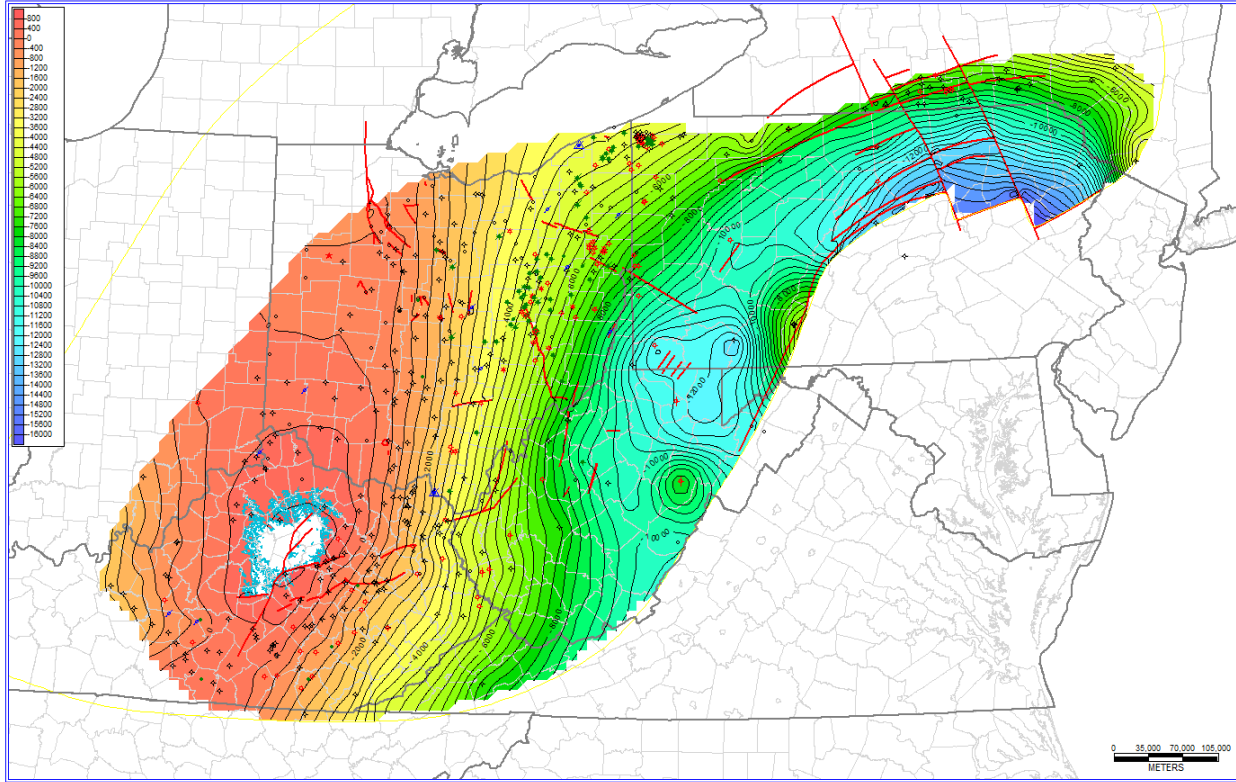


Figure 5-21. Areal extent and structure map (400-ft contour interval) on top of the Point Pleasant Formation (modified from Patchen and Carter, 2015). Major basement faults are indicated by red lines.

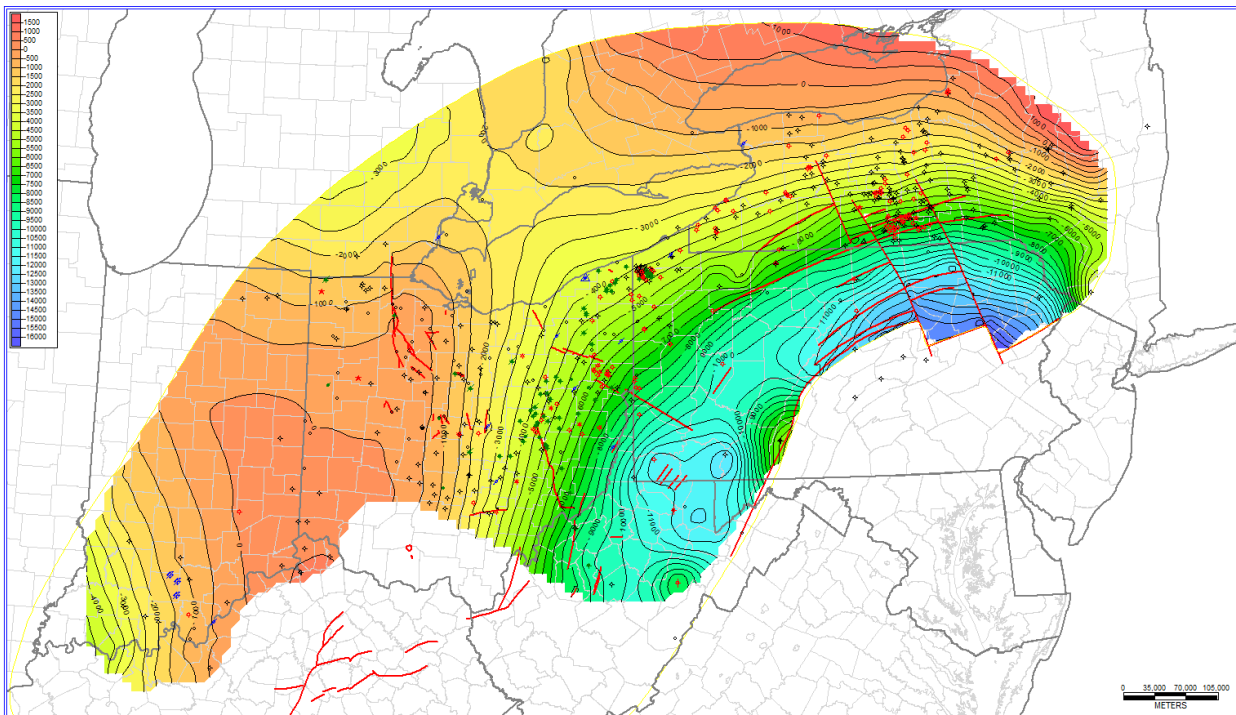


Figure 5-22. Areal extent and structure map (500-ft contour interval) on top of the Utica Shale (modified from Patchen and Carter, 2015). Major basement faults are indicated by red lines.

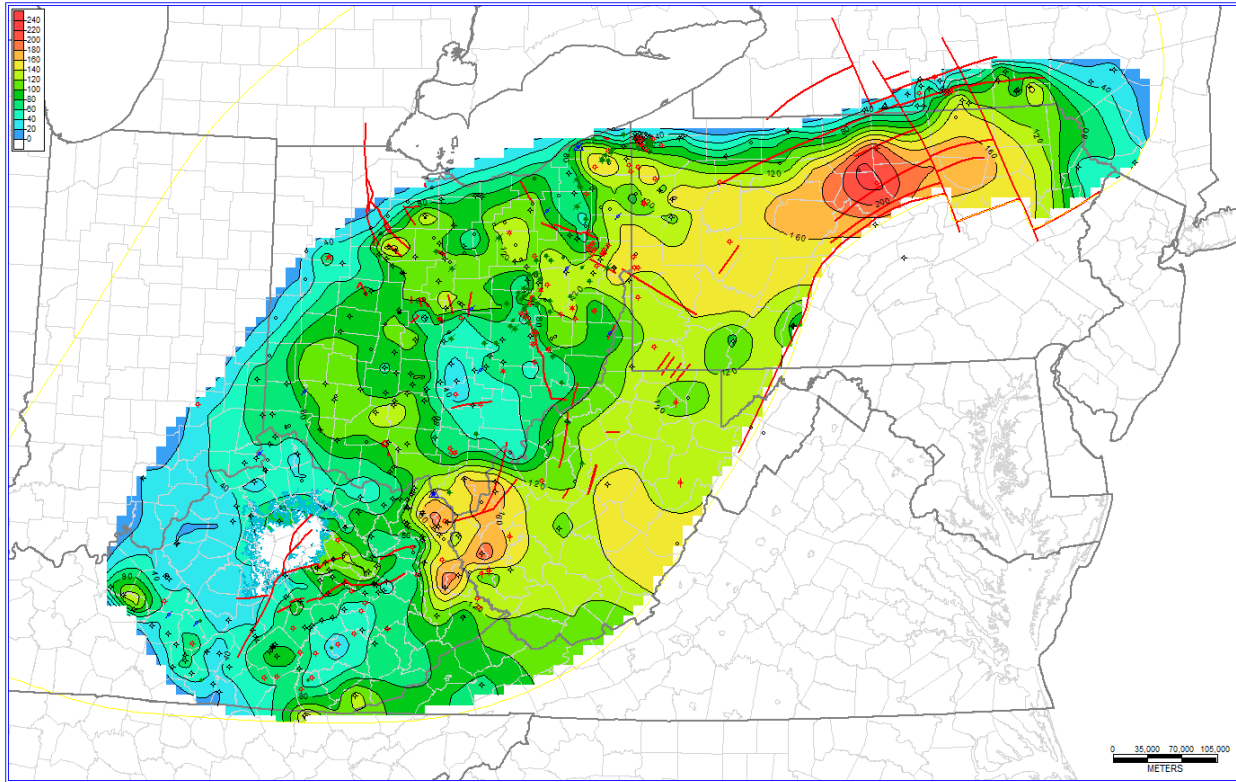


Figure 5-23. Gross thickness map (20-ft contour interval) of the Point Pleasant Formation (modified from Patchen and Carter, 2015). Major basement faults are indicated by red lines.

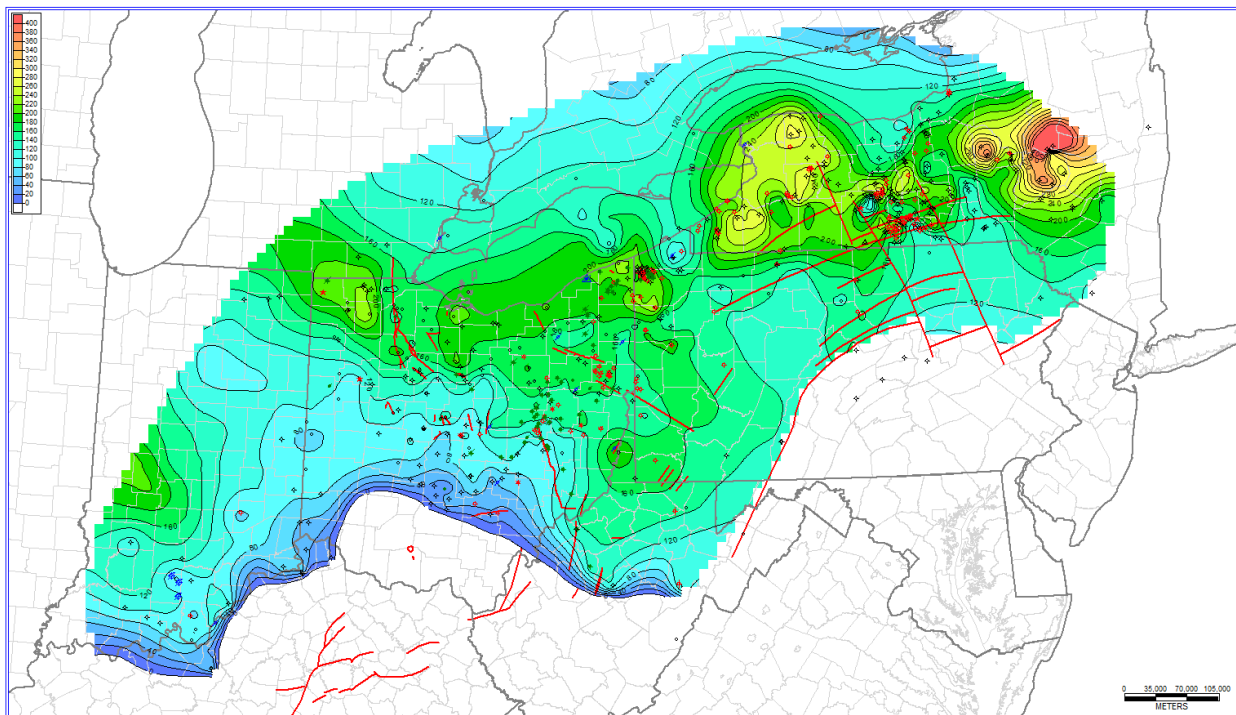


Figure 5-24. Gross thickness map (20-ft contour interval) of the Utica Shale (modified from Patchen and Carter, 2015). Major basement faults are indicated by red lines.

The Utica/Point Pleasant interval has been interpreted to comprise marine shales deposited in a succession of cratonward-migrating sub-basins related to deformational loading on the continental margin in association with the Taconic Orogeny (Ettensohn, 1991; Ettensohn and Lierman, 2012; Lehmann et al., 1995). During Late Ordovician time, tectonic flexure and forebulge migration is inferred to have steepened and deepened the carbonate ramp of the underlying Trenton carbonates. As in the Devonian, deepening is interpreted to have led to at least periodically stratified water columns, which created dysoxic to anoxic bottom-water conditions in which organic-rich shales could be preserved (Lehmann et al., 1995; Obermajer et al., 1999). Water-column stratification, however, was considerably variable and likely did not occur at great depths (Berry and Finney, 2010), with possibly seasonal changes in anoxia (Smith, 2013). Black shales of the Utica/Point Pleasant interval are also associated with sea-level changes and at least in some cases, condensed sections (Lehmann et al., 1995), similar to their Devonian counterparts.

Despite certain similarities, the Ordovician black shales also exhibit significant differences from their Devonian counterparts. Black shales in the Utica/Point Pleasant interval generally have much lower TOC values than do Middle Devonian Marcellus and Upper Devonian Ohio and Chattanooga shales in the basin (e.g., Ryder et al., 1998). Upper Ordovician black shales are interbedded with carbonates rather than siliciclastics, with significantly higher calcite content and lower clay content than their Devonian counterparts (Bai et al., 2016; Saboda and Lash, 2014; Wilson et al., 2016). Also, land plants had not yet evolved in the Ordovician so there was no contribution of organic matter from the terrestrial biome. Organic geochemistry studies of organic matter in Utica/Point Pleasant shales and oils suggests likely marine planktonic bacterial and/or algal origins (Hoffman et al., 1987; Jacobson et al., 1988; Longman and Palmer, 1987; Reed et al., 1986).

5.4.2 Data

Assessment of the carbon storage potential for the Utica/Point Pleasant interval differs from the approach used for more organic-rich shales like the Marcellus. Carbon storage in this interval is expected to occur as “free” gas in matrix porosity and as adsorbed gas associated with organic matter.

KGS prepared well-based stratigraphic interpretations using PETRA[®] software. Stratigraphic tops data were compiled from digital data files supplied by Geoteam members in New York, Ohio, Pennsylvania and West Virginia. As with the Marcellus Shale assessment, a series of reviews and quality control parameters were used to select a subset of available downhole logs and laboratory-derived TOC values for assessment of the Utica/Point Pleasant interval.

5.4.2.1 Utica Shale Play Book Study

The information utilized for the current study incorporated much information from another database prepared by the Utica Shale Appalachian Basin Exploration Consortium, who published the Utica Shale Play Book Study (Patchen and Carter, 2015). That study's PETRA® project database and associated gridded data, shapefiles and digital logs for were downloaded from the WVGES website (http://www.wvgs.wvnet.edu/utica/playbook/pb_12.aspx) for use in the current work. The project database contained location and header information for 10,416 wells across the five-state study area and the bordering regions of Indiana, Michigan and southern Ontario, Canada (Figure 5-25), a majority of which (>8000) represented Lexington/Trenton or deeper penetrations.

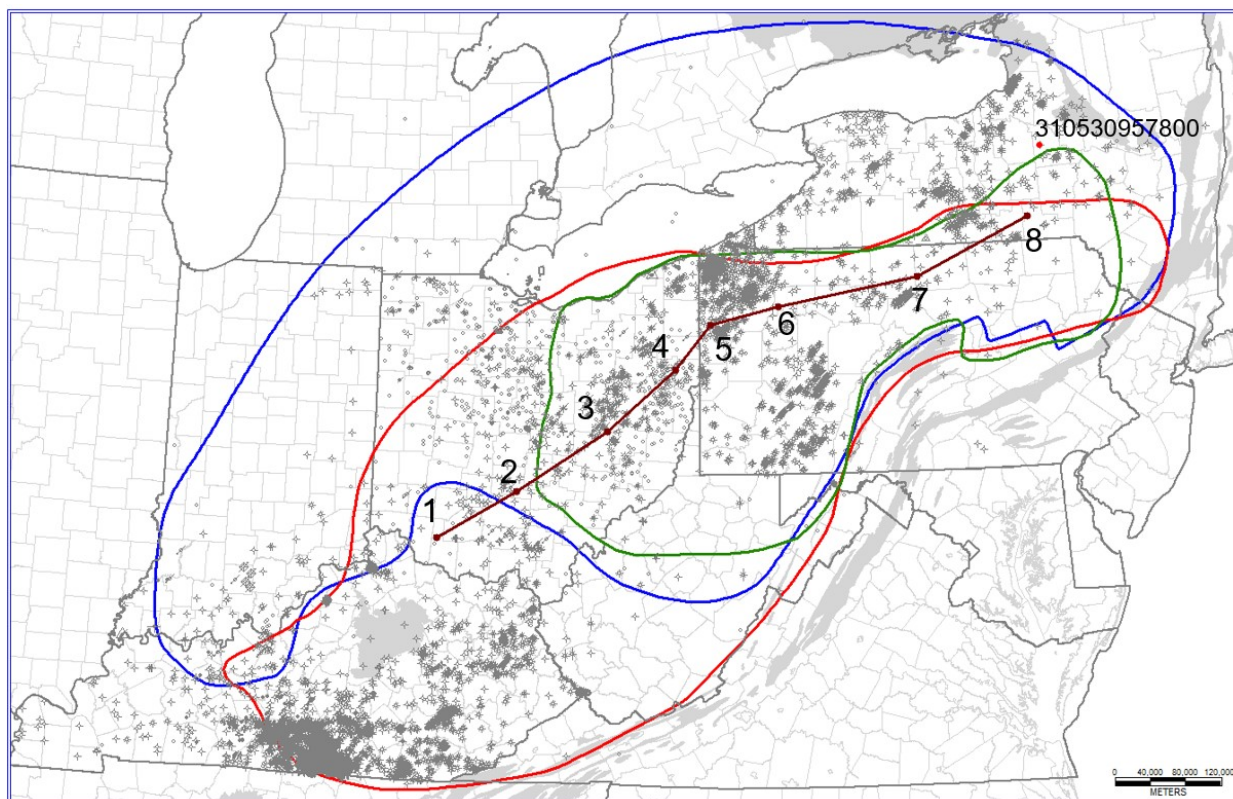


Figure 5-25. Well coverage utilized by the Utica Shale Play Book Study (modified from Patchen and Carter, 2015). The approximate extents of the Utica and Point Pleasant formations are shown by the blue and red outlines, respectively. The green outline represents the Utica/Point Pleasant play area. The red well and API number is the location of an example well used in the report. Light gray shaded polygons represent Ordovician outcrop areas.

Figure 5-25 shows the approximate areas of the Utica Shale (blue line) and Point Pleasant Formation (red line) used in the Utica Shale Play Book Study. The organic-rich portions of these units are much smaller than their overall extent. The Study's combined Utica/Point Pleasant play area (green line in Figure 5-25), where the northern, eastern and southern boundaries represent the organic-rich parts (defined as 25 ft or more shale >1 percent TOC) of the interval, and encompass the oil, wet gas and gas assessment units. The western margin of the play area appears to be a depth restriction and is close to the -2500 ft contour on the top of the Utica Shale (Figure 5-22).

5.4.2.2 Utica Shale Databook

A new PETRA® project of 1125 wells (the Utica Shale databook) was created using a subset of data from the 2015 Utica Shale Play Book Study. For example, some shallower, less mature, organic-rich parts of the Utica/Point Pleasant interval mapped by the Study in east-central Ohio were not included in the current study's databook, nor was data from wells shallower than the Utica/Point Pleasant interval or wells with incomplete digital geophysical log control. A total of 1020 geophysical well logs were loaded into the PETRA® project to prepare log-based correlations and calculations for the current assessment (Figure 5-26).

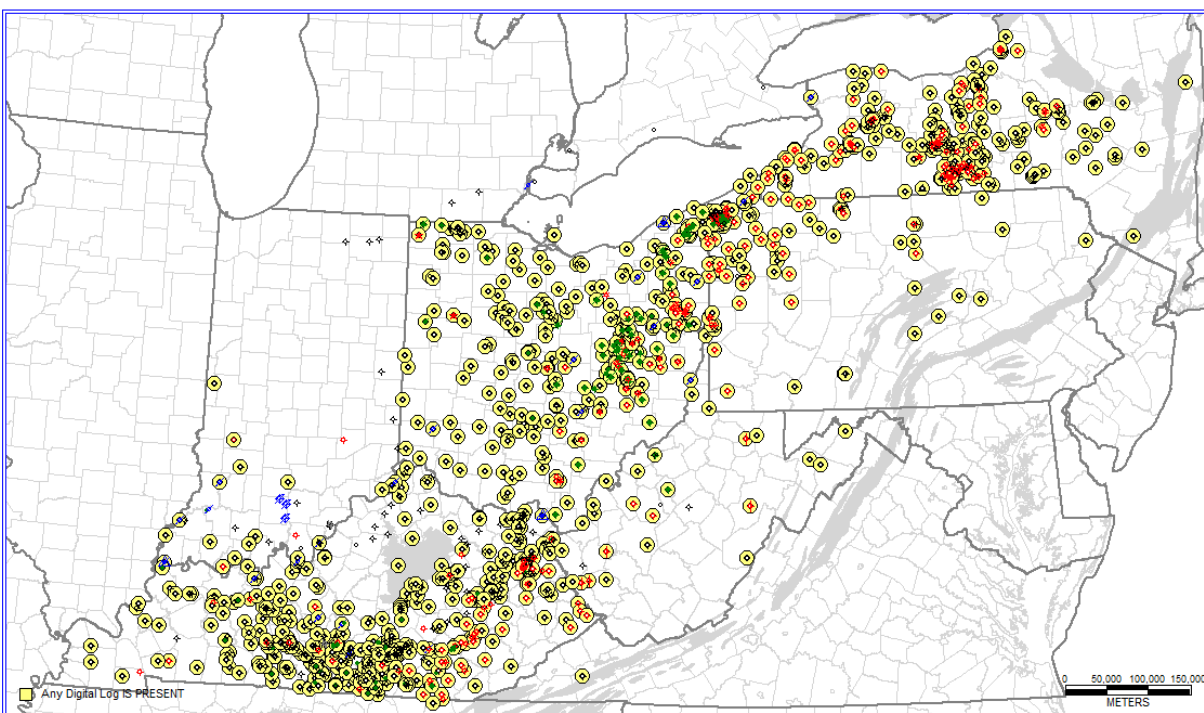


Figure 5-26. 1125 wells associated with the Utica Shale databook. Yellow circles (1020) are wells with digital geophysical log data files (LAS); non-digital well locations used in the study lack circles; red=gas show or production; green=oil show or production, black=dry hole, blue=salt-water disposal well. Gray shaded polygons represent Ordovician outcrop areas.

5.4.3 Data Review and Management

The Utica Shale Play Book Study had incorporated data from Devonian- to Cambrian-age geologic units, and therefore, required processing and filtering to focus on the Upper Ordovician units that were the focus of the current assessment. For the current assessment, KGS extended well-log-based stratigraphic interpretations for the Kope Formation, Utica Shale, Point Pleasant Formation, upper Lexington (Trenton) Limestone and Logana and Curdsville members of the Lexington (Trenton) Limestone as defined in Patchen et al. (2006). The generalized schema of stratigraphic nomenclature defined by Patchen and Carter (2015) was then adopted for the current work (Figure 5-18).

Patchen and Carter (2015) provided a spreadsheet-format catalog of measured TOC values. A total of 9515 TOC values were reported for 355 wells. No laboratory-determined RHOB data were included in this collection of TOC data so RHOB data were collected from available digital geophysical logs. The Utica Shale databook includes 2089 digital geophysical logs, but not all of

these are found within the current study area. Some wells outside the play area were retained for modeling purposes. Most of the available LAS files include GR and RHOB curve data. Both NPHI and PE curves could provide additional lithologic information potentially related to TOC, but the Utica Shale Play Book Study dataset included only one well with both measured TOC values and LAS file with a NPHI curve. A processed file of the data compiled for analysis in this study is supplied in Appendix C.

The Utica Shale Play Book Study's analytical data were identified by a plethora of stratigraphic names unique to different research team members and not necessarily consistent with the Study's correlation chart. A uniform set of stratigraphic nomenclature was adopted for the current assessment by mapping the Study's data file entries to equivalent formation names currently in use by KGS (http://www.uky.edu/KGS/emsweb/kyogfaq/stratcode_list.pdf). For example, TOC data for Upper Ordovician formations were variously identified in the Study's database as being associated with such units as the Ashlock, Drakes, Fairview, Calloway Creek, Garrard, Clays Ferry, "Ordovician," Kope, Reedsville, Martinsburg and Utica. These names were all mapped to Kentucky-equivalent formation names and then grouped together for statistical analyses as the: (1) Lexington (Trenton) Limestone; (2) Point Pleasant Formation; (3) Utica Shale; and (4) Kope and other formations. The Kope and other formations group includes all other Upper Ordovician units except for the Lexington (Trenton) Limestone, Point Pleasant Formation and Utica Shale. A "Utica" Formation designation was included in this group because for many wells in New York the Utica Formation name was assigned to all analyses (177) from the laboratory identified as "Humble." The Study's dataset also included 5441 analyses where the formation name was not identified (i.e., designated as unknown or missing and given a blank value).

A script was developed to process the Humble laboratory data entries for New York and the data entries with unknown or missing stratigraphic designations. The script matched the sample depths in the TOC dataset to formation tops data available from the Study's PETRA® project database. Thirty-one of the Humble observations and 3220 unknown or blank records were assigned updated formation and group names.

For TOC model assessment and development, data were selected for the: (1) Kope and other; (2) Utica; and (3) Point Pleasant stratigraphic intervals. The Lexington (Trenton) samples were excluded from this work. When filtered for the three selected intervals, the dataset included information for 1541 TOC observations and associated LAS files for a total of 130 wells (Figure 5-27). Most (87 percent) of these data are from New York and Ohio samples, and 77 percent represent samples collected from the Utica and Point Pleasant formations.

Summary statistics of the TOC data reported by Patchen and Carter (2015) are provided in Table 5-2. In total, 9502 TOC values were reported for 355 wells and ranged from 0.008 to 31.174 percent. For the Kope through Logana Member of the Lexington Formation, 6998 TOC values were reported for 300 wells and ranged from 0.008 to 7.931 percent. The ranges of TOC values for these units are illustrated in Figure 5-27. Of note, the observed magnitude and range of TOC values in the Logana Member of the Lexington (Trenton) Limestone suggest its organic matter content is comparable to that of the Point Pleasant Formation. While not currently a target of interest for hydrocarbon development, the Logana Member might have future potential (although thin).

Table 5-2. Descriptive statistics of TOC data in the Utica Shale databook grouped by stratigraphic categories. Samples were grouped as Logana Member if they were an organic-rich shale in the Lower Trenton (Lexington) Limestone. All Upper Ordovician non-Point Pleasant and Utica samples above the Trenton were placed in the Kope and other formations grouping.

System	Grouped Units	Count	Mean TOC	Standard Deviation	Min	Percentiles			Max
						25th	50th	75th	
Devonian	Ohio Shale	48	1.95	1.86	0.25	0.522	0.995	3.12	6.56
	Rhinestreet Shale	2	2.38	2.2	0.82	1.6	2.38	3.15	3.93
Silurian	Onondaga Limestone	4	1.93	1.04	1.02	1.2	1.69	2.42	3.33
	Oriskany Sandstone	2	0.247	0.211	0.098	0.173	0.247	0.322	0.396
	Crab Orchard Formation	1	0.104	--	0.104	0.104	0.104	0.104	0.104
	Brassfield Dolomite	2	0.136	0.004	0.133	0.134	0.136	0.137	0.138
Ordovician	Kope and other formations	1285	0.704	0.669	0.008	0.247	0.408	0.993	6.08
	Utica Shale	2031	1.28	0.764	0.012	0.597	1.21	1.8	4.19
	Point Pleasant Formation	951	1.71	0.998	0.009	0.93	1.61	2.43	7.28
	Lexington (Trenton) Limestone	1991	1.12	0.978	0.044	0.379	0.757	1.68	7.19
	Logana Member (and equivalents)	740	1.53	1.2	0.01	0.437	1.4	2.36	7.93
	Black River Group	228	0.357	0.376	0.01	0.128	0.225	0.414	2.46
	Wells Creek Formation	14	0.183	0.107	0.067	0.108	0.135	0.268	0.44
	Knox Group	48	0.291	0.266	0.01	0.17	0.22	0.297	1.32
Cambrian	Copper Ridge Formation	2	0.175	0.05	0.14	0.158	0.175	0.193	0.21
	Conasauga Group	4	0.168	0.045	0.13	0.138	0.155	0.185	0.23
	All Upper Ordovician units	6998	1.212	0.952	0.008	0.41	0.972	1.81	7.931
	Unknown	2149	1.24	1.64	0.01	0.32	0.74	1.61	31.174
	All observations	9502	1.195	1.151	0.008	0.37	0.868	1.75	31.174

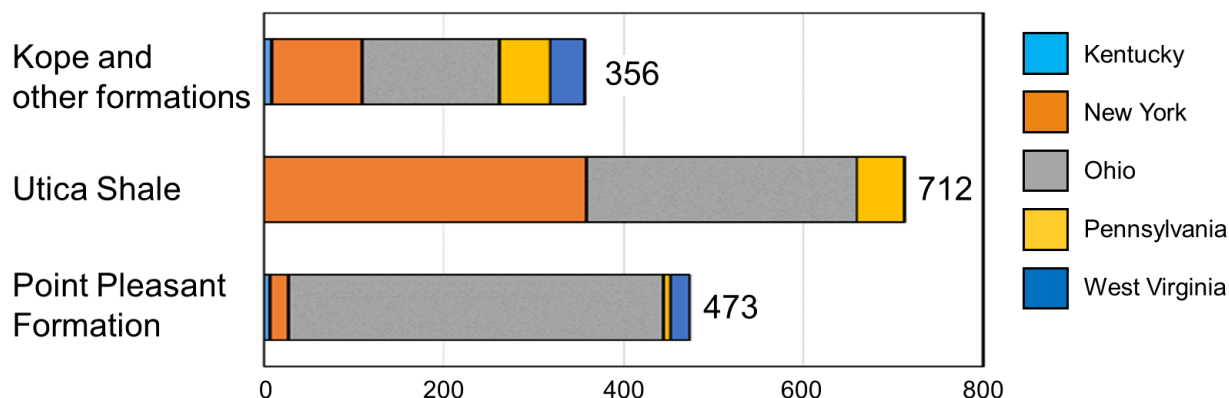


Figure 5-27. Measured TOC observations associated with RHOB data by state for Point Pleasant Formation, Utica Shale and Kope and other formations.

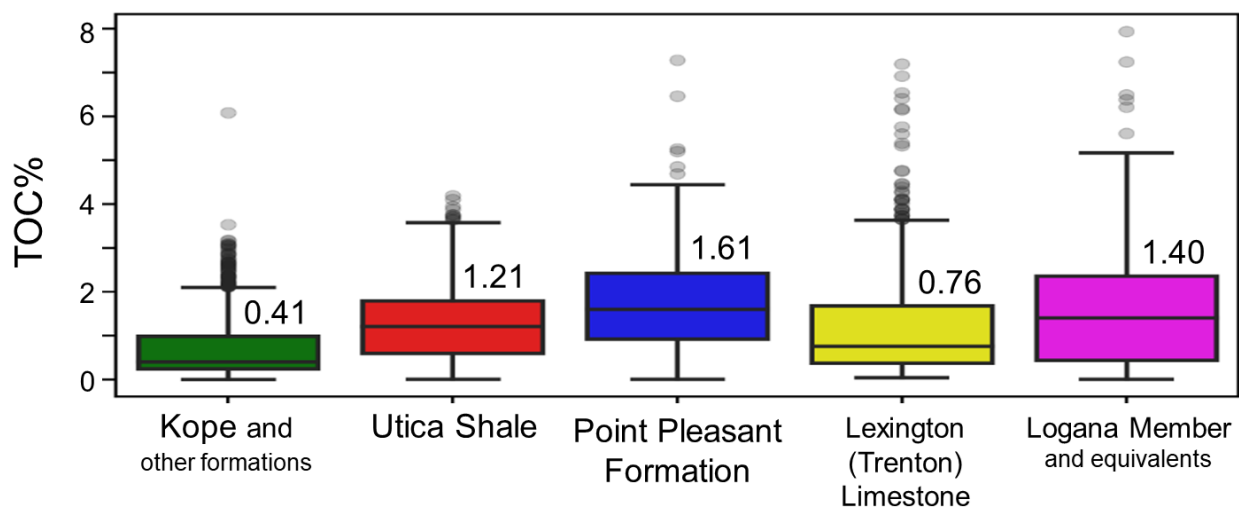


Figure 5-28. Distributions of TOC for selected Upper Ordovician units by stratigraphic group showing fiftieth percentile TOC values. See Table 5-2 for number of samples from each interval. Data from the Lexington (Trenton) Limestone, and Logana Member (and equivalents) of the lower Lexington (Trenton) Limestone, were not used for additional regional analyses.

5.4.4 Methods

Studies by Godec (2013c) and Patchen and Carter (2015) examined carbon storage and hydrocarbon volumetrics relative to organic-rich shale formations, respectively. The current study utilizes methods similar to those research efforts.

5.4.4.1 TOC Models

Laboratory-derived TOC values reported in the Utica Shale Play Book Study were acquired from either well cuttings or cores. Samples taken from whole core or rotary sidewall core were assumed to be representative of their given sample depth and the GR and RHOB values at that depth were extracted from the LAS file for the well. The TOC value provided for well cuttings with a reported sample interval required a different approach, however. The TOC data were assumed to represent the average TOC for the sample interval with a cited top and base depth. A sample measured depth was assigned to be the midpoint of that interval. The GR and RHOB values for the same depth interval were extracted from LAS files, and the average value over

that interval was assigned to the interval midpoint depth. Once paired with TOC data, a total of 1442 GR and 1538 RHOB values from 130 wells were available for analysis and modeling as part of the current assessment.

In Middle and Upper Devonian organic-rich shales, there is a strong relationship between TOC and GR and RHOB log response (Figure 5-1). Predicting TOC in the Utica and Point Pleasant formations from geophysical data, however, has proven more challenging (Godec, 2013c; Patchen and Carter, 2015; Wang et al., 2016). Correlation coefficients were calculated using TOC, GR and RHOB data from the Utica Shale Play Book Study for the (1) Kope and other; (2) Utica; and (3) Point Pleasant intervals. Data for these intervals were selected from the Study where digital data from both GR and RHOB logs could be depth-matched with TOC observations (1356 observations from 124 wells). The results show the best observed correlation was that between TOC and RHOB (Table 5-3). With a coefficient of only -0.5, however, this is a moderate correlation at best. The correlation between TOC and GR response is also weak.

Crossplots were generated for each grouping of stratigraphic units to further examine relationships between basic geophysical data and TOC. No R value for any of the grouped units exceeded 0.2 in either of the GR vs. RHOB or GR vs. TOC crossplots (Figure 5-29A and B), indicating no correlation or a weak correlation.

The R values in the RHOB vs. TOC crossplot (Figure 5-29C) indicate a weak correlation for the Utica Shale and a moderate correlation for the Point Pleasant. Nonetheless, the correlation coefficients are statistically significant for both stratigraphic groupings. There is essentially no correlation between TOC and RHOB for the Kope and other formations grouping. Based on the correlation coefficients (Table 5-3) and the crossplots, three assumptions were used to guide TOC modeling:

- The Kope and other formations grouping represents a baseline unit without significant organic content.
- GR data show little to no systematic response to changes in TOC.
- TOC is more strongly related to RHOB.

Table 5-3. Correlation coefficients (R) between TOC, RHOB and GR for 1356 observations from 124 wells (using data from Patchen and Carter, 2015).

	TOC	RHOB	GR
TOC	1	-0.5	-0.17
RHOB	-0.5	1	0.062
GR	-0.17	0.062	1

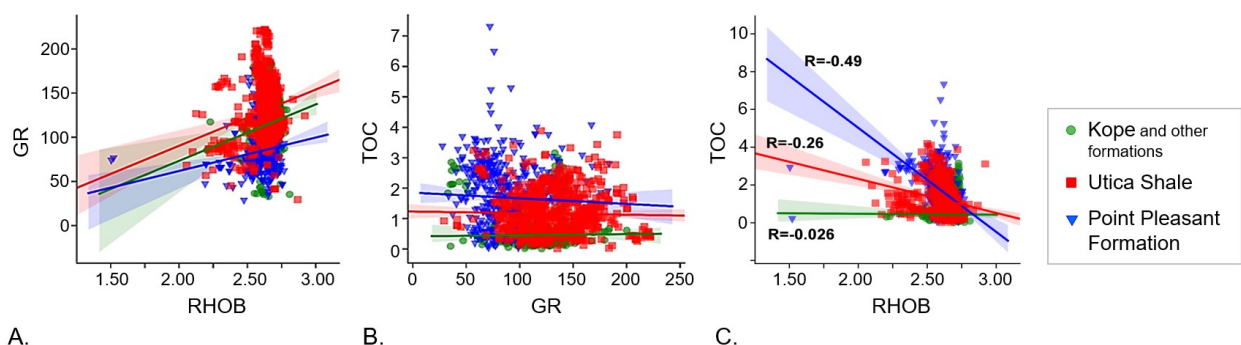


Figure 5-29. Crossplots of Kope and other (green), Utica (red) and Point Pleasant (blue) geophysical and TOC data: A) GR and RHOB; B) TOC and GR; and C) TOC and RHOB. Panel C includes R values for each of the grouped stratigraphic units.

Initially, two models that had been used for the Marcellus assessment and two models previously suggested for the Utica Shale and Point Pleasant formations were selected for calculating TOC from geophysical logs in the Utica/Point Pleasant interval:

- The Schmoker model (Schmoker, 1979, 1993), which was developed using primarily the Upper Devonian Ohio Shale in the Appalachian Basin (Equation 8).
- TOC_{inreg} is an OLS linear regression model based on the laboratory TOC and RHOB data in the Pennsylvania databook (Equation 9).

Godec (2013c) presented an OLS regression model developed from TOC and RHOB data for the Utica/Point Pleasant interval. This equation differs by only a few least significant digits from a similar analysis shown in Appendix C for active wells in the Utica Shale Play Book Study.

$$TOC_{Godec} = \frac{(RHOB - 2.73)}{-0.05} \quad \text{[Equation 13]}$$

Wang et al. (2016) provided a TOC model based an OLS regression using the inverse of RHOB for the Utica and Point Pleasant intervals.

$$TOC_{Wang} = \frac{(238.1)}{RHOB} - 89.1 \quad \text{[Equation 14]}$$

Calculations were performed using these four models to estimate TOC from RHOB data for the Utica and Point Pleasant grouped formations. The correlation coefficients between the measured and modeled TOC values were statistically significant.

The distributions of residuals computed using models from Equations 8, 9, 13 and 14 show deviations from what might be considered optimum predictions (Figure 5-30). Ideally, the distribution of residuals should be symmetrically distributed with respect to a value of zero and thus tending to minimize the difference between measured and calculated TOC values.

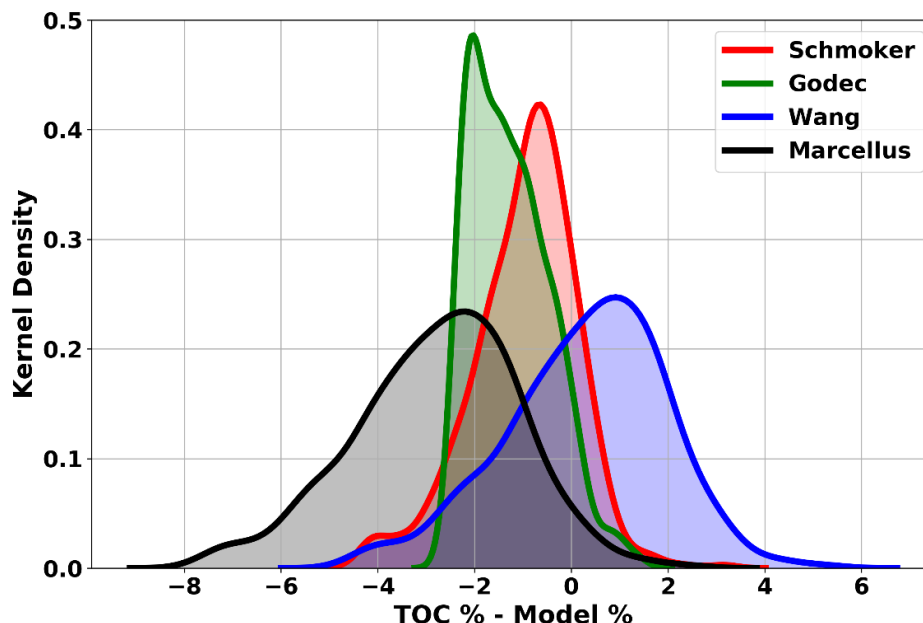


Figure 5-30. The distribution of the difference between measured and modeled TOC (residuals) in the Utica and Point Pleasant formations as determined using TOC estimated from RHOB using four models.

For the Schmoker (Equation 8), Marcellus OLS linear regression (Equation 9) and Godec (Equation 13) models, the estimated TOC values tend to overestimate the predicted TOC by 1 to 3 percent. The Wang (Equation 14) model predicted values that tend to underestimate the TOC by 1 percent. Considering the generally low range of observed TOC values for the Utica/Point Pleasant interval, this suggests these models might not be optimal for estimating TOC.

To improve the existing models for Utica Shale and Point Pleasant Formation TOC estimations using geophysical log data, the two existing formulas were modified, and two new models were tested. These four new models were applied to see if they might better predict TOC:

- A modification of the Schmoker (1979, 1993) relationship:

$$TOC_{SchUticMod} = 32.5 * \left(\frac{2.73}{RhoB} - 1 \right) \quad \text{[Equation 15]}$$

- A modification of the Wang et al. (2016) relationship:

$$TOC_{WangMod} = \frac{(49.331)}{RhoB} - 17.327 \quad \text{[Equation 16]}$$

- A non-parametric linear regression model was derived using the Theil-Sen estimator (Wilcox, 2010):

$$TOC_{TS} = -8.137 * RhoB + 22.746 \quad \text{[Equation 17]}$$

- A multi-variate linear regression model was derived from RHOB and GR using machine learning techniques (James et al., 2013).

$$TOC_{MV} = 18.415 - 6.444 * RhoB - 0.00049 * GR \quad \text{[Equation 18]}$$

The Schmoker (1979, 1993) and Wang et al. (2016) models (Equations 15 and 16, respectively) were each tuned to the available laboratory TOC and geophysical RHOB data using the Excel linear solver to alter both the constant and Rho_{max} values to minimize the RMSE between the observed and computed TOC contents.

The Theil-Sen estimator (Equation 17) is a robust regressor (i.e., relatively insensitive to outliers) and is derived by finding the median (P50) of the slopes between all pairs of observations (Wilcox, 2010). The y-axis intercept parameter is determined by using the median RHOB and solving the standard linear equation for the intercept.

A multi-variate linear regression model (Equation 18) was derived using the train-test-split method from machine learning techniques (James et al., 2013). Random selection is used to split the data into two sets: a training set equal to 30 percent of the observations and a test set with the remaining observations. An OLS linear regression is performed on the training data. This regression is then applied to the test data set and the coefficient of determination and RMSE between the observed and calculated TOC values are calculated to check the quality of the fit. Performing the train-test-split calculation sequence multiple times with differing randomly selected training sets enables calculation of model parameters that provide criteria to either maximize the coefficient of determination (r^2 approaching one) or minimize the RMSE. Figure 5-31 is a plot of the residuals from 1000 iterations of the train-test-split technique. This procedure will not necessarily generate a unique or optimal model. The solution can best be characterized as complying with one or both model fitness criteria given the selected subsets (training and testing) of the data. Table 5-4 provides the values of the measures for goodness of fit for the models considered for the Utica/Point Pleasant interval.

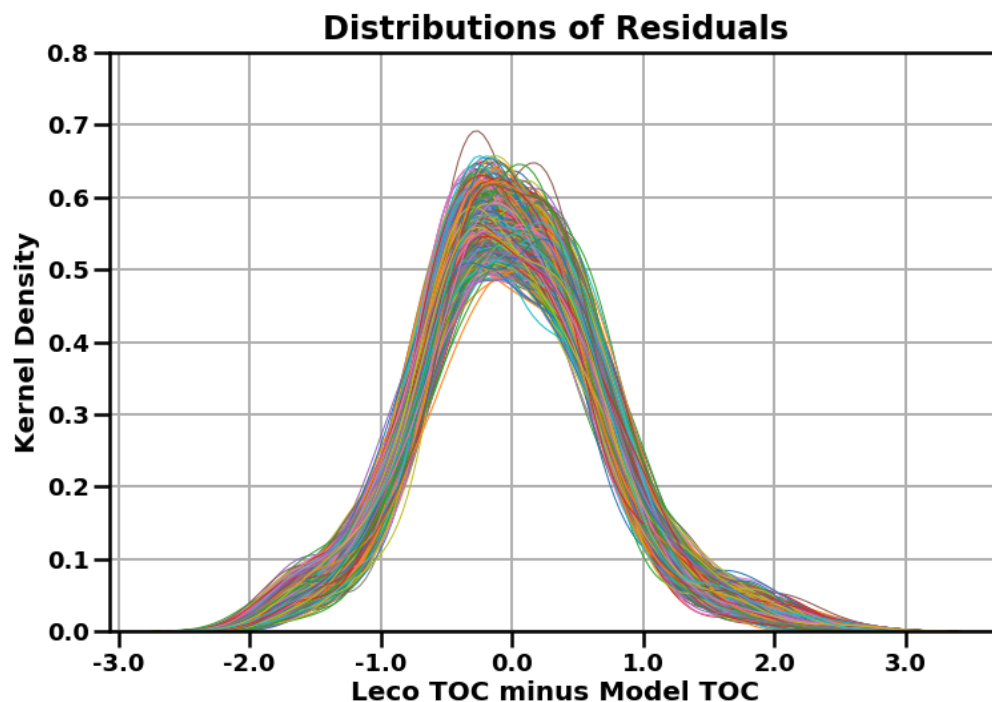


Figure 5-31. Distributions of residuals generated by multiple train-test-split iterations to determine multivariate regression parameters for modeling TOC in the Utica and Point Pleasant formation groups.

5.4.5 Results and Discussion

5.4.5.1 TOC Models

Three models, the Thiel-Sen regression (Equation 17), modified Wang equation (Equation 16) and the multivariate regression of RHOB and GR (Equation 18) all perform better than the other models considered in the current assessment. The multivariate regression model exhibited both the minimum RMSE value of 0.58 and the maximum r^2 value of 0.41 for a run of 10,000 train-test-split computations (Table 5-4).

The distribution of residuals for the four new proposed models (Figure 5-32) shows an acceptable variance within a range of +/- 0.5 percent. The CNG Shepard No. 1 well (API No. 310530957800) illustrates model performance on a single-well basis. Figure 5-33 shows a box and whisker plot

(top of figure) of the distribution of observed TOC values and the kernel density distributions for each of the four models (bottom) to help visualize variations between laboratory-derived TOC and modeled TOC estimates. For this well, the modified Schmoker (Equation 15) model tends to underestimate the TOC content while the modified Wang (Equation 16) and multivariate (Equation 18) models tend to overestimate the TOC content. The Thiel-Sen model

Table 5-4. Fit statistics for the eight models investigated to calculate TOC from geophysical log data in order by the coefficient of determination (r^2) and minimum RMSE. Highlighted values emphasize models with better predictive power.

Model	Equation	r^2	RMSE
TOC _{linreg}	10	-15.86	3.39
TOC _{Wang}	14	-4.32	1.90
TOC _{Schmoker}	8	-1.21	1.23
TOC _{Godec}	13	-0.98	1.16
TOC _{SchUtlicMod}	15	-0.03	0.84
TOC _{TS}	17	0.25	0.71
TOC _{WangMod}	16	0.28	0.70
TOC _{MV}	18	0.41	0.58

(Equation 17) appears to provide the best match with observed TOC distribution. Figure 5-34 plots the GR, RHOB and TOC curve data with depth, demonstrating the more organic-rich character of the Utica Shale in this well.

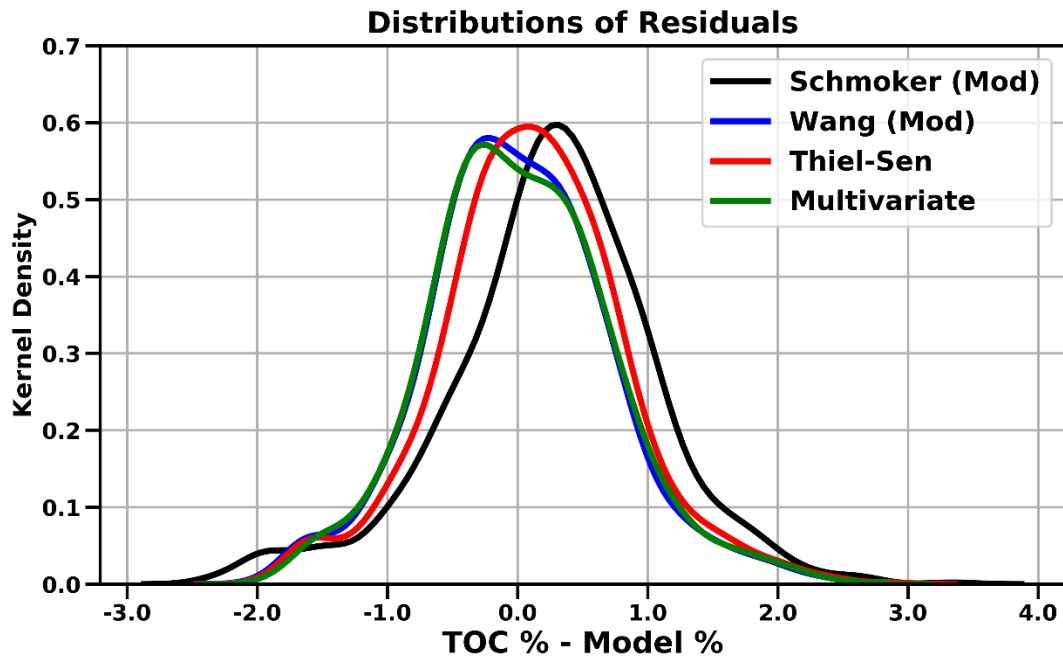


Figure 5-32. Distribution of residuals between measured and predicted TOC for four proposed models for the Utica/Point Pleasant interval.

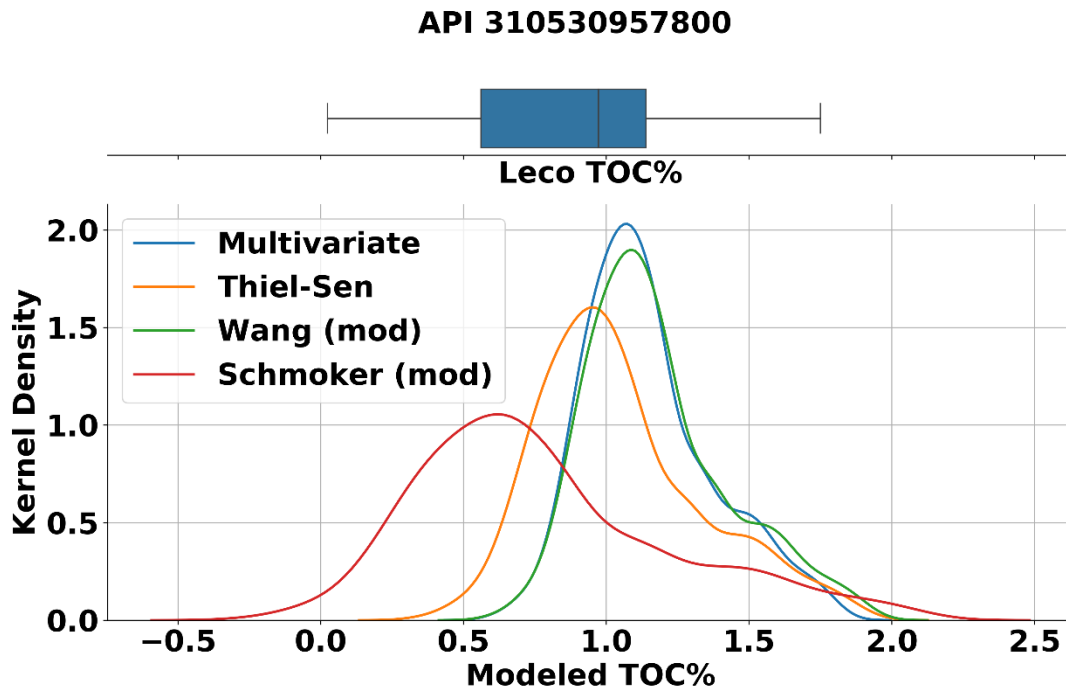


Figure 5-33. Example model performance for the CNG Shepard No. 1 well (Madison County, New York), showing the distribution of measured TOC values (box and whisker chart, top) and TOC calculated from geophysical log data (kernel distribution plots, bottom).

API: 310530957800

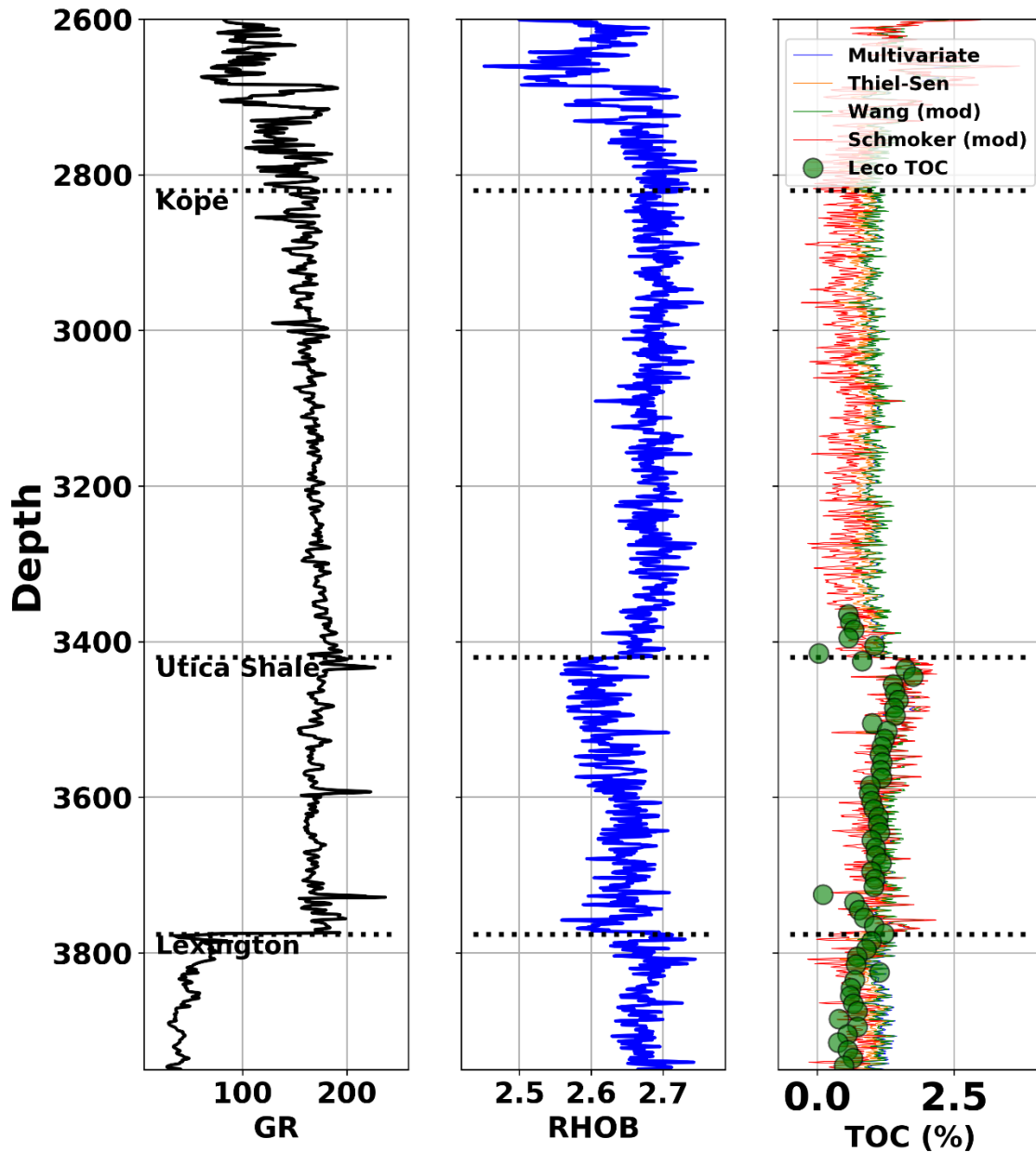


Figure 5-34. GR and RHOB logs for the CNG Shepard No. 1 well (Madison County, New York), with measured TOC data and calculated TOC curves. Note the Multivariate (blue) and Wang (mod) (green) TOC curves plot close together, so appear as only a green line.

Using the Utica Shale databook, descriptive statistics for new TOC model curves (minimum, maximum, mean and the tenth –P10, fiftieth – P50, and ninetieth – P90 percentiles) were calculated using PETRA® software, and the median (P50) was gridded to produce TOC distribution maps. A map of laboratory-measured TOC calculated across all intervals is presented in Figure 5-35. For this map, the mean value of available laboratory TOC analyses in each well was used. The map is constrained by the limited number of wells with laboratory data. The new digital log-based models can be used to generate TOC estimates from well data with a broader coverage across each unit's extent.

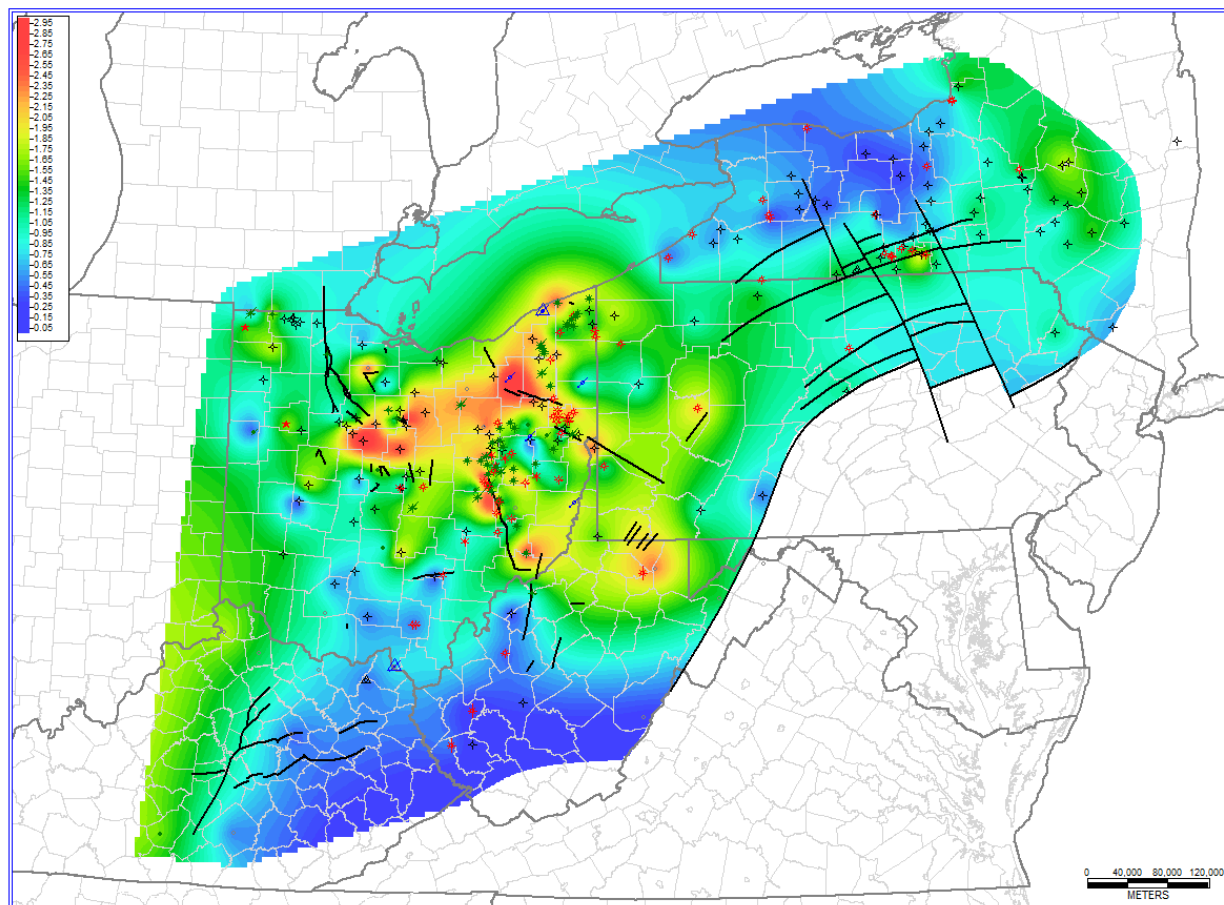


Figure 5-35. Map of Utica Shale and Point Pleasant Formation TOC from the Utica Shale databook. Contours represent mean measured TOC values for 264 wells. TOC values range from 0.05 percent (dark blue) to more than 2.95 percent (red).

5.4.5.2 CO₂ Storage in the Matrix

The storage of free CO₂ (i.e., not adsorbed on organic matter) in the Utica/Point Pleasant interval is a function of three factors: (1) total porosity is an upper limit of the space available for storage; (2) reservoir depth and pressure affect the phase and thus density of stored CO₂; and (3) water saturation affects the fraction of pore space available for storage. Godec (2013c) presented a detailed assessment of both adsorbed and free CO₂ storage in the Utica/Point Pleasant interval; this assessment has drawn heavily from Godec's data and approach. Potential effects related to acidification of the carbonate reservoir and changes in the hydrocarbon fluid properties by interactions of CO₂ with existing connate or bound waters were not addressed by Godec (2013c) or the current work.

RHOB data are used to calculate density porosity (DPHI). RHOB data in LAS format were available for 390 wells in the study area. Observed densities ranged from a minimum of 1.12 g/cm³ to 3.8 g/cm³, with a median of 2.66 g/cm³. The standard model for calculating matrix porosity from RHOB data is documented by Asquith and Krygowski (2004):

$$\phi = \frac{\rho_{matrix} - \rho_{bulk}}{\rho_{matrix} - \rho_{fluid}} \quad [\text{Equation 19}]$$

where ϕ is DPHI; ρ_{matrix} is matrix density (limestone basis = 2.71 g/cm³); ρ_{bulk} is RHOB from the geophysical log; and ρ_{fluid} is the density of borehole fluid (assumed = 1).

In cases where the observed RHOB is greater than the selected matrix density, the calculated DPHI is less than zero. Very low RHOB values typically indicate either washouts or possibly fractures. Differentiating washouts and fractures was not attempted here, so these low RHOB values were discarded. Thus, statistical outliers were first identified and dropped according to guidelines suggested by Wilcox (2010). Any remaining negative DPHI values were also dropped from the analysis. Plots of the resulting filtered RHOB data show the Utica Shale (orange line) is generally denser with less matrix porosity than the Point Pleasant Formation (blue line) (Figure 5-36). The density of stored CO₂ varies with pressure and temperature according to the change of state equation. For storage calculations based on geophysical logs, the equation of state was highly generalized to yield a CO₂ density at a given depth, as shown in Table 5-5.

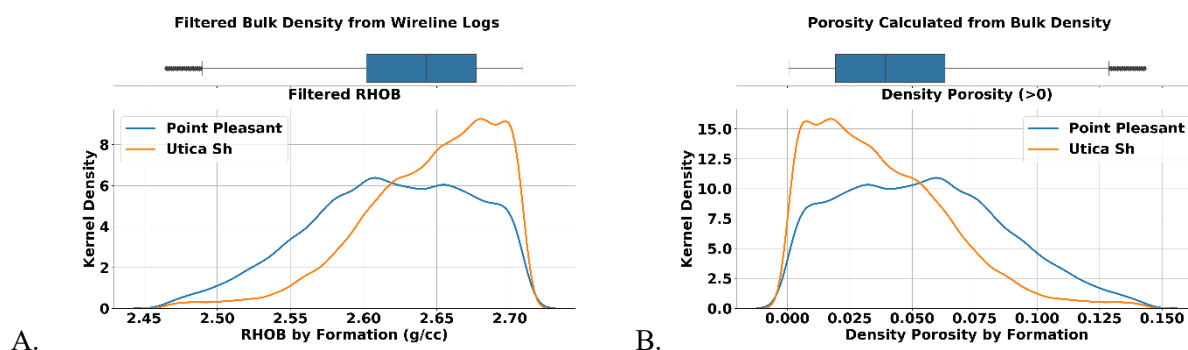


Figure 5-36. Distribution of RHOB and calculated DPHI from geophysical logs processed to remove outliers and observations with calculated DPHI <0: (A) raw RHOB values; (B) calculated DPHI (decimal fraction).

Table 5-5. Generalized CO₂ density values for calculating free gas in pore space.

Depth (ft)	Density (g/cm ³)	CO ₂ State	Density (short tons/ac-ft)	Density (tonnes/ac-ft)
<2500	0.155	Vapor	210.0	190.5
2500 – <5000	0.735	Liquid	1000.0	907.2
≥ 5000	0.777	Supercritical fluid	1056.0	958.0

Using a typical water saturation value of 0.73 (decimal fraction of pore space) estimated from data in Godec (2013c), calculation of matrix CO₂ storage resource in units of short tons for each 0.5-ft interval in the geophysical data proceeds in a straightforward manner using Equation 20:

$$CO2_{matrix} = CO2Density_{depth} * DPFI * (1 - S_w) * 0.5 * ef \quad [\text{Equation 20}]$$

where CO₂Density_{depth} is the density at a depth from Table 5-5; DPFI is the calculated density porosity (decimal fraction); S_w is an estimated water saturation (decimal fraction); 0.5 is the interval thickness in ft; and ef is a storage displacement efficiency factor.

Storage resource in short tons of CO₂ per ac-ft for each well was then derived by summing the tons per ac for the Utica/Point Pleasant interval and dividing by the interval thickness. Short tons were then converted to metric tonnes by multiplying the number of short tons by 0.907185. To facilitate grid operations and calculations, storage resource values for 3 and 10 percent efficiency factors (as suggested by Carr et al., 2008) were extrapolated to short tons per grid-ft by multiplying by a factor of 2203.95, the number of ac in each cell of a 3000-m x 3000-m grid.

5.4.5.3 CO₂ Storage as Adsorbed Gas

Carbon dioxide will also be stored as adsorbed gas associated with organic matter. Equation 18 was used to calculate the percent TOC when both GR and RHOB log data were available, and Equation 17 was used where only RHOB log data were available. As with the matrix porosity, RHOB outliers (in this case density values less than 2.0) were dropped from the analysis. Figure 5-37 shows the distributions of TOC data by formation.

Godec (2013c) presents a composite model for calculating adsorbed gas content based on TOC and reservoir pressure:

$$CO2_{scf/ton} = \frac{(37.1 * \frac{TOC}{100.0} * ReservoirPressure)}{510 + ReservoirPressure} \quad [\text{Equation 21}]$$

Both the Utica and Point Pleasant formations are overpressured across much of their extent. Using data from Godec (2013c), an estimated average pressure gradient of 0.54 pounds per square inch (psi) per ft was used to calculate a reservoir pressure for each depth, and the equation was applied using the modeled TOC to determine the theoretical maximum CO₂ storage in standard cubic feet per short ton of rock material. Figure 5-38 illustrates the distributions of calculated theoretical maximum CO₂ storage of adsorbed gas and free gas in the matrix porosity of both formations. These data, calculated by well, were gridded using PETRA[®] and ArcGIS[®] software.

Carbon storage was calculated from gridded thickness and capacity data for the Utica Shale and Point Pleasant Formations separately. In general, the storage resource estimate in short tons was calculated for each grid cell:

$$CO2_{\frac{tons}{cell}} = CO2_{\frac{tons}{acreft}} * 2,203.95 \frac{acres}{cell} * net_thickness_ft * efficiency \quad [\text{Equation 22}]$$

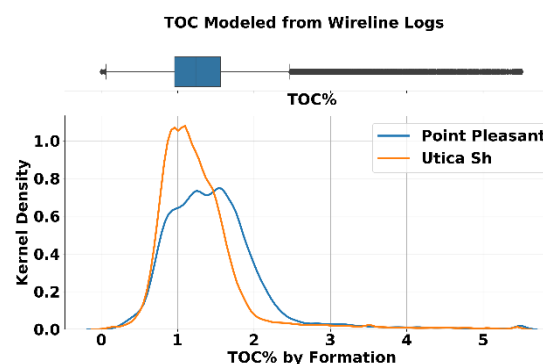


Figure 5-37. Distributions of TOC calculated from RHOB log data by formation (with outliers removed and TOC greater than zero). The overall distribution for both formations is shown by the box and whisker plot at the top.

The CO₂ storage estimates in short tons per grid cell at 3 percent and 10 percent efficiency factors were converted to tonnes by multiplying by 0.907185. These values were then summed across formations and areas to provide an estimate of the total storage in tonnes.

5.4.5.4 CO₂ Volumetrics

Using information from the Utica Shale databook, Utica Shale and Point Pleasant Formation TOC values were calculated from RHOB logs for 368 wells, and the median (P50) value was mapped for four variations of the combined or separate stratigraphic intervals based on regional variations in the distribution of the units (Figure 5-39 and Figure 5-40). Figure 5-39 is the median calculated TOC for the combined Utica Shale/Point Pleasant Formation interval across the entire study area, for wells in the dataset that had tops for either or both units. The next three maps are plots of subsets of these composite data. Figure 5-40A shows the regional variation of calculated TOC for wells in which only the Point Pleasant Formation top was included. Figure 5-40B shows the variation of calculated TOC for wells where a Utica Shale top was included, but a Point Pleasant top was not. It is generated from 276 wells. Figure 5-40C shows the variation of calculated TOC for wells that included both a Utica Shale and Point Pleasant Formation top, but does not include wells that had only a Utica, or only a Point Pleasant top. Differences in the four maps highlight variations in trends of TOC within the Utica and Point Pleasant individually, as well as showing differences in combined trends that result from using different data sets.

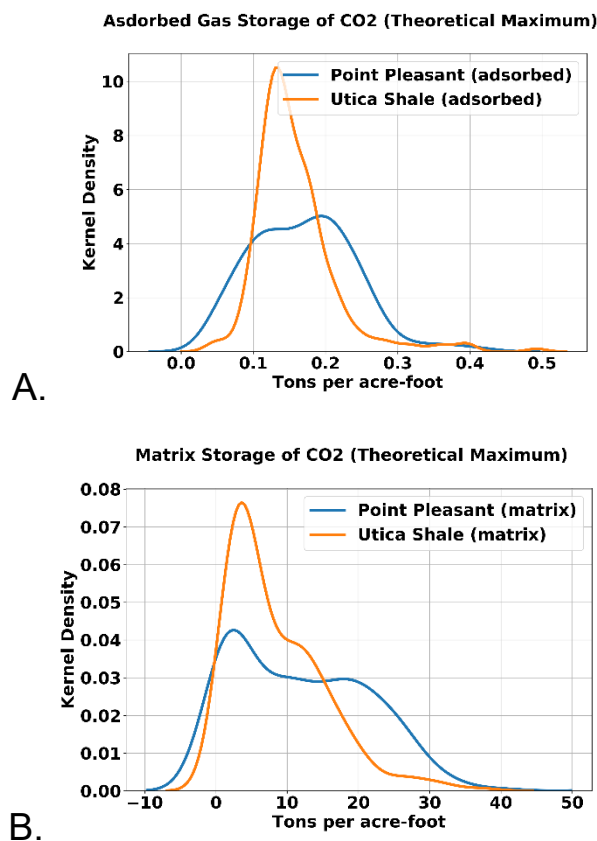


Figure 5-38. Distribution of calculated theoretical maximum CO₂ storage quantities in tons per acre foot for adsorbed gas (A) and free gas in matrix porosity (B) for the Utica Shale and Point Pleasant Formation.

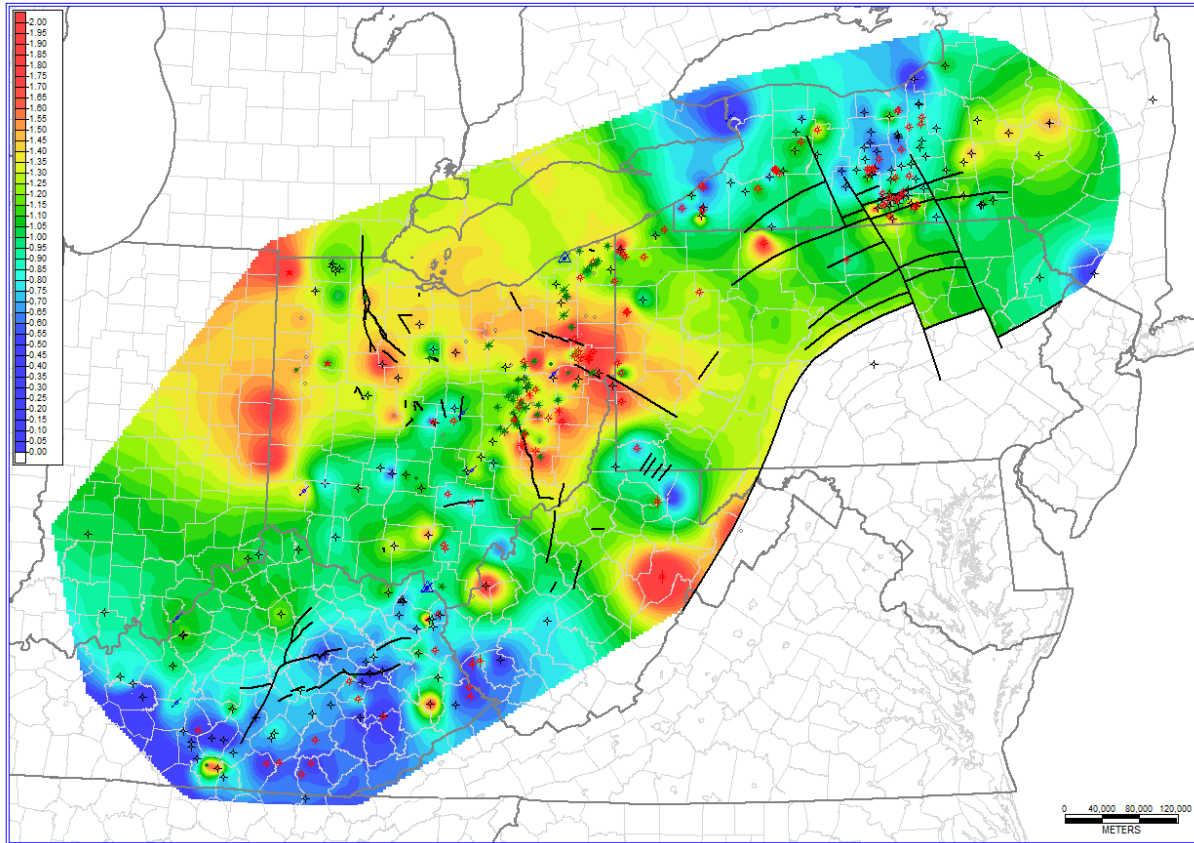


Figure 5-39. Map of TOC (P50) calculated from geophysical logs for the Utica Shale and Point Pleasant Formations to top of the Trenton/Lexington Formation interval for data with either or both Utica and Point Pleasant tops (368 wells). Color values range from 2.0 (red) to 0 (dark blue). Black lines are basement faults.

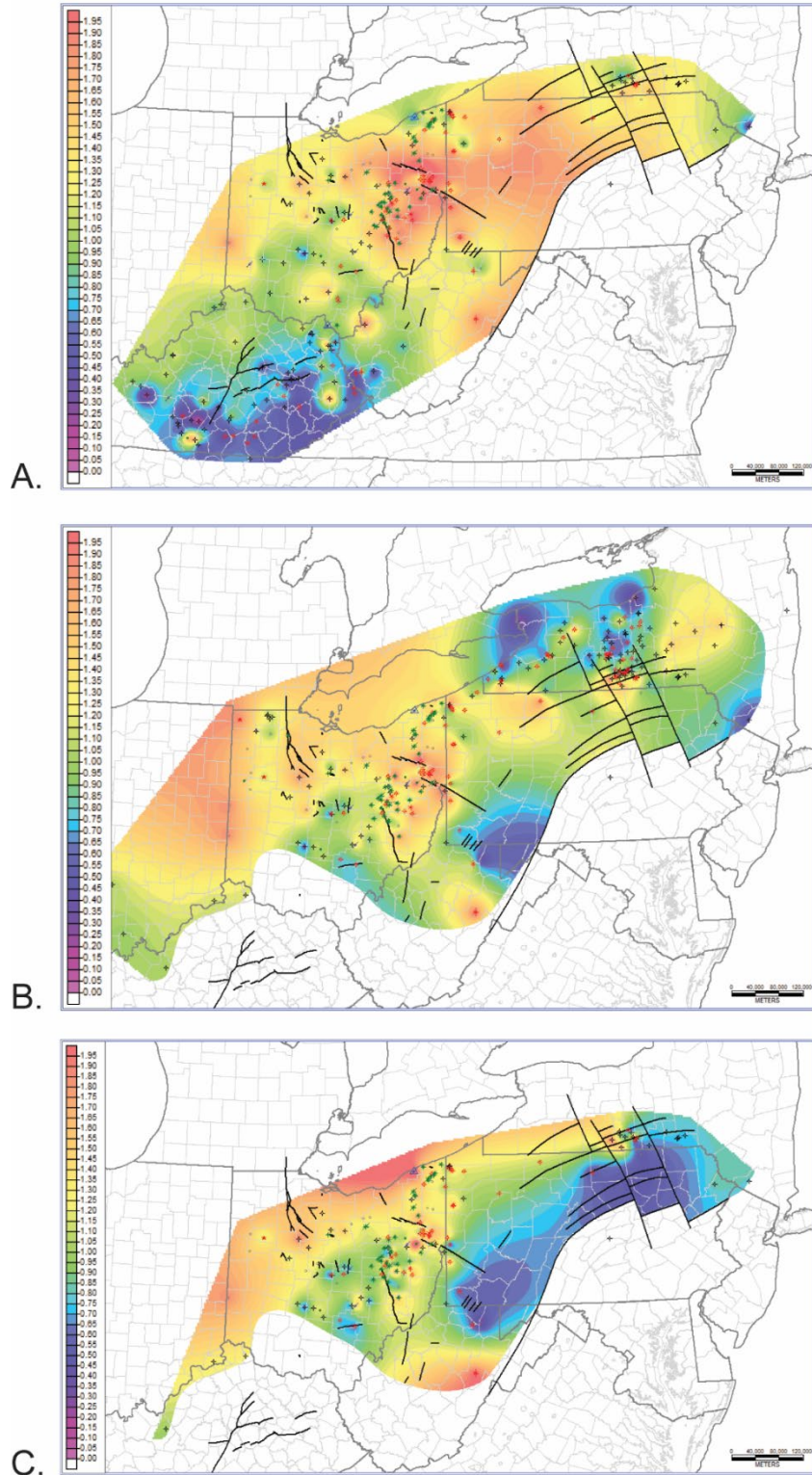


Figure 5-40. Subset maps of TOC (P50) calculated from geophysical logs for the Utica and Point Pleasant formations to top of the Trenton/Lexington Formation interval. (A) Point Pleasant TOC only, no Utica present or mapped (254 wells); (B) Utica TOC only, no Point Pleasant present or mapped (276 wells); (C) Utica TOC where both Utica and Point Pleasant intervals present (162 wells). Black lines are basement faults.

Figure 5-41A and Figure 5-41B show the areas of investigations and TOC-gridded area for the Utica Shale and Point Pleasant Formation, respectively. The Utica Shale's area of investigation (blue line) and Point Pleasant area of investigation (red line) are the approximate extents of these units from the Utica Shale Play Book Study. The gridded areas in Figure 5-41A and Figure 5-41B represent net thickness maps of each unit with TOC exceeding 1.5 percent and were compiled using PETRA[®] volumetric software tools. For the Utica Shale, a total of 276 wells were available (same wells used to map TOC variation for the Utica in Figure 5-40B) and net thickness was determined using 169 wells. For the Point Pleasant Formation, a total of 254 wells were available (same wells used to map TOC variation for the Point Pleasant in Figure 5-40A) and net thickness was determined using 181 wells. Table 5-6 summarizes the total areas of investigations, and the acreage and estimated total rock volumes of the gridded areas for each of the units mapped in Figure 5-41.

The gridded net thickness distributions of the Utica Shale and Point Pleasant Formation intervals were tabulated to compute a totaled net thickness isopach map of the combined interval (Figure 5-42). Volumetrics are reported for the combined interval in Table 5-7. The extent of the separate grids in Figure 5-41 is not the same as the grid extent in Figure 5-42 so volumetrics are not strictly additive. The volumetrics data for the three net thickness isopach maps illustrate the range of potential CO₂ storage resource for each respective area (Utica Shale, Point Pleasant Formation and combined Utica Shale and Point Pleasant interval).

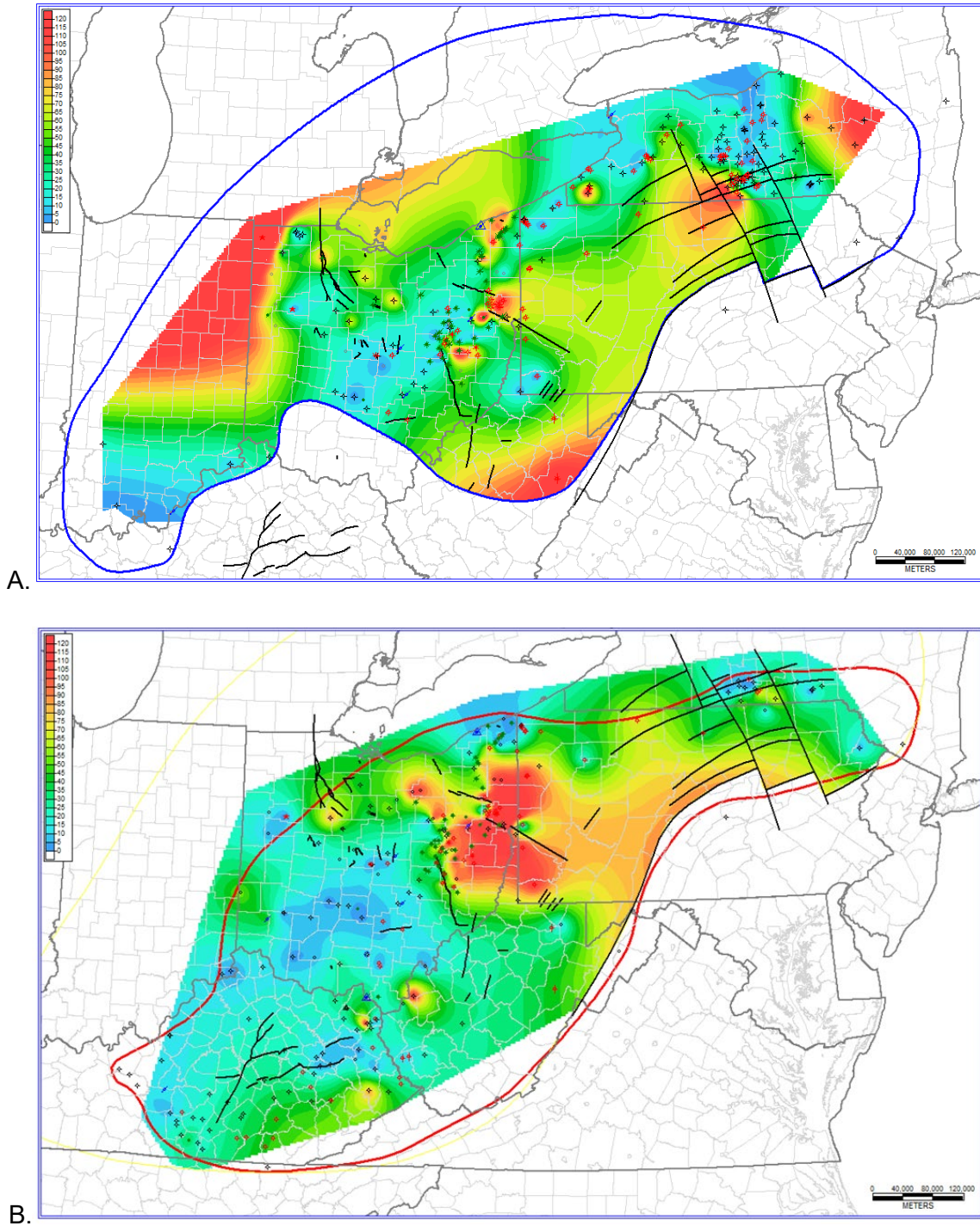


Figure 5-41. Isopach maps of net thickness with TOC greater than 1.5 percent by unit: (A) Utica Shale map interval (169 wells); (B) Point Pleasant Formation map interval (181 wells); Color values range from 0 (dark blue) to 120 ft (red) in both maps. Black lines are basement faults.

Table 5-6. Volumetrics using net thickness of the Utica Shale and Point Pleasant intervals separately with median (P50) TOC greater than or equal to 1.5 percent.

Assessment Area	Total Area (billion ac)	Gridded Area (billion ac)	Volume (billion ac-ft)	Average Thickness (ft)	Figure
Utica Shale	116.2	82	4.28	52.23	5.41A
Point Pleasant	80.6	72.8	3.13	43.02	5.41B

Table 5-7. Volumetrics using net thickness in ft, illustrating potential CO₂ storage resource of the combined Utica Shale-Point Pleasant intervals with (P50) TOC greater than or equal to 1.5 percent with reference to the area shown in Figure 5-42.

Assessment Area	Total Area (billion ac)	Gridded Area (billion ac)	Volume (billion ac-ft)	Average Thickness (ft)
Utica Shale	116.2	88.8	5.79	65.17
Point Pleasant	80.6	74.1	4.52	60.96

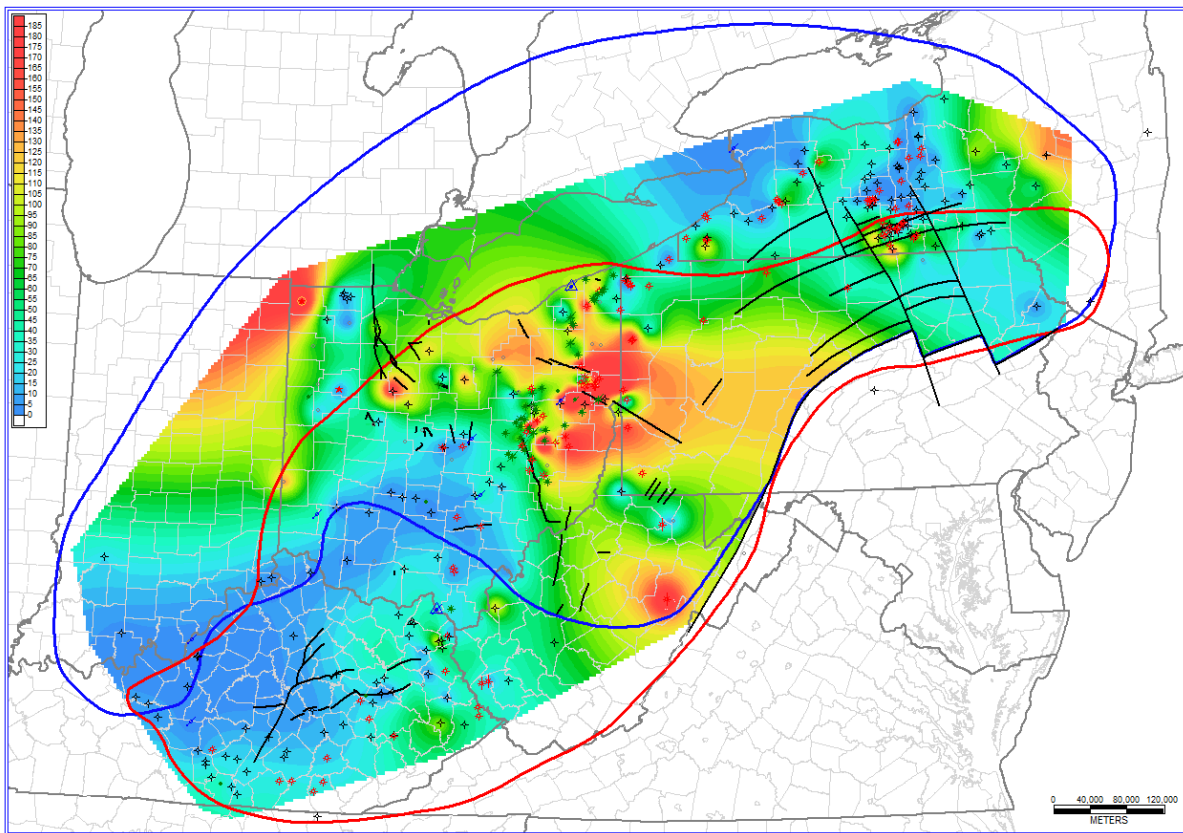


Figure 5-42. Net isopach map of the combined Utica Shale and Point Pleasant Formation with TOC greater than 1.5 percent. Blue outline illustrates the Utica Shale area of investigation. Red outline illustrates Point Pleasant Formation area of investigation. Color values range from 0 (dark blue) to 185 ft (red). Black lines are basement faults.

5.5 Carbon Storage Potential

Estimates of carbon storage potential were prepared at storage efficiency factors of 3 and 10 percent. While these efficiency factors are somewhat arbitrary, they are likely representative of the expected range of efficiencies in low-permeability geologic units. The storage resource estimates presented in this chapter are conservative when compared to previously published estimates of theoretical maximum storage values (Godec, 2013b, 2013c). Several factors contribute to the differences between previous efforts and those of the current study:

- The assessment area extents are not exactly coincident.
- RHOB and GR logs were processed with differing petrophysical cutoff values for computing such items as net thickness.
- The methodologies for modeling TOC content from petrophysical data differ.
- Assumptions about CO₂ properties and their variation with depth differ.

The final estimates, however, are generally the same order of magnitude when converted to the same units (million tonnes of CO₂) and applying the selected efficiency factors.

5.5.1 Middle Devonian Marcellus Shale

The regional distribution of estimated storage on the basis of short tons per unit volume (i.e., the volume of each 8895.8-ac grid cell - 6000 m x 6000 m) is illustrated in Figure 5-43. Total estimated CO₂ storage for the Middle Devonian Hamilton Group/Marcellus Shale interval ranges from 804.3 million tonnes (886.5 million short tons) at a 3 percent efficiency factor to 2680.8 million tonnes (2955 million short tons) at a 10 percent efficiency factor (Table 5-8).

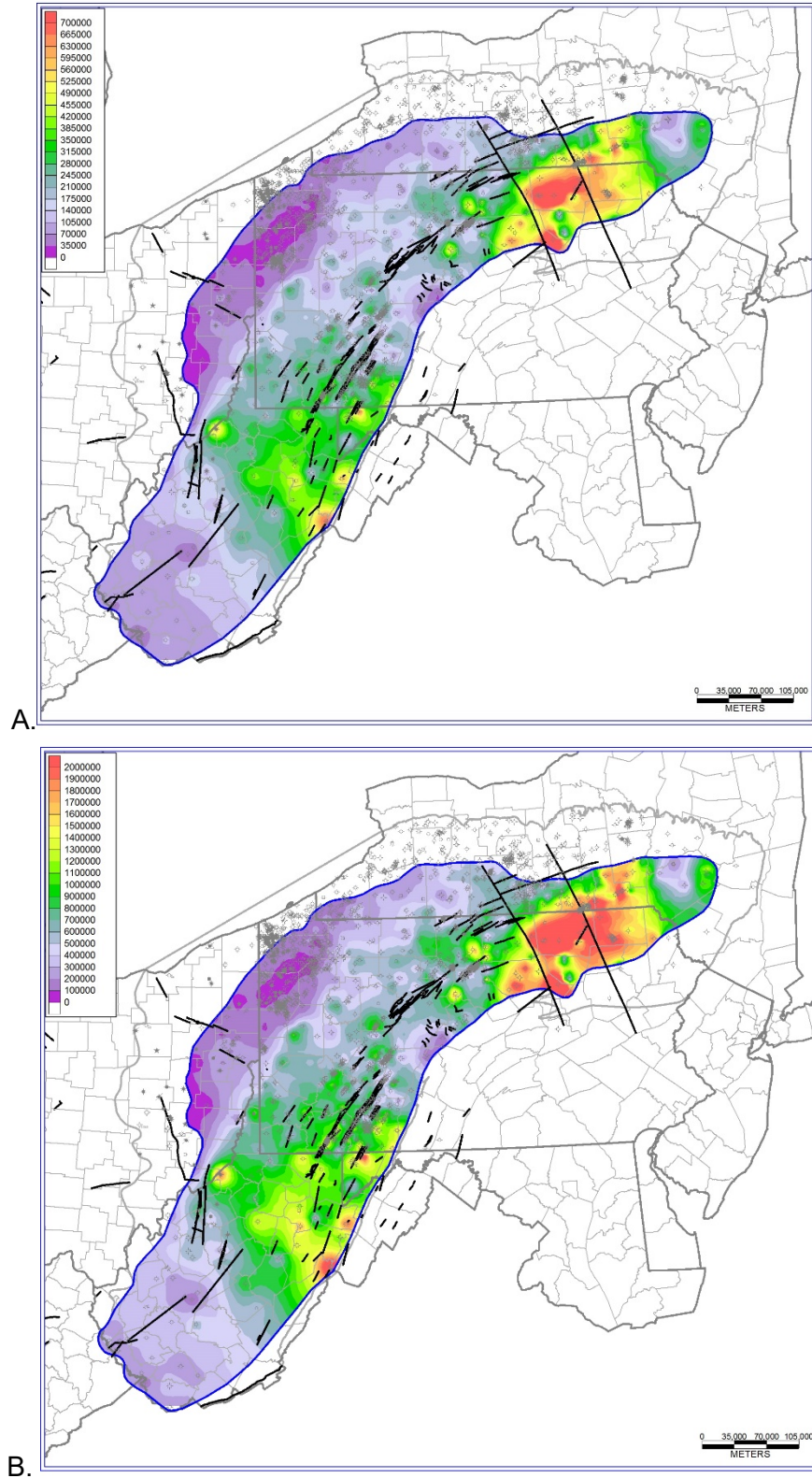


Figure 5-43. Regional distribution of carbon storage potential for the Middle Devonian Hamilton Group/Marcellus Shale interval at efficiency factors of (A) 3 percent and (B) 10 percent. Estimated storage potential ranges from 0 (purple) to more than 700,000 short tons (red). (One short ton equals 0.907185 tonnes). Black lines represent basement faults.

Table 5-8. Estimated CO₂ storage by state for the Middle Devonian Marcellus Shale interval.

CO ₂ Storage Marcellus Shale (million tonnes)		
State	3% Efficiency Factor	10% Efficiency Factor
Kentucky	0.8	2.6
Maryland	17.3	57.5
New York	112.8	375.9
Ohio	21.5	71.7
Pennsylvania	402.9	1343.1
Virginia	0.3	1.1
West Virginia	248.6	828.8
Total	804.2	2680.8

5.5.2 Upper Ordovician Utica Shale/Point Pleasant Formation Interval

The Utica Shale play area as defined in Patchen and Carter (2015) was chosen as the assessment area for carbon storage in the current assessment and should provide conservative estimates of potential CO₂ storage volumes based on the area in which oil and gas production is most likely to occur. Storage estimates for the Utica Shale/Point Pleasant interval were determined for each unit individually and for the combined units at both 3 percent and 10 percent storage efficiencies. Additionally, free gas in matrix porosity and adsorbed gas were separately assessed for the individual and combined units. Figure 5-44A and 5.44B shows the regional distribution of estimated CO₂ storage volume using 3 percent and 10 percent efficiencies, respectively. Estimated storage potential ranges from 0 to more than 300,000 short tons (272, 156 tonnes) per grid cell in Figure 5-44A, and from 0 to more than 900,000 short tons (816,467 tonnes) per grid cell in Figure 5-44B. As summarized in Table 5-9, estimated carbon storage potential of the combined Utica Shale/Point Pleasant interval ranges from 1879.6 million tonnes (2071.95 million short tons) at a storage efficiency of 3 percent to 6265.5 million tonnes (6906.54 million short tons) at a 10 percent efficiency.

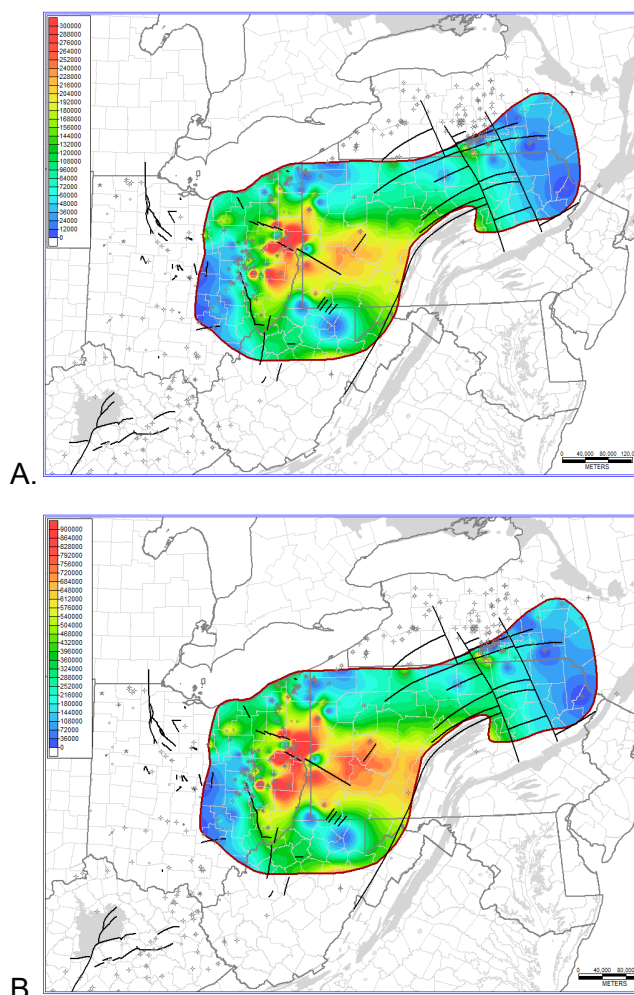


Figure 5-44. Regional distribution of estimated CO₂ storage (short tons) in the combined Utica Shale/Point Pleasant interval at efficiency factors of (A) 3 percent and (B) 10 percent. (One short ton equals 0.907185 tonnes).

Table 5-9. Estimated CO₂ storage by state as adsorbed gas and free gas in matrix porosity for the Utica Shale/Point Pleasant interval in millions of tons at 3 and 10 percent efficiencies.

CO ₂ Storage at 3 percent Efficiency Factor (million tonnes)									
State	Utica Shale			Point Pleasant			Combined		
	Adsorbed	Matrix	Total	Adsorbed	Matrix	Total	Adsorbed	Matrix	Total
Maryland	0.2	25.2	25.5	0.2	17.2	17.4	0.5	42.4	42.9
New York	0.7	42.3	42.9	0.3	19.0	19.3	0.9	61.2	62.2
Ohio	2.0	141.9	143.9	3.8	331.0	334.7	5.8	472.9	478.6
Pennsylvania	5.1	396.3	401.5	8.1	616.5	624.6	13.2	1012.8	1026.0
West Virginia	1.4	137.0	138.5	2.0	129.5	131.5	3.4	266.5	269.9
Total	9.5	742.8	752.2	14.3	1113.1	1127.4	23.8	1855.9	1879.6

CO ₂ Storage at 10 percent Efficiency Factor (million tonnes)									
State	Utica Shale			Point Pleasant			Combined		
	Adsorbed	Matrix	Total	Adsorbed	Matrix	Total	Adsorbed	Matrix	Total
Maryland	0.8	84.2	84.9	0.8	57.3	58.0	1.5	141.4	143.0
New York	2.2	140.9	143.1	0.9	63.3	64.2	3.1	204.1	207.2
Ohio	6.6	473.0	479.6	12.6	1103.2	1115.8	19.2	1576.2	1595.4
Pennsylvania	17.1	1321.1	1338.2	27.0	2055.0	2082.0	44.1	3376.0	3420.1
West Virginia	4.8	456.8	461.6	6.5	431.7	438.2	11.3	888.5	899.8
Total	31.5	2475.9	2507.4	47.7	3710.4	3758.1	79.2	6186.3	6265.5

5.6 Enhanced Recovery

Employing CO₂ to enhance gas, oil and liquids recovery from low-permeability, organic-rich rocks like the Marcellus, Utica and Point Pleasant formations is an intriguing possibility. The availability of abundant, reliable and economically feasible CO₂ in the future balanced by favorable commodity prices will influence the willingness of industry to implement enhanced recovery projects in unconventional shales using CO₂. Long-term storage of CO₂ could be a beneficial side-effect of this type of enhanced recovery project. At this time, data are not available for the units being studied to estimate the ratio of gas and liquids that might be produced under the influence of injected CO₂.

For the Marcellus Shale, the U.S. Geological Survey estimated a mean undiscovered resource of 84.2 trillion cubic feet (TCF) of natural gas and 3.4 billion barrels of natural gas liquids (NGLs) (Coleman et al., 2011). A “huff-and-puff” cyclic injection and production scenario likely has the best chance of successful implementation for enhanced recovery with CO₂ in the Marcellus Shale (Karmis et al., 2018; Schepers et al., 2009). Nuttall et al. (2009) found that CO₂ adsorption in the Upper Devonian Ohio Shale was approximately 5.3 times that of methane. Given a similar ratio, 17.25 million cubic feet (MCF) CO₂ per short ton of CO₂ (15.65 MCF CO₂ per tonne of CO₂), and CO₂ displacement efficiencies of 3 and 10 percent, the incremental gas recovery in the Marcellus could range from 2.9 TCF to 9.6 TCF natural gas if all the undiscovered resource was produced.

Enhanced natural gas recovery through displacement of adsorbed gas in the Utica Shale/Point Pleasant Formation interval could range from 87.0 billion cubic feet (BCF) to 287.5 BCF at 3 percent and 10 percent efficiency factors, respectively.

Enhanced recovery of hydrocarbons in the Utica Shale and Point Pleasant Formation is anticipated to be more along the lines of a conventional miscible flood rather than being dominated by the behavior of adsorbed gasses. In 2012, the U.S. Geological Survey provided estimates for the mean total undiscovered resources of the Utica Shale at 940 million barrels of oil (MMBO), 38.2 TCF natural gas and 208 million barrels (MMBLS) of NGLs (Kirschbaum et al., 2012). In 2015, the Utica Shale Play Book Study estimated original oil-in-place (OOIP) at approximately 82,903 MMBO and original gas-in-place at approximately 3192.4 TCF using a volumetric approach (Patchen and Carter, 2015). Given the magnitude of these various estimates for the Utica play, a probable enhanced recovery scenario therefore is likely to concentrate on oil and liquids production. There are many options for conducting hydrocarbon pore volume and flooding projects using CO₂ (Melzer, 2007; Verma, 2015). The wide range of project options indicates a possible approach for estimating incremental recoveries would be a generalized assessment based on CO₂ utilization factors. Melzer (2007) suggests an average CO₂ utilization of 7 MCF per barrel (BBL) of oil for existing CO₂-EOR projects. Reflecting the existing uncertainty, calculations using that CO₂ utilization factor leads to a greater volume of liquids recovered than has been estimated to remain in place by a significant factor. An alternative approach is that a four percent incremental recovery could be expected based on the estimated CO₂-EOR potential in the Illinois and Michigan basins (Advanced Resources International, 2006). Assuming a “state-of-the-art” miscible flood, the Utica Shale and Point Pleasant Formation could possibly produce an additional 50.9 MMBO and NGLs.

5.7 Conclusions

Carbon storage in the Middle Devonian Marcellus Shale is expected to occur as mostly adsorbed gas associated with organic matter. Therefore, storage is dependent on TOC, reservoir depth (which influences both reservoir pressure and CO₂ phase) and the total shale volume. Total carbon storage estimates were limited by confining the assessment to areas where drilling depth to the top of the shale was at least 2500 ft and applying a cutoff criteria of net shale thickness with at least two percent TOC and a GR value of 180 API or greater. A median (P50) TOC curve was determined for wells with digital GR and RHOB data using multiple TOC models. These data were then gridded and processed to produce an estimated carbon storage volume of from 804.3 million tonnes at a 3 percent efficiency factor to 2680.8 million tonnes at a 10 percent efficiency factor. Nearly two thirds of this storage potential are located in northeast Pennsylvania and southern New York.

Carbon storage in the Upper Ordovician Utica and Point Pleasant shales is expected to occur as a free gas in the matrix porosity of the units and as adsorbed gas associated with the organic matter. Free gas storage is more important in these units than in the Marcellus Shale (i.e., 98 percent versus 2 percent) because of their lower overall organic content. Storage is thus dependent on TOC, reservoir depth, total reservoir volume and porosity. Storage estimates were moderated by confining the assessment to areas where drilling depth to the top of the units was at least 2500 ft and a cutoff criteria of net shale thickness with at least 1.5 percent TOC. Several classic models from literature for determining TOC for organic-rich shales from geophysical logs were tested and determined to be not optimally representative of available laboratory-measured TOC values. Two of the previous models were adjusted and two new models were derived and applied based on whether both GR and RHOB or only RHOB digital geophysical log data were available. These data were then gridded and processed to produce an estimated carbon storage volume of from 1879.6 million tonnes to 6265.5 million tonnes. Nearly 60 percent of the total storage is estimated to occur in the Point Pleasant Formation due in part to the formation's larger calculated volume. An estimated 80 percent of the storage is situated in the tri-state area (see next chapter).

EGR in the Marcellus shale could range from 2.9 to 9.6 TCF.

Insufficient data and modeling results are available to adequately assess the enhanced oil, natural gas and NGL production potential of the Utica Shale/Point Pleasant Formation interval. EGR from these units could range from 87.0 to 287.5 BCF. Based on estimated undiscovered reserves and by assuming a possible analogue to the Illinois and Michigan basins, incremental production from CO₂-EOR could be 50.9 million barrels of oil and NGLs. For the Utica Shale and Point Pleasant Formation, CO₂ utilization factors, sweep efficiencies and the variety of enhanced recovery project designs suggests reservoir simulation and engineering are required to properly address this topic.

6.0 Evaluation of CCUS Opportunities

6.1 Overview

PAGS has prepared a focused assessment of potential CCUS opportunities in the tri-state area of Ohio, Pennsylvania and West Virginia. This part of the MRCSP region is home to more than two dozen CO₂ point-sources and encompasses an area of approximately 17,000 sq mi (Figure 6-1). The area is home to both shallow and deep depleting oil and gas fields that are still actively produced; fields considered to be depleted; fields that have been converted to natural gas storage; and unconventional shale gas and oil/condensate fields. By the numbers, the tri-state area includes 453 oil fields, 4338 gas fields, and 69 gas storage fields. This mix of activity offers an array of potential options for miscible and immiscible enhanced recovery and/or carbon storage in the Ohio River Valley.

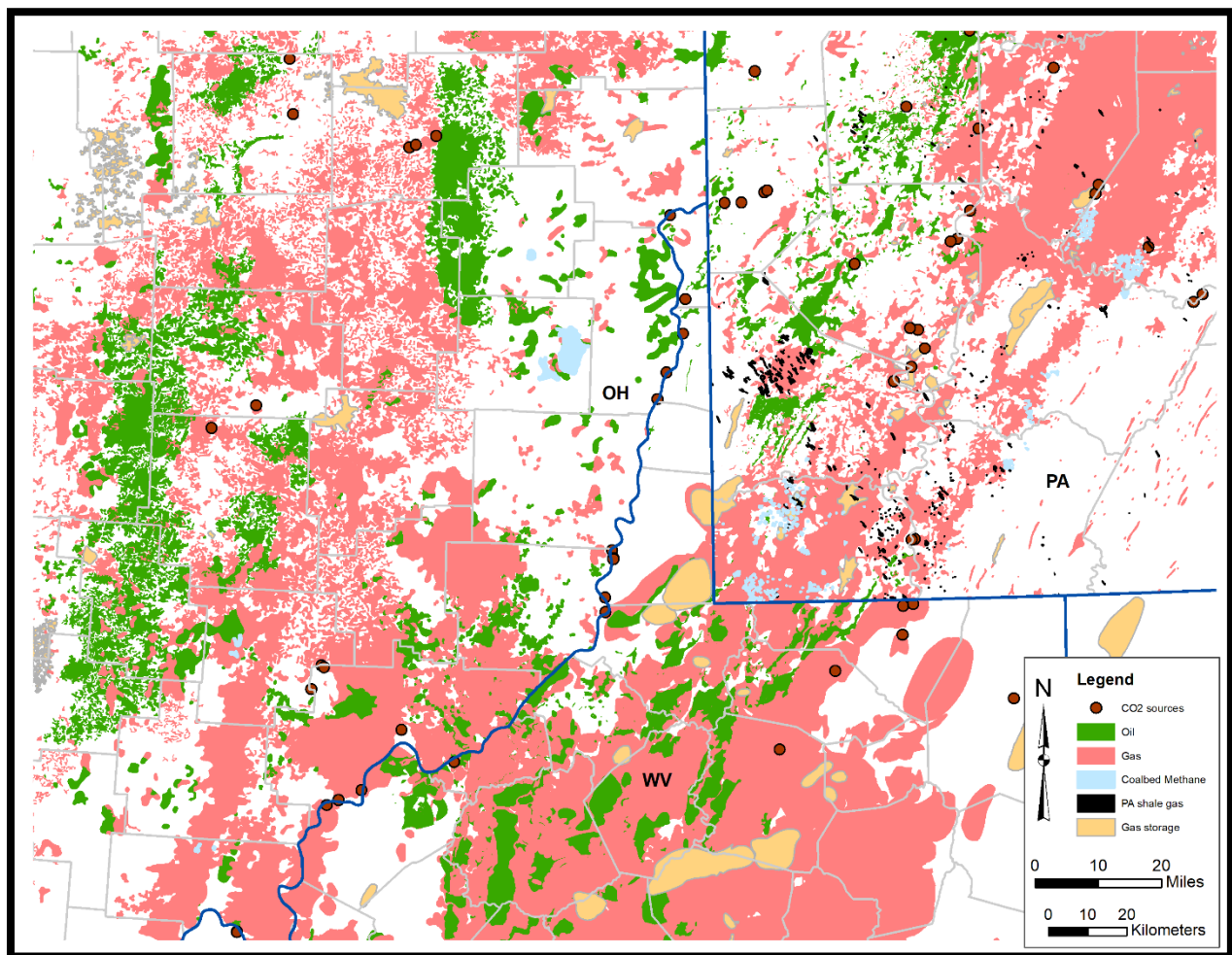


Figure 6-1. Tri-state study area, showing historical and active oil, gas and storage fields.

Based on this assessment, several prospects exist in the tri-state area that contain top-rated oil-producing reservoirs and exhibit varying degrees of stacked potential for both utilization and storage applications. These prospects have been identified by field name and are presented on a state by state basis as examples of how end users may apply the MRCSP Region's subsurface geologic and reservoir data associated with this report to their own CO₂-EOR and/or carbon storage considerations.

6.2 Subsurface Geology of the Tri-State Area

The subsurface geology of the tri-state area includes multiple oil and gas-bearing units of Pennsylvanian through Cambrian age (Figure 6-2). For more than 100 years, this region has produced oil and gas from shallow Devonian, Mississippian and Pennsylvanian deposits. By the early 1920s, Lower Devonian and Silurian reservoirs were also being tapped for natural gas in Ohio, and by the late twentieth century, Cambro-Ordovician sandstone and carbonate reservoirs were being developed for natural gas in the region as well. As many of the shallower gas fields in the region became depleted (ca 1930s to 1970s), they were converted to natural gas storage fields by gas utilities, and some are still in use today. Unconventional gas production from shallow coal seams became popular in the 1990s, and the discovery of the modern Marcellus Shale gas play in Washington County, Pennsylvania, in 2004 spawned the development of the shale gas industry throughout the region, with Interstate I-79 serving as an approximate boundary between dry Marcellus gas to the east and liquids-rich Marcellus gas to the west. The Utica Shale was first drilled in the tri-state area about a decade ago, although more recent activity farther west in Ohio represents the very lucrative, liquids-rich area of this unconventional play.

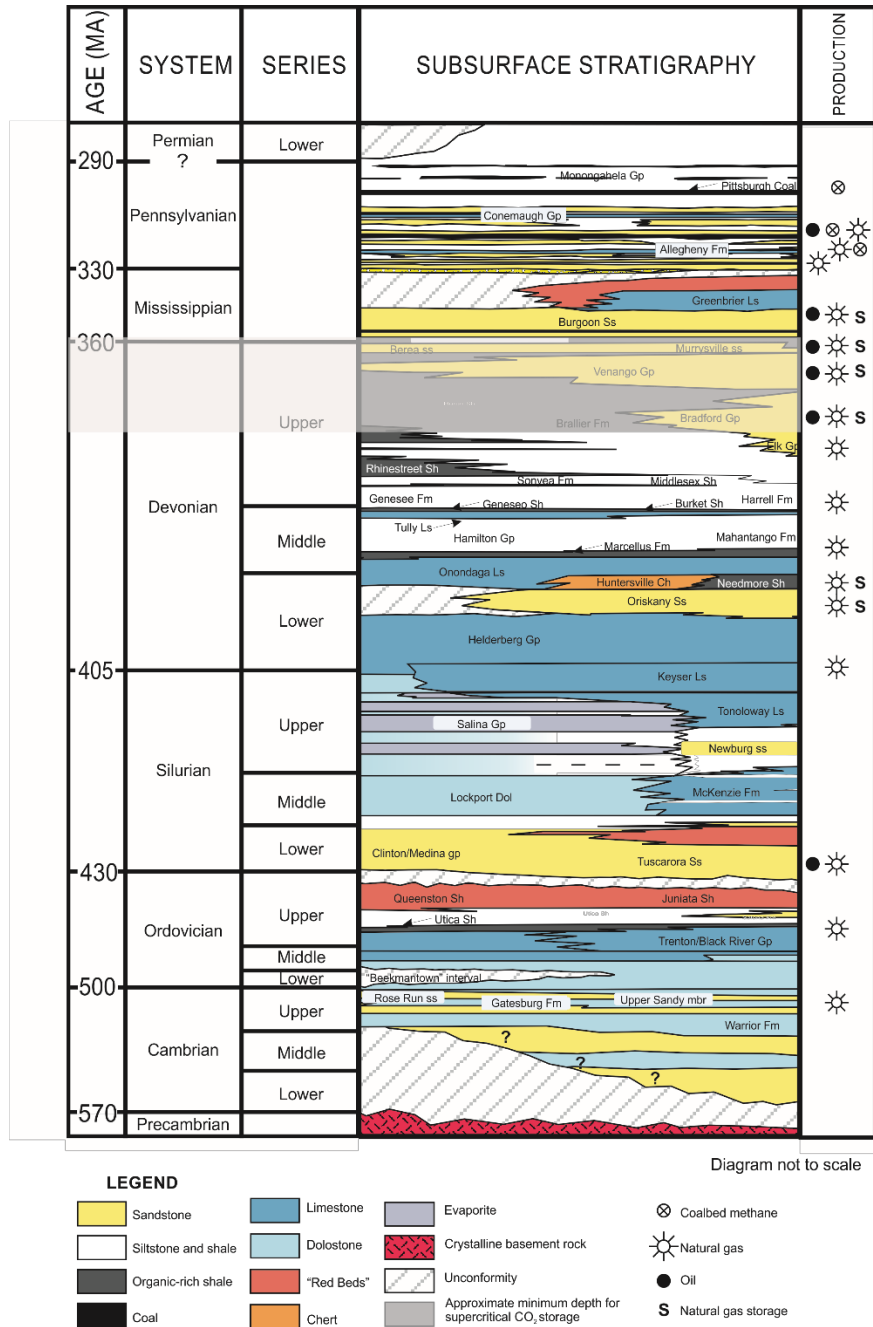


Figure 6-2. Generalized correlation chart for subsurface geologic units in the tri-state area using Pennsylvania terminology.

Figure 6-2 is not to scale, but the translucent gray bar references the approximate minimum depth interval at which supercritical CO₂ storage may be expected – that is, Devonian Venango Group and deeper units. Shallower units (the Mississippian Burgoon Sandstone and sandstones of the Mississippian-Devonian transition) are generally in the immiscible depth range for CCUS applications. Pennsylvanian units (mainly the coal measures) are mostly less than 1000 ft deep – too shallow to be considered for CCUS applications by this study.

Two regional cross sections – one in the dip direction and one along strike – have been prepared to illustrate the lithologic, stratigraphic and structural characteristics of subsurface geologic units in the tri-state area (Appendix D). These cross sections provide a more detailed representation of this area’s geologic resources and serve to augment the regional cross sections prepared by Dinterman et al. (2019).

6.3 Rating Enhanced Recovery Reservoirs

PAGS rated potential EOR and EGR reservoirs in the tri-state area of Ohio, Pennsylvania, West Virginia and Maryland panhandle based on several attributes. See Table 6-1 and Table 6-2 for the oil and gas field rating criteria, respectively. As expected, reservoir data availability played a significant role in completing this exercise.

Table 6-1. Rating criteria used to assess CCUS opportunities for oil fields in the tri-state area.

Item #	Value	Criteria	Item #	Value	Criteria
1		Average depth	10		Cumulative oil production
	0	≤1000 ft		0	no data or ≤1,000,000 BBL
	1	>1000 ft but ≤2500 ft		1	>1,000,000 BBL but ≤15,000,000 BBL
	2	>5000 ft		2	>15,000,000 BBL but ≤30,000,000 BBL
	3	>2500 ft but ≤5000 ft		3	>30,000,000 BBL
2		Acreage	11		Remaining oil
	0	≤500 ac		0	no data or ≤10,000 BBL
	1	>500 ac but ≤1000 ac		1	>10,000 BBL but ≤75,000,000 BBL
	2	>1000 ac but ≤5000 ac		2	>75,000,000 BBL but ≤150,000,000 BBL
	3	>5000 ac		3	>150,000,000
3		Net thickness	12		Potential oil recovery
	0	≤1 ft		0	no data or ≤10,000 BBL
	1	>1 ft but ≤10 ft		1	>10,000 BBL but ≤5,000,000 BBL
	2	>10 ft but ≤20 ft		2	>5,000,000 BBL but ≤10,000,000 BBL
	3	>20 ft		3	>10,000,000 BBL
4		Average porosity	13		Oil saturation reported (fractional)
	0	≤1%		0	no data
	1	>1% but ≤5%		1	>0 but ≤0.33
	2	>5% but ≤10%		2	>0.33 but ≤0.66
	3	>10%		3	>0.66
5		Permeability	14		Gas saturation reported (fractional)
	0	No data		0	no data
	1	≤10 mD		1	>0 but ≤0.33
	2	>10 mD but ≤1000 mD		2	>0.33 but ≤0.66
	3	>1000 mD		3	>0.66
6		Trap integrity	15		Salinity
	0	No data		0	no data
	1	Limited data on trap characteristics		1	>100,000 ppm
	2	Inferred lithologic and/or structural closure		2	≥ 0 ppm but ≤100,000 ppm
	3	Documented lithologic and/or structural closure			
7		Legacy well penetrations	16		Water saturation (fractional)
	0	No data or ≥20 wells per 1000 ac		0	no data
	1	≥5 wells per 1,000 ac but <20 wells per 1000 ac		1	>0.66
	2	≥2 wells per 1,000 ac but <5 wells per 1000 ac		2	>0.33 but ≤0.66
	3	<2 wells per 1000 ac		3	≥0 but ≤0.33
8		Stacked opportunity(ies)	17		Pressure minus estimated MMP
	0	No other intervals in same footprint		0	all P - MMP <0 or no data
	1	1 other interval in same footprint		1	$P_{\text{maximum}} - \text{MMP} > 0$
	2	2 or 3 other intervals in same footprint		2	$P_{\text{calculated}} - \text{MMP} > 0$
	3	4 or more intervals in same footprint		3	$P_{\text{reported}} - \text{MMP} > 0$
9		Mode CO₂ storage (computed)	18		Number of producing wells per acre
	0	≤10,000 tonnes		0	0 or ≥700 wells per 1000 ac
	1	>10,000 tonnes but ≤100,000 tonnes		1	>0 wells per 1000 ac but <300 wells per 1000 ac
	2	>100,000 tonnes but ≤1,000,000 tonnes		2	≥300 wells per 1000 ac but <500 wells per 1000 ac
	3	>1,000,000 tonnes		3	≥500 wells per 1000 ac but <700 wells per 1000 ac

Table 6-2. Rating criteria used to assess CCUS opportunities for gas fields in the tri-state area.

Item #	Value	Criteria	Item #	Value	Criteria
1		Average depth	8		Stacked opportunity(ies)
	0	≤2500 ft		0	No other intervals in same footprint
	1	>5000 ft		1	1 other interval in same footprint
	2	>2500 ft but ≤3500 ft		2	2 or 3 other intervals in same footprint
	3	>3500 ft but ≤5000 ft		3	4 or more intervals in same footprint
2		Acreage	9		Mode CO₂ storage (computed)
	0	≤500 ac		0	≤10,000 tonnes
	1	>500 ac but ≤1000 ac		1	>10,000 tonnes but ≤100,000 tonnes
	2	>1000 ac but ≤5000 ac		2	>100,000 tonnes but ≤1,000,000 tonnes
	3	>5000 ac		3	>1,000,000 tonnes
3		Net thickness	10		Oil saturation reported (fractional)
	0	≤1 ft		0	no data
	1	>1 ft but ≤10 ft		1	>0 but ≤0.33
	2	>10 ft but ≤20 ft		2	>0.33 but ≤0.66
	3	>20 ft		3	>0.66
4		Average porosity	11		Gas saturation reported (fractional)
	0	≤1%		0	no data
	1	>1% but ≤5%		1	>0 but ≤0.33
	2	>5% but ≤10%		2	>0.33 but ≤0.66
	3	>10%		3	>0.66
5		Permeability	12		Salinity
	0	No data		0	no data
	1	≤10 mD		1	>100,000 ppm
	2	>10 mD but ≤1000 mD		2	≥ 0 ppm but ≤ 100,000 ppm
	3	>1000 mD			
6		Trap integrity	13		Water saturation (fractional)
	0	No data		0	no data
	1	Limited data on trap characteristics		1	>0.66
	2	Inferred lithologic and/or structural closure		2	>0.33 but ≤0.66
	3	Documented lithologic and/or structural closure		3	≥0 but ≤0.33
7		Total penetrations	14		Pressure minus estimated MMP
	0	No data or ≥20 wells per 1000 ac		0	all P - MMP <0 or no data
	1	≥5 wells per 1000 ac but <20 wells per 1000 ac		1	P _{maximum} - MMP >0
	2	≥2 wells per 1000 ac but <5 wells per 1000 ac		2	P _{calculated} - MMP >0
	3	<2 wells per 1000 ac		3	P _{reported} - MMP >0

Eighteen different criteria were used to assess oil fields for their EOR potential (Table 6-1). These criteria were developed based on other work performed by the geological surveys (Carter and Patchen, 2017; Carter, 2013), and tailored to assessing oil field prospects by incorporating information from the MRCSP Phase II EOR report (Riley et al., 2010), related references and direct consultation with Geoteam members. Some of the criteria represent reservoir attributes (i.e., average depth, net thickness, porosity, permeability and pressure), while others are related to the location, size and overall likelihood that a field may produce more hydrocarbons (i.e., remaining oil, oil saturation, salinity, etc.) or serve as a viable storage reservoir (i.e., acreage, stacked opportunity and mode CO₂ storage). Some criteria were not included in this evaluation due to the similarity in values among fields (e.g., oil gravity, which is reported at 13-55° API for all oil fields in the tri-state area). A large portion of the data used for this exercise is derived from the petroleum fields geodatabase of Lewis et al., 2019.

Most of the rating criteria in Table 6-1 scale with increasing acreage, net thickness, etc.; however, certain items require some further explanation.

- **Criterion #1 – Average depth:** While EOR can generally be considered regardless of average depth, this project established a minimum depth of 1000 ft for field-level assessment purposes. Injected CO₂ is used to drive oil to recovery wells and can do so whether it is in a miscible or immiscible state.
- **Criterion #8 – Stacked opportunity(ies):** This criterion reflects an area's potential to offer options for a combination of CCUS and CO₂ storage activities. In the Appalachian Basin, enhanced recovery activities will likely focus on shallower oil-producing fields, with permanent CO₂ storage accomplished through injection into deeper depleted/depleting oil fields or saline formations.
- **Criterion #10 – Cumulative oil production:** Due the length of time many of the basin's oil fields have been in operation relative to the timing of modern oil and gas regulatory oversight, field-level production data are limited in many areas. For this reason, cumulative oil production volumes were calculated for the oil fields in this study, as opposed to having been provided by operators. Fields with less than 1,000,000 BBL of cumulative oil production were ranked zero because that level of production had been used as a minimum cutoff in the MRCSP Phase II EOR report (Riley et al., 2010).
- **Criterion #11 – Remaining oil:** For the reasons stated above, remaining oil volumes were also calculated. Fields with less than 10,000 BBL of remaining oil or potential oil recovery were ranked zero because that was the OOIP threshold used by Riley et al. (2010) to identify economic fields.
- **Criterion #15 – Salinity:** The formation-dependent effects of this parameter on CO₂-EOR operations were considered (Abdulrahman et al., 2017), as was the inversely proportional relationship between salinity level and CO₂ diffusion rates (Zarghami, Boukadi and Al-Wahaibi, 2016), in the development of the 100,000-parts per million (ppm) rating threshold.
- **Criterion #17 – Pressure minus estimated MMP:** Fields were rated greater than zero if the pressure in the database minus the computed MMP was a positive value, meaning that CO₂ would likely be subjected to supercritical conditions in that field (regardless of absolute measured depth). Ratings of 1, 2 and 3 were assigned if the source of the pressure data was maximum pressure, calculated pressure or reported pressure, respectively. The possibility that enhanced recovery operations for a given reservoir in one area could be miscible while immiscible in another makes the computed MMP data in the geodatabase and this rating criterion particularly important for planning field operations.

- **Criterion #18 – Number of producing wells per acre:** Well density is important for designing a successful CO₂-EOR program. Monson, Korose and Frailey (2014) recommended a spacing of 25 producing wells per 40 acres (ac). This is equivalent to 625 production wells per 1000 ac, which was a guiding factor in establishing the rating values for this criterion.

Oil gravity and permeability measurements were the most underrepresented variables in the MRCSP enhanced recovery datasets. The lack of oil gravity data was of concern because it can play an integral part in initial screening of oil fields for EOR potential. Statistical methodology was used to fill in these missing data where necessary. Takacs et al. (2011) stated that oil gravity <22 API can weaken the oil's ability to become miscible with CO₂. Riley et al. (2010) advised that an oil gravity ≤55 API was ideal. Increasing data density for these parameters and updating critical information will be particularly important to future evaluation of the basin's petroleum reservoirs. Oil field rating results are provided in Appendix D of this report.

Fourteen criteria were used to assess existing gas fields for their EGR potential (Table 6-2). A majority of these are identical to the oil rating criteria used for this project (e.g., permeability, trap integrity, salinity, etc.), while two criteria have been modified to reflect CO₂ miscibility conditions pertinent to gas fields, as described below.

- **Criterion #1 – Average depth:** As previously stated, average depth is an important consideration relative to the miscibility/immiscibility of CO₂ when injected for CCUS. In the case of gas fields, CO₂ miscibility is a necessity for both EGR and ultimate storage. For this reason, a minimum depth of 2500 ft (i.e., the upper miscibility limit of CO₂) was incorporated into the average depth criterion.
- **Criterion #7 – Total penetrations:** While this criterion's rating scheme is the same for both oil and gas fields, there is a distinction in how the counts were made. For oil fields, any well that was drilled in a given field, regardless of depth, was identified as a 'legacy well' and included in the well tally. For gas fields, any well that was drilled to a depth equal to or greater than the depth of the gas reservoir under consideration was identified as a 'penetration' and included in the well tally. In either case, the greater the number of wells in a given field, the more investigatory work that may be needed to determine well integrity and address potential migration pathways prior to CO₂ injection activities.
- **Criterion #8 – Stacked opportunity(ies):** This criterion reflects an area's potential to offer options for a combination of CCUS and CO₂ storage activities. In the Appalachian Basin, enhanced recovery activities may focus on shallower gas-producing fields, with permanent CO₂ storage accomplished through injection into deeper depleted/depleting gas fields or saline formations. In this regard, the most prevalent deep formations in the tri-state area include the Marcellus Shale, Oriskany Sandstone and Utica Shale.

Rating values were derived such that the better the reservoir property or field characteristic, the higher the rating for that criterion. Rating values were summed to generate an overall rating for each field; the higher the rating, the more promising the CCUS opportunity. Data contained in the TORIS and the petroleum fields geodatabase (Lewis et al., 2019) were particularly instrumental in applying rating criteria to several thousand oil and gas fields in the study area. Gas field rating results are provided in Appendix E of this report.

Using this methodology and considering the subsurface geologic conditions of the area, PAGES evaluated CCUS prospects by applying ratings to 453 oil fields and 1307 gas fields in the tri-state area (Appendices D and E, respectively). Of these, ten of the highest rated oil fields were selected for case study assessment as part of the current work. Three of these are located in eastern Ohio, three are in southwestern Pennsylvania and four are in northern West Virginia (Figure 6-3). The producing reservoirs associated with these fields are Silurian (“Clinton” and “Medina” sandstones of the Medina group), Devonian (Venango Group) and Mississippian (Burgoon Sandstone) in age (Table 6-3).

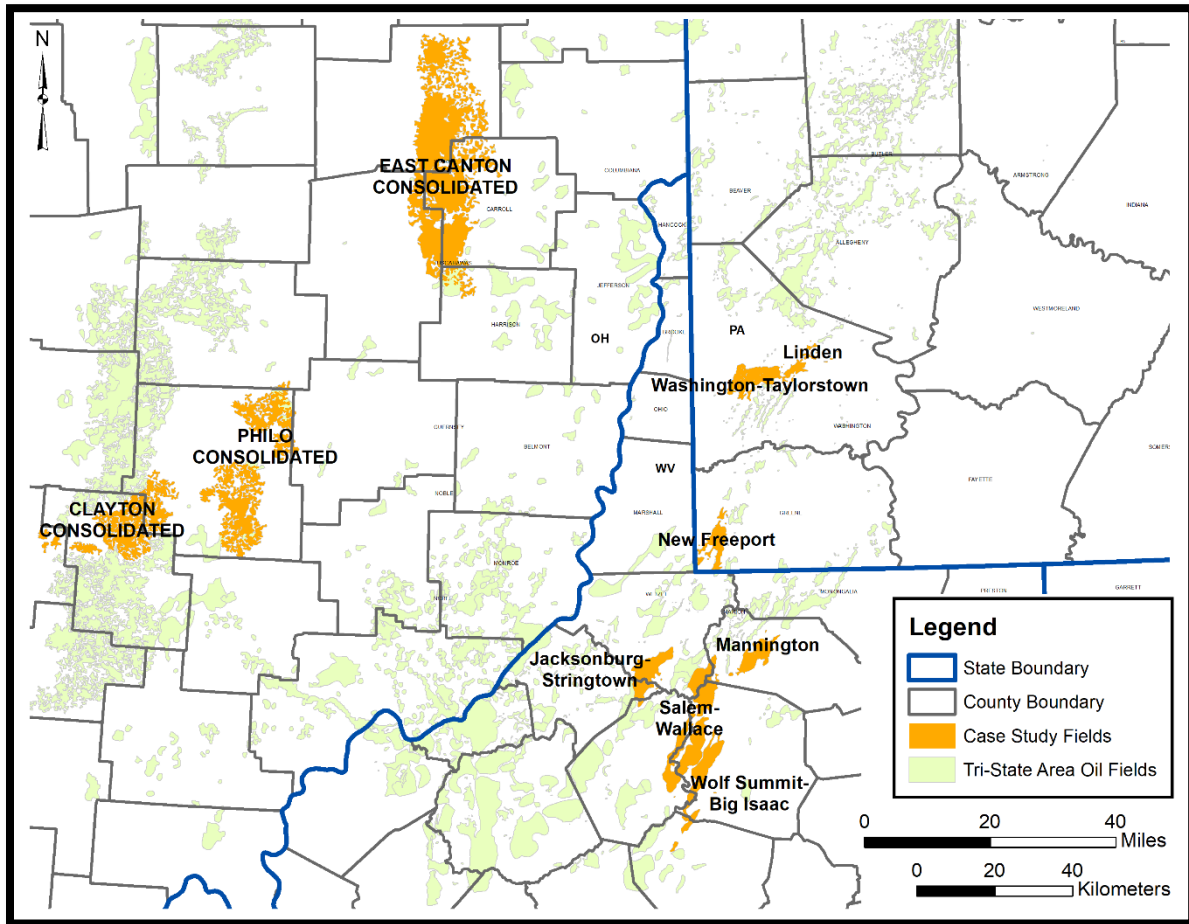


Figure 6-3. Oil fields selected for case study assessment.

Table 6-3. Oil fields selected for case study assessment in the tri-state area.

Field	State	Producing Unit(s)
Clayton Consolidated	Ohio	“Clinton”
East Canton Consolidated	Ohio	“Clinton”
Philo Consolidated	Ohio	“Clinton” / “Medina”
Linden	Pennsylvania	Venango Group (Gantz, Gordon, Fourth, Fifth)
New Freeport	Pennsylvania	Venango Group (Nineveh, Gordon, Fourth)
Washington-Taylorstown	Pennsylvania	Venango Group (Gantz, Fifty-Foot, Gordon, Fourth, Fifth)
Jacksonburg-Stringtown	West Virginia	Venango Group (Gordon)
Mannington	West Virginia	Burgoon Sandstone (“Big Injun”), Venango Group (Gordon, Fifth)
Salem-Wallace	West Virginia	Venango Group (Gordon)
Wolf Summit-Big Isaac	West Virginia	Venango Group (Gordon, Fifth)

6.4 Ohio Case Studies

6.4.1 Overview

The East Canton Consolidated, Clayton Consolidated and Philo Consolidated fields in eastern Ohio were selected as case studies for potential EOR using CO₂. They produce oil from the Grimsby Sandstone, known to drillers as the “Clinton,” part of the Medina group that is found at elevations ranging between -1400 to -4800 ft MSL (Figure 6-4). In addition, the Philo Consolidated Field produces from the drillers’ “Medina,” which is equivalent to the Whirlpool Sandstone that is found at the base of the Medina group (Figure 6-5). These oil-producing sandstones offer the possibility of stacked production and storage potential.

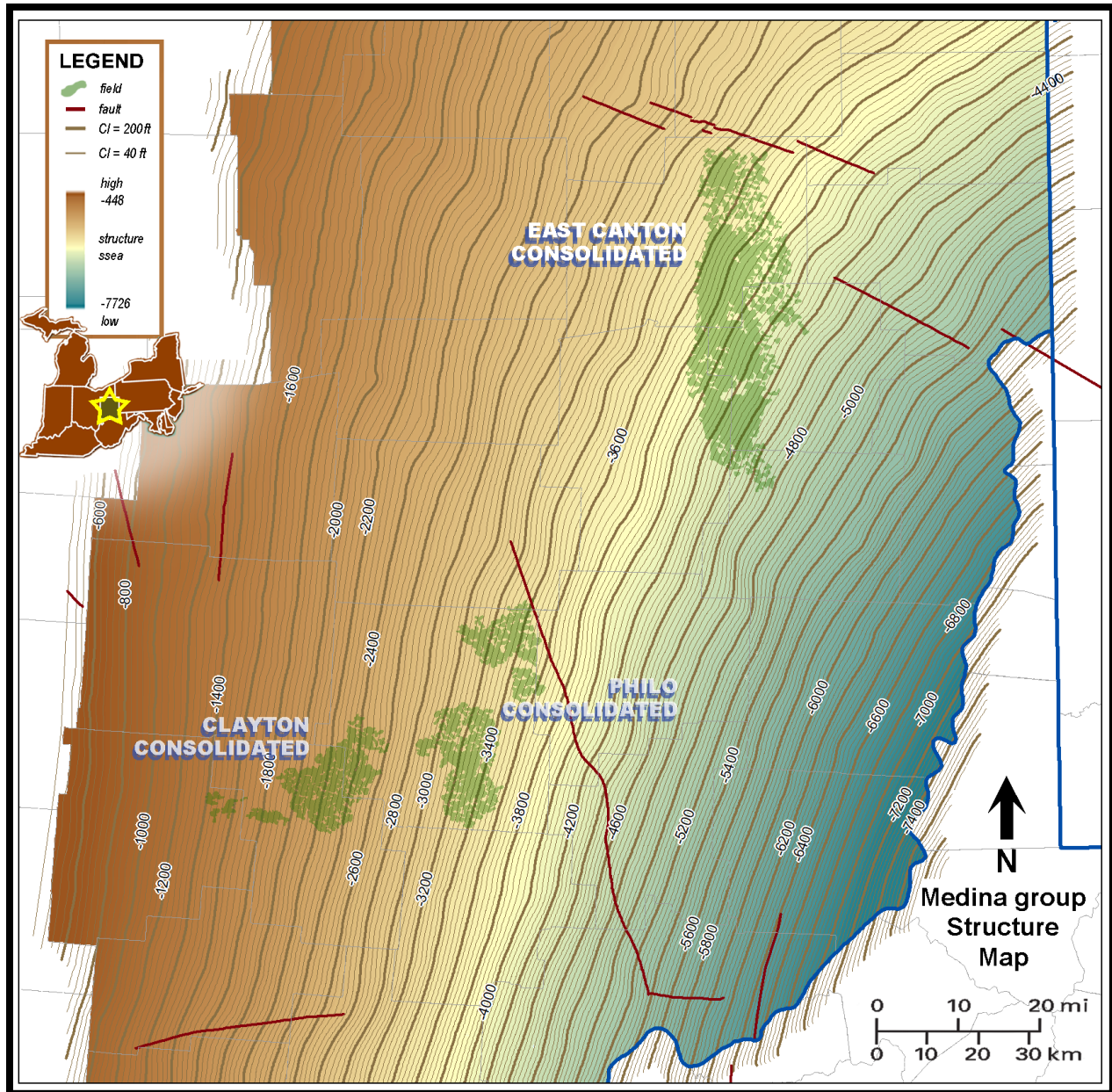


Figure 6-4. Structure map (200-ft contour intervals highlighted) on top of the Medina group showing field location (green) evaluated for CO₂-EOR potential. The structure in eastern Ohio forms a monocline dipping eastward into the Appalachian Basin, with pre-existing basement and Ordovician faults (red) mostly cutting across the regional dip (modified from Solis and Bloxson, 2019).

6.4.2 Lithostratigraphy

The Lower Silurian Medina group is highlighted green in a correlation diagram of the tri-state area's subsurface rock formations, with the expanded section presented as a geophysical type log from the East Canton Consolidated Field (Figure 6-4). Formal terminology and corresponding drillers' names are given for the sandstone, siltstone and shale units within the Medina group, a clastic interval sandwiched between marine units of the Middle Silurian Dayton Dolomite above and Upper Ordovician Queenston Shale lying unconformably below.

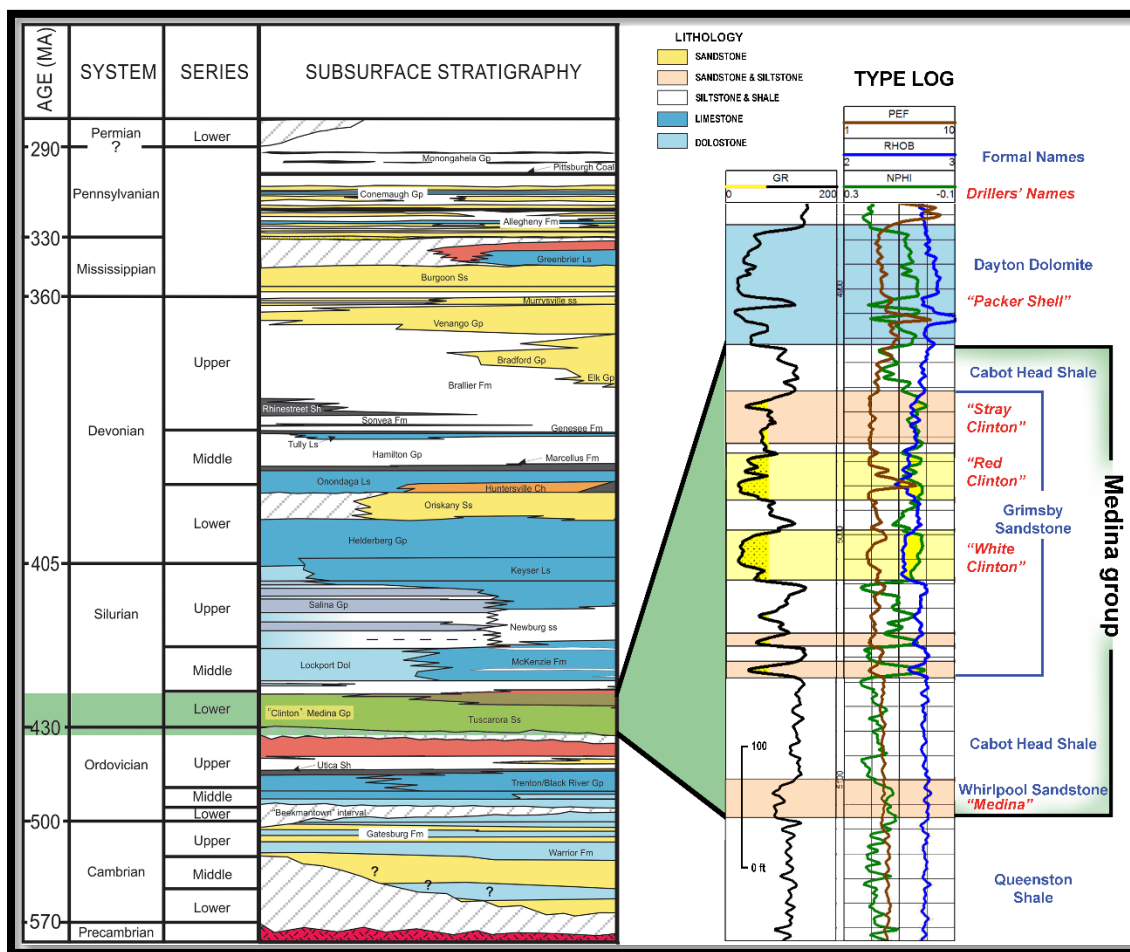


Figure 6-5. Regional correlation chart with Medina group type log (modified from Mishra, 2015), illustrating triple-combo curves [GR, RHOB and NPHI], along with a PE curve.

The "Red" and "White Clinton" intervals (yellow) of the Grimsby Sandstone are the main oil producing reservoirs in the case study areas. Highlighted darker yellow on the type log are intervals where the GR curve is less than 75 API units and where there is crossover between NPHI and RHOB less than 2.55 g/cm³. Siltstone units above and below develop occasional "stray" sandstone lenses (light orange) which intertongue (in eastern Ohio) with clastic prodelta sediments of the Cabot Head Shale. The basal "Medina" (pale orange) is a marine shelf deposit distal to the Whirlpool Sandstone of Pennsylvania and New York, forming non-reservoir calcareous shale in these field study areas (McCormac et al., 1996).

The thickness of the Medina group's siliclastic wedge in eastern Ohio, as measured from the base of the Dayton Dolomite to the top of the Queenston shale, ranges from less than 140 ft at

the western edge of Clayton Consolidated Field to more than 200 ft thick in portions of the Canton Consolidated Field (Figure 6-6). Preexisting Precambrian fault systems have influenced overlying Paleozoic deposition. If consistent trends are identified on each structure or thickness map for a given geologic unit or interval, then a deeper structural influence is the most likely cause of thickness variations in that area (Gray et al., 1982). The Medina group thins in the Philo and Clayton Consolidated fields west of the Cambridge Arch cross-structural discontinuity (CSD) and thickens east of it. The Medina group thins dramatically north of Canton Consolidated Field, where it is bounded by the Akron-Suffield-Smith fault system.

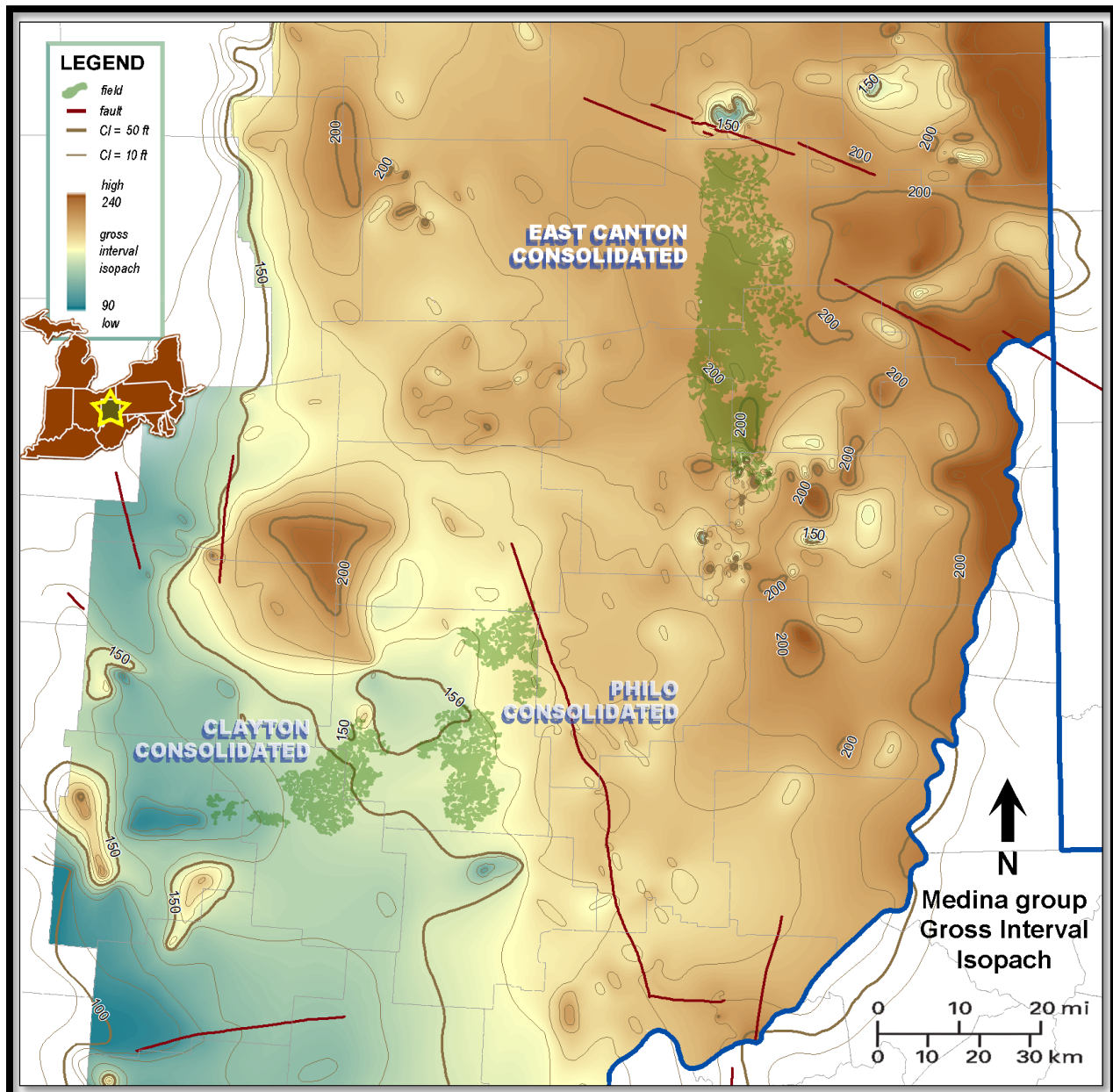


Figure 6-6. Gross thickness map (50-ft contour intervals highlighted) of the Medina group clastic wedge relative to case study fields (green) and influence on deposition from the pre-existing fault systems (modified from Solis and Bloxson, 2019).

Measured depth maps were prepared using data from Lewis et al. (2019) to determine whether Medina sandstones lie between the regional minimum miscible depth (2500 ft) and a lower limit for injectability postulated at 10,000 ft. The case study areas are all within this miscible range. Lineaments, structural nosing and variations in surface topography are better defined in fields with numerous geophysical well control points, as illustrated in the measured depth map for the top of the “Clinton” sandstone (CLNN) (Figure 6-7). The area between the East Canton Consolidated Field and the Clayton and Philo Consolidated fields (i.e., between measured depth contours of 3000 to 5000 ft) illustrates an example of the detail necessary to assess reservoir potential when moving from regional- to field-scale efforts.

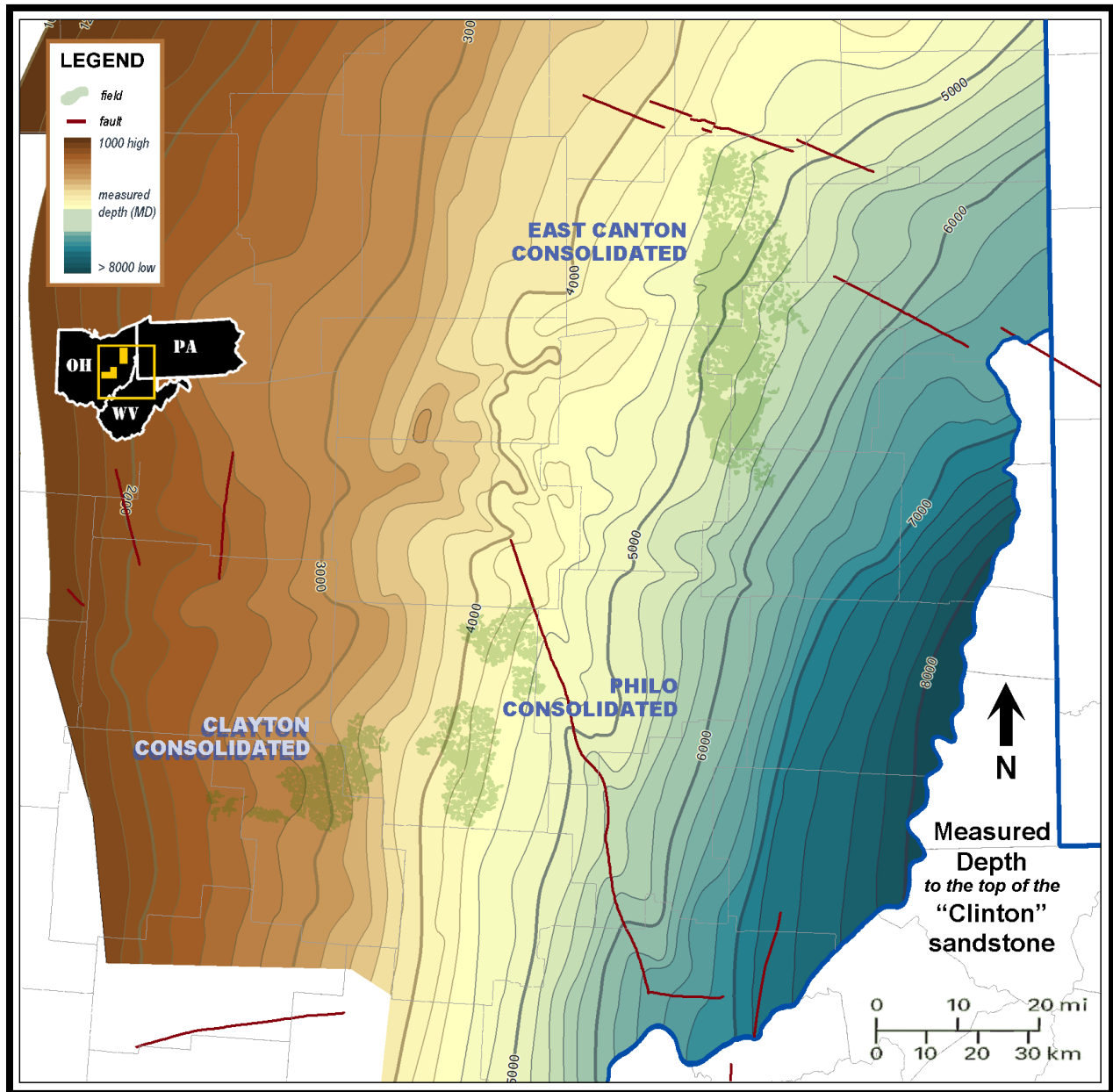


Figure 6-7. Measured depth to the top of the “Clinton” sandstone (200-ft contour interval).

Outcropping in northwestern New York at the Niagara escarpment (Figure 6-8), the Medina group is a near-shore depositional system producing hydrocarbons from tide-dominated shoreline facies (Laughrey, 1984; Laughrey and Harper, 1986; McCormac et al., 1996). The mixed influence of channel transport of sediment, tidal-current reworking and wave modification combined with post-depositional diagenetic processes make a detailed comparative study necessary to determine the reservoir characteristics that govern field production.

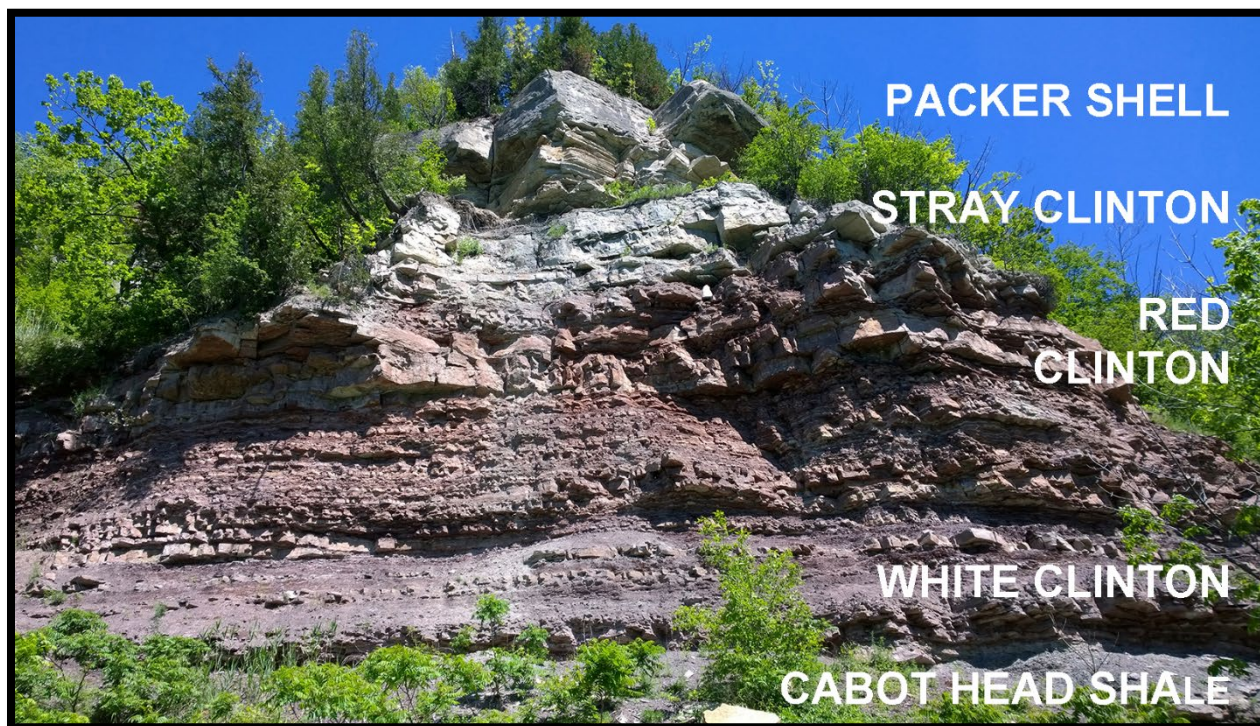


Figure 6-8. Medina group outcrop at the Niagara escarpment in western New York State. The photograph illustrates the contact of the Grimsby Sandstone with overlying dolomite and underlying shale, using equivalent drillers' terms from eastern Ohio.

6.4.3 East Canton Consolidated Field

6.4.3.1 Production and Status

In late 1966, extension of the (already large) Canton gas field in into the East Canton area resulted in commercial oil production in Osnaburg Township, Stark County, and initiated a period of frantic lease acquisition and drilling through the spring 1968, with approximately 600 permits issued. Market saturation at the time ultimately slowed Medina development to a steadier pace (Knight, 1969). Since then, East Canton Consolidated Field has produced approximately 95 MMBO, with estimated 10 MMBLS of primary recovery remaining. An OOIP estimate of 1.5 billion barrels (Riley et al., 2011, Mishra, 2014) indicated primary recovery to have been approximately 6 percent. Figure 6-9 graphs the production decline curve for the East Canton Consolidated Field. Mishra (2014) reported that average oil production has declined by an average of 3.9 percent since 1990. Developed with hydraulically fractured vertical wells on 40 acre-spacing, this oil field contains 3128 producing wells in a 164,000-acre footprint (Lewis et al., 2019), of which 1818 wells show production (Anonymous, 1999; Mishra, 2014). Carbon dioxide huff-n-puff tests and reservoir modeling of CO₂-EOR have estimated that 76 to 279 MMBLS of additional oil could be produced from this field through secondary recovery.

Operators are currently pursuing pilot waterfloods along with horizontal and vertical infill wells (Riley et al., 2011).

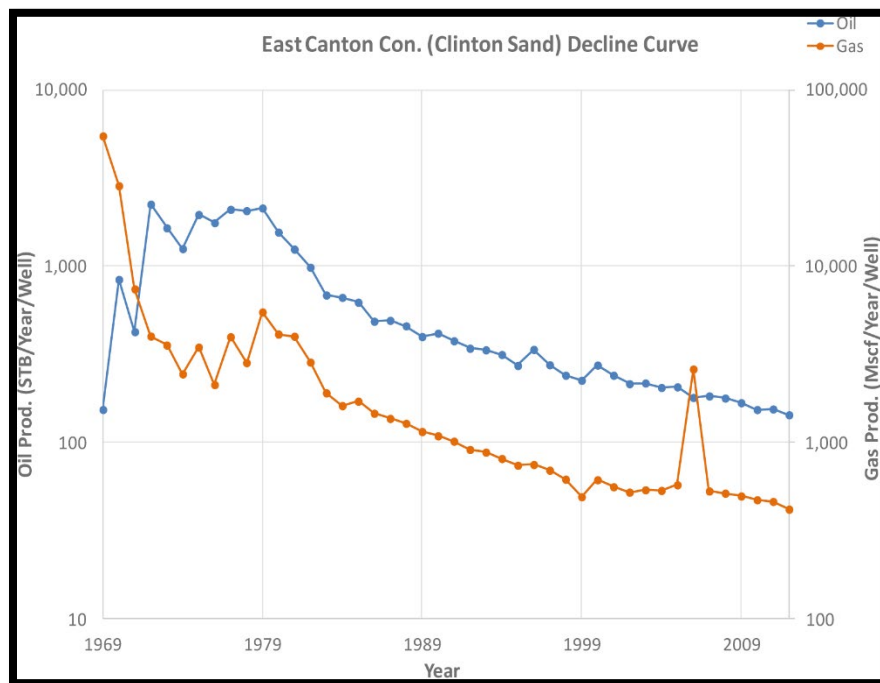


Figure 6-9. East Canton Consolidated Field production decline curve (Mishra, 2014).

6.4.3.2 Pay Zones

Knight (1969) attributed the primary trapping mechanism in the East Canton Consolidated Field to stratigraphic traps produced by updip thinning and pinchout of “Clinton” sandstone lenses (McCormac et al., 1996), as this was the usual mechanism in older “Clinton” fields developed from more permeable sandstones encountered to the west at the beginning of the twentieth century. But, with more than 50 years of production, modern log suites, technological advancements and analyses, combined with old-fashioned geological mapping, a more in-depth picture of structural controls, fluid movement through time and sandstone diagenesis has emerged to refine the understanding of factors contributing to production from this interval. These factors and determination of their relative importance will be useful in designing efficient Medina group CO₂-EOR operations.

Distinct log patterns can be traced from well to well due to the abundance of geophysical log control in this field. Mishra (2015) and Riley et al. (2011) utilized this well control to divide the “Clinton” sandstone based upon interpretation of flooding surfaces (shales) between the units (Figure 6-10). This approach uses reservoir compartmentalization by these shale confining layers to enable modeling of porosity and permeability distribution as it may affect fluid flow (Mishra, 2015; Riley et al., 2011). This sets the stage geologically for subsequent engineering design.

These intervals, referred to in both studies as CLNN, are numbered 1 through 5, starting at the base of the “Clinton” sandstone. CLNN 3 (i.e., drillers’ “White Clinton”) and CLNN 4 (i.e., drillers’ “Red Clinton”) are the main pay zones (yellow) in the Medina group, representing maximum reservoir development in the field. Historically, the best production has come from the “Red” and uppermost portion of the “White” (McCormac et al., 1996). CLNN 4 is the highstand systems

tract [i.e., coarsening-upward type B sequence of Castle (1998, 2001)] as it progrades basinward during regression (Mishra, 2015; Riley et al., 2011).

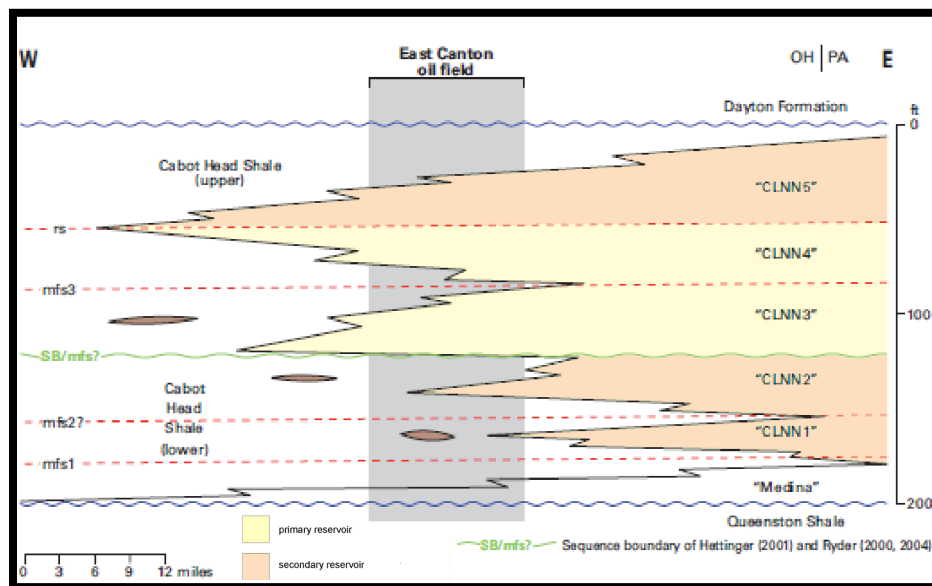


Figure 6-10. Diagram delineating facies relationship of the “Clinton” sandstone (CLNN) as it intertongues with the Cabot Head Shale in eastern Ohio, with relation to the East Canton Consolidated Field (modified from Riley et al., 2011).

6.4.3.3 Core-Derived Data

Mishra (2015) studied the full “Clinton” core section from the Smith and Evans well (API No. 34019202560), obtained from the Ohio Division of Geological Survey (ODGS) core repository. The “White Clinton” (CLNN 1-3) appears to have a very fine- to fine-grained texture while the overlying “Red Clinton” (CLNN 4) has a very fine/fine to medium-coarse grained texture. Figure 6-11 shows core from the “Red Clinton” (CLNN 4) interval in the portion of the East Canton Consolidated Field evaluated by Mishra (2015), while Figure 6-12 shows core from the “White Clinton” (CLNN 3) interval in that part of East Canton Consolidated Field evaluated by Riley et al. (2011).

A distinct color difference is observed among the CLNN 5, 4 and 3 intervals. CLNN 5 (“Stray Clinton”) is white. Sample core photos show the CLNN 4 (“Red Clinton”) to be red (Figure 6-11A), but the color gradually changes to white at the basal section of CLNN 4 (Figure 6-11B). The red color is arguably a result of subaerial exposure and a corresponding increase in iron content, as from hematite cement replacing quartz overgrowths (Knight, 1969). Subaerial exposure is plausible if CLNN 4 represents the highstand systems tract. There is a major flooding surface (~0.5 ft thick) that separates the CLNN 4 from CLNN 3 interval. This interval could possibly act as a barrier, compartmentalizing the two reservoir units. Sample core photos of the “White Clinton” (CLNN 3 in Figure 6-12) show both an open fracture, which suggests enhanced permeability, and a mineralized fracture, which suggests thermal fluids may have migrated through these rocks during hydrocarbon generation and migration, becoming slowly plugged with precipitated minerals so that it now acts as a seal to trap the oil in place.

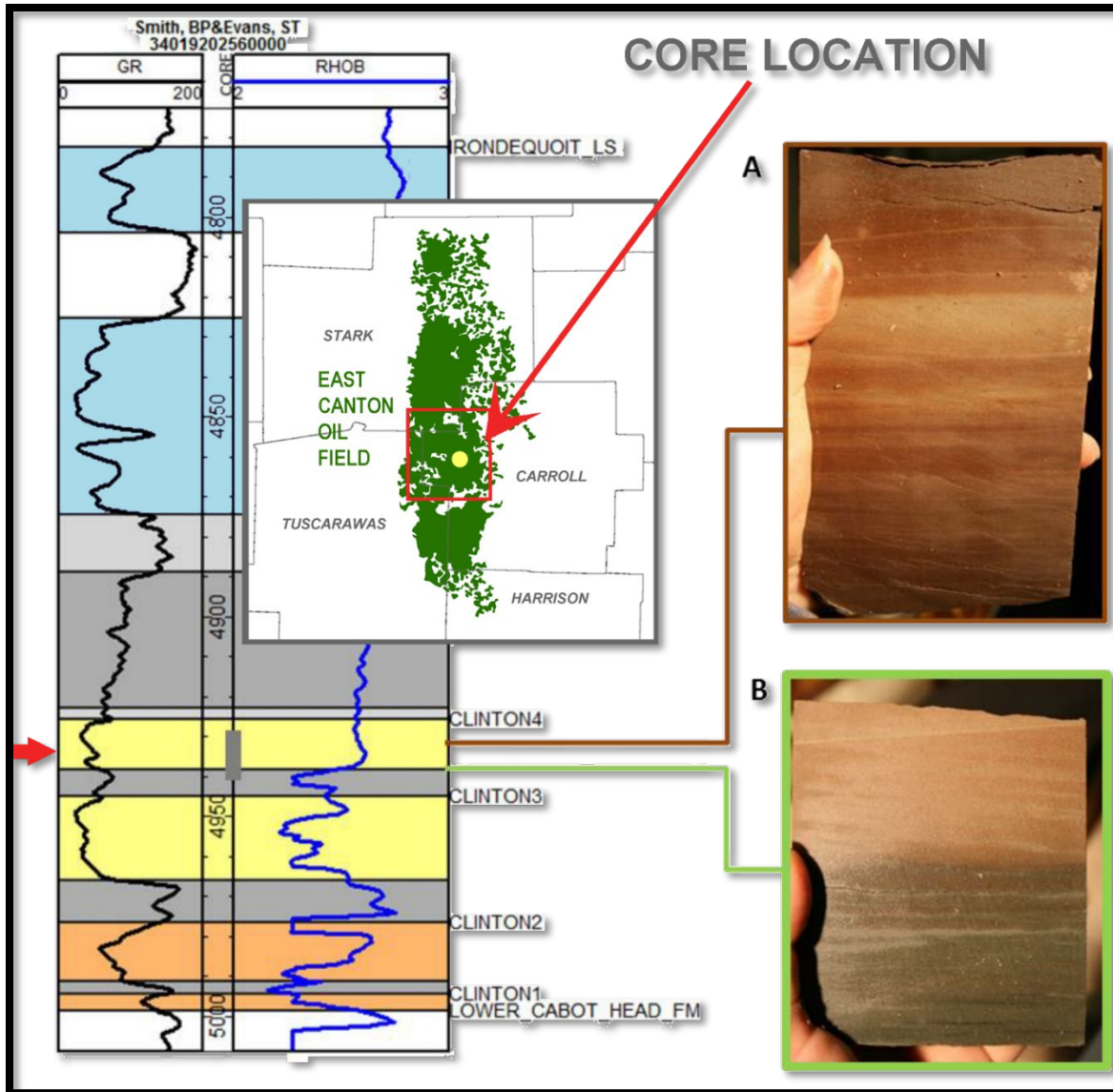


Figure 6-11. “Red Clinton” core photographs and geophysical log for the Smith and Evans well (API No. 3401920256). A) Vertically oriented core of the CLNN 4 and associated red beds. B) Vertically oriented core sample of basal section of CLNN 4 and associated dark-colored flooding surface separating CLNN 4 and CLNN 3. Arrow points to core sampling interval. Flooding surface between CLNN 4 and CLNN 3 is shown with dark gray shading (modified from Mishra, 2015).

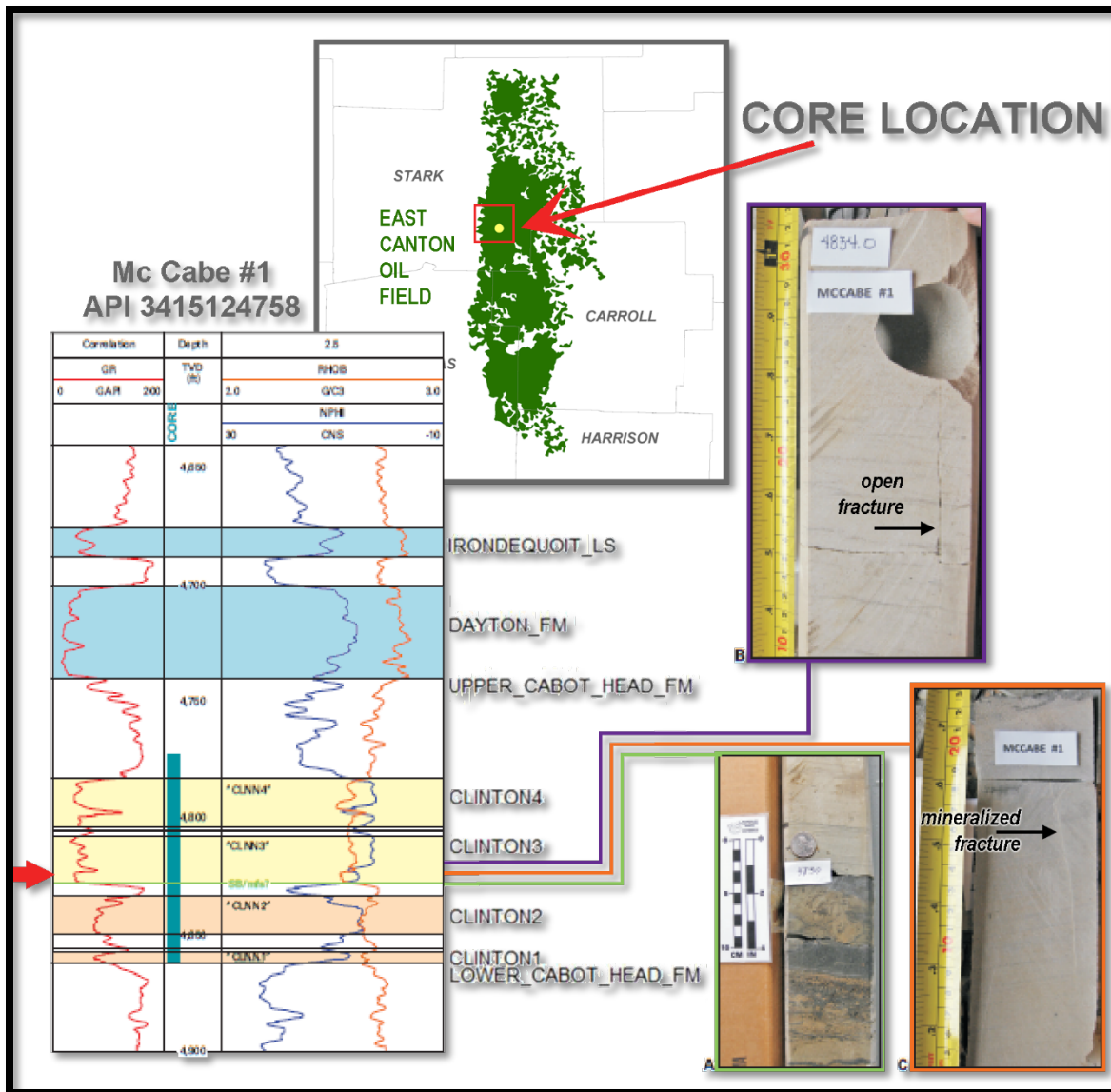


Figure 6-12. “White Clinton” core photographs and geophysical log for the McCabe No. 1 well (API No. 3415124758) Photos of the oriented core show A) the contact at the base of the CLNN 3 with underlying shale, B) an open fracture, and C) a mineralized fracture. Red arrow points to core sampling interval (modified from Riley et al., 2011).

6.4.3.4 Petrology

Most sandstone in the “Clinton” interval is well cemented by quartz overgrowths. Petrographic data indicate that primary porosity has been reduced by growth of quartz, carbonate and clay minerals during burial (Laughrey, 1984; Castle and Byrnes, 2005). Secondary porosity is predominantly from dissolution of unstable cement minerals (Ryder and Zagorski, 2003). Locally occurring hematite causes the reddish coloration in the “Red Clinton” and is the principal cementing material where the silica cement is limited or absent (Knight, 1969). Where hematite is the primary cementing agent, less quartz overgrowths are typically present. This is hypothesized to have minimized negative impacts to “Red Clinton” reservoir porosity and permeability.

6.4.3.5 Structural and Stratigraphic Framework

To better understand the depositional systems and geometry of sandstone distribution over the entire East Canton Consolidated Field, a net sandstone map was constructed by Riley et al. (2011) using 834 GR logs to identify lithology based on their deflection from the shale baseline. The GR curve was chosen for regional mapping because of the abundance of wells with this particular log, and the paucity of wells with RHOB curves. The shale base (100 percent shale) is plotted as 0 percent deflection, and the maximum deflection (100 percent) occurs in the Dayton Dolomite (see example in Figure 6-13). A deflection of less than 25 percent is considered to indicate shale. A deflection between 25 and 50 percent is used to indicate siltstone, while more than 50 percent deflection (in a clastic sequence) is indicative of sandstone (Knight, 1969).

Figure 6-14 plots the net thickness of clean sandstone (yellow) in the “Clinton” interval, based on a 75 percent deflection from the shale base line using GR logs. In East Canton Consolidated Field, mapping illustrates three delta lobes or distributary systems. The two northernmost lobes are roughly oriented east-west, and the southernmost lobe is oriented southeast-northwest. Net sand thicknesses range from less than 10 ft (primarily in the offshore marine and inter-channel depositional setting) to more than 50 ft (deltaic tidal channel setting). Sandstones are thickest where stacked distributary tidal channels occur, marking the CLNN 3 and CLNN 4 reservoirs. The paleo-shoreline is oriented roughly north-south, and the western boundary of the field approximately trends parallel to this feature (Riley et al., 2011).

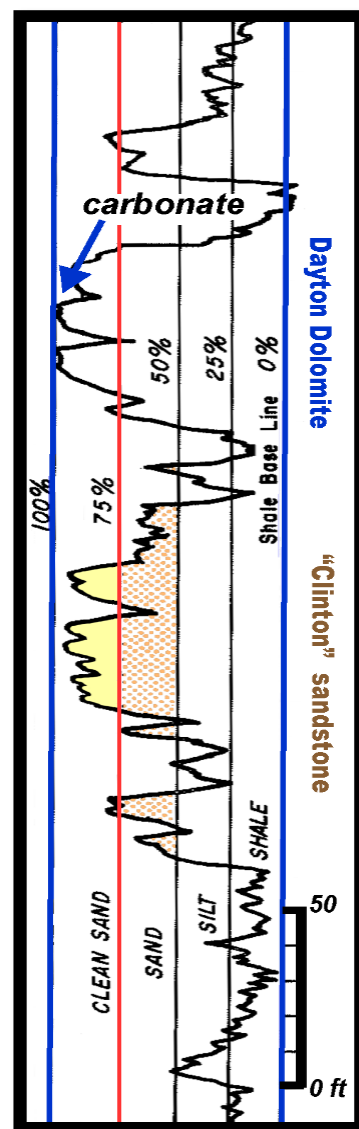


Figure 6-13. Lithologic analysis of the Medina group using the GR log from a well in Osnaburg Township, Stark County, Ohio. This traditional method works well in older fields where the standardized triple-combo log suite is not available for analysis (modified from Knight, 1969).

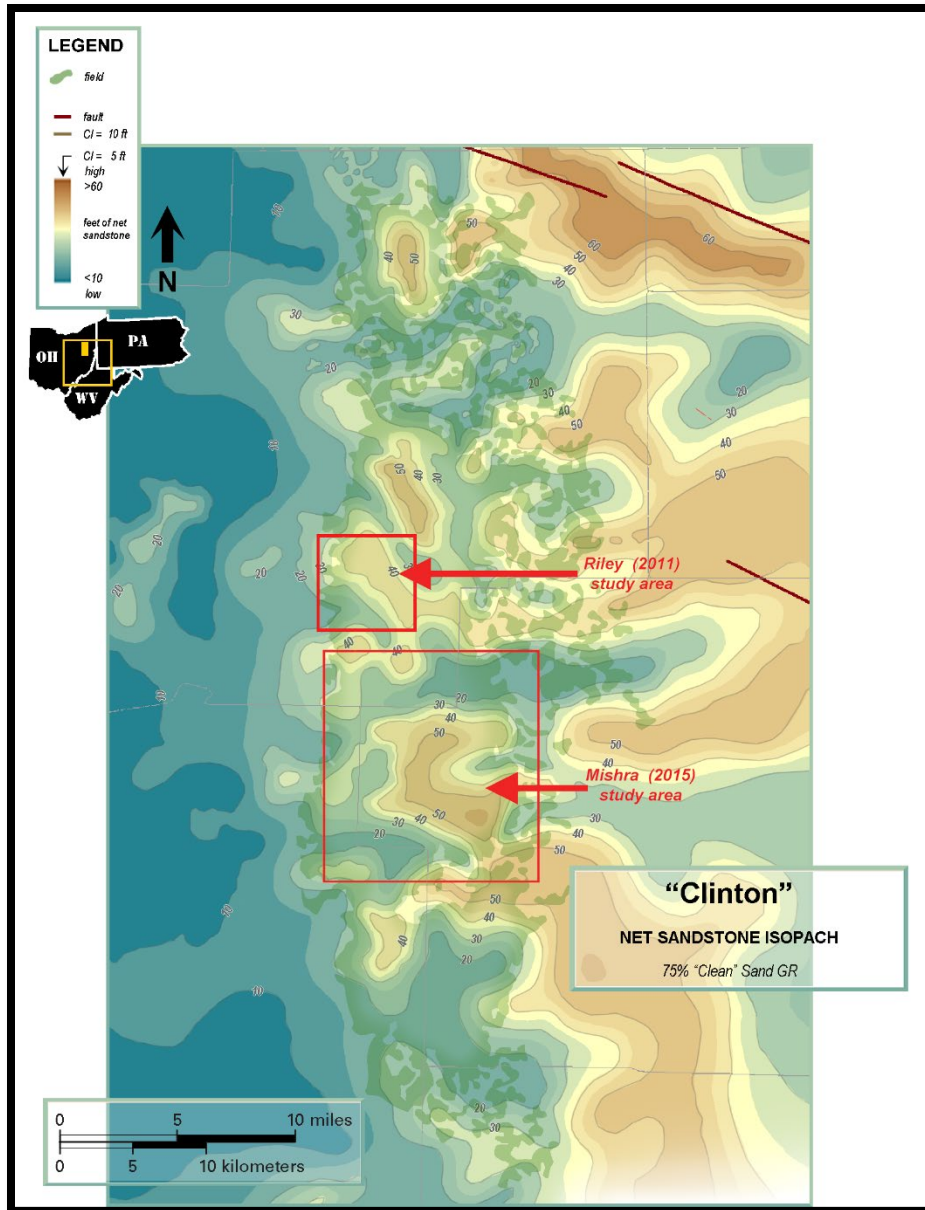


Figure 6-14. Net (75 percent) clean sandstone thickness map (modified from Riley et al., 2011), illustrating the regional depositional setting for the “Clinton” sandstone in East Canton Consolidated Field. Three distributary systems intersect the field, and its western margin bounded by the limits of the paleo-shoreline.

The surface representing the measured depth to top of the “Clinton” sandstone is mapped in Figure 6-15. The Riley and Mishra field study footprints are outlined in red, representing approximately one-fourth of the acreage of East Canton Consolidated Field. In this area, the “Clinton” is found an average of 10 to 20 ft below the base of the Packer Shell and in Ohio, is separated from it by the upper Cabot Head Shale (see Figure 6-5). According to Riley et al. (2011), the upper Cabot Head may thicken locally to as much as 40 ft where the CLNN 5 interval has been eroded. This thickening, in addition to local structural features, faults and surface topography, are expressed as irregularities in the measured depth map, beyond the overall monoclinal dip eastward into the Appalachian Basin. Encountered at 4500 ft below ground surface in the shallow northwestern corner of the Eastern Canton Consolidated Field, the “Clinton” sandstone dips to the southeast, where it is ultimately encountered at a depth of nearly 6000 ft at the southeasternmost tip of the field. Average producing depth is reported at 5300 ft (Lewis et al., 2019), where the main reservoir units occur. These depths are well within the miscible range for CO₂.

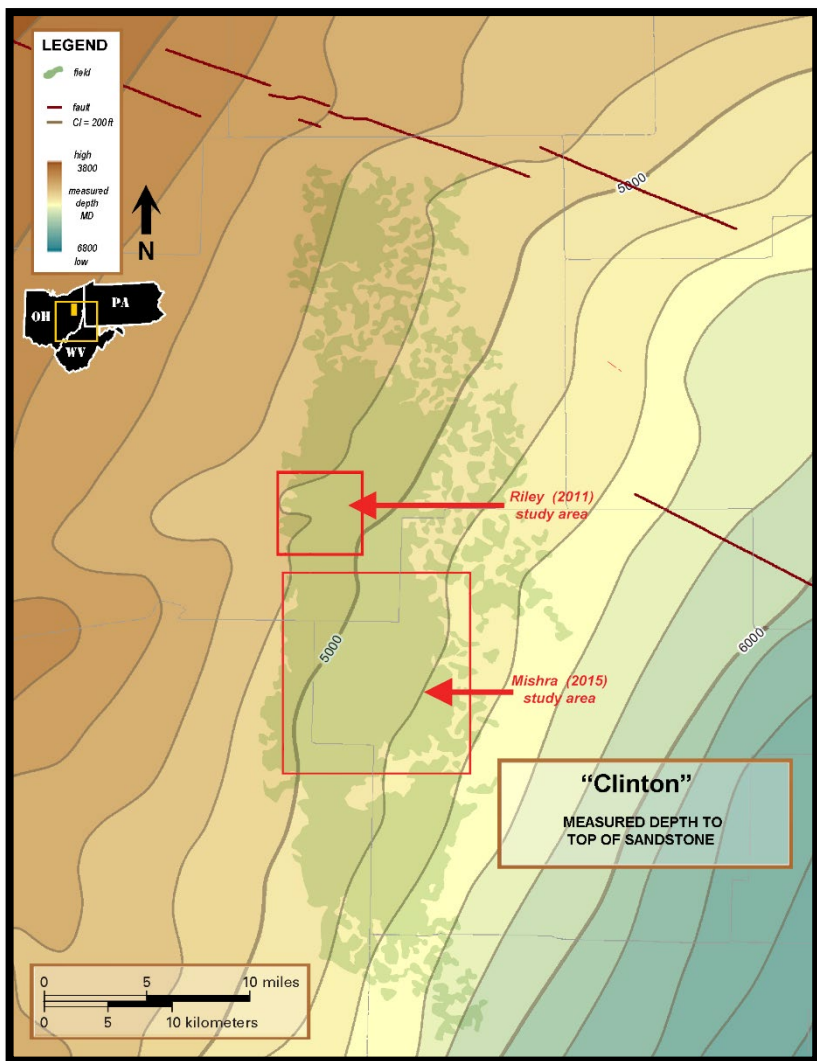


Figure 6-15. Measured depth to the top of the “Clinton” sandstone.

6.4.3.6 Field-Level Analysis Methodology

Using the regional framework described above, a more detailed analysis can be conducted using wells with modern triple-combo log suites (GR, RHOB and NPHI) to further define reservoir parameters at the field level. Ideal well candidates will also have PE curves for lithologic control and resistivity log curves for water saturation that span the depths at which both injection targets and confining caprocks occur.

Riley et al. (2011) prepared such a study on a 10,240-ac footprint in the north-central portion of East Canton Consolidate Field, initially constructing a more regional grid of 32 cross sections

with GR and RHOB log control, using an 8-percent porosity cutoff for reservoir mapping, to define a detailed 700-ac model area using 16 logs. This study established a methodology that was followed by Mishra (2015), who conducted a detailed reservoir study using 30 logs with a standard triple-combo log suite in the south-central portion of the field, covering approximately a quarter of the field's footprint. The footprints of both studies are provided in Figure 6-14 and Figure 6-15.

For the current investigation, reservoir maps from the Riley et al. (2011) study area were layered to conduct a comparative analysis of production and lineaments to structure, net sandstone, water saturation and porosity. The results of this effort are provided in subsequent sections and illustrated in Figure 6-16 through Figure 6-21. Reservoir parameters that appear to follow production trends are contrasted to reservoir parameters with less apparent connection. Stratigraphically, only the primary productive reservoirs (CLNN 3 and CLNN 4) have been considered. Structural and tectonic elements have also been assessed. Although covering a smaller footprint than Mishra (2015), mapping from Riley et al. (2011) was utilized in this assessment, as it contains the necessary regional sandstone, structural and tectonic elements to determine production controls (which can then be extrapolated to remaining field areas).

Geologic cross sections (Figure 6-22 through Figure 6-26) were constructed in PETRA[®] using geophysical logs available for East Canton Consolidated Field. These sections depict four areas of the field (north, north-central, south-central and south), as separated by natural breaks in the field's footprint and serve to tie the detailed local studies into the larger field area framework. These breaks occur in a cross-strike direction, suggesting that similar reservoir controls found in the published study areas exist across the entire field. Local strike and dip cross sections representative of Mishra (2015) highlight CLNN 3 and CLNN 4 reservoir heterogeneity in the main producing sandstones (Figure 6-24).

This field-level analysis concludes with a series of maps and discussion of legacy well issues relative to the implementation of CO₂-EOR in the East Canton Consolidated Field.

6.4.3.7 Structure and Tectonics

Oil producibility in East Canton Consolidated Field is related to subsurface structure and the presence of cross-structural lineaments. Lineaments are areas of increased fracture permeability that lead to vertical hydrocarbon and fluid migration (Rodgers and Anderson, 1984). Structure on the base of the Dayton Dolomite (i.e., "Packer Shell") shows a distribution and frequency of natural fracture trends from Landsat and LiDAR imagery (Figure 6-16). Core measurements and basin tectonic features suggest a northwest-southeast (i.e., cross-structural) trend for those natural fractures not related to the current stress field. The structure map on the base of the Dayton Dolomite (Figure 6-16) also illustrates a correlation between oil production and a 200-ft depth range, with the greatest concentration of high-yield wells found between -3600 to -3700 ft MSL. This may reflect the gas-oil-water contacts within the field (i.e., updip grading into the field is gas-prone while downdip becomes more water-saturated). It may also indicate a higher fracture density in the current stress field (discussed below). The highest oil production along this structural trend falls where two or more fault and/or fracture systems intersect.

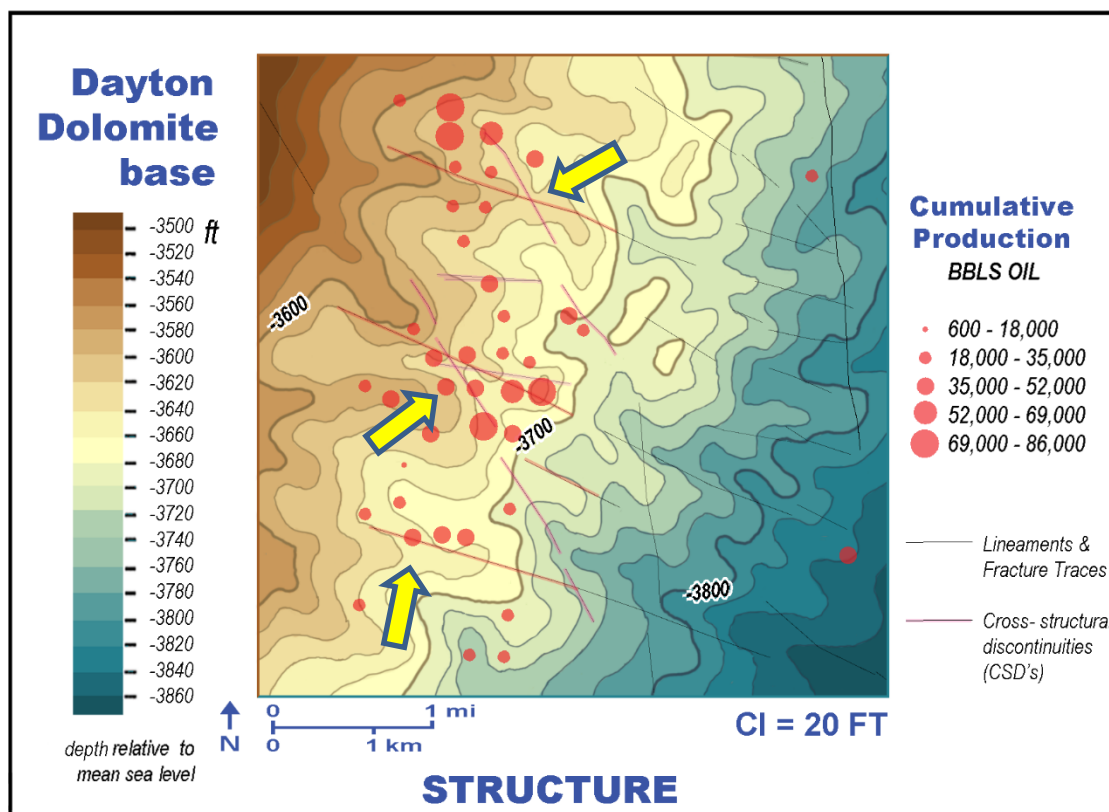


Figure 6-16. Structure map on the base of the Dayton Dolomite (i.e., "Packer Shell") compared to cumulative production (modified from Riley et al., 2011). Yellow arrows point toward lineaments (fracture trends) in this interval that appear to be associated with the highest oil production (red bubbles). Mapped study area is outlined in Figure 6-4 and Figure 6-15.

A body of research exists to substantiate the influence of lineaments and natural fractures on sediment deposition, post-burial diagenesis and fluid migration intermittently through geologic time. Subsurface structures were caused by stress orientations changing frequently during the formation of the Appalachian Mountains. When these stresses encountered pre-existing crustal weaknesses with favorable orientations, movement along these weaknesses occurred (Solis and Bloxson, 2019). This process generated fracture trends. Even if these fracture trends do not line up with the current stress regime, or are currently active, the timing of fluid movement along CSDs is related to the timing of motion along fractures (Wegweiser et al., 1998; Boyce and Morris, 2002). Thus, research suggests that when these fracture trends were active, they influenced the thickness of active deposition and created pathways for fluid migration and structural traps in subsurface rocks. Increased fracture permeability and vertical migration of hydrocarbons has been linked to the Tyrone-Mt. Union lineament in Crawford County, Pennsylvania (Lavin et al., 1982). If various natural fracture orientations in the East Canton Consolidated Field functioned similarly as intermittent conduits for fluid migration during the hydrocarbon generation process, increasing mineralization of a subset of those orientations during diagenesis may have functioned (along with vertical and horizontal facies variations) to substantively seal trapped hydrocarbons in place.

6.4.3.8 Net Sandstone

Figure 6-17 and Figure 6-18 map the net thickness of sandstone in the CLNN 4 and CLNN 3 intervals, respectively, along with cumulative oil production. Greater oil production is found where the thickest net sandstone intersects the central CSD (yellow arrows). Here, greater hydrocarbon production is apparent on one side of the fracture trace as opposed to the other, suggesting pairs of fracture traces delineate separate fault blocks. The southernmost CSD shows oil production along the lineament even though the net sandstone is thin (Figure 6-17), but the most oil production is along the central and northern CSDs where thick sand occurs in conjunction with the structural and tectonic elements (Figure 6-17 and Figure 6-18).

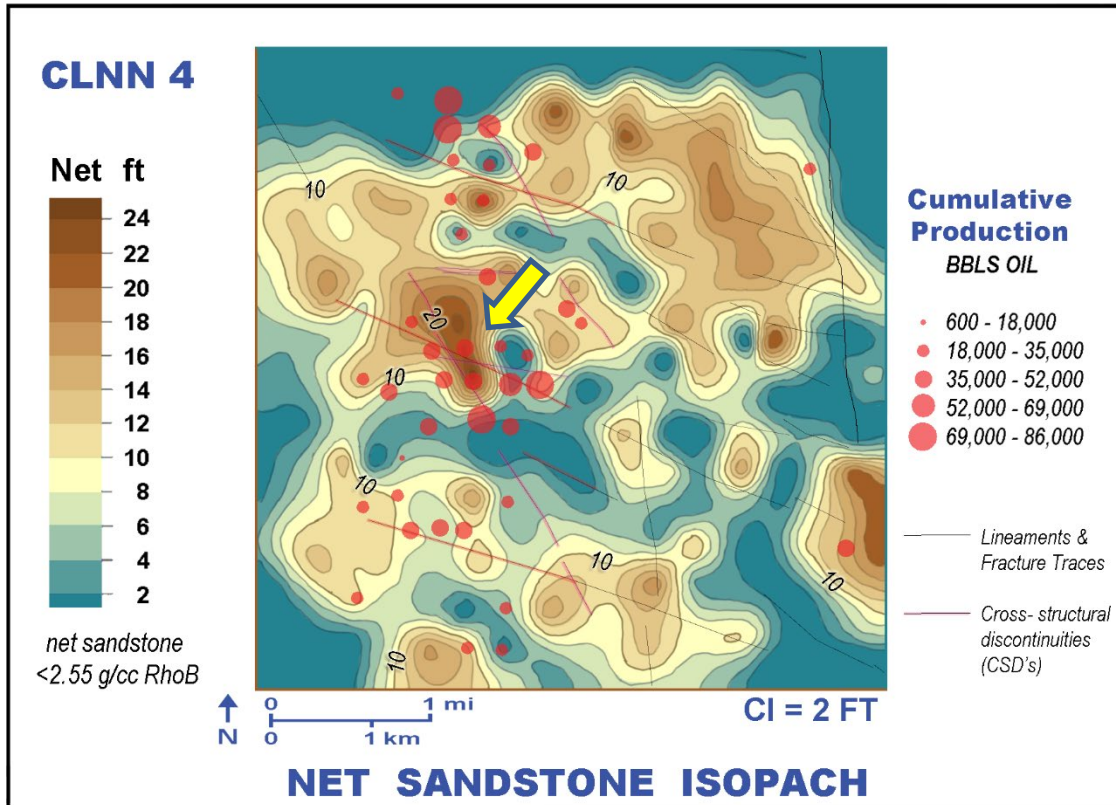


Figure 6-17. Yellow arrow points to the high cumulative oil production near two CSDs and one east-west fault, which intersect the thickest local accumulation of net sandstone in the CLNN 4 ("Red Clinton") reservoir (modified from Riley et al., 2011).

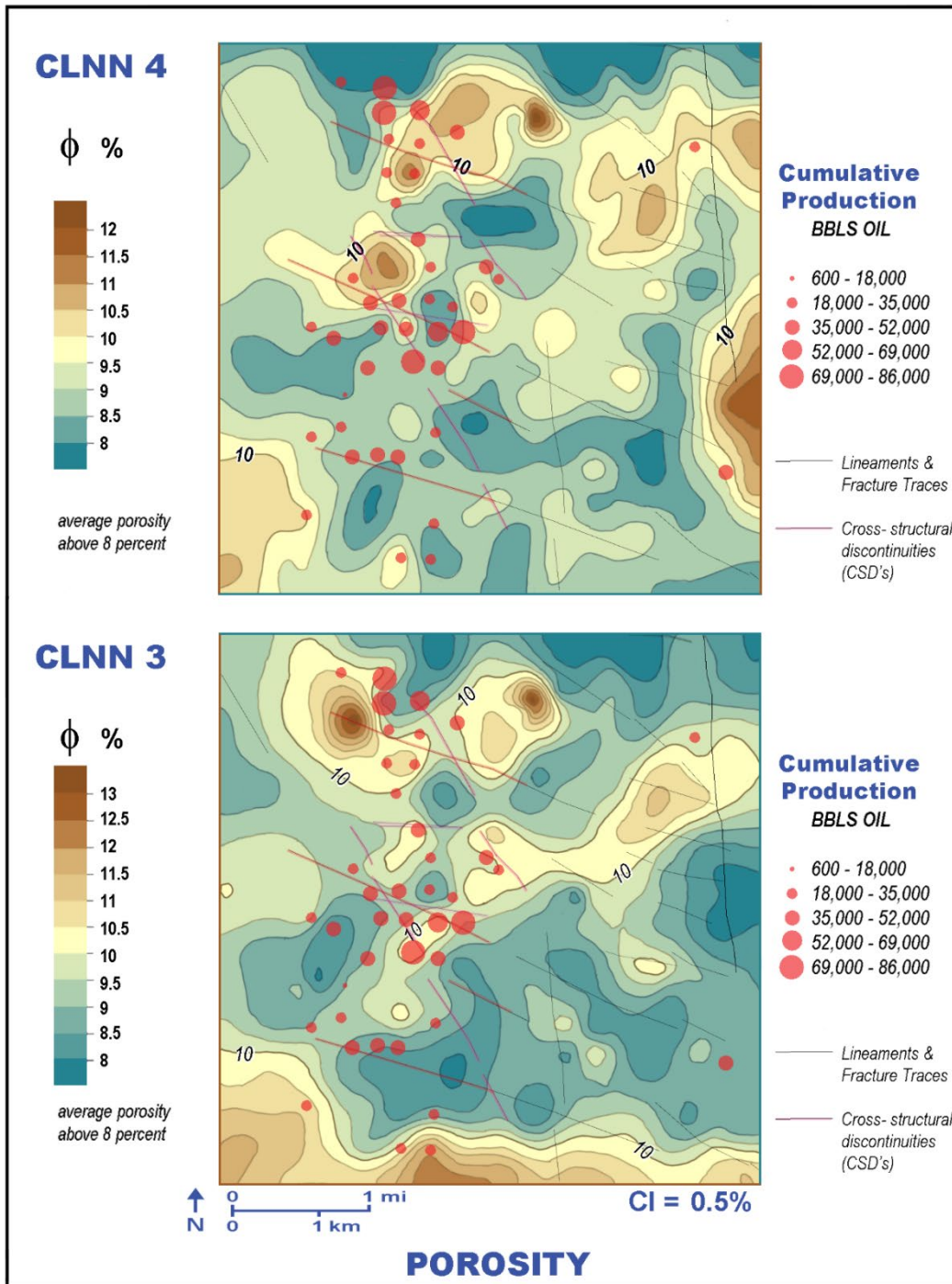


Figure 6-19. RHOB maps for the CLNN 4 and CLNN 3 intervals, compared to cumulative oil production (modified from Riley et al., 2011).

6.4.3.10 Water Saturation

Water saturation measurements for the CLNN 3 (“White Clinton”) and CLNN 4 (“Red Clinton”) intervals are mapped in Figure 6-20. Typically, water saturation increases in the downdip direction (as water molecules are heavier than methane and oil molecules), but as illustrated in Figure 6-20, there is a distinct area for each CLNN interval where higher water saturation values are found updip (yellow arrows) between areas of lower saturation and bounded by two CSDs. The offset in areas of high water saturation between the CLNN 4 and 3 intervals suggests that the persistent shale separating these two units may influence fluid flow within the reservoir, and that EOR projects may encounter separate flow regimes between them, as postulated by Riley et al. (2011).

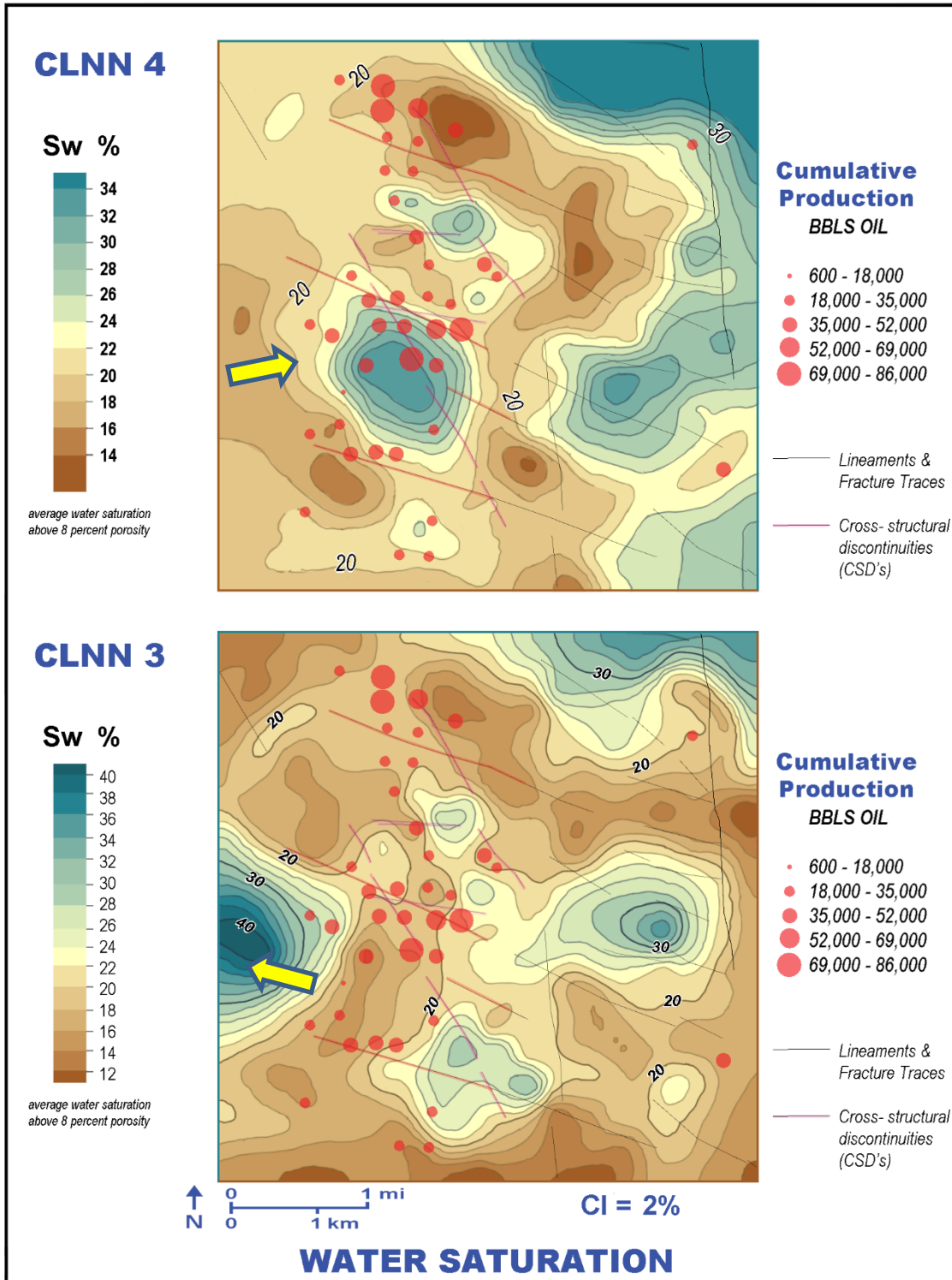


Figure 6-20. Water saturation in the CLNN 4 and CLNN 3 intervals. Yellow arrows point to areas of higher water saturation bounded by two CSDs (modified from Riley et al., 2011).

6.4.3.11 Hydraulic Fractures and the Current Stress Field

Based on published reports, the induced fracture direction (created by hydraulic fracturing during well completion) in the “Clinton” is N63°E, with a microseismic test in the Eastern Canton Consolidated Field showing a preferential direction of N55°E. Anecdotal evidence from other hydraulic fracture treatments in the field and limited observations of communication between wells confirms this general orientation (Riley et al., 2011). The best evidence for fluid communication between wells is from artificially induced hydraulic fractures, which trend in the direction parallel to the northeast-southwest contemporary stress field.

A comparison of oil production to surface lineament locations, which are parallel to sub-parallel to the current stress field, is shown in Figure 6-21, along with a structure map on the base of the Dayton Dolomite. Both fracture trace density and oil production in excess of 600 BBL are greatest in the -3600 to -3700 ft MSL contour interval.

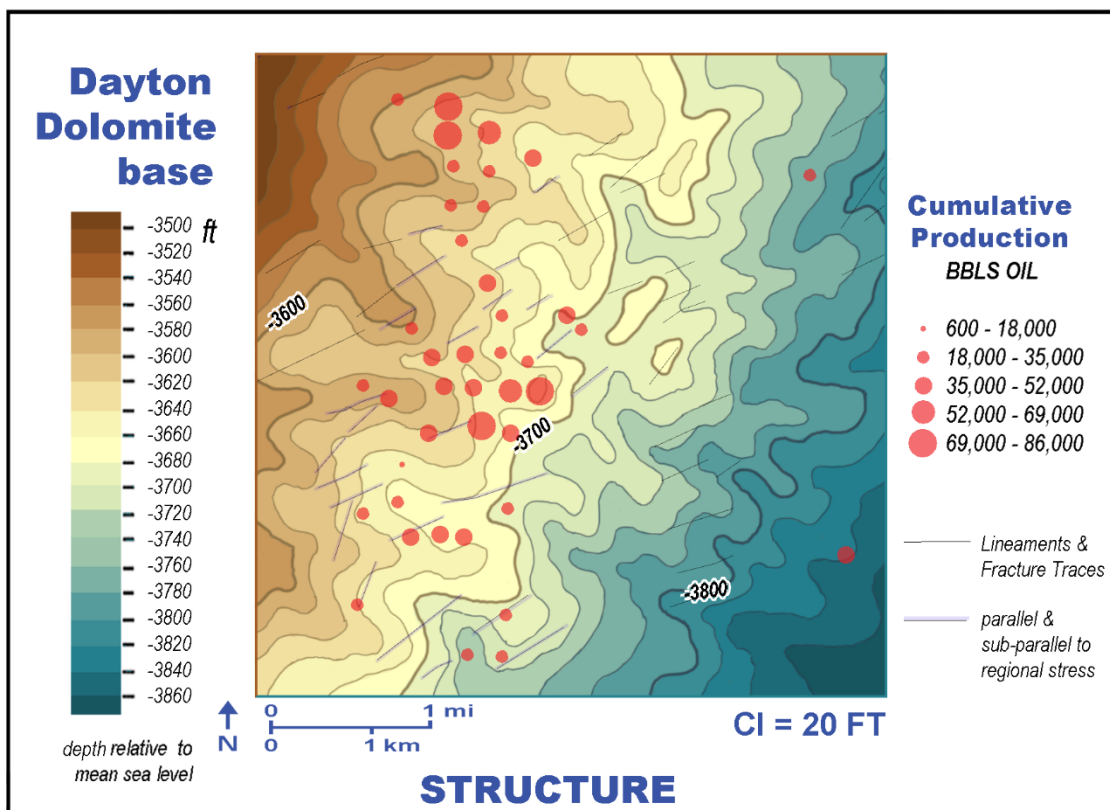


Figure 6-21. Surface lineament locations and cumulative oil production plotted on a structure map of the Dayton Dolomite base (modified from Riley et al., 2011).

6.4.3.12 Area Cross Sections

The East Canton Consolidated Field was divided into four areas (north, north-central, south-central and south), based on the presence of cross-cutting CSDs, for the purpose of constructing representative cross sections for each area of the field. A cross section along depositional strike, following the edge of the paleo-shoreline, was constructed from north to south along the entire length of the field, and several dip cross sections, parallel to distributary (tidal channel) direction and clastic wedge progradation, were developed from west to east for each of the four areas. Figure 6-22, Figure 6-23, Figure 6-25, and Figure 6-26 (this study) and Figure 6-24 (Mishra, 2015) provide annotated illustrations of subsurface “Clinton”/Medina group geology and reservoir characteristics for each area.

6.4.3.13 Legacy Wells

The East Canton Consolidated Field, intentionally developed on 40-acre spacing, has 3128 producing wells but also contains an additional 2114 non-producing wells (i.e., plugged and abandoned wells, dry holes and a handful of water injection wells). This equates to a total legacy well count of 5242, or 1.28 wells/40 ac. Most non-producing wells were part of the initial field development to tap the oil reserves of the “Clinton” sandstone. In the southern portion of the field, shallow Berea wells have been mostly plugged and abandoned, while Cambro-Ordovician wells show stacked potential in the north area. The types of wells, their status and producing formations are provided for each geographic area (north, north-central, south-central and south) in Figure 6-27 through Figure 6-30.

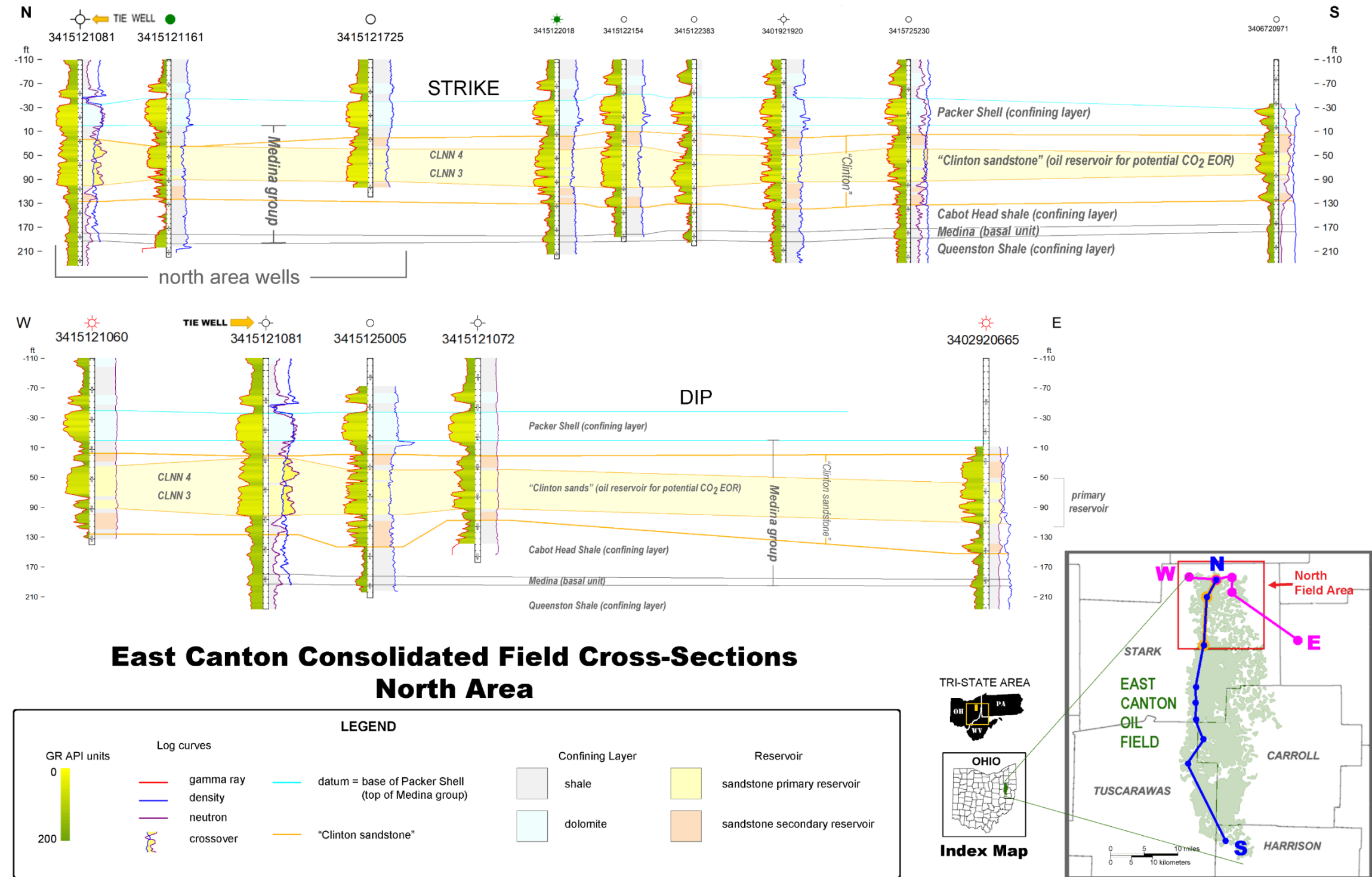


Figure 6-22. Development of the thickest sandstones occurred along the paleo-shoreline edge (N-S strike section). Heterogeneity is somewhat more pronounced in the W-E dip section, where a combination of distributary sandstones and tidal flat shales are present. Sandstone tends to be most developed where the distributary system intersected the paleo-shoreline. Shading is based upon GR API units, with lower values (yellow) representing cleaner sandstones in the clastic lithologies and dolomites in carbonate lithologies, higher values (green) representing increasing shale content. Formation and lithological divisions follow those of Mishra (2015) based on Riley et al. (2011).

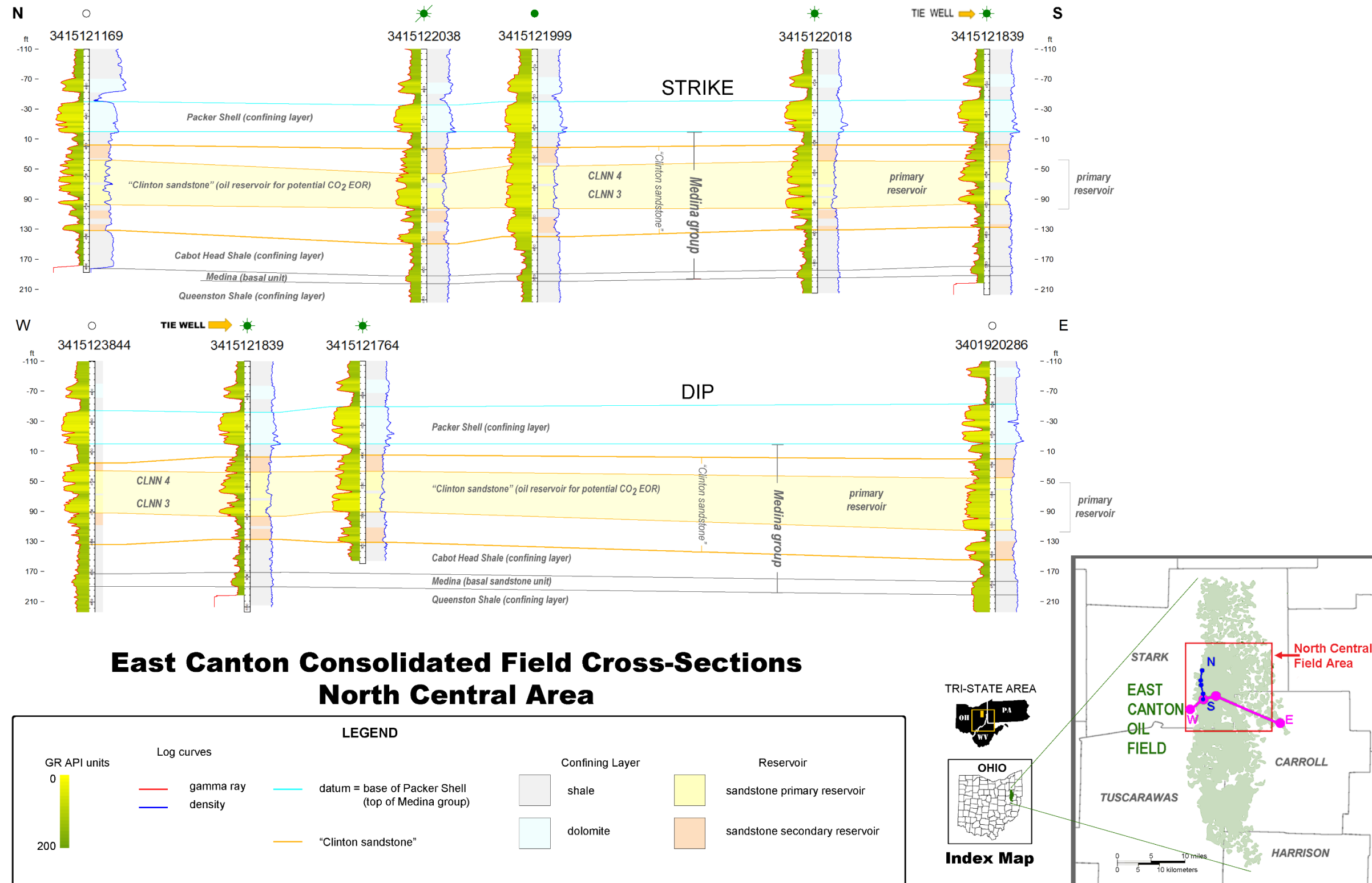


Figure 6-23. N-S strike and W-E dip sections using geophysical log control (shading as described in Figure 6-22). The log character displayed in these sections illustrate the complexity of facies distribution encountered by Riley et al. (2011) in their detailed study of the west-central portion of East Canton Consolidated Field.

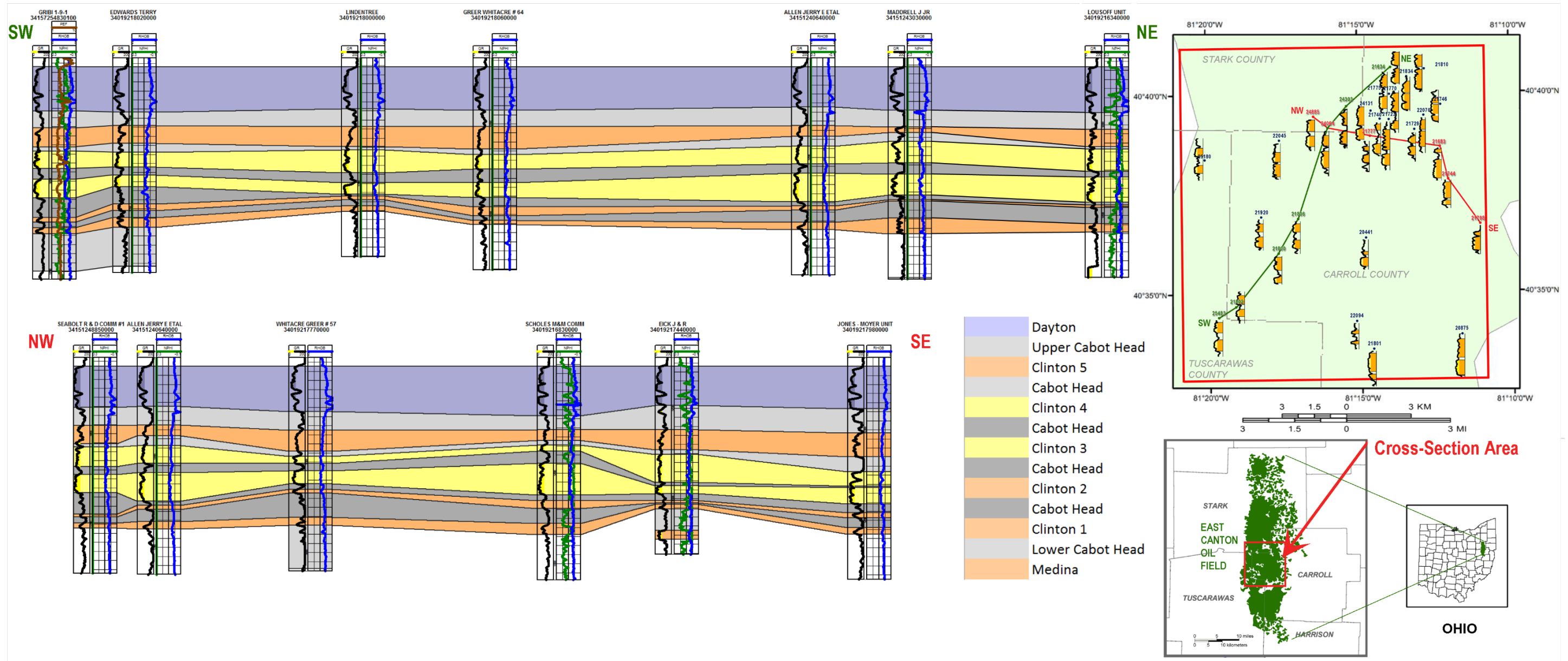


Figure 6-24. Cross sections in the south-central portion of East Canton Consolidated Field, as modified from Mishra (2015). SW-NE section in the south-central quadrant of the field (see inset map, top right) follows basin strike and is subparallel to the north-south trend of the paleo-shoreline. Both the upper CLNN 4 (“Red Clinton”) and the lower CLNN 3 (“White Clinton”) intervals (highlighted in yellow) show gradual thickening and thinning along the shoreline trend. Thicker shoreline sandstones occur where fed by the distributary channels illustrated in the NW-SE dip section, which intersects the general east-west trend of tidal channels (see Figure 6-14) as they weave through the delta plain to the shoreline. Thick sandstone in the middle of the distributary (tidal channel) facies in one well differs from that of delta plain siltstones encountered in an offset well at the same stratigraphic interval. This creates a “zig-zag” effect, enhanced by Mishra’s color scheme, where the solid yellow delineating the reservoir makes “Clinton” heterogeneity more apparent. The index map (top right) shows GR log signatures for the 30 control wells having standardized triple combo logs for the two major producing intervals (CLNN 4 and CLNN 3), separated by the flooding surface identified by Riley et al. (2011). Modern log control in this portion of the field and a smaller area to the north allows for detailed mapping and assessment of production controls. These findings may allow for extrapolation of reservoir parameters thought to influence production to areas where modern log suites are less abundant, or not available at all.

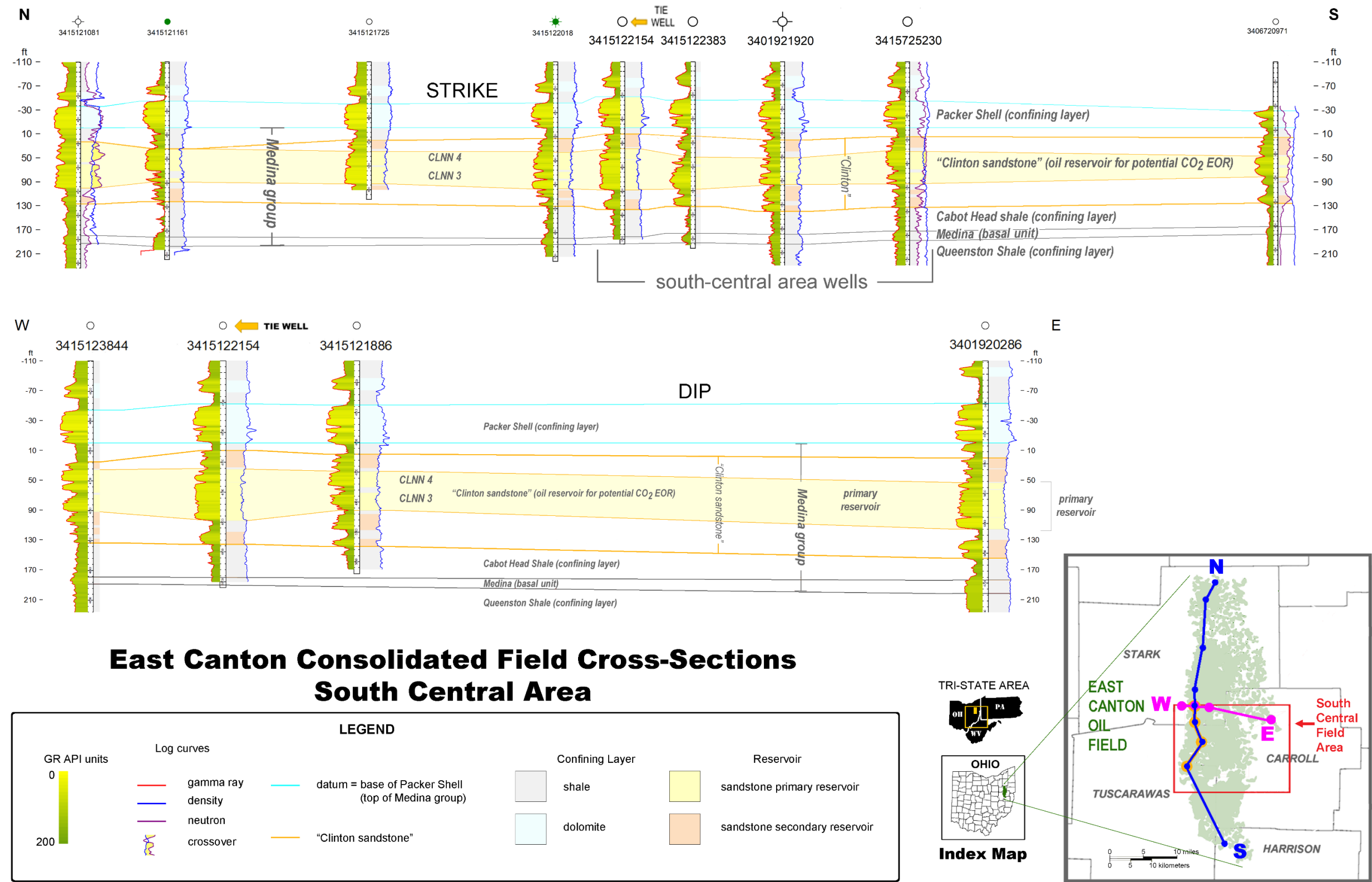


Figure 6-25. N-S strike and W-E dip sections over the same area as Figure 6-24, using geophysical log control to emphasize the clean sandstone to shale aspect within "Clinton" reservoirs.

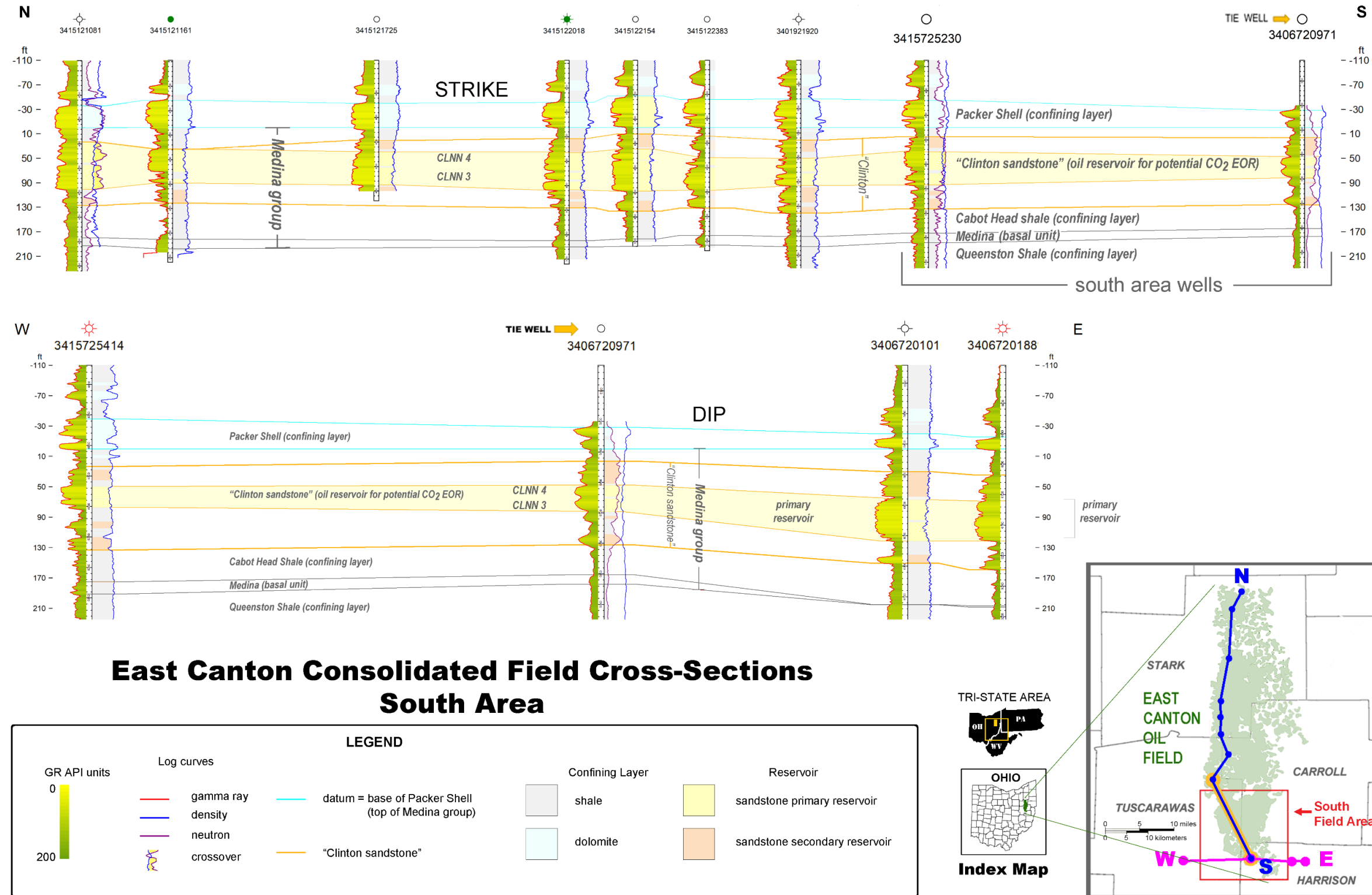


Figure 6-26. N-S strike section shows that clean CLNN 4 and CLNN 3 intervals thin and become more shaley at the southern terminus of the field. Dry holes separate the thin reservoir unit from thicker sandstones downdip to the east, suggesting the presence of good lateral stratigraphic seals. The sandstone character does not change in the updip direction, but legacy wells (see Figure 6-30C) transition from mostly oil producers to gas producers moving updip.

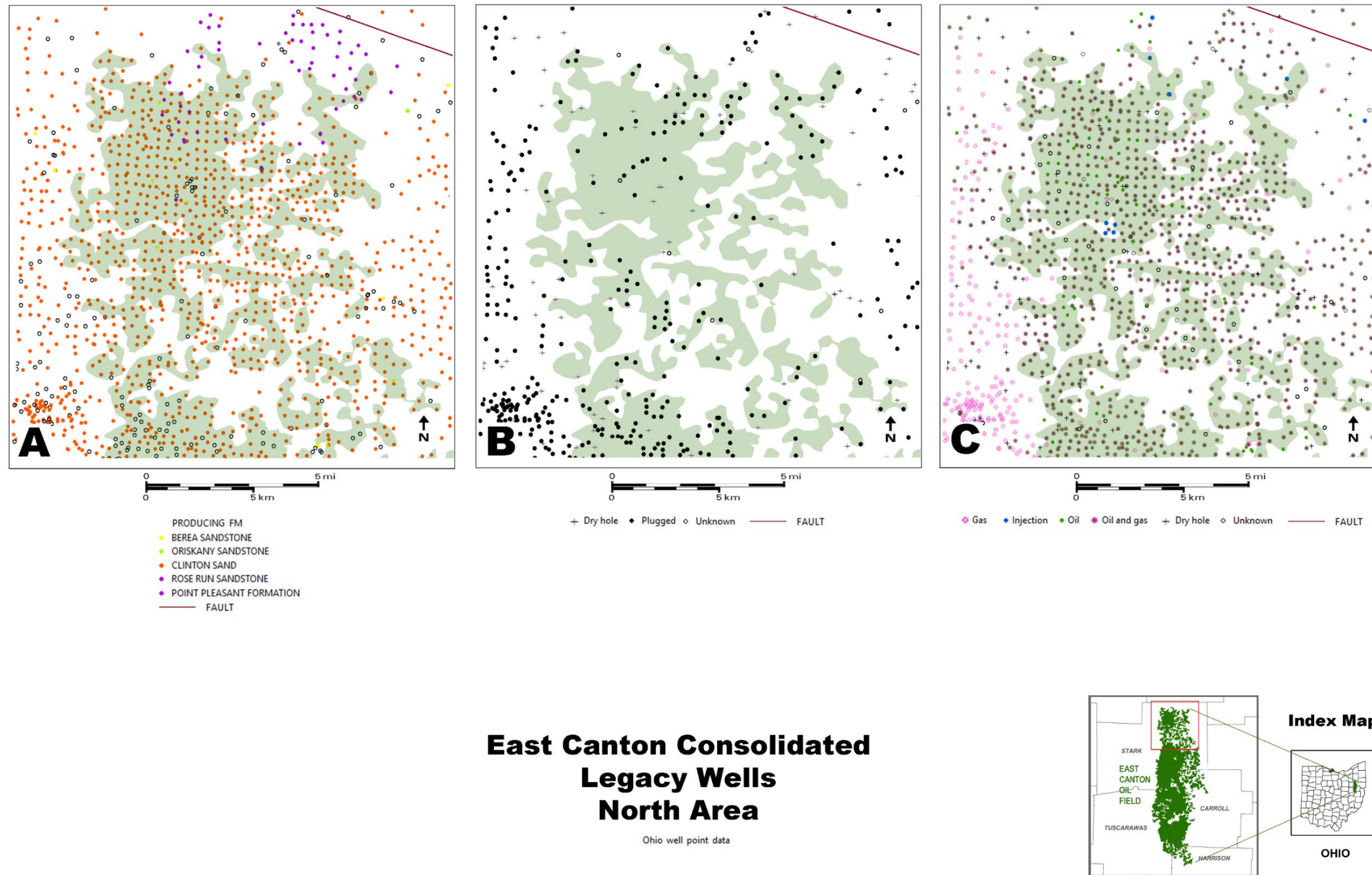


Figure 6-27. Legacy wells in the north area of East Canton Consolidated Field. A) Producing formation – Most wells produce from the “Clinton” sandstone (orange). Rose Run producers (purple) at top right of map indicate a stacked opportunity (see Section 6.5.5). B) Plugged wells and dry holes – Several dry holes at right edge of field may indicate increasing water saturation and decreasing permeability in the “Clinton” downdip area, forming a lateral seal. C) Well type – Water injection wells (blue) indicate beginning of secondary recovery operations in this field. Gas-oil contact in the “Clinton” sandstone is visible at the western edge of the field.

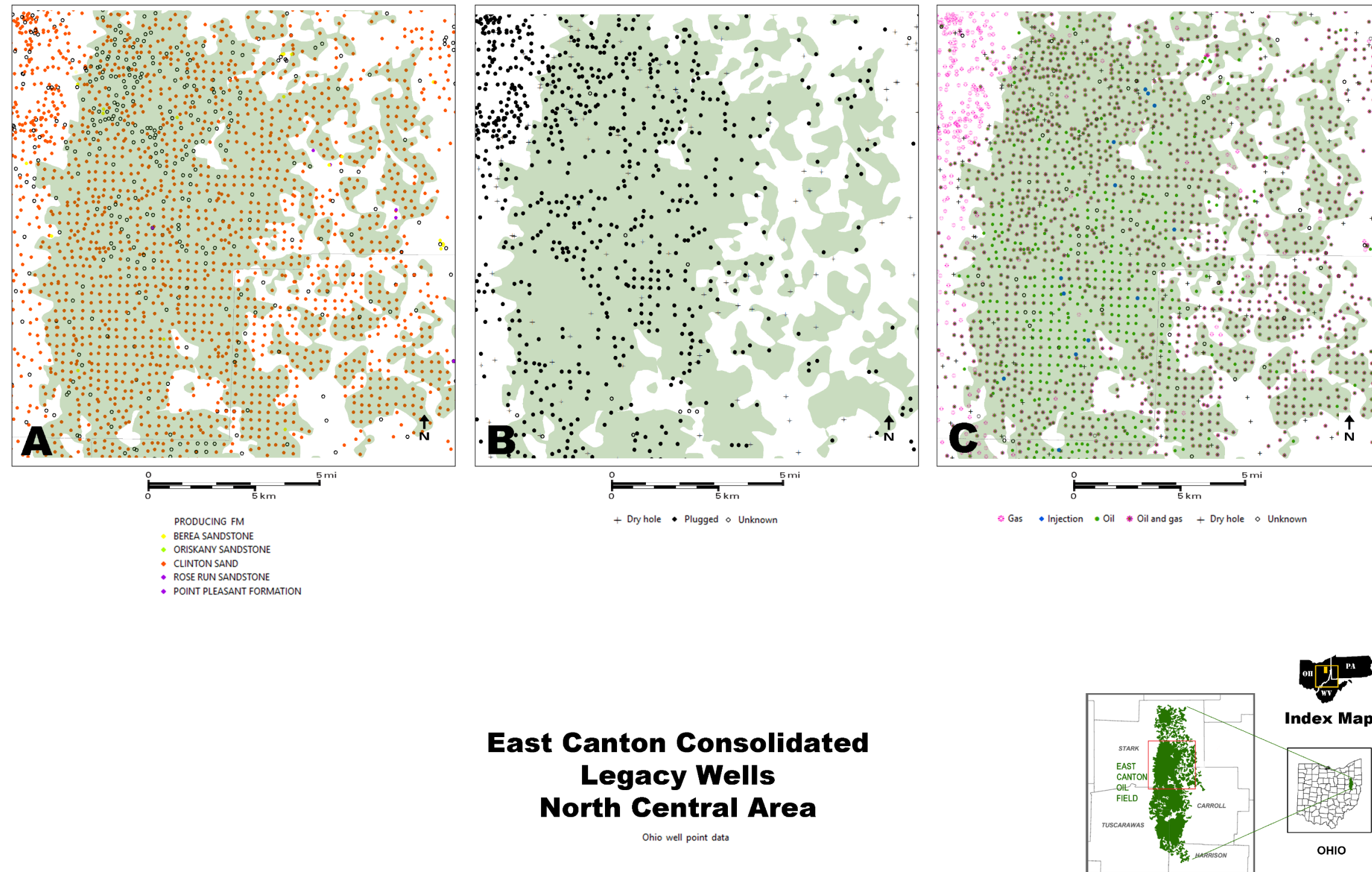
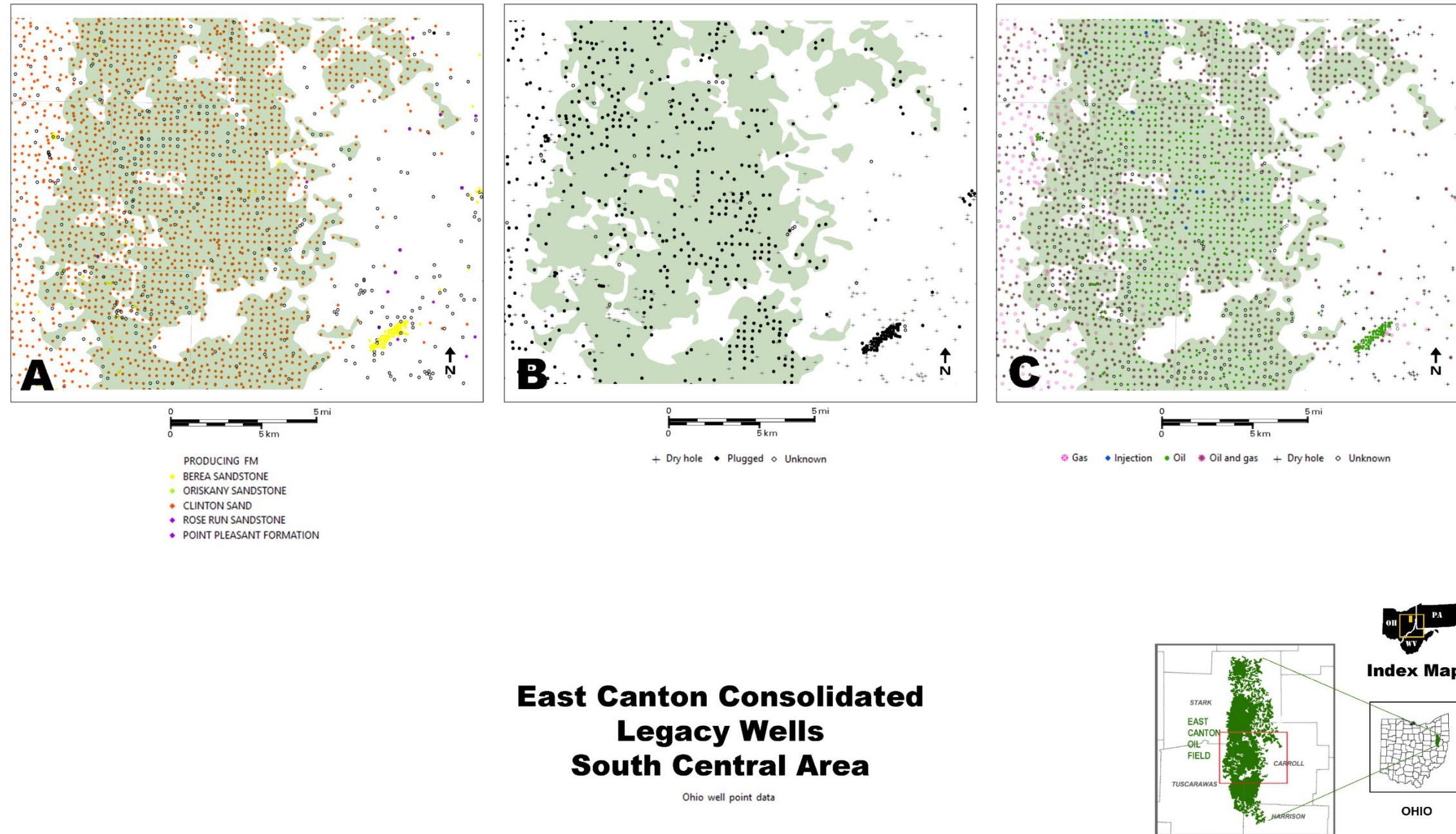


Figure 6-28. Legacy wells in the north-central area of East Canton Consolidated Field. A) Producing formation – A majority of wells produce from “Clinton sandstone” (orange). A handful of deep wells (purple) to the east are Rose Run/Beekmantown producers, representing stacked potential (see Section 6.5.5). A deep well (purple) in the heart of the “Clinton” oil field is producing from the Point Pleasant Formation. B) Plugged wells and dry holes - Forty percent of wells have been plugged. Dry holes mark the eastern field boundary. C) Well type – Note the gas contact to the west and pilot waterflood operations (blue) in the center of the oil field.



East Canton Consolidated Legacy Wells South Central Area

Ohio well point data

Figure 6-29. Legacy wells in the south-central area of East Canton Consolidated Field. This area was studied by Mishra (2015). A) Producing formation – A majority of wells produce from “Clinton” sandstone (orange). Point Pleasant organic-rich shale wells (purple) produce to the east just outside of the field footprint, and maps (see Section 6.5.5) indicate this deeper formation may exist as stacked potential within the field itself. Immiscible shallow Berea oil wells (yellow) inside and outside of the field (gray/green) boundaries exist, although most of these have been plugged. B) Plugged wells and dry holes –Approximately 40 to 50 percent of formerly producing wells have been plugged. Dry holes mark the eastern field boundary, indicating a good lateral seal in the form of porosity, permeability, lithology and structural barriers. C) Well type – Note the gas contact to the west. McCormac et al. (1996) noted poor communication between East Canton and Canton Consolidated (west) portions of the field. Note the oil wells and limited waterflood operations in the center of the field footprint.

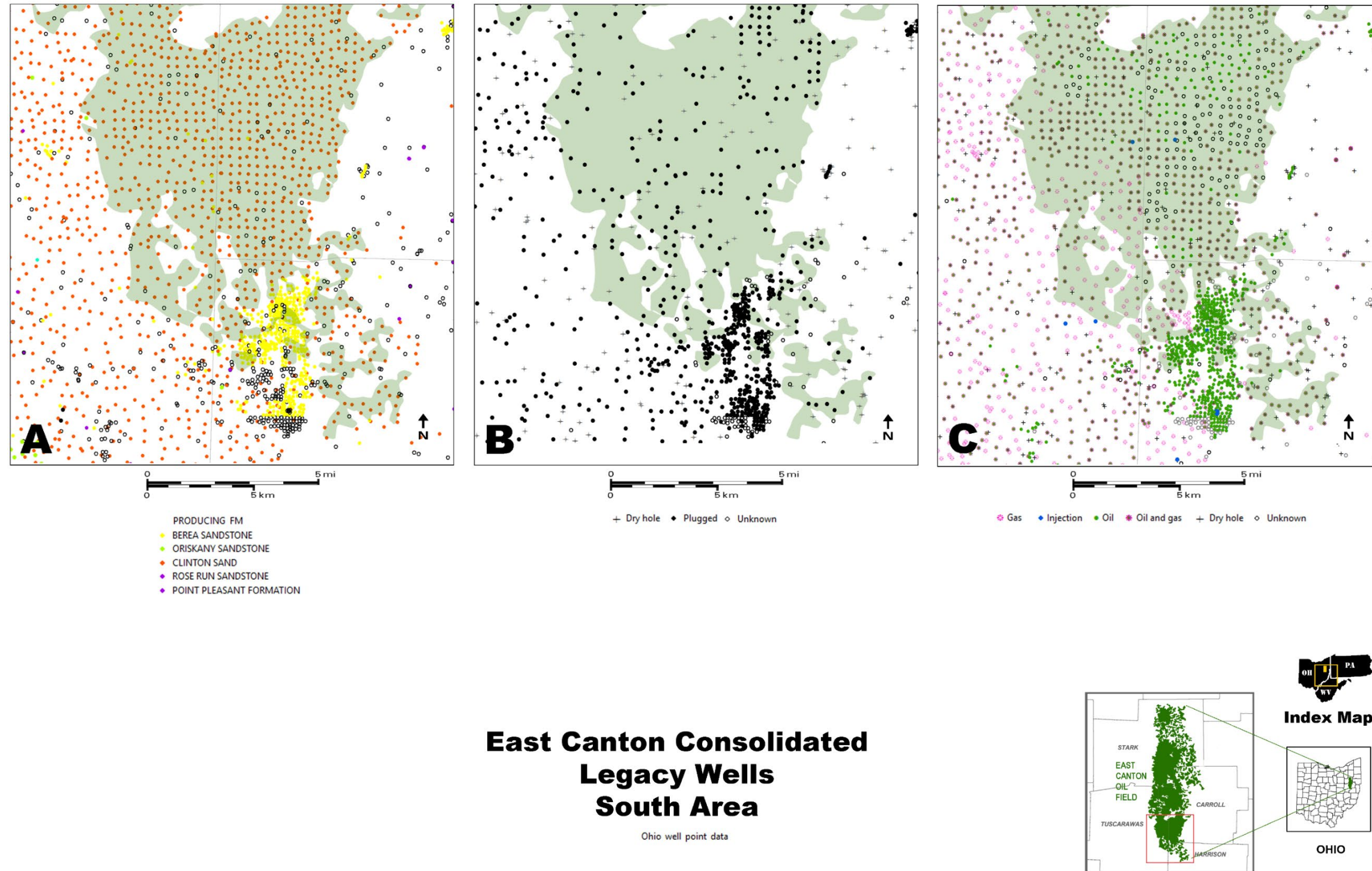


Figure 6-30. Legacy wells in the south area of East Canton Consolidated Field. A) Producing formation – A large, immiscible shallow Berea Sandstone oil field has been mostly plugged to the south. Most wells within the field are producing or have produced from “Clinton” sandstone (orange). Organic-rich shale wells targeting the Point Pleasant Formation (purple) produce to the east of the field footprint. B) Plugged wells and dry holes – Dry holes mark the eastern boundary, as in the other areas of the field, but also wrap around to the south and partially to the west, marking the field terminus. C) Well type – Most oil producers occur in the eastern half of the field, with combination oil and gas wells grading into the gas contact (Canton Consolidated Field) updip to the west.

6.4.4 Clayton and Philo Consolidated Fields

6.4.4.1 Production and Status

The 50,000-ac Clayton Consolidated Field, discovered in 1910, has produced 14 MMBLS oil from the “Clinton” sandstone with an OOIP of 197 MMBLS, which represents a primary recovery of 7 percent. The 165,000-ac Philo Consolidated Field, discovered in 1928, has produced 19 MMBLS oil from the “Clinton” sandstone (Figure 6-31) with an OOIP of 326 MMBLS, representing 6 percent primary recovery. Poor primary recovery efficiency, as in the case of both fields, makes them promising candidates for CO₂-EOR, as much oil remains to be produced and therefore, much pore space remains for associated storage of CO₂.

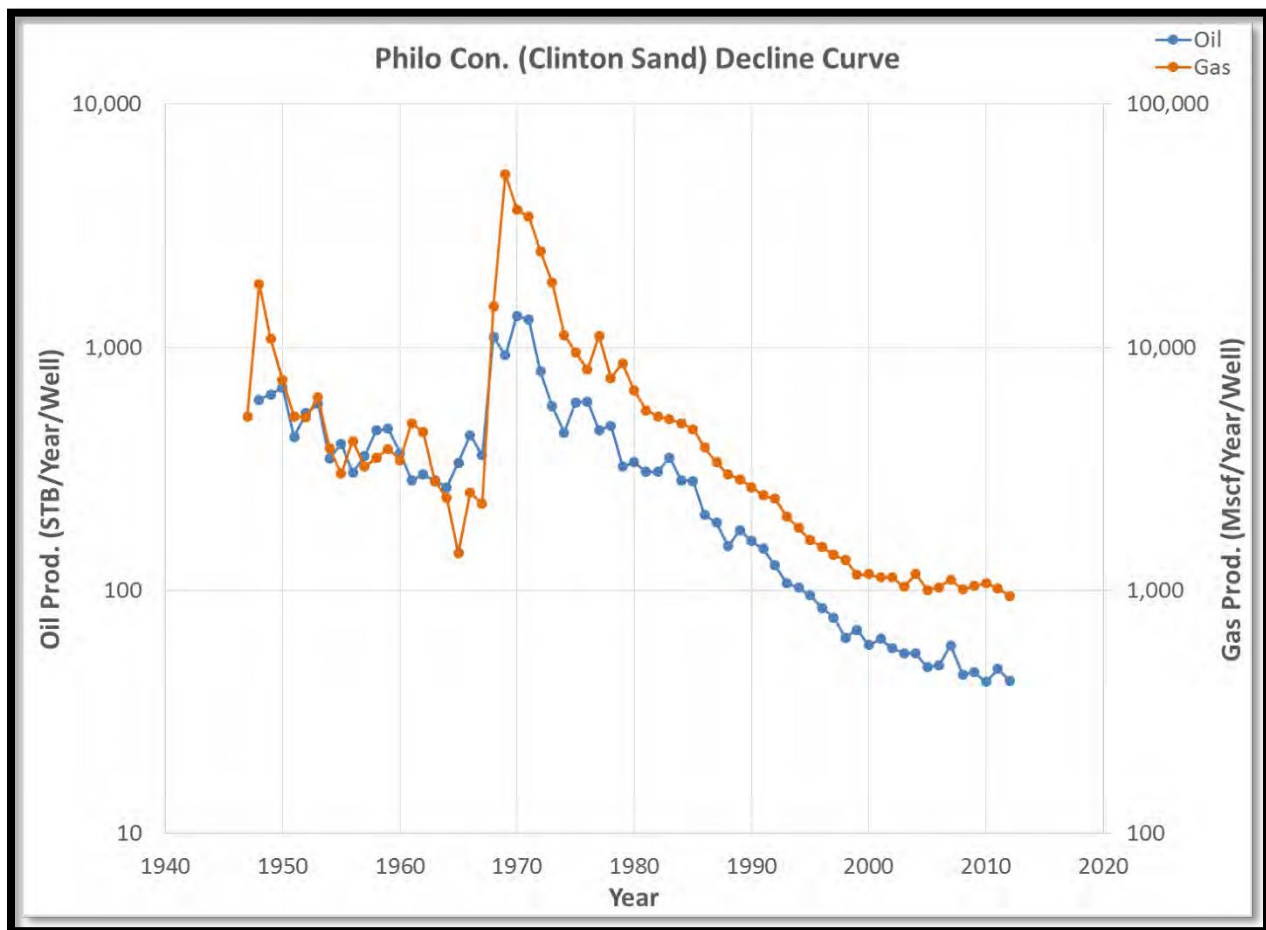


Figure 6-31. Production decline curve for the Philo Consolidated Field, from Mishra (2014) indicates secondary recovery operations starting in the mid-1960s.

Another consideration for CO₂-EOR is the relationship between initial pressure (IP), which relates to depth, and MMP of CO₂ in that reservoir. The higher the IP and lower the MMP, the more CO₂ may be stored. During carbon storage, ambient pressure of a depleted reservoir is raised toward its IP, therefore, IP provides an upper limit to pressure that can be achieved (Mishra, 2014). Producing from an average depth of 3230 ft, the Clayton Consolidated Field has a reported pressure of 1100 psi with MMP at 967 psi and formation temperature of 90°F. Producing from an average depth of 4650 ft, the Philo Consolidated Field has a reported pressure of 1400 psi, with MMP at 1155 psi and formation temperature of 100°F (Lewis et al.,

2019). Reported pressure-at-depth values may not represent IPs in older fields, as this measurement may be acquired at some point after discovery. Calculated IPs are higher (i.e., 1399 psi for Clayton Consolidated and 2013 psi for Philo Consolidated) than reported pressures in Lewis et al. (2019), closely following the upper bound linear regression trend IP in Figure 6-32 calculated by Mishra (2014).

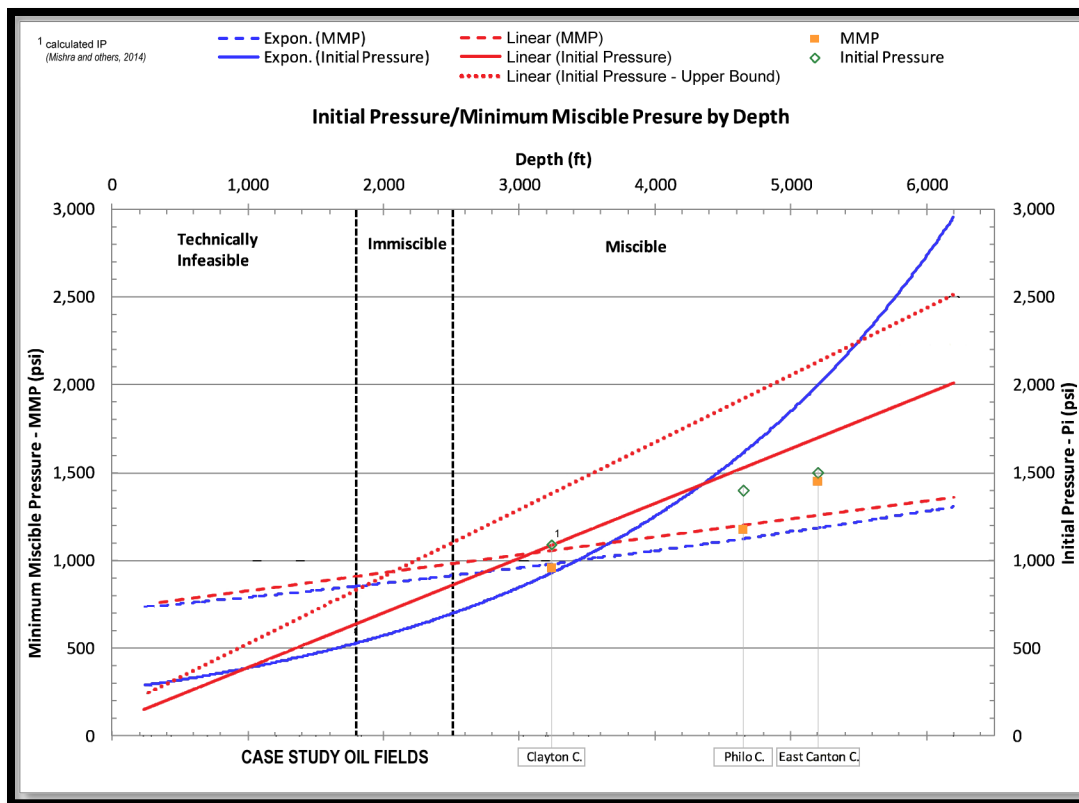


Figure 6-32. IP and MMP for the case study fields in Ohio. Linear and exponential IPs and MMPs are graphed. Calculated IPs from Lewis et al. (2019) correlate well with the upper bound IP of Mishra (2014).

6.4.4.2 Structural and Stratigraphic Framework

The measured depth to the top of the “Clinton” sandstone within and between the Clayton and Philo Consolidated fields is mapped in Figure 6-33. Measured depths range from 2400 ft (i.e., just below the miscible depth of CO₂ at 2500 ft) in the western fringe of Clayton Consolidated Field to 5400 ft at the eastern edge of Philo Consolidated Field. These fields, developed prior to hydraulic fracturing, were discovered in a narrow zone parallel to the updip pinchout in central Ohio. They tend to delineate trends of maximum porosity and permeability (McCormac et al., 1996).

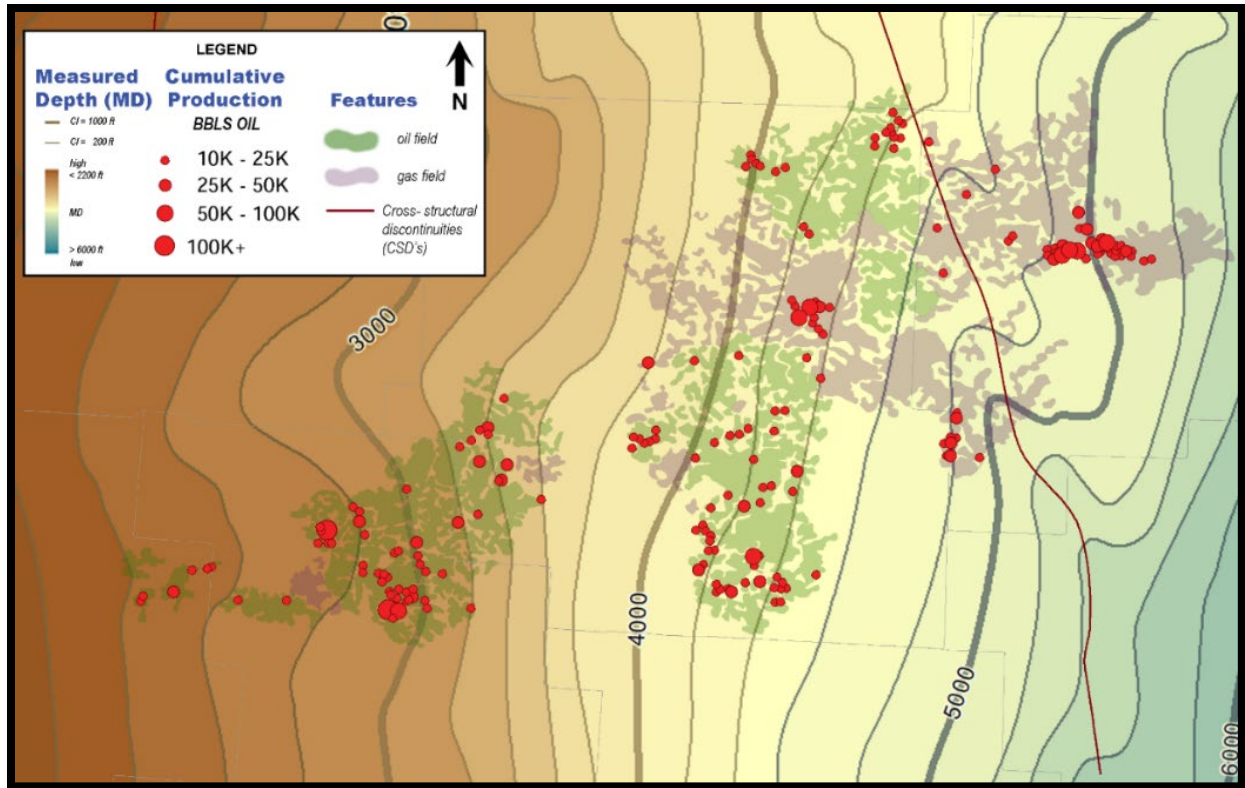


Figure 6-33. Measured depth to the top of the “Clinton” sandstone in Clayton and Philo Consolidated fields (MRCSP database). Cumulative oil production bubble map indicates possible structural influence along the Cambridge CSD (dark red line).

Mishra (2014) reported net average pay thicknesses of 27 ft in Clayton Consolidated Field, with average porosity and oil saturation values of 9 and 38 percent, respectively. The Philo Consolidated Field has similar reservoir characteristics, with an average pay thickness, porosity and oil saturation values of 20 ft, 7 percent and 40 percent, respectively. A net sand thickness map was prepared using available geophysical log data, using a sand cutoff of 75 API and RHOB cutoff of 2.6 g/cm³ (Figure 6-34).

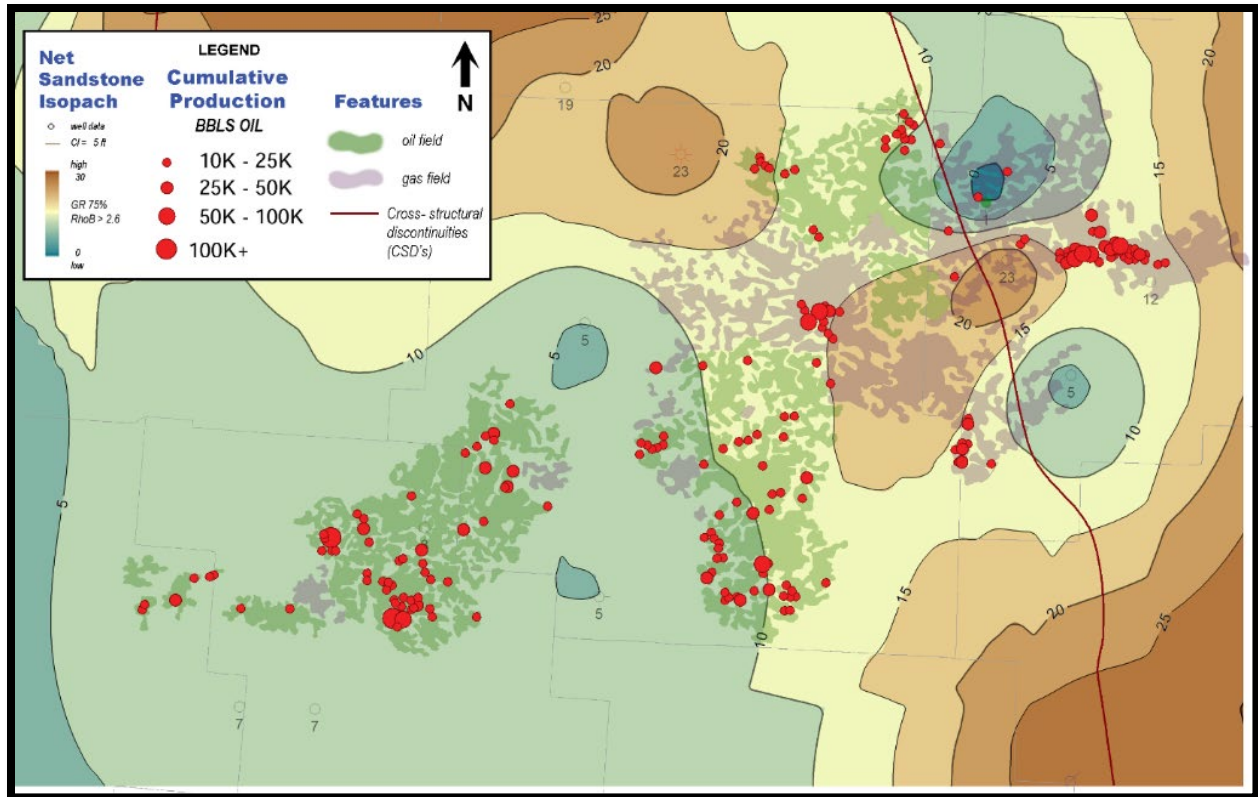


Figure 6-34. Net clean sandstone thickness map of the “Clinton” sandstone in Clayton and Philo Consolidated fields (MRCSP database). Cumulative oil production bubble map may be indicative of thicker, cleaner and/or more permeable sandstones. Note that some of the higher cumulative production occurs in gas-prone areas (purple).

Comparison of Figure 6-34 to the gross interval thickness map in Figure 6-6 reveals that isolated, locally thick buildups of sandstone occur in proximity to the updip pinchout of the “Clinton” to the west. As this pinchout represents the farthest westward progradation of the “Clinton” deltaic clastic wedge, the buildups may be the result of wave action as the sea transgressed over the shoreline, truncating the sands and leaving isolated deposits where thicker sands (such as a distributary channel) may have been preserved below wave base. Conversely, these buildups could represent sequence stratigraphy as described by May (2019), whereby sands accumulate both along the shelf margin and toward the bottom of the delta slope in the same time horizon. These time horizons may contribute to discrete permeability changes within the prograding sand body that may not be evident from the lithostratigraphy. Proximity to the sandstone pinchout creates a good lateral and vertical trap. These older fields, which pre-date modern stimulation techniques, also have relatively higher porosity and permeability than more recently developed conventional reservoirs. Combined with less efficient extraction methods, this results in ample pore space volume and remaining oil to make CO₂-EOR an attractive option.

Based on the findings of Mishra (2015) and Riley et al. (2011), certain structural control can be inferred from the cumulative oil production bubble map in Figure 6-33. Higher production volumes occur along structural nosing trends in Clayton and Philo Consolidated fields, particularly where they widen and before the contours plunge. An east-west trend of higher production east of the Cambridge CSD along with anomalous changes in gas/oil field designation, which also occur in an east-west trend across the Philo Consolidated Field

(Figure 6-33 and Figure 6-34), may be indicative of structural controls. In a clay-cake Reidel experiment, faults in the overburden are, in fact, secondary structures generally directly rooting down to the preexisting basement fault (Dooley and Schreurs, 2012). Physical clay-cake modelling of strike-slip fault systems using kaolin with water content between 45 to 54 percent yields a structural pattern containing elements similar to both the northwest-southeast trending Cambridge CSD and an apparent east-west fracture system inferred by production. Harper (1989) reported that fields with anomalously heavy oils in northwestern Pennsylvania have been found along lineaments. Another east-west lineament may represent the southern terminus of both fields, with concurrent changes in net sandstone and nosing trends.

6.4.4.3 Area Cross Sections

A southwest-northeast cross section over the northern edge of Clayton Consolidated and Philo Consolidated fields illustrates the “Clinton” sandstone pinchout to the west (Figure 6-35). A similarly oriented cross section from Gore Consolidated Field (to the south) through the central field area illustrates a buildup of locally thick, discontinuous sandstone (Figure 6-36). Such thick, discontinuous sandstone lenses may have been captured with greater log control used by the Mishra (2015) study, thereby increasing the average pay thickness reported for Clayton Consolidated Field. Northwest to southeast cross sections use a closer well spacing to illustrate local continuity of sandstone lenses which helps to trace individual units as they progress from sandy to more shaley facies (Figure 6-37 through Figure 6-39).

6.4.4.4 Legacy Wells

Figure 6-40, Figure 6-41 and Figure 6-42 map legacy well locations by producing formation, well type and non-producing wells (i.e., both plugged wells and dry holes) for the Clayton Consolidated Field, and Figure 6-43 through Figure 6-45 provide similar maps for the Philo Consolidated Field. The Clayton Consolidated Field has 567 producing wells within a footprint of 52,121 ac. Another 2524 wells (plugged, dry or other) have also been identified here, which equates to a total legacy well count of 5242 wells, or 59 wells/1000 ac. The Philo Consolidated Field, with an acreage of 164,962 ac, has 956 producing wells and 2184 additional wells. This equates to a total legacy well count of 3140 wells, or 19 wells/1000 ac.

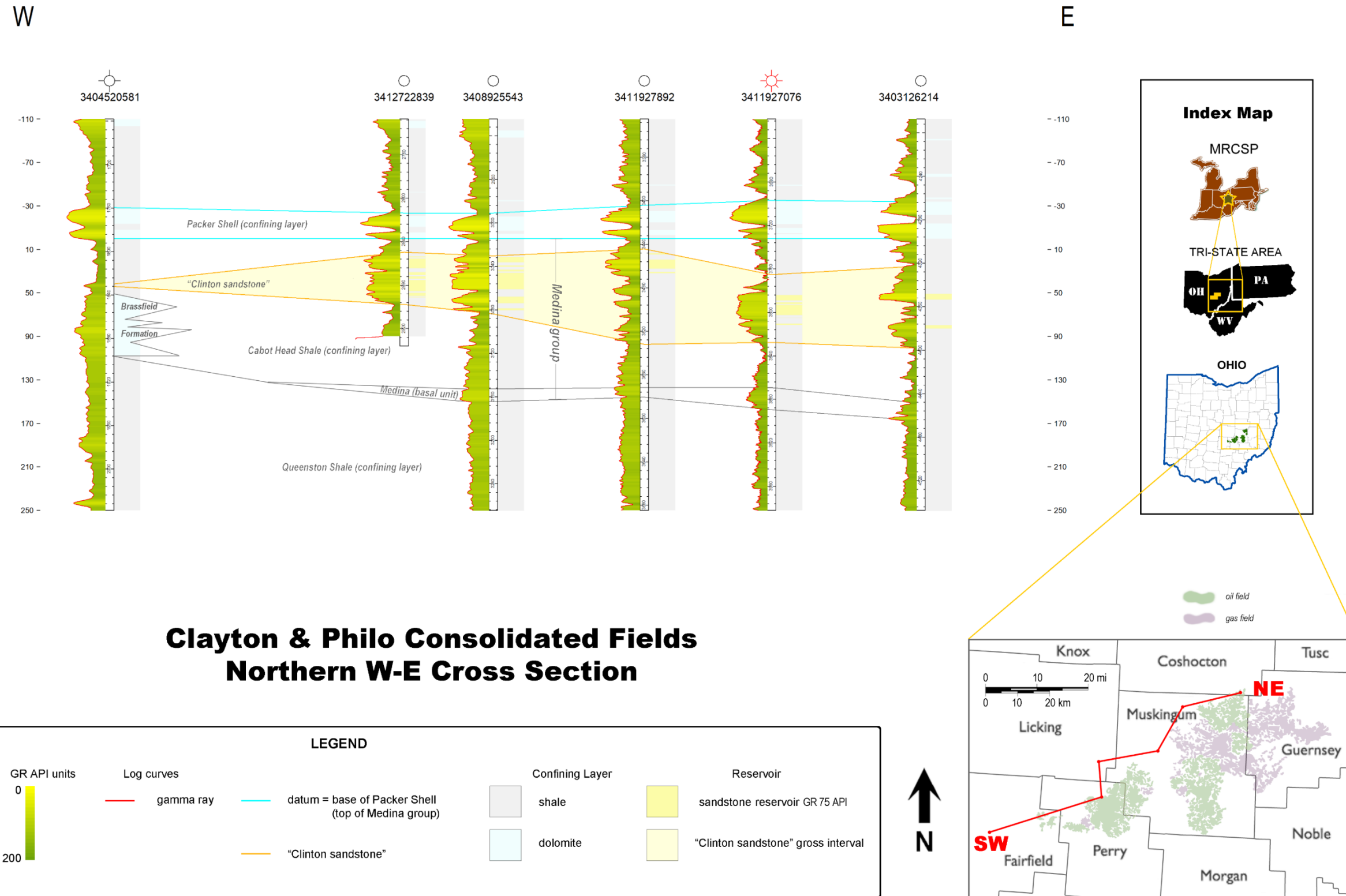


Figure 6-35. Cross section from southwest to northeast over the northern edge of Clayton Consolidated and Philo Consolidated fields, illustrating the "Clinton" sandstone pinchout to the west.

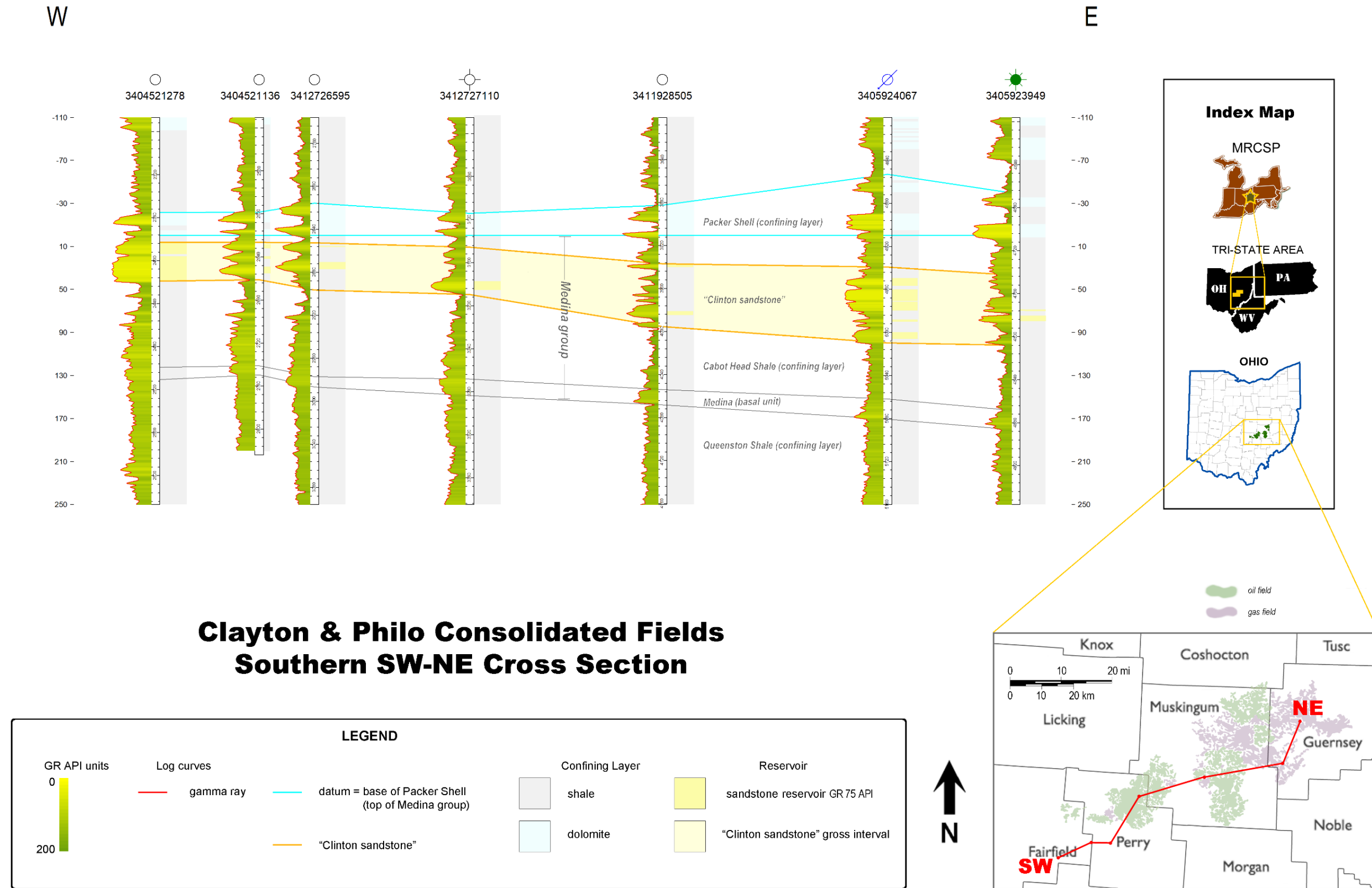


Figure 6-36. Cross section from southwest to northeast through the central field area, illustrating generally thin sandstone lenses with discontinuous, locally thick accumulations of sandstone in some places.

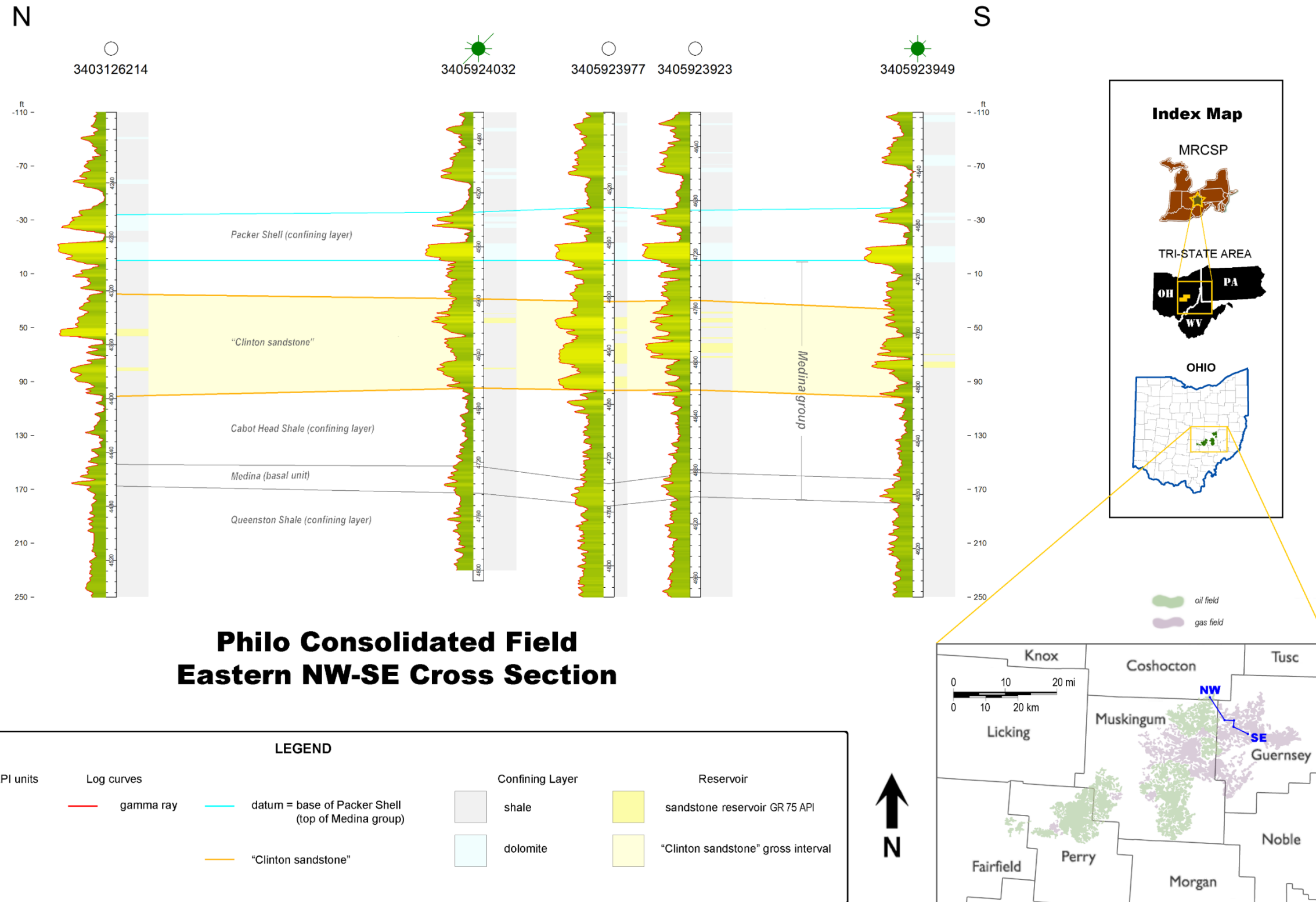


Figure 6-37. Individual "Clinton" sandstone units can be traced as they thicken and thin (and become increasingly sandy or more shaley), using denser well control in this particular cross section.

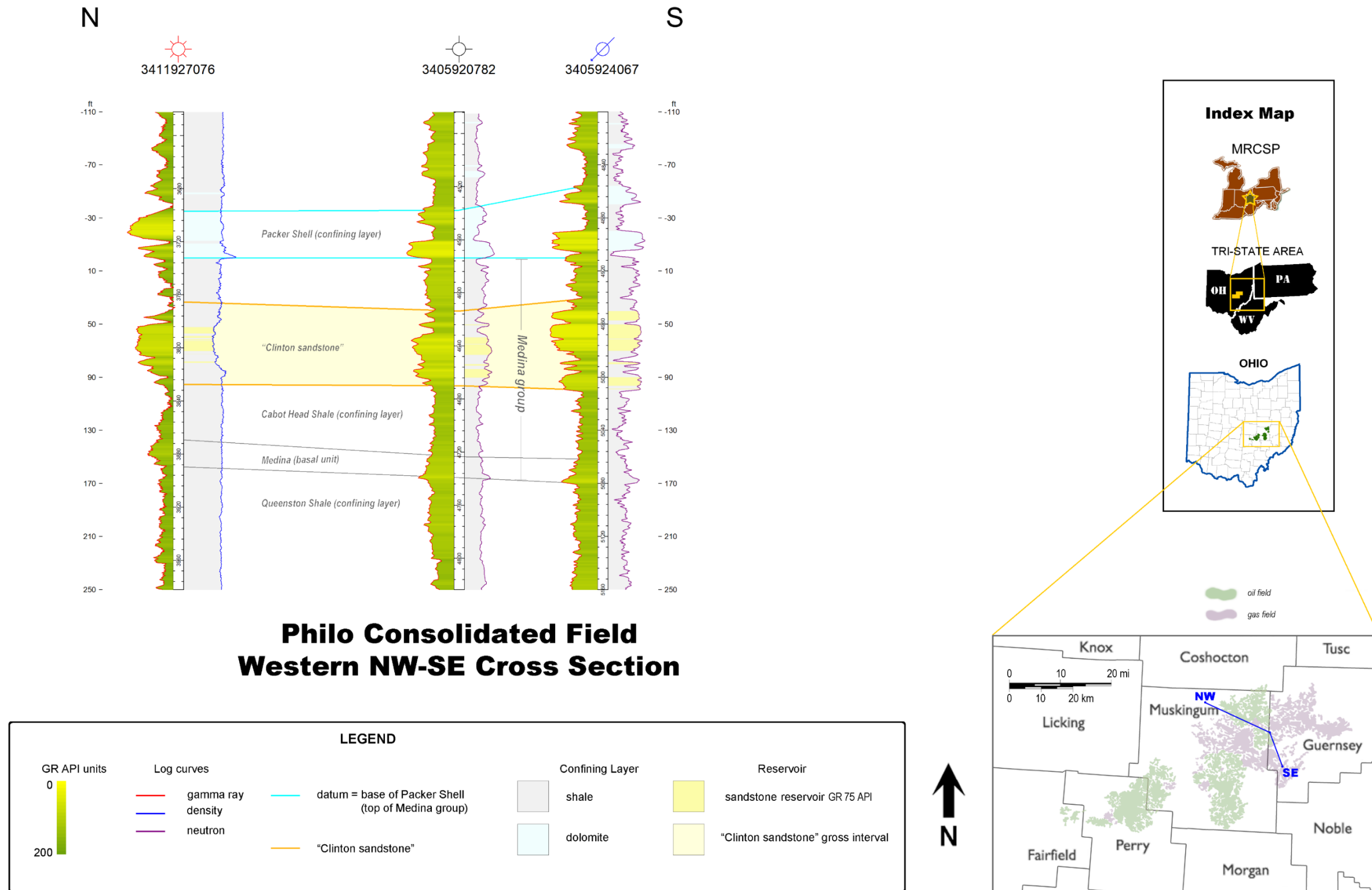


Figure 6-38. Disconnected sandstone bodies, in addition to the structural position and pressure drop during production, may influence the division between oil- and gas-producing areas of the field.

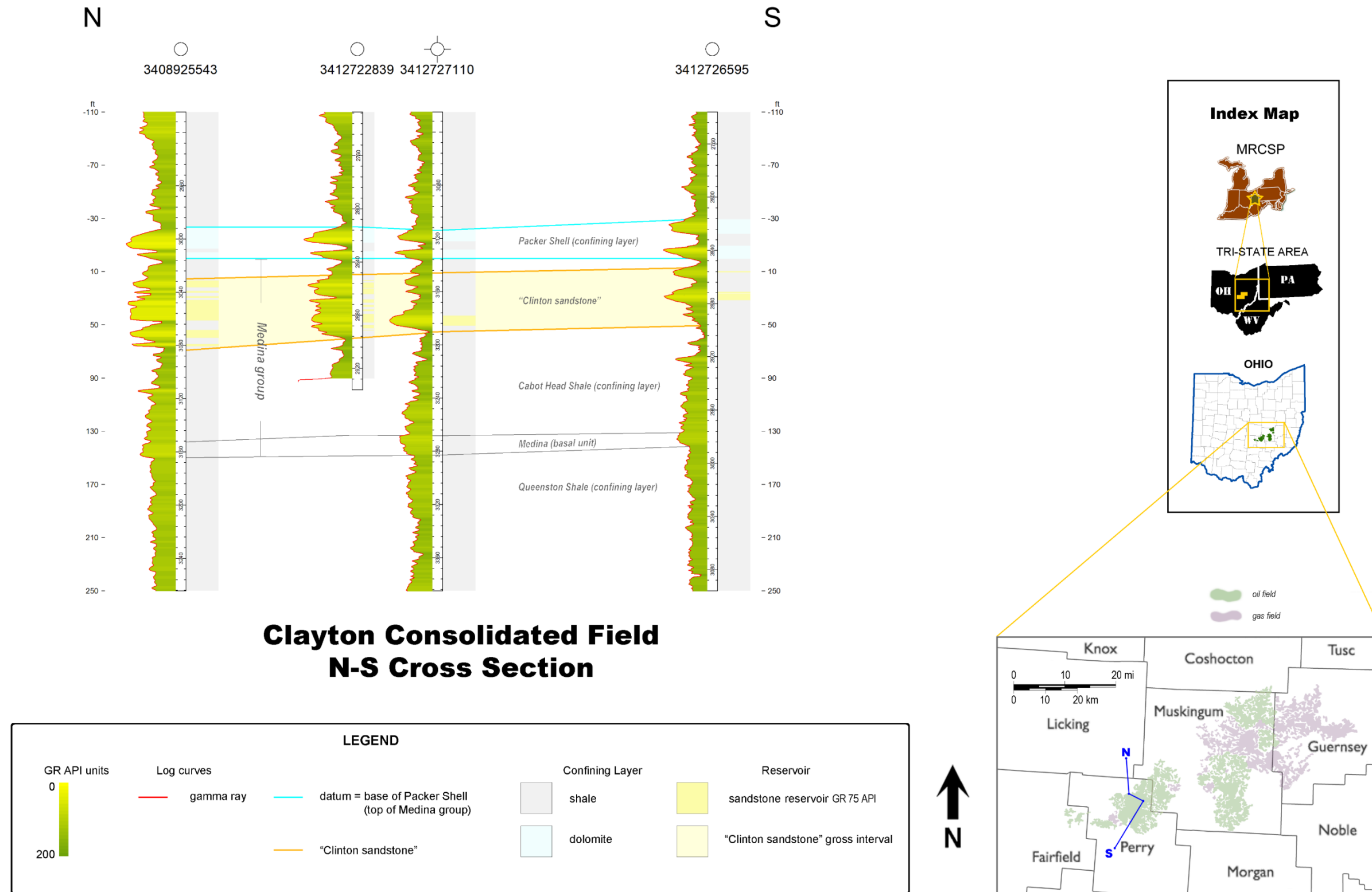


Figure 6-39. Permeability barriers due to structural and diagenetic controls may have influenced field footprints as much as sandstone development (indicated by the GR log signatures).

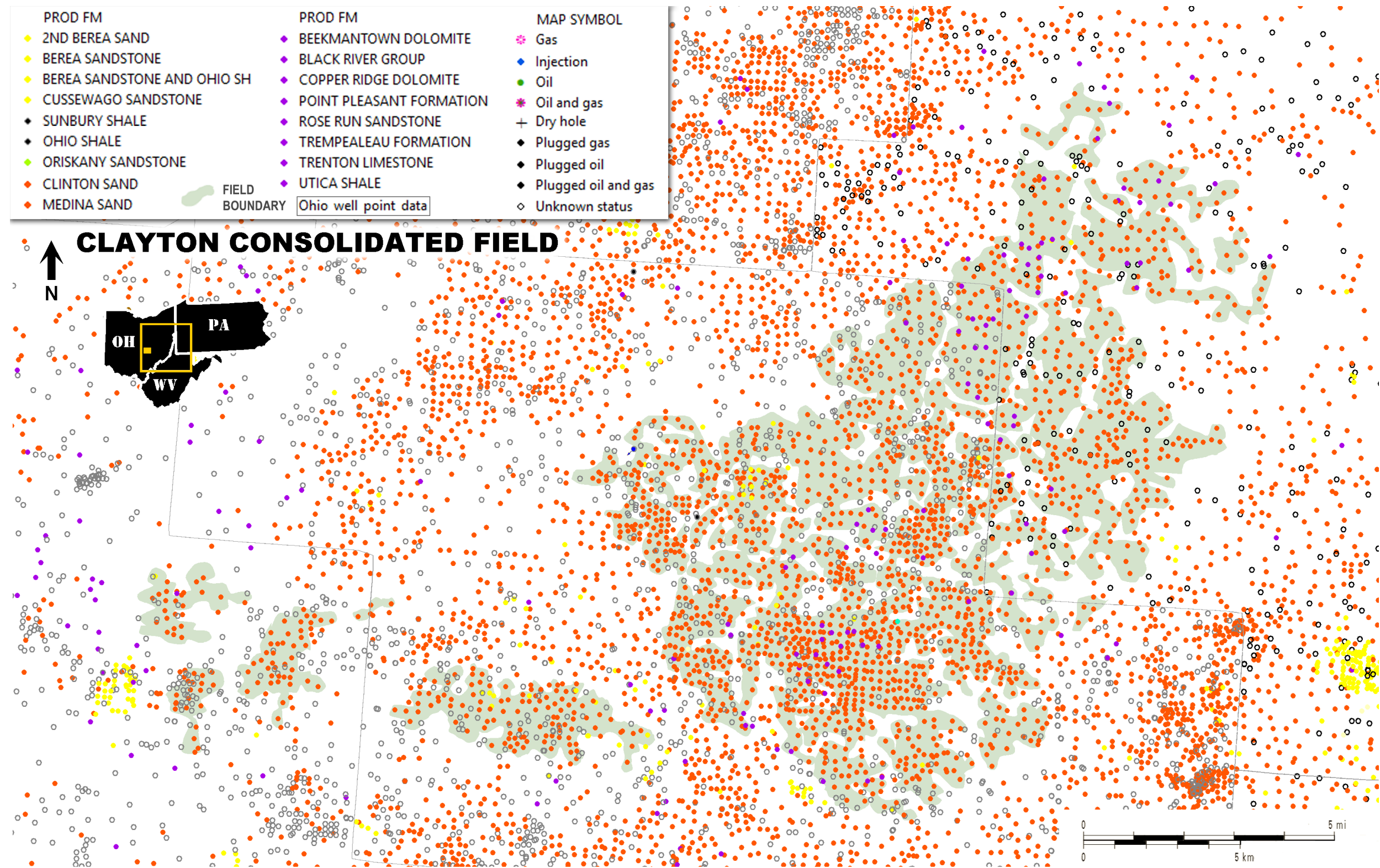


Figure 6-40. The most significant feature of this producing formation legacy well map is relatively large number of wells targeting the Rose Run Formation (purple) both inside and outside the field footprint (Clayton Consolidated Field straddles the Cambro-Ordovician Rose Run subcrop). "Clinton" producing wells are shown with orange dots. Yellow dots represent shallow, immiscible Berea Sandstone producers, and only one injection well (blue) is present.

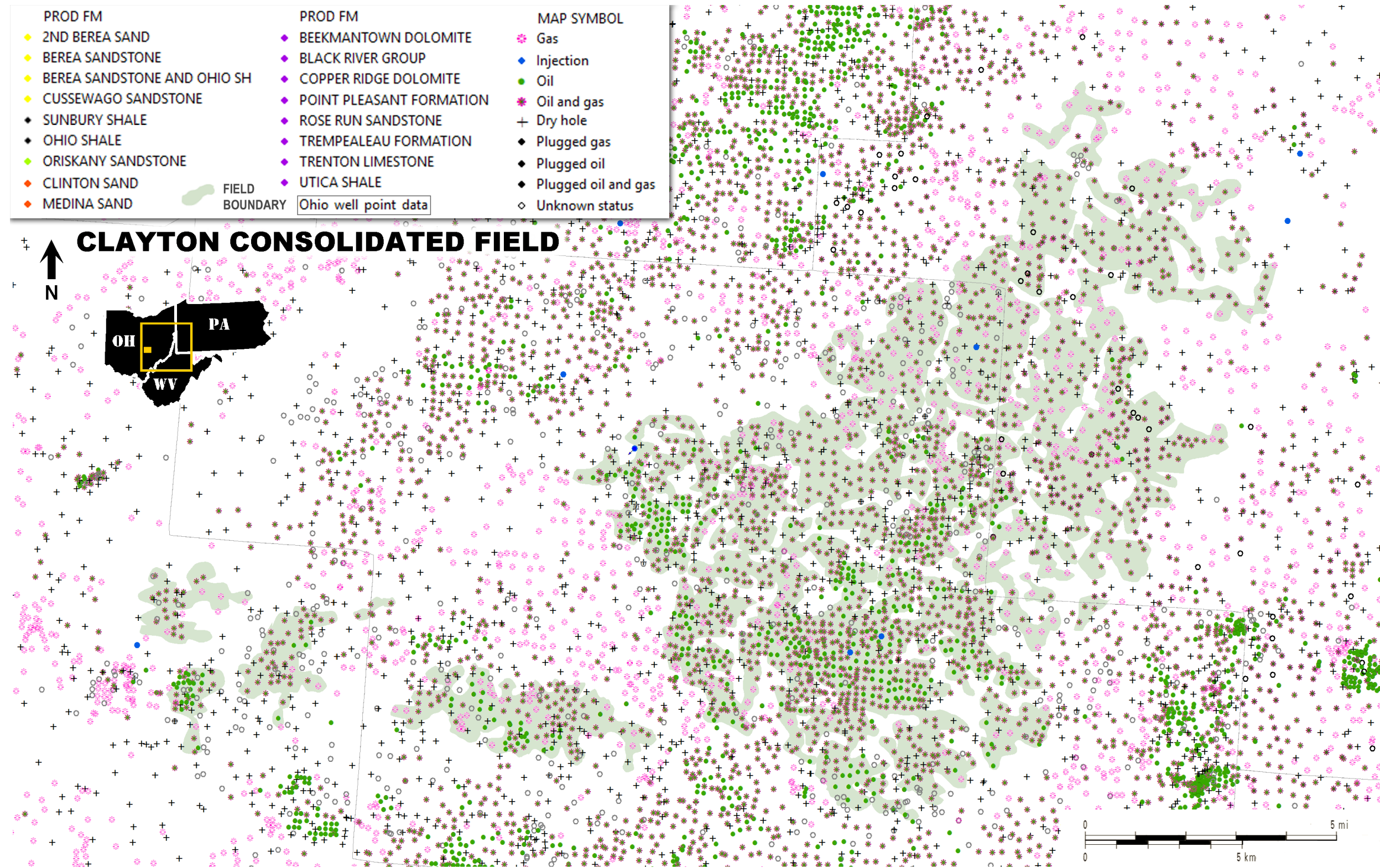


Figure 6-41. From this well type legacy map, the geographic separation between oil producing wells and other types of hydrocarbon production is evident, suggesting that Clayton Consolidated Field may have the trapping mechanisms necessary for CO₂-EOR. Multiple water injection wells (blue) are visible. Shallow, immiscible Berea oil wells are represented by dense masses of green dots.

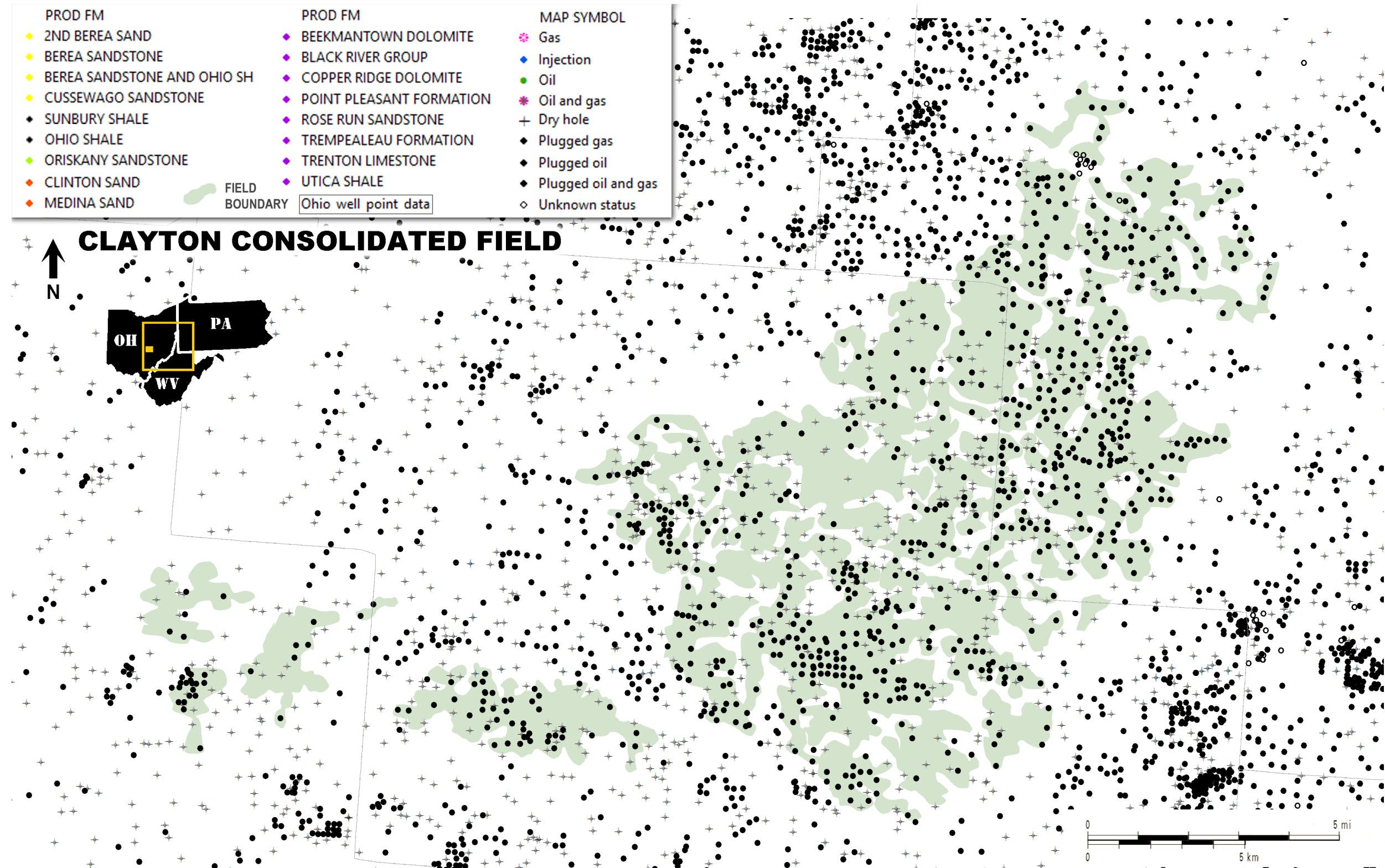


Figure 6-42. Several dry holes exist in the Clayton Consolidated Field, indicative of either the age of these wells (i.e., pre-modern-day stimulation techniques) and/or areas of thin sandstone between thicker, discontinuous lenses. The number of plugged wells relative to producing wells is quite high, especially in some of the oil producing areas. Nearly all shallow Berea Sandstone wells have been plugged.

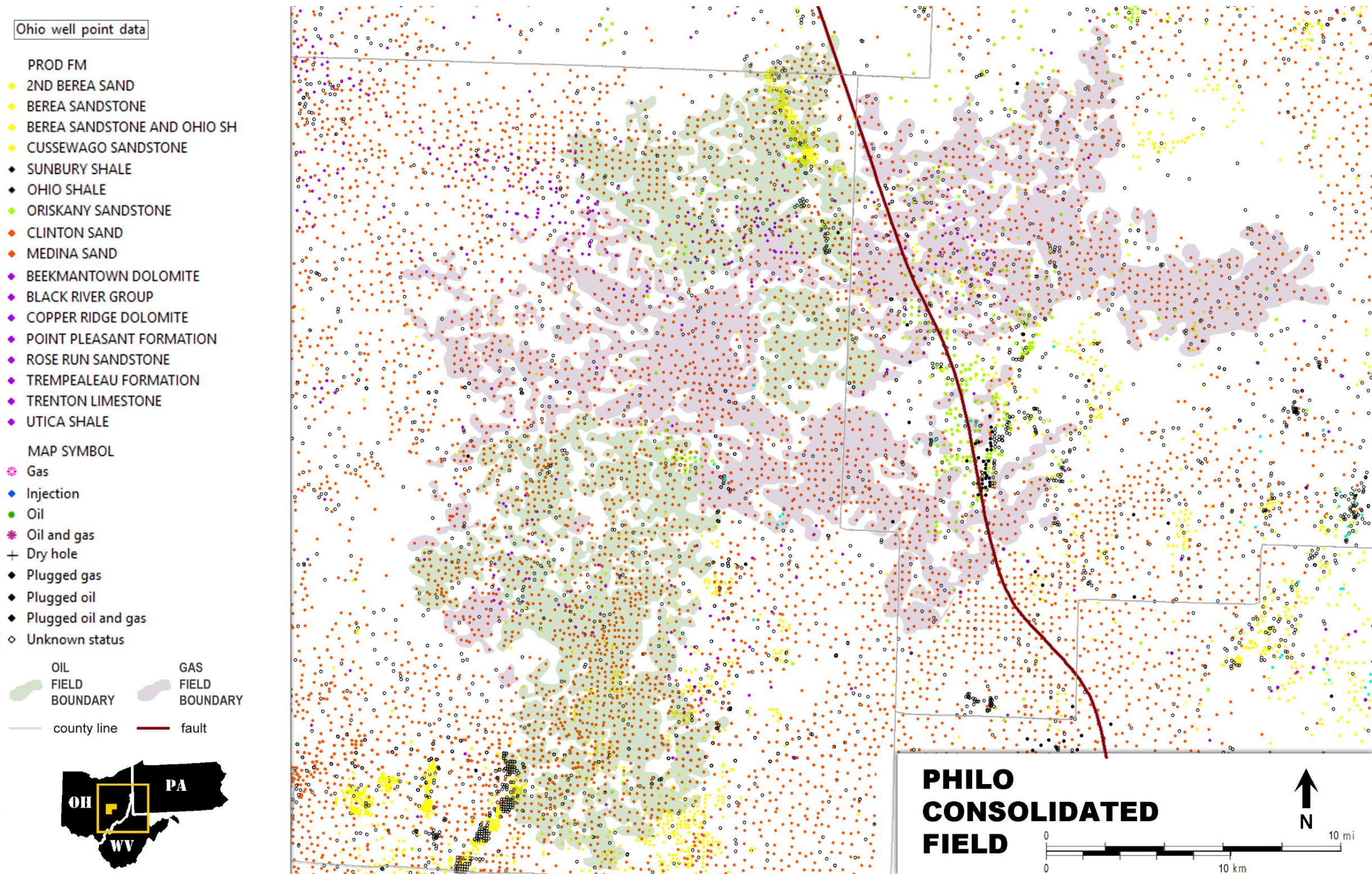


Figure 6-43. The producing formation legacy well map shows several wells targeting the Rose Run or Beekmantown formations along a west/north-east to east/southeast trend that also corresponds to some Oriskany Sandstone wells and to the divisions between oil and gas footprints in the “Clinton” sandstone. This strongly suggests the presence of a major structural feature (possibly a wrench fault because of the lack of visible throw; see Figure 6-33). There are also several wells targeting the Oriskany along the Cambridge CSD. Shallow, immiscible Berea Sandstone wells are present in thin, well-defined bands.

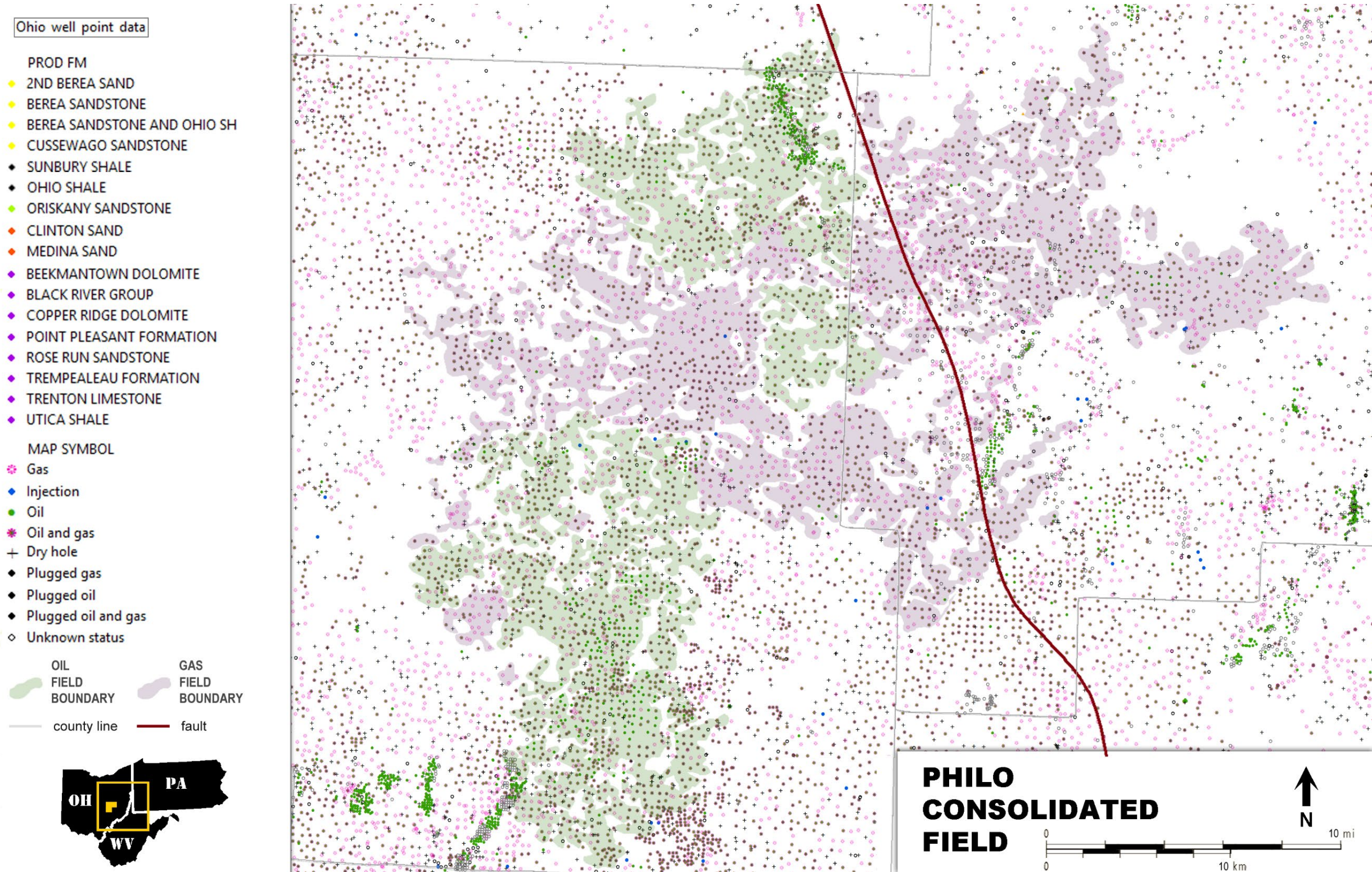


Figure 6-44. This well type legacy map shows most of the current “Clinton” oil producers to be in the southern portion of Philo Consolidated Field. Gas-prone areas have many gas wells, but oil, gas and combination oil and gas wells are present in both the oil and gas field footprints. The shallow Berea wells are primarily oil wells. A few, isolated injection wells are visible.

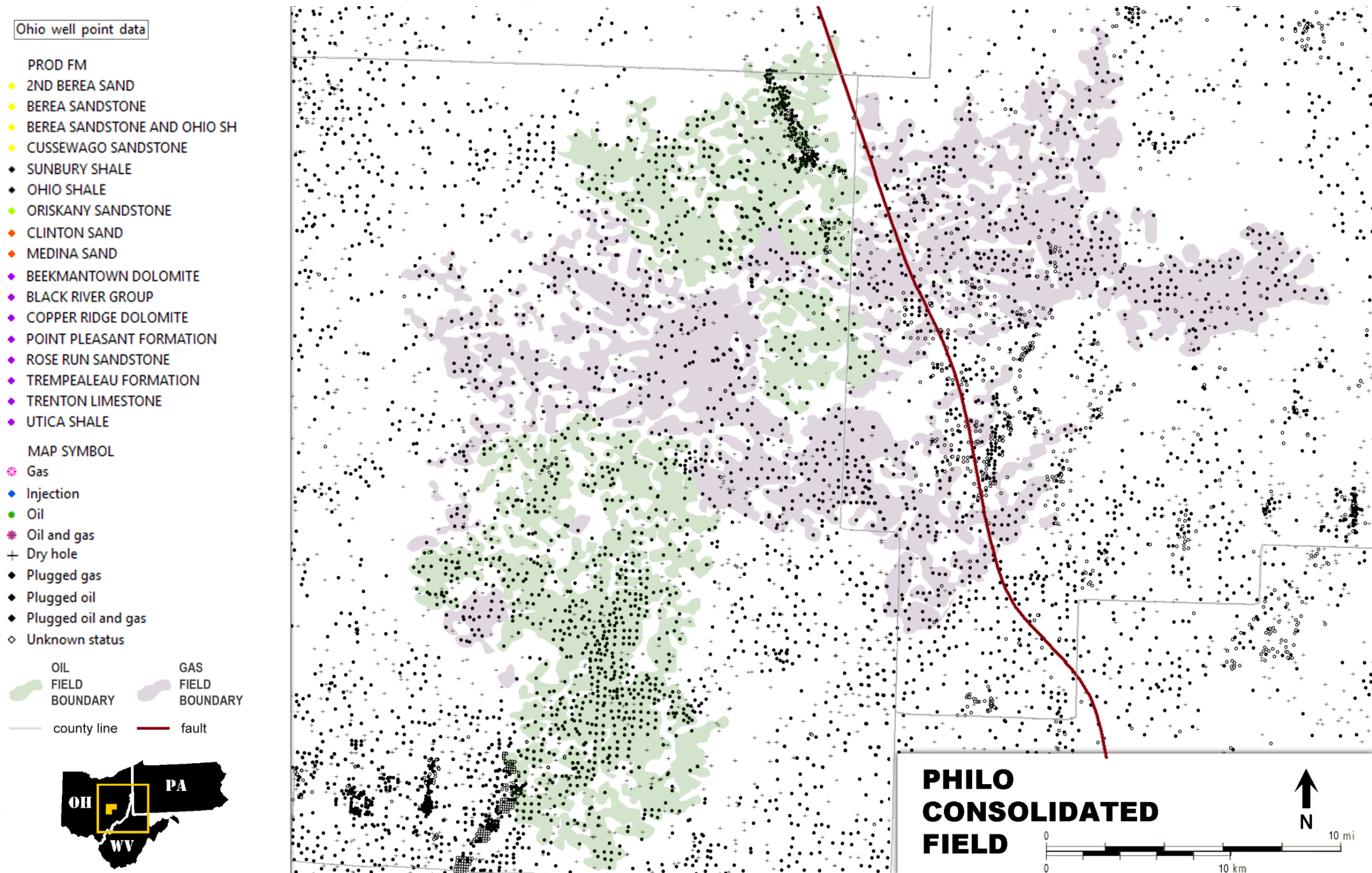


Figure 6-45. This map of plugged wells and dry holes illustrates that dry holes occur with greater frequency around the margins of Philo Consolidated Field. However, there are also several producing “Clinton” wells of the same well type (mostly combination oil and gas wells) connecting this field to adjacent fields, such that trap integrity would have to be carefully evaluated. The highest cumulative oil producers in the gas footprint, which all occur in a narrow west-east trend, have been plugged. It is unclear whether oil production in this case was entirely associated with fracture permeability or whether matrix permeability also exists. Most oil wells in the oil footprints of this field have also been plugged, which may require additional drilling or possibly horizontal drilling access to the “Clinton” sandstone for CO₂-EOR.

6.4.5 Stacked Opportunities

In addition to oil reservoirs which may benefit from CO₂-EOR, the stratigraphic section between 2500 and 10,000 ft has several thousand feet of seals or barriers to keep CO₂ from migrating out of zone, along with a handful of formations which may function as reservoirs to store CO₂, either in pore spaces of depleted natural gas reservoirs or saline formations or adsorbed onto organic-rich shales. Where stacked above and below oil fields used in the case studies reported herein, these formations represent potential additional CCUS opportunities (Figure 6-46 through Figure 6-48).

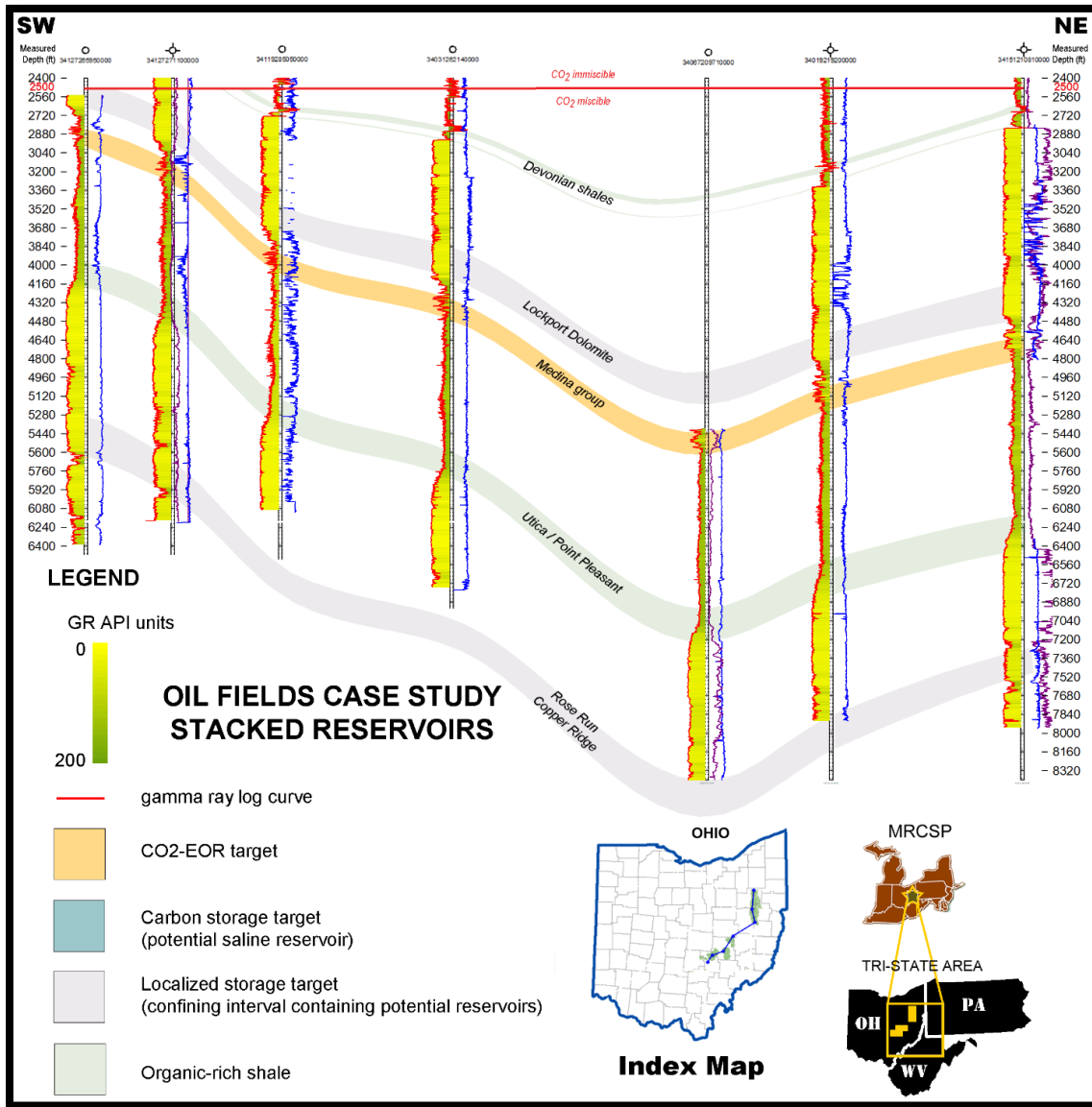


Figure 6-46. Stacked opportunities for CCUS occur above and below the “Clinton” sandstone (orange) from Cambro-Ordovician carbonates and sandstones through organic-rich Devonian shales. Southwest-northeast cross section runs from Clayton and Philo Consolidated fields to East Canton Field.

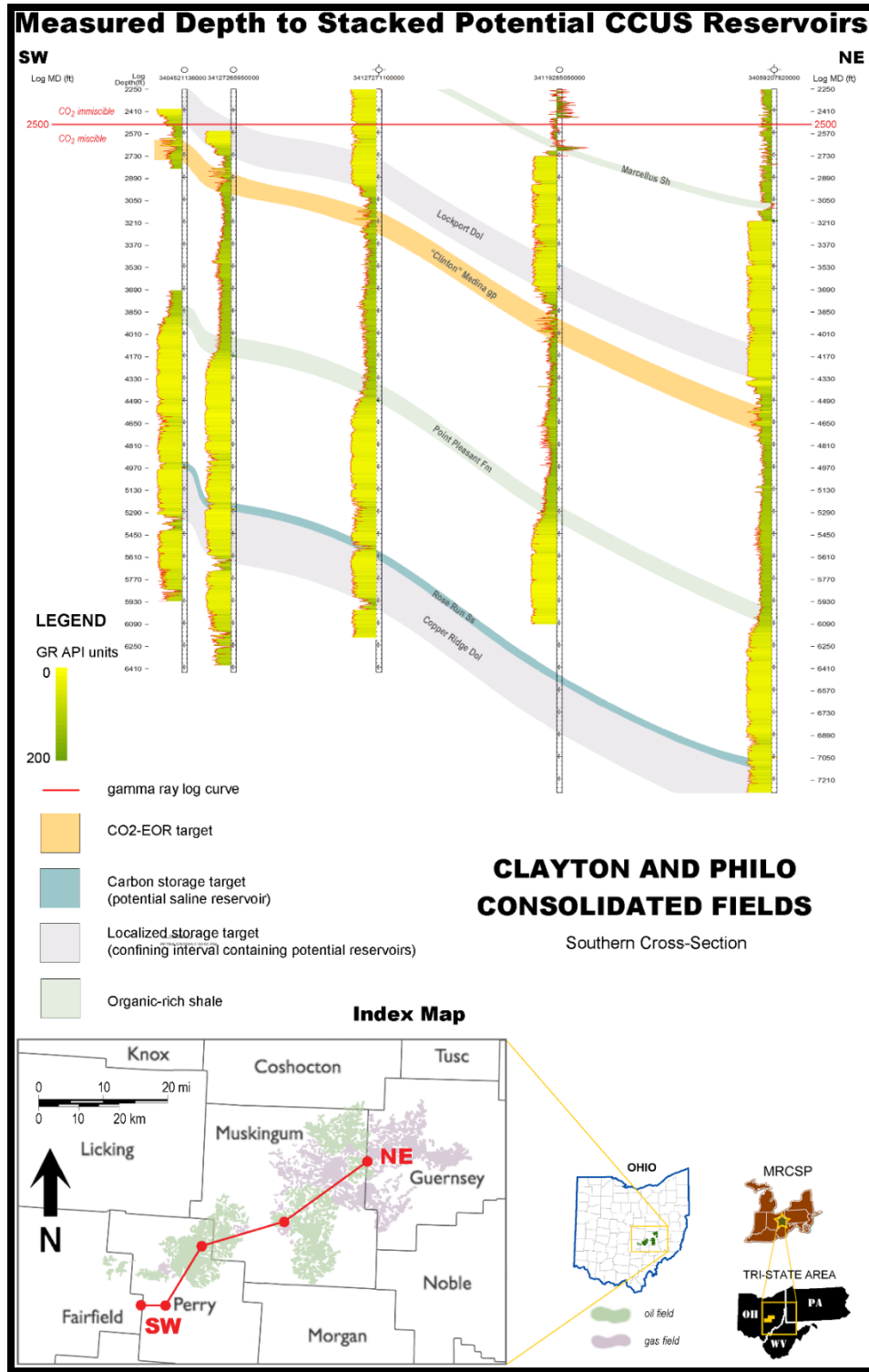


Figure 6-47. Cross section through the center of the Clayton and Philo Consolidated fields, illustrating stacked formations with CO₂-EOR and CCUS potential in this area.

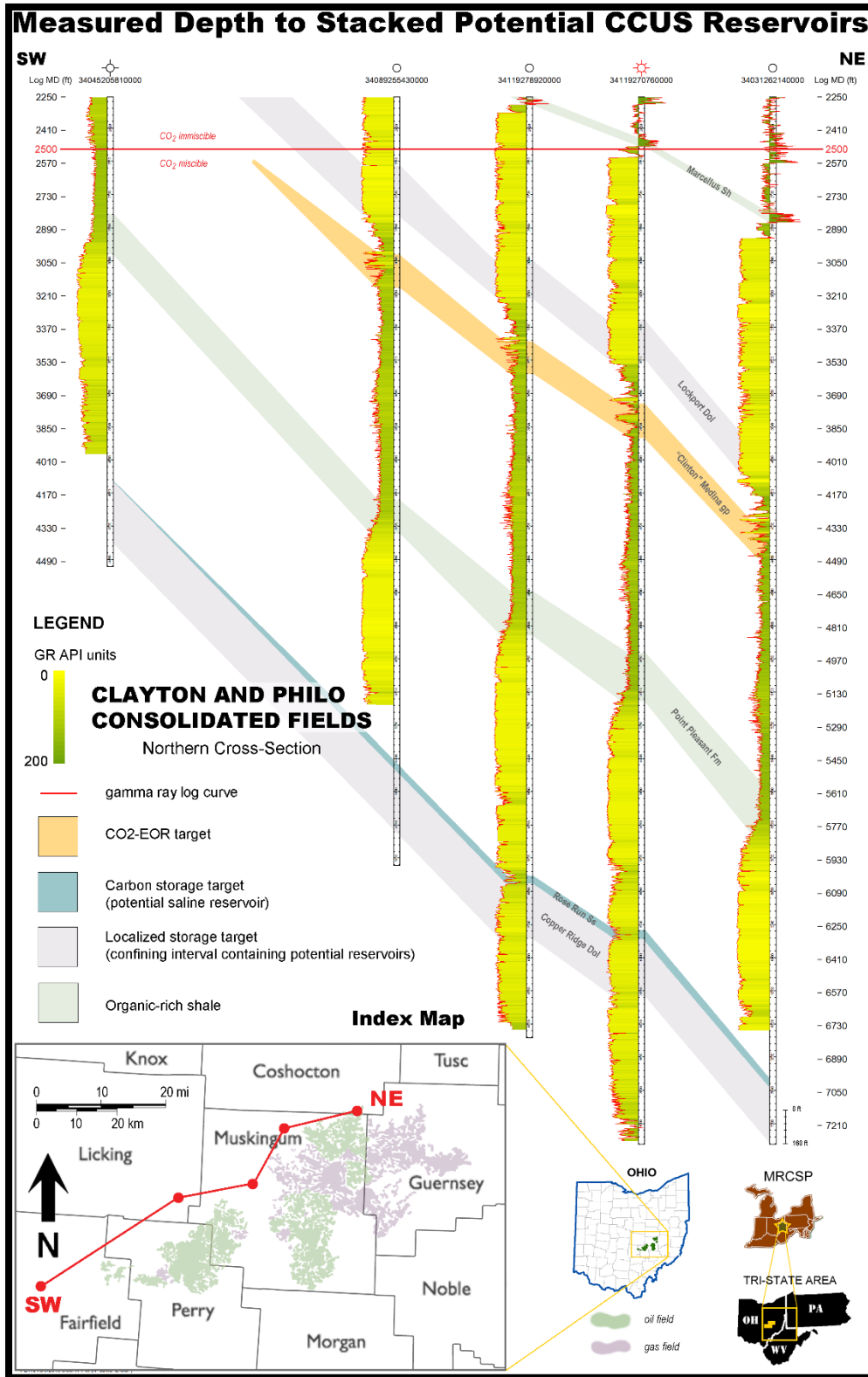


Figure 6-48. Cross section along the northern edge of the Clayton and Philo Consolidated fields area, illustrating the updip pinchout of the “Clinton” sandstone and subcrop of the Rose Run Formation.

6.4.5.1 Rose Run Formation

The Upper Cambrian Rose Run produces from porous sandstone erosional remnants that subcrop along the Knox unconformity in the band shown in Figure 6-47. To the west, the underlying Copper Ridge dolomite is truncated by the unconformity, while to the east, increasingly thick layers of the overlying Ordovician Beekmantown dolomite are present. Each of these formations can develop intergranular to vugular porosity where present at or near the Knox unconformity, thought to be associated with subaerial exposure surfaces (Wickstrom et al., 2011). This individual Rose Run remnant, or monadnock, generally occupies 80 ac or less (Riley et al., 1993). Rose Run legacy wells are present over most of the Clayton Consolidated Field, portions of the Philo Consolidated and the northernmost quadrant of the East Canton Consolidated Field (Figure 6-49). Most of the Clayton Consolidated Field has more than 100 ft of Rose Run sandstone, and legacy wells (Figure 6-40) show several producers in this field. Measured depths to this unit range from about 5000 to 7000 ft over the Clayton and Philo Consolidated fields area (Figure 6-44 through Figure 6-48), deep enough for permanent, miscible storage of CO₂.

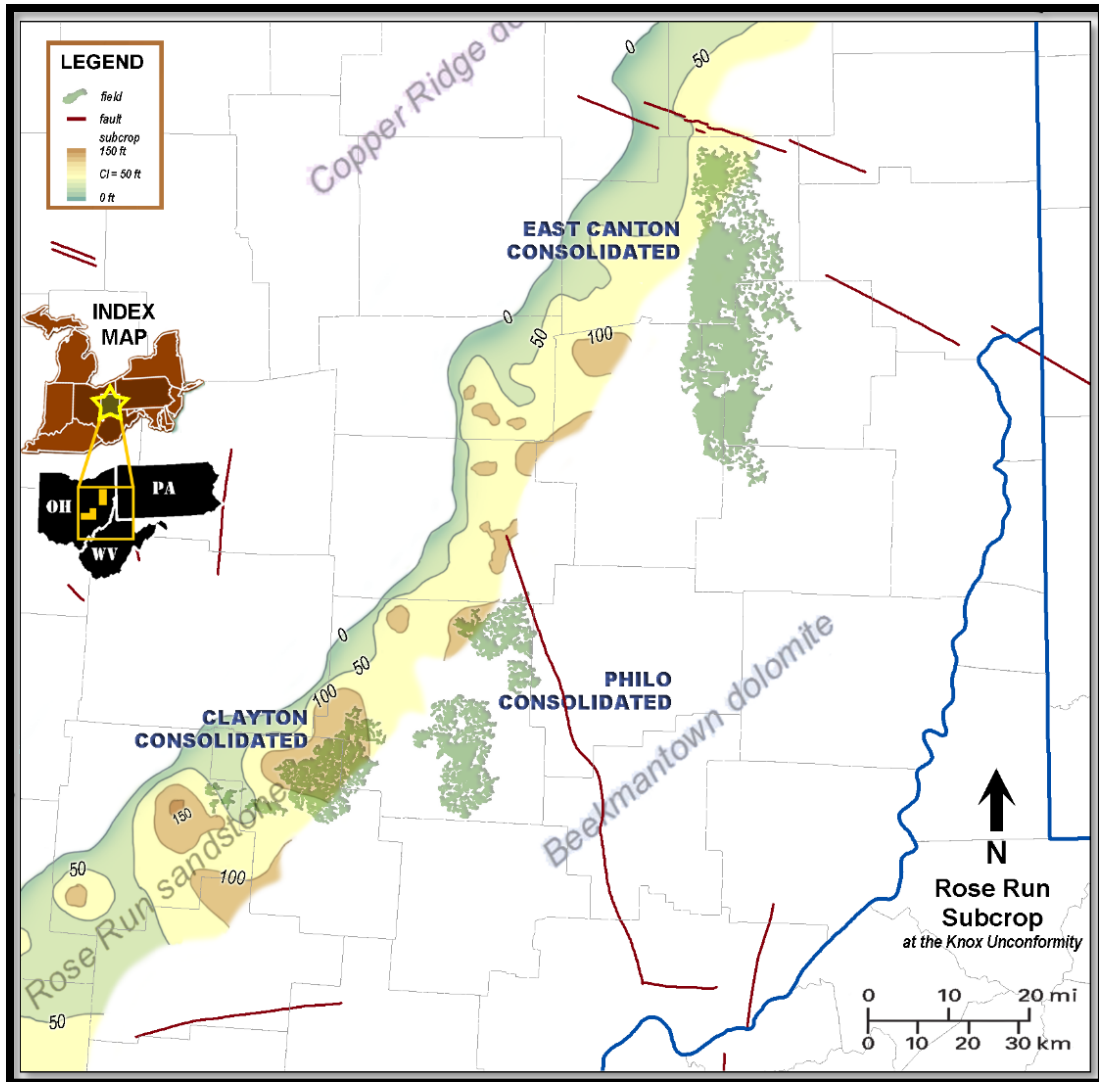


Figure 6-49. Gross thickness map (50-ft contour interval) of the Rose Run sandstone where it subcrops at the Knox unconformity in the case study area. Depleted hydrocarbon reservoirs with CCUS potential occur in the horizontally and vertically sealed erosional remnants (modified from Riley et al., 1993).

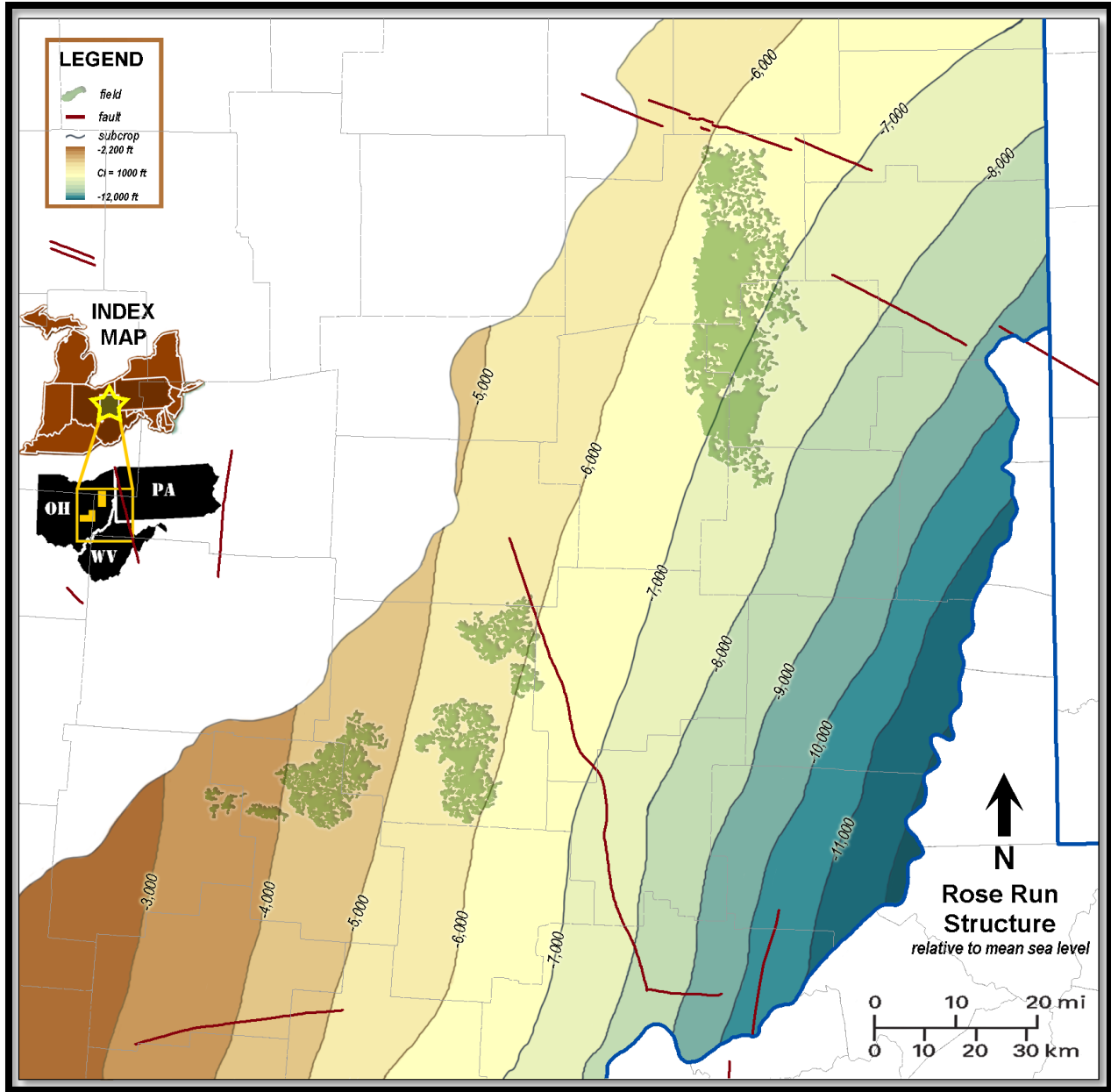


Figure 6-50. Structure map (100-ft contour interval) on top of the Rose Run Formation in eastern Ohio.

The Upper Cambrian Rose Run Formation consists of well-developed beds of white to light gray, fine- to coarse-grained, sub- to well-rounded quartz sandstones, interbedded with thin beds and lenses of low-porosity bioclastic dolostones. The dolostones act as baffles to fluid flow and create fluid-flow compartments within the Rose Run (Riley et al., 1993). The sandstone intervals are cemented with dolomite and minor amounts of clay and quartz (Mishra, 2014; Wickstrom et al., 2005, 2011). Based on cores and geophysical log correlations, as many as five Rose Run sandstone units, separated by non-porous dolostones, may be present, although they are not regionally persistent (Riley et al., 1993). As an example, a description of Rose Run remnants along the subcrop fairway in south-central Ohio in neighboring Pickaway County (Morris, 1995), west-southwest of the Clayton and Philo Consolidated fields, consists of a basal carbonate or dolomite approximately 50 ft thick, sometimes capped with a blocky sand section ranging in thickness from 0 to 50 ft. When a full section of sandstone is present, a thickness of Beekmantown dolomite caps the unit. A portion of the Tuscarawas County geophysical log illustrating the type section of the Rose Run Formation is shown in Figure 6-51. Peak porosities range between 20 and 30 percent (Morris, 1995), making this reservoir an attractive target for carbon storage or CO₂-EOR, depending upon type of hydrocarbon production noted in a given area.

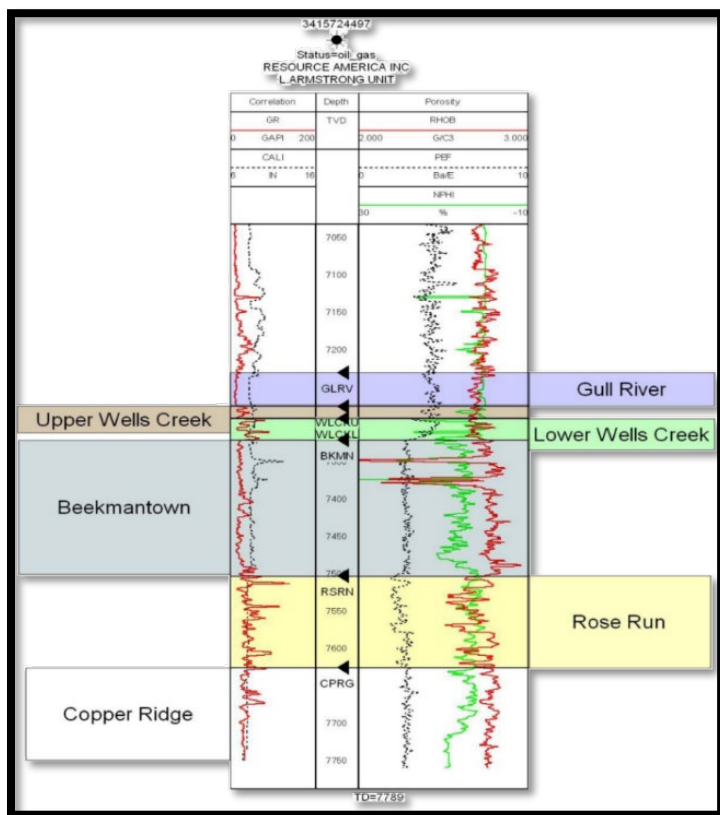


Figure 6-51. Rose Run type section (Flood, 2011).

Examination of legacy wells in the Clayton Consolidated Field (Figure 6-40) shows several wells completed in the Rose Run sandstone throughout the field footprint. Copper Ridge Dolomite producers are also present in the western portions of the field where the Rose Run thins and the unconformity starts to impact that underlying formation. In the Philo Consolidated Field, Rose Run legacy wells are restricted to a well-defined band in the southern portion of the northern oil field footprint, which appears to be structurally controlled by an east-west lineament and which extends into adjacent gas producing areas of the field (Figure 6-43). Less numerous are Rose Run wells in the East Canton Consolidated Field, which occur in the north field area, at depths of about 7200 ft (Figure 6-46). The Rose Run subcrop play extends beyond the East Canton Consolidated Field footprint to the north and appears to be influenced by the Suffield/Akron/Smith fault system (red lines north of the field in Figure 6-50). Evaluation of geologic and seismic data indicates that fracturing and small-scale faulting, due to reactivation of the Suffield fault system, controlled reservoir heterogeneity in the producing Rose Run wells (Riley et al., 1993) in this area.

Most Rose Run sandstone wells are gas to combination oil/gas producers. Typically, the overlying Beekmantown has low porosity and permeability and is a good seal. However, it can develop reservoir quality where it was subaerially exposed at the Knox unconformity surface (Figure 6-49). Porosity types observed in core include intergranular, vugular and fracture (Smosna et al., 2005). Hydrocarbon production is reported for the Beekmantown Dolomite in the field footprints. Overlying carbonates above the Knox unconformity (which drape around the monadnocks) also form a seal (Figure 6-51). The Rose Run thickens to more than 700 ft in Pennsylvania, but reservoir potential in the deep saline portion remains untested.

6.4.5.2 Point Pleasant Formation

The Upper Ordovician Point Pleasant Formation (Figure 6-52) is an interbedded limestone and organic-rich shale, currently producing hydrocarbons in eastern Ohio, that has deeper stacked potential. It is found an average of 5500 ft MSL in the East Canton Consolidated Field. Cole et al. (1987) postulated the Point Pleasant Formation as the source rock for the “Clinton” sandstone (McCormac et al., 1996). The inset map adjacent to the field shows seismic time mapping on basement reflectors and a southwest-northeast seismic line also runs across this area. The central block is bounded on the south by the west/northwest-east/southeast trending Highlandtown fault, which appears reverse with significant vertical displacement and possible lateral (wrench) movement, and on the north by the west/northwest-east/southeast trending Pittsburgh-Washington lineament, which appears normal with vertical displacement and lateral (wrench) movement. Detailed information in large 3D data volumes can provide insight into structural events and timing and possible depositional influences for younger sediments. The Highlandtown fault is offset at “Clinton” reflectors (Torry, 2014). The central block can be traced seismically from basement through Ordovician Point Pleasant reflectors, forming a high area. The edges of the fault block line up with breaks in the field footprint. This could suggest early oil expulsion and migration updip into overlying Lower Silurian “Clinton” sediments, with late-stage hydrothermal diagenesis sealing the fractures, creating permeability barriers evidenced by production breaks in the field footprint.

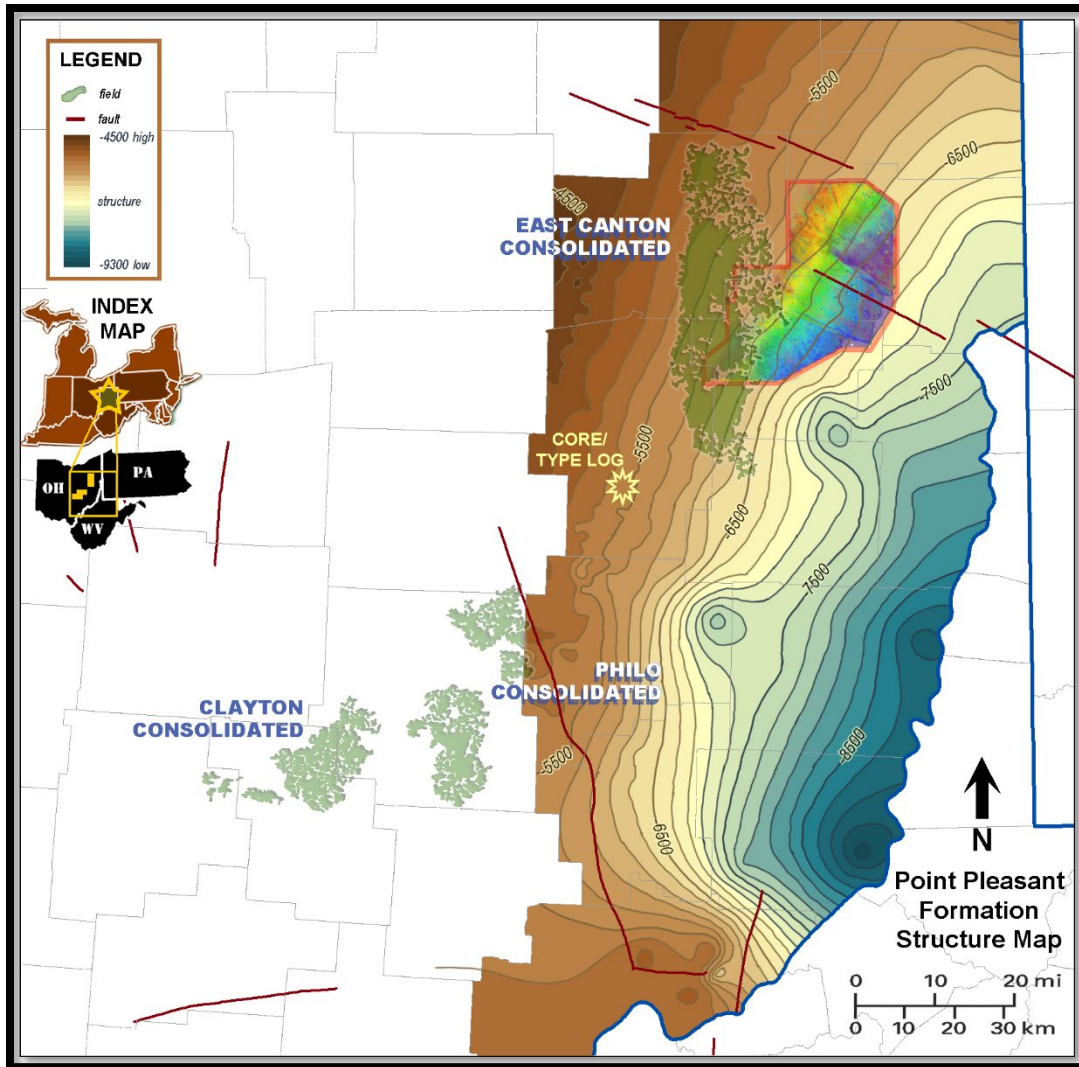


Figure 6-52. Structure map (100-ft contour interval) on the top of the Point Pleasant Formation in eastern Ohio. Inset map outlined in red adjacent to the East Canton Consolidated Field is derived from seismic time data, showing near-basement structure over an area producing from the Utica/Point Pleasant (modified from Torry, 2014).

Hydrocarbon production using horizontal drilling and stimulation via staged, high-volume hydraulic fracturing must occur prior to a geologic carbon storage operation (Levine et al., 2016; Sanguinito et al., 2018). Horizontal Utica-Point Pleasant activity in Ohio (Figure 6-53) shows current operations mostly confined to eastern Ohio. However, there has been some activity in this field and near the Philo Consolidated Field. Since current shale production (Figure 6-53) adjacent to the field case study areas is in the oil/condensate/wet gas window, potential also exists for eventual CO₂-EOR.

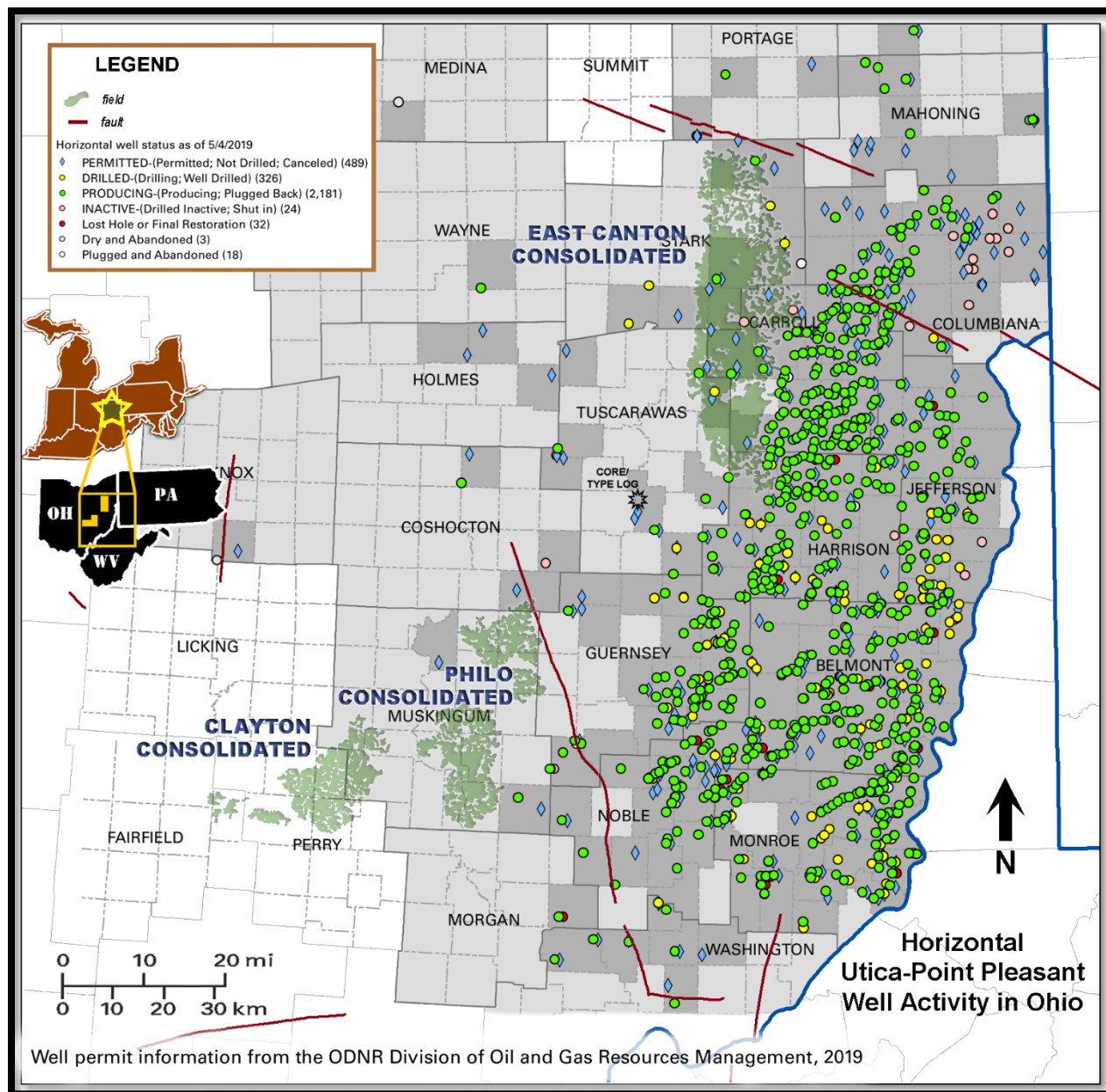


Figure 6-53. Horizontal Utica-Point Pleasant activity (ODNR, 2019) shows producing wells in and near case study field locations in eastern Ohio.

S₁ is a measurement of the free hydrocarbons already generated that are volatilized out of the rock without cracking the kerogen. An S₁ of greater than 1 is considered a good source rock. Figure 6-54 shows the main Utica-Point Pleasant play area and the best potential development areas in Ohio based on S₁. Yellow through red represent very good to excellent potential. The East Canton Consolidated Field falls into this window. The Clayton Consolidated and the Philo Consolidated fields show less activity (Figure 6-53) and less potential (Figure 6-54) at this time.

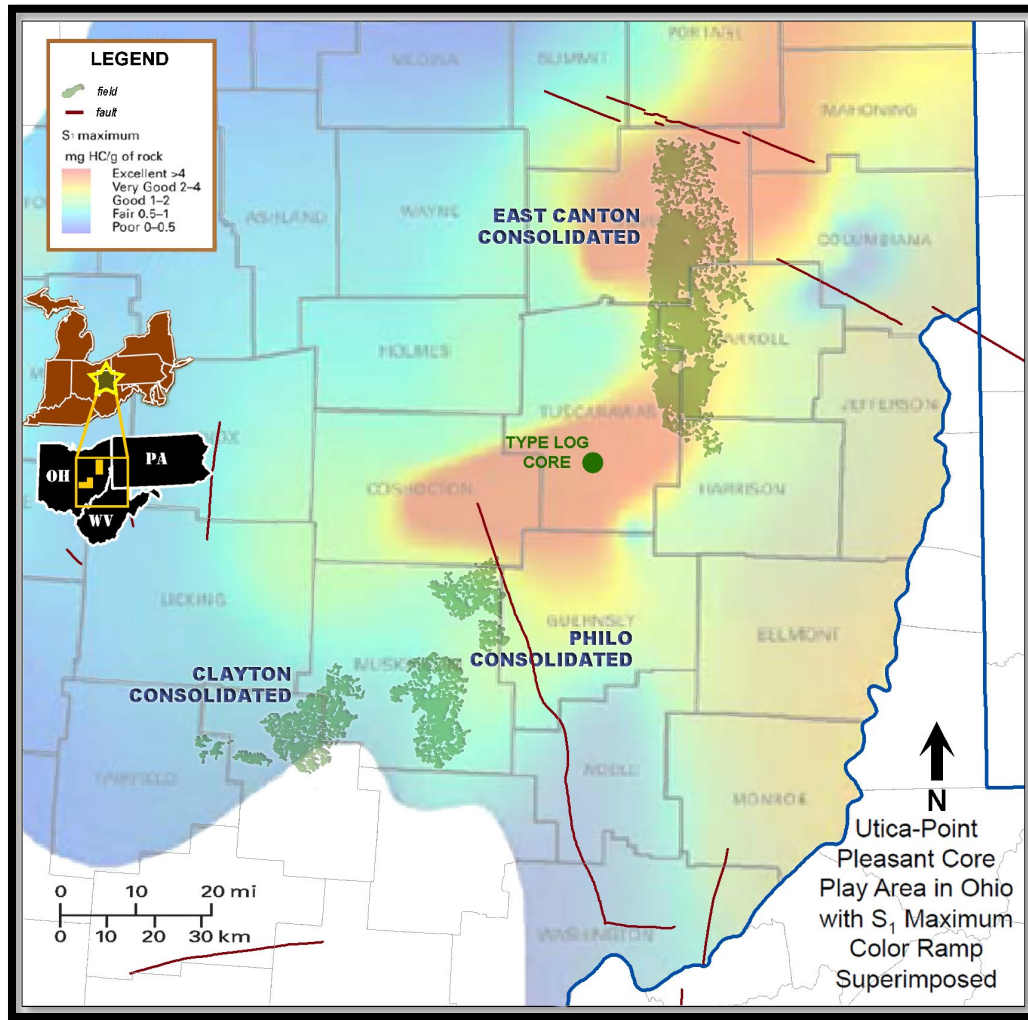


Figure 6-54. Utica-Point Pleasant play area in Ohio (modified from Wickstrom et al., 2012) showing case study fields relative to S₁ data. To date, development of the shale play has occurred mainly east of the case study fields.

Figure 6-55 shows a geophysical type log from Tuscarawas County, with Utica-Point Pleasant TOC measurements derived from core (Riley et al., 2010), compared the standard type log from the Utica Shale Playbook Study (Patchen and Carter, 2015).

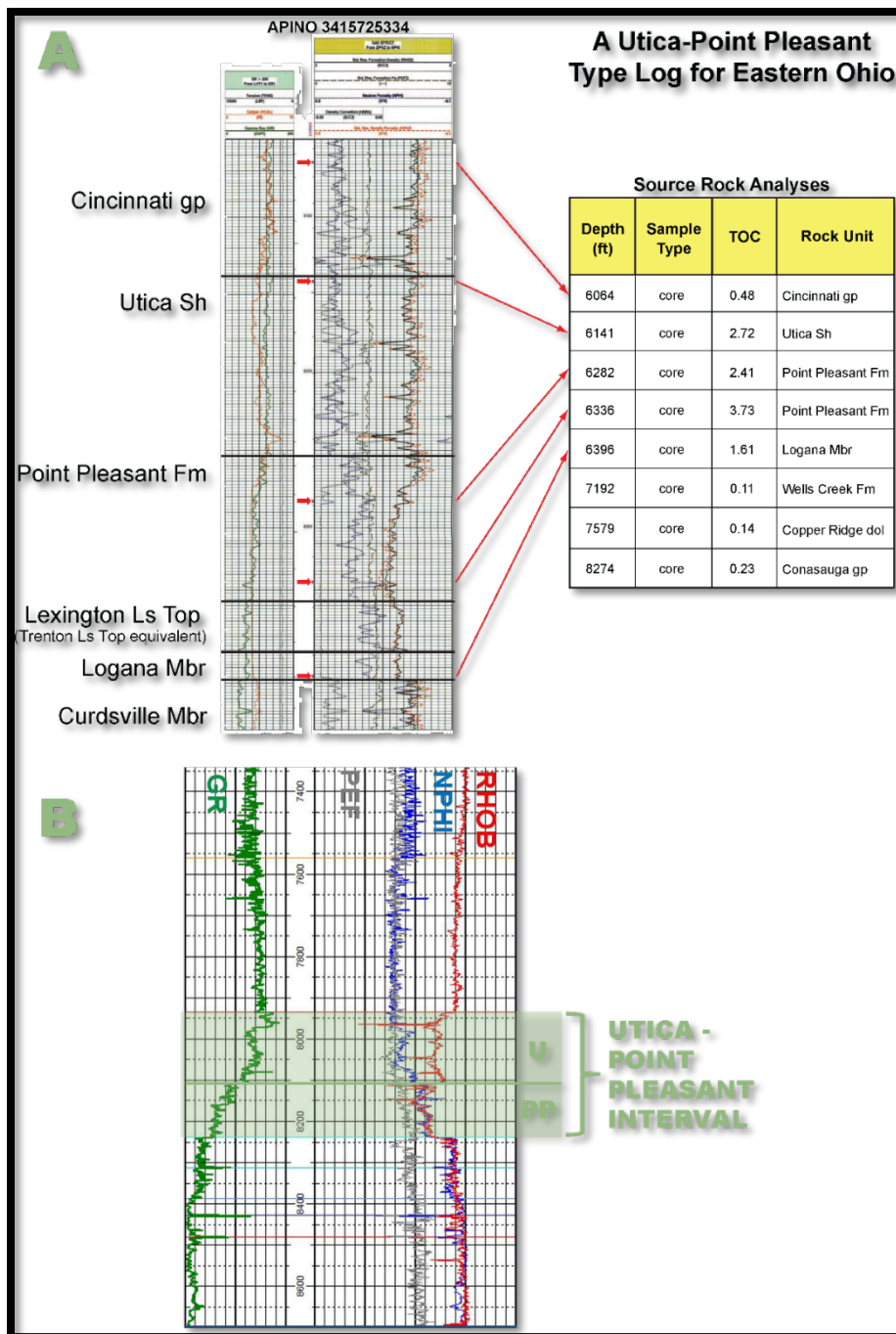


Figure 6-55. A) Type section for the Utica/Point Pleasant interval from Tuscarawas County (modified from Riley et al., 2010) located midway between case study fields. B) Comparison to type log from the Utica Play Book (modified from Patchen and Carter, 2015).

6.4.5.3 Lockport Dolomite

Successful gas well completions in the Lockport Dolomite began in 1889 in southern Ontario, Canada, and spread south through Ohio. Cumulative production, extrapolated from limited production data of 38 BCF gas from 213 wells, was estimated to be at least 100 BCF gas, which was produced from 917 wells (Noger et al., 1996). In central and eastern Ohio, portions of the

Lockport are often referred to as the “Newburg” by Ohio drillers and represent any significant porosity zone (Wickstrom et al., 2011). It occurs from 2500 ft deep at the western margin of Clayton Consolidated Field to 5100 below ground surface in the East Canton Consolidated Field.

The Silurian Lockport Dolomite is a fine- to medium-crystalline, slightly argillaceous and fossiliferous dolomite that was deposited in a carbonate shelf setting. During the Upper Silurian, several patch reef trends extended southwestward from Ontario, Canada, to eastern Kentucky. Associated depositional facies included ooid bars, skeletal sand shoals, patch reef bioherms, lagoons, mud banks, and sabkhas. The location and extent of these facies were likely influenced by changes in sea level, relict topographic highs and syndepositional fault movements (Smosna et al., 1989). Patch reef bioherms, consisting of corals, stromatoporoids, bryozoan and crinoids, formed gas reservoirs (Figure 6-56), which are now depleted and can be considered for carbon storage.

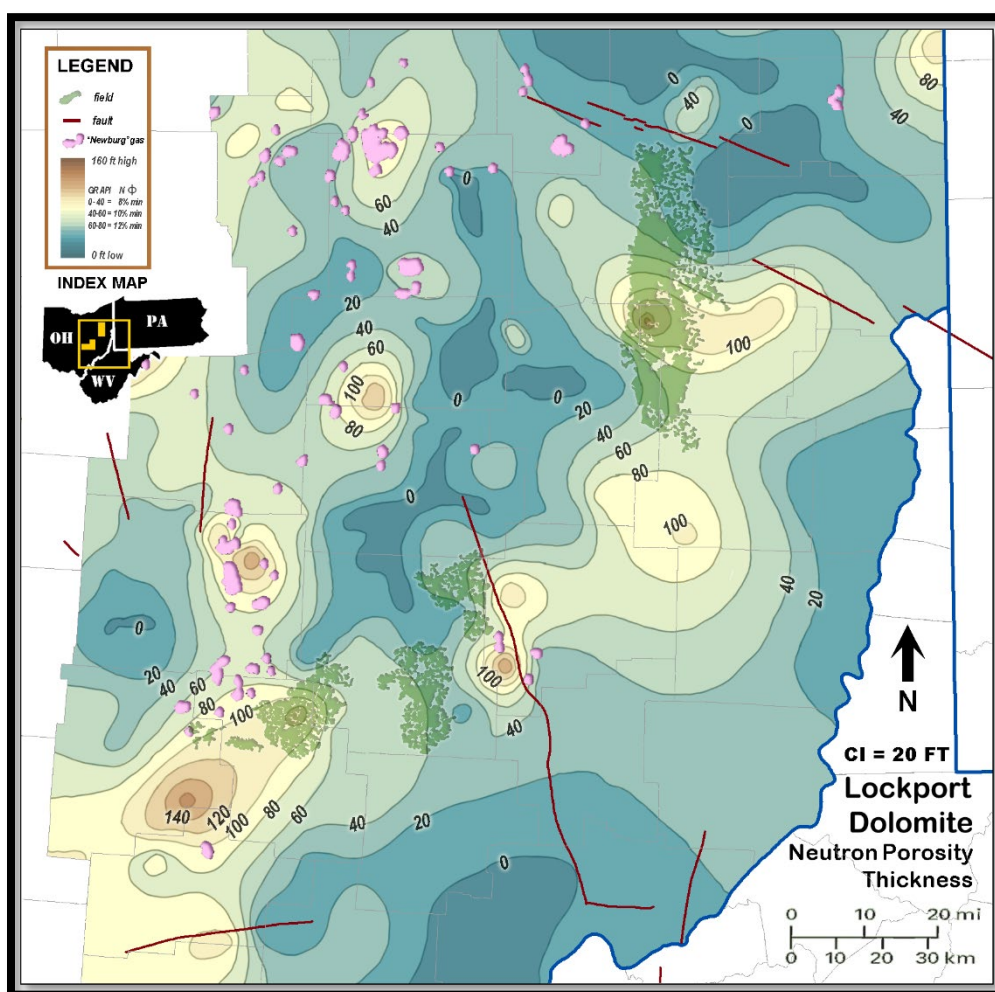


Figure 6-56. NPHI thickness (Bloxsom, 2017) overlain with “Newburg” gas fields (pink, from Noger et al., 1996). Clayton Consolidated Field appears to be on trend, although lack of gas development suggests it may be more brine saturated than gas depleted.

The NPHI thickness (Figure 6-56) along the western edge of the map lines up with the “Newburg” trend, possibly because of the gas effect shown by the NPHI log. The Clayton

Consolidated Field lies along this trend of existing “Newburg” gas fields, although lack of gas development over the field itself may be due to its structural position slightly downdip in the Parkersburg-Lorain syncline between the Cincinnati Arch to the west and the Cambridge CSD to the east. Potential may exist for carbon storage in the saline formation along the patch reef bioherm facies, although the reservoir may be more brine-rich than gas-depleted.

Less potential appears to exist with the remaining two fields. Fracturing associated with the Cambridge CSD along the eastern edge of the Philo Consolidated Field and possible syndepositional fault movement associated with the Akron-Suffield-Smith fault along the northern edge of the East Canton Consolidated Field may create limited storage opportunity, and likely concerns with seal integrity. The thickness of the porous interval increases in the south-central area of the field, which may create issues with high water saturations. Another concern is that casing string cement within “Clinton” wells may not cover this interval, leading to corrosion and leakage. Figure 6-57 illustrates the thickness of the Lockport Dolomite and location of patch reef bioherms in Lockport to “Newburg” gas-producing areas. There may be several factors involved in permeability development, including structure, facies, timing of tectonic events and sea level fluctuations.

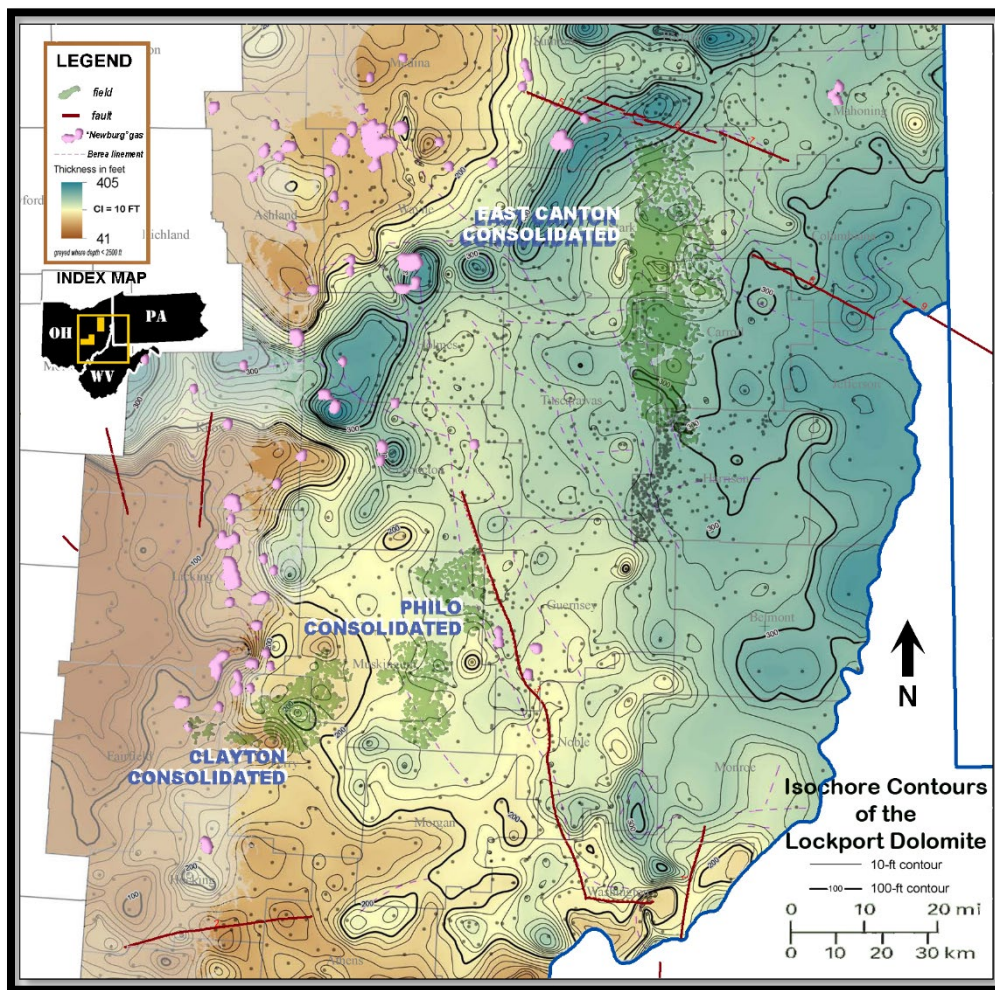


Figure 6-57. Isochore Contours of the Lockport Dolomite (Solis and Bloxson, 2019), overlain with “Newburg” gas fields (pink, from Noger et al., 1996), shows the location of patch reef bioherms

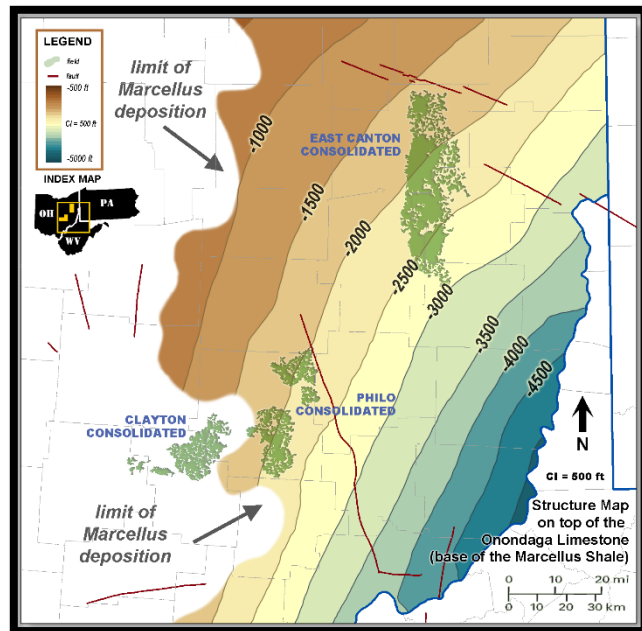
(darkest turquoise, indicating greatest thickness, in the north-central portion of map) in the Lockport to “Newburg” gas fields.

6.4.5.4 Oriskany Sandstone

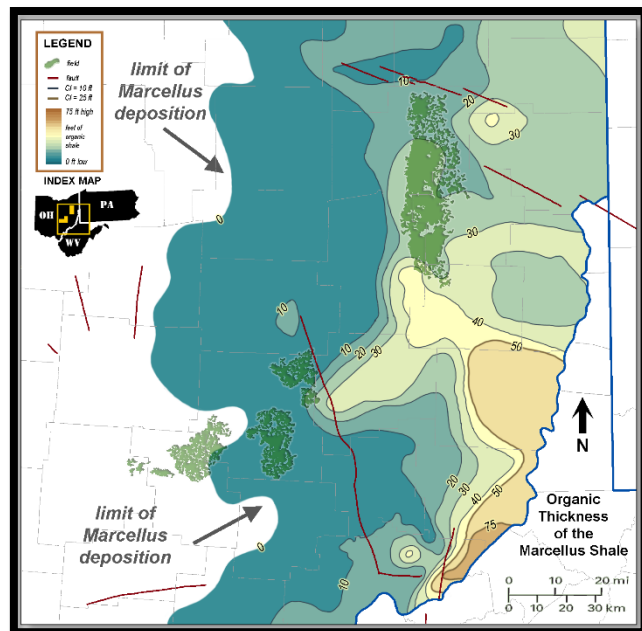
This Devonian sandstone unconformably overlying the Helderberg Formation and underlying the Onondaga Limestone develops localized reservoir potential from structural traps in the Philo Consolidated Field, primarily along the Cambridge CSD, and in small, isolated patches marked at the “Clinton” level by changes from oil footprint to gas footprint.

6.4.5.5 Devonian Shales

Averaging 2000 ft MSL (Figure 6-58A), organic-rich Devonian shales have limited potential in the case study areas. Less than 2500 ft deep to about 4000 ft deep over the field footprints, the Middle Devonian Marcellus ranges from 0 to 30 ft thick (Figure 6-58B), with a thicker interval of Upper Devonian Rhinestreet Shale above (about 50 ft in Philo Consolidated Field), as the shales thin and coalesce at the western margin of the Appalachian Basin (Figure 6-59).



A.



B.

Figure 6-58. Although in the oil window in Ohio, most of the Upper Devonian shales are too shallow to support miscible storage of CO₂. Of those that are, the Marcellus is absent to very thin throughout the case study area (B), which lies 1500 to 3000 ft below sea level where present (A).

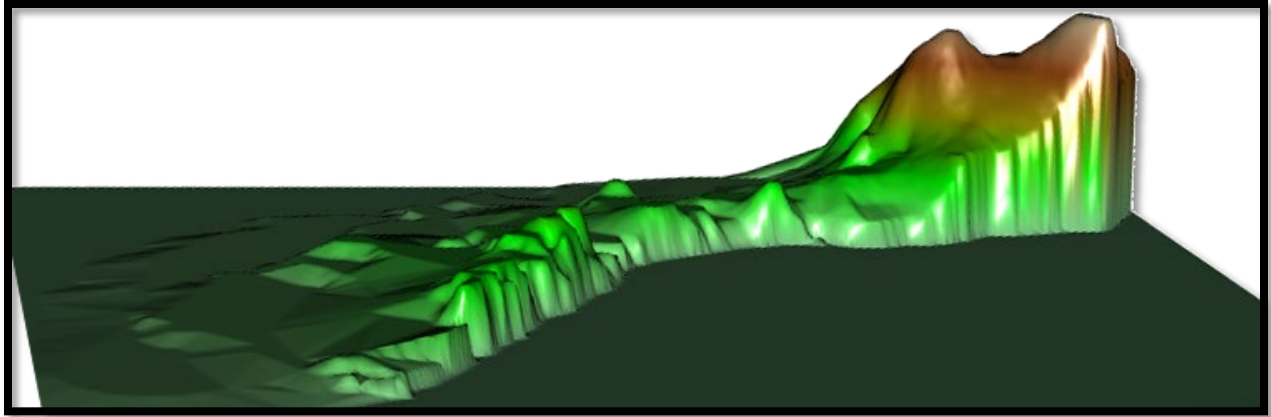


Figure 6-59. Current development of the Marcellus is restricted to the extreme southeastern edge of Ohio in Jefferson, Belmont and Monroe counties, where the formation thickens rapidly, as seen in this 3D model (The Energy Consulting Group-accessed online 5/2019).

6.4.6 Summary

Ohio's East Canton Consolidated Field has produced 95 MMbbls oil from the Medina group's "Clinton" Sandstone since 1966, with another 10 MMbbls primary recovery remaining. EOR using CO₂ creates economic benefit by extracting previously unrecoverable oil reserves while providing environmental benefit by storing carbon in the "Clinton" a mile underground. Reservoir modeling of CO₂-EOR estimates an additional 76 to 279 MMbbls oil could be recovered.

Engineering an effective recovery operation is dependent on understanding how this oil reservoir was formed geologically through time. Diagenesis of heterogeneous Silurian deltaic clastic facies accounts for a fair to poor correlation of geophysical log porosity to oil production. Thus, an integrated geologic analysis of East Canton Consolidated Oil Field was performed to assist engineers in designing a more effective CO₂-EOR operation. This case study utilized published reports, public data and the MRCSP-derived data to perform a comparative analysis of factors thought to influence production. Portions of the field studied by Riley et al. (2011) and Mishra (2015) were reevaluated using comparative analysis. Case study findings suggest that engineering models should incorporate fluid migration pathways through geologic time into the CO₂-EOR modeling. In Ohio, where cross-structural lineaments often define these pathways, creating a rectangular bounding-box in the orientation of the fracture system may serve to compartmentalize the fluid flow such that the model more accurately reflects heterogeneity in fluid flow.

The highest oil yield is found to occur in alignment with two or more cross-structural fracture sets with thick sandstone distributary systems in a 100-ft structural depth interval where a greater than average density of modern stress field fractures occurs. This case study proposes that CSDs served as a conduit for fluid migration during episodic tectonic events when aligned with the paleo-stress field, first filling pore spaces in permeable sandstones with oil expelled from underlying Point Pleasant source rock. Later-stage hydrothermal fluids forming diagenetic cements along the CSDs trapped the oil in place. The monoclinical structure dipping eastward into the Appalachian Basin segregated fluids into gas updip and water downdip of the oil reservoir, and the current stress field fractures enhance permeability.

Laterally extensive vertical seals will likely constrain CO₂ used to move oil, and include the overlying “Packer Shell” dolomites, interbedded Medina group shales and the underlying Queenston shale. These findings can be extrapolated to the entire 164,000-ac field while the comparative analysis methodology can be used to evaluate CO₂ in other “Clinton” oil fields.

6.5 Pennsylvania Case Studies

6.5.1 Overview

The Washington-Taylorstown, Linden and New Freeport fields of Greene and Washington counties were the focus of Pennsylvania’s case study work (Figure 6-60). Each of these fields produce from multiple intervals within the Venango Group (Table 6-2). In this southwestern corner of the state, nearly 20,000 wells have been drilled since the late 1800s to produce petroleum hydrocarbons from conventional and unconventional reservoirs (EDWIN, 2019). Data for approximately 15,000 wells were used in some form or fashion to evaluate subsurface geology in this area, with approximately 2200 wells accounted for by the three case study fields.

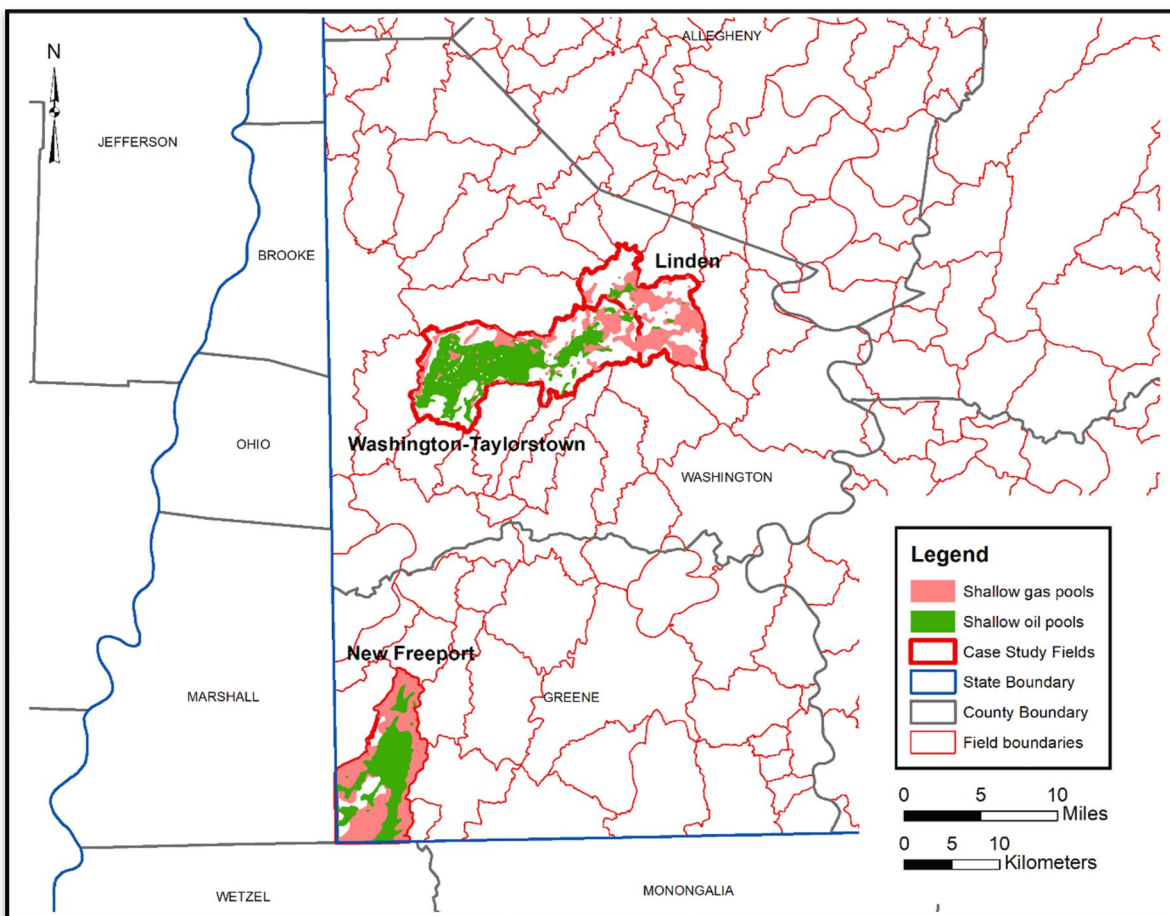


Figure 6-60. Pennsylvania case study locations.

The oil and gas activity in this part of the state has been well studied by PAGS over the years. In his assessment of Pennsylvania's crude oil reserves, Lytle (1950) reported total oil in place volumes of 49.2 MMBO for Washington-Taylorstown and Linden fields (combined) and 3.1 MMBLS for New Freeport Field as of January 1, 1947. Fettke et al. (1946) prepared a mineral resource report for North Strabane Township, Washington County, including the area of Linden Field. In this report, Fettke described shallow (Pennsylvanian, Mississippian and Upper Devonian) oil and gas sandstones; prepared localized structure maps, thickness maps and cross sections for the Gordon sandstone; and reported on core and rock cuttings samples available for the area. McGlade (1967)'s mineral resource report on the Amity and Claysville quadrangles of Washington County provided a thorough assessment of the area's oil and gas geology, including Washington-Taylorstown Field and the surrounding area. McGlade included descriptions of shallow subsurface stratigraphy and structure; prepared a detailed accounting of oil and gas wells drilled in the area; reported on the general reservoir and production characteristics of Pennsylvanian, Mississippian and Upper Devonian oil- and gas-bearing rocks found here; prepared core and rock cuttings descriptions for multiple wells; and included laboratory analyses of selected oil samples taken from local Venango Group sandstones. Harper and Laughrey (1987) expanded on the discussion of oil- and gas-bearing units in southwestern Pennsylvania by incorporating the activity of southern Beaver and Allegheny counties into their assessment, as well as including the subsurface geology, structure and prospects of deeper Middle and Lower Devonian reservoir rocks. Their study is, by far, the most comprehensive oil- and gas-related assessment to be prepared for this corner of the state. It not only compiled salient information regarding subsurface stratigraphy, oil and gas production and related industry activity in area fields, but also evaluated the petrology and depositional history of Venango Group sandstones and explored the potential effects of deep structure on shallow oil and gas reservoir characteristics. Most recently, PAGS identified sandstones of the Venango Group in Washington County as prospective carbon storage reservoirs, given their attractive porosity and permeability characteristics (PA DCNR, 2009).

6.5.2 Venango Group Lithostratigraphy

The oil fields of southwestern Pennsylvania are well-known for their Venango Group production, although the number of productive intervals varies from place to place. Figure 6-61 provides a generalized GR log curve and stratigraphic chart for the Venango Group in the study area, where as many as five productive zones (informally named the Hundred-Foot, Nineveh, Gordon, Fourth and Fifth) are present in the subsurface.

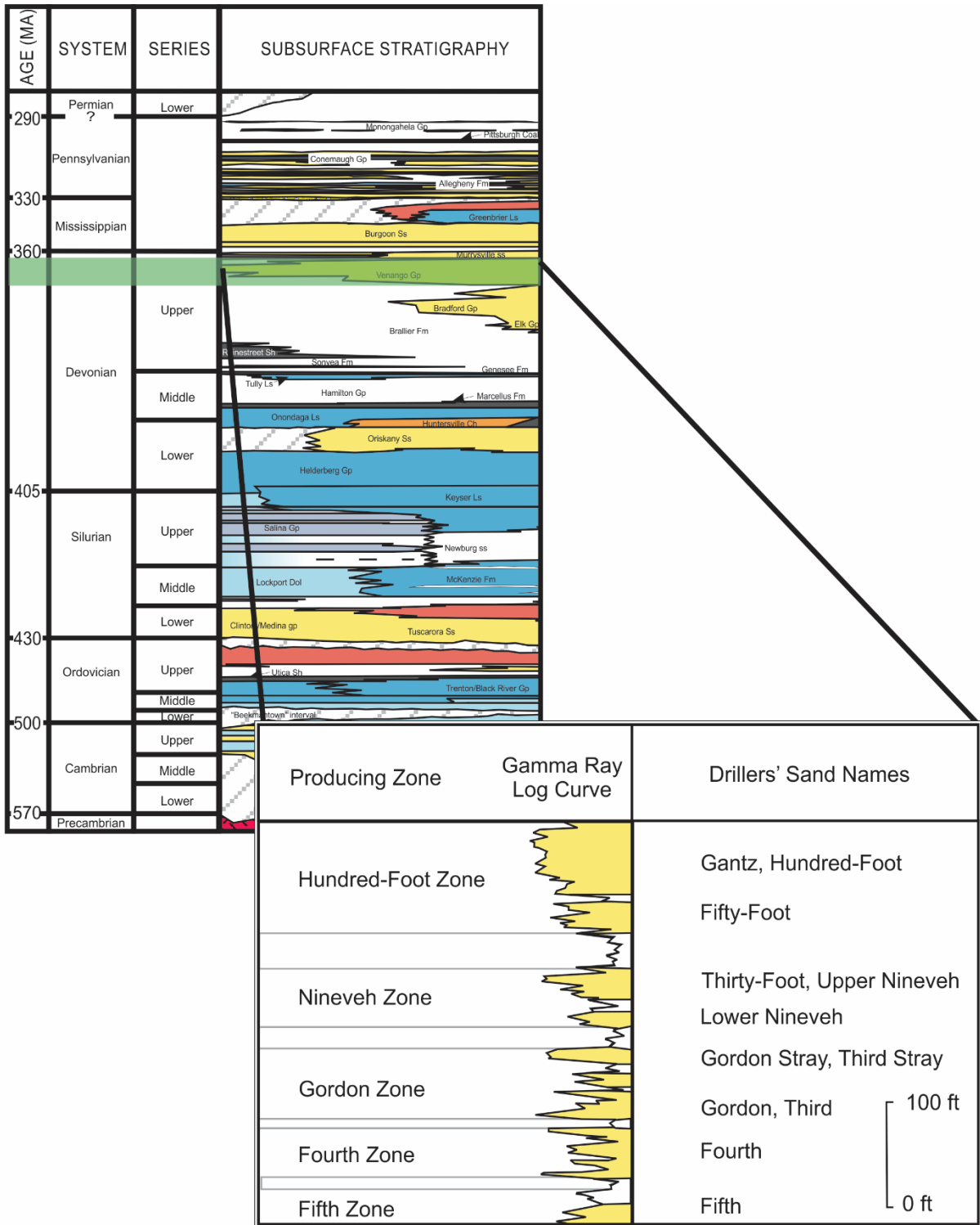


Figure 6-61. Generalized subsurface stratigraphic chart, highlighting Venango Group lithostratigraphy as used in southwestern Pennsylvania.

Lithostratigraphic correlations of these informal sandstone units were prepared for 140 wells in southwestern Pennsylvania. These wells were selected based on their geographic coverage, as well as the availability of modern geophysical logs that penetrated most, if not all, of the Venango Group interval. See Appendix F for the regional geologic cross sections that provided interpretive backbone against which all wells were correlated in advance of mapping and reservoir characterization. Lithostratigraphic correlations were based on GR, RHOB, NPHI and/or DPHI logs, as available. Both tops and bottoms were correlated for the major producers in the study area (i.e., Gantz, Fifty-Foot and Gordon sandstones), and tops were selected for the Murrysville, Nineveh, Gordon Stray, Fourth and Fifth sandstones, as appropriate.

As reported by McGlade (1967), the Gordon Zone is “probably the most complex unit in the Upper Devonian” of Washington County. More specifically, lithostratigraphic correlation of sandstones in the Nineveh and Gordon zones can prove challenging, as the Lower Nineveh sandstone can be confused with the upper portion of the Gordon Zone (i.e., the Gordon Stray) in some areas. The correlating cross sections in Appendix G (particularly D-D’ and E-E’) confirm the stacked morphology of sandstones in these intervals, where some of the Gordon tops interpreted for this study could arguably be identified as the top of the Gordon Stray. For the purposes of this study, Gordon picks represent the larger “Gordon Zone” of McGlade (1967), rather than the Gordon sandstone proper (i.e., the lower sandstone of the Gordon Zone).

The reservoir characteristics of Venango Group sandstones, as determined by this study, are provided in Table 6-4. Formation tops data were interpreted from wells with geophysical log control. Net thicknesses were determined applying a 100-API cutoff on the GR curve to the gross thickness interval. Average porosity values were computed for net sandstone intervals using DPHI or NPHI curves, or both (average value).

Table 6-4. Unit-specific reservoir characteristics of the Venango Group, Washington and Greene counties, Pennsylvania.

Drillers' Sand Name	Top Formation (ft)			Thickness (ft)		Porosity		
	Min	Max	Avg	Gross	Net	Density (%)	Neutron (%)	Average (%)
Hundred-Foot	1813	3306	2563	81	55	11	6	9
Gantz	1813	3306	2633	18	11	14	6	10
Fifty-Foot	1839	3342	2591	60	48	7	6	7
Nineveh	1968	3395	2708	39	23	12	7	10
Gordon Stray	2018	3451	2745	13	7	9	9	9
Gordon	2050	3482	2792	43	30	11	7	9
Fourth	2116	3555	2896	26	16	8	6	7
Fifth	2175	3611	2979	40	29	11	6	9

Based on the average formation top depth data, Venango Group reservoirs may offer both CO₂-EOR and permanent storage targets throughout the study area. Looking at the range of minimum and maximum depths, however, any decisions regarding CCUS should be made in conjunction with site-specific assessments at potential field sites. In other words, what may be miscible CO₂-EOR in a given unit at one location may be immiscible CO₂-EOR at another, and the prospects for permanent storage at the end of enhanced recovery operations will undoubtedly vary.

The structure on top of the Venango Group was mapped using formation top data from area wells with geophysical log control (Figure 6-62). Shallower depths are represented in shades of orange and yellow, and greater depths are mapped with shades of green. The elevation of the top of the Venango Group ranges from -600 to more than -1800 ft MSL. The interval is present throughout the study area, and gradually deepens from north to south. Interpreted basement faults (Gold et al., 2005) are associated with the deep structure of the Rome Trough in this part of the Appalachian Basin. Venango Group deposition appears to have been influenced by deep structure, as evidenced by the orientation, gradient and deflection of contours in the vicinity of these faults (Figure 6-62).

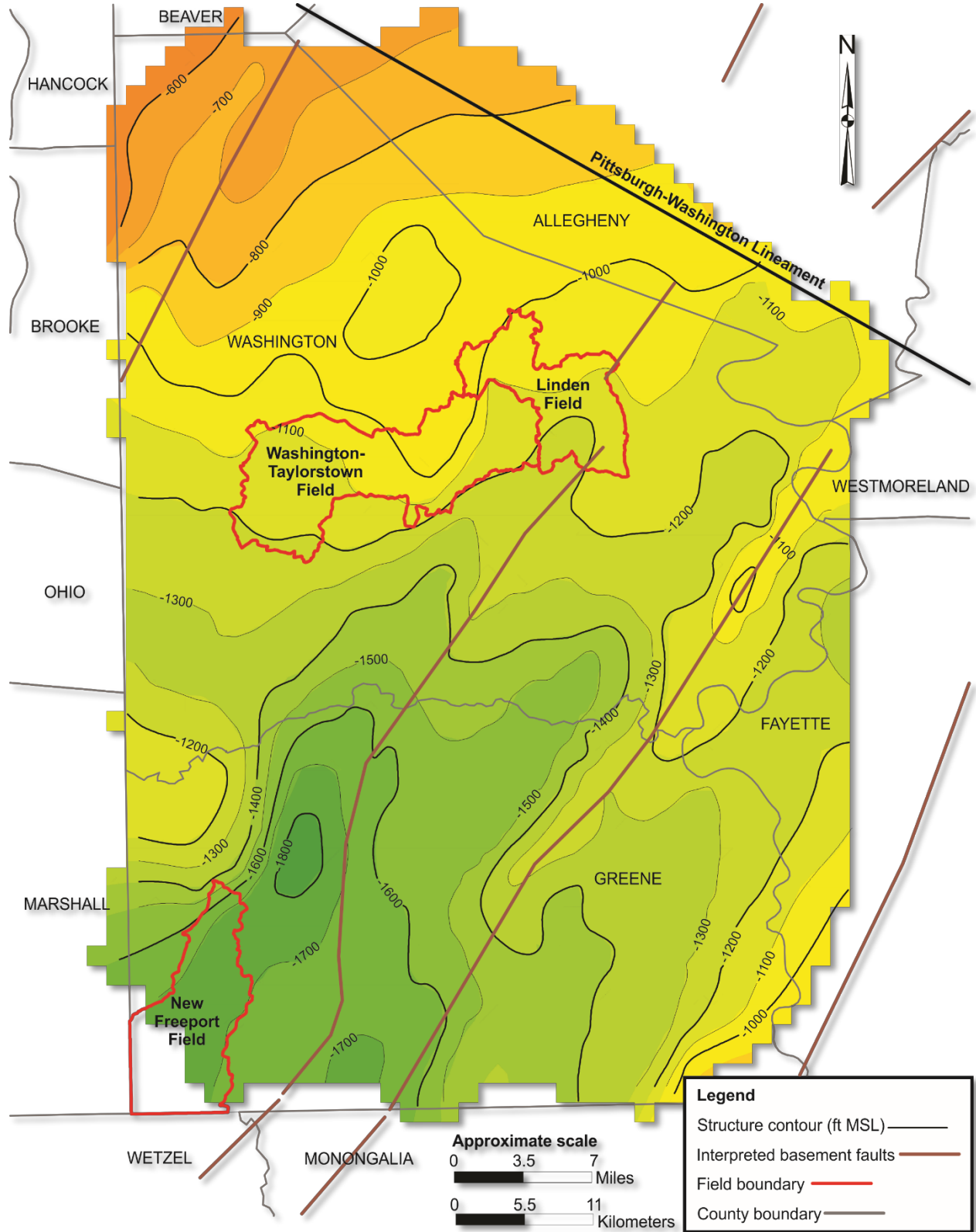


Figure 6-62. Structure map (100-ft contour interval) on top of the Venango Group in southwestern Pennsylvania.

Of all the hydrocarbon-bearing units in southwestern Pennsylvania, the Gantz and Fifty-Foot (“Hundred-Foot” where both occur) and Gordon sandstones have been the most productive. Figure 6-63, Figure 6-64 and Figure 6-65 map the gross thicknesses of these units in Greene and Washington counties. Thicker areas of sandstone are represented with pale yellow to brown shading, and thinner areas are represented with purple shading. The Gantz sandstone (Figure 6-63) is thickest (30-50+ ft) in central and eastern Washington County (including the area of Washington-Taylorstown and Linden fields), although a marginally thicker area (25-30 ft) exists in southeastern Greene County. This uppermost unit of the Venango Group is absent in the western portion of the study area.

Much like the structure contour lines associated with the top of the Venango Group (Figure 6-62), variations in thickness of Venango Group sandstones (Figure 6-63 through Figure 6-65) generally correspond to locations of basement faulting. Please note that the Geoteams did not preferentially select well control, nor use extensive interpretive license, with these deep structures in mind. Well locations were chosen based on the availability of geophysical log data alone (Figure 6-66). Even so, it is very possible that operators may have sited their Venango Group well locations in this area based on confidential information (e.g., seismic data) that provided them more guidance on the locations of subsurface structure and areas of favorable unit thicknesses, in essence creating similar results with respect to these map’s contours.

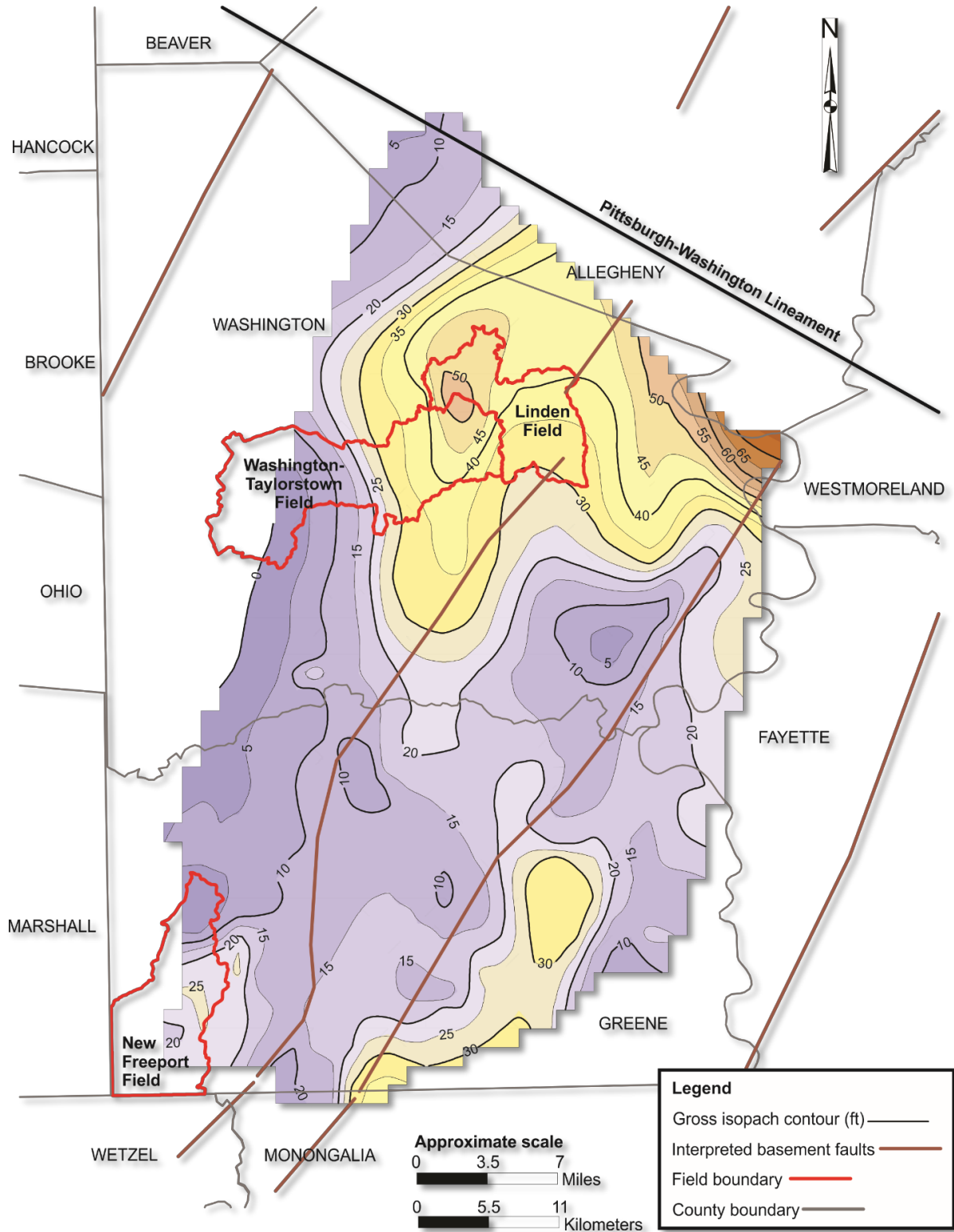


Figure 6-63. Gross thickness map (5-ft contour interval) of the Gantz sandstone in Greene and Washington counties.

The underlying Fifty-Foot sandstone (Figure 6-64) is present throughout the study area, thinner in the west and thicker to the east. The areas of thickest (60-110+ ft) Fifty-Foot sandstone occur in eastern Greene and Washington counties and coincide with areas that have experienced basement faulting.

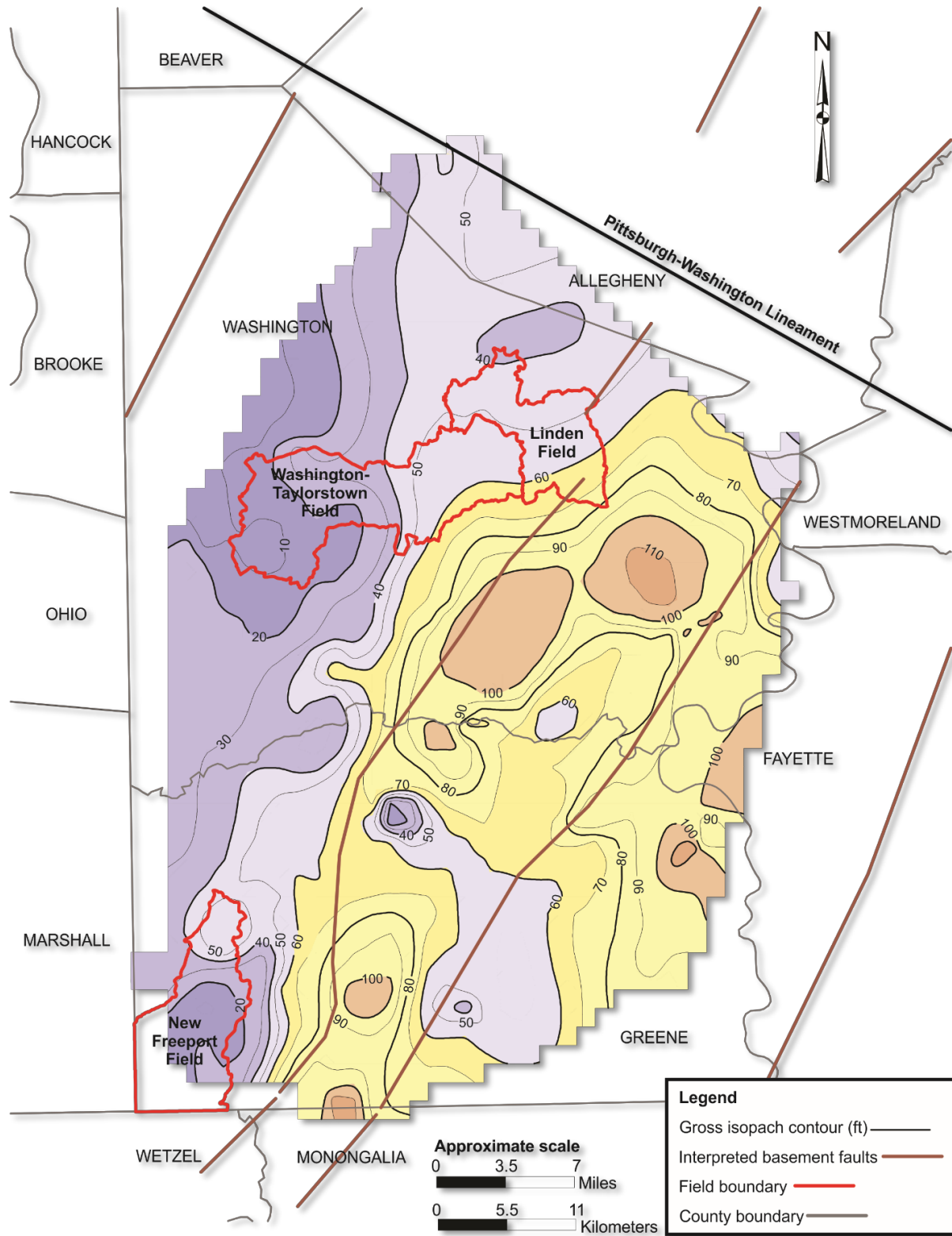


Figure 6-64. Gross thickness map (10-ft contour interval) of the Fifty-Foot sandstone in Greene and Washington counties.

The Gordon sandstone (Figure 6-65) is found throughout the study area and extends farther west than any other Venango Group sandstone in southwestern Pennsylvania. The Gordon is thickest (60-110+ ft) in central/southern Washington and northern/western Greene counties, although a marginally thicker area occurs in southeastern Washington County.

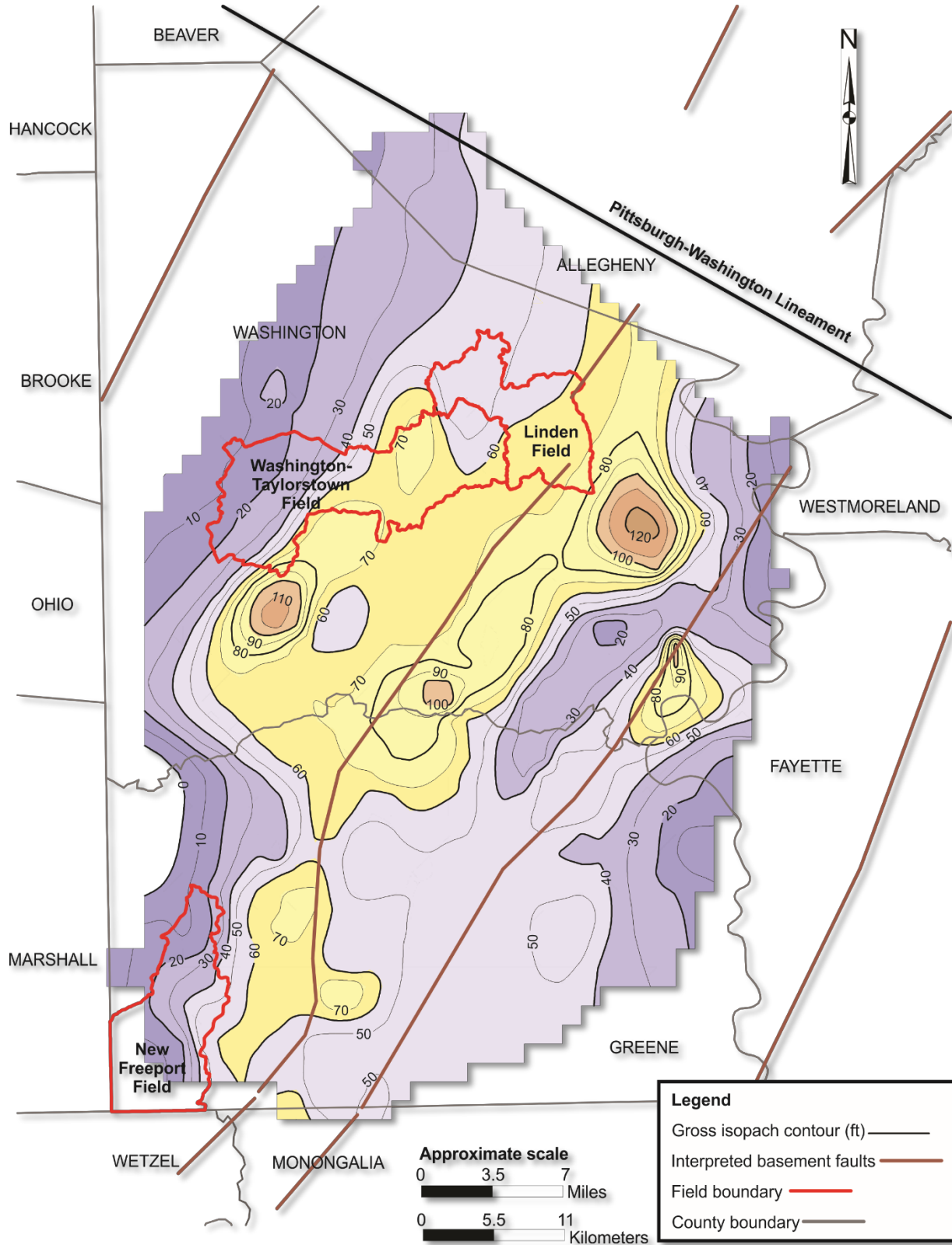


Figure 6-65. Gross thickness map (10-ft contour interval) of the Gordon sandstone in Greene and Washington counties.

6.5.3 Area Cross Sections

Four geologic cross sections were generated to illustrate the variability in depth, thickness and extent of Venango Group units in the study area (Figure 6-66). The orientation and extent of lines A-A', B-B', D-D' and F-F' are generally consistent with those of similarly named correlating cross sections (Appendix G), although these four have been prepared to horizontal scale and incorporate a smaller number of wells than those in Appendix G. The cross sections sit on the base of the Gordon sandstone (i.e., the relative depth of 0 ft), and correlate several geologic units: the Murrysville, Gantz, Fifty-Foot, Nineveh, Gordon, Fourth and Fifth sandstones. This illustrates 750 ft of subsurface geology for the study area – from approximately 200 ft above the top of the Murrysville sandstone to 200 ft below the Gordon sandstone. The GR curves on Track 1 (left side of geophysical log grid) use a shaded pattern to differentiate among clean sandstones (yellow), mixed siliciclastic units (green) and shales (dark green). DPHI (green) and NPHI (blue) curves, when available, have been plotted on Track 2 (right side of geophysical log grid). The wells plotted in Figure 6-66 represent those 140 locations with geophysical log control that have been incorporated into this study.

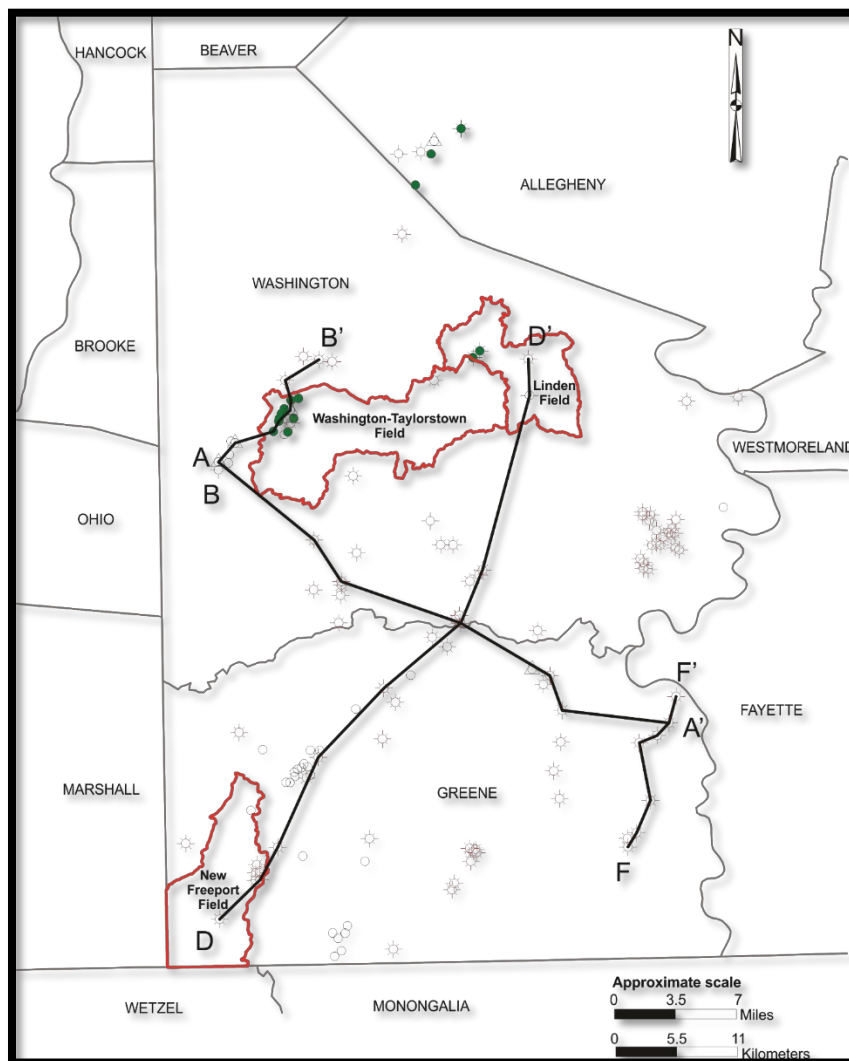


Figure 6-66. Location of well control and geologic cross sections prepared for the Venango Group interval in Greene and Washington counties.

Geologic cross section A-A' (Figure 6-67) is a dip section running from western Washington County to northeastern Greene County. A-A' shows an eastward thickening of sandstones associated with the Venango's Hundred-Foot Zone (that is, where the Gantz and Fifty-Foot are both present), but particularly with respect to the Fifty-Foot sandstone (Figure 6-64), as the Gantz is locally absent (Figure 6-67). The Gordon Zone, as shown in A-A', is thinnest in the west, absent in the east and illustrates a "triple sand" character with thicknesses on the order of 50-70 ft along this line of cross section, excepting API No. 3712521147, where the Gordon exceeds 100 ft. Just as previous workers (Boswell et al., 1996) have reported, the Gordon extends farther westward than any other Venango Group sandstone unit in southwestern Pennsylvania.

The remaining geologic cross sections – B-B', D-D' and F-F' (Figure 6-66) – were generated perpendicular to A-A' to illustrate differences in Venango Group sandstone thickness and character along strike. B-B' (Figure 6-68) includes oil wells subjected to enhanced recovery operations in western Washington-Taylorstown Field; D-D' (Figure 6-69) begins in New Freeport Field (Greene County) and ends in Linden Field (Washington County); and F-F' (Figure 6-70) is in Greene County, near the eastern edge of the study area. Each of these are discussed in turn below, moving from west to east through the study area.

B-B' (Figure 6-68) shows the subsurface geology just to the west and north of Washington-Taylorstown Field. The presence of sandstones here is generally limited, and where sandstone units exist, they tend to be thin. Specifically, both the Fifty-Foot and Gordon sandstones remain thin (~10-20 ft thick) along the entire section, and no Gantz sandstone is present here. The two service wells in this cross section (API Nos. 3712520107 and 3712520044) were completed in the Gordon sandstone to store natural gas; hence, geophysical log curves stop at the bottom of the Gordon Zone. The three oil wells (API Nos. 3712521889, 3712521890 and 3712521895) and enhanced recovery injector well (API No. 3712522289) exhibit clean sandstones with "single sand" character that are just a bit thicker than those in neighboring wells. The utilization of the Gordon sandstone for natural gas storage and EOR activity in this part of Washington County suggests abundant porosity and permeability, especially given the limited thickness of the unit here.

D-D' (Figure 6-69) is situated in the central portion of the study area, approximately 15 mi east of dip section B-B'. Both the Gantz and Fifty-Foot sandstones of the Hundred-Foot Zone are present in most locations, excepting only API Nos. 3712522251 and 3712522059. Hundred-Foot thicknesses range from about 50 to 100 ft. The Gordon sandstone thickens from ~20 ft in New Freeport Field (southwest) to upwards of 60-70 ft in Linden Field (northeast), and is thickest (~90 ft) in API No. 3712522059, the well that serves as the tie to dip section A-A'. The character of the Gordon varies from a "double sand" to "triple sand" to "massive" character along this line of section. Geologic cross sections prepared for Linden Field by Fettke (1946), drawn approximately parallel and perpendicular to the inferred shoreline orientation at the time of deposition, also illustrate the Gordon Zone as comprised of one or more sand bodies, depending on location (and presumably the focus of deposition). In addition, the Nineveh sandstone, which is situated between the Hundred-Foot and Gordon zones (Figure 6-61), is noticeably thick and relatively clean in New Freeport Field (and Greene County in general). Even sandstones of the Fourth and Fifth zones display relatively clean sandstones along this line of section. Given the crossover (blue shading) exhibited by NPHI and DPHI curves for one of the wells in New Freeport Field (API No. 3705924540), gas production from wells in this area are likely from multiple sandstones – the Gantz, Fifty-Foot, Nineveh and Gordon.

F-F' (Figure 6-14) is located about 15 mi east of dip section D-D' and is the easternmost line of section prepared for this study. The Hundred-Foot Zone is present along the entire length of this cross section, with relatively clean Gantz and Fifty-Foot sandstones combining to offer a consistently thick interval of 100 ft or more. The Gordon sandstone maintains a relatively consistent "double sand" character and thickness (20 ft or less) in most places (i.e., the Gordon is absent in API No.3705923139). Murrysville and Nineveh sandstones are present in some locations along this line of section, although they are certainly not as clean or thick as the Hundred-Foot and Gordon zones. Sandstones of the Fourth and Fifth zones are present in greater thicknesses in this section (relative to cross sections B-B' and D-D'), although they are siltier here in eastern Greene County. The NPHI and DPHI curves in API No. 3705921572 exhibit crossover in the Gantz, Fifty-Foot, Nineveh and Gordon sandstones, suggesting these are good gas-bearing intervals within the Venango Group here.

Interpretations of unit depth, thickness and extent, as illustrated in Figure 6-67 through Figure 6-70, are consistent with the plan view gross thickness maps for the Gantz, Fifty-foot and Gordon sandstones in Figure 6-63, Figure 6-64 and Figure 6-65. In addition, variations in unit presence (or absence) and thickening (or thinning) of Venango Group geologic units in these sections generally occur near areas where basement faulting has been interpreted to exist – in particular, note sections B-B' and D-D.' The data presented here is consistent with the results of previous studies (e.g., Harper, 1989; Wagner, 1976), which have postulated the periodic reactivation of deep structures affected depositional patterns, structural fabric and other characteristics of shallower sedimentary rocks over geologic time. While these deep basement structures helped to shape Appalachian Basin morphology and may have influenced the depth, thickness and extent of certain subsurface formations (including the Venango Group) at the time of their deposition, the faults themselves terminate at depths well below those reservoirs described in this case study.

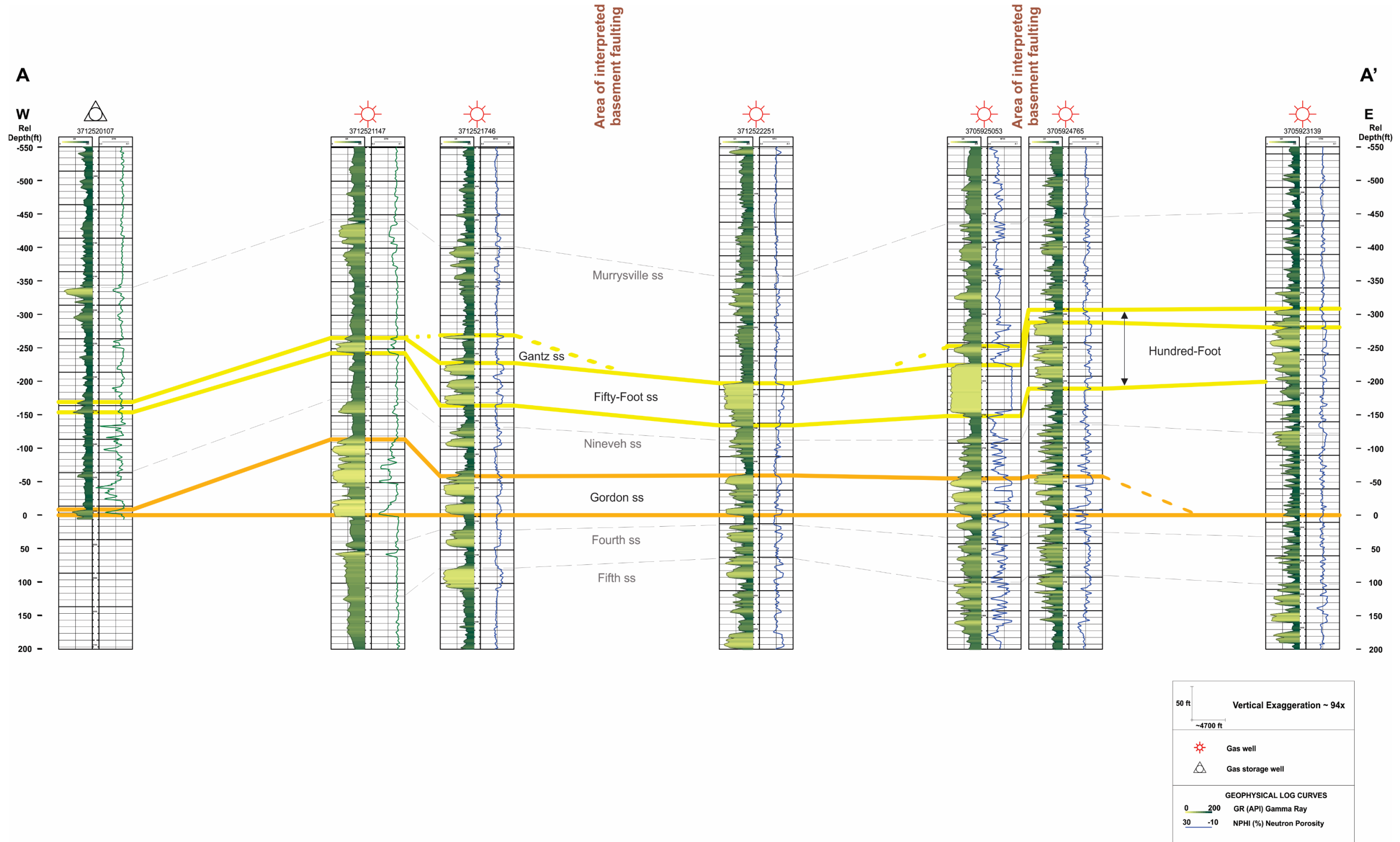


Figure 6-67. Dip cross section A-A', western Washington County through eastern Greene County.

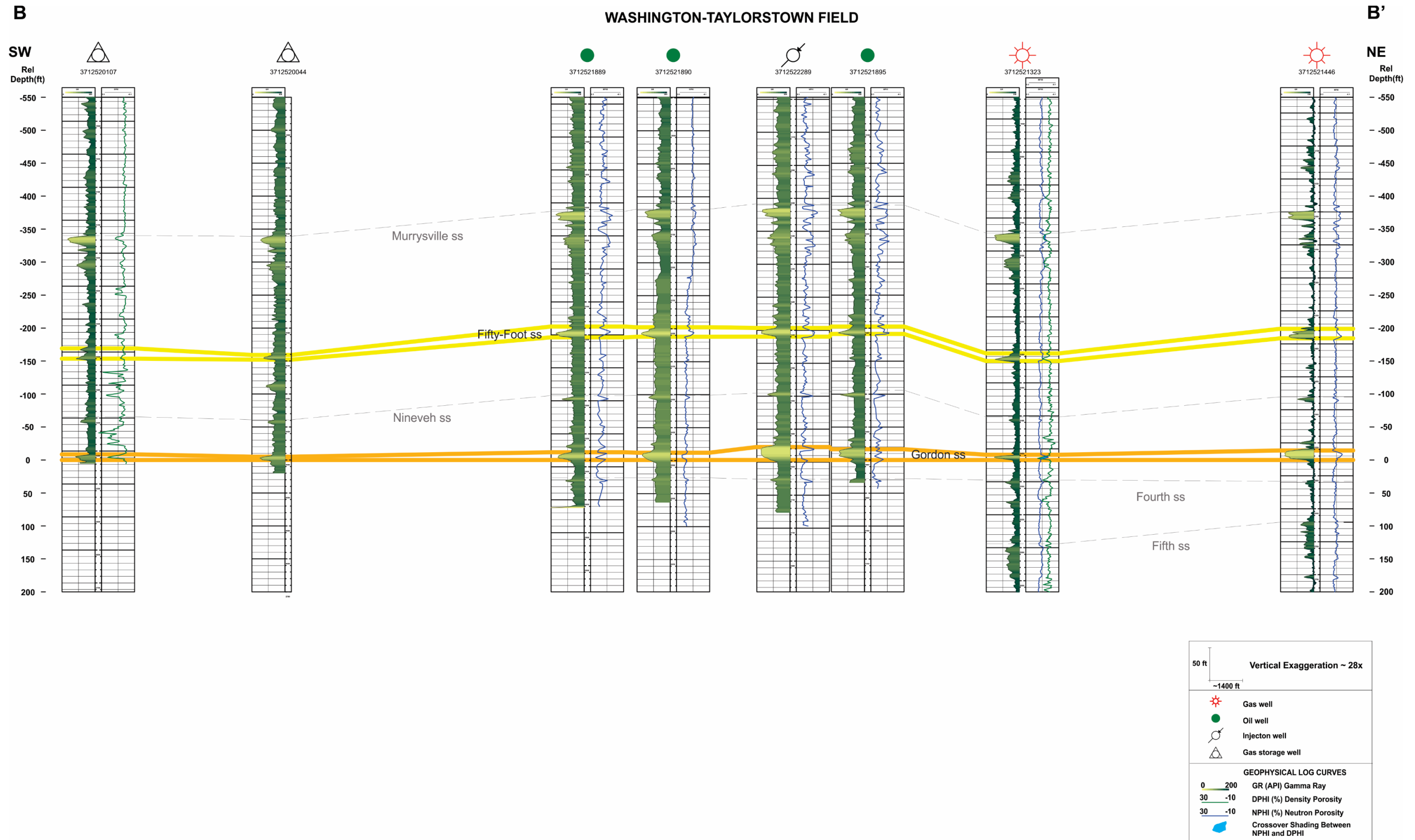


Figure 6-68. Strike cross section B-B', including the western portion of Washington-Taylorstown Field and points farther north.

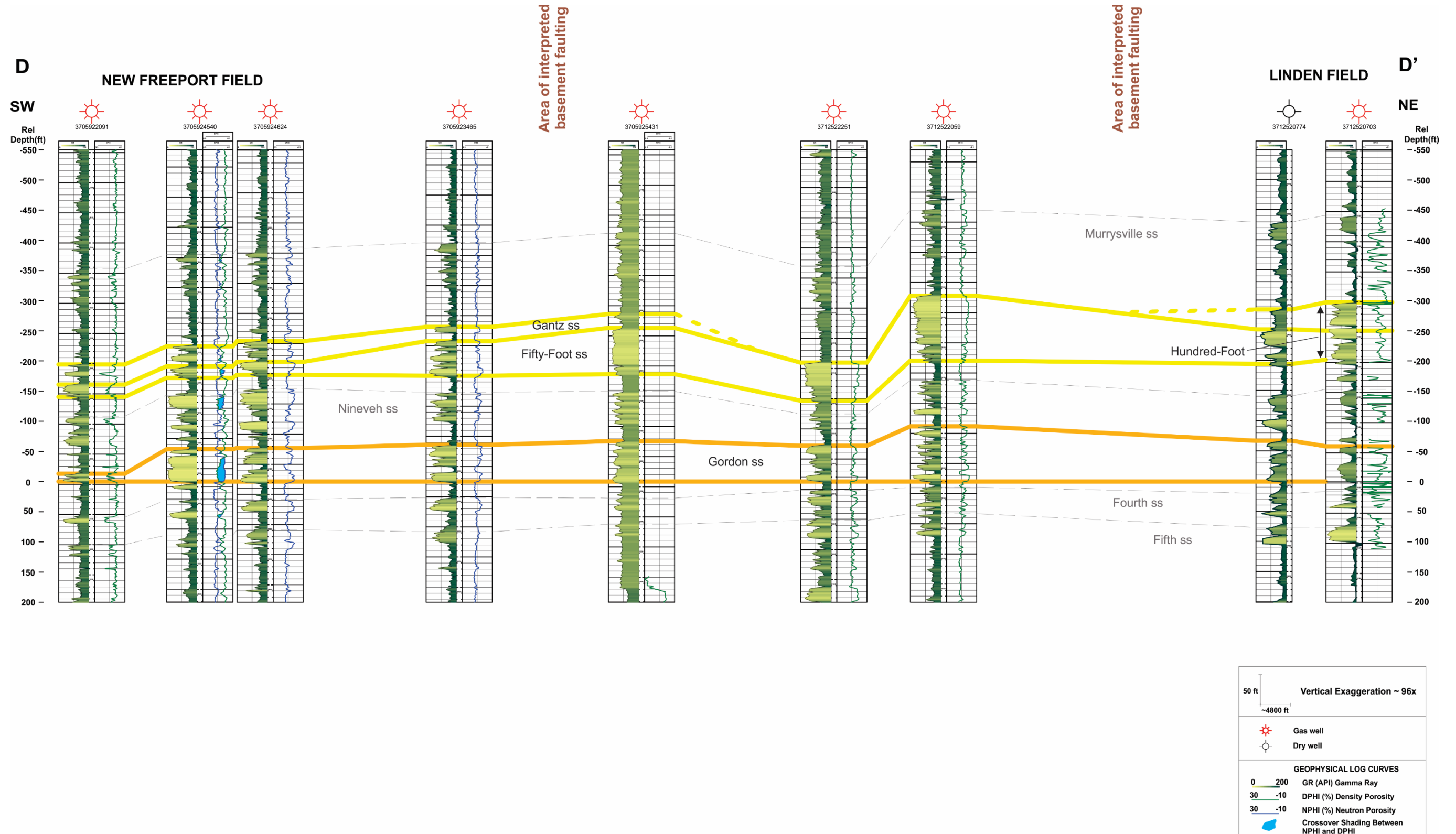


Figure 6-69. Strike cross section D-D', New Freeport Field to Linden Field.

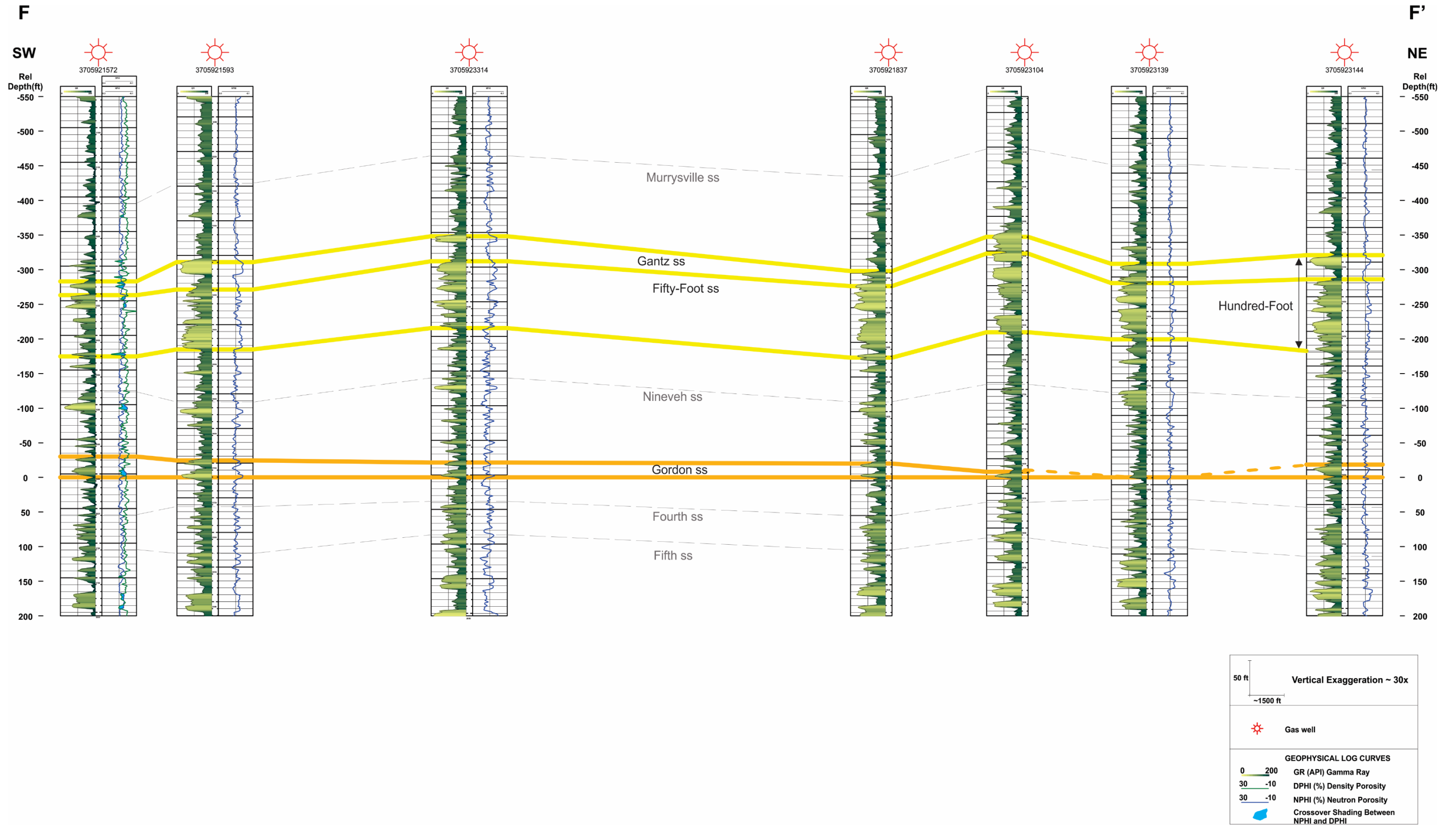


Figure 6-70. Strike cross section F-F', eastern Greene County.

6.5.4 Washington-Taylorstown Field

The Washington-Taylorstown Field (Figure 6-71), situated in central Washington County, Pennsylvania, was discovered with the completion of the Gantz No. 1 (API No. 3712591695) by the Citizens Natural Gas Company on January 1, 1885. Drilled to a depth of 2191 ft, this well reported production of approximately 20 barrels of oil per day (BOPD) from the coffee-colored sandstone at the base of the well, named the “Gantz sand” for the farm on which it was drilled. The Gantz Well not only discovered the Washington-Taylorstown Field, it was the first commercially productive oil well in Washington County, was the first well to export oil out of the county to neighboring areas and spurred extensive oil and gas drilling activity in the greater Washington area for decades to come (Figure 6-72).

A second notable discovery in the Washington-Taylorstown Field occurred in the Summer 1885. The Manufacturers Heat and Light Company completed the Gordon No. 1 (API No. 3712590428) to a depth of 2408 ft on August 21, 1885. This well was located on the Gordon farm, about a mile northwest of the Gantz well, and it produced more than 100 BOPD (Carll, 1887; Boyle, 1898; McGlade, 1967). The oil-producing unit in this well was a 16-ft-thick sandstone aptly named the “Gordon sand.” At the turn of the 20th century, the Gordon well had the distinction of being the deepest oil-producing well in the world. The notoriety and productivity of the Gordon well provided further incentive for active oil exploration and development in Washington County and surrounding areas (Carll, 1887; McGlade, 1967).

The first oil discovery in the western portion of the Washington-Taylorstown Field was the John McMannis No. 1 (API No. 3712501587). This well was completed in the Gordon sandstone in late 1885 (Harper and Laughrey, 1987), and Munn (1912) reported a production rate of 90 BOPD for this well. Subsequent oil development in the greater Taylorstown area joined with activity in the Washington area, ultimately creating the merged field as we know it today.

Shallow oil and gas production, mainly from Venango Group sandstones, was the mainstay of Washington-Taylorstown Field activity throughout the twentieth century (excepting a very short list of unsuccessful tests for shallow CBM and deep Oriskany Sandstone gas). The most recent, notable activity in the greater Washington area was the production of shale gas from the Renz No. 1 (API No. 3712522074) in Hickory Field, northwestern Washington County, which discovered the modern Marcellus Shale gas play and reinvigorated the region’s oil and gas industry. Marcellus Shale gas is currently being produced along the northwestern limits of Washington-Taylorstown Field (Figure 6-72).

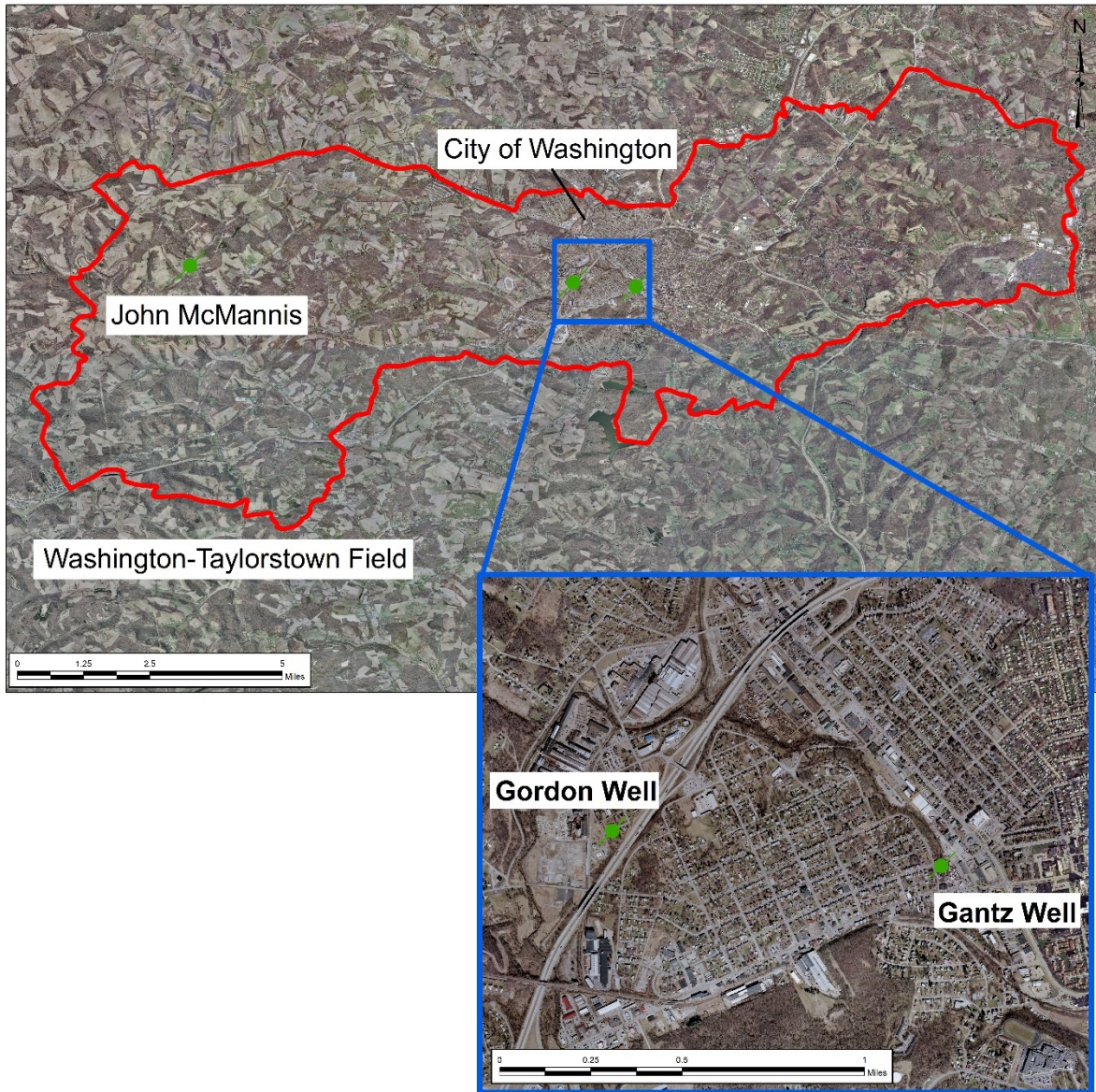


Figure 6-71. Washington-Taylorstown Field and its prominent discovery wells.

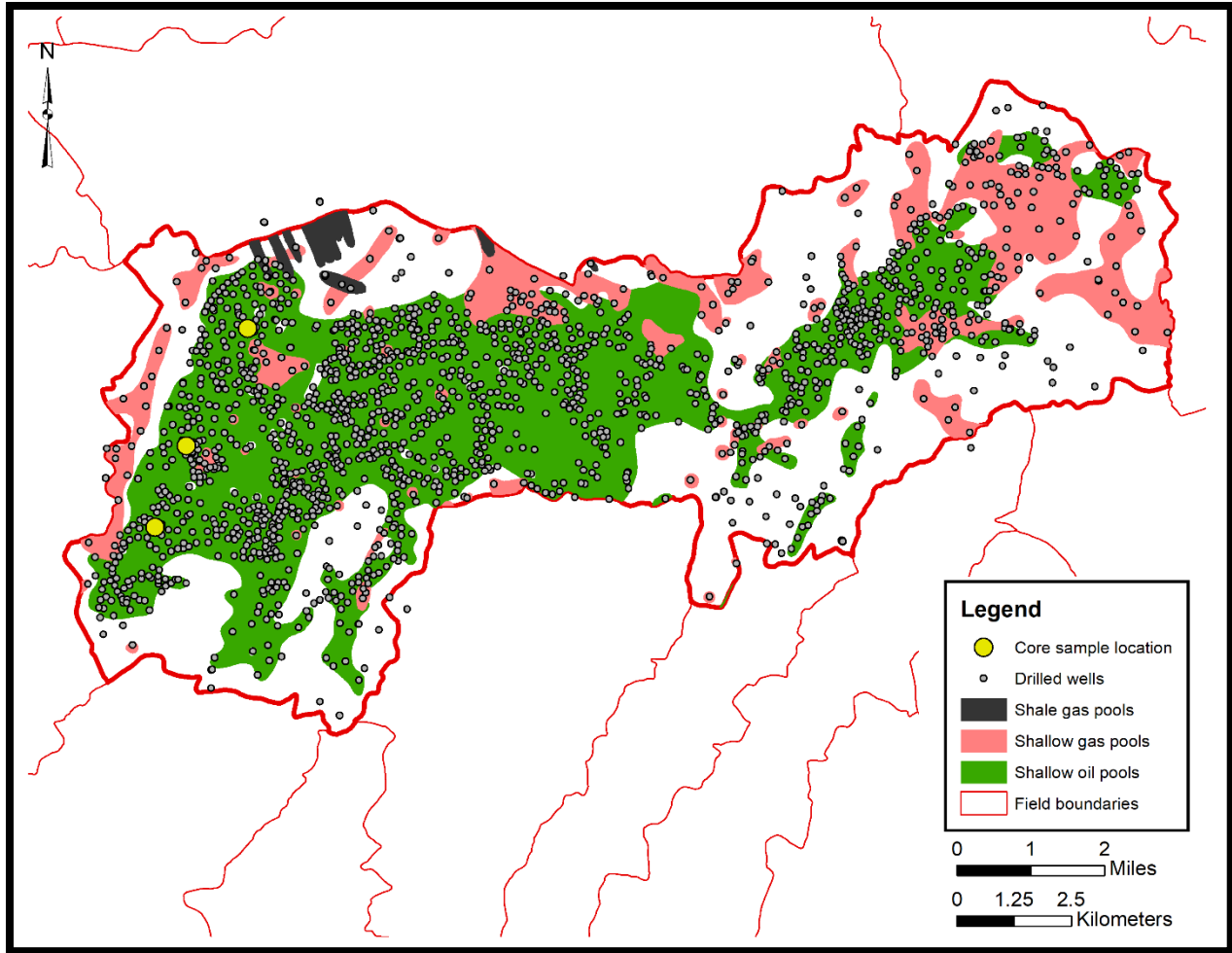


Figure 6-72. The Washington-Taylorstown Field has produced oil, gas and shale gas from more than 1500 wells (EDWIN, 2019).

6.5.4.1 Reservoir Data from Geophysical Logs

Venango Group sandstone reservoir characteristics have been determined using well control specific to this field (Table 6-5). Formations tops and gross thickness data were compiled from several hundred wells for which either geophysical logs or reliable drillers log reports were available. Net thickness values were determined by applying a 100-API GR curve cutoff to the gross thickness interval for those wells with geophysical log control. Average porosity values were computed for net sandstone intervals using NPHI curves; no RHOB or DPHI curves were available for wells in this field.

Table 6-5. Unit-specific reservoir characteristics for the Venango Group in Washington-Taylorstown Field.

Drillers' Sand Name	Top Formation (ft)			Thickness (ft)		Average Neutron Porosity (%)
	Min	Max	Avg	Gross	Net	
Gantz	1930	2640	2310	32	--	--
Fifty-Foot	2059	2716	2404	37	12	10
Gordon	2250	2865	2588	17	13	16
Fourth	2319	2913	2668	20	3	11
Fifth	2390	3015	2708	17	--	--

Based on the average formation top depth data, Gordon and deeper sandstones may offer miscible CCUS opportunities, while shallower units (the Gantz and Fifty-Foot) will likely provide immiscible CCUS prospects. Net thicknesses for both the Fifty-Foot and Gordon sandstones exceed 10 ft, with average NPHI values of 10 percent or more.

6.5.4.2 Core-Derived Data

Venango Group sandstones were the focus of rock coring efforts in central Washington County during the first half of the twentieth century. Three of these core locations are situated on the western limb of Washington-Taylorstown Field and were collected from wells completed in the 1940s. The James McMannis No. 9 (Table 6-6) was completed in 1942 to a depth of 2520 ft and produced oil from the Gordon sandstone. Core from this well spanned both the Gordon Stray and Gordon intervals. The Gordon Stray, a locally present and relatively thin unit, reported an average permeability of 0.45 mD and average porosity of 7.97 percent, while the thicker and more laterally persistent Gordon reported average permeability and porosity values of 106.37 mD and 20.47 percent, respectively (Table 6-4). An average permeability of 100 mD was also reported for the John McMannis No. 1 (API No. 3712501587; the discovery well of the former Taylorstown Field) as part of reservoir modeling and water flood tests conducted in 2001 and 2002 (Farias et al., 2003).

Table 6-6. Gordon stray and Gordon sandstone core test results for the James McMannis No. 9 (API No. 3712501189).

Sample	Depth (ft)	Permeability (mD)	Porosity (%)
Gordon Stray			
X-1	2471.2	0.23	11.82
X-2	2743.3	0.68	1.21
X-3	2474.4	0.44	12.63
X-4	2475.4	ND	11.54
X-5	2478.0	ND	2.63
	Minimum	0.23	1.21
	Maximum	0.68	12.63
	Average	0.45	7.97
Gordon			
X-6	2492.2	2.47	13.19
S-1	2492.5	6.30	17.37
S-2	2493.0	3.62	15.24
X-7	2493.9	20.75	18.08
S-3	2494.7	26.83	19.17
X-8	2495.3	37.04	21.59
S-4	2495.9	108.32	20.59
S-5	2496.5	0.16	17.25
X-9	2497.0	182.10	22.50
S-6	2497.5	221.92	25.91
S-7	2498.0	239.69	20.00
X-10	2498.5	188.85	23.44
S-8	2499.0	284.54	28.29
S-9	2499.5	166.65	23.94
	Minimum	0.16	13.19
	Maximum	284.54	28.29
	Average	106.37	20.47

The Lemon Carson No. 10 was drilled to a depth of 2575 ft in 1944 and completed to produce oil from the Gordon sandstone. The Gordon was cored over a five-ft interval and submitted for permeability, porosity and saturation (oil and water content) testing (Table 6-7). In this well, the Gordon reported an average permeability and porosity of nearly 300 mD and 27 percent, respectively. Saturation analyses indicate that the pore spaces of the Gordon contain from 0 up to about 22 percent oil and 67 to almost 100 percent water, depending on the depth interval tested (Table 6-7). Given this information, the oil content of the Gordon sandstone ranges from 0 (at depths fully saturated with water) to 435 barrels per acre-foot (BBL/ac-ft), where approximately 20 percent of the pore space is filled with oil. Average oil content was reported at 268 BBL/ac-ft.

Table 6-7. Gordon sandstone core test results for the Lemon Carson No. 10 (API No. 3712501137).

Sample	Depth (ft)	Permeability (mD)	Porosity (%)	Saturation (% pore volume)		Oil Content (BBL/ac-ft)
				Oil	Water	
Gordon	2548.0	0.7	5.99	0.00	99.67	0
	2548.7	195.4	25.15	5.96	92.07	116
	2549.5	242.0	26.66	7.67	80.33	159
	2550.5	14.0	24.22	13.07	78.77	245
	2551.5	2.4	24.69	21.95	68.04	420
	2552.0	1.2	27.11	20.67	69.33	435
	2552.5	276.5	25.99	19.84	70.71	400
	2553.0	297.6	26.67	17.76	67.06	367
	Minimum	0.7	5.99	0.00	67.06	0
	Maximum	297.6	27.11	21.95	99.67	435
	Average	128.7	23.31	13.37	78.25	268

Finally, the James Hodgins No. 13 was completed to a depth of 2560 ft in 1946 and produced oil from the Gordon sandstone. As with the Lemon Carson No. 10, Gordon core from this well was submitted for permeability, porosity and saturation (oil and water content) analysis (Table 6-8). Permeability ranged from 4.2 to 328.2 mD, averaging 144.6 mD. Porosity ranged from 9.68 to 27.19 percent, averaging 20.16 percent. Saturation analyses show that Gordon sandstone pore spaces contain anywhere from 0 to almost 14 percent oil and about 60 to 96 percent water, depending on the depth interval. The oil content, as determined from these data, ranges from 0 to 250 BBL/ac-ft, with an average oil content of 154 BBL/ac-ft.

Table 6-8. Gordon sandstone core test results for the James Hodgins No. 13 (API No. 3712501175).

Sample	Depth (ft)	Permeability (mD)	Porosity (%)	Saturation (% pore volume)		Oil Content (BBL/ac-ft)
				Oil	Water	
Gordon	2551.0	4.8	11.72	12.49	81.35	114
	2551.5	16.4	11.07	0.00	89.84	0
	2552.7	314.2	26.37	10.38	79.36	212
	2553.4	328.2	27.19	10.81	77.75	228
	2553.8	285.3	26.80	10.41	79.81	217
	2554.5	290.9	26.41	12.21	75.46	250
	2355.0	61.7	21.81	13.87	84.42	235
	2555.5	106.8	23.17	9.86	77.00	177
	2556.0	33.1	17.38	7.94	59.74	107
	2557.3	4.2	9.68	0.00	96.06	0
	Minimum	4.2	9.68	0.00	59.74	0
Maximum	328.2	27.19	13.87	96.06	250	
Average	144.6	20.16	8.80	80.08	154	

6.5.4.3 Summary

The Washington-Taylorstown Field is both an historically and economically important field in Pennsylvania's oil belt. Here, the Gantz and Gordon sandstones of the Venango Group were first discovered in 1885 and provided the impetus for regional development of Venango Group reservoirs into the twentieth century. Multiple units (the Gantz, Fifty-Foot, Gordon, Fourth and Fifth sandstones) in the field have produced oil and gas from average depths of 2300 to 2700 ft, falling in the immiscible/miscible CCUS depth range. Net sandstone thicknesses and average porosities, as determined from available geophysical log data, range from 3 to 12 ft and 10 to 16 percent, respectively (Table 6-3).

The Washington-Taylorstown Field is uniquely situated in the center of Washington County, with the City of Washington overlying the midpoint of the field, where the top of the Venango Group is its shallowest and earliest oil production occurred (Figure 6-71). In contrast, the western and eastern limbs of the field, where suburban to rural land use dominate, have supported a majority of the twentieth century production activities, including that of the Marcellus Shale.

The western limb of the field has supported EOR from Venango Group reservoirs for decades. Here, the top of the Venango Group (which essentially represents the top of the Fifty-Foot sandstone, as the Gantz is largely absent here) ranges from about 2100 to 2600 ft deep,

averaging 2400 ft. The most prolific oil-bearing sandstones include the Fifty-Foot and Gordon sandstones, which are generally thin (Figure 6-64 and Figure 6-65) but typically clean (Figure 6-68), likely offering an updip facies (sand bar or other shoreface deposit) pinchout as a trapping mechanism. Core samples taken from the Venango Group's Gordon Zone in several locations (Figure 6-72) report average porosities and permeabilities on the order of 20 to 23 percent and 106 to 145 mD, respectively. Where fluid saturation analyses were conducted, the Gordon was found to offer hundreds of barrels of oil per ac-ft of reservoir (Table 6-7 and Table 6-8).

The eastern limb of the field is associated with thicker deposits of Gantz and Fifty-Foot sandstones (the "Hundred-Foot" Zone; Figure 6-63 and Figure 6-64) as well as relatively thick Gordon deposits (Figure 6-65). In this part of the field, the top of the Venango Group is approximately 1800 to 2700 ft deep, averaging 2300 ft below ground surface (BGS). Here, the Gantz, Fifty-Foot and Gordon sandstones are the largest oil producers. Based on core analyses available for a well in neighboring Linden Field (see Section 6.5.5), the Gordon sandstone offers an average porosity of 7.24 percent, average permeability of 9.2 mD and an oil content in excess of 125 BBL/ac-ft.

Local natural gas storage operations also corroborate favorable Venango reservoir characteristics in this part of Washington County. The Mehaffy Field's Donegal storage pool (just west of Washington-Taylorstown Field) has been used to store methane in the Gordon Stray sandstone since it was converted to this usage in 1934. The oil and gas industry's repurposing of depleted/depleting sandstone reservoirs for storage applications suggests that the favorable trapping mechanisms, injectability and deliverability needed for successful CCUS operations may be here as well, with reservoir depth determining whether utilization and storage will ultimately be miscible or immiscible.

6.5.5 Linden Field

The Linden Field (Figure 6-73), situated in North Strabane Township, Washington County, is considered a northeastern extension of Washington-Taylorstown Field. This area experienced drilling activity as early as 1886, in response to the Gantz and Gordon oil discoveries made in Washington (Fettke et al., 1946). Early gas wells produced from the "First Salt sand" of the Pottsville Formation, the "Big Injun sand" of the Burgoon Formation and multiple Venango Group sandstones (Gantz, Fifty-Foot, Gordon, Fourth and Fifth), while oil production came mostly from the Gantz and Gordon zones (Fettke et al., 1946). Exploratory activity waned in the 1890s but picked up again in 1945 when a flowing well was completed on the George A. Ackroyd farm (API No. 3712592758), with an estimated production of 100-170 BOPD from the Gordon sandstone (Fettke et al., 1946). For the remainder of the twentieth century, activity in this field was limited to shallow Venango Group well completions, but most recently, the production of oil and gas from the Upper Devonian Brallier Formation (ca 2010) and shale gas from the Middle Devonian Marcellus Shale (ca 2015) have been reported (NOTE: shale gas pools are not illustrated in Figure 6-73 due to limited data availability at the time the petroleum field geodatabase was finalized).

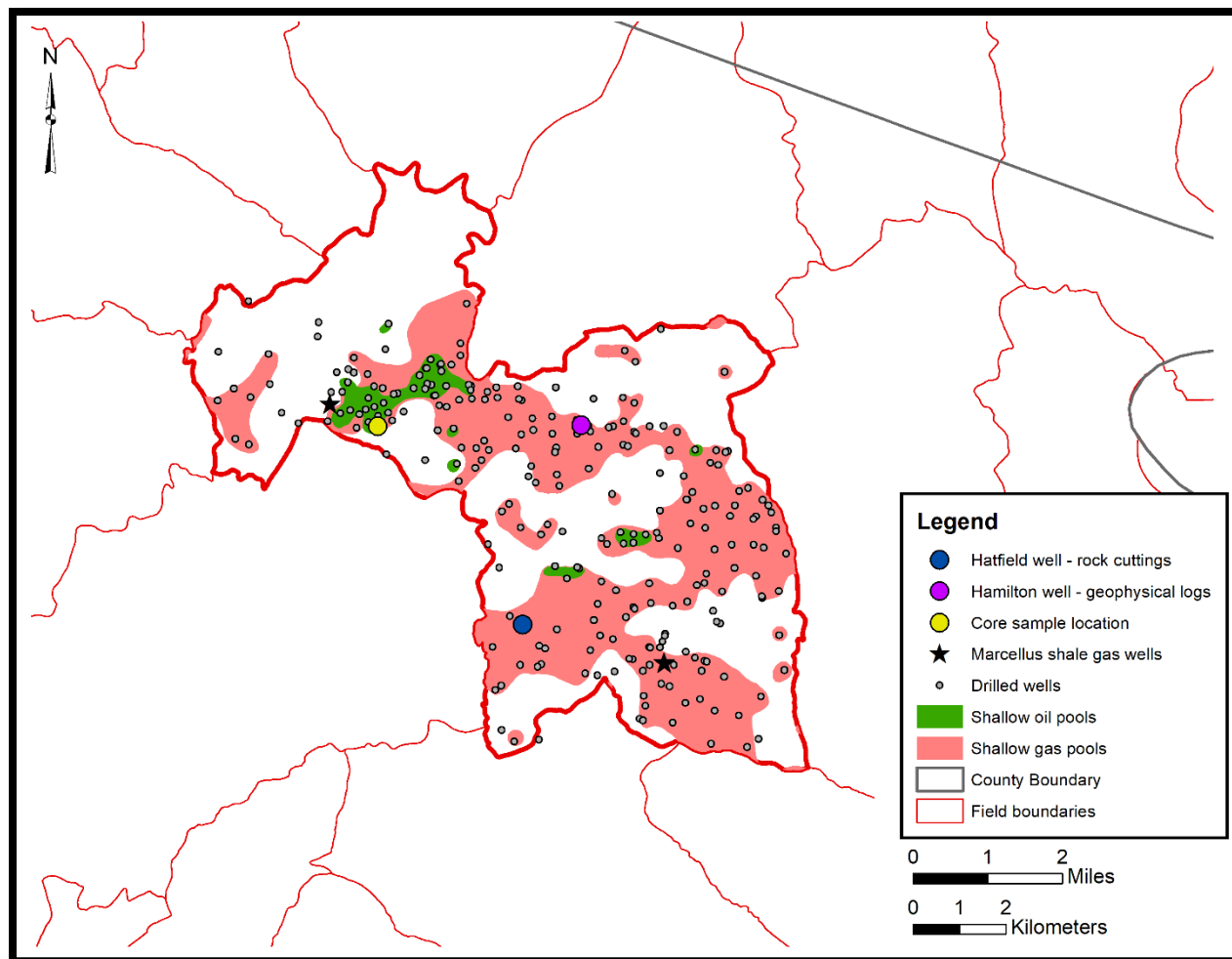


Figure 6-73. The Linden Field has produced shallow oil and gas from more than 200 wells (EDWIN, 2019).

6.5.5.1 Reservoir Data from Geophysical Logs

Venango Group sandstone reservoir characteristics have been determined using available well control (Table 6-9). Formations tops and gross thickness data were compiled from dozens of wells for which either geophysical logs or reliable drillers log reports were available. Net thickness values were determined by applying a 100-API GR curve cutoff to the gross thickness interval for those wells with geophysical log control. Average porosity values were computed for net sandstone intervals using DPHI curves; no NPHI curves were available for wells in this field.

Table 6-9. Unit-specific reservoir characteristics for the Venango Group in Linden Field.

Drillers' Sand Name	Top Formation (ft)			Thickness (ft)		Average Density Porosity (%)
	Min	Max	Avg	Gross	Net	
Gantz	1985	2500	2240	55	34	9
Gordon	2288	2769	2507	48	28	9
Fourth	2326	2740	2530	26	9	8
Fifth	2401	2788	2557	27	14	9

Based on the average formation top depth data in Table 6-9, Gordon and deeper sandstones may offer miscible CCUS opportunities, while the shallower Gantz will likely provide immiscible carbon storage and/or CO₂-EOR opportunities. Net thicknesses for these units range from 9 to 34 ft and offer porosities of 8 to 9 percent.

6.5.5.2 Core-Derived Data

PAGS cored a complete section of the Gordon sandstone in the J.L. Kenamond No. 1, a Linden Field oil well completed to a depth of 2610 ft in 1945. The reader is referred to Fettke et al. (1946) for detailed lithologic descriptions, porosity and permeability profiles and laboratory analytical results associated with this core. The Gordon was cored from 2423 to 2502 ft (79 ft total) and submitted for permeability, porosity and saturation testing (Table 6-10).

Table 6-10. Gordon sandstone core test results for the J.L. Kenamond No. 1 (API No. 3712592783).

Sample	Depth (ft)	Permeability (mD)	Porosity (%)	Saturation (% pore volume)		Oil Content (BBL/ac-ft)
				Oil	Water	
Gordon	2427.7	0.3	2.49	25.62	72.02	50
	2428.4	0.9	2.28			
	2432.5	0.3	3.62	15.89	80.41	45
	2443.1	1.5	4.47			
	2448.1	0.4	3.54			
	2450.0	1.0	7.87			
	2452.7	0.7	4.59			
	2459.5	9.6	6.57			
	2462.1	11.6	11.21			
	2462.7	3.9	11.19			
	2462.8	96.0	10.11			
	2465.7	0.9	8.14	25.59	14.22	162
	2468.3	2.5	11.69	24.86	27.16	226
	2469.6	1.9	10.31			
	2470.4	0.8	9.24	17.16	32.60	123
	2472.2	1.1	8.48			
	2473.1	0.9	9.16	14.47	45.08	103
	2475.6	3.2	7.72			
	2477.1	1.0	8.37	25.80	41.95	168
	2478.5	71.5	7.82	22.60	13.09	137
	2479.5	1.1	7.68			
	2484.2	0.4	4.52			
2486.0	0.4	5.55				
	Minimum	0.3	2.28	14.47	13.09	45
	Maximum	96.0	11.69	25.80	80.41	226
	Average	9.2	7.24	21.50	40.82	127

The average permeability of the Gordon sandstone in this well was 9.2 mD, notably less than the values reported for the same unit in Washington-Taylorstown Field (i.e., ~106-145 mD). The average core-derived porosity was reported at 7.24 percent, generally consistent with average density porosities derived this study's geophysical logs (8 to 9 percent) but less than half that reported for Gordon core in Washington-Taylorstown Field (~20 to 23 percent). Saturation analyses indicate that Gordon pore space contains about 15 to 26 percent oil and 13 to 80 percent water (Table 6-10). Given this information, the oil content of the Gordon sandstone ranges from 45 to 226 BBL/ac-ft, where approximately 25 percent of the pore space is filled with oil. Average oil content was reported at 127 BBL/ac-ft.

6.5.5.3 Other Studies

Mineralogy and Porosity Investigation

A PAGES geology intern worked with PAGES staff to prepare an independent study of rock cuttings and geophysical logs from two of the older wells completed in Linden Field (Kanavy, 2018; Appendix H). Rock cuttings from the Harry Hatfield No. 1 (API No. 3712590083) and recently received geophysical and sample logs for the Hamilton No. 3299 (API No. 3712520703) were evaluated as part of this work.

Gantz and Gordon sandstone samples were obtained from the PAGES cuttings library for the Harry Hatfield No. 1 and subjected to sieve analysis, bulk mineralogy testing and scanning electron microscopy (SEM) analysis as per the methods described in Appendix H. Sieve analysis determined that both sandstone units consist mostly of fine-grained sand, with lesser amounts of medium-coarse sand; fine to medium sand; and silt-size particles. XRD analyses determined the bulk mineralogy of the Gantz sandstone to contain 75 percent quartz and 25 percent clay minerals, while the Gordon sandstone consisted of 72 percent quartz, 23 percent clay and 5 percent carbonate minerals.

SEM analyses were performed on multiple sample depths from the Gantz (2420-2424 ft) and Gordon (2672-2700 ft) intervals in the Harry Hatfield No 1, with the intent of visualizing the mineral and pore space characteristics of these reservoir rocks. Given that the source material was comprised of rock cuttings (as opposed to core) and the SEM requires intact samples, the samples collected for this work were preferentially comprised of rock chips with mixed mineralogic content. Cleaner sandstone fractions could not be sampled for SEM analysis due to particle size – they were broken into individual sand grains, either during the drilling process itself or over time while in storage.

As viewed under the SEM, samples from both geologic units contained an abundance of platy clay minerals (Figure 6-74). No visual porosity was noted for samples from the Gantz sandstone, but some was observed in the Gordon sandstone (Figure 6-75).

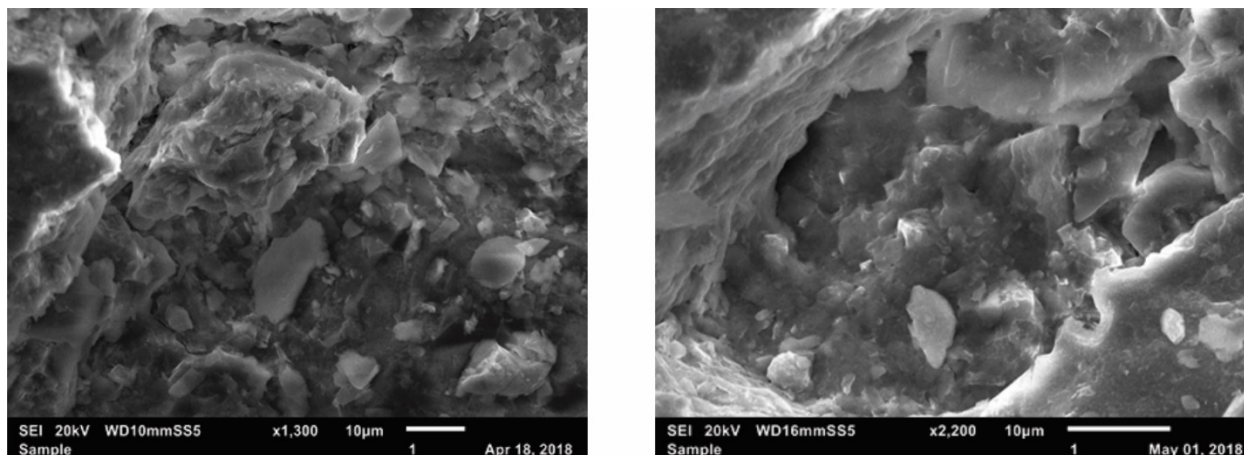


Figure 6-74. SEM images (secondary electron imaging) of the Gantz sandstone at 2420-2424 ft (left) and Gordon sandstone at 2672-2680 ft (right). Platy clay minerals are visible in both samples.

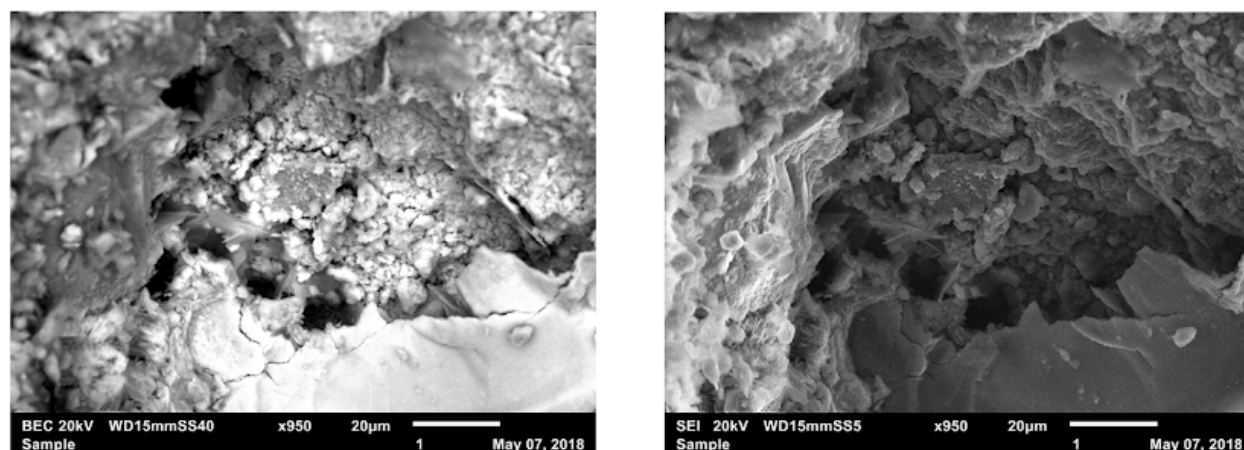


Figure 6-75. SEM images of porosity (dark spots with dimension) in the Gordon sandstone at 2690-2700 ft (backscatter electron composition, left; secondary electron imaging, right).

The presence of platy clay minerals on and between mineral grains, as reported here for the Gordon sandstone, is consistent with the results of thin section analyses prepared by Fettke et al. (1946) for the Kenamond No. 1 (API No. 3712592783). Specifically, Fettke reported (Fettke et al., 1946, p. 35):

“Examination under a polarizing microscope of thin sections, prepared from samples of the sandstone cut from the 2458-2480 interval in the Kenamond core representing the various textural types, revealed that the low porosities and relatively low permeabilities are due to two causes. In some instances, considerable quantities of clay minerals, up to 20 percent by volume, fill the space between the quartz grains. More frequently, however, cementation by the recrystallization of quartz in a manner similar to that described by Waldschmidt (1941) was observed.”

In the first scenario postulated by Fettke et al. (1946), primary intergranular porosity would be largely destroyed as clay minerals filled intergranular pore space during compaction. In the second scenario, however, primary porosity would be reduced, but not completely obliterated, by quartz precipitation during burial. In fact, as part of the petrologic study of Venango Group

sandstones performed by Harper and Laughrey (1987), cementation by secondary minerals (not just silica, but also calcite, dolomite, chlorite, smectite and sericite) was observed to reduce, but not destroy, the porosity of these units. Harper and Laughrey (1987) went on to report that secondary porosity in Venango Group sandstones is mainly the result of dissolution of carbonate cement and, to a lesser extent, of feldspar and chert grains. The effective porosity is a hybrid of reduced primary pore space and secondary void space of dissolution origin. This interpretation of Venango sandstone porosity is based on petrographic studies and is supported by the observed scatter in permeability when plotted against porosity (Figure 6-76).

Geophysical and geological sample logs were obtained for the Hamilton No. 3299 as part of a large corporate donation of geophysical logs to PAGES in 2017. Kanavy (2018) digitized and interpreted the Hamilton logs to further describe the reservoir characteristics of the Gantz and Gordon sandstones in Linden Field. Figure 6-77 summarizes the results of this work. The digitized GR curve is shown on the left, and the geological sample log is in on the right. The top of the Venango Group is defined as the top of the Gantz sandstone at 2250 ft. The top of the Gordon sandstone is a few hundred feet below, at a depth of 2570 ft. This well is also included as the northernmost well in geologic cross section D-D' (Figure 6-69).

Sample descriptions for the Gantz and Gordon sandstones in this well are summarized as follows: (1) Gantz – very light gray to white sandstone, fine-grained, occasionally coarse to very coarse-grained, subangular, poorly sorted, friable and poor to fair intergranular porosity; (2) Gordon – very light gray sandstone, fine-grained, subangular, fair sorting, friable, slightly calcareous and poor intergranular porosity. Using geophysical log data for the Hamilton No. 3299, average bulk densities of the Gantz and Gordon were determined to be 2.48 g/cm³ and 2.51 g/cm³, respectively. The average porosity of the Gantz and Gordon intervals were 8.25 and 7 percent, respectively.

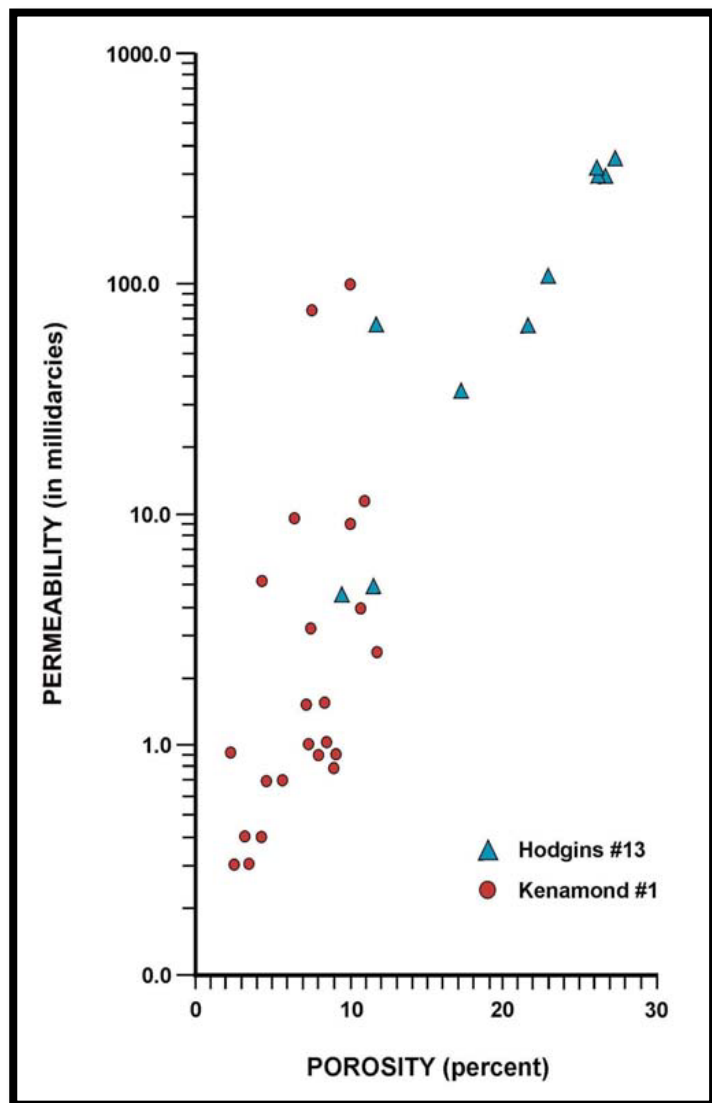


Figure 6-76. Porosity-permeability crossplot, using Gordon sandstone core data from Washington County wells (Hodgins No. 13, API No. 3712501175; Kenamond No. 1, 3712592783; PA DCNR, 2009).

Unit Depth and Pore Space Investigation

A PAGES intern prepared an undergraduate thesis on reservoir attributes of the Gantz and Gordon sandstones in Linden Field (Remis, 2018; Appendix I). This study was conducted using formation top data reported by operators in their well record filings, as opposed to interpretations of downhole geophysical logs. Remis (2018) prepared measured depth and gross isopach maps for the Gantz and Gordon units, and used this information to calculate anticipated pore space volumes that may exist in these rocks. Perhaps most helpful to those considering miscible and/or immiscible CCUS applications in Linden Field is the inventory of the tops data Remis extracted from the Exploration and Development Well Information Network (EDWIN), and the gross thicknesses derived from these data, which is provided in Remis' Appendix A (Appendix I).

6.5.5.4 Summary

The Linden Field is a northeastern extension of Washington-Taylorstown Field, with drilling activity dating back to 1886. Early exploratory activities were focused on finding oil in the Gantz and Gordon sandstones, which occur at depths of about 2200 to 2500 ft (putting them in the immiscible/miscible CCUS depth range). Through the years, however, gas was found in shallower formations, other sandstones of the Venango Group and even deeper units in this area. The completion of a flowing Gordon oil well on the Ackroyd farm (API No. 3712592758) in 1945 provided renewed interest in

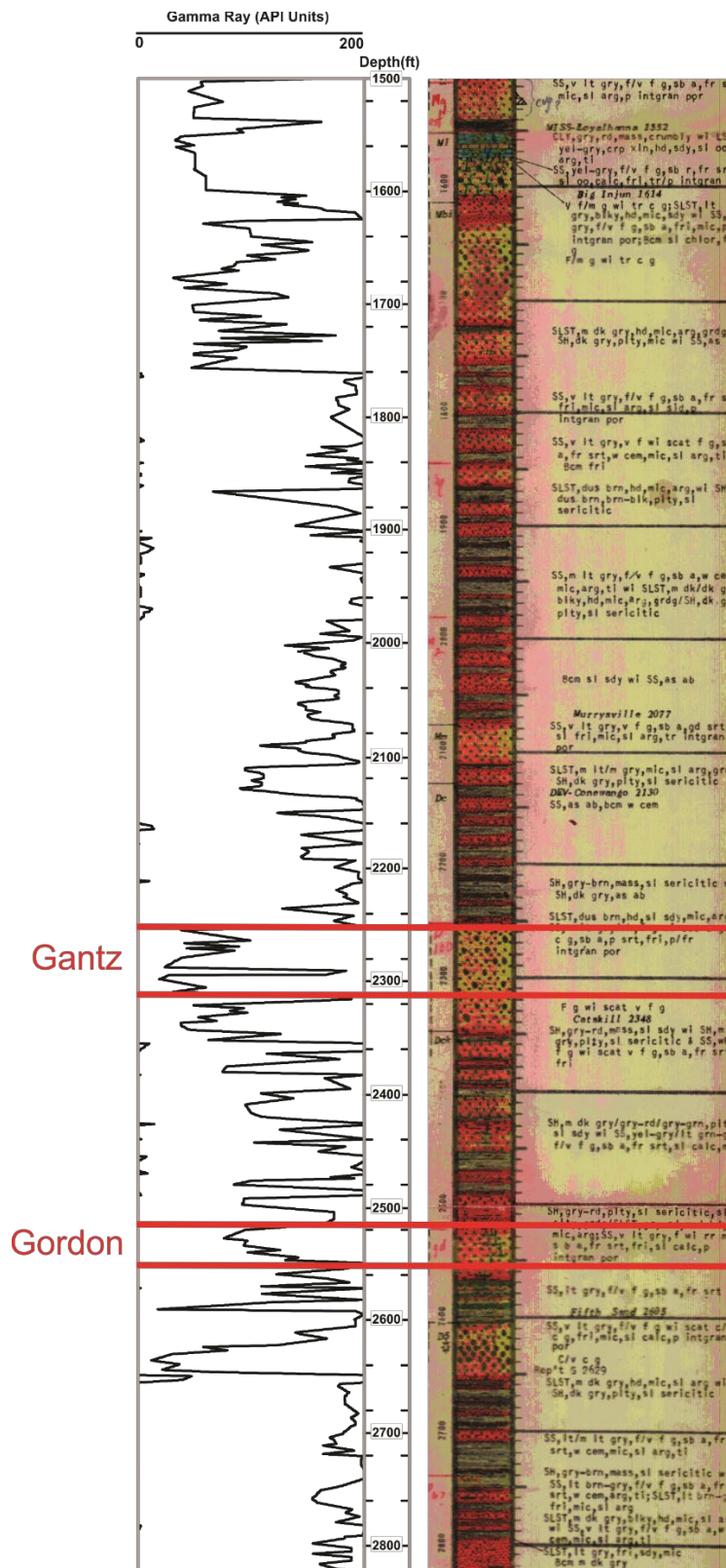


Figure 6-77. Hamilton No. 3299 (API No. 3712520107) GR and sample logs.

this fledgling field, including that on the part of the PAGS, which prepared a mineral resource report to define, describe and interpret the geology and oil and gas resources of the area (Fettke et al., 1946). The most recent activity in Linden Field has included the development of the Middle Devonian Marcellus Shale in North Strabane Township (north) and Somerset Township (south) (Figure 6-73).

The Linden Field has supported shallow oil and gas production from multiple Venango Group units, with the Gantz and Gordon providing the lions' share of the field's oil production over time. Here, the top of the Venango Group (represented by the omnipresent Gantz sandstone; see Figure 6-63) ranges from 1985 to 2500 ft in depth, averaging 2240 ft. Net sandstone thicknesses and average porosities, as determined from available geophysical log data, range from 9 to 24 ft and 8 to 9 percent, respectively (Table 6-9). Core analyses of the Gordon sandstone from the Kenamond No. 1 (API No. 3712592783) report an average porosity of 7.24 percent, comparable to that determined from local geophysical logs, an average permeability of 9.2 mD and an oil content greater than 125 BBL/ac-ft.

Although the Washington-Taylorstown and Linden fields are adjacent to one another, we have observed at least a few differences between them, mainly related to lithology, lithostratigraphy and petroleum hydrocarbon production trends. First, unlike Washington-Taylorstown Field, the Gantz sandstone of Linden Field represents the top of the Venango Group over its entire footprint, with a gross average thickness of 50 ft (Figure 6-63 and Table 6-9). In other words, the "Hundred-Foot" Zone is present throughout the subsurface of Linden Field. In the Washington-Taylorstown Field, the Gantz sandstone is thinner, and even absent in places along its western limb (Figure 6-63). Second, the Fifty-Foot sandstone of Linden Field does not produce oil as it does in Washington-Taylorstown; instead, it has been reported to produce only minor gas (Fettke et al., 1946). Third, and perhaps most importantly from a CCUS injectivity standpoint, the Gantz and Gordon sandstones of Linden Field are thicker (both gross and net values), with silty and shaley lenses separating cleaner reservoir intervals (see Figure 6-67, Figure 6-68 and Figure 6-69). This mixed lithology is corroborated by the sieve, mineralogy and SEM sample studies performed as part of the current work (Kanavy, 2018, and Figure 6-74 and Figure 6-75).

6.5.6 New Freeport Field

The New Freeport Field (Figure 6-78) is situated in the southwestern corner of Greene County, Pennsylvania and has the deepest Venango Group sandstone deposits (Figure 6-62) of all three Pennsylvania case studies. Petroleum exploration began here in 1896, and oil and gas drilling and production from these units has continued to the present time. In the early 1990s, some methane was produced from coal seams of the Permian Dunkard and Pennsylvanian Monongahela groups, and most recently, shale gas production from the Middle Devonian Marcellus Shale (ca 2013) has been documented (NOTE: shale gas pools are not illustrated in Figure 6-78 due to limited data availability at the time the petroleum field geodatabase was finalized).

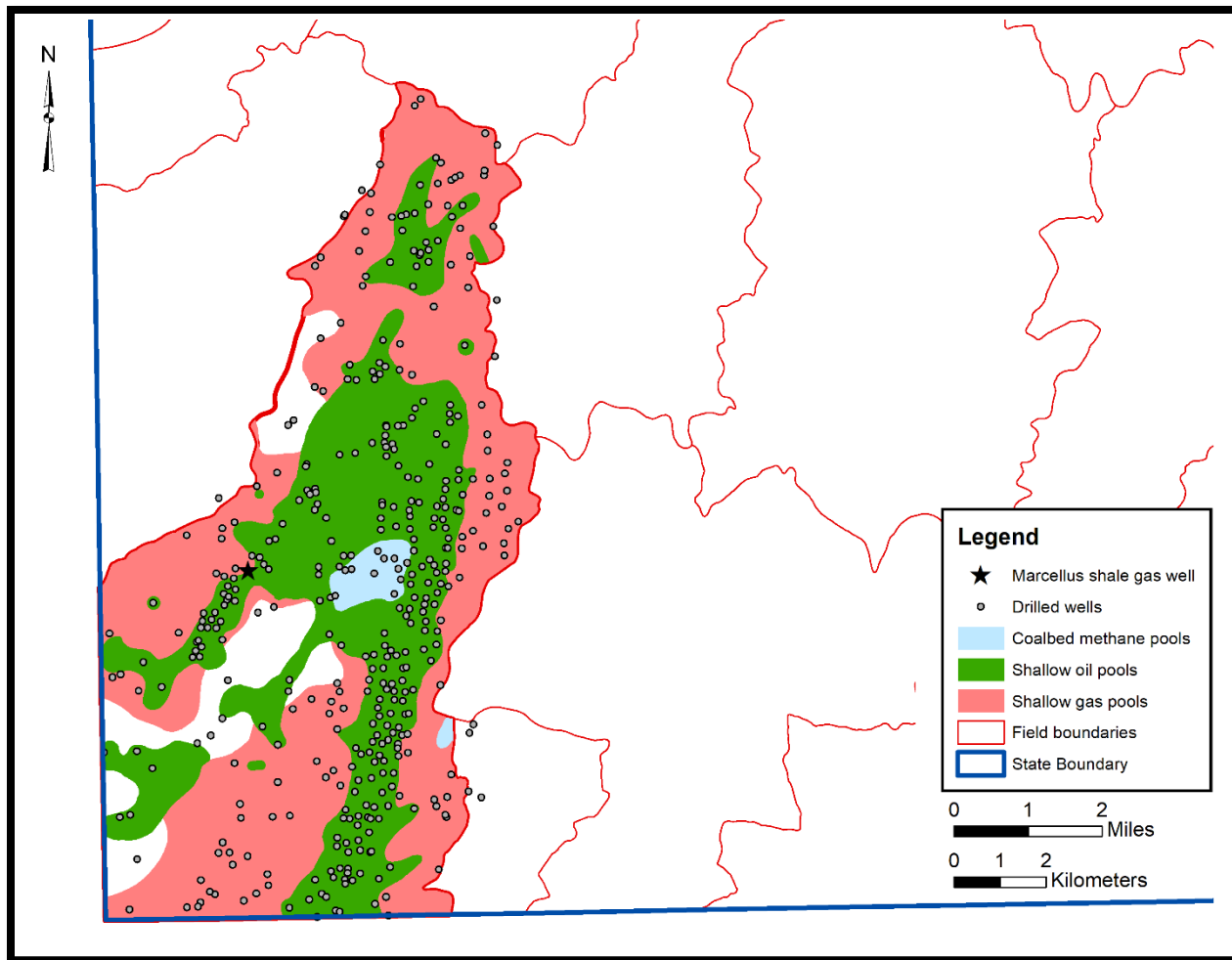


Figure 6-78. The New Freeport Field has produced shallow oil and gas (including some CBM) from approximately 400 wells (EDWIN, 2019).

6.5.6.1 Reservoir Data from Geophysical Logs

Venango Group sandstone reservoir characteristics have been determined using well control specific to this field (Table 6-11). Formations tops and gross thickness data were compiled from a limited number of wells (≤ 31) for which either geophysical logs or reliable drillers log reports were available. Net thickness values were determined by applying a 100-API GR curve cutoff to the gross thickness interval for those wells with geophysical log control. Average porosity values were computed for net sandstone intervals using DPHI or NPHI curves, or both (average value).

Table 6-11. Unit-specific reservoir characteristics for the Venango Group in New Freeport Field.

Drillers' Sand Name	Top Formation (ft)			Thickness (ft)		Porosity		
	Min	Max	Avg	Gross	Net	Density (%)	Neutron (%)	Average (%)
Nineveh	2833	3395	3153	57	43	18	6	12
Gordon	2892	3476	3209	44	51	10	3	7
Fourth	2950	3553	3278	15	11	8	5	7

Based on these data, the Nineveh, Gordon and Fourth sandstones offer miscible targets for CCUS applications. Net thicknesses range from 11 to 51 ft, while average porosities range from 7 to 12 percent. The New Freeport Field lacks publicly available core data, so none is reported herein.

6.5.6.2 Summary

The New Freeport Field has experienced shallow oil and gas development since 1896, and within the past few decades, shallow CBM and Marcellus Shale gas have also been produced here. This field is situated within what can be called the Gordon fairway – that northeast-southwest trending area between the Washington-Taylorstown Field and oil fields described for northern West Virginia in the next section of this report – that have produced significant volumes of oil from the Gordon Zone over a period of decades.

The top of the Venango Group in New Freeport Field ranges from about 2700 to 3300 ft deep, averaging almost 3100 ft, and so all Venango Group sandstones in this corner of the state fall in the miscible depth range for CCUS applications. The Gantz is either very thin or absent here (Figure 6-63), and the underlying Fifty-Foot sandstone occurs at thicknesses of 50 ft or less (Figure 6-64).

The Nineveh, Gordon and Fourth sandstones, all known for their oil production in the New Freeport Field, occur at average depths of 3100 to 3300 ft. Based on geophysical log data, these sandstones have gross thicknesses of 15 to 57 ft, net thicknesses of 11 to 43 ft and average porosities of 7 to 12 percent (Table 6-11). The three New Freeport wells in geologic cross section D-D' (Figure 6-69) corroborate these data by illustration. Here, the Nineveh sandstone is relatively thick and exhibits a stacked sandstone appearance, with minor siltstone and shale breaks between the sandstone intervals, and the Fourth sandstone, although relatively thin (20 ft or less), is clean. These three sandstone intervals may offer stacked CCUS opportunities, as described in Section 6.6.9.

6.5.7 History of EOR in Southwestern Pennsylvania

An historical summary of Pennsylvania's EOR activities was included in Riley et al. (2010), MRCSP's Phase II Task Report on CO₂-EOR and sequestration opportunities in regional oil and gas fields. Although many of the commonwealth's oil fields have undergone various recovery projects over the decades, including both secondary (vacuum, air/gas drive and water flooding) and tertiary (chemical flooding and thermal stimulation) efforts, most of the success stories are associated with water flood projects in the Northern District, and in particular, Bradford Oil Field (Riley et al., 2010).

With respect to southwestern Pennsylvania, EOR operations have been performed using air/gas drive and water flood techniques, or some iterative combination of these, over the past century. Some have been successful, while others have not (Figure 6-79).

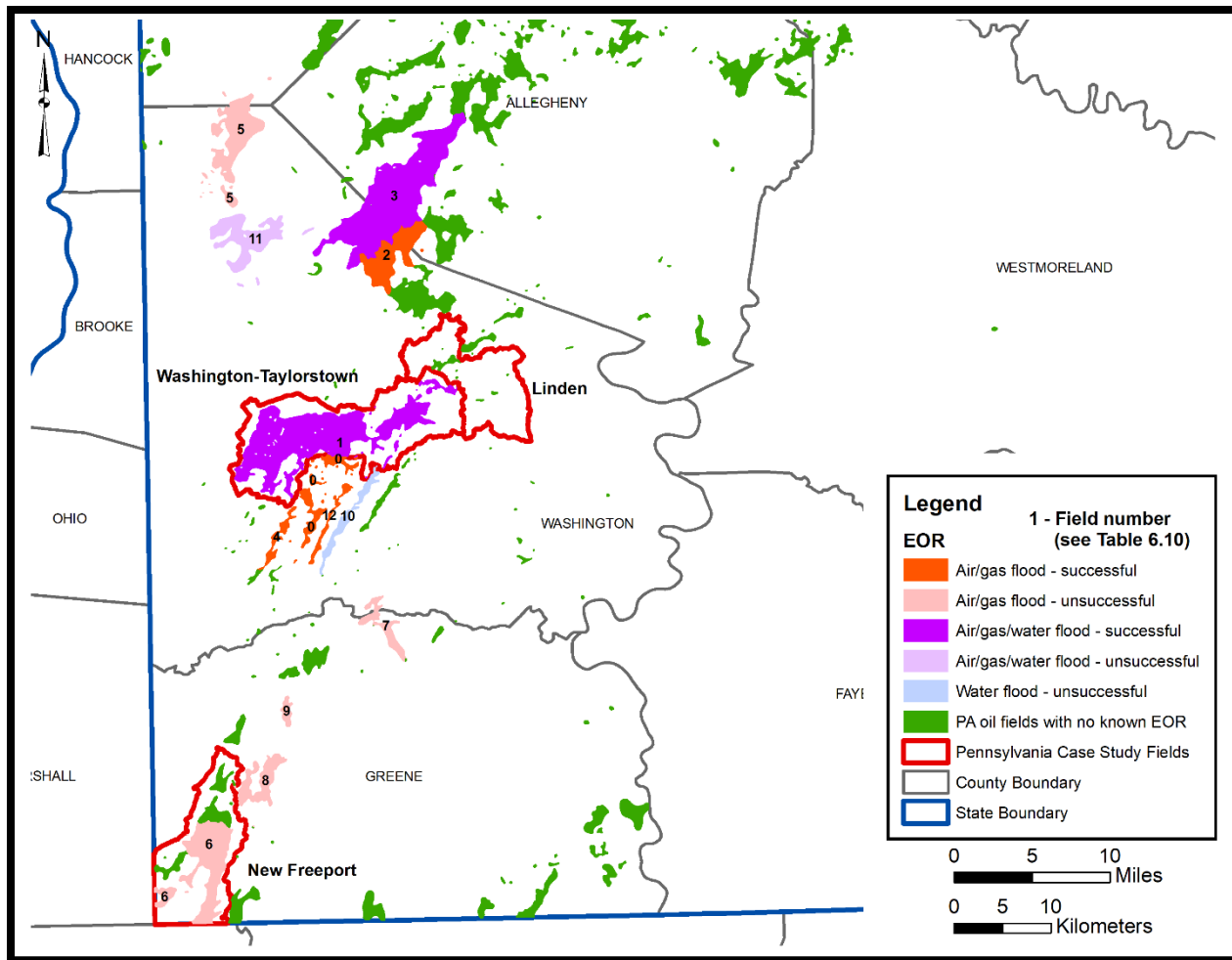


Figure 6-79. EOR activities in southwestern Pennsylvania (modified from Riley et al., 2010).

The historical data regarding EOR practices and target reservoirs in the study area are based largely on information reported by Lytle (1960), Lytle (1976) and Harper and Laughrey (1987) and are provided in Table 6-12. All producing reservoirs that have been targeted for EOR in Washington and Greene counties are associated with the Upper Devonian Venango Group and occur at average depths of 1900 to 3300 ft below ground surface. Six of the thirteen EOR projects completed in this area have been successful (Field #s 0, 1, 2, 3, 4 and 12 in Figure 6-79). All projects incorporated air/gas drive methods, and two of the six – Washington-Taylorstown Field (#1) and McDonald-McCurdy Field (#3) – have also implemented successful water flood projects at some point in time (Table 6-12).

Table 6-12. EOR activity in Southwestern Pennsylvania oil fields.

Field	Pool	Map #	EOR Method	Success?	EOR Producing Unit(s)	Reported Depth (ft)
Amity	Fonner	7	Air/gas flood	no	Gantz sandstone	2700
Bristoria	Unnamed	8	Air/gas flood	no	Upper Nineveh sandstone	3100
Burgettstown	Unnamed	11	Air/gas/water flood	no	Hundred-Foot interval	2050
Florence-Five Points	Unnamed	5	Air/gas flood	no	Hundred-Foot interval	1900
Grays Fork	Unnamed	9	Air/gas flood	no	Upper Nineveh sandstone	3150
Lagonda	Unnamed	0	Air/gas flood	yes	Fifth sandstone	2632
Lagonda	Crafts Run	12	Air/gas flood	yes	Fifth sandstone	2750
McDonald-McCurdy	Unnamed	3	Air/gas/water flood	yes	Gordon and Fifth sandstones	2150
New Freeport	Unnamed	6	Air/gas flood	no	Upper Nineveh sandstone	3300
Pleasant Grove	Unnamed	4	Air/gas flood	yes	Fifth sandstone	2650
Point Lookout	Unnamed	10	Water flood	no	Fifth sandstone	2813
Venice	Unnamed	2	Air/gas flood	yes	Fourth sandstone	2384
Washington-Taylorstown	Unnamed	1	Air/gas/water flood	yes	Gantz and Gordon sandstones	2546

The remainder of this section explores the history of secondary oil recovery in Washington-Taylorstown Field using air/gas drive and water flood methods.

6.5.7.1 Washington-Taylorstown Field

The Washington-Taylorstown Field was estimated to have 49.2 MMBLS total oil in place as of 1947, with 1.1 MMBLS determined recoverable by primary methods and another 10.6 MMBLS potentially recoverable by intensive air or gas drive methods (Lytle, 1950). These reserve estimates undoubtedly tempted operators, who employed various enhanced recovery methods in this field to extract oil over the years. Gas drive methods were employed as early as 1923 and continued through about 1970. McGlade (1967) reported 15 gas injection projects in Washington-Taylorstown Field as of 1967 – 14 targeting the Gordon sandstone in the Taylorstown (western) portion of the field and one targeting the Gantz and Fifty-Foot sandstones (Hundred-Foot Zone) just northeast of the City of Washington. Figure 6-80 provides a graphical history of these activities relative to annual oil production volumes for the field. Early (pre-1940) production data were obtained by McGlade (1967), and more recent (1991-present) production data were obtained from EDWIN (2019). Figure 6-81 shows the location of modern (post-1950) EOR wells in Washington-Taylorstown Field that were still considered active and producing as of the early 1990s.

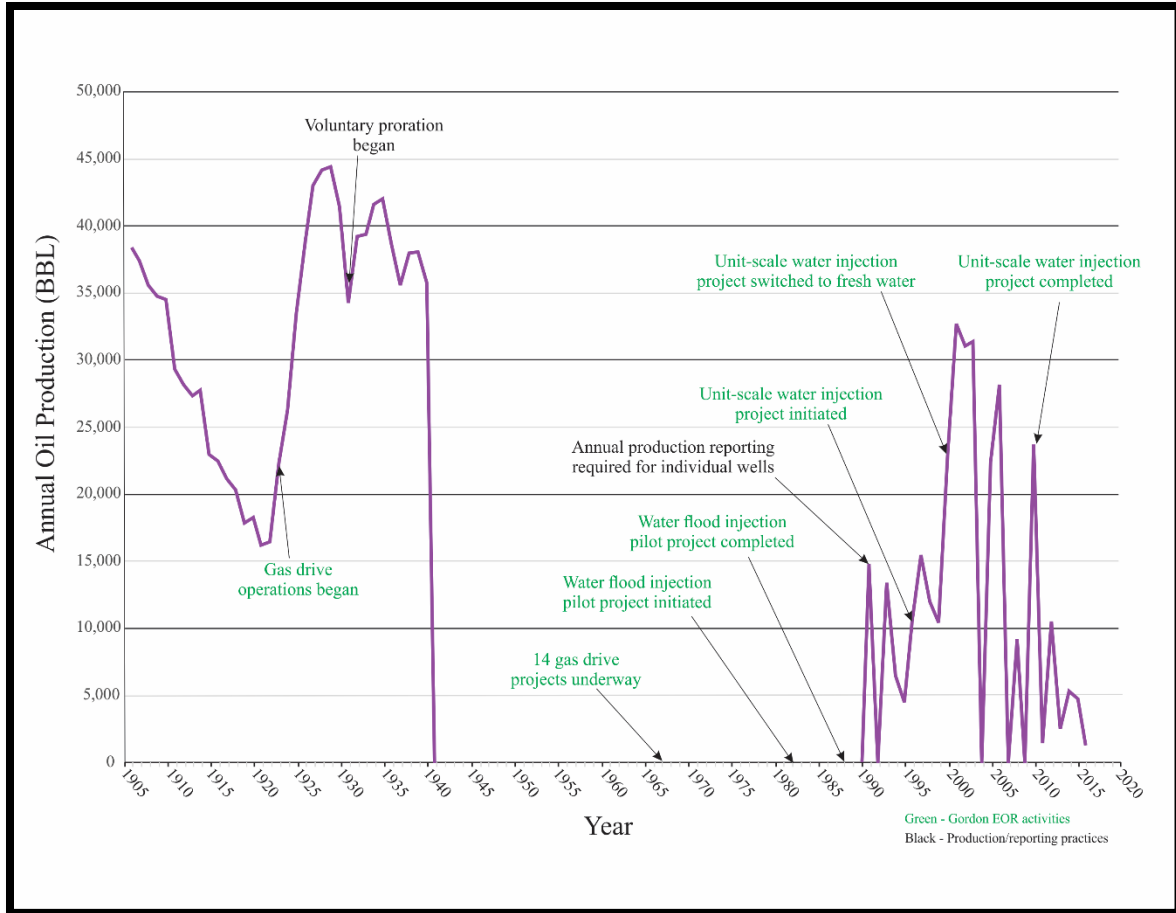


Figure 6-80. Oil production and EOR activities in Washington-Taylorstown Field.

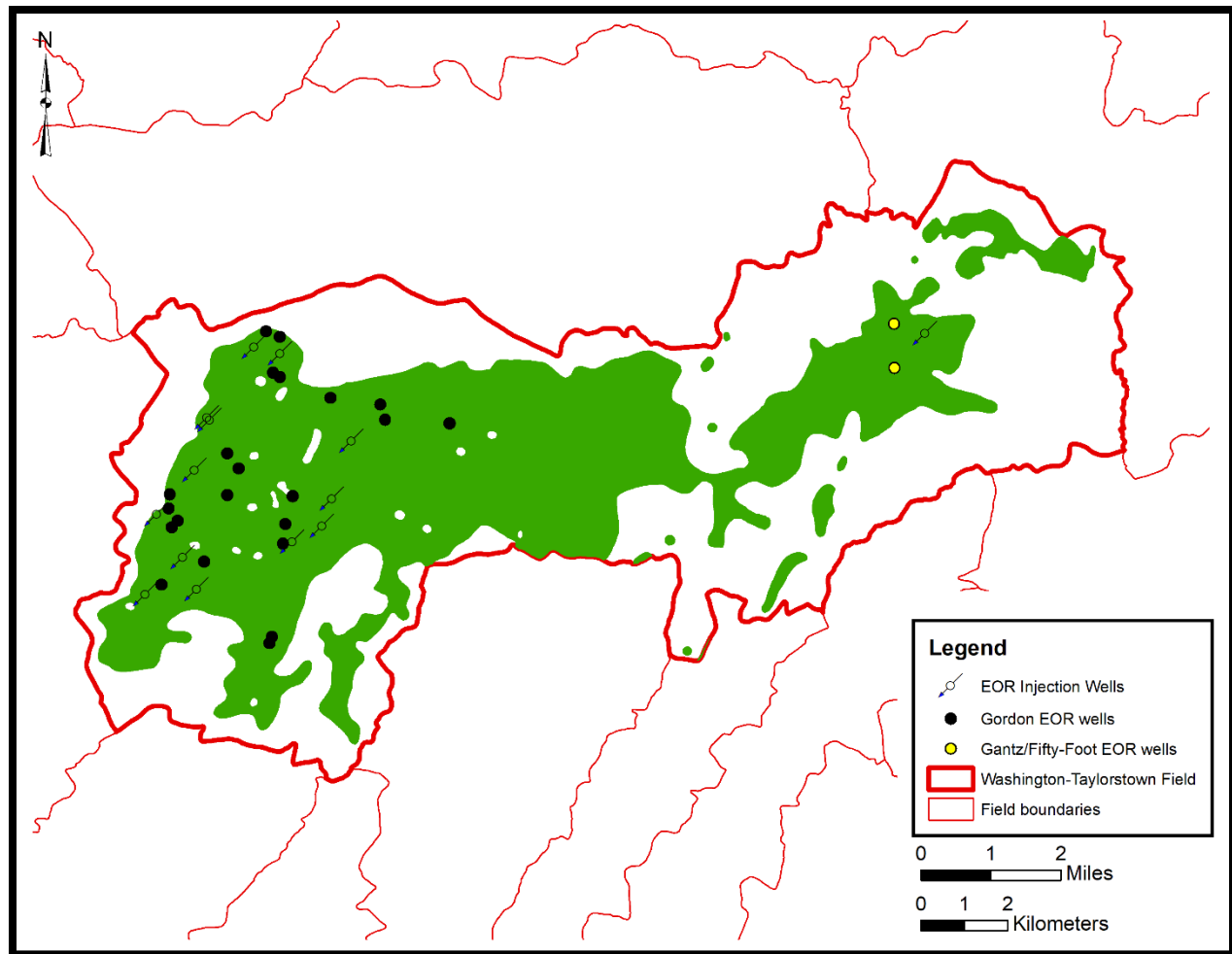


Figure 6-81. Modern EOR operations in Washington-Taylorstown Field.

Early oil wells in the Washington-Taylorstown Field commonly reported initial production rates of 2000 BOPD or more (McGlade, 1967), and at the turn of the twentieth century, the field was producing approximately 4500 BOPD (Farias et al., 2003). As Figure 6-80 illustrates, twentieth century oil production was successfully enhanced using air/gas drive techniques (McGlade, 1967; Harper and Laughrey, 1987) and remained significant, even with the institution of voluntary proration in 1931, which limited oil production at the wellhead to some amount below its ultimate capacity to produce. By 1940, approximately half of oil wells producing from the Gordon, Fourth and Fifth sandstones in this field were deemed inactive (Lytle, 1950), which accounts for the drop off in annual oil production at that time (Figure 6-80).

Industry activity picked up again in the 1980s, but this time, water flood techniques were employed. A pilot project was conducted in the Taylorstown (western) area of the field to enhance production from the Gordon sandstone (Figure 6-81). The project began in 1982 and lasted for seven years. Two contiguous five-spot patterns were used to inject 1.2 MMBSL water into the Gordon Zone, producing 6.4 MMBSL oil (Farias et al., 2003). Based on the success of this pilot project, a full-scale injection project using a line-drive pattern was initiated in 1996. For the first three years of this project, however, wastewaters (e.g., formation brines, coalmine water, etc.) were used as the injection fluid with not much increase in oil production. In fact, the injectivity into the Gordon sandstone decreased from 4.6 MMBSL per day to only 600 BBL per

day during this time (Farias et al., 2003). Farias et al. (2003) attributed the decline in injectivity to several factors, including the introduction of unfiltered solids and formation of emulsions that filled pore spaces and blocked pore throats near injection wellbores. In other words, the introduction of wastewaters into the reservoir modified the physical and chemical characteristics of the near-bore pore environment, creating 'skin damage' that impacted the reservoir's overall productivity. In 1999, the operator began to use fresh water as the injection fluid, which increased injectivity somewhat and had a positive impact on annual oil production (Figure 6-80). This water flood project continued through ca 2010, at which time the operator began to plug and abandon both injection and production wells associated with the project (Rectenwald, personal communication, 2019). Based on information available in EDWIN (2019), however, some of these oil wells have reported production post-2010 (Figure 6-80) and have not yet been formally reported as plugged and abandoned.

6.5.8 Stacked CCUS Potential

Southwestern Pennsylvania presents stacked opportunities for both CO₂-enhanced oil and gas production and permanent carbon storage (Figure 6-82). Enhanced production of petroleum hydrocarbons from conventional oil, conventional gas and perhaps even unconventional shale gas may be pursued here, with permanent storage in the Oriskany Sandstone as well as conventional reservoirs post-production. Although not included in this study due to lack of data control, siliciclastic units of Late Cambrian age might also serve as carbon storage targets in the area.

Figure 6-83 illustrates important geologic features (shallow oil and gas accumulations, Oriskany trapping methods, shallow Venango Group structure and deeper structure/interpreted faults) and demarcates three areas (A, B and C) to facilitate the discussion of CCUS opportunities relative to the location of case study fields.

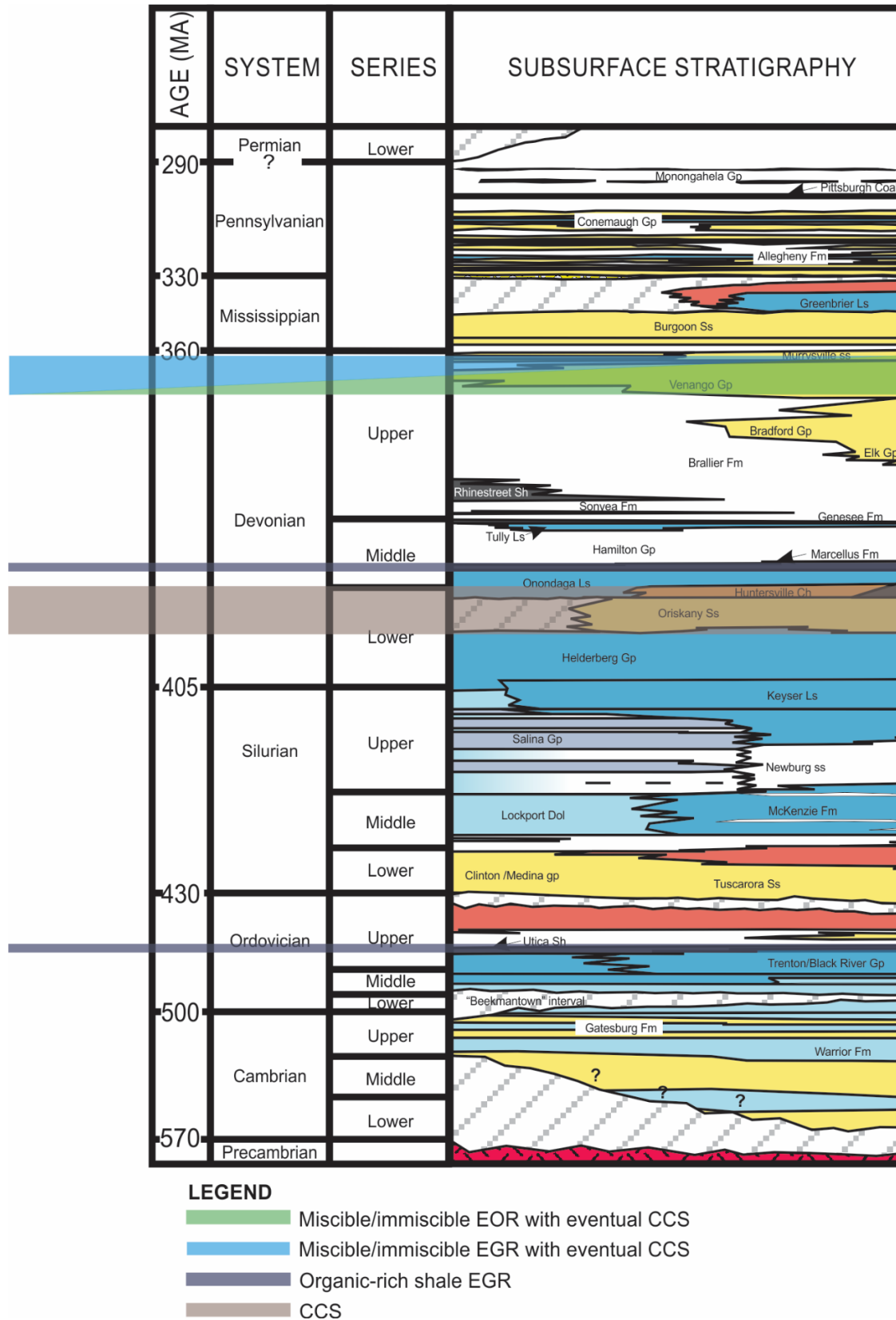


Figure 6-82. Stratigraphic representation of stacked CCUS potential in southwestern Pennsylvania.

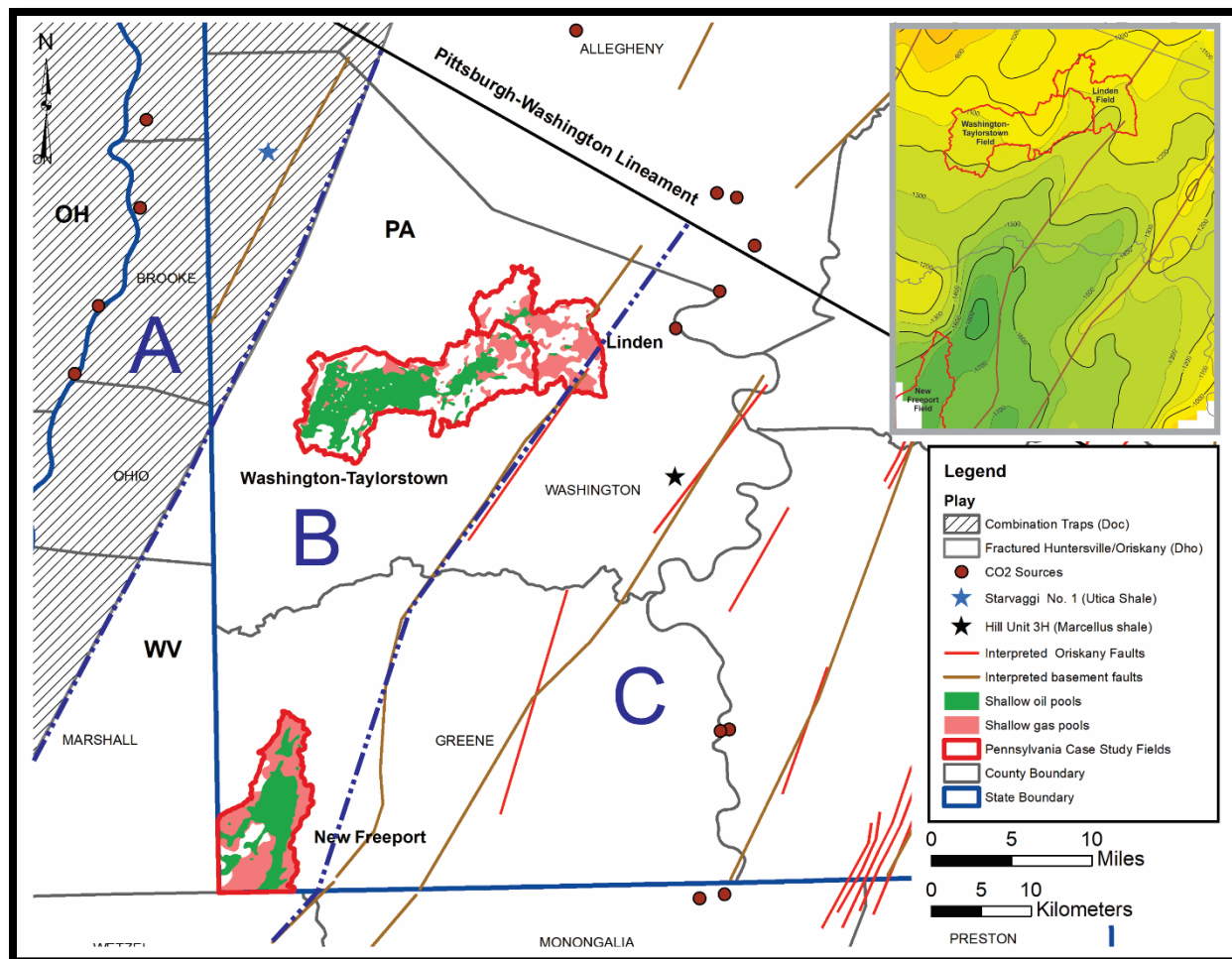


Figure 6-83. Southwestern Pennsylvania's stacked storage potential is defined by the lithology, structure and hydrocarbon trapping mechanisms of its subsurface rocks, as well as the geologic history of the area (inset structure contour map from Figure 6-63).

6.5.8.1 Upper Devonian Enhanced Recovery with Eventual CCS

The oil fields of southwestern Pennsylvania are prominent fixtures in the shallow oil belt that extends from northwestern Pennsylvania to northern West Virginia. Here, sandstones of the Upper Devonian Venango Group produce oil and gas, as illustrated by overlapping pools in the Washington-Taylorstown, Linden and New Freeport fields (Figure 6-83). As described in Section 6.5.2, there are several Venango-producing zones in southwestern Pennsylvania where hydrocarbons may be produced from multiple layers in the same geographic space. The geologic maps, cross sections and reservoir attributes prepared for this study, as well as the history of EOR activities reported herein, can be used to identify discrete reservoir intervals that may be assessed as potential CCUS prospects at specific locations in this corner of the state.

Area B in Figure 6-83, referred to as the Gordon fairway in this report, represents that portion of southwestern Pennsylvania and the adjacent West Virginia panhandle most likely to provide miscible and/or immiscible CO₂-EOR or CO₂-EGR from the Gordon sandstone, with opportunities for eventual carbon capture and storage (CCS) in those depleted fields deeper than 2600 ft. Table 6-13 provides the minimum, mode and maximum CO₂ storage estimates for the three case study fields, based on information in the petroleum fields geodatabase compiled

by Lewis et al. (2019). These estimates are inclusive of multiple Venango Group sandstones, with a large majority of the oil reservoir resource associated with the Gantz and Gordon sandstones. Storage resource estimates for gas reservoirs in these three fields are generally associated with sandstones from most, if not all, of the Venango Zones.

Table 6-13. Storage resource estimates for case study fields.

Field	Product	CO ₂ Storage Resource Estimates (million tonnes)		
		Minimum	Mode	Maximum
Washington-Taylorstown	oil	7.58	12.59	23.09
	gas	2.60	4.31	7.91
Linden	oil	0.06	0.10	0.18
	gas	0.83	1.37	2.52
New Freeport	oil	1.39	2.32	4.24
	gas	2.99	4.97	9.11

6.5.8.2 Lower Devonian CCS

The top of the Oriskany Sandstone ranges from -4000 ft MSL in Jefferson County, Ohio, and Hancock County, West Virginia, to -7000 ft MSL in eastern Washington and central Greene counties, Pennsylvania (Figure 6-84). Throughout the study area, the Oriskany is found at depths of at least 5500 ft, and generally dips toward the southeast. In Area C, the unit reaches depths of 7000 ft or more (Carter et al., 2010; Carter and Patchen, 2017).

Roen and Walker (1996) described four natural gas plays associated with the Oriskany Sandstone, and two of these exist in the study area (Figure 6-84). The combination traps play is found in Area A, while the fractured Huntersville Chert/Oriskany Sandstone play spans Areas B and C (Figure 6-83). The Oriskany Sandstone's storage potential as a saline formation in southwestern Pennsylvania was previously evaluated by Carter (2013) and Popova et al. (2013). This high-level assessment determined that the Oriskany may provide ~6 to 30 million tonnes of CO₂ storage in Washington County alone.

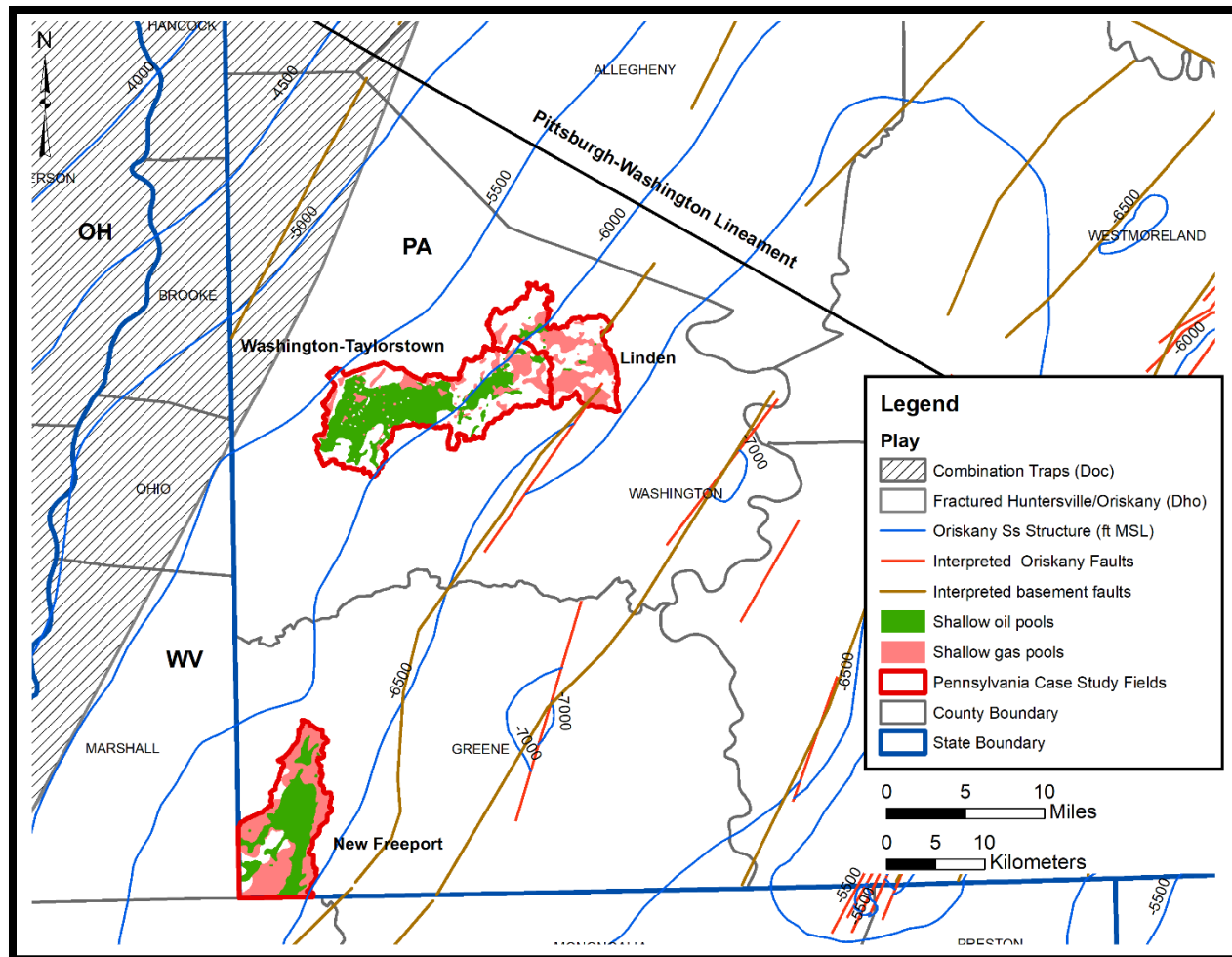


Figure 6-84. Oriskany Sandstone structure and plays in southwestern Pennsylvania (modified from Kostelnik and Carter, 2009).

Based on an analysis by Kostelnik and Carter (2009), the combination traps play area (hatched pattern in Figure 6-84) offers a more promising carbon storage target than the fractured Huntersville Chert/Oriskany play (remainder of the mapped area in this figure). Kostelnik and Carter (2009) evaluated core and geophysical log data in concert with petrographic analyses to determine that the Oriskany Sandstone of the combination traps play has porosities on the order of 5 percent, comprised mostly of secondary porosity derived from the dissolution of carbonate grains and cement. Their evaluation of the fractured Huntersville Chert/Oriskany play area found high fracture porosity in places but noted a certain level of structure complexity that would likely require additional analysis before selecting the best geographic area for CO₂ injection. Consequently, although it can be said that the Oriskany Sandstone may be developed as a storage reservoir throughout the area, it is in Area A (Figure 6-83) where the Oriskany probably offers the most favorable storage opportunities.

6.5.8.3 Organic-Rich Shale EGR with Eventual CCS

The tri-state study area is home to some of the most vigorous shale gas activity in the Appalachian Basin. Both the Middle Devonian Marcellus Formation and Upper Ordovician Utica Shale are being developed here, and in fact, northern Washington County is considered the

birthplace of the modern Marcellus Shale play, as the Renz No. 1 (API No. 3712522074) was completed here in 2004.

In southwestern Pennsylvania, the Marcellus Shale occurs at depths of a mile or more, and as illustrated in Figure 6-85, the top of the unit ranges from -4000 to -7000 ft MSL. The Marcellus Shale is at its lowest elevation in eastern Greene and Washington counties, as well as Fayette and Westmoreland counties east of the study area. With respect to petroleum hydrocarbon production, wet Marcellus gas (i.e., methane plus natural gas liquids) is generally produced west of Interstate I-79 and the City of Washington (Figure 6-85), with dry gas being produced to the east.

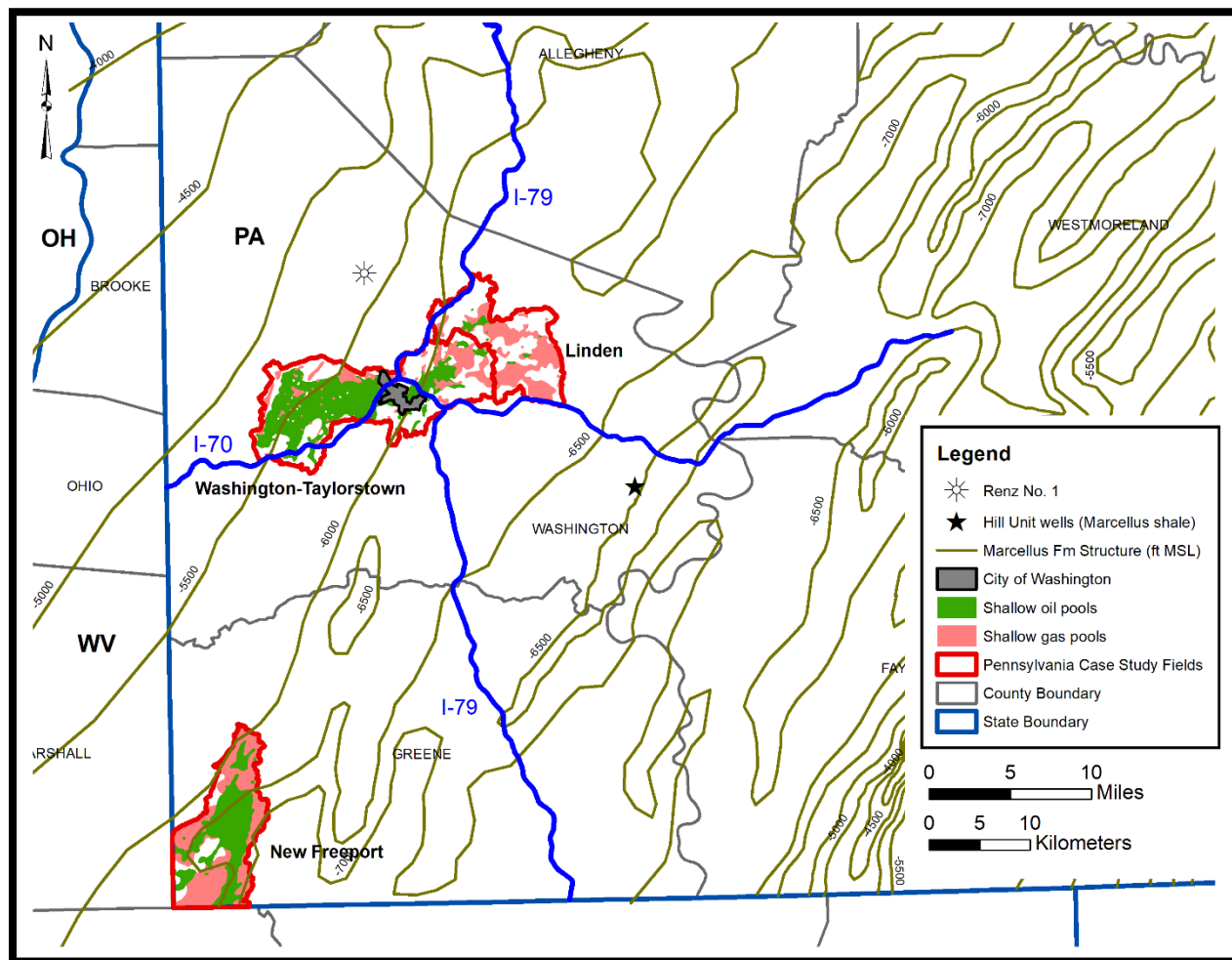


Figure 6-85. Marcellus Shale structure contour map for southwestern Pennsylvania (modified from Harper et al., 2017).

Two separate Marcellus Shale studies have been prepared as part of the current work using rock cuttings samples obtained from the Hill Unit 2H (API No. 3712523880) and 3H (API No. 3712523879) wells in eastern Washington County. The first study (Opsitnick, 2015; Appendix J) was an independent undergraduate research project that interpreted the lithostratigraphy of the Marcellus Formation and adjacent units and characterized the bulk mineralogy of this interval. The second (Cooney, 2016; Appendix K) used organic petrographic methods to evaluate the thermal maturity of the Marcellus in these same wells. Figure 6-86 and Figure 6-87 provide

graphical depictions of the mineralogic content of the vertical portions of the Hill Unit 2H and Hill Unit 3H wells, respectively. Figure 6-87 includes a stratigraphic interpretation of subsurface rock units encountered in this well, based on geophysical log control and consistent with the regional interpretations of Harper et al. (2017) for Middle and Upper Devonian shales.

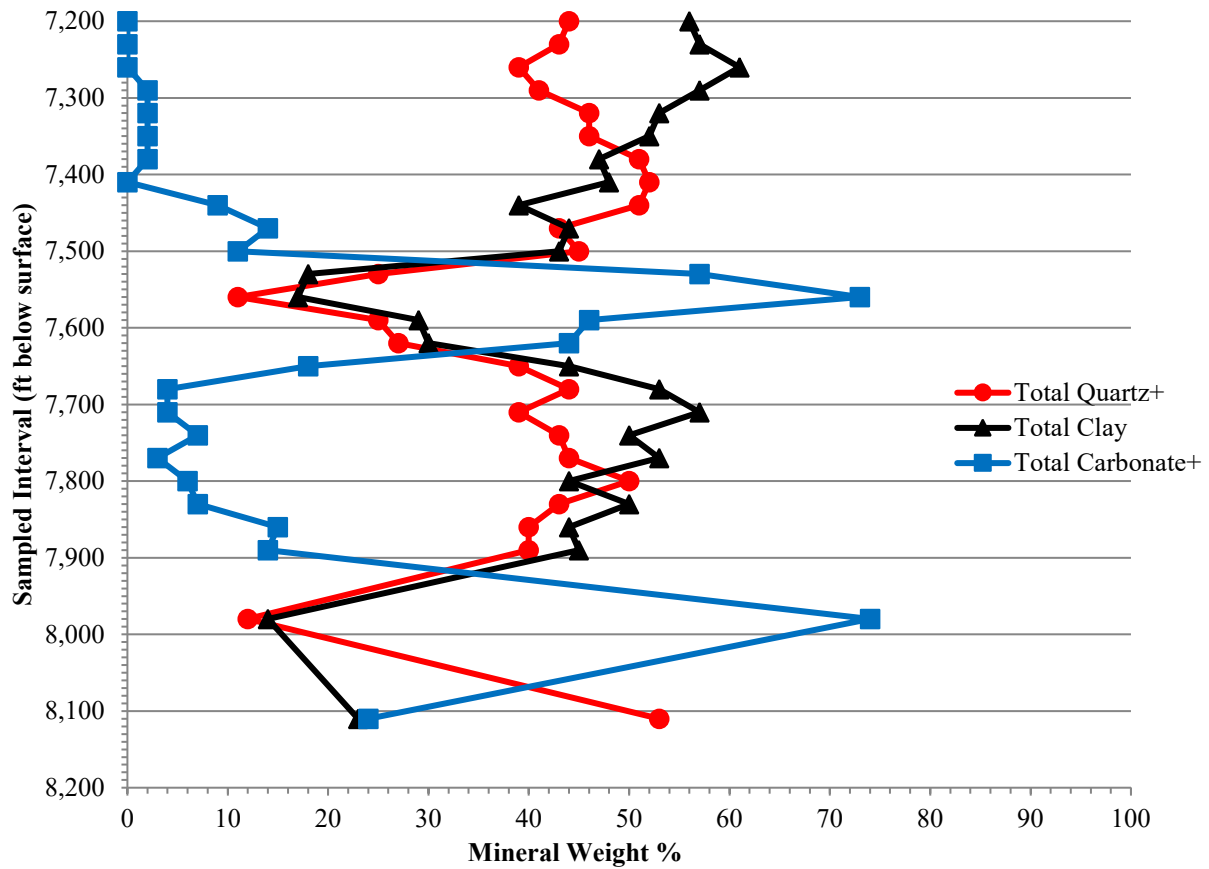


Figure 6-86. Mineralogy analysis of the vertical section of Hill Unit 2H, API No. 3712523880, Washington County, PA (modified from Opsitnick, 2015).

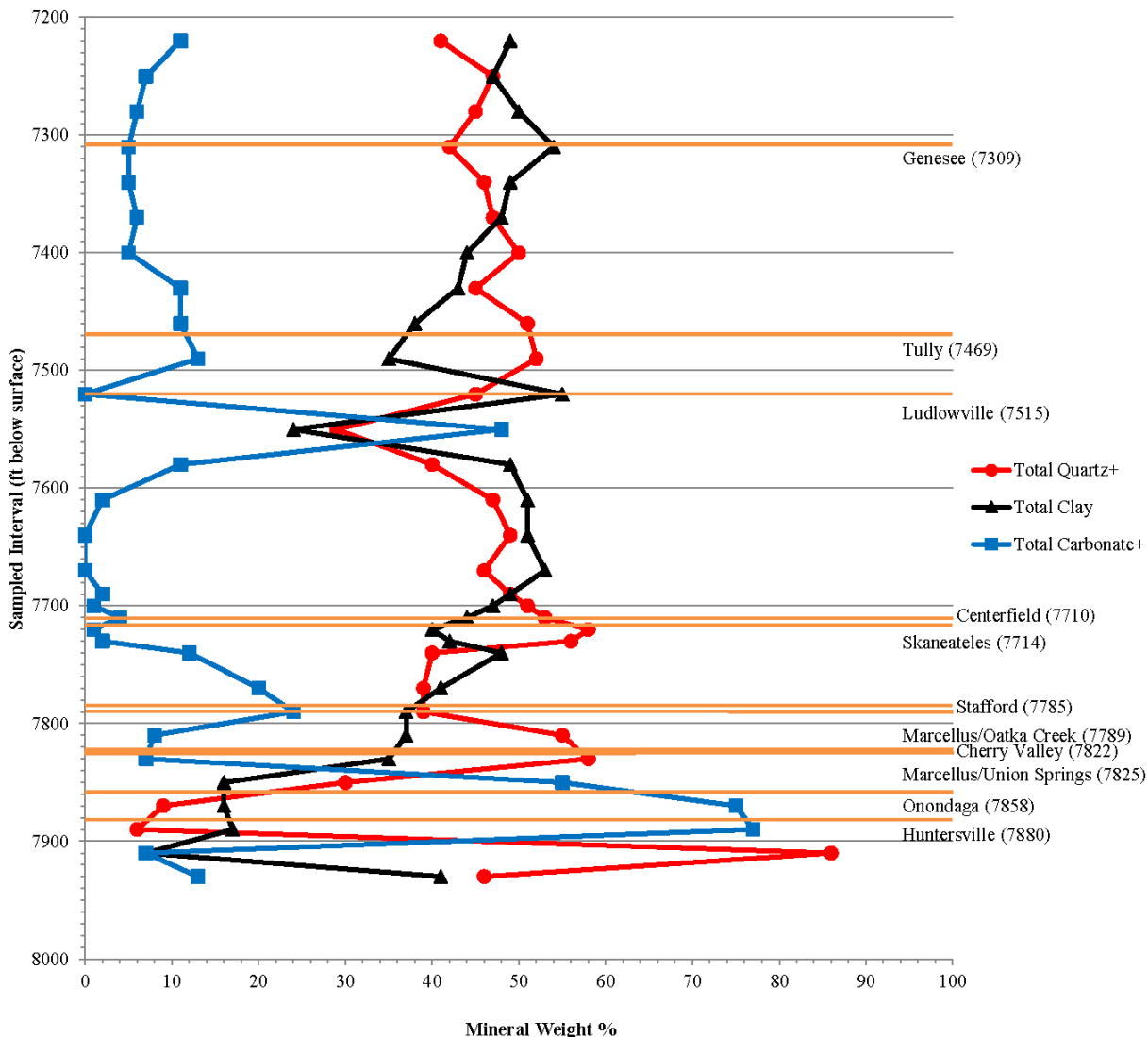


Figure 6-87. Mineralogy analysis of the vertical section of Hill Unit 3H, API No. 3712523879, Washington County, PA (modified from Opsitnick, 2015).

Table 6-14 summarizes the average results of bulk mineralogy (relative proportions of quartz, clay and carbonate minerals) and vitrinite reflectance (Ro%) analysis of Marcellus Shale samples collected from the horizontal laterals of Hill Unit 2H and 3H. The clay mineral content of these samples falls in the 20 to 60 percent range, with varying percentages of quartz minerals and generally lesser proportions of carbonate minerals. Vitrinite reflectance data for both wells (1.13 to 2.22) indicate the Marcellus is within the dry gas window (see Dow, 1977). Additional Marcellus rock cuttings samples from these two wells were submitted to the U.S. Geological Survey for analysis of conodonts. The samples were found to contain a few conodont fragments with a color alteration index (CAI) in the range of 2.5 to 3 (Repetski, personal communication, 2015). Both the vitrinite reflectance and CAI results from the Hill Unit wells are consistent with data reported for this same area of southwestern Pennsylvania by Repetski et al. (2008) and corroborate the observed production of dry Marcellus Shale gas from these wells.

Table 6-14. Average mineralogy and vitrinite reflectance data for the Marcellus Shale in two Washington County wells (modified from Cooney, 2016).

(a) Hill Unit 2H (API No. 3712523880)

Mineralogy				Vitrinite Reflectance	
Depth	Quartz (%)	Clay (%)	Carbonate (%)	N	Mean Ro%
7600	5	20	74	108	1.56
7990				44	1.68
8620	39	33	27	38	1.76
9010				35	1.77
9490				18	1.72
9610	45	52	2	55	1.67
10,000				32	1.68
10,600	40	60	0	28	1.73
10,990				33	1.13
11,624	49	50	1	54	1.54

(b) Hill Unit 3H (API No. 3712523879)

Mineralogy				Vitrinite Reflectance	
Depth	Quartz (%)	Clay (%)	Carbonate (%)	N	Mean Ro%
11,010	63	30	6	46	1.93
11,900				6	1.76
11,910				100	2.06
12,000	57	29	14		
12,030				55	1.77
12,990	43	16	42	127	2.22

In southwestern Pennsylvania, the Utica Shale occurs at depths of up to 10,000 ft or more. Figure 6-88 provides a structure contour map on top of the Utica relative to ft MSL. Here, the top of the unit ranges from -7600 to -11,800 ft MSL. The Utica Shale is at its lowest elevation in eastern Greene County and parts of Fayette County east of the study area.

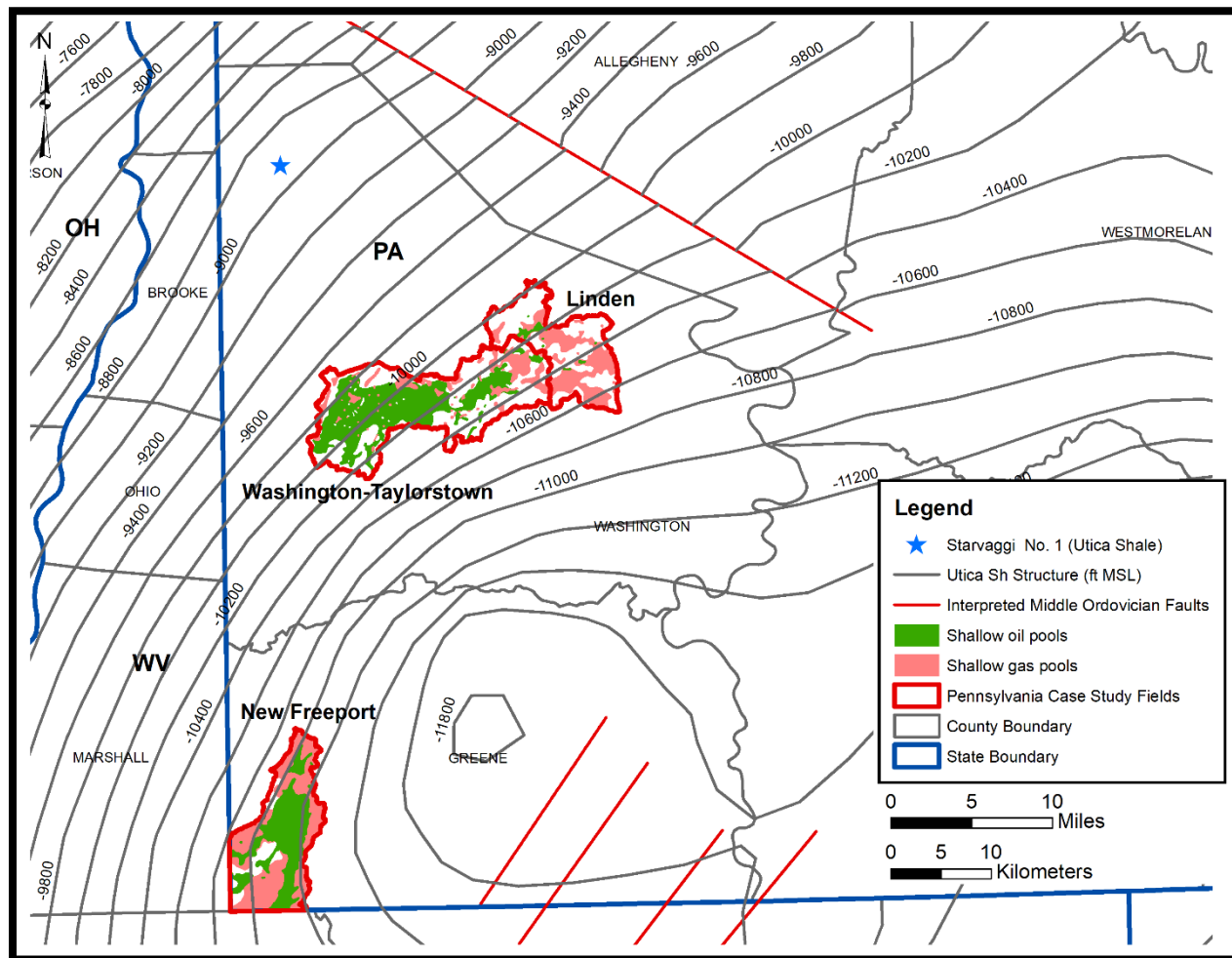


Figure 6-88. Utica Shale structure contour map for southwestern Pennsylvania (modified from Patchen and Carter, 2015).

A case study report was prepared for the Utica Shale (Carter, 2017; Appendix L) based on findings reported by Patchen and Carter (2015) for the Starvaggi No. 1 (API No. 3712522278). The case study report summarizes the bulk mineralogy, organic content and thermal maturity of the Utica/Point Pleasant interval in northwestern Washington County (see Figure 6-83 for location). Figure 6-89 illustrates the relative proportions of quartz, clay and carbonate minerals with depth for the Kope, Utica, Point Pleasant and Lexington/Trenton formations. Deflections in clay and carbonate mineral percentages mark clear boundaries between geologic units.

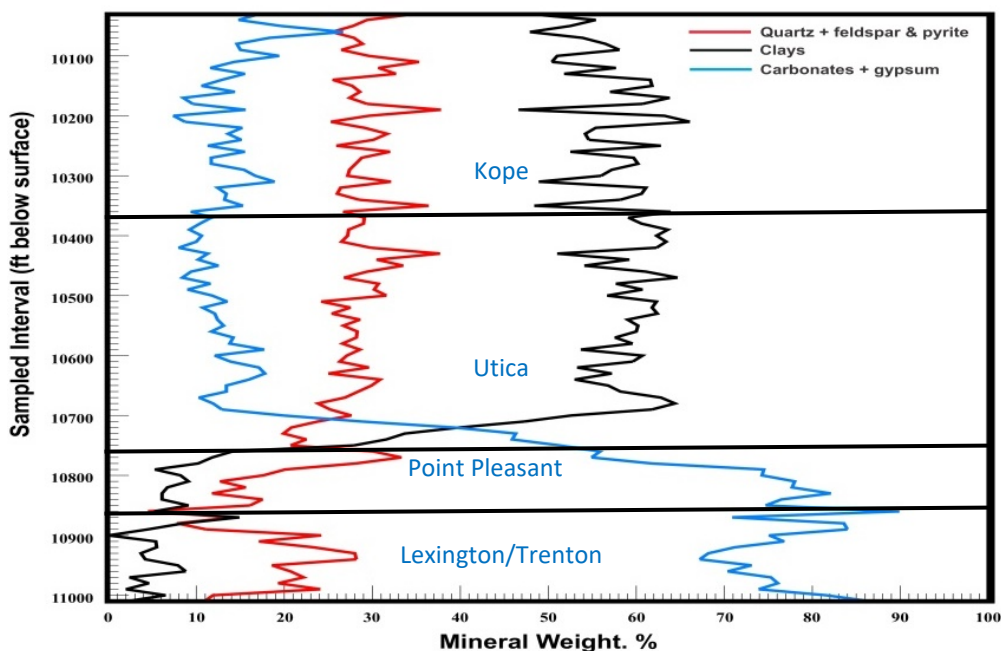


Figure 6-89. Mineralogy versus sample depth for the Starvaggi No. 1 (modified from Patchen and Carter, 2015).

Table 6-15 summarizes aggregated TOC content results for Utica and Point Pleasant samples collected from the Starvaggi No. 1. In this part of the Appalachian Basin, both the Utica and Point Pleasant formations are considered part of the “Utica Play,” and the Point Pleasant oftentimes has a higher percent TOC than the Utica itself.

Table 6-15. Starvaggi No. 1 TOC results (modified from Patchen and Carter, 2015).

Formation	Total Organic Content (%)			
	Minimum	Maximum	Average	No. Samples
Utica Shale	0.47	4.11	1.36	39
Point Pleasant Formation	1.51	4.19	3.22	10

With respect to the thermal maturity of this unconventional reservoir, organic petrography studies of the Utica and Point Pleasant formations in the tri-state area by Kentucky and Pennsylvania research team members suggest a trend of wet gas production in southeastern Ohio to dry gas production in southwestern Pennsylvania (Patchen and Carter, 2015). The Utica reflectance results reported by Kentucky for the Starvaggi No. 1 ranged from 1.75 to 1.85, which fall in the dry gas window (see Dow, 1977). This analysis corroborates the observed production of dry gas from the Utica/Point Pleasant interval in Washington and Greene counties.

As of the writing of this report, use of CO₂ to enhance natural gas production from unconventional shale reservoirs has not been applied in the Appalachian Basin. However, Chapter 5 of this report addresses the potential of Marcellus and Utica shales as CO₂ storage reservoirs. In addition, Soeder (2017) provided a cursory discussion of the prospects of geologic carbon storage in depleted shale reservoirs. The higher adsorptive capacity of CO₂ to shale mineral surfaces (compared to that of methane) and the availability of production infrastructure (i.e., well pads, hydraulically fractured boreholes, pipelines and the like) that could be

repurposed for CO₂ injection at the end of an area's gas production phase are two positive aspects of performing CCUS in shale formations. Important engineering considerations that might limit the viability of using shale gas reservoirs for carbon storage applications center around reservoir pressure conditions.

Soeder (2017) reported a need for both laboratory experiments and field tests to assess the potential effects of post-production reservoir pressures on carbon storage. Once natural gas has been removed from overpressured reservoirs like the Marcellus and Utica shales, there is a net increase in the formation's overburden pressure. This may adversely impact the reservoir's porosity and permeability, hampering the ability of fluids to move through the rock, and therefore, limiting CO₂ injectivity. In addition, the fact that shales are subject to hysteresis (i.e., the inability to restore a reservoir's permeability characteristics by repressuring the rock to its original state of stress) means that hydraulically fractured shale formations may experience permanent pore damage and/or destruction once depleted. Using such formations for carbon storage would require special attention to reservoir pressure management during shale gas production.

6.5.9 Summary

The case studies prepared for the Washington-Taylorstown, Linden and New Freeport fields highlight specific CCUS opportunities for southwestern Pennsylvania. These include (1) both miscible and immiscible CO₂-EOR and CO₂-EGR for Upper Devonian Venango Group reservoirs; (2) permanent carbon storage in the Lower Devonian Oriskany Sandstone; and (3) possible future opportunities for CO₂-EGR and permanent storage in the Middle Devonian Marcellus and Upper Ordovician Utica shale reservoirs. These fields are proximal to regional CO₂ sources derived from the power and industry sectors, which are located along the Ohio River to the west and Monongahela River to the east (Figure 6-83).

All three case study fields are situated in the Gordon fairway (Area B in Figure 6-83). The western limb of the Washington-Taylorstown Field offers miscible CO₂-EOR opportunities in the Gordon sandstone, which has porosities on the order of 20% and permeabilities ranging from 106 to 145 mD. The eastern limb of this field and adjoining Linden Field offer immiscible CO₂-EOR opportunities in the Gantz and Gordon sandstones, and CO₂-EGR in the Fifty-Foot sandstone. Here, the Gordon sandstone is not as clean as it is to the west, however, and has much lower average porosities (7 percent) and permeabilities (9 mD). Mineralogy and petrography studies of Gantz and Gordon sandstones sampled from Linden Field reported clay minerals in intergranular spaces and the presence of secondary minerals that further occluded the pore space in these rocks. Based on the work of Lytle (1950), it is estimated that approximately 10 MMBLS of additional oil could be produced from Washington-Taylorstown Field using air/gas drive methods. Like Washington-Taylorstown Field, the New Freeport Field offers miscible CO₂-EOR in the Gordon sandstone, but what's more, the overlying Nineveh and underlying Fourth sandstones also serve as miscible CO₂-EOR targets, since the Venango Group is deeper in this part of Pennsylvania. Based on the carbon storage estimates prepared by WVGES, oil and gas reservoirs of the Washington-Taylorstown, Linden and New Freeport fields may offer 9 to 23 million tonnes of CO₂ storage in depleted oil reservoirs and 6 to 11 million tonnes of storage in depleted gas reservoirs (Table 6-13).

Based on the geologic and reservoir assessments reported herein, Area C of Figure 6-83 may offer multiple CCS opportunities for area carbon sources. The depth to top of Venango Group is greater here (Figure 6-63), particularly in southern Greene County, and given the documented productivity of multiple Venango sandstones, stacked carbon storage may be possible in eastern Washington and Greene counties. The thickness of the Fifty-Foot sandstone in this area

(Figure 6-65) suggests that more studies of this unit's porosity and permeability are warranted. In addition, the presence of the underlying Oriskany Sandstone offers a deeper storage target when some Venango Group sandstones might be in the immiscible depth range (e.g., the Gantz sandstone).

The Oriskany Sandstone, present in the subsurface at depths of 5500 ft or more, offers a permanent carbon storage opportunity for the tri-state area, as well as stacked potential with shallower enhanced recovery operations that may be pursued in southwestern Pennsylvania. Based on evaluations by Kostelnik and Carter (2009), the most favorable area for permanent storage in the Oriskany Sandstone occurs in Area A of Figure 6-83, where this unit has produced gas from a combination traps play.

The prospect of using shale formations for CO₂-EGR and eventual storage of carbon, although yet untested in the Appalachian Basin, could bring an important nuance to CCUS applications in the tri-state area in years to come. Based on certain reservoir engineering and economic considerations, it is recommended that utilization of CO₂ for enhanced recovery from these formations focus on areas of wet gas production and do so at the latter stages of shale gas development rather than waiting for reservoir depletion. Because the majority of Washington and Greene counties fall in the dry gas window for both the Marcellus and Utica plays, this recommended approach for CO₂-EGR would likely be most successful in the western portion of these counties for enhanced recovery of wet gas from the Marcellus, and adjacent to or west of the Ohio River for enhanced recovery of wet gas from the Utica Shale.

6.6 West Virginia Case Studies

6.6.1 Overview and Area Geology

Four oil fields in northern West Virginia were selected as case studies for potential EOR using CO₂. They include the Jacksonburg-Stringtown, Mannington, Salem-Wallace and Wolf Summit-Big Isaac fields. All four are fewer than 20 mi from CO₂ point-sources, including coal-fired power plants (Moore et al., 2013). The fields were discovered in the late 1890s and produce oil from Upper Devonian siliciclastics, primarily the Gordon sandstone. This area is also situated in the Gordon fairway, a northeast-southwest trending area of multiple, vertically stacked sandstone bodies. In addition to the Gordon sandstone, the Mannington Field produces from the Mississippian "Big Injun" (Burgoon Formation) and the Upper Devonian Fifth sandstone. The Wolf Summit-Big Isaac Field also produces from both the Gordon and Fifth sandstones.

Figure 6-90 illustrates the regional subsurface stratigraphy and expands on the Mississippian and Upper Devonian section using common drillers' names. This depiction is intended to show the morphology of the siliciclastic beds in the study area and should not be construed to represent relative position of the source material and/or the direction of transport. In this area, multiple oil- and gas-producing reservoirs have been penetrated from the Mississippian Greenbrier Limestone through the Upper Ordovician Utica Shale. Red arrows point to horizons that may provide CCUS opportunities.

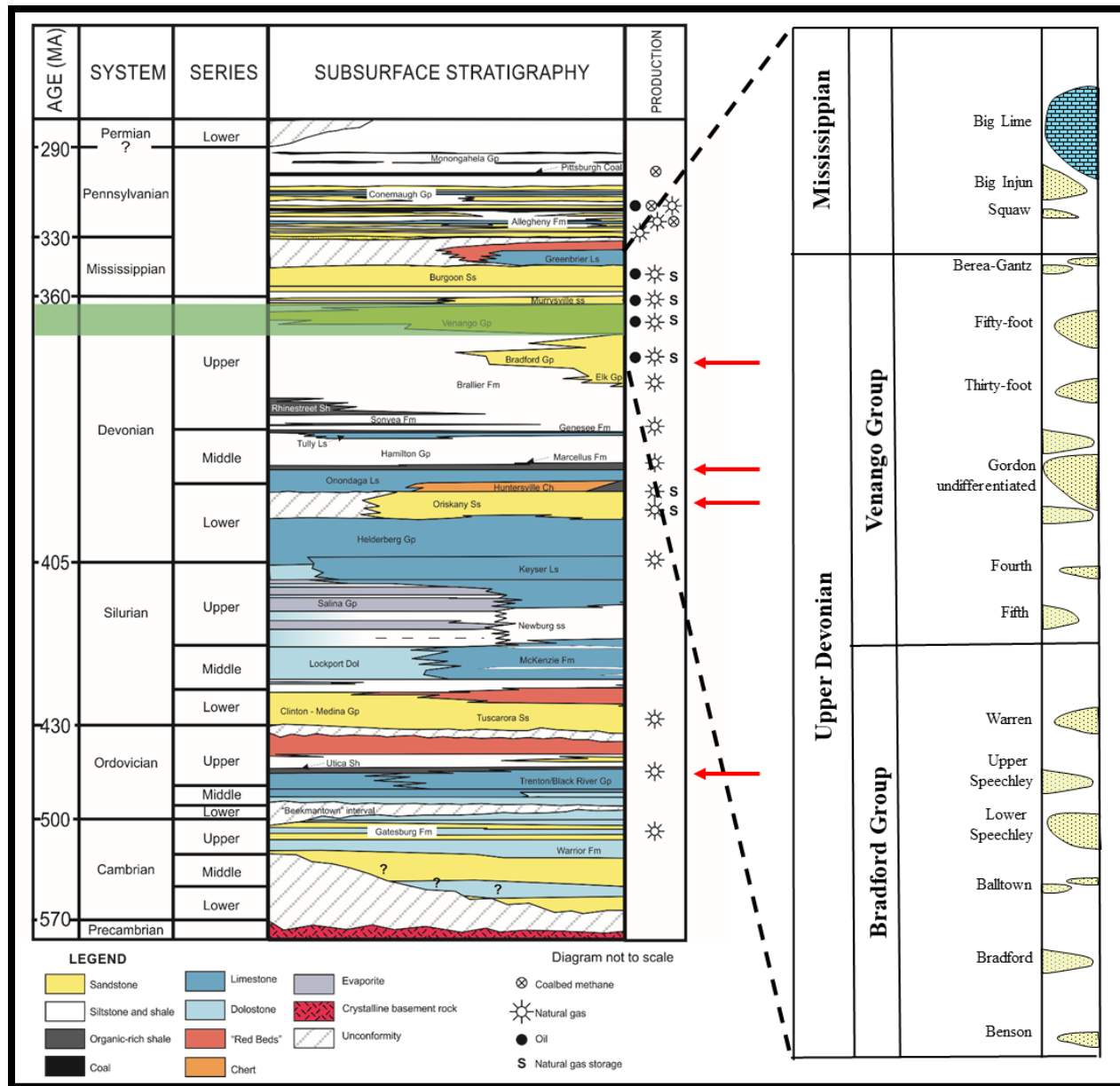


Figure 6-90. Regional Stratigraphic chart with local stratigraphic column with drillers' names on the right. Red arrows highlight potential CCUS horizons.

Figure 6-91 illustrates the regional location of the Jacksonville-Stringtown, Mannington, Salem-Wallace, and Wolf Summit-Big Isaac fields in north-central West Virginia relative to local anticlines and synclines. The Jacksonville-Stringtown Field lies between the Littleton Anticline and the Burchfield Syncline; the Salem-Wallace Field parallels the Robinson Syncline; the Wolf Summit-Big Isaac Field lies between the Robinson Syncline and the Wolf Summit Anticline; and the Mannington Field lies just north of the Wolf Summit Anticline. Oil production in the four fields results from either a combination of structural and stratigraphic traps or strictly stratigraphic traps.

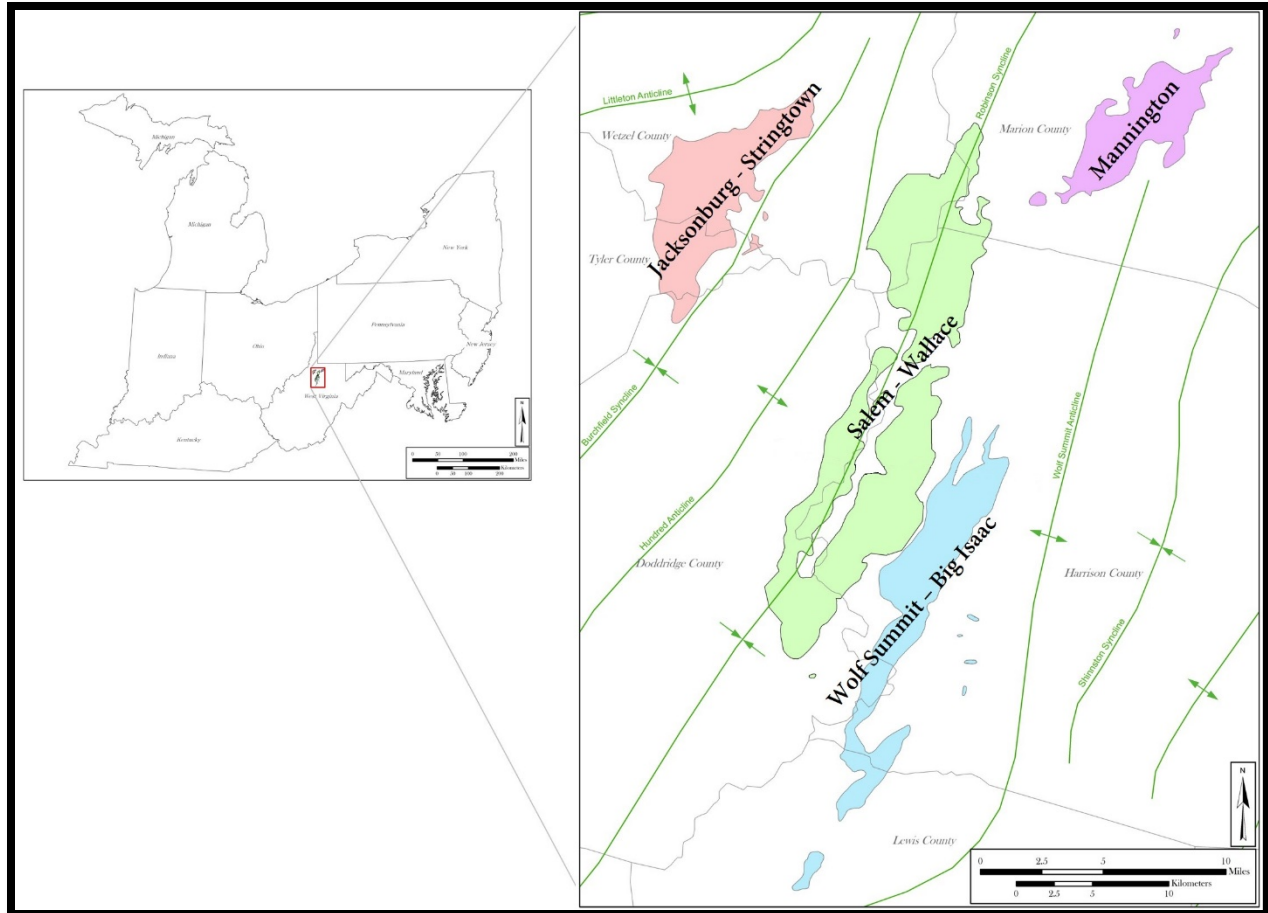


Figure 6-91. Four case study fields mapped with regional anticlines and synclines (modified from Moore et al., 2013).

The overall structural trend in the case study area is a general shallowing to the southeast (Figure 6-92), with anticlines and synclines trending in a southwest to northeast direction. In the northwest corner of this area, the base of the Gordon sandstone is about -1800 ft MSL near the Littleton Anticline. This deepens to -2100 ft MSL in the Jacksonburg-Stringtown Field approaching the Burchfield Syncline and then shallows to -1700 ft MSL along the Hundred Anticline in Doddridge County. The base of the sandstone deepens to -1900 ft MSL along the Robinson Syncline in the Salem-Wallace Field. The elevation of the base of the Gordon is shallowest (-800 ft MSL) along the Wolf Summit Anticline.

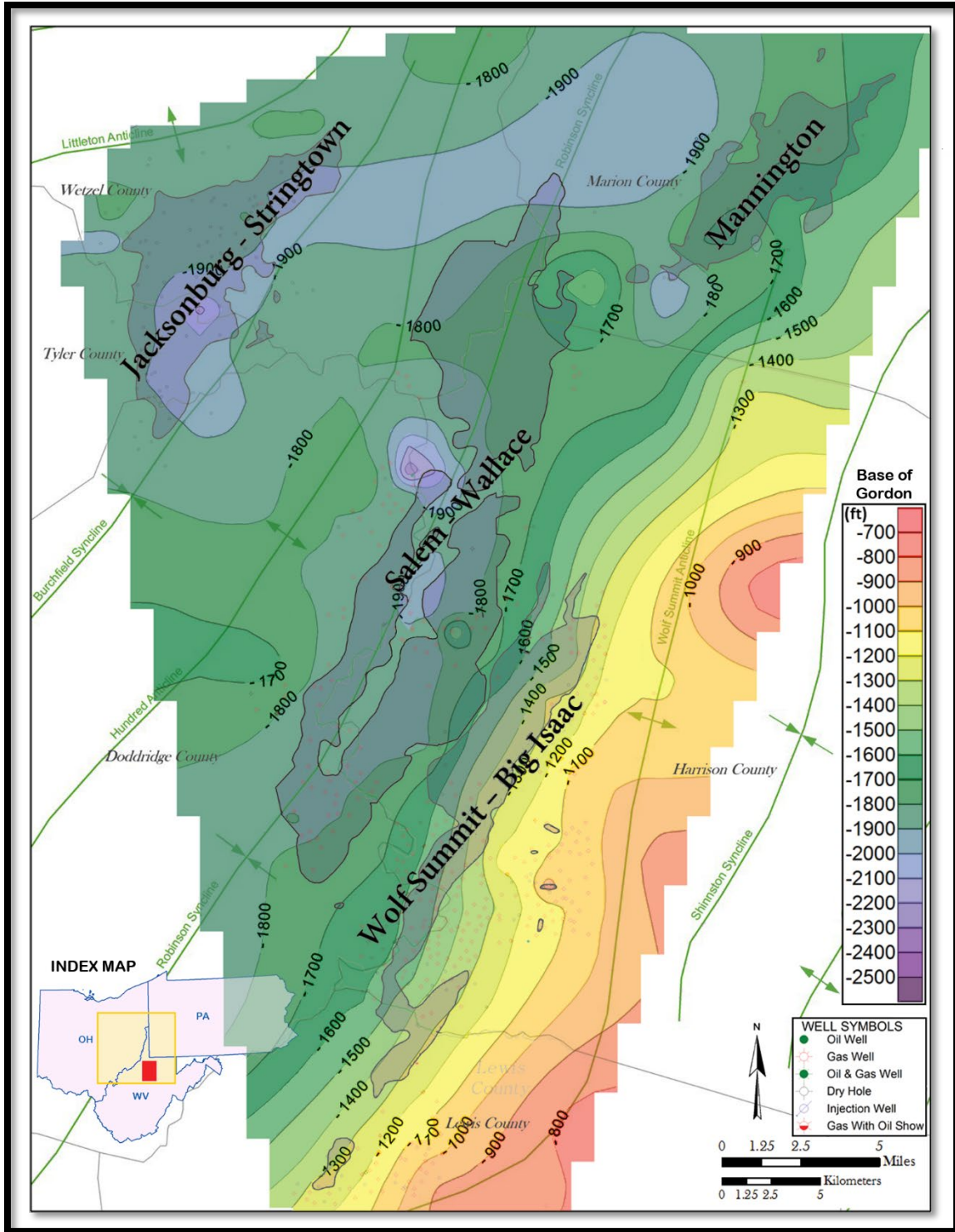


Figure 6-92. Case study fields with regional anticlines and synclines and structure map (100-ft contour interval) on the base of the Gordon sandstone (modified from Moore et al., 2013).

The Gordon sandstone of northern West Virginia consists of multiple stacked sandstones (Figure 6-93). Boswell (1988) postulated that stacked Gordon sandstones are the result of basement subsidence in the Rome Trough, believed to be active during Late Devonian time, in conjunction with an abundant sediment supply created from uplift of the Acadian mountains. This subsidence and accommodation space at the ancient shoreline environment resulted in vertical stacking of sandstone lenses. Stacking patterns become less pronounced and sandstone lenses thin from east to west across the study area.

Net thicknesses reported for the Gordon sandstone in the West Virginia case study fields seem low compared to those illustrated in cross sections and used in other reports (e.g., Moore et al., 2013 and Ober and Eckert, 2014). The source of net thickness data used in this report is Lewis et al. (2019), which comprises information from multiple source and vintages, including information reported when the field was discovered. It is also possible that the thickness reported in legacy well reports is a “pay” thickness, which could represent neither net nor gross thickness of the sandstone body. In the case of the Gordon Stray sandstone in the Jacksonburg-Stringtown field, McBride (2004) reported that most of the production in the field is within the lower upper shoreface and upper lower shoreface subfacies of the barrier island complex. These subfacies exhibit the highest porosity and permeability, ranging from 25 to 250 mD, and it may be more helpful to think of them as “swept zones” for the purpose of CCUS applications. Field-level reservoir evaluations have evolved over time through subsequent exploration, geologic interpretations and data acquired since the field discovery. In the case of the four West Virginia fields herein, subsidence and accommodation (Boswell, 1988) seems to have played a critical role in the accumulation of multiple Gordon and other sandstone units of Mississippian and Late Devonian age. This would not have been recognized when the fields were drilled in the late 1800s.

6.6.2 Jacksonburg-Stringtown Field

The Jacksonburg-Stringtown Field was discovered in 1895 and produces oil from the Gordon sandstone (Hohn, 2001a). At the time of this study, 1584 wells were identified in this field, which comprises 15,895 ac (Figure 6-94) in parts of Wetzel, Tyler and Doddridge counties. Depths to the top of the Gordon range from 2800 to 2825 ft (Cardwell and Avary, 1982), placing this EOR target in the miscible CO₂ range. The field is on the western flank of the Burchfield Syncline (Avary, 2001; Figure 6-92), and Matchen (2001) interpreted an east-west fault that isolates oil production from the Gordon sandstone in the southern portion of this field (Figure 6-95). The current operator of the field, Ascent Resources, acknowledges that Matchen (2001) identified a fault in this area but maintains in a 2017 Class II Underground Injection Control (UIC) permit renewal application that the fault, if present, has “no effect on water injectivity or the ability of the confining shale section to isolate the Gordon sand.” Figure 6-95 represents the operator’s portion of the Jacksonburg-Stringtown Field when Matchen (2001) was published. This area is of a similar extent to the modern area of secondary recovery operations (Figure 6-96).

Northern West Virginia

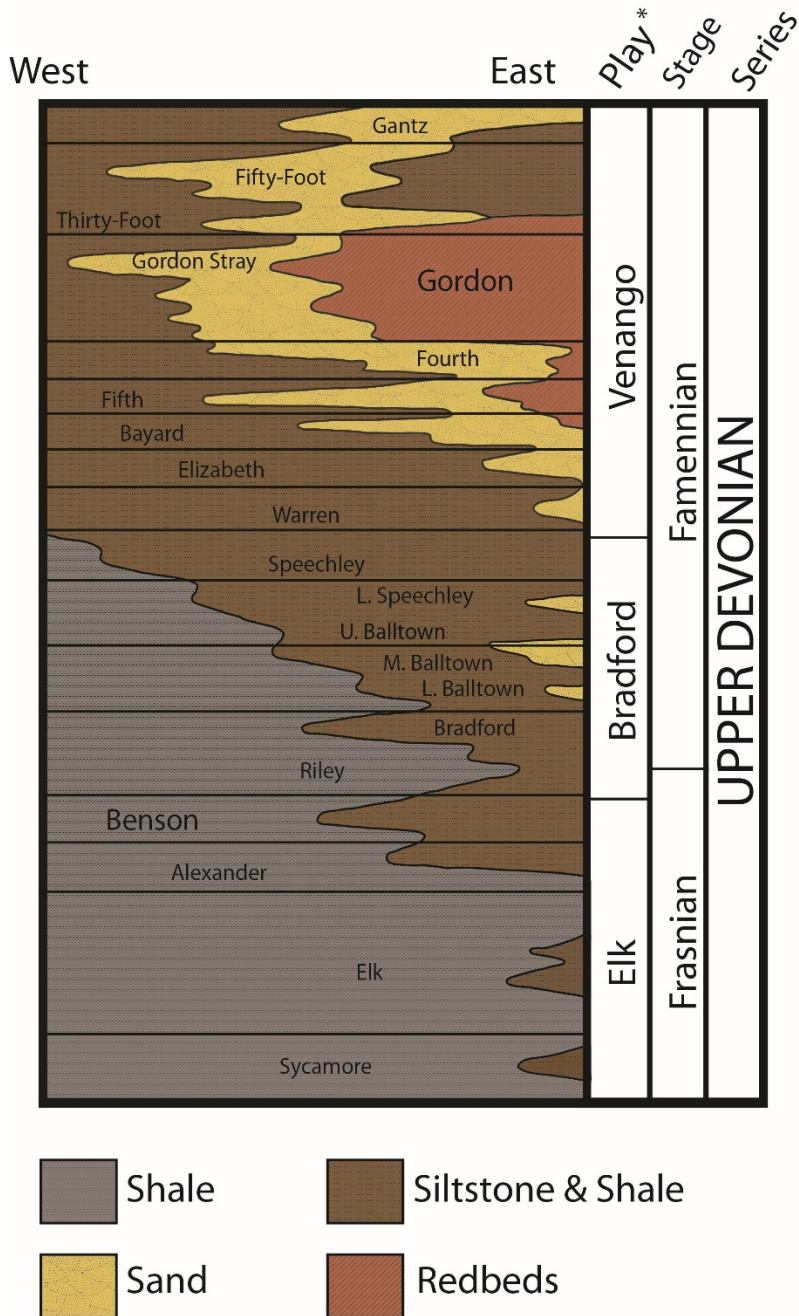


Figure 6-93. Stacked sandstones of the Venango, Bradford and Elk groups in northern West Virginia (modified from Boswell et al., 1996).

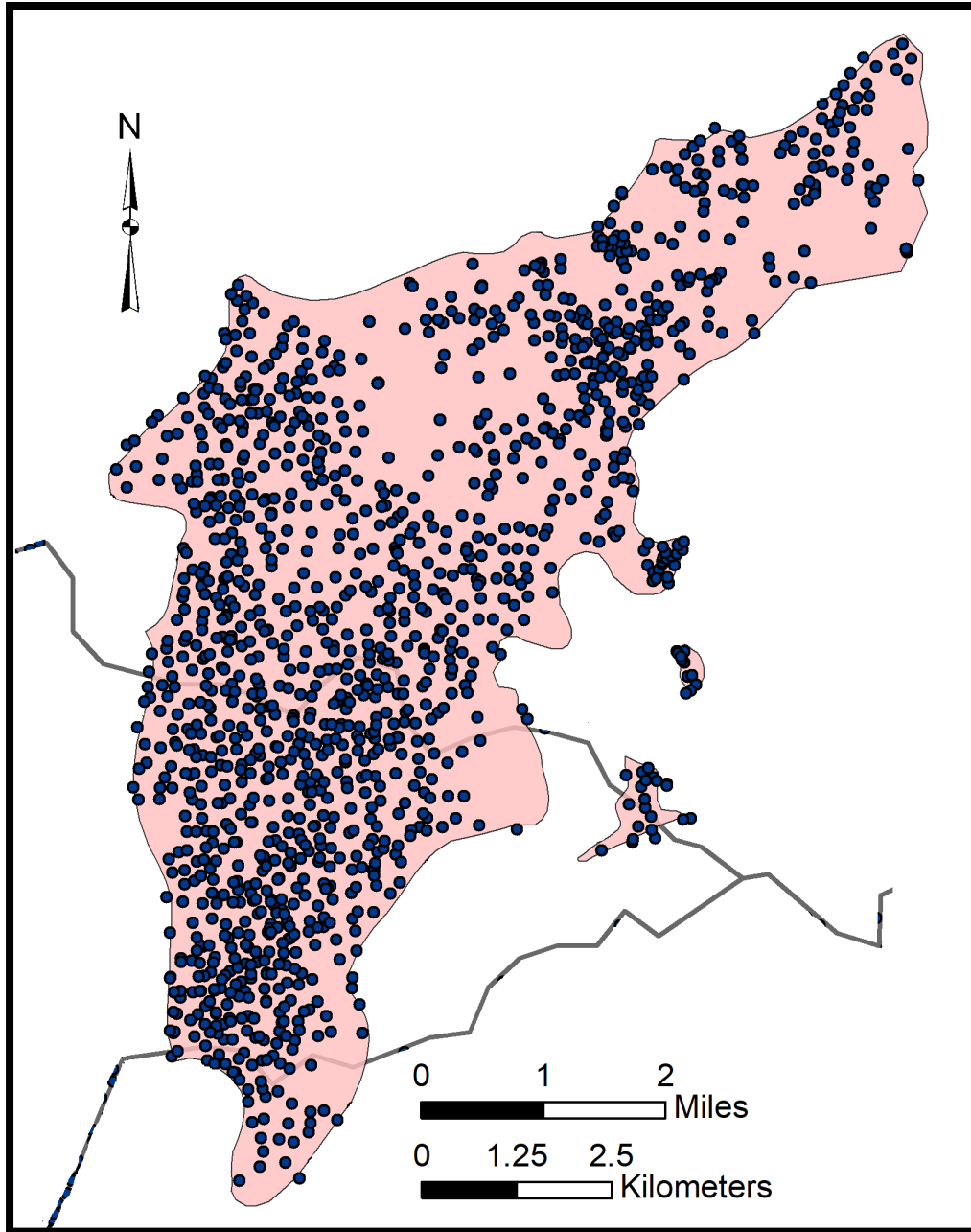


Figure 6-94. Oil and gas wells in the Jacksonburg-Stringtown Field.

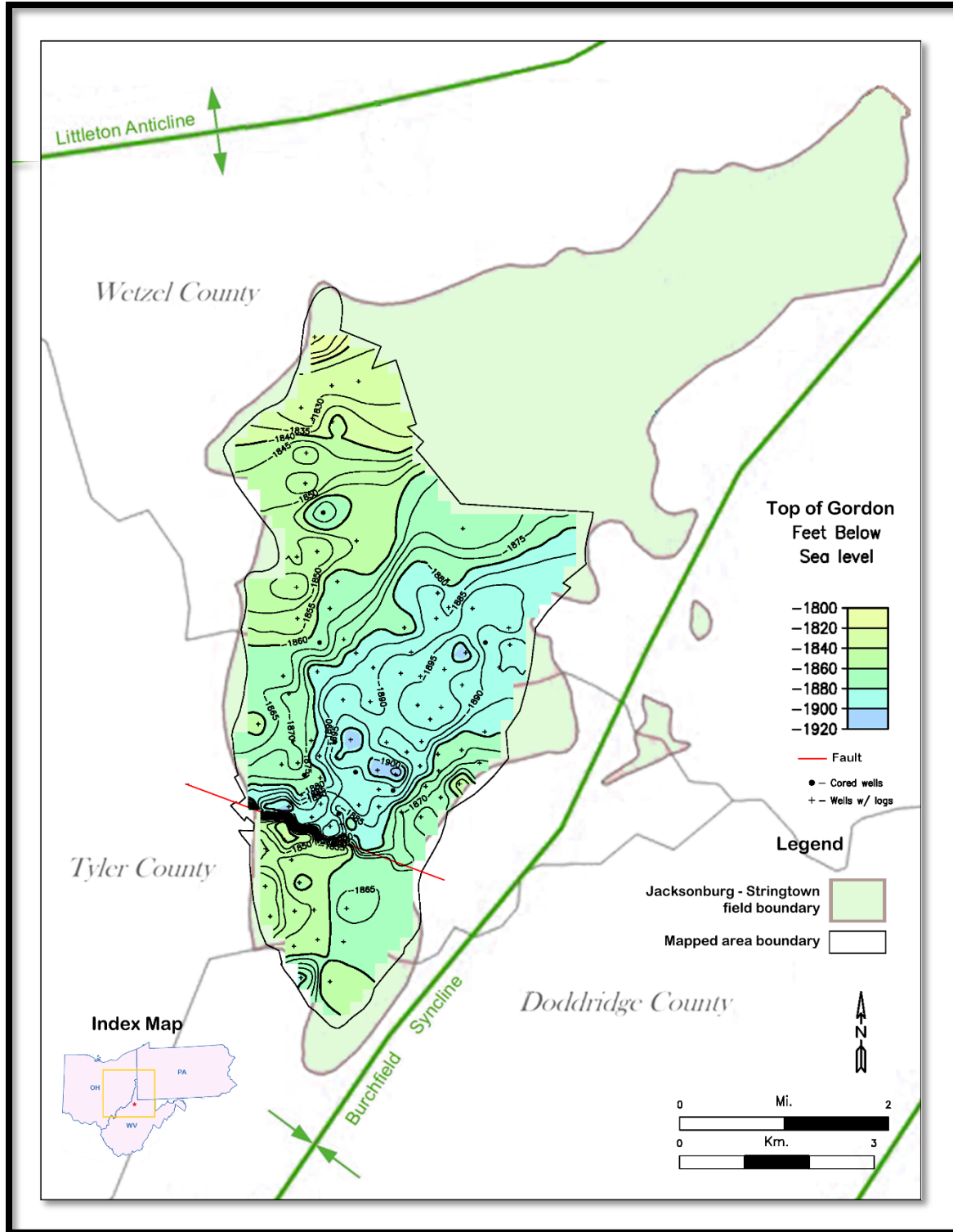


Figure 6-95. Structure map (20-ft contour interval) on the top of the Gordon sandstone (modified from Matchen, 2001, and Moore et al., 2013).

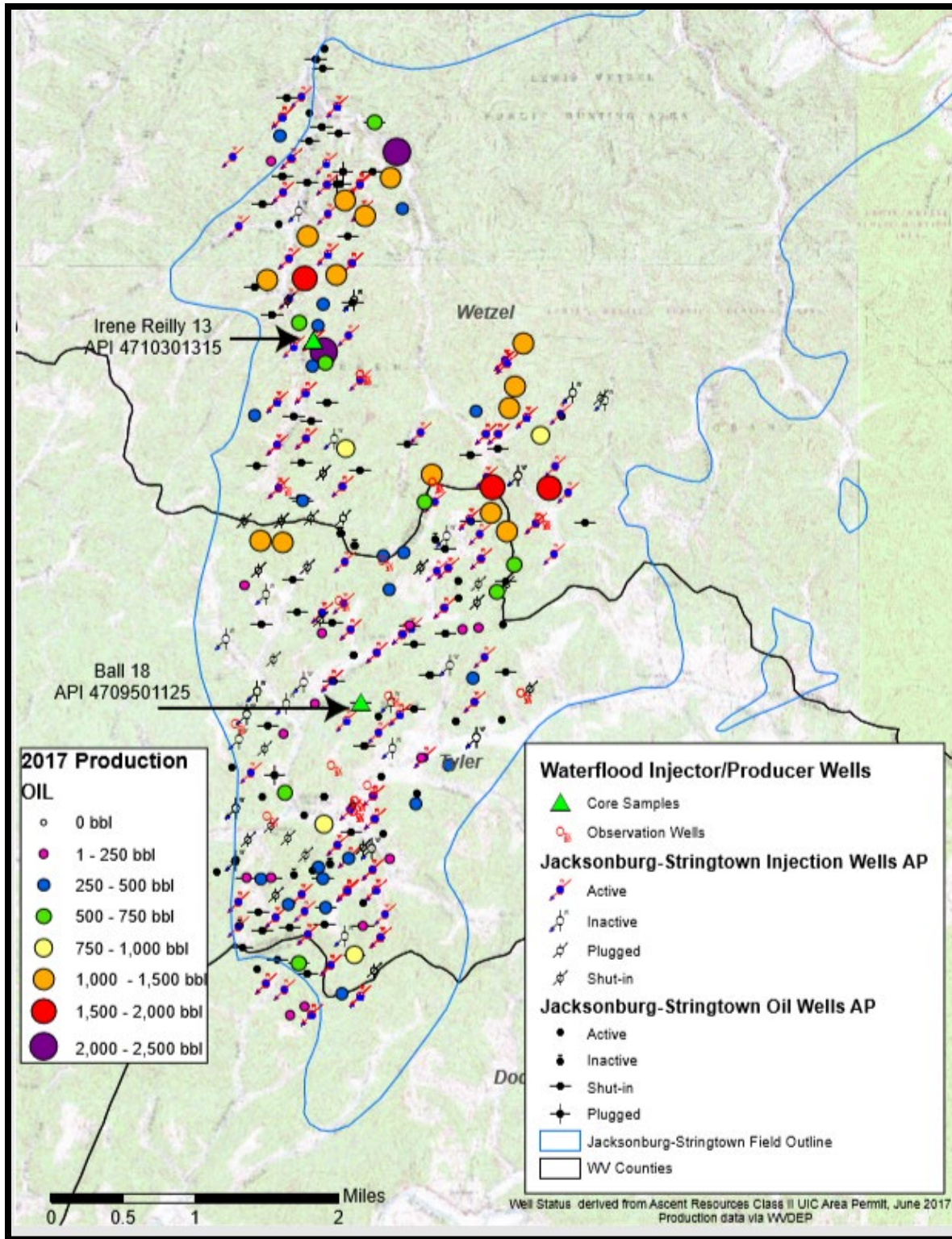


Figure 6-96. Status of wells associated with waterflood operations in the Jacksonburg-Stringtown Field, currently operated by Ascent Resources.

As an active waterflooding operation, more data are available for the Jacksonburg-Stringtown Field, primarily in the form of maps, well status reports and reservoir data submitted by the primary operator to the State of West Virginia in fulfillment of requirements associated with Class II UIC permit applications.

A Class II UIC permit application filed by Ascent Resources in June of 2017 is the source of the well status data presented on Figure 6-96. In addition to this information, the operator provided the following statement characterizing the injection zone:

“The perfect sandstone oil reservoir for waterflooding and, for that sake, water injection, is a thick, clean, homogeneous sandstone with high porosity, high permeability, and low water saturation. The Gordon Sand at Stringtown is far from a perfect candidate. It is neither homogeneous nor clean. It is characterized by narrow sand lenses between thin layers of clay and shale. The sand lenses are poorly sorted and contain clay in the porosity. The better sections exhibit approximately 20% porosity.

The overall Gordon Sand is approximately 60 feet thick. However, reservoir quality pay sand is six to twelve feet within the section. These sand lenses are not continuous across the Stringtown Field. Lenses come and go within 2-3 wellbores.”

The heterogeneous internal composition of the Gordon sandstone in the Jacksonburg-Stringtown Field precludes detailed identification of individual facies in most wells, even if geophysical logs are available. However, given the aggradational morphology of the sandstone lenses, Matchen (2001) divided the interval into three parasequences, each separated by thin shale beds. Five lithofacies associations were identified within the parasequences: laminated sandstone, conglomeratic sandstone, shale and heterolithic bioturbated lithofacies. This tripartite division is readily identified in electric logs from the field, as illustrated in Figure 6-97. Ascent Resources, in their 2017 UIC permit application, assert that the middle parasequence exhibits the best reservoir quality and is the zone completed in most wells. Matchen (2001) reports that only the featureless sand lithofacies exhibits “characteristics of pay.”

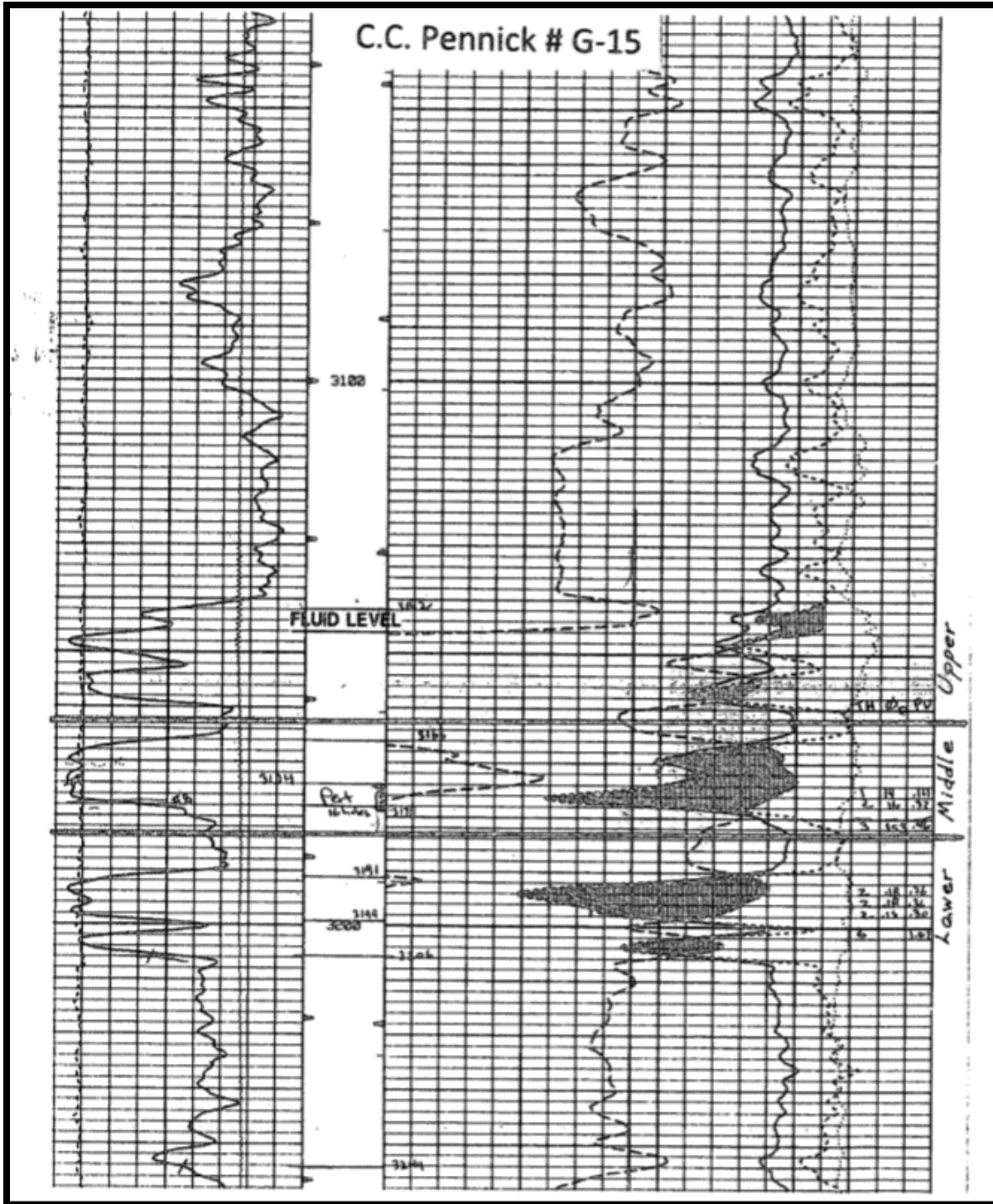


Figure 6-97. Well log submitted as part of the geologic review for Ascent Resources UIC Area Permit. Note the recognition of three individual parasequences in the Gordon Stray interval, each with a low GR signature and crossover of DPHI and NPHI logs, suggesting presence of hydrocarbons (WVDEP).

Several cores were collected from the Jacksonburg-Stringtown Field during the most recent phase of its development. McBride (2004) described ten of the cores in detail and suggested the Gordon Stray sandstone bed, often described as an “erratic rider sand,” was deposited as a barrier island complex at the leading edge of the Catskill Delta. Matchen (2001) suggests that this uppermost Gordon bed was deposited during a forced regression of sea level, which is the reason for its position westward of the main Gordon trend. Fluctuations of relative sea level exerted strong control on position, thickness and stacking patterns of individual sandstone bodies, resulting in high degrees of reservoir heterogeneity across the field. This heterogeneity is apparent from the core samples, two examples of which are presented below.

The Ball 18 well (API No. 4709501125), located in the central part of the field, was drilled by the Pennzoil Company in 1985 and recompleted in 1990. Depth of the completed well is 3089 ft. The Gordon interval is cored from 2977 to 3015 ft (Figure 6-98). In this core, McBride (2004) identifies a lower shoreface deposit (~13.4 ft thickness) overlain by upper shoreface (~9.8 ft), foreshore (~3.2 ft) and washover fan/lagoon (~11.5 ft) deposits (Figure 6-99). Conventional core plug analysis conducted by Core Labs (Table 6-16) identifies a zone of high porosity and permeability from 2992 to 3002 ft, which corresponds to the upper shoreface deposits identified by McBride, and the middle parasequence of Matchen (2001). The Ball 18 well has been an excellent oil producer, with a cumulative oil production of 124,451 BBL from 1991 to present.



Figure 6-98. Full-core photograph of the Ball 18 well (McBride, 2004).

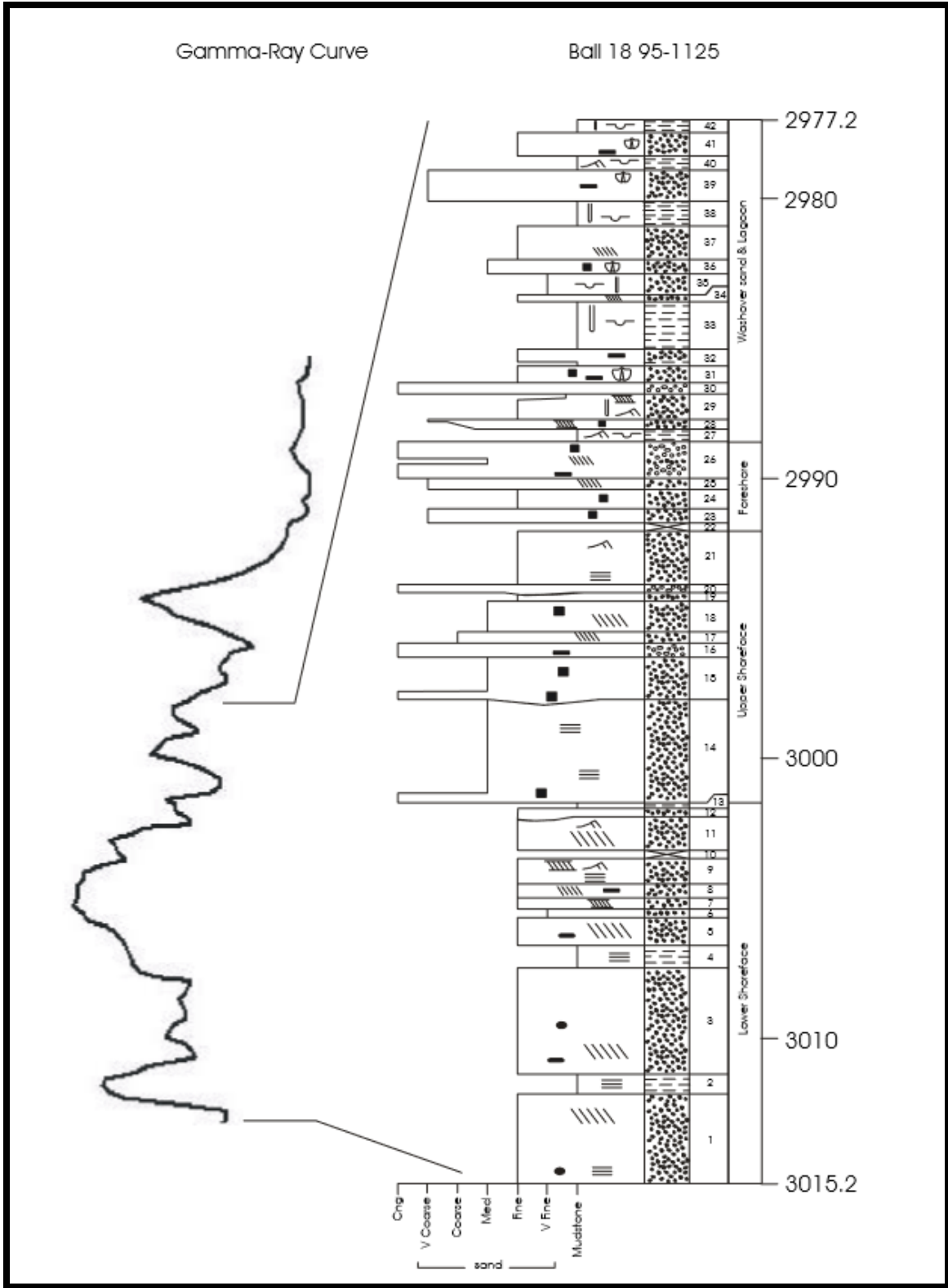


Figure 6-99. Core log of the Gordon Stray sandstone from the Ball 18 well, Jacksonburg-Stringtown Field (McBride, 2004)

Table 6-16. Core Analysis of the Gordon sandstone in Jacksonburg-Stringtown well F.R. Ball 18. Zone of highest porosity and permeability ranges from ~2992 to 3002 ft (WVGES Pipeline Plus).

47-095-01125		Operator: Pennzoil				Field: Jacksonburg-Stringtown				
F R Ball 18		Lab: Core Labs								
Formation: Gordon Sand		Conventional plug analysis								
Depth	Permeability (md)				Porosity (%)		Fluid Sats.		Grain Density (g/cc)	Description
	K _{a-1}	K _{a-2}	K _{a-3}	K _v	He		Oil (%)	Wtr. (%)		
2988.5-2989.0	0.26				6.3					
2989.0-2990.0	0.77			0.03	5.2					
2990.0-2991.0	0.06			0.04	4.2					
2991.0-2992.0	0.14			0.06	5.8				2.68	
2992.0-2993.0	28.00			49.00	21.7					
2993.0-2994.0	54.00			36.00	19.9					
2994.0-2995.0	42.00			48.00	16.5					
2995.0-2996.0	20.00	22.00	8.80	1.92	16.1					
2996.0-2997.0	226.00	182.00	189.00	215.00	24.1				2.66	
2997.0-2998.0	257.00	236.00	269.00	50.00	24.9					
2998.0-2999.0	207.00	324.00	239.00	190.00	24.0				2.66	
2999.0-3000.0	180.00	127.00	220.00	174.00	22.3					
3000.0-3001.0	178.00			115.00	24.9					
3001.0-3002.0	137.00			10.00	24.4					
3000.0-3003.0	0.06			0.06	10.9					
3002.0-3003.0	0.06			0.06	10.9					
3003.0-3004.0	0.05			47	11.2					
3004.0-3005.0	37			0.05	22.5					
3005.0-3006.0	0.1			0.18	10.4					
3006.0-3007.0	0.26			0.06	11					
3007.0-3008.0	0.07				11.7				2.67	
3008.0-3009.0	1.4				13.2					
3009.0-3010.0	1.5				12.3					
3010.0-3011.0	0.79			0.27	10.2					
3011.0-3012.0	0.25				9.8					
3012.0-3013.0	0.11			0.1	9.9					
3013.0-3014.0	0.26			0.24	8.8					
3014.0-3015.0	0.38			0.29	10.4					

Located approximately 2.5 mi north of the Ball 18 well, the Irene Reilly 13 well (API No. 4710301315) was drilled by the Pennzoil Company in 1984 and recompleted in 1986 and 1995. The total depth of the well is 2990 ft, and the Gordon Stray has been cored from 2865 to 2899 ft. In this core, McBride (2004) identified a thin shelf mud (~1.2 ft), overlain by lower shoreface (~2.4 ft), upper shoreface (~6.25 ft), and foreshore (~3.15 ft) deposits, which are then overlain by a 21 ft succession of interbedded washover channel and lagoon deposits (Figure 6-100). These lagoonal muds appear in sharp contrast to the clean sand bodies of both the shoreface, foreshore and washover channel sands (Figure 6-100).

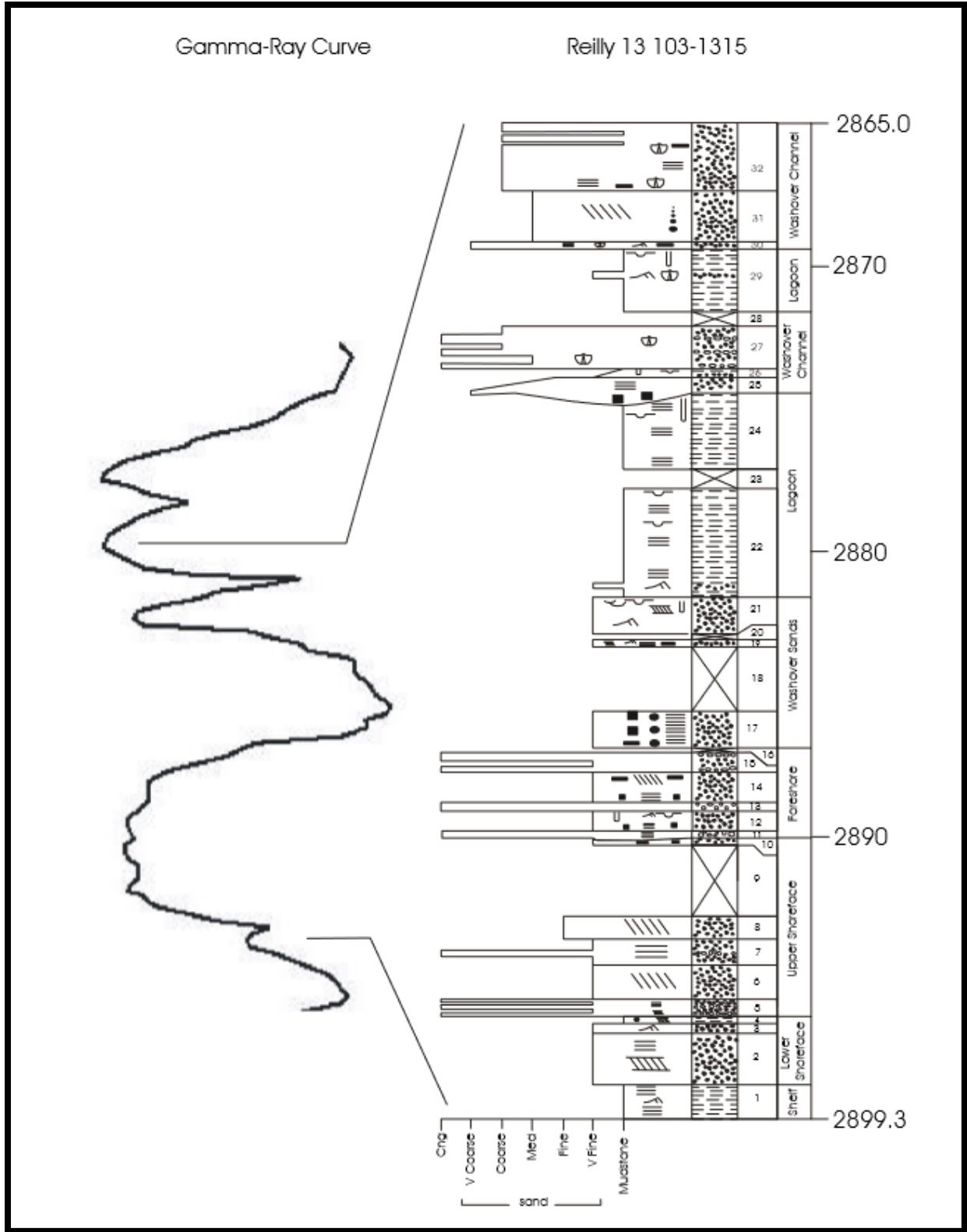


Figure 6-100. Core log of the Gordon Stray sandstone from the Reilly 13 well, Jacksonburg-Stringtown Field (McBride, 2004).



Figure 6-101. Full-core photograph of the Irene Reilly 13 well (McBride, 2004).

The Irene Reilly 13 core was also analyzed by Core Labs for porosity and permeability, although only core plugs from the lower, more sandstone-rich portion of the core (2880 to 2896 ft) were selected for analysis. Despite being collected from similar lithofacies as were observed by McBride (2004) in the Ball 18 well, porosity and permeability values are significantly lower. Porosity ranges from 4.9 to 9.8 percent, and permeability from <0.1 to 0.9 mD (Table 6-17). The Irene Reilly 13 well did not produce any oil and only a small amount of gas (9464 MCF from 1989 to 1995). However, the Irene Reilly 4, located 0.1 mi to the southeast, produced 2032 BBL oil in 2017 and has produced a cumulative 16,126 BBL since 1981.

Table 6-17. Core Analysis of the Gordon sandstone in Jacksonburg-Stringtown well Irene Reilly 13. Note relatively low porosity and permeability values, as compared to the Ball 18 well (WVGES Pipeline Plus).

47-103-01315		Operator: Pennzoil				Field: Jacksonburg-Stringtown						
Irene Reilly 13		Lab: Core Labs										
Formation: Gordon Sand												
Depth	Feet Analyzed	Permeability				Porosity		Fluid Sats.		Bulk Density (g/cc)	Grain Density (g/cc)	Description
		max (md)	90 deg (md)	vert (md)	ft (90) (md ft)	gex (%)	feet	Oil (%)	Wtr. (%)			
full diameter analysis with measured grain densities:												
2880.7-2882.0	0.67	<0.1	<0.1	<0.1	<0.10	7.7	5.15	3.5	30.2	2.55	2.67	ss,f/gr,gy
2882.0-2883.0	0.32	<0.1	<0.1	<0.1	<0.10	5.9	1.88	5.7	48.6	2.62	2.72	ss,f/gr,gy
2883.0-2884.0	0.64	0.1	<0.1	<0.1	<0.10	9.2	5.89	4.5	38.6	2.53	2.67	ss,f/gr,gy
2884.0-2885.0	0.5	<0.1	<0.1	<0.1	<0.10	8.8	4.36	29.4	24.9	2.52	2.66	ss,f/gr,gy
2885.0-2886.0	0.66	0.1	0.1	<0.1	0.07	8.8	5.77	30.2	25.9	2.53	2.67	ss,f/gr,gy
2886.0-2887.0	0.44	0.5	0.4	0.2	0.17	4.6	2.01	26.2	22.4	2.58	2.65	ss,f/gr,gy,pbly
2887.0-2888.0	6.7	1	0.9	0.3	0.6	8.6	5.73	19.2	11.9	2.51	2.64	ss,f/gr,gy,pbly
2888.0-2889.0	0.52	0.5	0.5	<0.1	0.26	9.8	5.05	23.2	14	2.49	2.64	ss,f/gr,gy,pbly
2889.0-2890.0	0.58	0.5	0.4	<0.1	0.23	9.3	5.4	25.6	15.4	2.5	2.64	ss,f/gr,gy,pbly
2890.0-2891.0	0.64	0.2	0.2	<0.1	0.13	6.3	4.05	15.3	26	2.54	2.64	ss,f/gr,gy,pbly
2891.0-2892.0	0.33	0.2	0.2	<0.1	0.07	6.3	2.07	14.5	25	2.54	2.64	ss,f/gr,gy,pbly
2892.0-2893.0	0.75	0.4	0.3	<0.1	0.22	7.8	5.83	15.7	26.9	2.52	2.64	ss,f/gr,gy,pbly
2893.0-2894.0	0.41	0.3	0.3	<0.1	0.12	5.5	2.27	8.3	25	2.56	2.64	ss,f/gr,gy,pbly
2894.0-2895.0	0.75	0.2	0.1	<0.1	0.08	7	5.26	19	16.1	2.53	2.64	ss,f/gr,gy,pbly
2895.0-2896.5	0.49	0.4	0.4	<0.1	0.2	4.9	2.41	8.4	24.9	2.56	2.64	ss,f/gr,gy,pbly

Here, the Gordon interval is made up of several roughly linear sandstone bodies that may be superimposed in some areas (Avary, 2001). These sandstones are interpreted as shoreline/shoreface sandstones because they were deposited at the western extent of the prograding Catskill Delta. This leading edge of the landmass was therefore very sensitive to fluctuations in relative sea level, as evidenced by the highly heterogeneous reservoir (Matchen, 2001). Stacking of these sandstone bodies controls thickness variations, as illustrated in Figure 6-102, and the GR log curves in Figure 6-103 and Figure 6-104 show variable stacking patterns in cross section.

The most widely recognized sandstone in Jacksonburg-Stringtown Field is the upper Gordon sandstone, which is commonly referred to as the "Gordon Stray" by local operators (Moore et al., 2013). The Gordon Stray is the uppermost sandstone bed of the Gordon succession and is often referred to as an erratic "rider sandstone" above the Gordon (McBride, 2004). The average net pay thickness of this unit is nine ft, and the average producing depth is 3000 ft, deep enough for CO₂ to exist in its supercritical state and be miscible with oil. The Gordon's

pore-derived permeability ranges from 10 to 200 mD, and the distribution of permeability within this zone is fairly uniform (Hohn, 2001b). Field-level reservoir data extracted from Lewis et al. (2019) for the Gordon sandstone are provided in Table 6-18.

Table 6-18. Field-level reservoir data for the Gordon sandstone in Jacksonburg-Stringtown Field.

Average Producing Depth (ft)	Net Thickness (ft)	Pressure (psi)	Porosity (%)	Water Saturation (%)	Remaining Oil (BBL)
3000	9	1000	15	26	69,447,862

Figure 6-105 presents a petrophysical analysis for Wetzel 568 (API No. 4710300568) in Jacksonburg-Stringtown Field. Here, the Gordon sandstone is particularly clean (yellow) with only minor shale (gray). Effective porosity (red) in the Gordon interval ranges from 20 to nearly 50 percent, and according to the petrophysical calculation, a sizeable quantity of hydrocarbons (orange) remain in this unit.

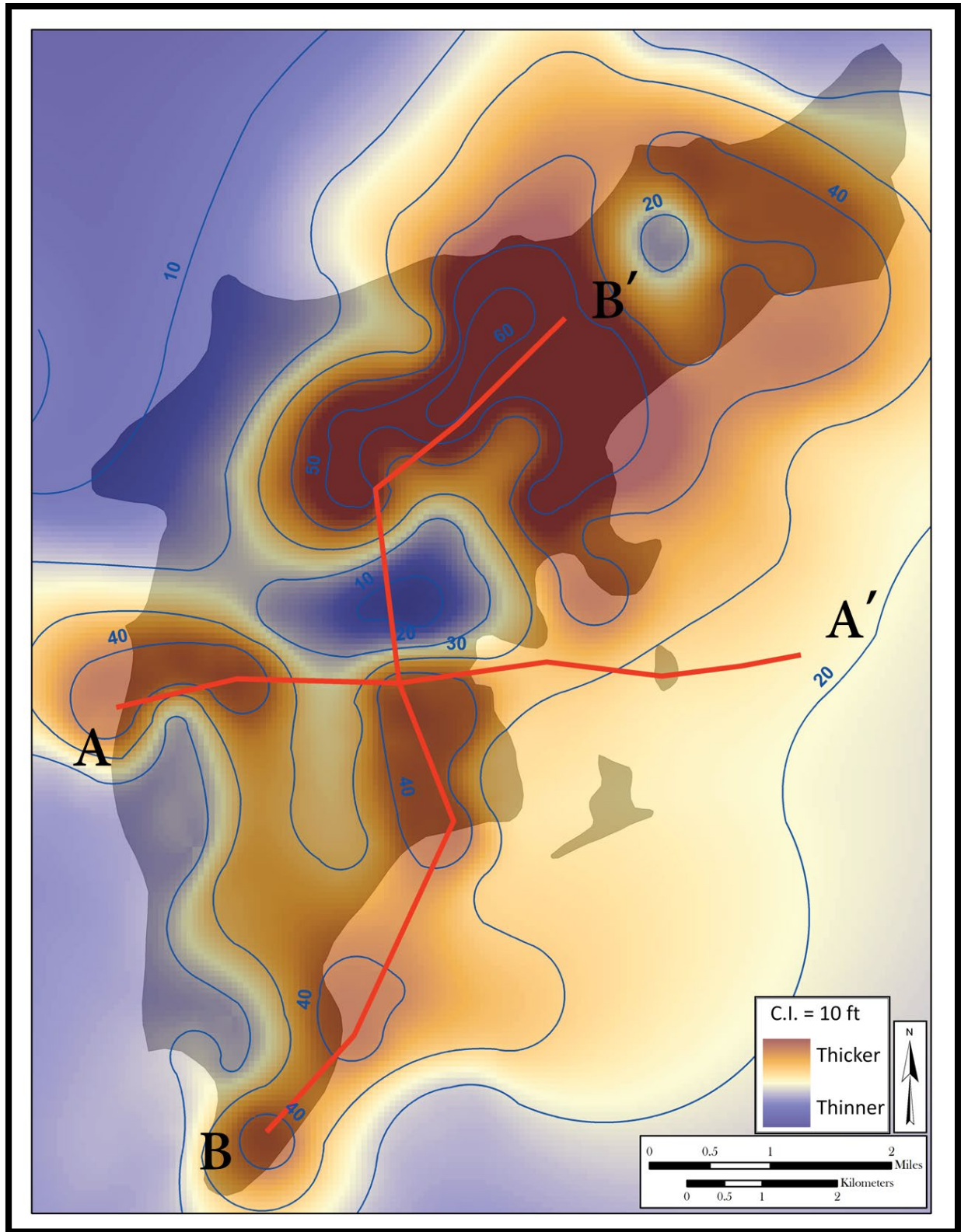


Figure 6-102. Gross thickness map (10-ft contour interval) of the Gordon sandstone in Wetzel, Tyler and Doddridge counties (Moore et al., 2013).

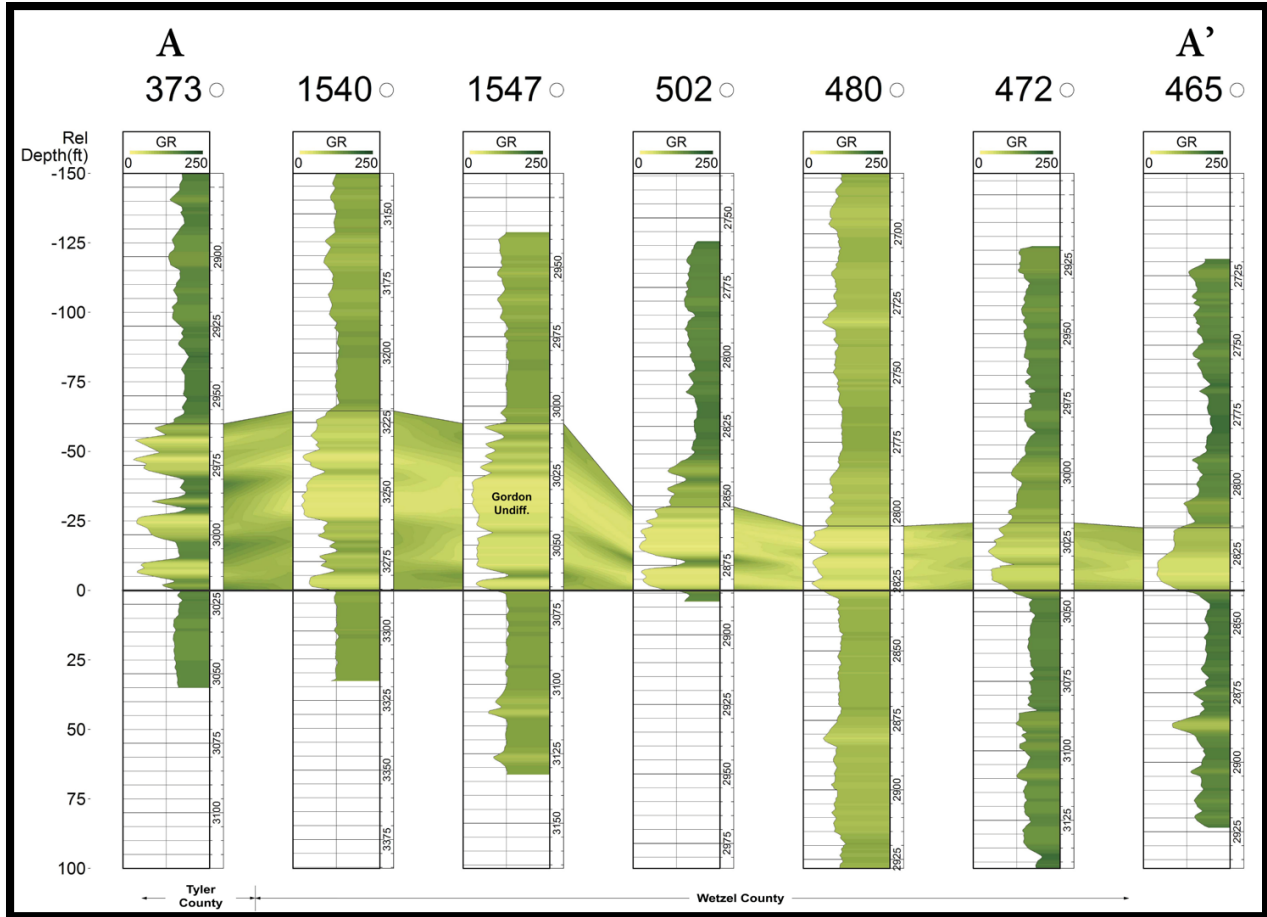


Figure 6-103. West to east Gordon cross section through Jacksonburg-Stringtown Field (Moore et al., 2013).

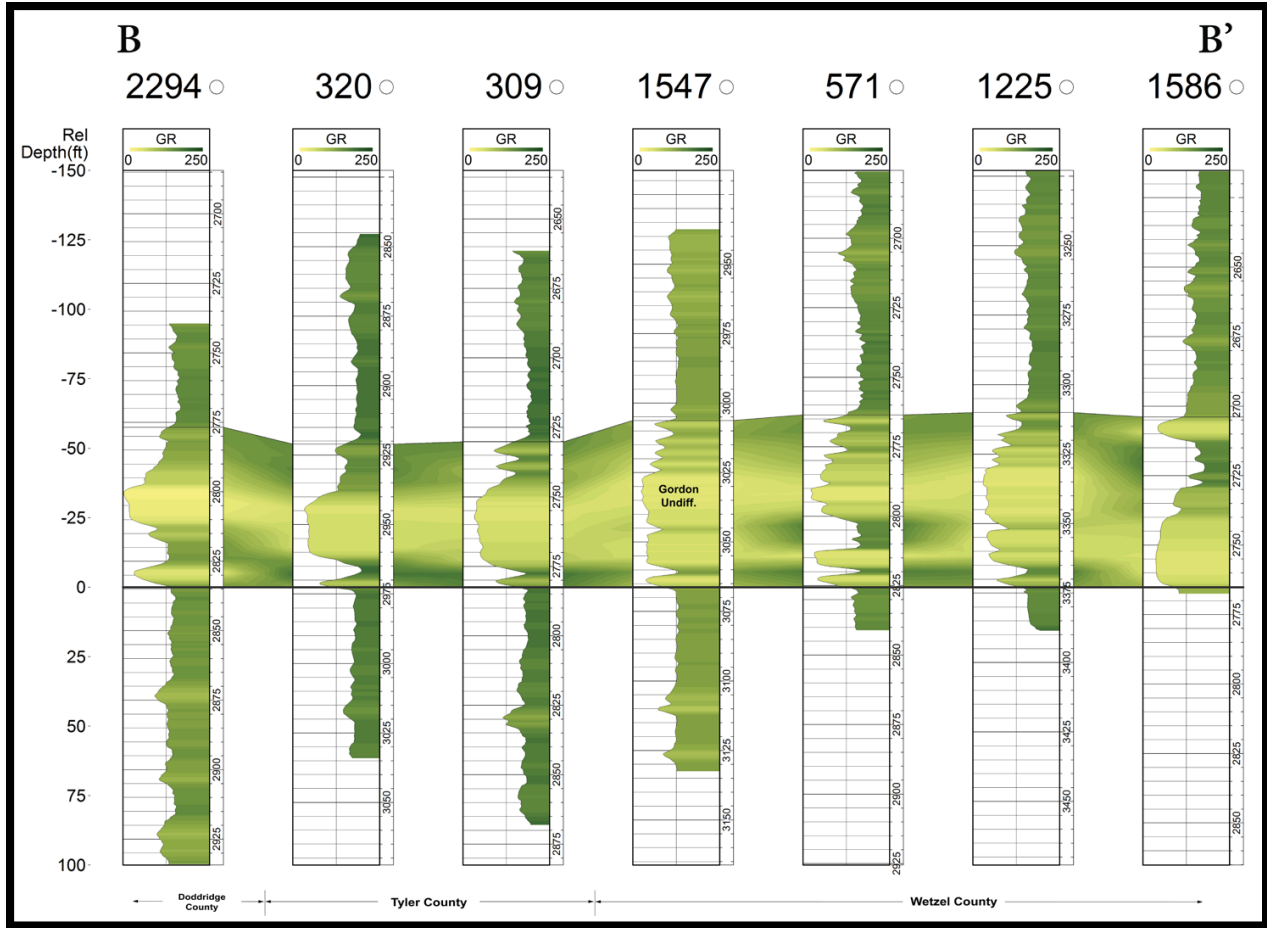


Figure 6-104. North to south Gordon cross section through Jacksonburg-Stringtown Field (Moore et al., 2013).

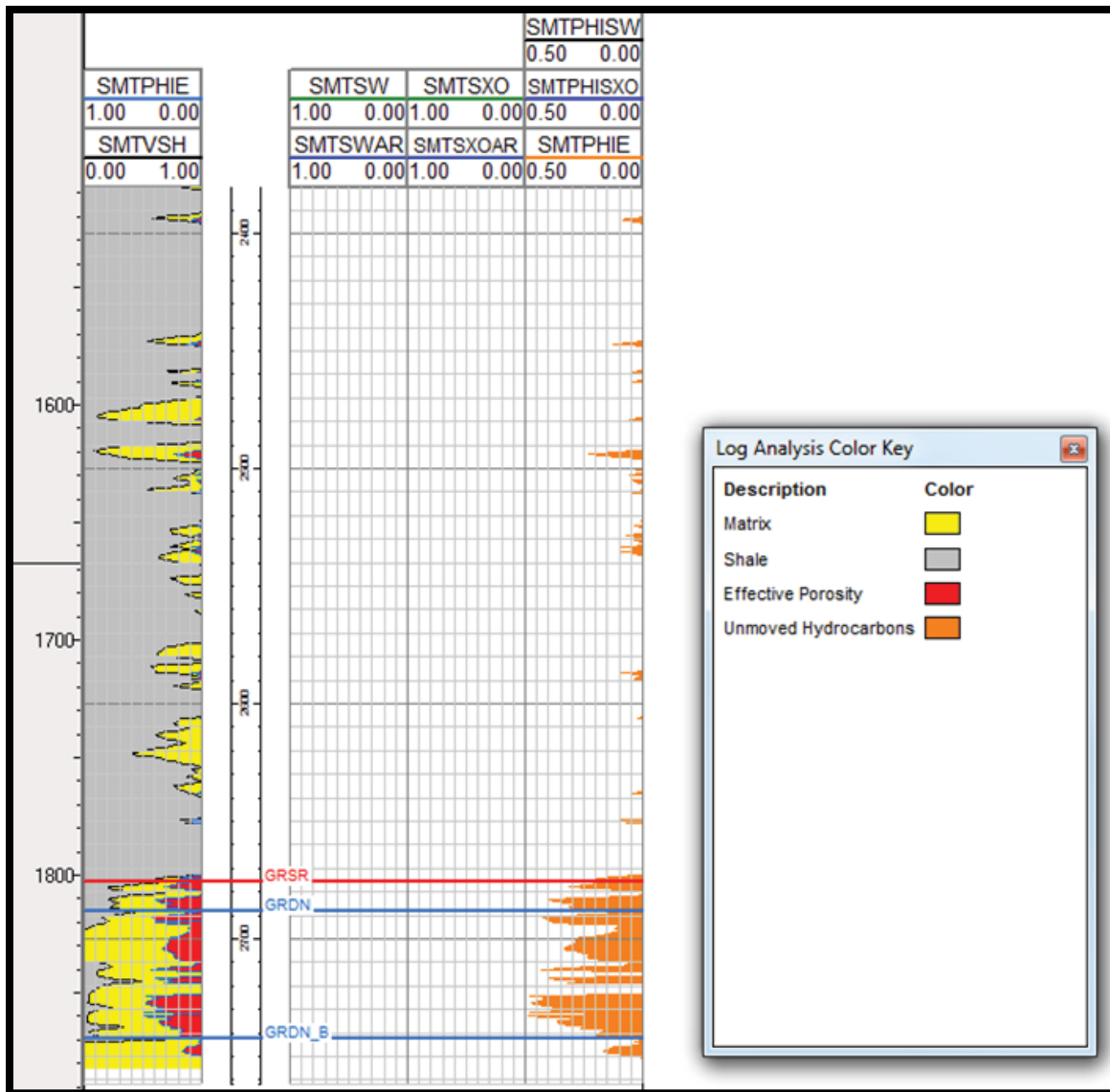


Figure 6-105. Petrophysical analysis of the Gordon Stray (GRSR) and lower Gordon sandstones (GRDN-GRDN_B) in Wetzel 568 (Moore et al., 2013).

6.6.2.1 Rating Discussion

The Jacksonburg-Stringtown Field was rated highly for depth and pressure, as the reported pressure is greater than the calculated MMP for CO₂ in this field. The field's trap integrity is well-documented by Hohn (2001a), and the field was also rated highly for its size and matrix porosity. In addition, oil saturation (40.6 percent), potential oil recovery (9 MMBO) and cumulative oil production (20 MMBO) make this field a favorable EOR target using tertiary recovery methods. The net reservoir thickness was rated low for this field. The number of legacy wells (estimated at 1428) will necessitate a field-level investigation prior to future EOR injection operations. Detailed rating results for this field is provided in Appendix D.

6.6.2.2 Secondary Recovery

Secondary recovery efforts are active in Jacksonburg-Stringtown Field. Full-scale waterflooding began in 1990 (Avary, 2001), with a total of 215 waterflood wells in this area (Figure 6-106). All waterflood wells were drilled to the Gordon sandstone. Figure 6-107 shows annual oil production with the number of waterflood wells completed for that year. Following the completion of 14 waterflood wells in 1990 and 11 waterflood wells in 1992, oil production increased five-fold from 36,107 BBL in 1992 to 181,877 BBL in 1993. Waterflood wells continued to be drilled through the early 1990s and production rose to 328,413 BBL in 1995. The drilling of waterflood wells slowed during the late 1990s and early 2000s, with oil production dropping to 221,099 BBL in 2002. Six waterflood wells were drilled in 2003, and 19 were completed in 2004. Oil production rose to 421,488 BBL in 2007. Production volumes appear low in 2009 due to lack of operator reporting in that year.

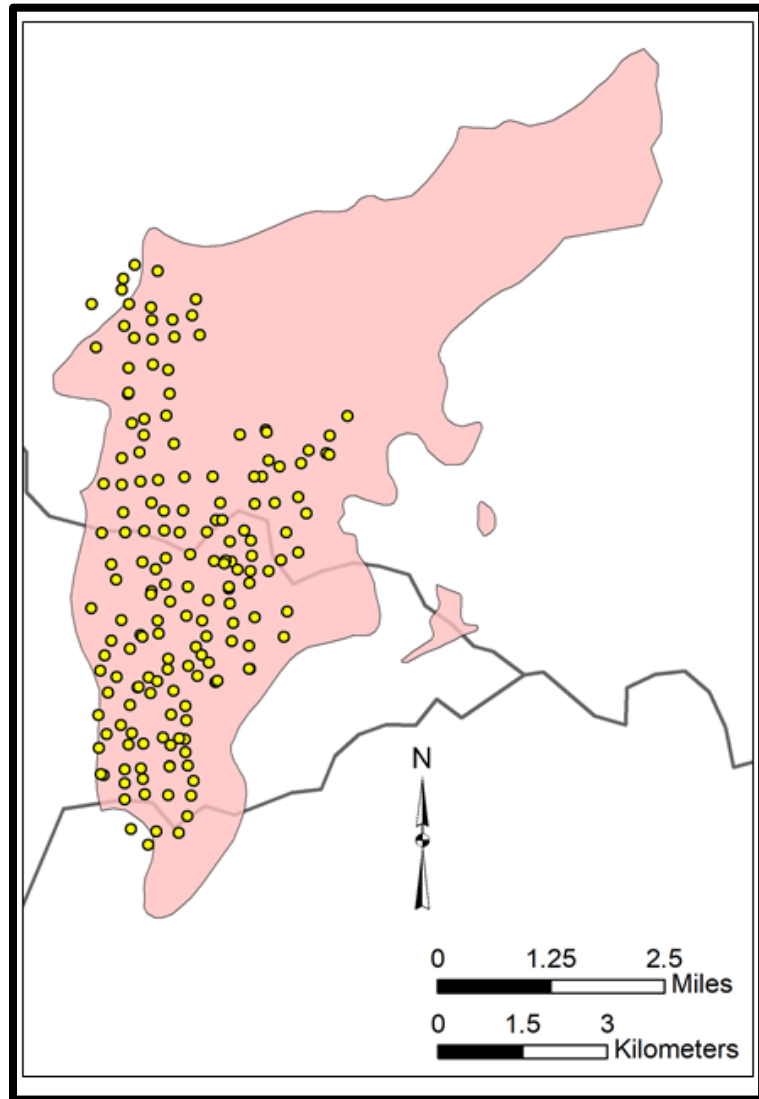


Figure 6-106. Waterflood wells in the Jacksonburg-Stringtown Field.

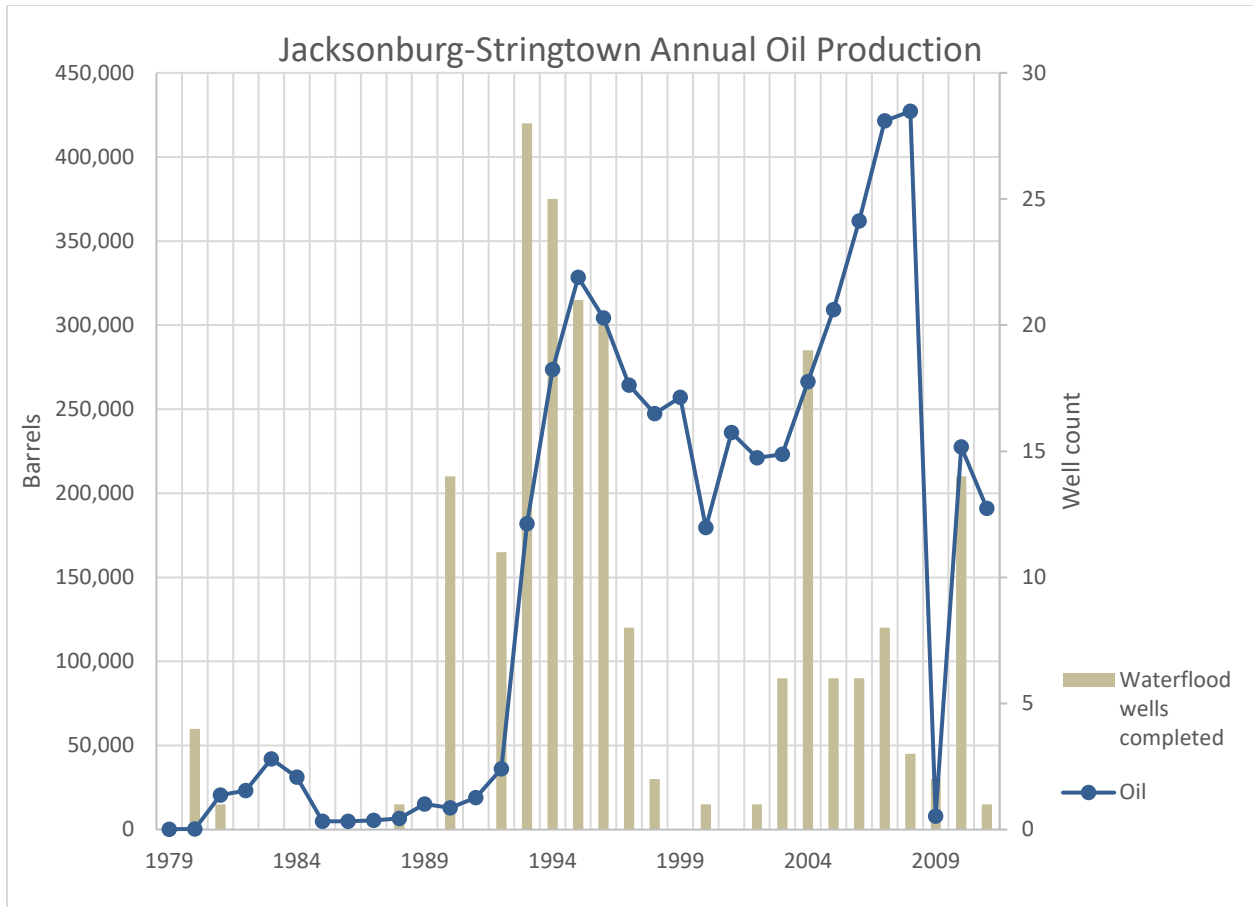


Figure 6-107. Annual oil production (DDS5, 2018) and waterflood well completions in Jacksonburg-Stringtown Field.

6.6.3 Mannington Field

The Mannington Field was discovered in 1886 and is situated just north of the Wolf Summit Anticline (Figure 6-91) in Marion County. The first well was drilled as a test of pioneering geologist I. C. White’s anticlinal theory of hydrocarbon accumulation (Dorsey, 2008). The field produces oil from three intervals – the “Big Injun,” Gordon and Fifth sandstones. Depth to producing zones range from 2000 to 3075 ft (Cardwell and Avary, 1982). At the time of this study, 638 wells were identified in this field (Figure 6-108).

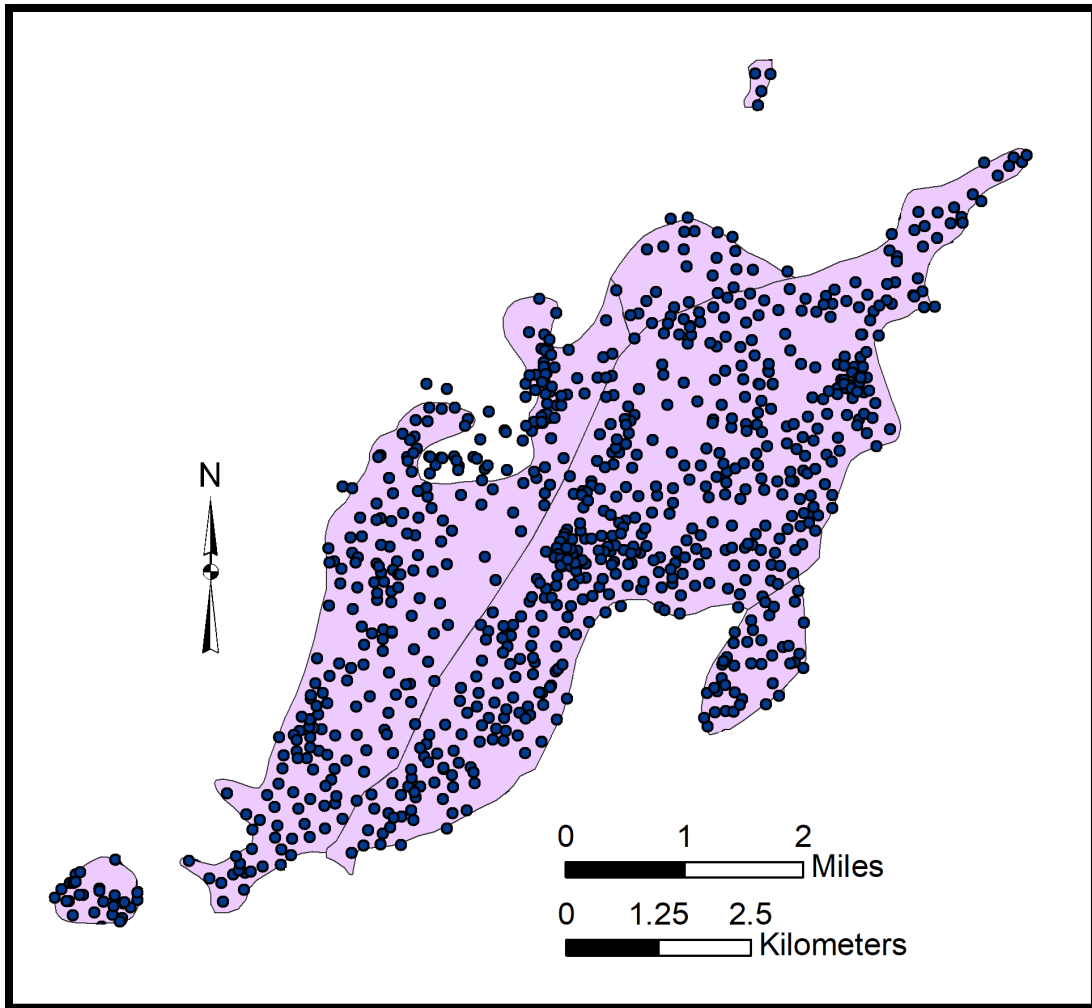


Figure 6-108. Oil and gas wells in the Mannington Field.

Figure 6-109 plots oil wells in Mannington Field by producing formation. Most of the “Big Injun” wells (blue) are situated in a northeast/southwest trend (gray dashed lines) through this area. Gordon wells (brown) are scattered throughout the field but mostly exist outside of the “Big Injun” trend. Wells producing from the Fifth sandstone (yellow) are limited to the northern part of this field.

The “Big Injun” sandstone covers an area of 5833 ac and produces oil from 71 wells in Mannington Field (Figure 6-109). Here, the unit ranges from approximately 25 to 100 ft thick (Figure 6-110), with most wells producing from the area where the “Big Injun” is 25 to 50 ft thick. The “Big Injun” has a net pay thickness of 18 ft, and its average depth is 2100 ft (Table 6-19).

Table 6-19. Unit-specific reservoir characteristics for the Mannington Field.

Unit	Average Producing Depth (ft)	Net Thickness (ft)	Pressure (psi)	Porosity (%)	Water Saturation (%)	Remaining Oil (BBL)
"Big Injun"	2100	18	909	15	48	86,201,936
Gordon	2700	5	1169	12	28	7,832,942
Fifth	3000	7	1299	17	7	3,914,376

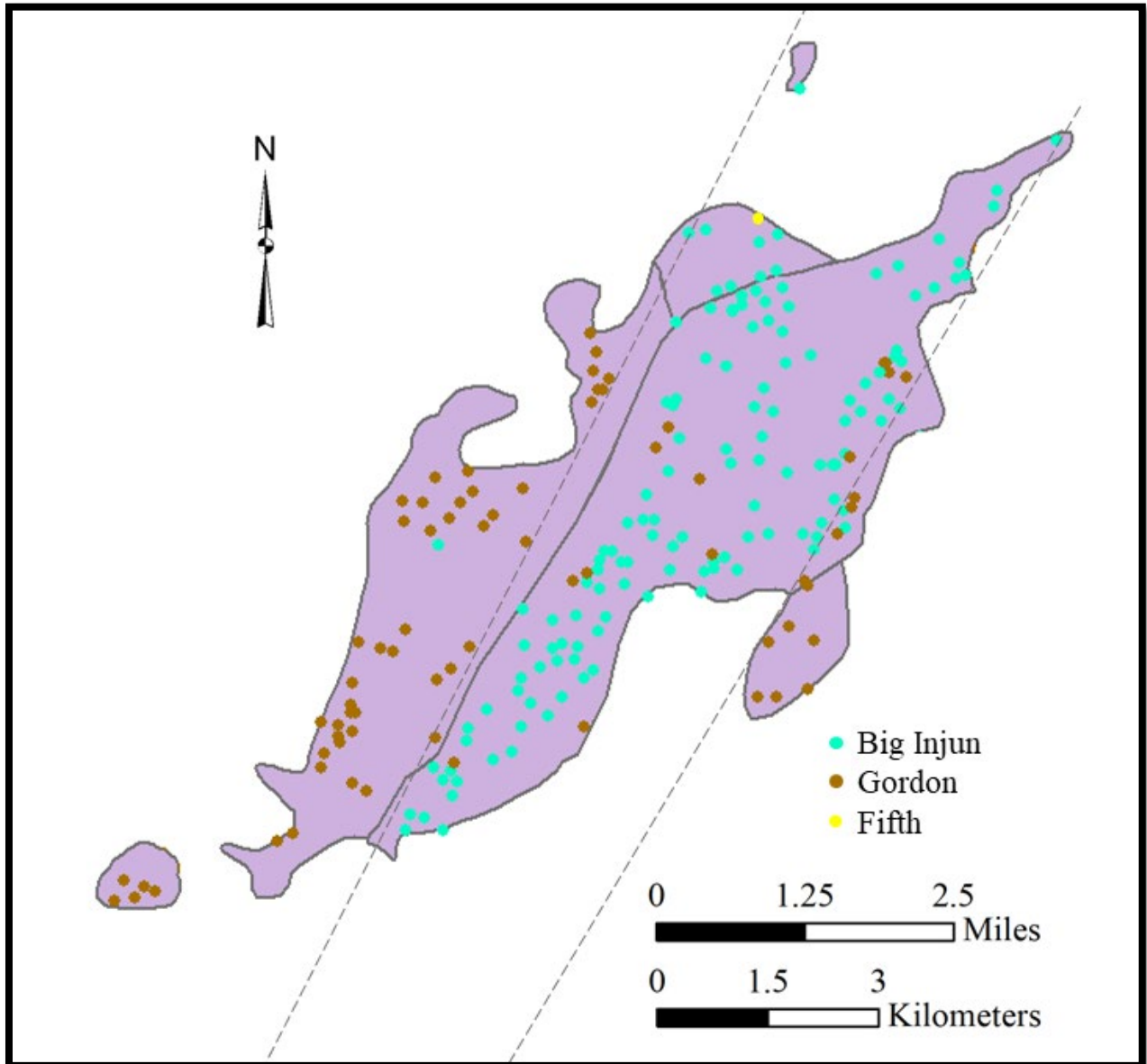


Figure 6-109. Oil wells of the Mannington Field.

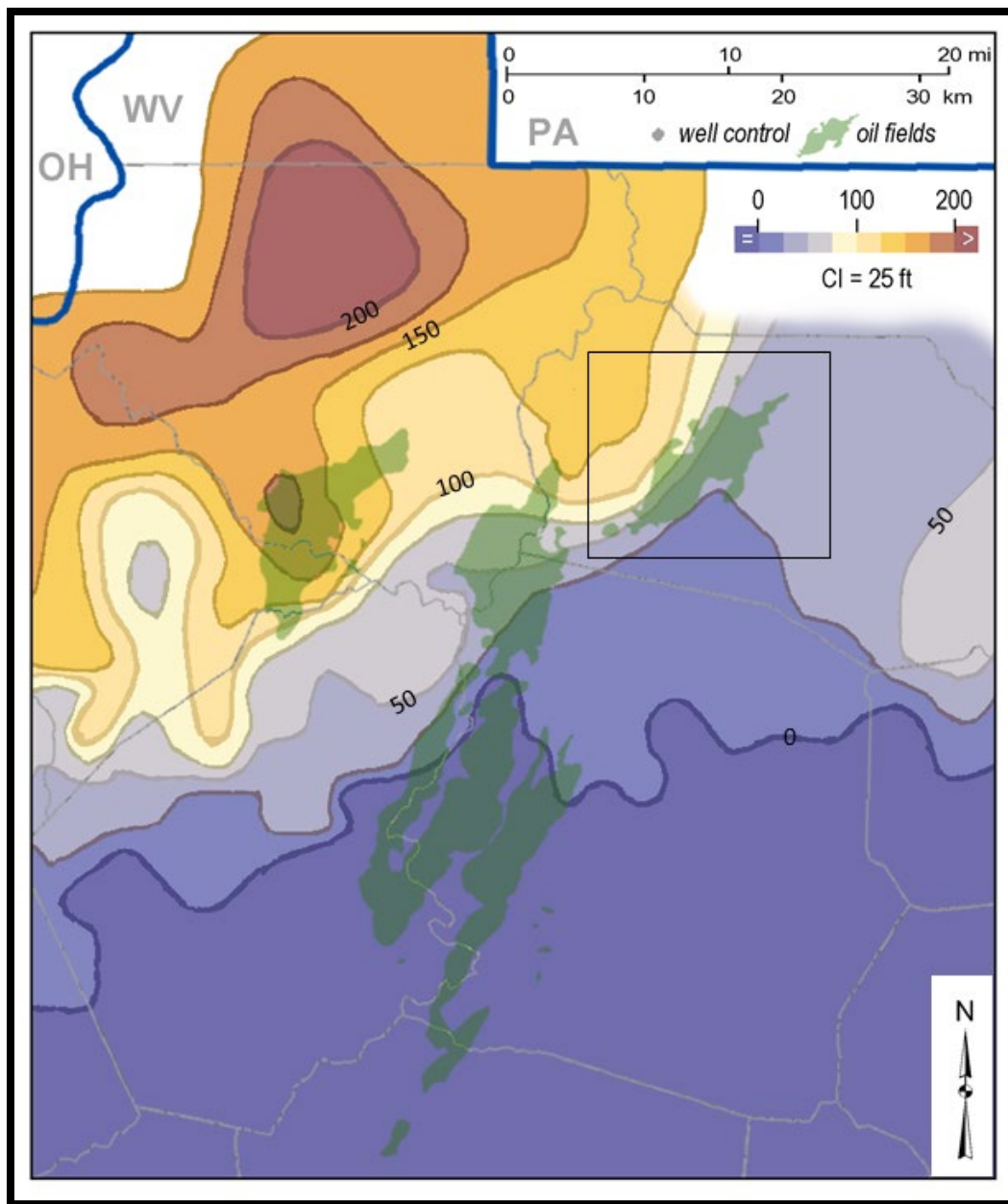


Figure 6-110. Gross thickness map (25-ft contour interval) of the “Big Injun” sandstone in northern West Virginia (modified from Vargo and Matchen, 1996). The Mannington Field shown in the rectangular box.

The Gordon sandstone produces from 20 wells in Mannington Field (Figure 6-109). The gross thickness of the undifferentiated Gordon ranges from about 175 to about 205 ft (Figure 6-111) within a footprint of 4179 ac. Northern thickening is likely a result of increased accommodation space during deposition, while rapid westward thinning may be structurally related (Moore et al., 2013). The average net pay thickness of the Gordon sandstone, as reported in Lewis et al. (2019) is five ft and its average depth is 2700 ft, deep enough for CO₂ to exist in its supercritical state and be miscible with oil. The elevation of the Gordon sandstone base ranges from -1600 to -1900 ft MSL in Mannington Field (Figure 6-92).

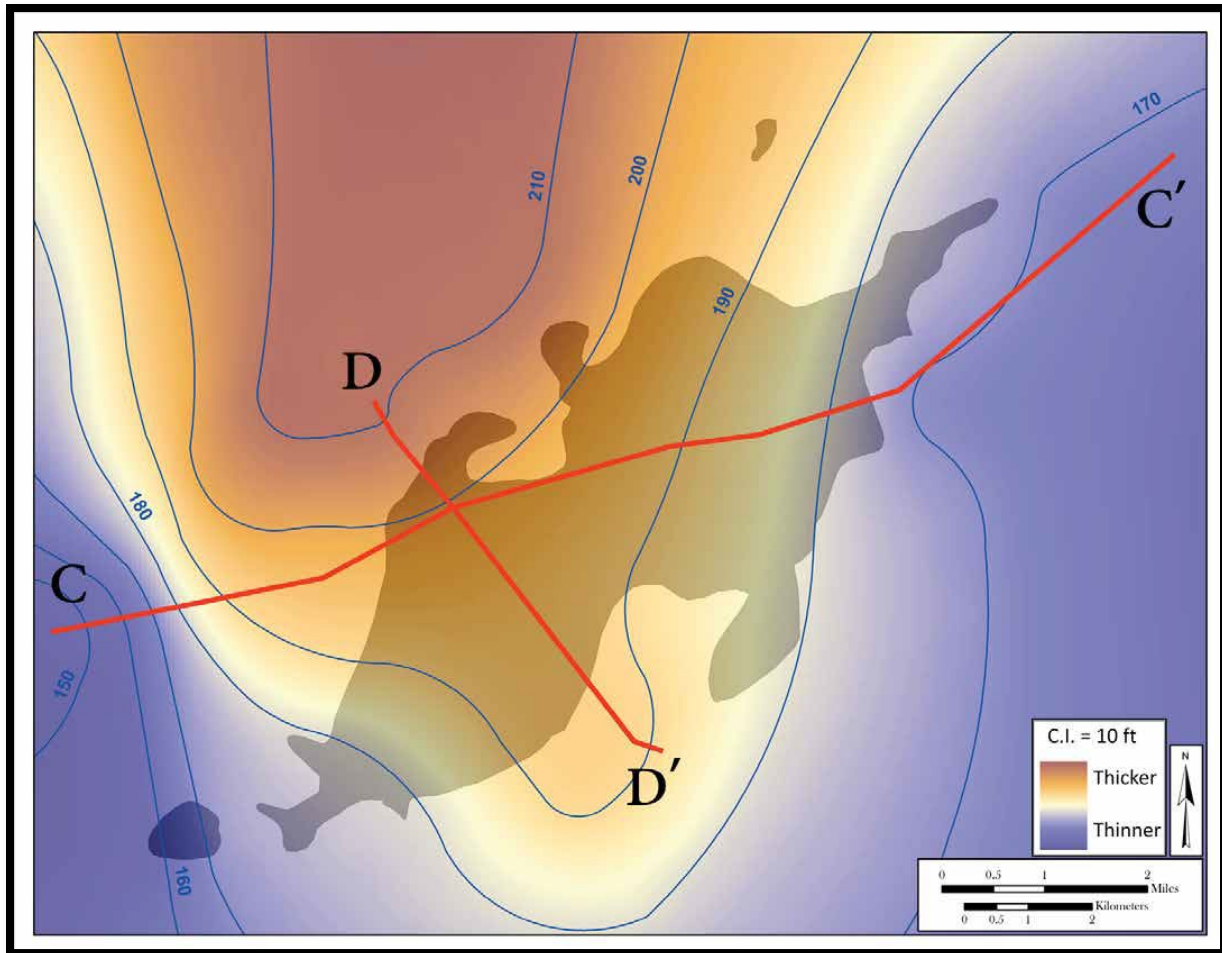


Figure 6-111. Gross thickness (10-ft contour interval) of the Gordon sandstone in Marion County (Moore et al., 2013).

The Fifth sandstone has a limited presence across Mannington Field (see cross sections in Figure 6-112 and Figure 6-113) and covers an area of only 496 ac. One well currently produces oil from the Fifth sandstone (Figure 6-109). Here, the average net pay thickness of the Fifth sandstone is seven ft and its average depth is 3000 ft (Table 6-19).

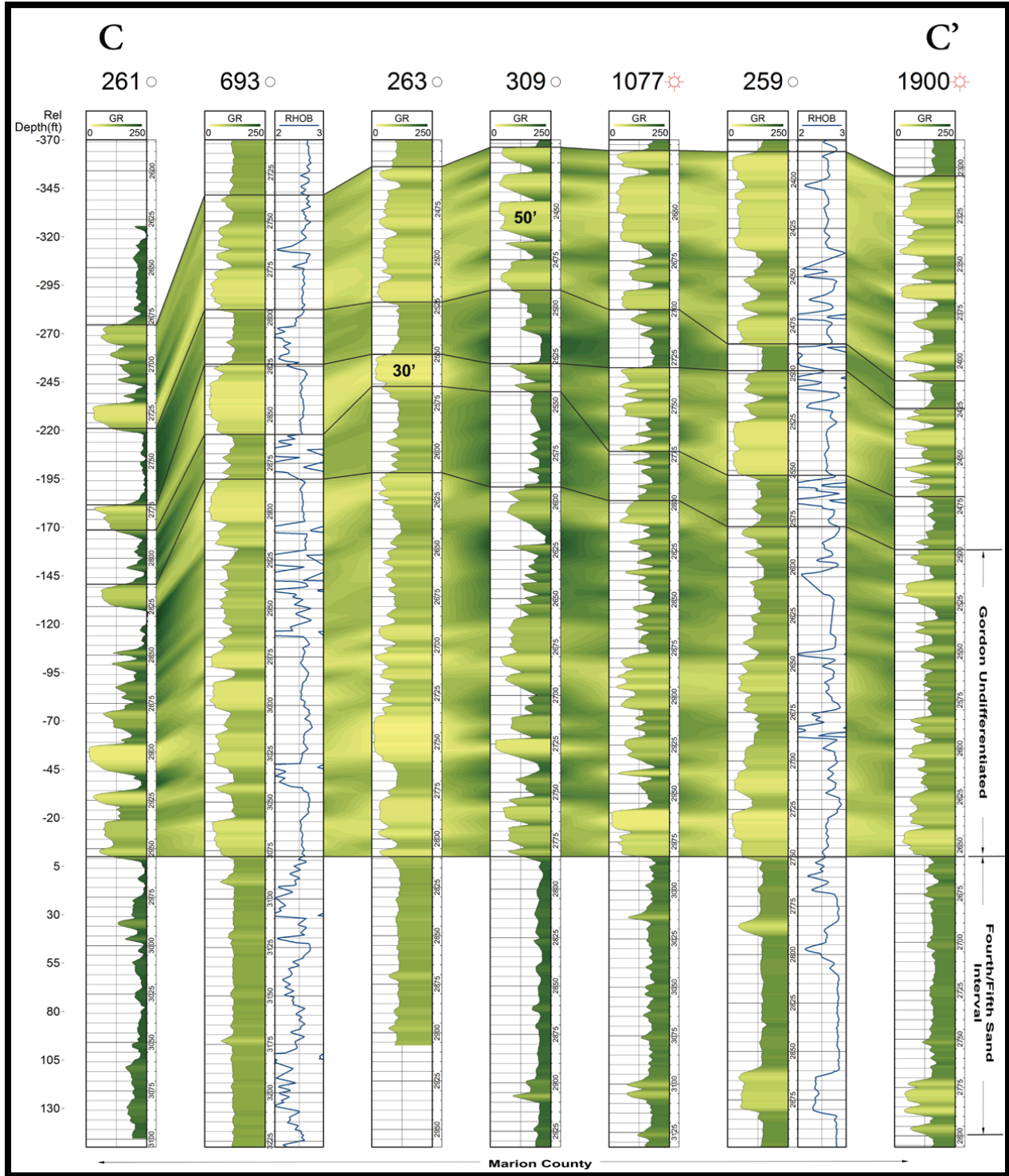


Figure 6-112. Southwest to northeast stratigraphic cross section of the Gordon sandstone in Marion County, flattened on the base of the Gordon sandstone interval (Moore et al., 2013).

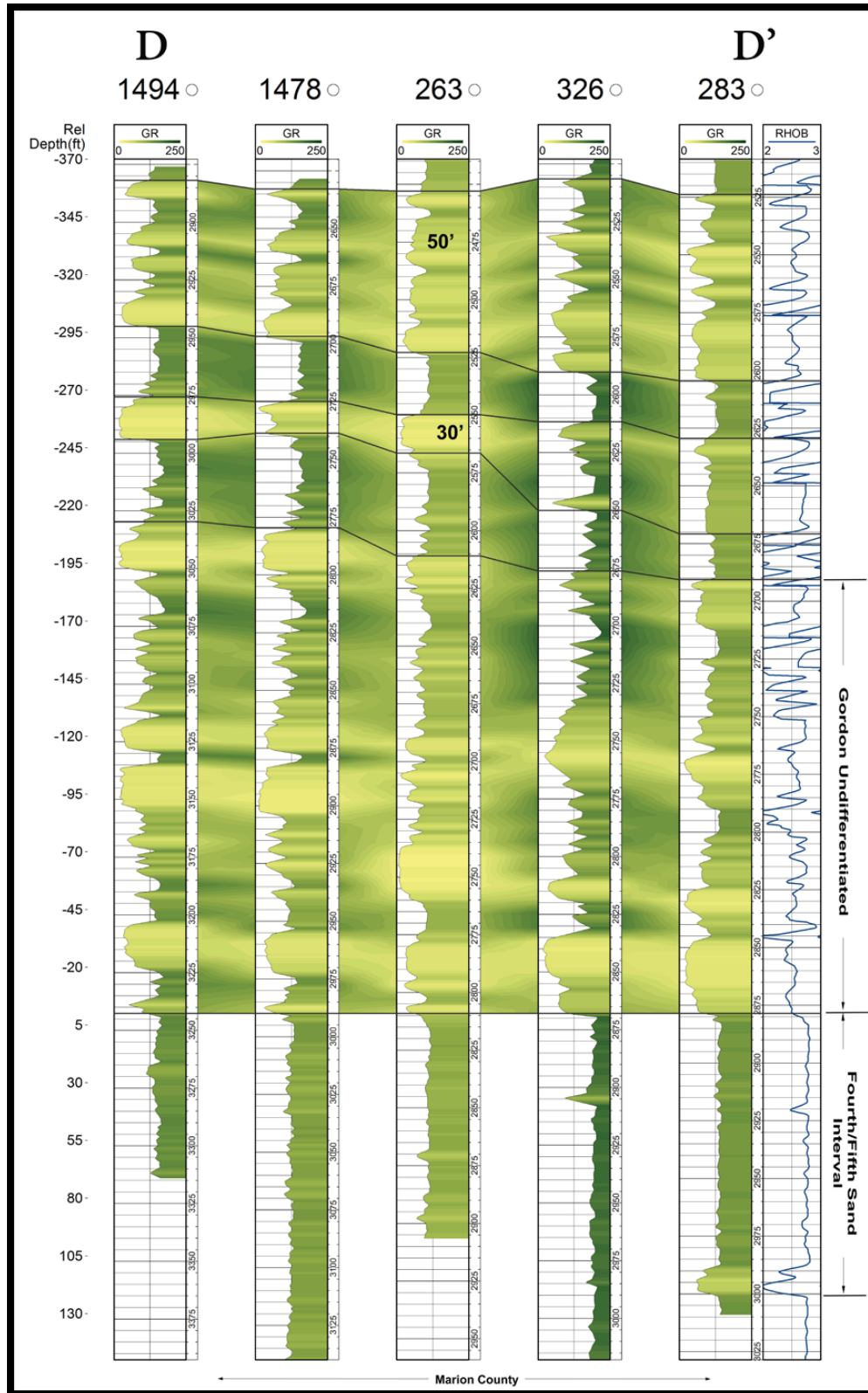


Figure 6-113. Northwest to southeast stratigraphic cross section of the Gordon sandstone in Marion County, flattened on the base of the Gordon sandstone interval (Moore et al., 2013).

Figure 6-114 presents a petrophysical analysis for Marion 1077 (API No. 4704901077) in the Mannington Field. This analysis shows the Gordon sandstone interval to be relatively clean (yellow), with some shale interbeds (gray) and effective porosity values of up to 10 percent (red). Remaining hydrocarbons and bulk water volume are shown in orange and blue, respectively. Several potential oil recovery targets are present in the Gordon interval.

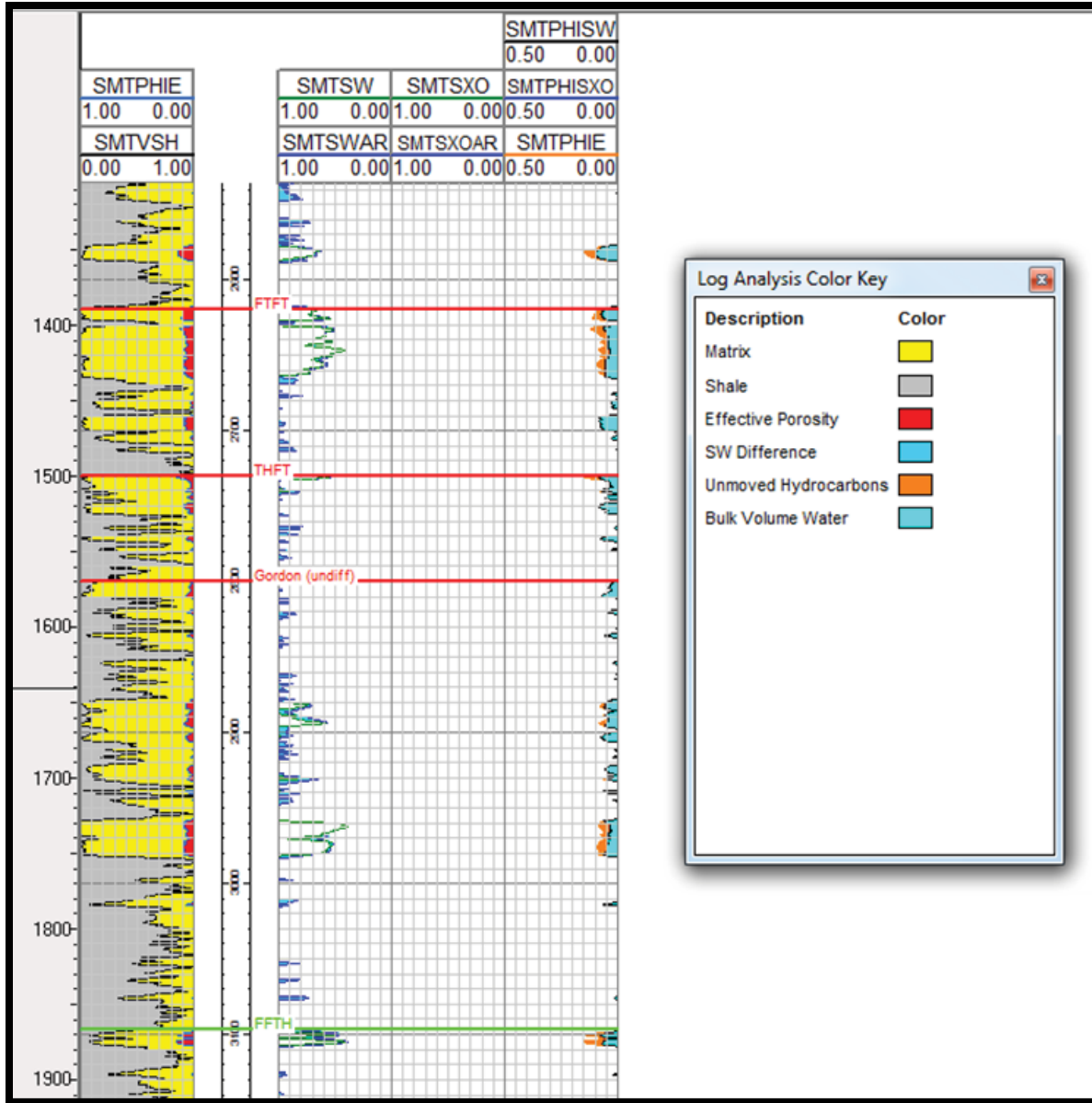


Figure 6-114. Petrophysical analysis of Venango Group sandstones in Marion 1077 (Moore et al., 2013).

6.6.3.1 Rating Discussion

Each producing interval in Mannington Field was rated individually (Appendix D) for these results). The “Big Injun” sandstone rated the highest overall, and the intermittent Fifth sandstone rated the poorest. All three horizons were rated highly for porosity (with field-level porosities exceeding 10 percent), and all three were rated favorably for depths within the miscible CO₂ range. The “Big Injun,” however, received the poorest rating for depth, as it is the shallowest of the three reservoirs in this field. With respect to thickness, cumulative oil production (32 MMBO) and trap integrity, however, the “Big Injun” received better ratings than the other two intervals across the board. Oil saturation ratings were favorable for the “Big Injun” (35 percent) and good for the Gordon (76 percent); the Fifth sandstone lacked saturation data for rating purposes. The legacy well rating was low for all three intervals. The Fifth sandstone is penetrated by 22 legacy wells over an area of 496 ac; the Gordon is penetrated by 618 legacy wells over 4179 ac; and the “Big Injun” is penetrated by 470 legacy wells over 5833 ac.

6.6.3.2 Secondary Recovery

Pennzoil operated a pilot waterflood project in the Mannington Field in 1964. The company drilled four water injection wells around an old production well in a normal five-spot pattern. The approximate area covered by these wells was 40 ac. The pilot project was never expanded, and permits were obtained to abandon some of the pilot wells in 1970 (Pease and Watts, 1979). No data for this particular project was available for review.

Records do exist, however, for eight waterflood wells associated with a secondary recovery operation initiated in 1979 (Figure 6-115). Five wells were drilled to the Fourth sandstone, two were drilled to the Gordon, and one was drilled to an unidentified Upper Devonian target. All waterflood wells were completed as open hole borings.

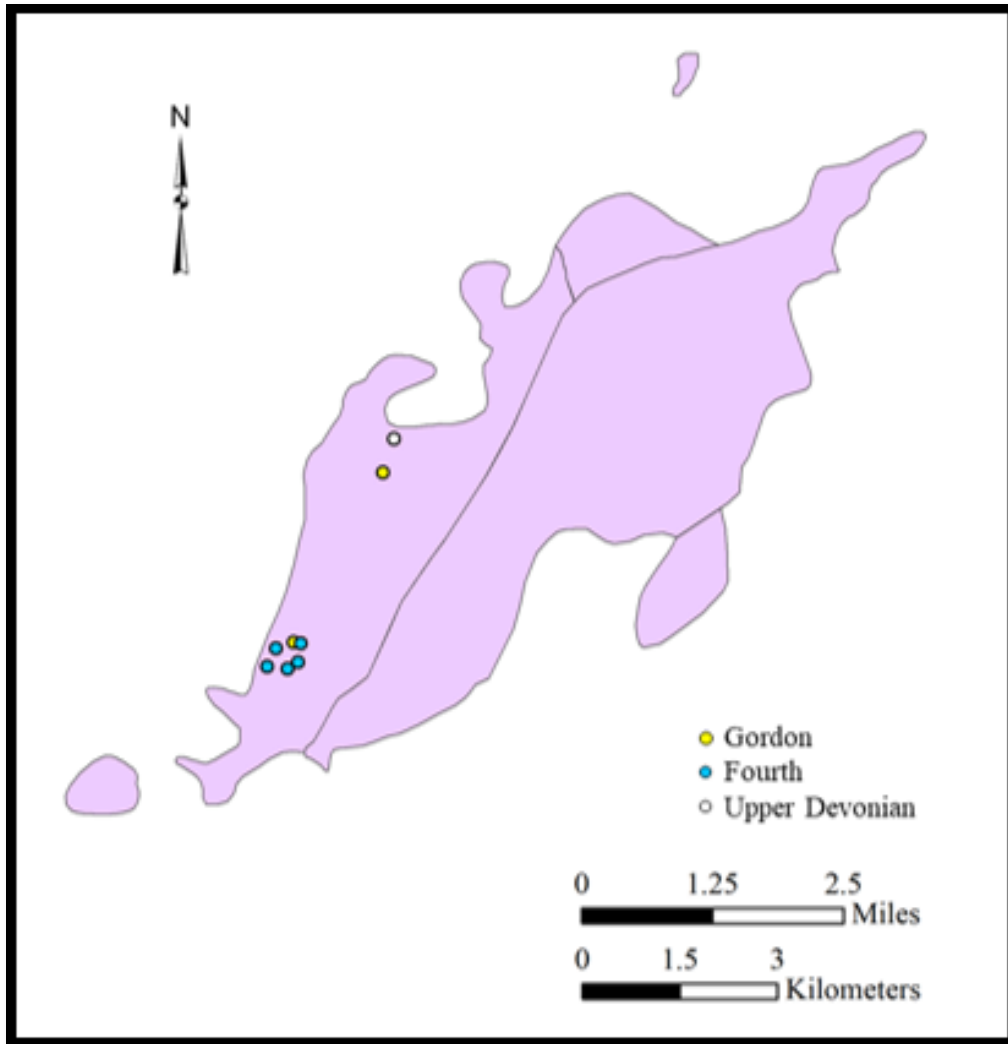


Figure 6-115. Waterflood wells in Mannington Field. The different colors represent total depth formations as reported by drillers.

Figure 6-116 plots annual oil production with the number of waterflood wells completed in Mannington Field between 1979 and 2011. Oil production increased by 22,056 BBL in 1981 following the drilling of six waterflood wells in 1979 and 1980. The overall production increase is much smaller than increases observed in the Jacksonburg-Stringtown Field but is comparable to increases seen in the Wolf Summit-Big Isaac Field. It is also possible that the relatively small size of Mannington Field led to project termination.

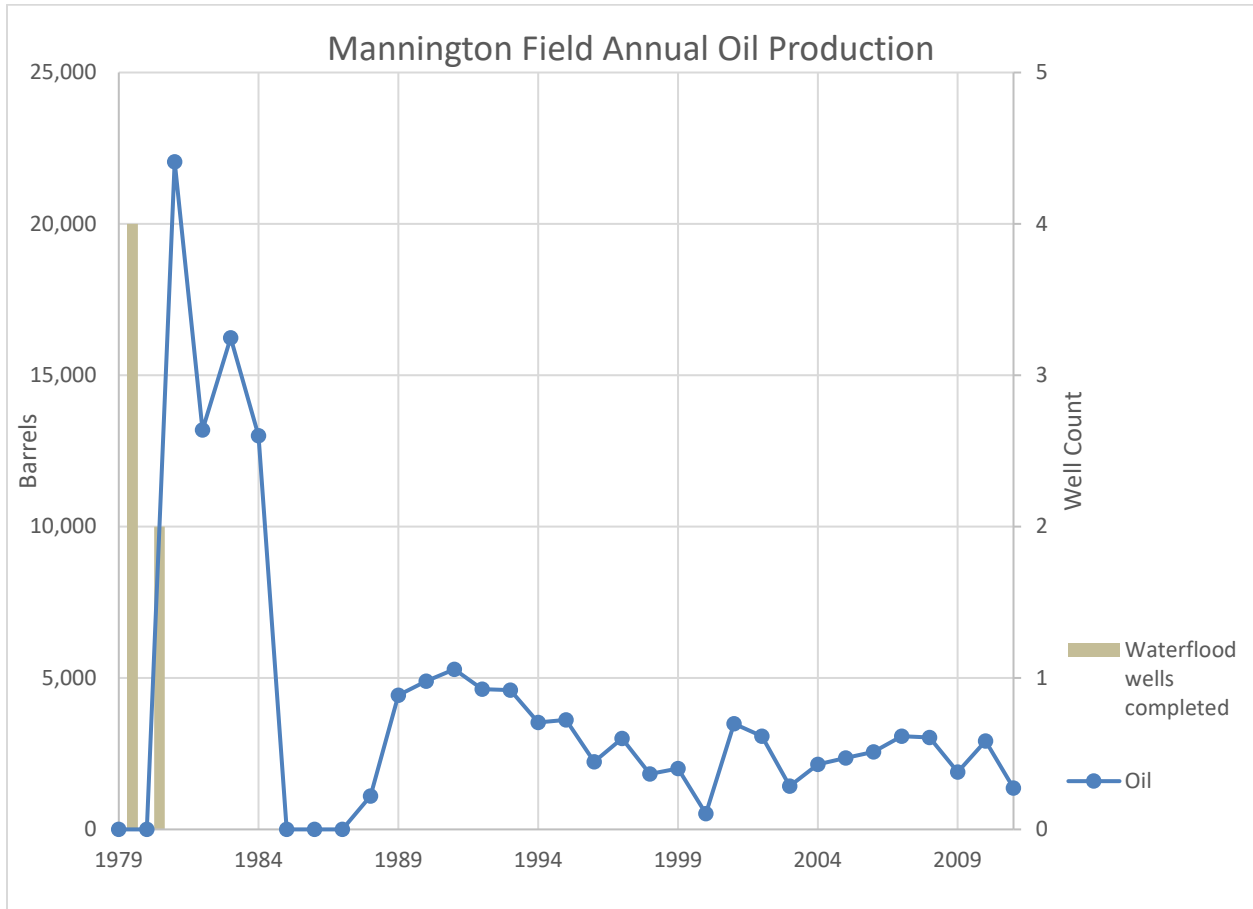


Figure 6-116. Annual oil production (DDS5, 2018) and waterflood well completions in the Mannington Field (1979-2011).

6.6.4 Salem-Wallace Field

The Salem-Wallace Field was discovered in 1899 and produces oil from undifferentiated sandstones of the Gordon interval in Doddridge, Harrison and small portions of Marion and Wetzel counties. The field is 39,645 ac in size and has been penetrated by nearly 3000 wells. Figure 6-117 shows well locations for both the Salem-Wallace (left center) and Wolf Summit-Big Isaac (right center) fields. The Robinson Syncline bifurcates the Salem-Wallace Field (Figure 6-91). This field has elements of both structural and stratigraphic trapping mechanisms where the Gordon pinches out to the west. Oil is produced along the flanks of the Robinson Syncline (Cardwell, 1982).

The gross thickness of the undifferentiated Gordon interval is illustrated in Figure 6-118. Thicknesses range from about 120 to 150 ft. Figure 6-119 displays the Gordon sandstone and intermittent Fourth/Fifth interval sandstones in cross section. Three stacked sandstone layers are present here, with greater thicknesses to the north. Individual Gordon sandstones become thinner and more isolated southward.

Field level reservoir data extracted from Lewis et al. (2019) are given in Table 6-20. The Salem-Wallace Field contains 147 producing wells. No secondary recovery projects (waterflooding or other methods) have occurred here. The producing depth of the

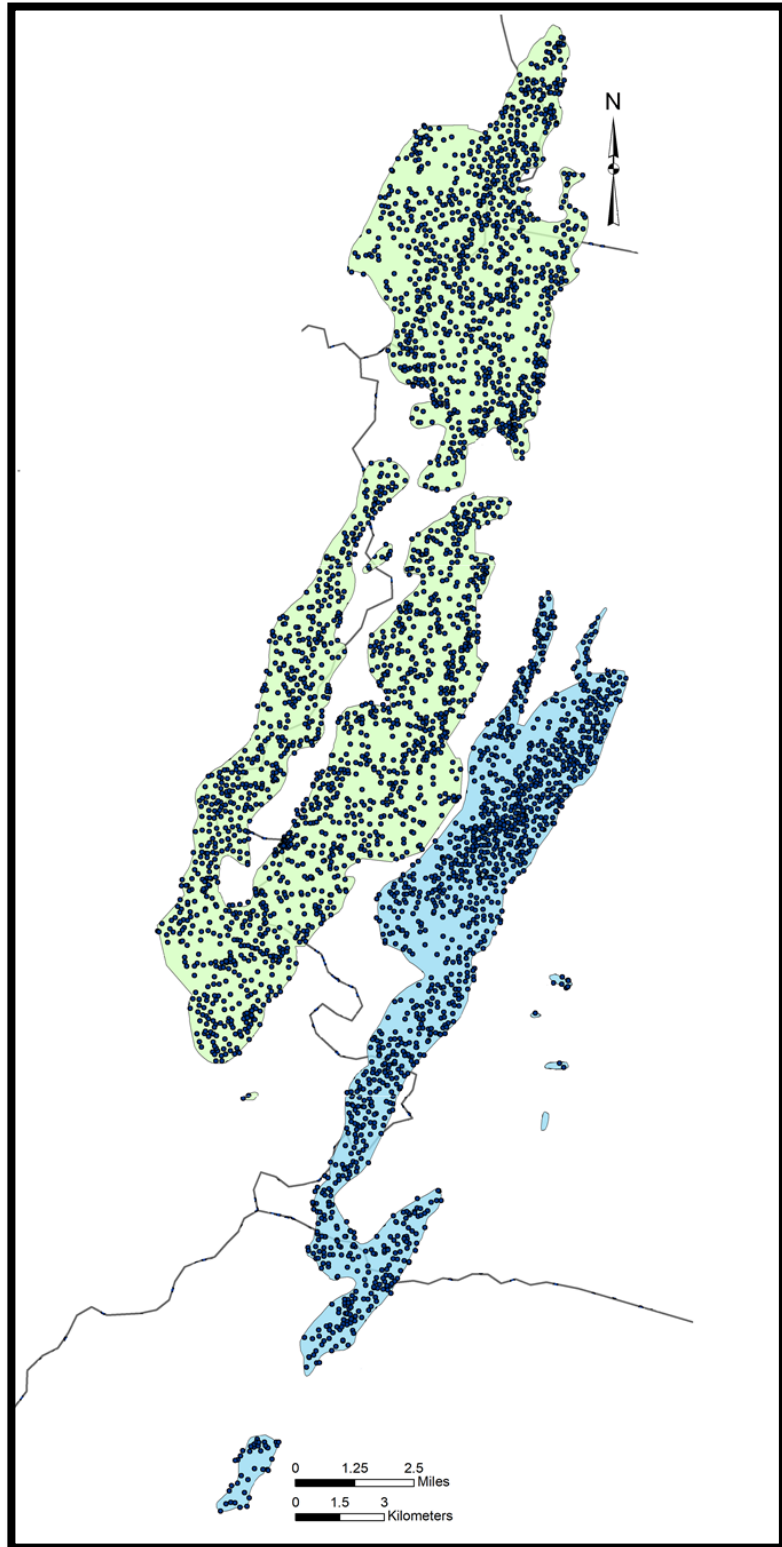


Figure 6-117. Map of wells in Salem-Wallace (green) and Wolf Summit-Big Isaac (blue) fields.

Gordon averages 2800 ft, and reservoir pressure is reported at 1200 psi, so CO₂ would be expected to remain in a supercritical state post injection.

Table 6-20. Field-level reservoir data for the Gordon sandstone in Salem-Wallace Field.

Average Producing Depth (ft)	Net Thickness (ft)	Pressure (psi)	Porosity (%)	Water Saturation (%)	Remaining Oil (BBL)
2800	8	1200	12	20	132,731,398

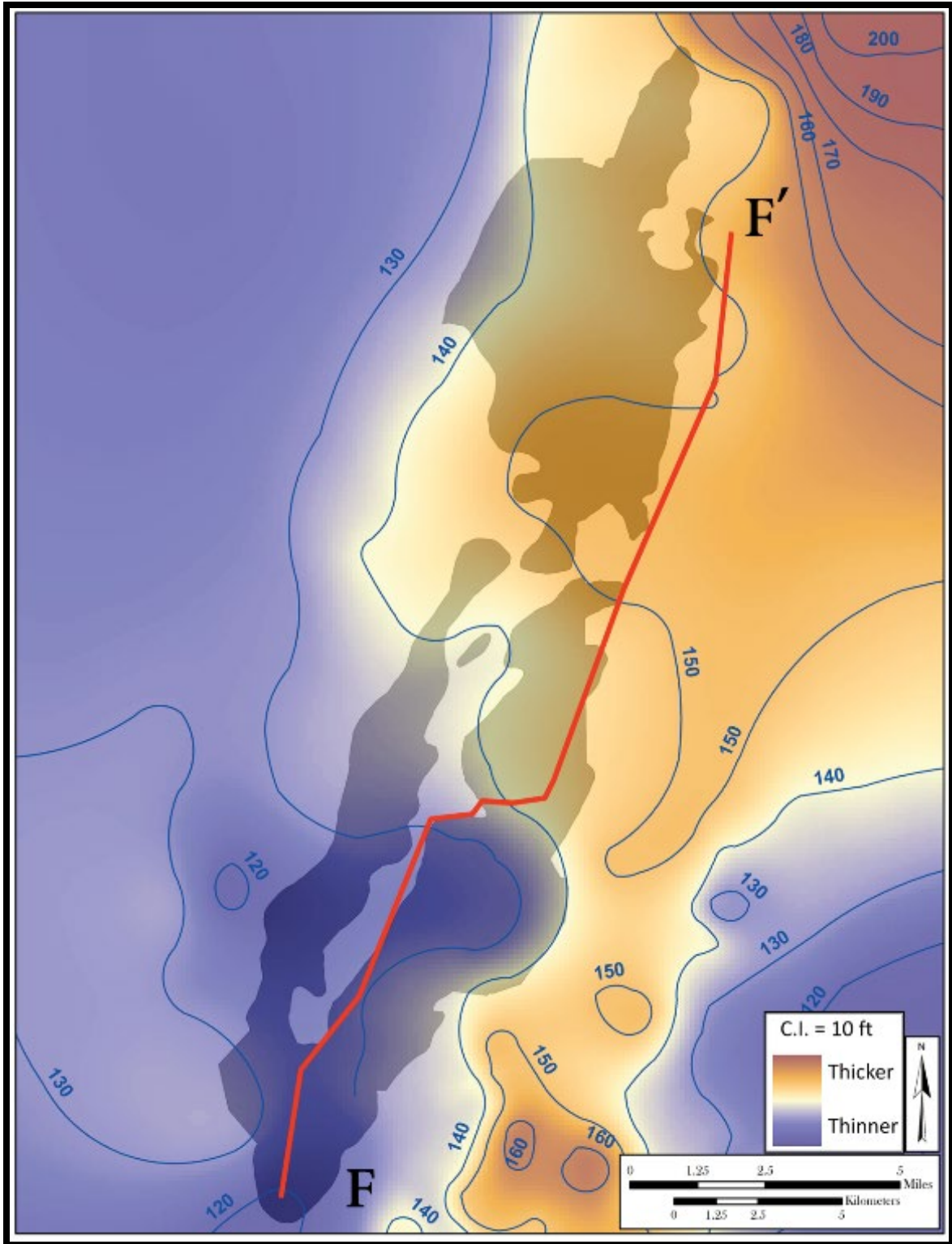


Figure 6-118. Gross thickness map (10-ft contour interval) of the Gordon interval in the Salem-Wallace Field (Moore et al., 2013).

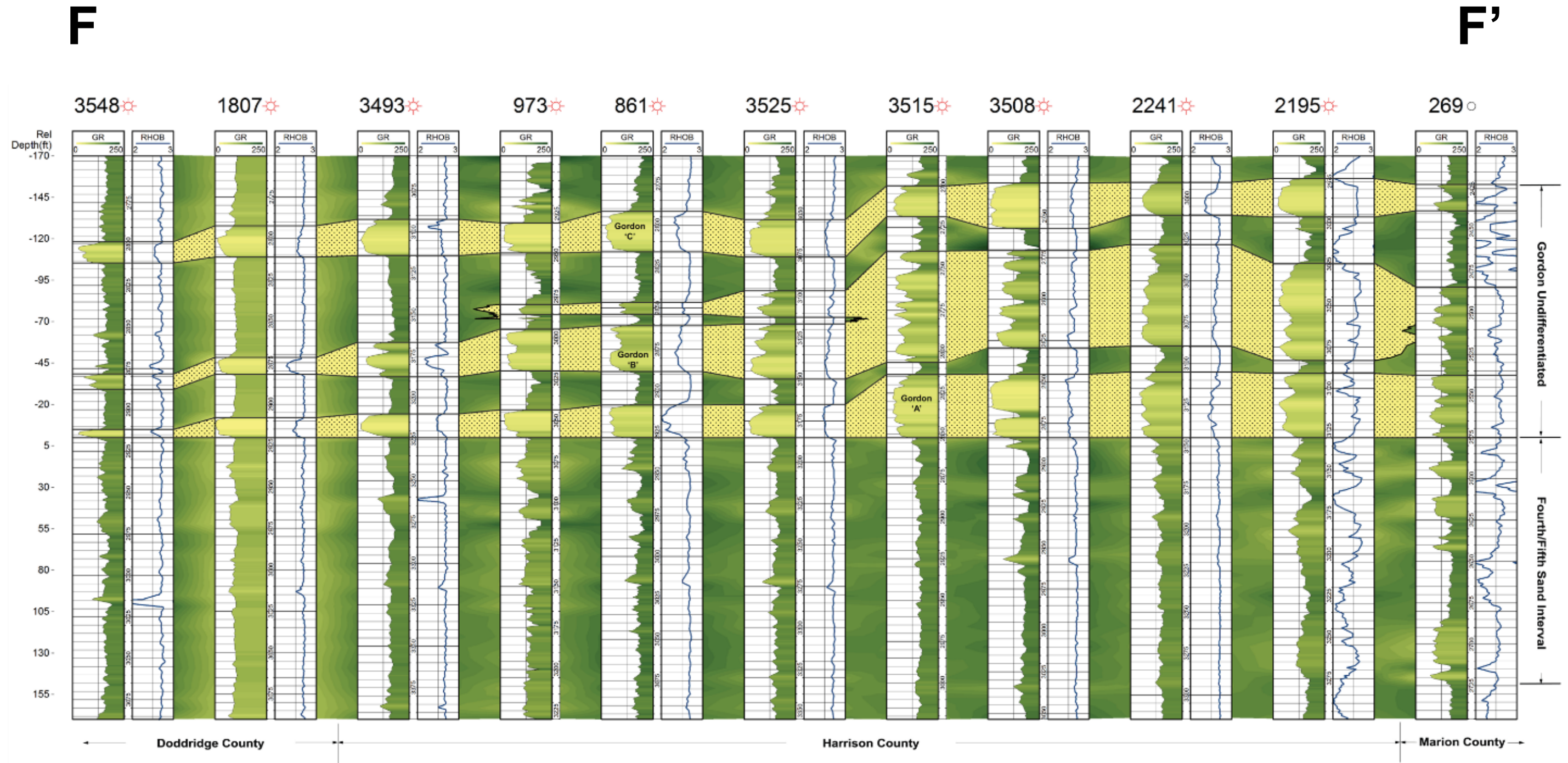


Figure 6-119. South to north Gordon stratigraphic cross section through the Salem-Wallace Field. Note the stacked sandstone layers of the Gordon in this area (Moore et al., 2013).

6.6.4.1 Rating Discussion

The Salem-Wallace Field received favorable ratings for a majority of the oil field rating criteria – depth, area, porosity, mode CO₂ storage, cumulative oil production (41 MMBO), water saturation, trap integrity and potential oil recovery (17 MMBO). The field rated poorly for its average net sand thickness (8 ft, as per Lewis et al., 2019). In addition, the number of legacy penetrations in this field are an issue and will require detailed investigation prior to an enhanced recovery operation.

Multiple Gordon pay zones have been discovered in Salem-Wallace Field over time. Ober and Eckert (2014) recognized relatively high net pay thicknesses resulting from the interpretation of stacked Gordon sandstone layers (89 ft versus nine ft as reported in this study). They also used a different API cutoff for net pay sand and included units that Moore et al. (2013) considered part of the Fourth/Fifth sandstone interval. Notwithstanding the different cutoff methodology, it is clear from their study that the Gordon interval in northern West Virginia and southwestern Pennsylvania includes multiple, stacked sandstone bodies. As the Salem-Wallace Field is one of the most highly rated oil fields (Appendix D), a higher net sand rating would only make this field an even more favorable EOR target.

In terms of petroleum hydrocarbon resources, Ober and Eckert (2014) used both decline curve and volumetric analyses to estimate remaining oil in place (Figure 6-121). Each method produced similar results and corroborate the earlier work of Whieldon and Eckard (1963). According to these studies, remaining oil in place for the Salem-Wallace Field is estimated at 200 MMBO.

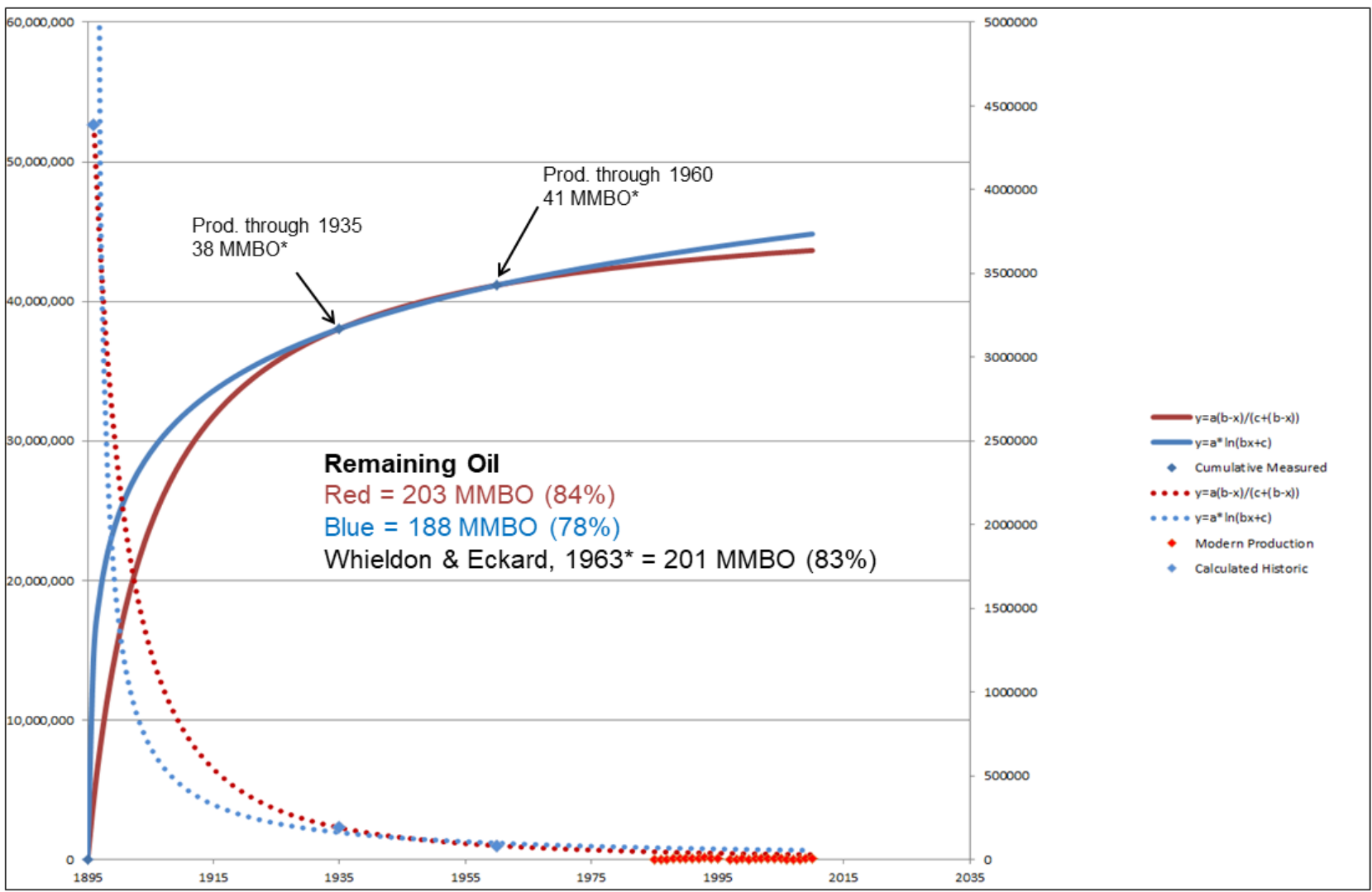


Figure 6-121. Salem-Wallace cumulative and decline curves on historical production with modern production data (from Ober and Eckert, 2014). *Data obtained from Rietz Tucker, Assistant State Geologist of West Virginia.

6.6.5 Wolf Summit-Big Isaac Field

The Wolf Summit-Big Isaac Field was discovered in 1896 and produces petroleum hydrocarbons from the Gordon and Fifth sandstone intervals primarily in Harrison and parts of Doddridge and Lewis counties. This field covers more than 16,000 ac and lies between the Robinson Syncline to the west and Wolf Summit Anticline to the east (Figure 6-92). Approximately 1900 wells are known to penetrate the field. Oil is produced along the western flank of the Wolf Summit Anticline (Caldwell, 1982), while gas is produced from Jarvisville Field to the east at structurally higher elevations. Figure 6-117 shows the location of both the Salem-Wallace and Wolf Summit-Big Isaac fields and drilled wells.

Oil production in the Wolf Summit-Big Isaac Field is from 143 wells completed in the Venango Group's Gordon and Fifth sandstones. Table 6-21 summarizes reservoir characteristics for both formations, based on values reported in Lewis et al. (2019). Depth to the Gordon sandstone averages 2575 ft (close to the upper miscible depth of CO₂), while the Fifth sandstone occurs at an average depth of 2900 ft (well within the depth range at which CO₂ will remain miscible with oil).

Table 6-21. Unit-specific reservoir characteristics for the Wolf Summit-Big Isaac Field.

Formation	Average Producing Depth (ft)	Net Thickness (ft)	Pressure (psi)	Porosity (%)	Water Saturation (%)	Remaining Oil (BBL)
Gordon	2575	18	1100	10.6	26.5	35,052,255
Fifth	2900	5	1300	20	47	29,665,582

Figure 6-122 plots oil wells in Wolf Summit-Big Isaac Field by producing formation. Most of these produce from the Fourth/Fifth (yellow) interval, with a lesser number producing from the Gordon (brown) interval. In general, Gordon-producing wells are concentrated along the western edge of the field, while wells producing from the Fourth/Fifth interval are found throughout the field.

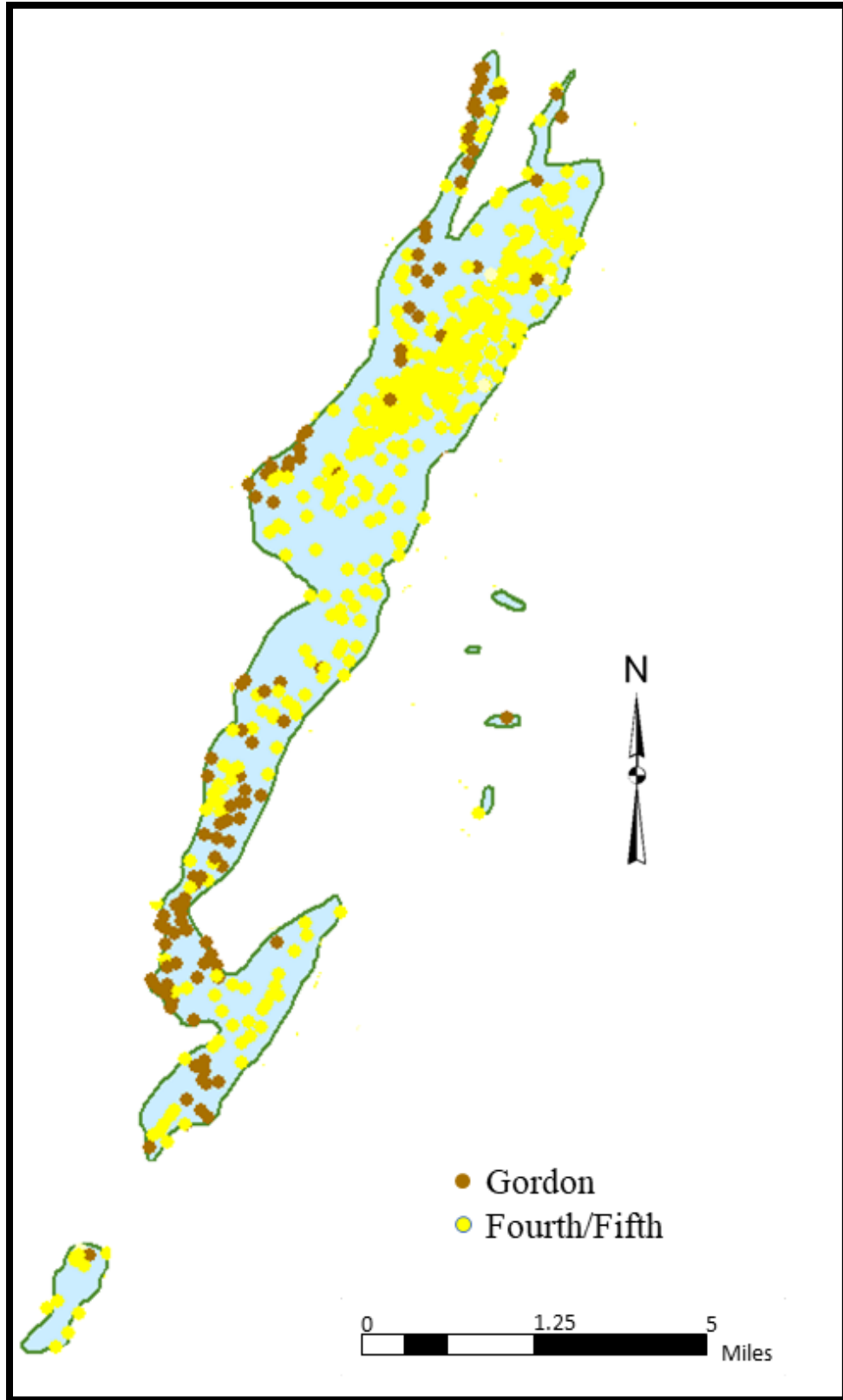


Figure 6-122. Oil wells in the Wolf Summit-Big Isaac Field.

Figure 6-123 depicts the gross thickness of the undifferentiated Gordon interval, which ranges from about 130 to 160 ft. The oil-producing Wolf Summit-Big Isaac Field includes the western portion of the thicker Gordon interval. The eastern section produces gas and is discussed in the stacked opportunities section of this case study. Figure 6-124 illustrates the thinning of the Gordon sandstone layers along the western and eastern margins of the field. Note the variable sandstone thicknesses of the Gordon interval from north to south along cross section G-G.' Thinning in the uppermost Gordon sandstone results in an overall decrease in net thickness to the south.

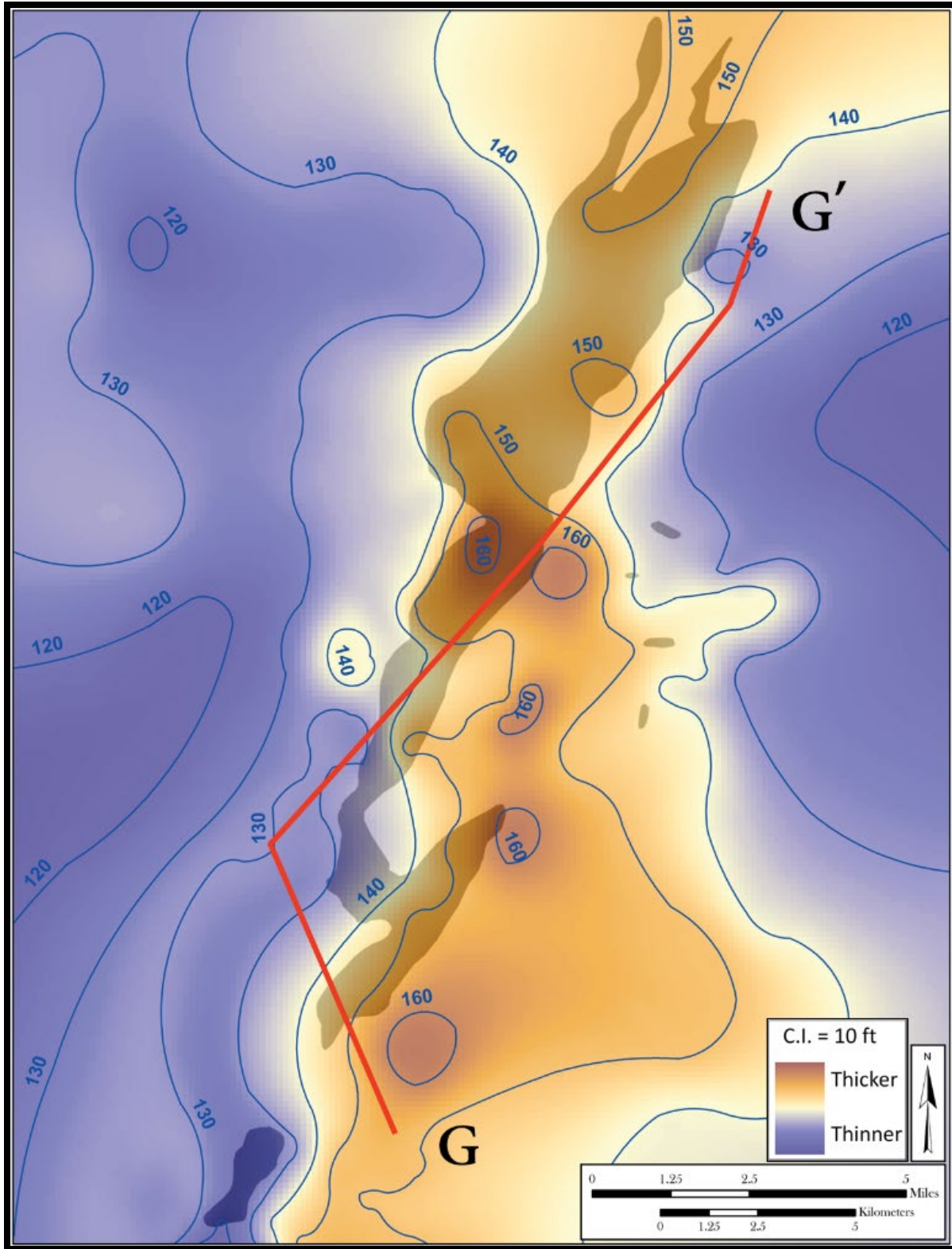


Figure 6-123. Gross thickness map (10-ft contour interval) of the Gordon interval in the Wolf Summit-Big Isaac Field (Moore et al., 2013).

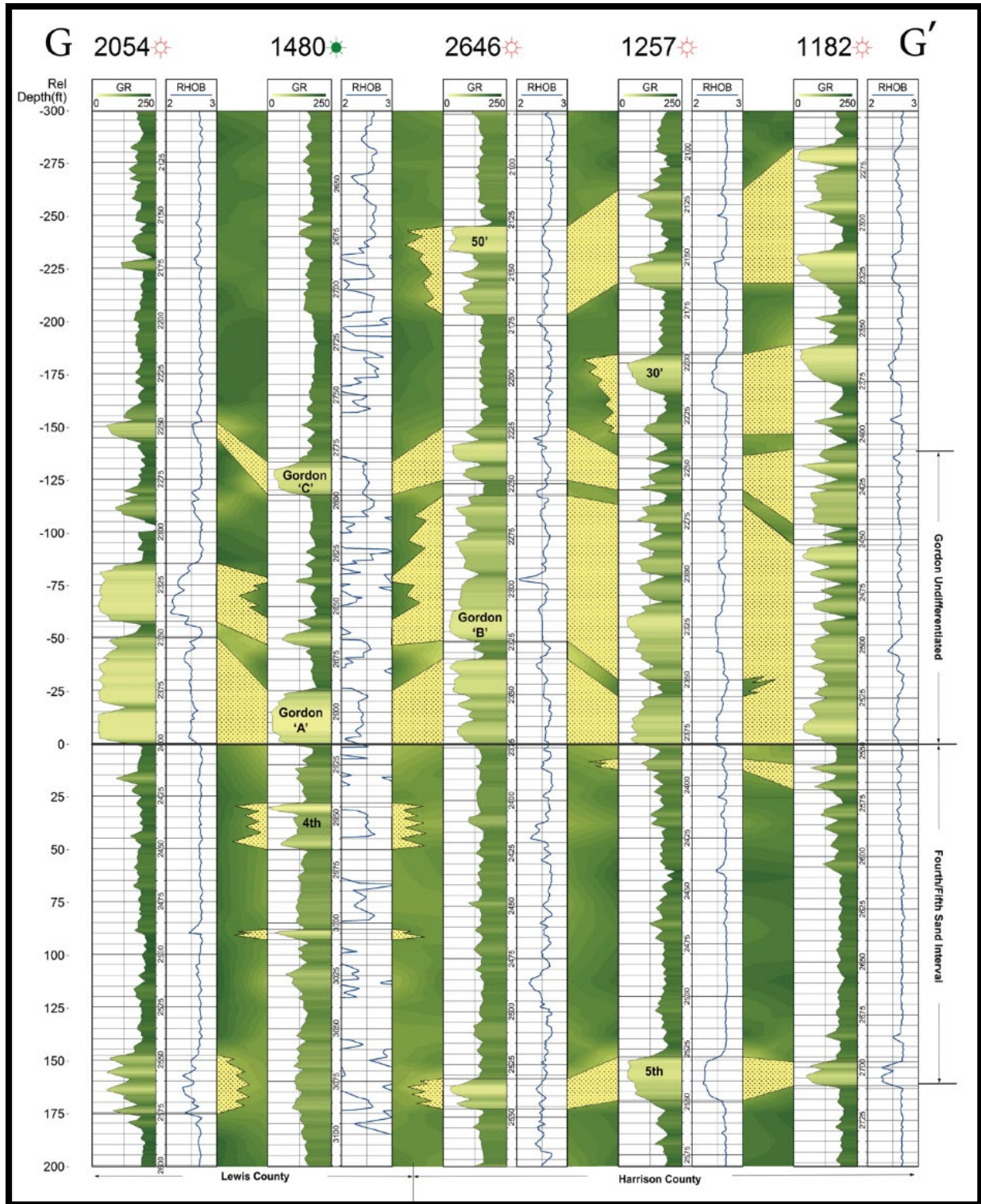


Figure 6-124. South to north cross section through the Wolf Summit-Big Isaac Field (Moore et al., 2013).

A petrophysical analysis from the Harrison 1156 well (API No. 4703301155) is provided in Figure 6-125. Here, the Gordon and Fifth intervals are very clean (yellow), with thicknesses exceeding 100 and 30 ft, respectively. Effective porosity (red) of the Gordon sandstone is approximately 10 percent, and that of the Fifth sandstone ranges from 10 to 20 percent. Remaining hydrocarbons (orange) are present in multiple intervals.

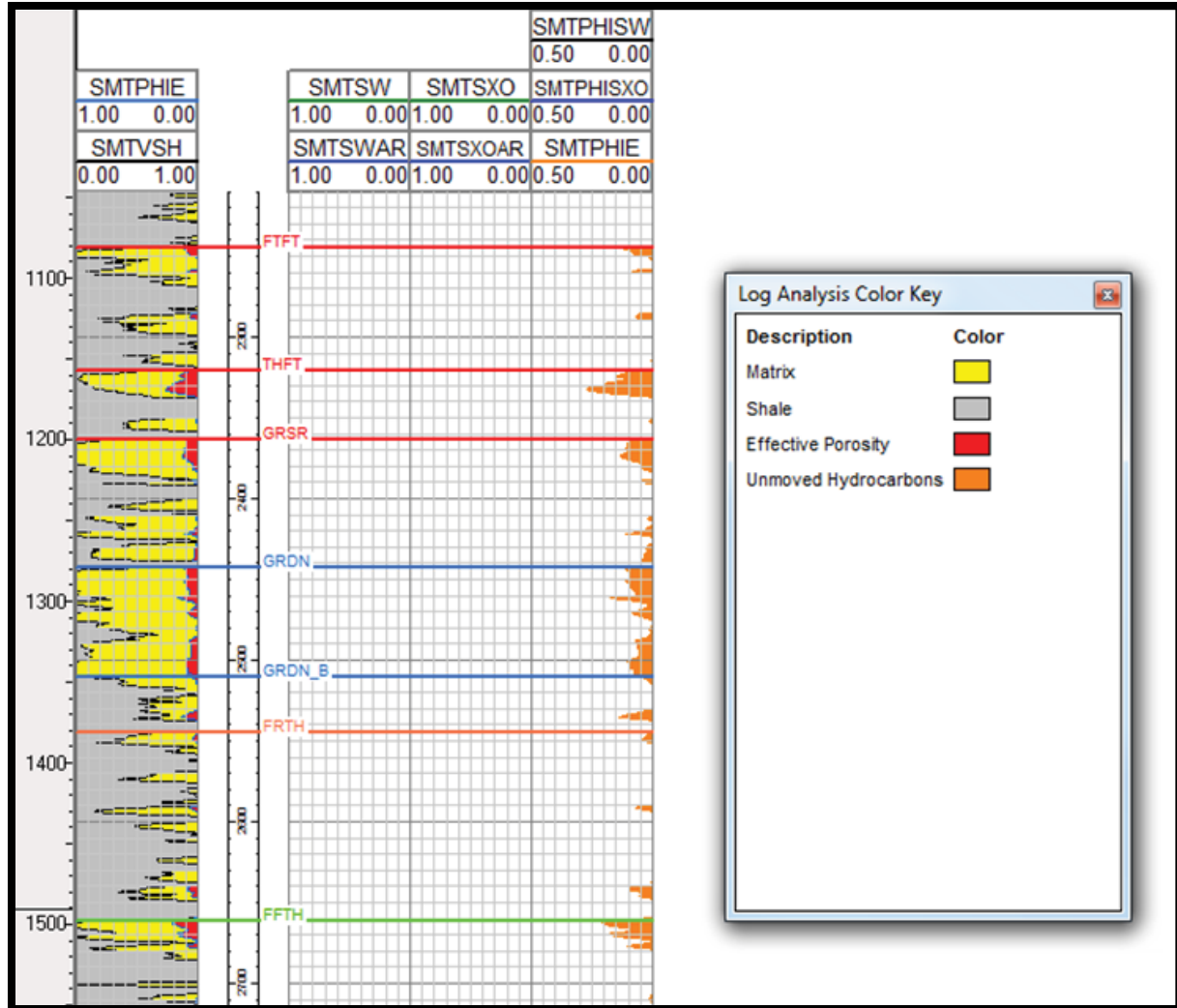


Figure 6-125. Petrophysical analysis of Venango Group sandstones in Harrison 1156 (Moore et al., 2013).

6.6.5.1 Rating Discussion

Each producing interval in the Wolf Summit-Big Isaac Field was rated individually. Despite its low acreage, the Fifth sandstone received a higher overall rating than the Gordon sandstone. Both units were highly rated for their porosities and pressures, and the Fifth sandstone was also rated favorably for permeability (no permeability data were available for the Gordon sandstone at this location). Cumulative oil production and recovery ratings were low for both intervals. Legacy wells will necessitate more detailed investigation at this location prior to enhanced recovery operations.

6.6.5.2 Secondary Recovery

Secondary oil recovery operations have been confined to the northern portion of Wolf Summit-Big Isaac Field, and have been accomplished using waterflood techniques. Sixty-five waterflood wells have been drilled in the Wolf Summit portion of the field between 1978 and 2011. Most of these were drilled to the Fifth sandstone, with only one drilled to the Fourth sandstone, one to the Hampshire Group and two to the underlying Benson (Figure 6-126).

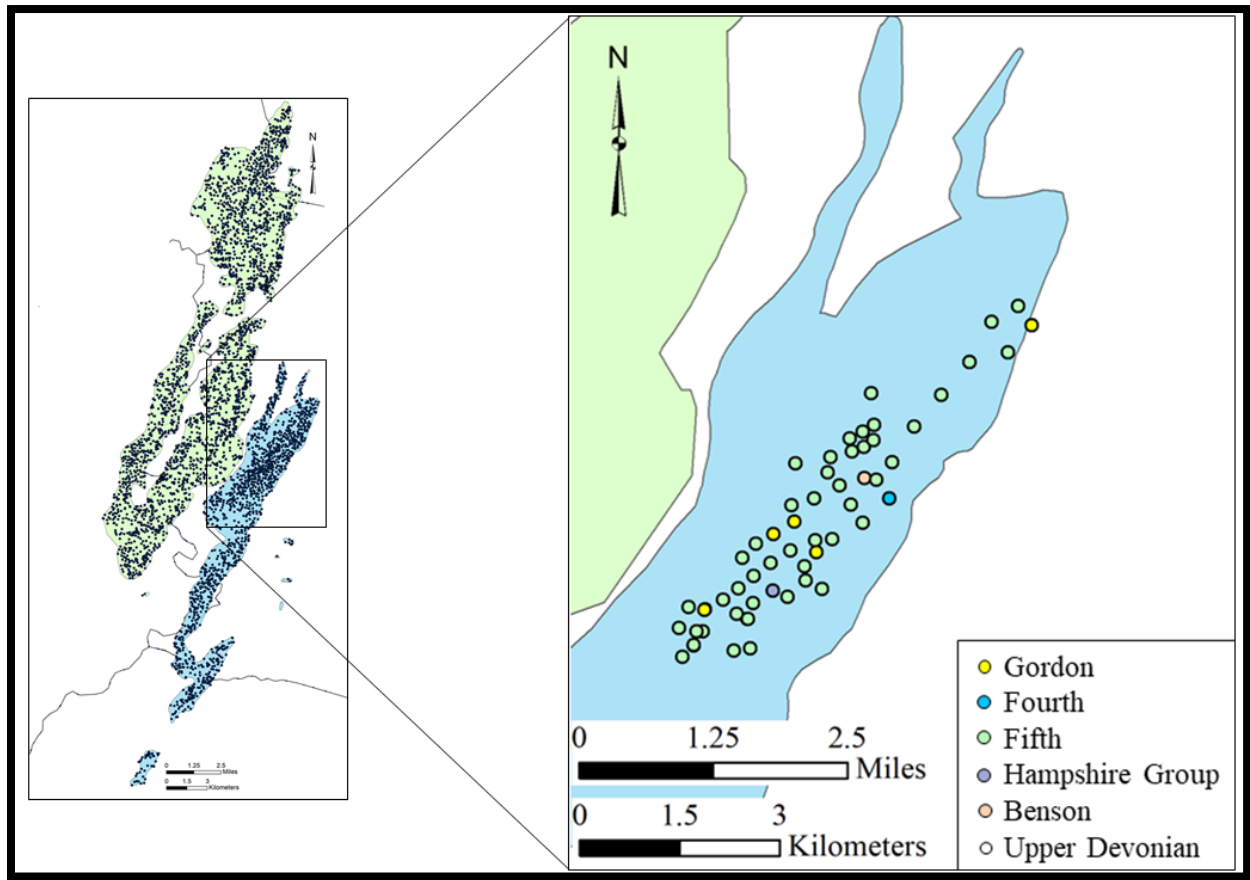


Figure 6-126. Secondary recovery waterflood well locations in the northern portion of Wolf Summit-Big Isaac Field.

Figure 6-127 plots annual oil production in Wolf Summit-Big Isaac Field with the number of waterflood wells. Increases in oil production lag behind the completion of waterflood wells. For example, a small increase in oil production in 1981 follows the completion of six waterflood wells in 1979; an increase in 1997 follows the completion of eight waterflood wells in 1994; and a large production increase in 2010 follows 15 waterflood wells drilled in 2008.

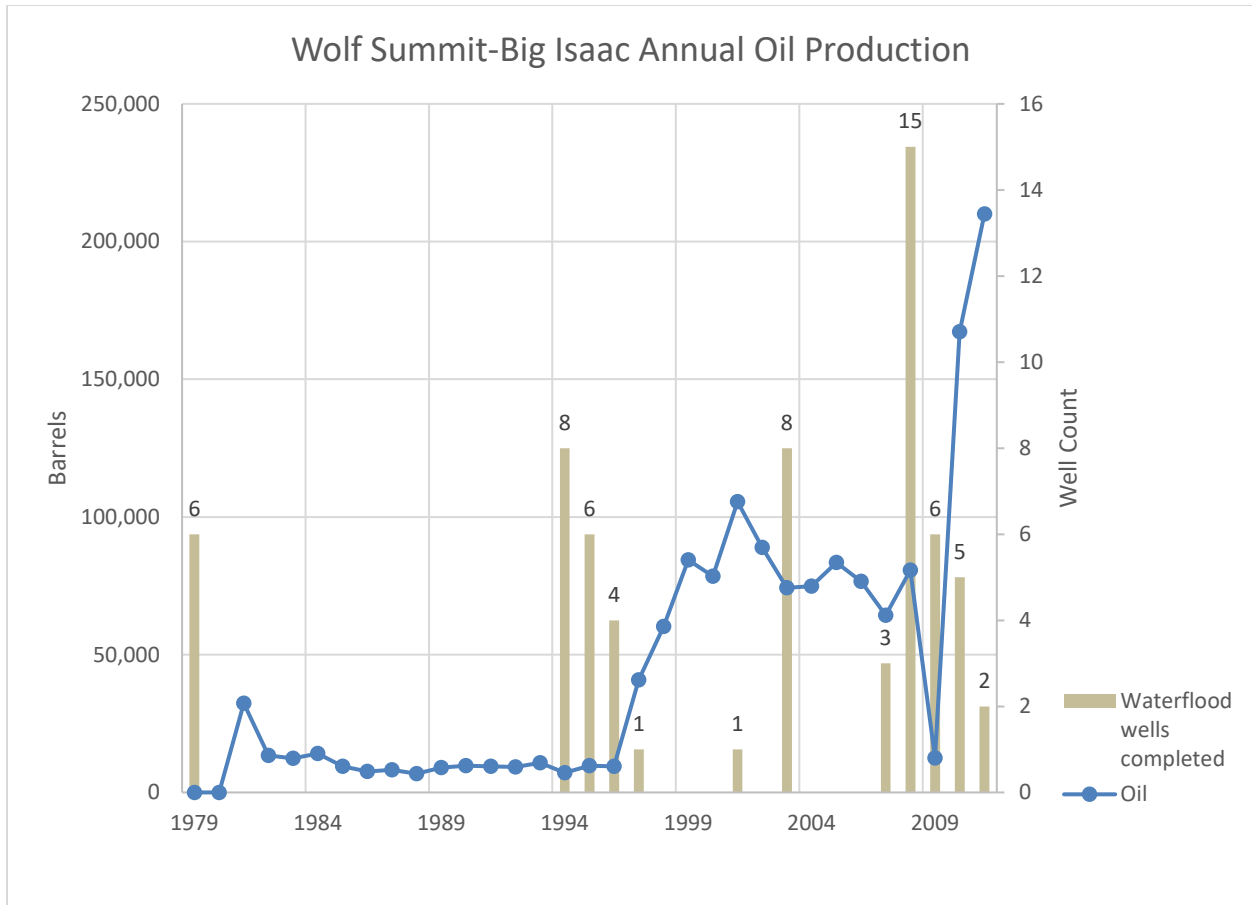


Figure 6-127. Annual oil production (DDS5, 2018) and waterflood well completions in the Wolf Summit-Big Isaac Field.

6.6.6 Summary of EOR Operations in West Virginia Case Study Fields

Secondary oil recovery has occurred in the Jacksonburg-Stringtown and Wolf-Summit-Big Isaac fields since the mid-1990s. Limited recovery efforts in the Mannington Field did not yield favorable results and have ceased. Figure 6-128 highlights the areas where secondary recovery operations were conducted in these three case study fields.

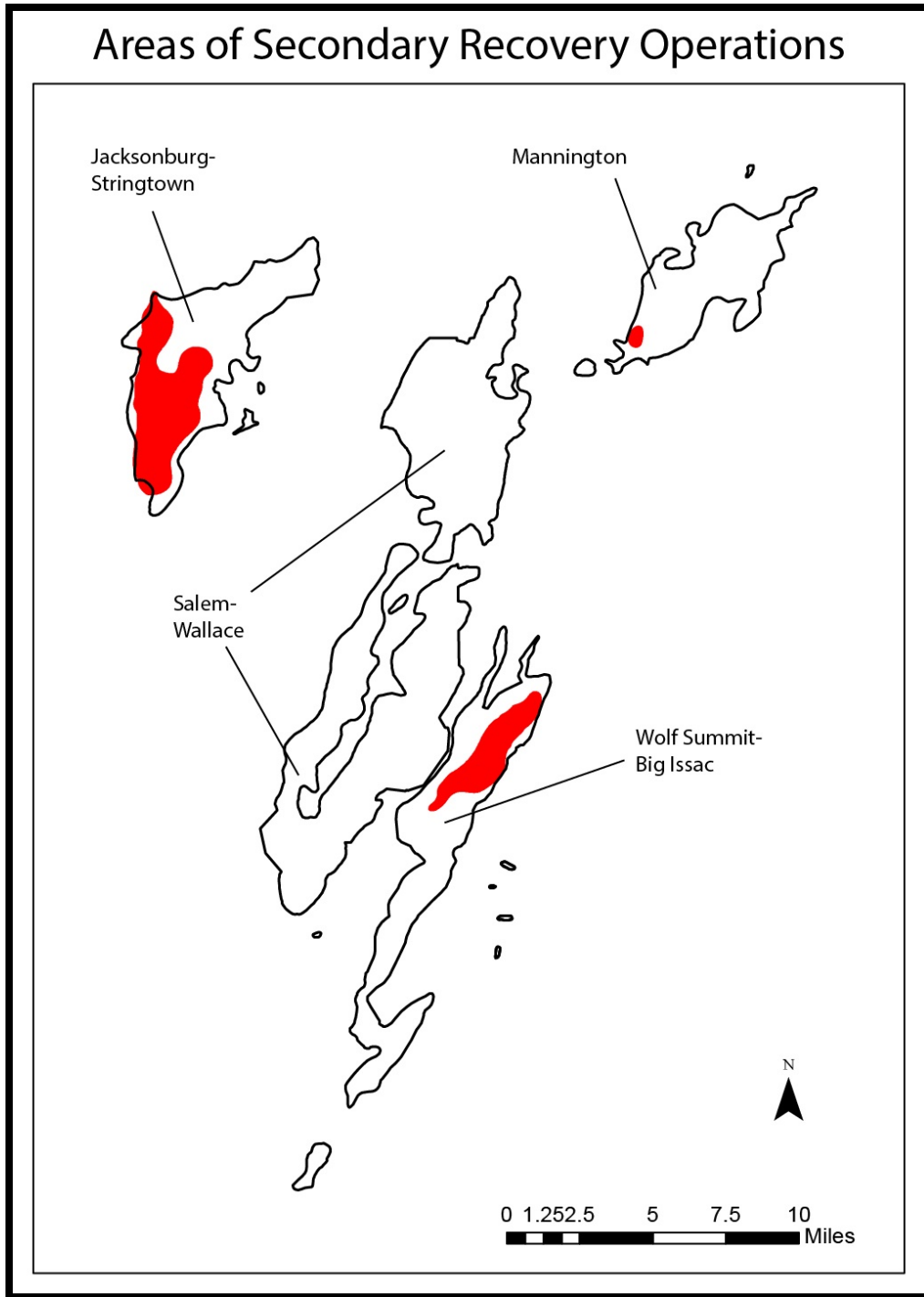


Figure 6-128. Secondary oil recovery operations via waterflooding (red). Recovery operations in Mannington Field have been discontinued (Moore et al., 2013).

Figure 6-129 plots annual oil production and waterflood well counts for the three fields with secondary oil recovery projects. The Jacksonburg-Stringtown Field produced more oil than the Wolf Summit-Big Isaac Field in all but two years (2009 and 2011) during secondary recovery operations but has three times the number of waterflood wells compared to Wolf Summit field. The Wolf Summit Field produced about 4000 to 7000 more BBL per year than Mannington Field from 1988 through 1996, prior to secondary recovery efforts. In 1997, that difference grew to more than 37,000 BBL per year after waterflooding commenced in the mid-1990s. Oil production in Mannington Field was slightly higher than that in Jacksonburg-Stringtown Field at the beginning of waterflooding in the late 1970s, but quickly dropped after secondary recovery efforts were discontinued. The apparent drop in production in 2009 is attributed to lack of production reporting on the part of operators.

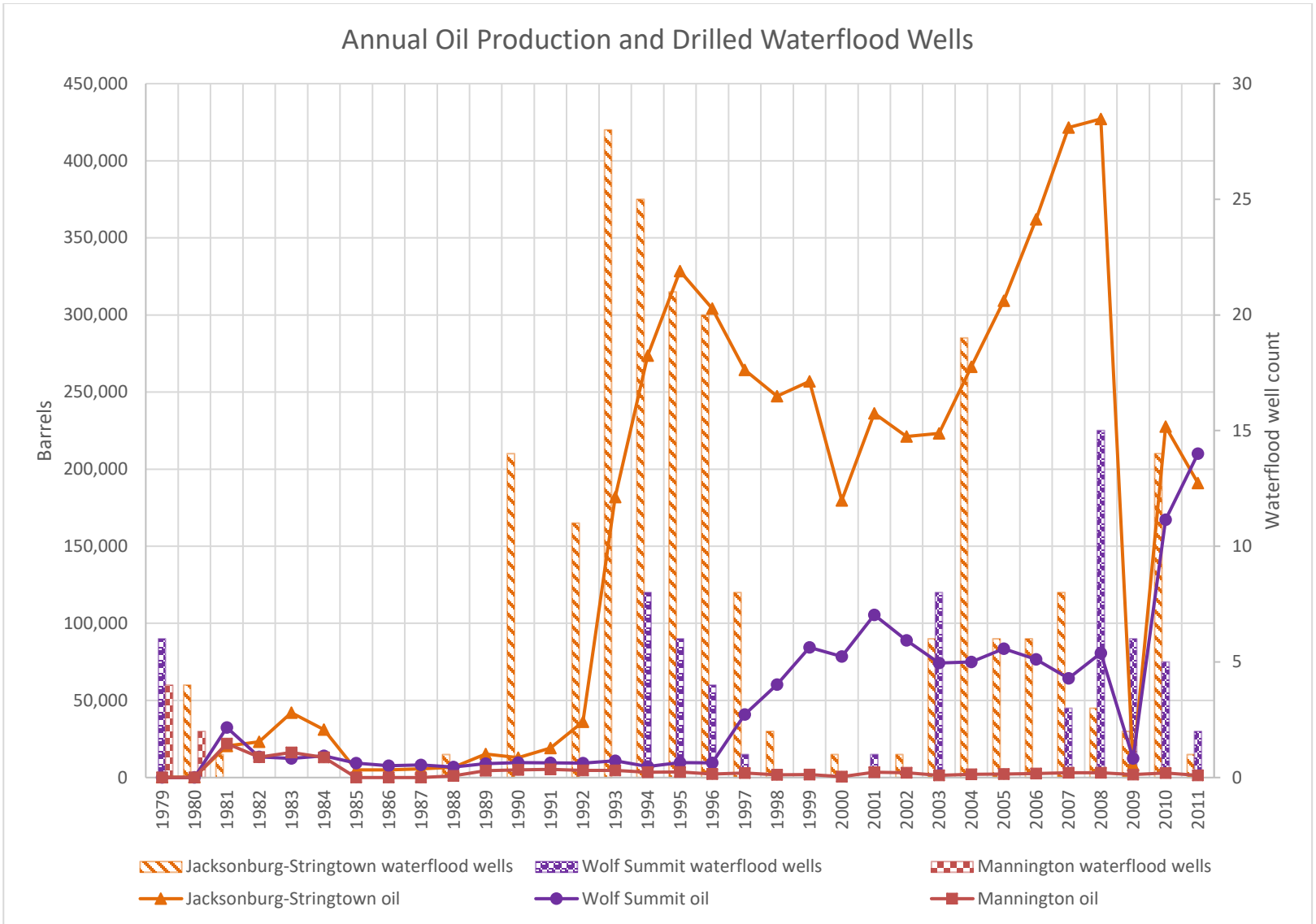


Figure 6-129. Annual oil production and waterflood wells drilled in Jacksonburg-Stringtown, Wolf Summit and Mannington fields.

To normalize the data shown in Figure 6-129, annual oil production was divided by the total number of wells reporting production for each year (Figure 6-130). The Jacksonburg-Stringtown Field has always produced more oil per well compared to the other fields, but production per well increased five-fold after active waterflooding began in 1990. The Wolf Summit and Mannington fields produced about the same amount of oil per well from 1989 through 1996, and in the case of Wolf Summit Field, a four-fold increase in well-specific production was observed after waterflooding commenced in the mid-1990s. Production in the Wolf Summit Field approached that of Jacksonburg-Stringtown Field after additional waterflood wells were drilled here in 2007. Again, the apparent drop in production in 2009 is attributed to lack of production reporting on the part of operators.

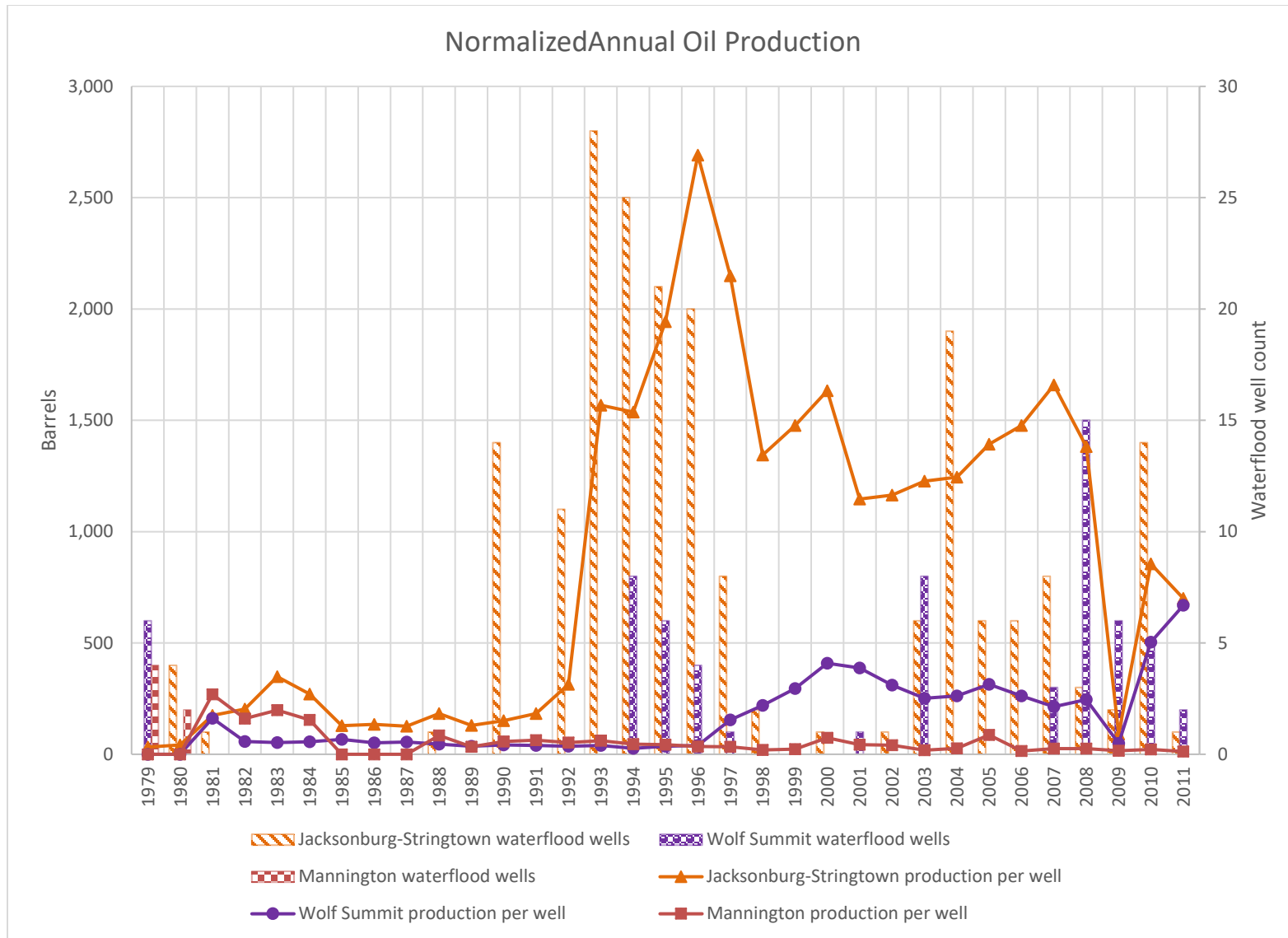


Figure 6-130. Normalized annual oil production and number of waterflood wells drilled in Jacksonburg-Stringtown, Wolf Summit and Mannington fields.

6.6.7 Legacy Wells

The Appalachian Basin has been producing petroleum hydrocarbons for more than 150 years. The Mannington Field, oldest of the West Virginia case study fields, began producing circa 1886, and exploration and production have continued here to the present day. One of the consequences of a century of activity is the large number of well penetrations in an area that will require investigation prior to the initiation of enhanced recovery operations. One way of evaluating potential impacts is determining the number of wells per ac, as shown in Table 6-22. The Salem-Wallace Field has the largest number of well completions of all fields evaluated by the current study, but also the largest total acreage. This accounts for the relatively low (71 wells per ac) well density reported for this field. In contrast, well density in the Wolf Summit-Big Isaac and Mannington fields, two other fields that produce from the Gordon sandstone interval, exceed 100 wells per ac (360 and 148, respectively).

Table 6-22. Wells per acre in the study area. Well counts current as of mid-2018 (WVGES).

Field	Producing Formation	Size (ac)	No. Producing Wells	Total No. Wells in Field	Wells/ 1000 ac
Jacksonburg-Stringtown	Gordon	15,895	1556	1428	90
Mannington	“Big Injun”	5833	71	470	81
Mannington	Gordon	4179	20	618	148
Mannington	Fifth	496	1	22	44
Salem-Wallace	Gordon	39,645	147	2796	71
Wolf Summit-Big Isaac	Gordon	119	4	43	360
Wolf Summit-Big Isaac	Fifth	16,448	139	1764	107

A presumption can be made that areas undergoing secondary recovery via waterflooding have already been investigated with respect to legacy well identification and plugging. An operator considering potential CO₂-EOR project would build on previously completed work. Nevertheless, legacy wells are a challenge to that will necessitate thorough research prior to commencement of EOR activities.

6.6.8 Stacked CCUS Potential

Northern West Virginia oil fields have potential for CO₂-EOR, EGR and CCS. Multiple studies have investigated the potential for CO₂ as a driver to increase oil production in the Upper Devonian Gordon and Fifth sandstones (e.g., Ameri et al., 2002; Bergerud, 2013; Moore et al., 2013; Pease and Watts, 1979; Zhong and Carr, 2016). Oil-bearing units are also present above this sandstone. Due to their shallow depths in the four fields, carbon storage potential is limited in the Lower Mississippian “Big Injun” sandstone, Upper Devonian Gantz and Fifty-Foot sandstones (i.e., the Hundred-Foot Zone of southwestern Pennsylvania) and Thirty-Foot sandstone (i.e., the Nineveh Zone) intervals that are above the Gordon sandstone interval. Most, if not all, lie above the 2500-ft miscible depth for CO₂. However, additional opportunities exist in the area for and carbon storage in deeper units. Potential targets include depleted sandstones in the Upper Devonian Bradford and Elk groups, the Middle Devonian Marcellus Shale, the Lower Devonian Huntersville Chert/Oriskany Sandstone and the Upper Ordovician Utica Shale (Figure 6-131). Although not included in this study due to lack of data control, siliciclastic units of Late Cambrian age might also serve as carbon storage targets.

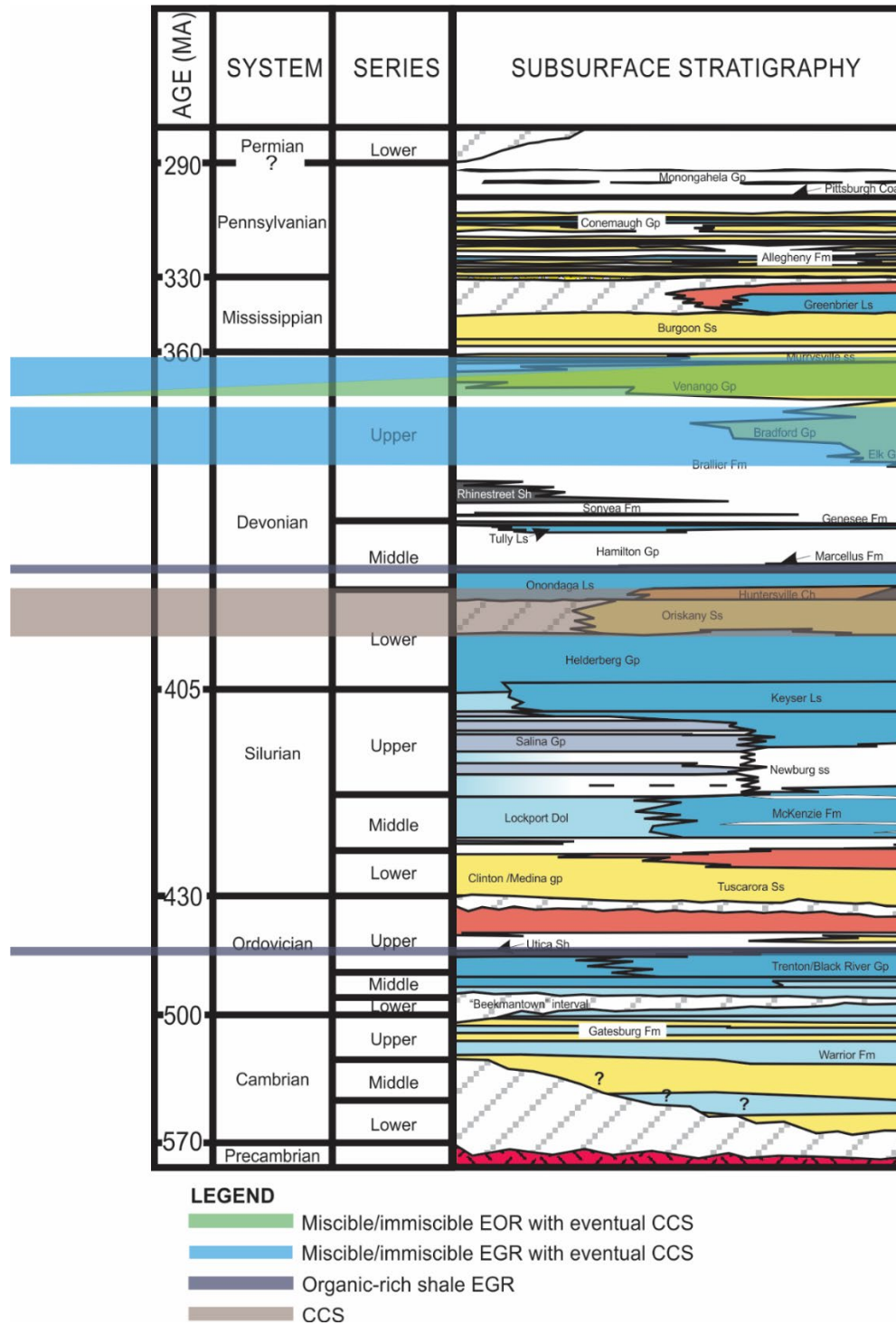


Figure 6-131. Stratigraphic column illustrating stacked CCUS potential in north-central West Virginia.

The oil-producing Gordon and Fifth sandstones in the four case study fields are deep enough to serve as permanent carbon storage reservoirs. Table 6-23 provides the minimum, mode and maximum CO₂ storage estimates for these oil-producing sandstones, based on information compiled by Lewis et al. (2019). These storage estimates are specific to the sandstones listed in the table and use the net thicknesses reported in the database.

Table 6-23. Storage resource estimates for case study fields.

Field	Formation	Depth (ft)	CO ₂ Storage Resource Estimates (million tonnes)		
			Minimum	Mode	Maximum
Jacksonburg-Stringtown	Gordon	3000	2.55	4.24	7.77
Mannington	Gordon	2700	0.29	0.47	0.87
	Fifth	3000	0.09	0.15	0.27
Salem-Wallace	Gordon	2800	4.85	8.05	14.76
Wolf Summit- Big Isaac	Gordon	2575	0.03	0.04	0.08
	Fifth	2900	1.39	2.32	4.25

6.6.8.1 Upper Devonian EGR with Eventual CCS

Fields in proximity to the case study areas produce gas from sandstones in the Bradford and Elk groups. The Brown Lumberport Field borders the eastern side of Salem-Wallace Field. It also overlaps the northern extent of the Wolf-Summit-Big Isaac Field. The Jarvisville Field borders the Brown Lumberport Field to the north and most of the eastern side of Wolf-Summit-Big Isaac Field (Figure 6-132). The sandstones in these two groups are deep enough to have potential for both CO₂-EGR and CCS.

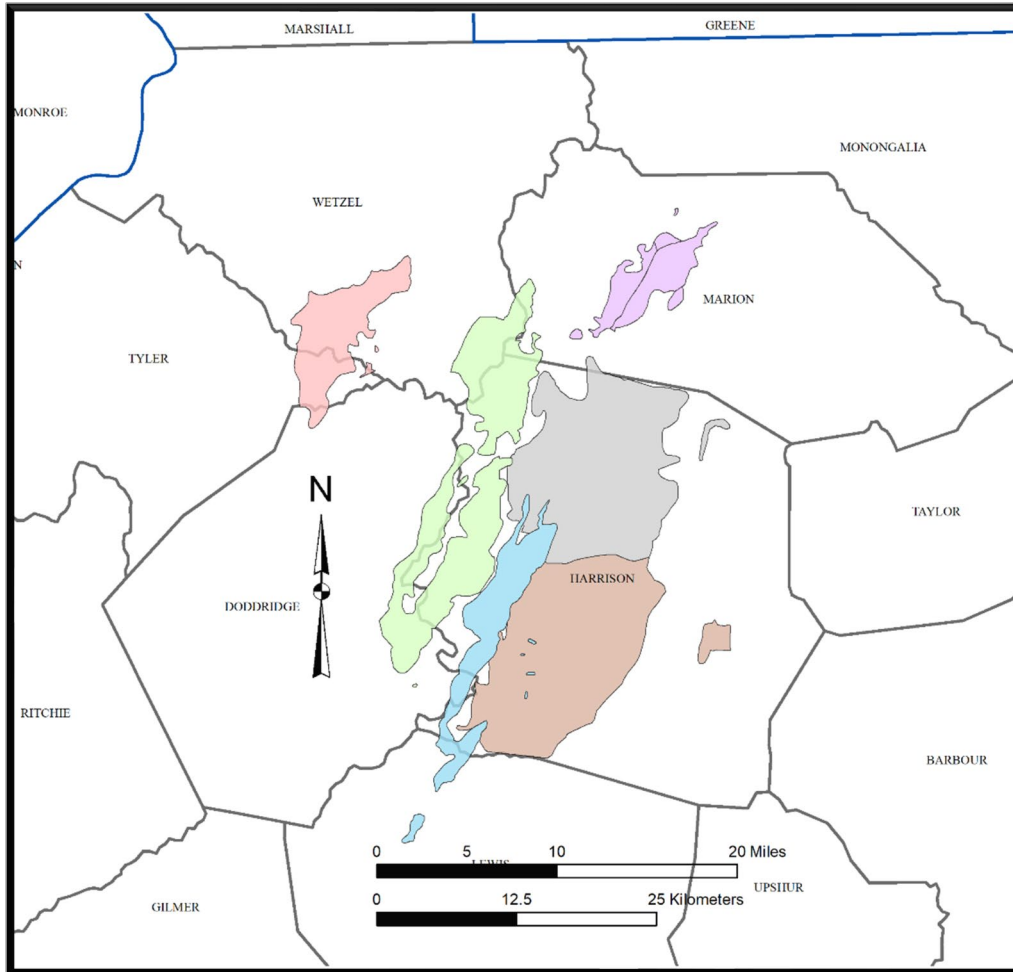


Figure 6-132. Case study fields with Brown Lumberport (gray) and Jarvisville (tan) fields producing gas from the Bradford and Elk groups.

Gas-bearing sandstones of the Bradford and Elk groups also have higher CO₂ storage estimates than the Venango oil-bearing units. The large footprint of their associated fields greatly influences volumes. Table 6-24 lists the CO₂ storage estimates for these deeper Upper Devonian sandstones.

Table 6-24. Storage resource estimates for gas-producing fields near the case study areas.

Field	Formation	Depth (ft)	CO ₂ Storage Resource Estimates (million tonnes)		
			Minimum	Mode	Maximum
Brown-Lumberport	Bradford Group	3326	14.10	23.43	42.95
	Elk Group	4597	3.25	5.40	9.89
Jarvisville	Bradford Group	3158	27.69	45.99	84.32
	Elk Group	4525	4.61	7.65	14.02

6.6.8.2 Lower Devonian CCS

Roen and Walker (1996) described four natural gas plays associated with the Oriskany Sandstone. The fractured Huntersville Chert/Oriskany Sandstone play is associated with northern West Virginia. Gas fields in this play are located along faulted and offset anticlines in the Allegheny Plateau Province (Flaherty, 1996). Several Huntersville/Oriskany fields lie mainly to the east of the case study area (Figure 6-133). Available well data suggests high fracture porosity (Kostelnik and Carter, 2009). Variations in porosity, lithology, presence and degree of fractures and healing along with structural complexity do not allow for broad generalizations. These factors, as well as seal integrity, will require detailed analysis to assess storage suitability.

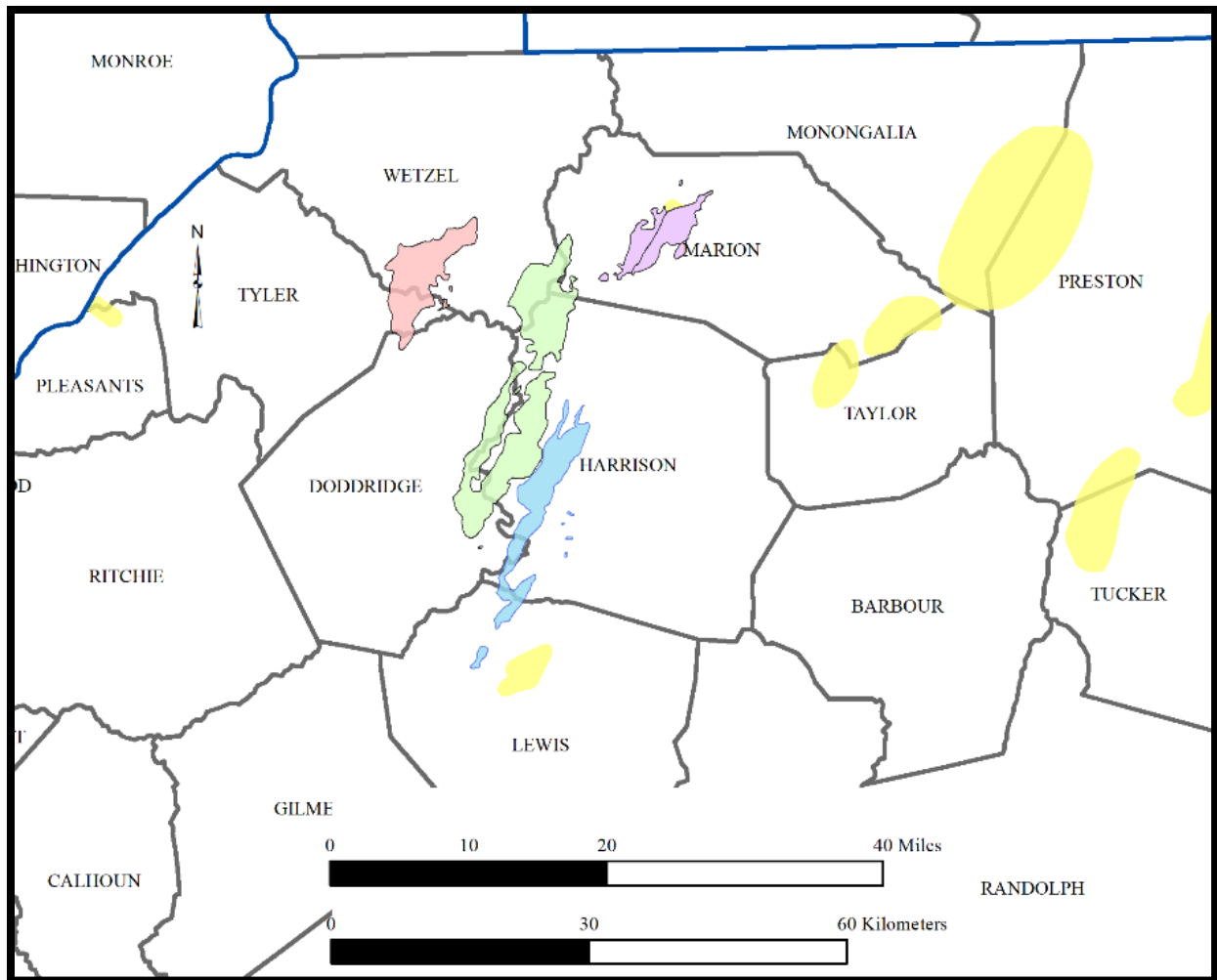


Figure 6-133. Huntersville Chert/Oriskany Sandstone fields (yellow) in the case study area.

The top of the Oriskany Sandstone ranges from -6300 ft MSL at the north eastern tip of the Mannington Field in Marion County to -5600 ft MSL on the south side of the Wolf Summit-Big Isaac Field in Lewis County (Figure 6-134). Regional dip is to the north and east (Figure 6-134). Production in the Huntersville/Oriskany play is primarily from fractures (Flaherty, 1996), responsible for both gas migration and accumulation. Oriskany Sandstone thickness ranges from 100 to 150 ft while the Huntersville Chert interval in the study area, including Doddridge and Harrison counties, exceeds 250 ft (Oliver et al., 1971).

Nearby Huntersville/Oriskany fields have CO₂ storage estimates ranging from 0.38 to 188.08 million tonnes (Table 6-25). Porosity is reported at 7 to 9 percent for these fields. The field with the most CO₂ storage potential (South Burns Chapel Field) lies east of the study area along the border of Monongalia and Preston counties.

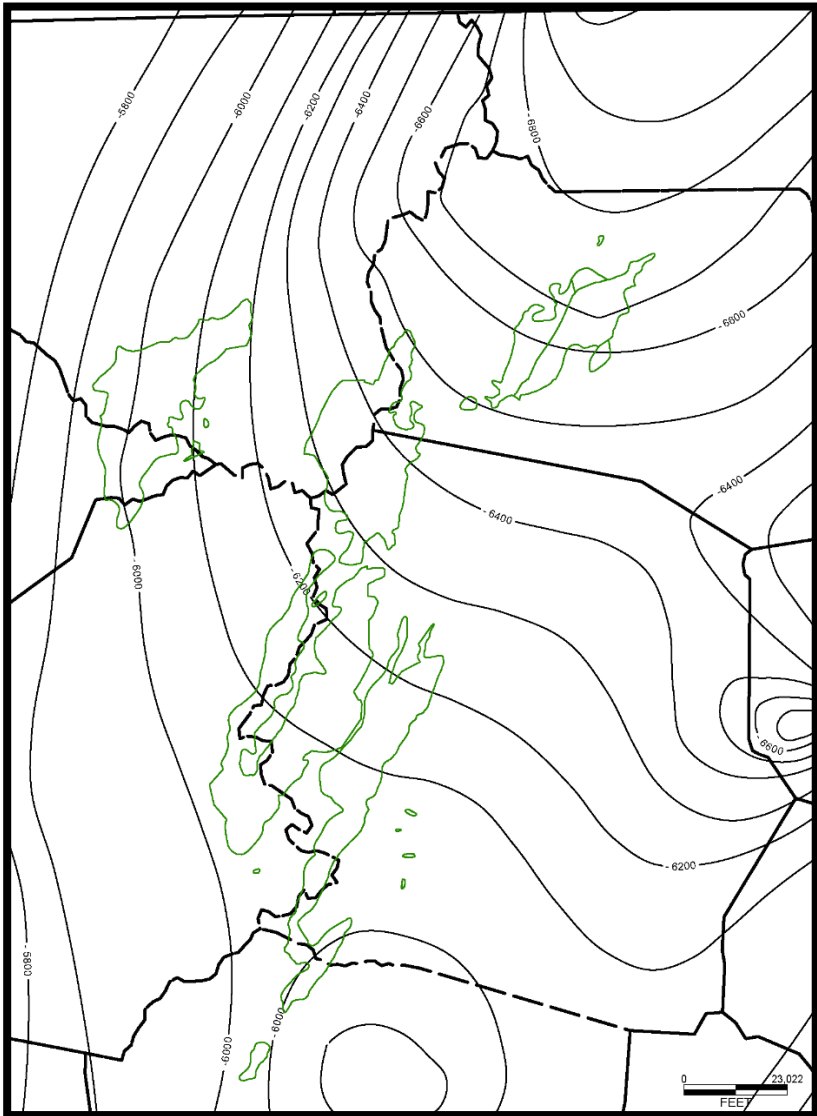


Figure 6-134. Structure map (100-ft contour interval) on top of the Oriskany Sandstone in northern West Virginia.

Table 6-25. Storage resource estimates for area Huntersville Chert/Oriskany Sandstone gas fields.

Field	Formation	Depth (ft)	CO ₂ Storage Resource Estimates (million tonnes)		
			Minimum	Mode	Maximum
Bens Run	Oriskany	5914	0.38	0.63	1.15
Bunners Ridge	Huntersville /Oriskany	7326	4.63	7.70	14.11
Etam	Huntersville /Oriskany	4879	3.64	6.05	11.08
Murphy Creek	Huntersville /Oriskany	6838	0.42	0.70	1.29
Quiet Dell	Huntersville /Oriskany	7407	2.35	3.90	7.15
South Burns Chapel	Huntersville /Oriskany	7634	61.76	102.59	188.08

6.6.8.3 Organic-Rich Shale EGR with Eventual CCS

Chapter 5 addresses the potential of Marcellus and Utica shales to serve as both enhanced recovery and carbon storage targets. With infrastructure from an EOR project in place, these deeper storage zones may become attractive for EGR with eventual CCS as shallow CO₂-EOR operations cease.

The base of the Middle Devonian Marcellus Shale is 3000 ft or more below shallow oil-producing reservoirs in northern West Virginia (Figure 6-135). The four counties that comprise most of the study area (i.e., Doddridge, Harrison, Marion and Wetzel) are among the top ten counties producing from the Marcellus Shale in 2017 (Figure 6-136; Dinterman, 2018). The wet/dry gas transition occurs near the Harrison/Doddridge County line, essentially in the middle of the Salem-Wallace Field. Therefore, Jacksonburg-Stringtown is considered to be in the wet gas area. Figure 6-137 illustrates the deviated shale well activity in the study area. These wells could include Upper Devonian, Marcellus

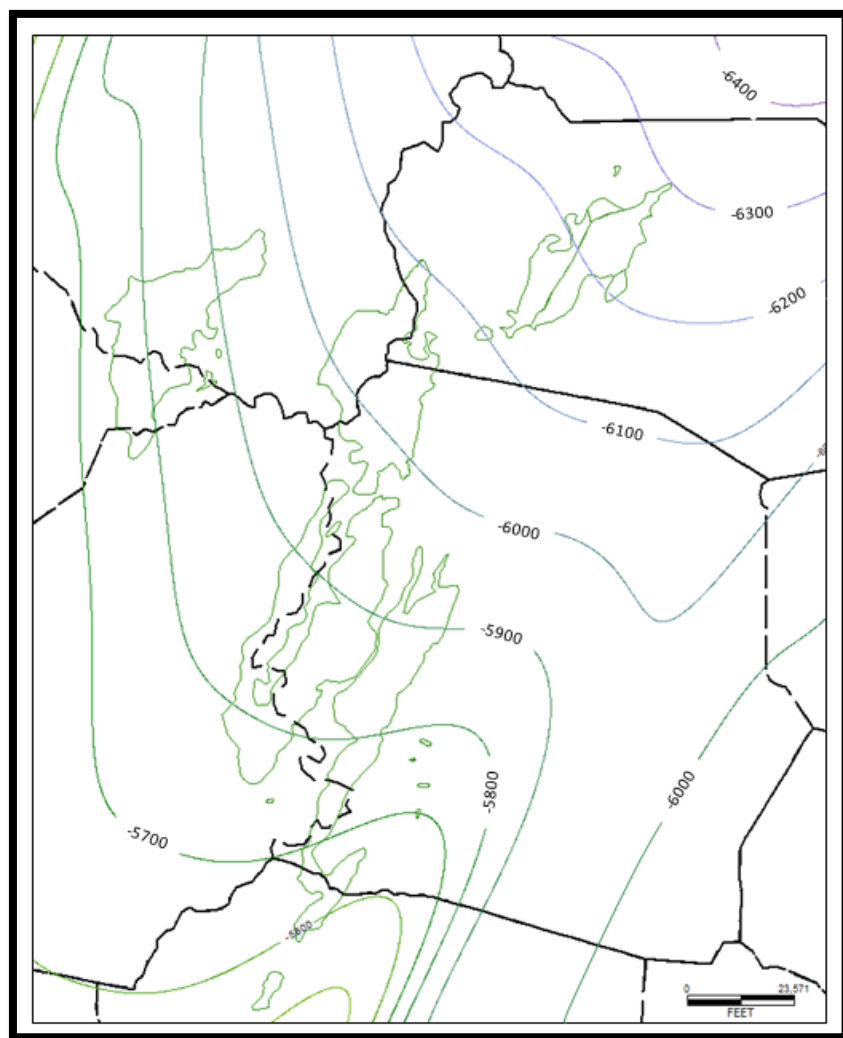


Figure 6-135. Structure map (100-ft contour interval) on the base of the Marcellus Shale in northern West Virginia.

and/or Utica completions, but are overwhelmingly Marcellus producers. These are more favorable targets for enhanced recovery than dry gas areas.

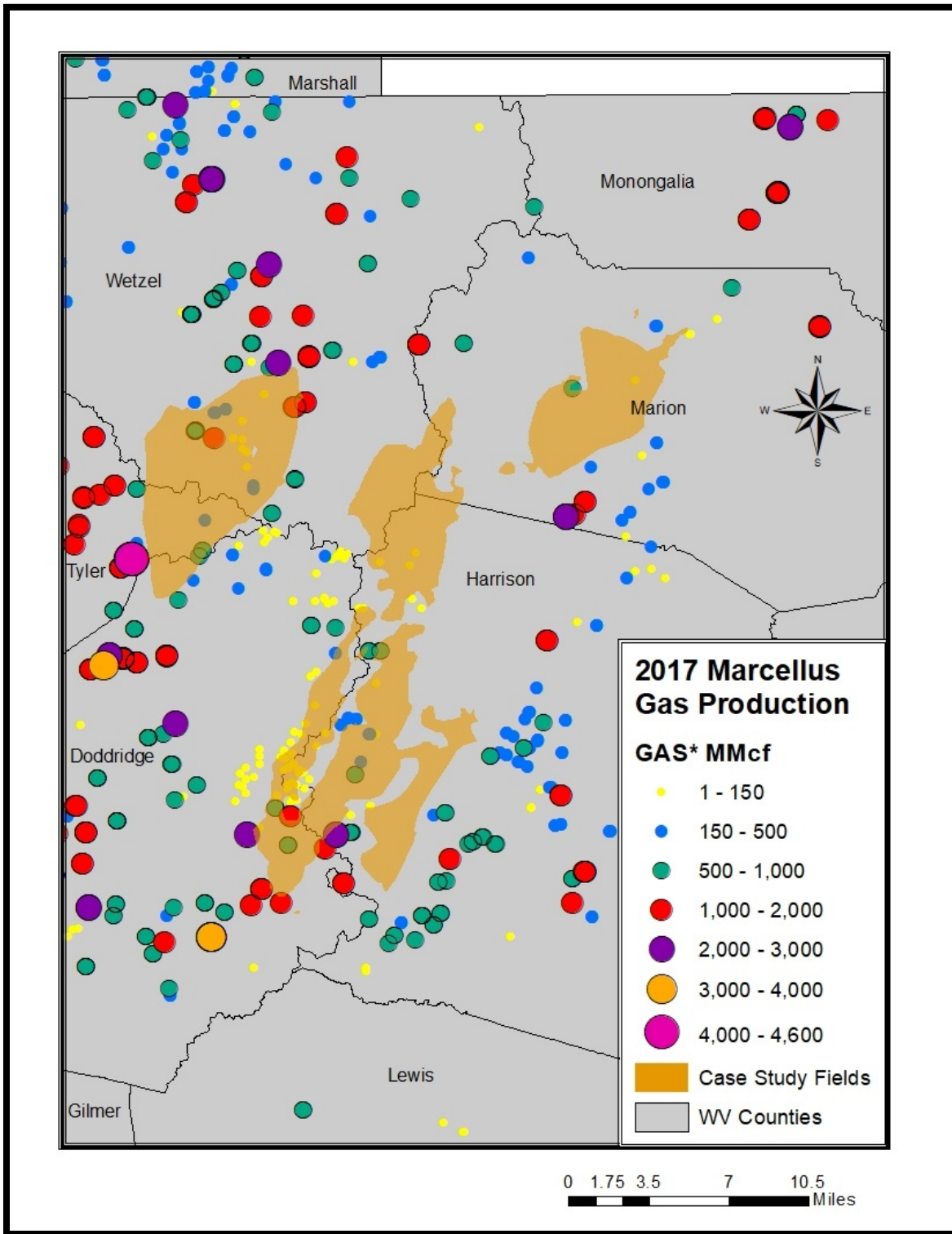


Figure 6-136. Bubble map of Marcellus Shale gas production in relation to the study area (modified from Dinterman, 2018).

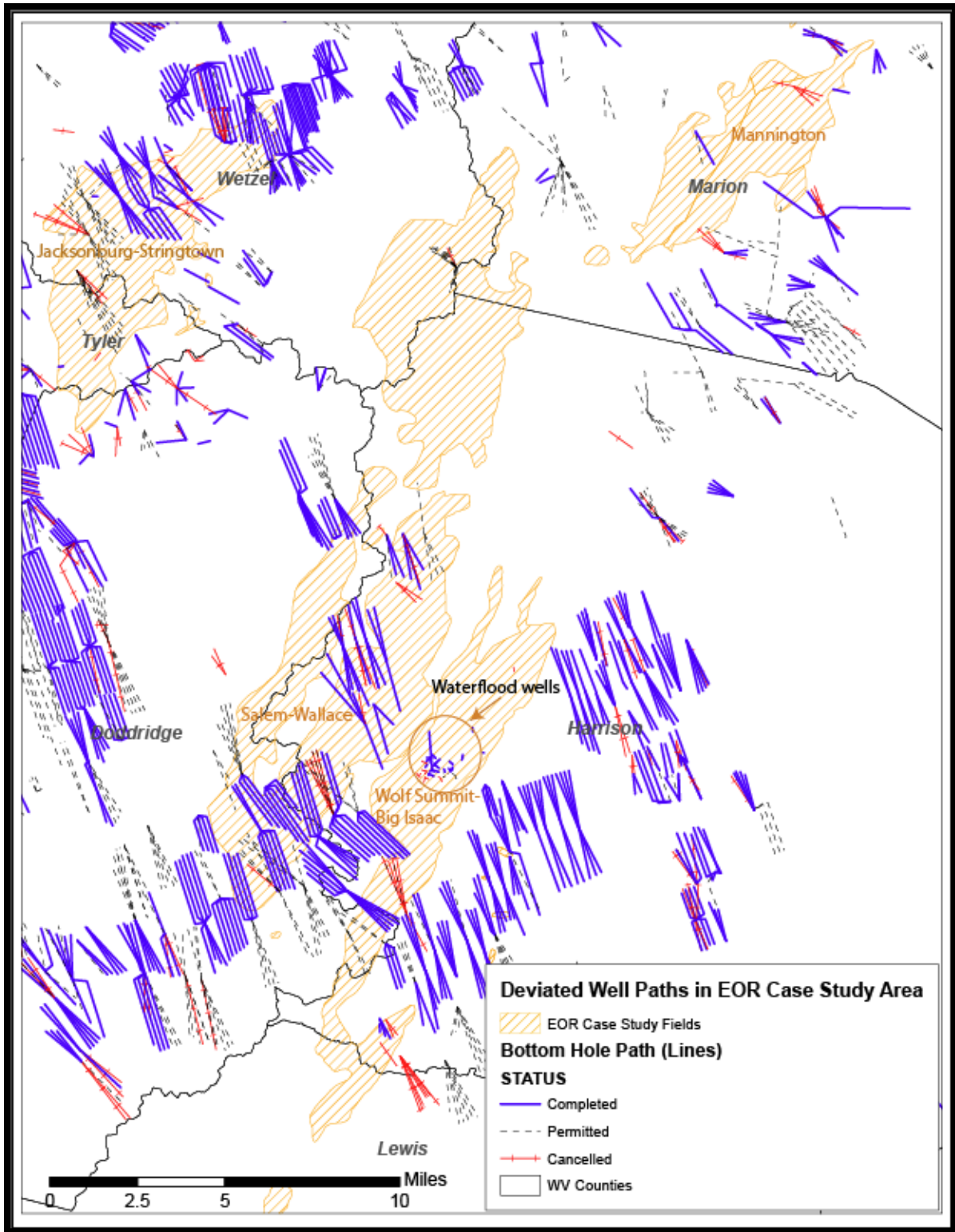


Figure 6-137. Deviated well paths (permitted, completed and cancelled) in the case study area. The Wolf Summit waterflood wells are circled.

The Utica Shale represents another potential storage reservoir, albeit deep. Two wells in Wetzel County near the Jacksonburg-Stringtown Field reported production from the Utica Shale in 2017, and more wells have been since been permitted in that area (Dinterman, 2018). In the area of the four case study fields, the top of the Utica is found at elevations of -10,000 to -11,200 ft MSL (Figure 6-138), which exceeds the CCUS measured-depth limit (i.e., 10,000 ft) considered by the current study.

6.6.9 Summary

The case studies prepared for the Jacksonburg-Stringtown, Mannington, Salem-Wallace and Wolf Summit-Big Isaac fields highlight specific CCUS opportunities for northern West Virginia. These include: (1) both immiscible and miscible CO₂-EOR for Mississippian and Upper Devonian reservoirs;

(2) miscible CO₂-EGR in Upper Devonian Bradford and Elk group reservoirs;

(3) permanent carbon storage in the Lower Devonian Oriskany Sandstone; and (4) possible opportunities for CO₂-EGR with eventual storage in the Middle Devonian Marcellus and Upper Ordovician Utica shale reservoirs. Each of these fields are less than 20 mi from potential CO₂ point-sources, including coal-fired power plants (Moore et al., 2013).

The Jacksonburg-Stringtown Field produces from the Gordon sandstone and is estimated to have more than 69 MMBO oil remaining, with 9 MMBO recoverable. Porosity averages 15 percent and pore-derived permeability ranges from 10 to 200 mD. Secondary oil recovery

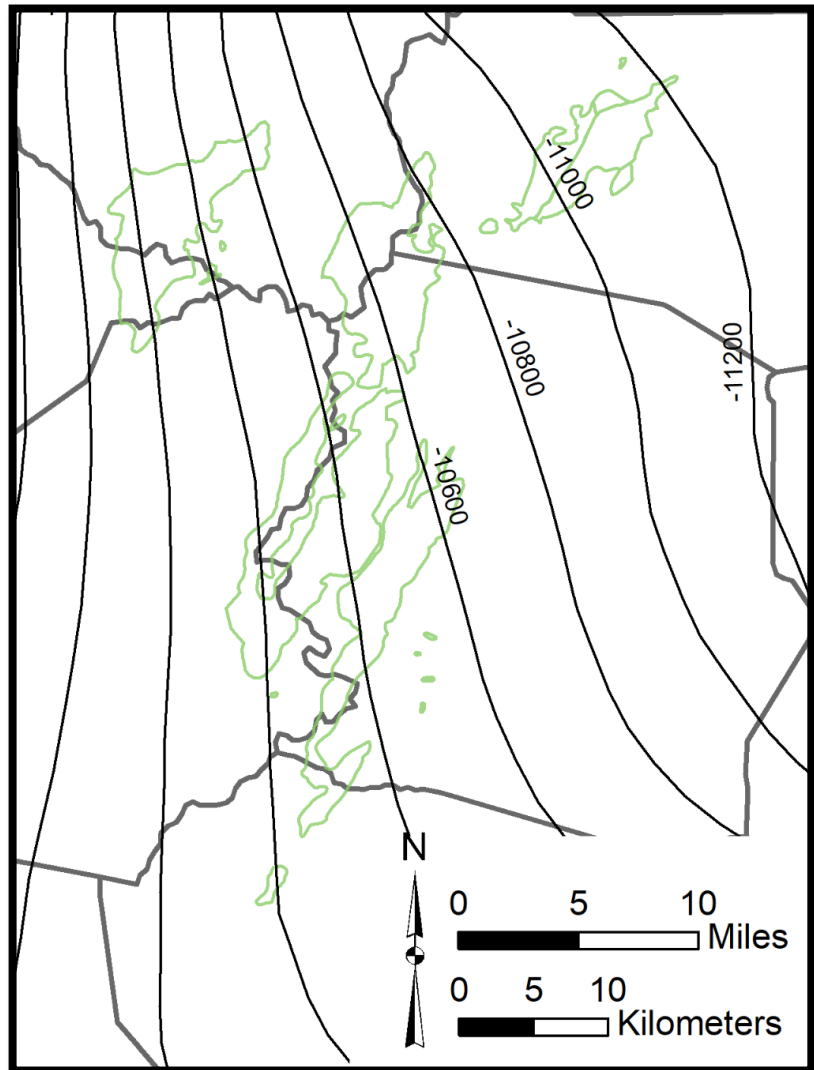


Figure 6-138. Utica Shale structure contour map for northern West Virginia (modified from Patchen and Carter, 2015).

efforts via waterflooding began in 1990 and have continued to the present day, resulting in increased oil production.

In addition to the Gordon sandstone, the Mannington Field also produces from the overlying “Big Injun” and underlying Fifth sandstones. The “Big Injun” is shallower than the regional CO₂ miscible depth of 2500 ft and is the producing formation for 75 percent of the oil wells in this field. The Fifth sandstone, with a limited production acreage, is in the miscible range with the Gordon sandstone. Secondary oil production from Venango Group sandstones via water injection was discontinued after a short time.

The Salem-Wallace Field produces oil in the CO₂-miscible-depth range in multiple, undifferentiated Gordon sandstones. Both stratigraphic and structural traps define this field. Remaining oil is estimated at more than 132 MMBO, with an estimated 17 MMBO recoverable. Sandstone porosity is approximately 12 percent.

Bordering the east-central portion of the Salem-Wallace Field, the Wolf Summit-Big Isaac Field has a combined 64 MMBO oil remaining in the Gordon and underlying Fifth sandstones. Porosity ranges from approximately 10 percent in the Gordon to 10 to 20 percent in the Fifth. Permeability in the Fifth sandstone is reported at 64 mD.

Sandstones of the Bradford and Elk groups have produced gas from adjoining fields and represent potential CO₂-EGR with subsequent CCS. The fractured Huntersville Chert/Oriskany Sandstone play in the study area will require detailed investigation of reservoirs and seals to determine its ultimate suitability for CCS.

Development of the Marcellus Shale play is largely co-located with the Venango oil fields evaluated by this study for miscible CO₂-EOR. Combined with the underlying Utica Shale, these shale gas formations hold potential for both CO₂-EGR and CCS. Here, the Marcellus Shale falls within the dry to wet gas transition zone, and the Utica remains mostly unexplored.

7.0 Discussion

The Appalachian Basin is situated in the heart of the MRCSP Region, producing coal, oil, gas and NGLs that provide power, fuels and feedstock for various industries, both domestically and abroad. The basin's unconventional shale resources (most notably the Marcellus and Utica shales) are world-class and offer both challenges and opportunities to the advancement of CCUS in the region. Furthermore, the longevity of the oil and gas industry in the Appalachian Basin, along with the many technological advances that have been developed here, provide a certain historical context and familiarity with subsurface activities that other areas of the United States may lack.

The geologic characterization efforts performed by Geoteam members as part of the MRCSP Phase III project period have been instrumental in filling data gaps; refining carbon storage resource estimates; developing and expanding approaches for desktop reservoir assessment; and providing a thoughtful evaluation of current CCUS opportunities by considering enhanced petroleum hydrocarbon recovery in concert with stacked storage options. A concise summary of the results of this integrated basin assessment is provided below.

7.1 Summary of Findings

7.1.1 Prospective Reservoirs

7.1.1.1 Regional Oil Field Opportunities

During the current phase of research, a master geodatabase of petroleum fields (Lewis et al., 2019) was compiled from pre-existing MRCSP datasets and newly derived field-level data. The result is a digital dataset consisting of more than 4000 oil and gas fields represented by nearly 19,000 rows of data for the entire MRCSP Region. This geodatabase includes data for 993 individual oil fields in the Appalachian Basin, which are represented by more than 1200 polygons of various size and reservoir attribute content. The geodatabase includes reported and/or calculated values for production depth; net thickness; reservoir pressure and temperature; water and oil saturation; cumulative production; remaining OOIP; permeability; oil saturation; and storage resource estimates for conventional targets. It is intended to help lower the technological barrier that stakeholders often face when evaluating a prospective CCUS target and serves as a repository for information collected over the 16-year period of MRCSP research.

WVGES used this geodatabase to identify oil fields in the Appalachian Basin where reservoir properties suggest EOR potential. Specifically, oil saturation, porosity, permeability and reservoir thickness data were screened to determine a short list of oil fields that may benefit from enhanced recovery operations. These include Kane Field in Pennsylvania and several fields (Cabin Creek, Centerpoint, Granny Creek-Stockly, Griffithsville, Jacksonburg-Stringtown, Salem-Wallace, Smithfield, Wolf Summit-Big Isaac and Yellow Creek Revere) in West Virginia. It should be noted that three of these fields – Jacksonburg-Stringtown, Salem-Wallace and Wolf Summit-Big Isaac – were also identified as CCUS prospects using the oil field rating criteria (Table 6-1) developed by PAGS for the current study. This suggests that these three West Virginia oil fields not only have favorable reservoir properties for a CO₂-EOR project, but also have characteristics that would be economically beneficial for an enhanced recovery operation with eventual carbon storage – namely, adequate remaining OOIP, a sizable footprint and stacked storage opportunities.

7.1.1.2 Ohio

Ohio is home to many oil fields that may serve as good CO₂-EOR candidates. Case studies prepared for three of these fields – East Canton Consolidated, Clayton Consolidated and Philo Consolidated – serve as examples of how to approach geologic and engineering assessments of Medina group reservoirs for enhanced recovery operations. Engineering models should incorporate fluid migration pathways through geologic time into the CO₂-EOR modeling process. Cross-structural lineaments often define these pathways, with higher oil yields typically occurring in alignment with two or more cross-structural fracture sets. Laterally extensive vertical seals above and below Medina group reservoirs will likely constrain the movement of CO₂ during recovery and storage operations.

The East Canton Consolidated and Clayton Consolidated fields produce from the Grimsby Sandstone (“Clinton” sandstone), and Philo Consolidated Field produces from the Whirlpool Sandstone (“Medina” sandstone). These units offer the prospect of both enhanced oil production and carbon storage. Primary oil production from these fields has been reported in the 6-7 percent range, indicating significant reserves remain in place. As an example, reservoir modeling has estimated that 76 to 279 MMBLS oil could be recovered from the East Canton Consolidated Field via CO₂-EOR, with eventual storage of CO₂ once production ceases.

Stacked storage potential exists in each of the three Ohio case study areas. In addition to the prospect of stacked storage within individual units of the Medina group, operators may choose to investigate both shallower (Oriskany Sandstone and Lockport Dolomite) and deeper (Rose Run Sandstone) units for carbon storage. The Utica Shale/Point Pleasant interval may also provide another opportunity – enhanced recovery of oil and NGLs with eventual carbon storage.

7.1.1.3 Pennsylvania

Case studies prepared for three Pennsylvania oil fields – Washington-Taylorstown, Linden and New Freeport – spotlight multiple CCUS opportunities in Greene and Washington counties (Figure 6-83). These include CO₂-EOR and CO₂-EGR (both miscible and immiscible scenarios) for conventional reservoirs, permanent carbon storage and CO₂-EGR for shale gas reservoirs.

Enhanced oil and gas recovery opportunities are associated with sandstones of the Venango Group and are situated in an area referred to as the Gordon fairway (Area B of Figure 6-83), which extends into northern West Virginia. Here, the Gordon sandstone’s porosity (~20 percent) and permeability (100 mD or more) make it the primary target for oil development, although the Gantz, Fifty-Foot, Nineveh, Fourth and Fifth sandstones have also produced oil and/or gas in the area. As an example, approximately 10 MMBO could be produced from the Gantz and Gordon in Washington-Taylorstown Field alone (Lytle, 1950). Over the past century, the Washington-Taylorstown Field has undergone both air/gas drive and waterflood enhanced oil recovery operations to recover additional oil; these have mostly focused on the field’s western limb. There are no active enhanced recovery operations in southwestern Pennsylvania at this time.

Permanent carbon storage may be pursued in the Oriskany Sandstone, which occurs at depths of a mile or more throughout southwestern Pennsylvania. Based on previous studies, the most favorable area for permanent storage in this unit may be Area A of Figure 6-83, where the Oriskany has produced gas from a combination traps play.

Stacked storage potential may be feasible using multiple sandstones of the Venango Group. By and large, this option may be pursued throughout the study area, as the Venango Group is comprised of four to five sandstone intervals in Greene and Washington counties. In Area C of

Figure 6-83, stacked storage potential may be particularly attractive, given the deeper depths of these units. The Oriskany Sandstone is also present in this area, and provided site-specific investigations determine fracture and/or matrix porosity sufficient to support injection activities, this deeper reservoir may serve as an additional stacked storage reservoir.

Although yet untested in the Appalachian Basin, performing CO₂-EGR in places where the Utica and/or Marcellus shale reservoirs have produced wet gas may be appealing to operators as these reservoirs approach the end of their development phase. As the majority of Washington and Greene counties fall in the dry gas window for both shale plays, CO₂-EGR would likely be most successful in western Greene and Washington counties for enhanced recovery of wet gas from the Marcellus, and adjacent to or west of the Ohio River for enhanced recovery of wet gas from the Utica Shale (Area A of Figure 6-83).

7.1.1.4 West Virginia

Case studies were prepared for four fields in West Virginia – the Jacksonburg-Stringtown, Mannington, Salem-Wallace and Wolf Summit-Big Isaac (Figure 6-91). All of these are situated in the Gordon Fairway and have produced oil from multiple, undifferentiated stacked sandstones of the Gordon Zone since the late 1800s. In addition, the Mannington and Wolf Summit-Big Isaac fields produce oil from the underlying Fifth sandstone, and the Mannington Field produces from the overlying “Big Injun” sandstone. Most of the CO₂-EOR opportunities in these case study fields appear to be in miscible range (i.e., depths \geq 2500 ft).

Core analysis from the Ball 18 well in Jacksonburg-Stringtown Field indicates very good reservoir porosity (>20 percent) and permeability (tens to hundreds of mD). More than 9 MMBO is estimated to be recoverable from the Gordon sandstone in this field. Salem-Wallace Field estimates of recoverable oil are 17 MMBO, with an effective porosity of 30 percent in parts of the reservoir (Moore et al., 2013). No enhanced oil recovery projects are known in this field as of the writing of this report. Porosities in Wolf Summit-Big Isaac Field average 10 percent in the Gordon sandstone and 20 percent in the underlying Fifth sandstone. In this field, the combined remaining oil is estimated at >64 MMBO.

Enhanced oil recovery efforts in the Jacksonburg-Stringtown and Wolf Summit-Big Isaac fields were initiated in the early 1990s and responded well to reservoir waterflooding techniques. Similar attempts in Mannington Field were not broadly pursued (Figure 6-129).

Stacked opportunities for additional CCUS exist in northern West Virginia. Adjoining fields producing gas from deeper Bradford and Elk Group sandstones have favorable storage estimates, due in part to their large acreage. The fractured Huntersville Chert/Oriskany Sandstone gas play is situated to the east of the case study fields. Detailed analyses of variable reservoir characteristics and structural complexities will be required to determine storage suitability in these locations and geologic intervals.

The wet/dry gas transition in the Marcellus Shale passes through the study area, with the Jacksonburg-Stringtown Field in the wet gas area. As noted in the Pennsylvania study, CO₂-EGR is an enticing prospect as primary production declines. Demand for NGLs is expected to increase in the region with the development of petrochemical plants and manufacturing demand. The deeper Utica Shale remains locally unexplored.

7.1.2 Storage Resource Estimates

Storage resource estimates were calculated for conventional oil and gas fields where the requisite field-level reservoir data were available. With respect to oil fields in the Appalachian

Basin (the focus of the current study), Ohio, Pennsylvania and West Virginia offer most of the potential carbon storage, with mode resource estimates ranging from ~100 – 400 million tonnes. Other basin states reported total mode storage resource estimates less than 100 million tonnes (Figure 4-6).

Mode carbon storage resource estimates were totaled by state and plotted using bar graphs (Figure 4-7). The oil fields of Ohio and Pennsylvania have the largest mode estimate totals (~200 – 400 million tonnes) of all states in the basin, and the gas fields of Pennsylvania and West Virginia have the largest mode estimate totals (2.8 – 4.6 billion tonnes).

The total storage resource estimate for all types of production was summed for each state and compared to what was reported in MRCSP's Phase II assessment (Figure 4-7). The current storage resource estimates are more conservative than those reported previously, not only due to the revision of field boundaries and field-level data prepared as part of the current work but also because shale gas fields were not included in this basin-wide assessment. Instead, Geoteam members assessed the storage potential of the Middle Devonian Marcellus and Upper Ordovician Utica shales separately, developing data transforms that may be used to assign TOC content to these units on a well by well basis. This effort is a necessary first step in determining the ability of these unconventional shales to adsorb CO₂ and/or store CO₂ in organic pores.

Carbon storage in the Marcellus Shale is expected to occur as mostly adsorbed gas associated with organic matter. A carbon storage volume was estimated at ~804 million tonnes (3 percent efficiency factor) to ~2680 million tonnes (10 percent efficiency factor) using reservoir depth, reservoir volume and modeled TOC data. A majority of this storage potential is located in northeast Pennsylvania and southern New York.

Carbon storage in the Utica/Point Pleasant interval is expected to occur as both a free gas in the units' matrix porosity and as adsorbed gas associated with the organic matter. Free gas storage is more important here than in the Marcellus Shale due to the lower overall organic content of these Ordovician units. Here, storage resource potential is dependent on TOC, reservoir depth, reservoir volume and porosity. An estimated carbon storage volume of ~1880 million tonnes (3 percent efficiency factor) to ~ 6300 million tonnes (10 percent efficiency factor). An estimated 80 percent of this storage is situated in the tri-state area of Ohio, Pennsylvania and West Virginia.

7.1.3 Challenges

The regional characterization work performed during the Phase III project period has served to consolidate and distill our understanding of the many challenges facing the Appalachian Basin with respect to the CCUS implementation. In this regard, the following subsections address legacy wells, modern horizontal drilling, pipeline infrastructure, prospective reservoir size and reservoir data gaps.

7.1.3.1 Legacy Wells

The Appalachian Basin's legacy stretches back to the birth of the modern petroleum industry, and the wells exist to prove it (if one can locate them, that is). Despite concerted efforts at the state level, hundreds of thousands of abandoned oil and gas wells remain unaccounted for or are incorrectly located due to mapping errors. On-ground reconnaissance is often difficult across rugged terrain and through decades of overgrowth, but modern techniques such as magnetic drone surveys and LiDAR produce high-resolution, remotely-sensed data that can be used to conduct surveys across relatively large areas (Hammack et al., 2016). Once orphaned

wells are identified, however, mitigation costs and responsibilities are usually transferred onto the state, resulting in a backlog of wells to be plugged. If improperly plugged, an abandoned borehole may serve as a conduit for fluid migration through the subsurface. Presence of unidentified wells may also affect re-pressurization efforts in EOR fields.

In areas of the Appalachian Basin co-located with modern horizontal drilling activities, orphaned and unidentified wells present a significant safety concern for operators. State regulations vary, but operators are typically required to plug wells that are encountered in proximity to drilling operations. Gas storage fields are federally regulated by the Pipeline and Hazardous Materials Safety Administration (PHMSA) and are required to account for all wells in the storage pool, including any legacy wells drilled by a third party.

7.1.3.2 Modern Horizontal Drilling

Organic-rich shales are often referred to as the “source kitchen” for the thermal maturation of kerogen to produce hydrocarbons, which then migrate through the subsurface and accumulate in conventional reservoirs. Modern horizontal drilling bypasses the conventional accumulation and instead produces from the source rock. This presents a problem for CCUS activities in depleted or depleting fields due to the proximity to the “source kitchen” currently being developed by large-scale drilling operations. The proximity not only presents technical challenges, such as maintaining the integrity of the local cap rocks (Sminchak et al., 2016), but also presents difficulties in acquiring the leases necessary to conduct CCUS operations. However, for existing operators or those with legacy leaseholds, the presence of EOR targets can also be evaluated as a type of behind-pipe pay, especially in marginal wells, or wells that are located near fields that have been identified as having significant remaining oil in place.

7.1.3.3 Pipeline Infrastructure

Addressing a lack of CO₂ pipeline infrastructure and the time required for permitting and construction of new infrastructure is critical to maximizing CCUS opportunities. Currently, the transport and delivery of CO₂ to a prospective CCUS target in the MRCSP Region is usually achieved via tanker truck and is often cost-prohibitive. Introduced on May 13, 2019, Senate Report 116-38 addresses this challenge. The “Utilizing Significant Emissions with Innovative Technologies” (USE IT) Act recognizes the need for a more robust CO₂ pipeline infrastructure and seeks to both clarify the appropriate role of federal and state regulatory bodies and streamline the permitting process. If the USE IT Act is passed, the statutory language for CCUS projects, including CO₂ pipelines, would be made explicit to consider construction of CO₂ pipelines as “covered projects” under Title XLI of the 2015 Fixing America’s Surface Transportation (FAST) Act. This designation as a “covered project” means that a proposed CO₂ pipeline would benefit from the oversight of the Federal Permitting Improvement Steering Council for improved efficiency and timeliness of the permit application process.

Successful passage of legislation such as the USE IT Act is an important first step in the creation of a network of pipeline infrastructure connecting point sources with potential storage and utilization targets, but work is also needed at the state level to maximize the benefit of the federal legislation. This is especially true for smaller, intrastate projects that would be primarily covered by state statute. For states with current oil and gas exploration and production in the Appalachian Basin, this could possibly be achieved by co-locating CO₂ pipelines in rights-of-way established for natural gas or NGL pipelines, thereby minimizing both the environmental footprint and streamlining the state permitting process.

7.1.3.4 Prospective Reservoir Size

Prospective reservoirs that are limited in size may be attractive CCUS targets for other reasons. For example, the Cabin Creek Field in southern West Virginia is an EOR target in the Berea Sandstone and located in proximity to active coal mining operations. As the mining operation moves progressively through the coal seam above the EOR target, all legacy oil and gas wells intersecting the mine are plugged, which significantly reduces an initial risk involved with injection activities. Other potential scenarios where a smaller-sized reservoir may present an attractive target are those located in proximity to a captured CO₂ source or those located in proximity to existing infrastructure.

7.1.3.5 Reservoir Data Gaps

Despite efforts made throughout the three phases of MRCSP to close data gaps wherever possible, a major finding of this report is that certain data gaps remain, within all of the reservoirs characterized, across all parts of the region that were assessed. This is especially apparent in the petroleum fields database (Lewis et al., 2019), where certain critical reservoir parameters, such as permeability, are reported for fewer than 10 percent of the fields, and oil gravity, which had to be estimated using data transforms due to the lack of direct measurements at the field level.

7.1.4 Opportunities

Based on the integrated assessment provided in this report, Geoteam members have identified many CCUS opportunities that may be pursued in the Appalachian Basin. The oil field and gas field rating criteria may be employed in conjunction with the petroleum fields geodatabase to develop desktop prospects, which can then be vetted through additional field-level investigations and site evaluations. The main premise in developing these data products and rating criteria was to provide a way to locate CCUS opportunities given the 3D “lay of the land.” In other words, when the geographic extent of a field, location of CO₂ sources and land use at ground level are considered in concert with subsurface geologic conditions and stacked storage opportunities, the result is much more likely to identify a viable enhanced recovery and/or carbon storage project.

The following examples illustrate how the methods and datasets of this topical report can be applied to facilitate the development of technically and economically feasible CCUS projects:

- The proximity of CO₂ point-sources to storage reservoirs (sinks) can be weighed against the potential volume of CO₂ to be injected to provide a “best match” for field-level operations. The petroleum fields geodatabase contains thousands of fields of different sizes and depths, so such an exercise should yield multiple opportunities. Such projects may take advantage of current Section 45Q tax credits, which require that project construction commences before January 1, 2024 and that a minimum 25,000 to 100,000 tonnes CO₂ is injected per year at the qualified project site (Tracy, 2019).
- Active shale gas well sites, which are relatively large compared to conventional well pads and currently abundant given Marcellus and Utica Shale activity in the tri-state area, can be assessed for enhanced recovery and/or carbon storage prospects using this report’s field-level data, rating criteria and methods for assessing organic-rich shales. Operators and industry partners can then determine whether CO₂ injection may be beneficial at their sites. Such piggyback activity could include CO₂-EGR in the depleting shale reservoir with eventual storage, or carbon storage in other geologic intervals.

- Fields where depleting/depleted oil and gas reservoirs exist could be reinvigorated with enhanced recovery operations, followed by eventual carbon storage in the same or deeper reservoirs. The proceeds from enhanced production in these fields may be used to offset the costs associated with implementing CO₂ injection at the site. In this manner, petroleum hydrocarbons are more fully developed, and the amount of carbon stored can be maximized by potentially utilizing stacked storage reservoirs.

7.2 Recommendations

As the submission of this topical report signals the end of the MRCSP Phase III project for Geoteam members, we offer the following recommendations for consideration of follow-on work. These are not intended to be an exhaustive listing. Instead, they provide a generalized summary of research pursuits that may advance industry's understanding of subsurface formations identified as prospective CCUS reservoirs by this report. Some recommendations may be easily implemented with little financial support needed, while others will require significant investments of time and funding.

- Determine field-level **TOC** data for shale formations, either from core-derived analyses or the log-based approaches reported in Chapter 5 of this report; update the petroleum geodatabase of Lewis et al. (2019) with this information and seek to refine storage resource estimates for these unconventional reservoirs.
- Seek field-level **pressure, permeability and oil gravity** data for CCUS target areas where prospective reservoir data are lacking; this will fill existing knowledge gaps regarding the injectivity of prospective reservoirs, and whether enhanced recovery operations will involve miscible or immiscible injection of CO₂.
- Support state-level **core repository operations** to include: (1) handheld permeameter measurements of prospective core; (2) encourage core donations to state surveys; and (3) facilitate core sampling and laboratory analysis of newly acquired and/or critical samples.

8.0 References Cited

- Abdulrahman, A. A., Amaf, A. M., Al-Zahrani, N. I., AlQarni, M. T., and AlShamrani, S. A., 2019, Low salinity water and CO₂ miscible flooding in Berea and Bentheimer sandstones: *Journal of King Saud University – Engineering Sciences*, v. 31, no. 3, p. 286-295.
- Advanced Resources International, 2006, Basin oriented strategies for CO₂ enhanced oil recovery: Illinois and Michigan Basins: Pittsburgh, Pennsylvania, National Energy Technology Laboratory, U.S. Department of Energy, 104 p.
- Algeo, T. J., and Scheckler, S. E., 1998, Terrestrial-marine teleconnections in the Devonian: links between the evolution of land plants, weathering processes, and marine anoxic events: *Philosophical Transactions Royal Society London, Part B, Biological Science*, v. 353, p. 113-130.
- Algeo, T. J., Berner, R. A., Maynard, J. B., and Scheckler, S. E., 1995, Late Devonian oceanic anoxic events and biotic crises: “rooted” in the evolution of vascular land plants?: *Geological Society of America, Geology Today*, v. 5, p. 64-66.
- Ameri, S., Aminian, K., Avary, K. L., Bilgesu, H. I., Hohn, M. E., McDowell, R. R., and Patchen, D.L., 2002, Reservoir characterization of Upper Devonian Gordon Sandstone, Jacksonburg, Stringtown oil field, northwestern West Virginia. United States: N. p., doi:10.2172/794279.
- Anonymous, 1999, POGO-Production of Oil and Gas in Ohio database: *Ohio Geology*, 1999, no. 2, p. 3., <http://geosurvey.ohiodnr.gov/portals/geosurvey/PDFs/Newsletter/1999No.2.pdf>, last accessed 6/13/2019.
- Asquith, George, and Krygowski, Daniel, 2004, Basic well log analysis: Tulsa, Oklahoma, American Association of Petroleum Geologists Methods in Exploration Series, no. 16, 244 p.
- Avary, K. L., 2001, Discovery and Development, chap. 2 of Hohn, Michael, ed., *Petroleum Geology and Reservoir Characterization of the Upper Devonian Gordon sandstone, Jacksonburg-Stringtown oil field, northwestern West Virginia*: West Virginia Geological and Economic Survey publication B-45, p. 7-18.
- Bachu, S., and Gunter, W. D., 1998, Storage capacity of CO₂ in geological media in sedimentary basins with application to the Alberta Basin, *in* Eliasson, B., Riemer, P.W.F., and Wokaun, A., eds., *Proceedings of the 4th International Conference on Greenhouse Gas Control Technologies: Interlaken, Switzerland*, Pergamon Press, p. 195-200.
- Bai, B., Sun, Y., and Liu, L., 2016, Petrophysical properties characterization of Ordovician Utica gas shale in Quebec, Canada: *Petroleum Exploration and Development*, v. 43, p. 74-81.
- Battelle, 2010, Midwest Regional Carbon Sequestration Partnership Phase II – Storage Capacity Potential Overview: Summary of Phase II Topical Reports, 8 p. plus appendices.
- Bergerud, B. D., 2013, Reservoir model of the Jacksonburg-Stringtown oil field; northwestern West Virginia: Potential for miscible CO₂ enhanced oil recovery: *American Association of Petroleum Geologists Search and Discovery*, Article 90182, [1]p., <http://www.searchanddiscovery.com/abstracts/html/2014/90182se/abstracts/berg.htm?q=%2BtextStrip%3Abergerud> (Abstract from the AAPG/SEG Student Expo, Houston. Texas, September 16-17, 2013. Accessed June 28, 2019.)
- Berry, W. B., and Finney, S. C., 2010, Black shales: an Ordovician perspective: *Geological Society of America, Special Papers*, v. 466, p. 141-147.
- Bloxson, J. M., 2017, Neutron porosity thickness of the Lockport Dolomite, where porosity is greater than 8%: unpublished manuscript, scale 1:500,000.

- Boswell, Ray, 1988, Stratigraphic expression of basement fault zones in northern West Virginia, *Geological Society of America Bulletin*, v. 100, p. 1988-1998.
- Boswell, Ray, 1996, Play UDs: Upper Devonian black shales, *in* Roen, J. B., and Walker, B. J., eds., *The Atlas of Appalachian gas Plays: West Virginia Geological and Economic Survey, Publication V-25*, p. 93-99.
- Boswell, Ray, Heim, L. R., Wrightstone, G. R., and Donaldson, Alan, 1996, Upper Devonian Venango sandstones and siltstones, *in* J. B. Roen, and B. J. Walker, eds., *The atlas of major Appalachian gas plays: West Virginia Geological and Economic Survey Publication V-25*, p. 63-69.
- Boyce, J. I., and Morris, W. A., 2002, Basement-controlled faulting of Paleozoic strata in southern Ontario, Canada: new evidence from geophysical lineament mapping: *Tectonophysics* 353, p. 151-171.
- Boyle, P. C., 1898, *The Derrick's handbook of petroleum: A complete chronological and statistical review of petroleum developments from 1859 to 1899: Oil City, Pennsylvania, Derrick Publishing Company, 1062 p.*
- Brett, C.E., McLaughlin, P.I., Cornell, S.R., and Baird, G.C., 2004, Comparative sequence stratigraphy of two classic Upper Ordovician successions, Trenton shelf (New York—Ontario) and Lexington Platform (Kentucky—Ohio): implications for eustacy and local tectonism in eastern Laurentia: *Palaeogeography, Palaeoclimatology, Palaeoecology*, v. 210, p. 295-329.
- Bruner, K. R., Walker-Milani, M. and Smosna, Richard, 2015, Lithofacies of the Devonian Marcellus shale in the eastern Appalachian Basin, USA: *Journal of Sedimentary Research*, v. 85, no. 8, p. 937-954.
- Byers, C. W., 1977, Biofacies patterns in euxinic basins: A general model, *in* Cook, H. E., and Enos, P., eds., *Deep water carbonate environments: Society of Economic Paleontologists and Mineralogists, Special Publication 25*, p. 5-17.
- Cardwell, D. H., 1982, Oil and Gas Report and Map of Doddridge and Harrison counties, West Virginia, *Bulletin B-16A, West Virginia Geological and Economic Survey.*
- Cardwell, D. H., and Avary, K. L., 1982, Oil and gas fields of West Virginia: *West Virginia Geological and Economic Survey Mineral Resources Series MRS-7B*, 119 p.
- Carll, J. F., 1887, Annual report of the Geological Survey of Pennsylvania for 1886: *Pennsylvania Geological Survey, 2nd Series, Part II, Oil and gas region*, 918 p.
- Carr, T., Frailey, S., Reeves, S. R., Rupp, J., and Smith, S., 2008, Methodology for development of geologic storage estimates for carbon dioxide, *in* *Carbon Sequestration Atlas of the United States and Canada: U.S. Department of Energy, Regional Carbon Sequestration Partnerships, NETL Carbon Sequestration Program, Capacity and fairways subgroup, geologic working group, Appendix B*, p. 115-132.
- Carter, K. M., 2013, Washington-Taylorstown field as a microcosm of the oil and gas industry in Pennsylvania: *American Association of Petroleum Geologists Annual Convention and Exhibition, Pittsburgh, Pennsylvania: Abstracts with Programs, #1555655.*
- Carter, K. M., Moore, M. E., Harper, J. A., Whitfield, T. G., Dunst, B. J., Anthony, R. V., Schmid, K. W. and Chipman, April 2015, Oil and gas fields and pools of Pennsylvania—1859–2011: *Pennsylvania Geological Survey, 4th ser., Open-File Report OFOG 15–01.3*, 10 p., personal geodatabase and shapefiles.
- Carter, K. M., 2017, Shale gas case study report: Starvaggi No. 1 (API No 3712522278), Washington County, Pennsylvania: Prepared for Midwest Regional Carbon Sequestration Partnership (MRCSP) Phase III, 95 p.

- Carter, K. M., Kostelnik, Jaime, Laughrey, C. D., Harper, J. A., et al., 2010, Characterization of geologic sequestration opportunities in the MRCSP Region: Middle Devonian-Middle Silurian formations, Phase II Topical Report, DOE Cooperative Agreement No. DE-FC26-05NT42589, OCDO Grant Agreement No. DC-05-13, 350 p.
- Carter, K. M. and Patchen, D. G., eds., 2017, A geologic study to determine the potential to create an Appalachian Storage Hub for natural gas liquids, Final report of the Appalachian Oil and Natural Gas Research Consortium, July 31, 2017, 162 p.
- Castle, J. W., 1998, Regional sedimentology and the stratal surfaces of a Lower Silurian clastic wedge in the Appalachian foreland basin: *Journal of Sedimentary Research*, v. 68, no. 6, p. 1201-1211.
- Castle, J. W., 2001, Foreland-basin sequence response to collisional tectonism: *Geological Society of America Bulletin*, v. 113, no. 7, p. 801-812.
- Castle, J. W. and Byrnes, A. P., 2005, Petrophysics of Lower Silurian sandstones and integration with the tectonic-stratigraphic framework, Appalachian basin, United States: *American Association of Petroleum Geologists Bulletin*, v. 89, no. 1, p. 41-60.
- Chen, R. and Sharma, S., 2016, Role of alternating redox conditions in the formation of organic-rich interval in the Middle Devonian Marcellus Shale, Appalachian Basin, USA: *Palaeogeography, Palaeoclimatology, and Palaeoecology*, v. 446, p. 85-97.
- Cole, G. A., Drozd, R. J., Sedivy, R. A. and Halpern, H. I., 1987, Organic geochemistry and oil-source correlations, Paleozoic of Ohio: *American Association of Petroleum Geologists Bulletin*, v. 71 no. 7, p. 788-809.
- Coleman, J. L., Milici, R. C., Cook, T. A., Charpentier, R. R., Kirschbaum, M. A., Klett, T. R., Pollastro, R. M., and Schenk, C. J., 2011, Assessment of undiscovered oil and gas resources of the Devonian Marcellus Shale of the Appalachian Basin Province, 2011: Reston, Virginia, U.S. Geological Survey, Fact Sheet 2011-3096, 2 p.
- Cooney, M. L., 2016, Vitrinite reflectance report: Antero Hill Unit 2H an Antero Hill unit 3H wells, Washington County, Pennsylvania: Prepared for Midwest Regional Carbon Sequestration Partnership (MRCSP) Phase III, 58 p.
- Core Laboratories, 2008, Gas shale evaluation, critical elements of reservoir characterization, Core Laboratories, 93 p.
- Crow, E. L., Davis, F. A., and Maxfield, M. W., 1960, *Statistics Manual*: New York, New York, Dover Publications, 288 p.
- DDS5: WVGES Oil and Gas Well Data for West Virginia (release 5/1/2018).
<http://www.wvgs.wvnet.edu/pipe2/OGDataSearch.aspx>
- De Witt, W., Jr., Roen, J. B., and Wallace, L. G., 1993, Stratigraphy of Devonian Black Shales and associated rocks in the Appalachian Basin, *in* Roen, J.B., and Kepferle, R. C., eds., *Petroleum geology of the Devonian and Mississippian Black Shale of eastern North America*, U. S. Geological Survey Bulletin 1909, U.S. Government Printing Office, p. B1-B57.
- Dinterman, P. A., 2018, 2017 Marcellus Shale and Utica-Point Pleasant production summary: West Virginia Geological and Economic Survey, 12 p.
<http://www.wvgs.wvnet.edu/www/datastat/Marcellus/WVGES2017%20Marcellus%20Production%20and%20Utica%20Summary.pdf> (accessed June 5, 2019).
- Dinterman, P., Greb, S., Lewis, E., Schmelz, W., Sparks, T., Solis, M., Medina, C., Carter, K., Barnes, D., Harper, J., Harrison, W., Moore, J., Miller, K., Hickman, J., Riley, R., McDowell, R., Rupp, J., Browning, J., and Gupta, N. 2020. Regional Geologic Cross Sections for Potential Storage and Containment Zones in the MRCSP Region. MRCSP topical report prepared for DOE-NETL project DE-FC26-05NT42589, Battelle Memorial Institute, Columbus, OH

- Dooley, T. P., and Schreurs, G., 2012, Analogue modelling of intraplate strike-slip tectonics: A review and new experimental results, *Tectonophysics*, 574-575, p. 1-71.
- Dorsey, Brenda, 2008, Wetzel County oil fields, *The Wetzel Chronical*, April 2, 2008
<http://www.wvgenweb.org/wetzel/communities/Wetzel-Co-Oil-Fields.html>
- Dow, W. G., 1977, Kerogen studies and geologic interpretations: *Journal of Geochemical Exploration*, v. 7, p.79-99.
- Dutta, N. C., 2016, Effect of chemical diagenesis on pore pressure in argillaceous sediment: *The Leading Edge*, v. 35, no. 6, p. 523-527.
- Environmental Protection Agency (EPA), 2017, Summary data collected by the Greenhouse Gas Reporting Program for 2017: data reported to EPA by facilities as of 08/19/2018, all emissions data presented in units of metric tonnes of CO₂ equivalent using GWP's from IPCC's AR4,
<https://www.epa.gov/ghgreporting/ghg-reporting-program-data-sets> (accessed 5/14/2019).
- Ettensohn, F. R., 1985, Controls on development of Catskill Delta complex basin-facies, *in* Woodrow, D. L., and Sevon, W. D., eds., *The Catskill Delta: Geological Society of America Special Paper 201*, p. 65-77.
- Ettensohn, F. R., 1991, Flexural interpretation of relationships between Ordovician tectonism and stratigraphic sequences, central and southern Appalachians, U.S.A., *in* Barnes, C. R., and Williams, S. H., eds., *Advances in Ordovician geology: Geological Survey of Canada Paper*, v. 90, no. 9, p. 213-224.
- Ettensohn, F. R., 1992, Controls on the origin of the Devonian-Mississippian oil and gas shales, east-central United States: *Fuel*, v. 71, p. 1487-1492.
- Ettensohn, F. R., and Barron, L. S., 1981, Depositional model for the Devonian-Mississippian black shales of North America: A paleoclimatic-paleogeographic approach, *in* Roberts, T. G., ed., *Economic geology, structure; Field Trip No. 3*, Geological Society of America Field Trip Guidebooks, American Geological Institute, Falls Church, Virginia, p. 344-361.
- Ettensohn, F. R., and Lierman, R. T., 2012, Large-scale tectonic controls on the origin of paleozoic dark-shale source-rock basins: Examples from the Appalachian Foreland Basin, Eastern United States, *in* Gao, D., ed., *Tectonics and sedimentation: Implications for petroleum systems: American Association of Petroleum Geologists Memoir*, v. 100, p. 95-124.
- Ettensohn, F. R., Miller, M. L., Dillman, S. B., Elam, T. D., Geller, K. L., Swager, G., Markowitz, G. D., Woock, F. D., and Barron, L. S., 1988, Characterization and implications of the Devonian-Mississippian black shale sequence, eastern and central Kentucky, U.S.A.: Pycnoclines, transgression, and tectonism, *in* McMillan, N. J., Embry, A. F., and Glass, D. J., eds., *Devonian of the World, II: Canadian Society of Petroleum Geologists, Memoir 14*, p. 323-345.
- Exploration and Development Well Network (EDWIN), 2019, Well location, completion, geophysical log and production data retrieved from the database of the Pennsylvania Geological Survey:
<https://EDWIN.onbaseonline.com> (accessed March 15, 2019).
- Farias M., Zaghoul, J., Ertekin, T., et al., 2003, Waterflooding in Gordon sandstone formation - Taylorstown Field, during the period 5/15/2001 to 11/30/2002: Work performed under Prime Award No. DE-FC26-00NT41025, Subcontract No. 2040-TPSU-DOE-1025, 47 p.
- Fettke, C. R., Stephenson, R. C., and Tignor, E. M., 1946, Oil and gas developments in the North Strabane area, Washington County, Pennsylvania: Pennsylvania Geological Survey, 4th Series, Mineral Resource Report 28, 62 p.
- Flaherty, K. J., 1996, Fractured Middle Devonian Huntersville Chert and Lower Devonian Oriskany Sandstone, *in* Roen, J. B., and Walker, B. J., eds., *The atlas of major Appalachian gas plays: West Virginia Geological and Economic Survey, Publication V-25*, p. 103-108.

- Flood, J., 2011, Detailed stratigraphic study of the Rose Run Sandstone in Coshocton, Holmes and Tuscarawas Counties, Ohio: A potential carbon dioxide injection horizon: Undergraduate Thesis, The Ohio State University, Columbus, OH, 23 p.
- Frone, Z.S., Blackwell, D.D, Richards, M.C., and Hornbach, M. J., 2015, Heat flow and thermal modeling of the Appalachian Basin, West Virginia: *GEOSPHERE*, v. 11, no. 5, p. 1279-1290.
- Gass, T. E., 1982, Geothermal heat pumps: Geothermal Resources Council Bulletin, v. 11, p. 3-8.
- Godec, M. L., 2013a, Assessment of factors influencing effective CO₂ storage capacity and injectivity in eastern gas shales: Final technical report: Arlington, Virginia, Advanced Resources International, Inc., U.S. DOE award DE-FE0004633, 469 p.
- Godec, M. L., 2013b, Volume 2, Basin-level characterization of enhanced gas recovery and CO₂ storage potential in the Marcellus Shale, *in* Godec, M. L., ed., Assessment of factors influencing effective CO₂ storage capacity and injectivity in eastern gas shales: Final technical report: Arlington, Virginia, Advanced Resources International, Inc., U.S. DOE award DE-FE0004633, 66 p.
- Godec, M. L., 2013c, Volume 3, Basin-level characterization of enhanced gas recovery and CO₂ storage potential in the Utica Shale, *in* Godec, M. L., ed., Assessment of factors influencing effective CO₂ storage capacity and injectivity in eastern gas shales: Final technical report: Arlington, Virginia, Advanced Resources International, Inc., U.S. DOE award DE-FE0004633, 63 p.
- Gold, D. P., Alexander, S. S., Cakir, R., and others, compilers, 2005, Basement depth and related geospatial database for Pennsylvania: Pennsylvania Geological Survey, 4th ser., Open-File Report OFGG 05-01.0, 1 map, scale 1:500,000.
- Goodman, Angela, Hakala, Alexandra, Bromhal, Grant, Deel, Dawn, Rodosta, Traci, Frailey, Scott, Small, Mitchell, Allen, Doug, Romanov, Vyacheslav, Fazio, Jim, Huerta, Nicolas, McIntyre, Dustin, Kutchko, Barbara, and Guthrie, George, 2011, U.S. DOE methodology for the development of geologic storage potential for carbon dioxide at the national and regional-scale: *International Journal of Greenhouse Gas Control*, v. 5, p. 952-965.
- Gray, J. D., Struble, R. A., Carlton, R. W., Hodges, D. A., et al., 1982, An integrated study of the Devonian-age black shales in eastern Ohio, Ohio Department of Natural Resources, Division of Geological Survey final report for U.S. Department of Energy Eastern Gas Shales Project: U.S. Department of Energy Report No. DOE/ET/12131-1399, 169 p.
- Hammack, R. W., Veloski, G. A., Hodges, D. G. and White, C. M., 2016, Methods for finding legacy wells in large areas: NETL-TRS-6-2016, EPA Technical Report Series: U.S. Department of Energy, National Energy Technology Laboratory, Pittsburgh, Pennsylvania, p. 28.
- Harper, J. A., and Laughrey, C. D., 1987, Geology of the oil and gas fields of southwestern Pennsylvania: Pennsylvania Geological Survey, 4th Series, Mineral Resource Report 87, 166 p.
- Harper, J. A., 1989, Effects of recurrent tectonic patterns on the occurrence and development of oil and gas resources in western Pennsylvania: *Northeastern Geology*, v. 11, p. 225-245.
- Harper, J. A., Anthony, R. V., Carter, K. M., Schmid, K. W., Dunst, B. J., and Cooney, M. L., 2017, Correlation of Middle and Upper Devonian shales in the Marcellus-producing regions of Pennsylvania: Joint 52nd Northeastern Annual Section/51st North-Central Annual Section Meeting, Geological Society of America: Abstracts with Programs, v. 49, no. 2, doi: 10.1130/abs/2017NE-289852.
- Herron, S. L., 1991, In-situ evaluation of potential source rocks by geophysical logs, *in* Merrill, R. K., ed., Treatise of petroleum geology: Handbook of petroleum geology, source and migration processes and evaluation techniques: Tulsa, Oklahoma, American Association of Petroleum Geologists, Treatise Handbook 1, p. 127-134.

- Hoffman, C. F., Foster, C. B., Powell, T. G., and Summons, R. E., 1987, Hydrocarbon biomarkers from Ordovician sediments and fossil alga *Gloeocapsamorpha prisca* Zalesky 1917: *Geochimica et Cosmochimica Acta*, v. 51, p. 2681-2697.
- Hohn, Michael, 2001a, Introduction, chap. 1 of Hohn, Michael, ed., *Petroleum Geology and Reservoir Characterization of the Upper Devonian Gordon sandstone, Jacksonburg-Stringtown oil field, northwestern West Virginia*: West Virginia Geological and Economic Survey Publication B-45, p. 1-6.
- Hohn, Michael, 2001b, Summary and Conclusions, chap. 8 of Hohn, Michael, ed., *Petroleum Geology and Reservoir Characterization of the Upper Devonian Gordon sandstone, Jacksonburg-Stringtown oil field, northwestern West Virginia*: West Virginia Geological and Economic Survey Publication B-45, p. 89-91.
- Hosterman, J. W., and Whitlow, S. T., 1981, Clay mineralogy of Devonian shales in the Appalachian Basin: U.S. Geological Survey, Professional Paper, v. 1298, 30 p.
- Ingall, E., and Jahnke, R., 1997, Influence of water-column anoxia on the elemental fractionation of carbon and phosphorus during sediment diagenesis: *Marine Geology*, v. 139, p. 219-229.
- Jacobson, S. R., 1991, Petroleum source rocks and organic facies, Chapter 1: Petroleum generation and migration, in Merrill, R.K., ed., *Treatise of petroleum geology: handbook of petroleum geology, source and migration processes and evaluation techniques*: Tulsa, Oklahoma, American Association of Petroleum Geologists, Treatise Handbook 1, p. 3-11.
- Jacobson, S. R., Hatch, J. R., Teerman, S. C., and Askin, R. A., 1988, Middle Ordovician organic matter assemblages and their effect on Ordovician-derived oils: *American Association of Petroleum Geologists Bulletin*, v. 72, no. 9, p. 1090-1100.
- James, G., Witten, D., Hastie, T., and Tibshirani, R., 2013, *An introduction to statistical learning with applications in R*: New York, Springer, 426 p.
- Jarvie, D. M., 1991, Total organic carbon (TOC) analysis, in Merrill, R. K., ed., *Treatise of petroleum geology: handbook of petroleum geology, source and migration processes and evaluation techniques*: Tulsa, Oklahoma, American Association of Petroleum Geologists, Treatise Handbook 1, p. 113-118.
- Kanavy, Lauren, 2018, Mineralogy and porosity report: #1 Harry Hatfield and #3299 Hamilton wells, Linden Field, Washington County, Pennsylvania: Prepared for Midwest Regional Carbon Sequestration Partnership (MRCSP) Phase III, 43 p.
- Karmis, M., Ripepi, N., Gilliland, E., Louk, A., Tang, X., Keles, C., Schlosser, C., Diminick, E., McClure, M., Hill, G., and Hill, B., 2018, Central Appalachian Basin unconventional (coal/organic shale) reservoir small scale CO₂ injection test: Virginia Polytechnic Institute and State University (Virginia Tech), Blacksburg, Virginia (United States), 701 p.
- Kirschbaum, M. A., Schenk, C. J., Cook, T. A., Ryder, R. T., Charpentier, R. R., Klett, T. R., Gaswirth, S. B., Tennyson, M. E., and Whidden, K. J., 2012, Assessment of undiscovered oil and gas resources of the Ordovician Utica Shale of the Appalachian Basin Province, 2012: Reston, Virginia, U.S. Geological Survey, Fact Sheet 2012-3116, 6 p.
- Knight, M. V., 1969, Historical and economic geology of Lower Silurian Clinton Sandstone of northeastern Ohio: *American Association of Petroleum Geologists Bulletin*, v. 53, no. 7. p. 1421-1452.
- Kostelnik, Jaime, and Carter, K. M., 2009, Unraveling the stratigraphy of the Oriskany Sandstone: a necessity in assessing its site-specific carbon sequestration potential: *Environmental Geosciences*, v. 16, no. 4, p.187-200.
- Kovscek, A. R., 2002, Screening criteria for CO₂ storage in oil reservoirs: *Petroleum Science and Technology*, v. 20:7-8, p. 841-866, DOI: 10.1081/LFT-120003717.

- Kuuskräa, V. A., Leeuwen, T. V., and Wallace, M., 2011, Improving Domestic Energy Security and Lowering CO₂ Emissions with 'Next Generation' CO₂-Enhanced Oil Recovery (CO₂-EOR): United States Department of Energy/National Energy and Technology Laboratory, DOE/NETL-2011/1504.
- Lash, G. G., and Blood, D. R., 2014, Organic matter accumulation, redox, and diagenetic history of the Marcellus Formation, southwestern Pennsylvania, Appalachian basin: *Marine and Petroleum Geology*, v. 57, p. 244-263.
- Laughrey, C. D., 1984, Petrology and reservoir characteristics of the Lower Silurian Medina Group sandstones, Athens and Geneva fields, Crawford County, Pennsylvania: Pennsylvania Geological Survey, 4th Series, Mineral Resource Report 85, 126 p.
- Laughrey, C. D., and Harper, J. A., 1986, Comparisons of Upper Devonian and Lower Silurian tight formations in Pennsylvania - geological and engineering characteristics, *in* Spencer, C. W., and Mast, R. F., eds., *Geology of tight gas reservoirs: American Association of Petroleum Geologists Studies in Geology* 24, p. 9-43.
- Lavin, P. M., Chaffin, D. L., and Davis, W. F., 1982, Major lineaments and the Lake Erie-Maryland crustal block: *Tectonics*, v. 1, no. 5, p. 431-440.
- Lehmann, D., Brett, C. E., Cole, R., and Baird, G., 1995, Distal sedimentation in a peripheral foreland basin: Ordovician black shales and associated flysch of the western Taconic foreland, New York State and Ontario; *Geological Society of America Bulletin*, v. 107, p. 708-724.
- Levine, J. S., Fukai, Isis, Soeder, D. J., and nine others, 2016, U.S. DOE NETL methodology for estimating the prospective CO₂ storage resource of shales at the national and regional scale: *International Journal of Greenhouse Gas Control*, v. 51, p. 81-94.
- Lewis, J. E., Carter, K. M., Dinterman, Philip, Sparks, T. N., Harrison, W. B., III, Medina, C. R., Moore, J. P., Ortt, R. A., Slater, Brian and Solis, M. P., 2019, An overview of the MRCSP Petroleum Fields 2019 Database: American Association of Petroleum Geologists Search and Discovery, Article 80686, [2]p., http://www.searchanddiscovery.com/pdfz/documents/2019/80686lewis/ndx_lewis.pdf.html?q=%252BauthorStrip%253Aeric+authorStrip%253Alewis+%252ByearSort%253A%255B2019+TO+2019%255D (Adapted from a poster presentation given at AAPG Annual Convention and Exhibition, San Antonio, Texas, May 21, 2019. Accessed June 28, 2019.)
- Longman, M. W., and Palmer, S. E., 1987, Organic geochemistry of mid-continent Middle and Late Ordovician oils: *American Association of Petroleum Geologists Bulletin*, v. 71, no. 8, p. 938-950.
- Lytle, W. S., 1950, Crude oil reserves of Pennsylvania: Pennsylvania Geological Survey, 4th Series, Mineral Resource Report 32, 256 p.
- Lytle, W. S., 1960, History, present status and future possibilities of secondary recovery operations in Pennsylvania: Pennsylvania Geological Survey, 4th Series, Mineral Resource Report 41, 42 p.
- Lytle, W. S., 1976, Oil fields of the Greater Pittsburgh Region: Pennsylvania Geological Survey, 4th Series, Mineral Resource Report 70, 119 p.
- Mastalerz, M., Schimmelmann, A., Drobniak, A., and Chen, Y., 2013, Porosity of Devonian and Mississippian New Albany Shale across a maturation gradient: insights from organic petrology, gas adsorption, and mercury intrusion: *American Association of Petroleum Geologists Bulletin*, v. 97, no. 10, p. 1621-1643.
- Matchen, D. L., 2001, Regional and local geology, chap. 3 of Hohn, Michael, ed., *Petroleum Geology and Reservoir Characterization of the Upper Devonian Gordon sandstone, Jacksonburg-Stringtown oil field, northwestern West Virginia*: West Virginia Geological and Economic Survey Publication B-45, p. 19-37.
- May, Jay, 2019, Using sequence stratigraphy to optimize target selection in unconventional reservoirs, oral presentation at Pittsburgh Association of Petroleum Geologists, May 16, 2019.

- McBride, P. S., 2004, Facies analysis of the Devonian Gordon Stray sandstone in West Virginia: Unpublished M.S. thesis, West Virginia University, 135 p.
- McCormac, M. P., Mychkovsky, G. O., Opritza, S. T., Riley, R. A., et al., 1996, Lower Silurian Cataract/Medina Group ("Clinton") sandstone play, *in* J.B. Roen, and B.J. Walker, eds., The atlas of major Appalachian gas plays: West Virginia Geological and Economic Survey Publication V-25, p. 156-163.
- McGlade, W. G., 1967, Oil and gas geology of the Amity and Claysville Quadrangles: Pennsylvania Geological Survey, 4th Series, Mineral Resource Report 54, 131 p.
- Melzer, L. S., 2007, EOR and the expanding field of CO₂ flooding: American Association of Petroleum Geologists, Eastern Section Annual Meeting, Workshop Notes, varied pagination.
- Meyer, B. L., and Nederlof, M. H., 1984, Identification of source rocks on geophysical logs by density/resistivity and sonic transit time/resistivity crossplots: American Association of Petroleum Geologists Bulletin, v. 68, no. 2, p. 121-129.
- Mishra, Srikanta, 2015, Midwest Regional Carbon Sequestration Partnership - CO₂ utilization for enhanced oil recovery and geologic storage *in* Ohio, Milestone Report #3, Data synthesis, geologic analyses and geologic framework modeling for East Canton and Morrow Consolidated oil fields, Ohio, OCDO Grant/Agreement 00E-CDO-D-13-24, 120 p.
- Mishra, Srikanta, 2014, Midwest Regional Carbon Sequestration Partnership - CO₂ utilization for enhanced oil recovery and geologic storage *in* Ohio, Milestone Report #2, Production history assessment, OCDO Grant/Agreement 00E-CDO-D-13-24, 74 p.
- Mitchell, C. E., Goldman, D., Bergstrom, S. M., Delano, J. W., and Samson, S. D., 1992, Chronostratigraphy of the Trenton Group and Utica Shale, Part 1: Preliminary revision of lithofacies and age relationships: Geological Society of America Abstracts with Programs, v. 24, no. 7, p. 196.
- Monson, C. C., Korose, C. P., and Frailey, S. M., 2014, Screening methodology for regional-scale CO₂ EOR and storage using economic criteria: Energy Procedia, v. 63, p. 7796-7808.
- Moore, J. P., Dinterman, P. A., Lewis, J. E., Luczko, J. L., and Pool, S. E., 2013, Assessing suitability of depleted fields for enhanced oil recovery in West Virginia: poster presented at AAPG annual convention and exhibition, May 19-22, 2013, Pittsburgh Pennsylvania.
http://www.wvgs.wvnet.edu/www/presentations/posters_presentations.htm
- Morris, J. R., 1995, Seismic detection, interpretation of Rose Run in south-central Ohio: Oil and Gas Journal, v. 93, no. 20 <https://www.ogj.com/articles/print/volume-93/issue-20/in-this-issue/exploration/seismic-detection-interpretation-of-rose-run-in-south-central-ohio.html> (accessed June 13, 2019).
- Munn, M. J., 1912, Claysville Folio, Pennsylvania: U.S. Geological Survey Geologic Atlas of the U.S., Folio 180, 14 p.
- Murphy, A. E., Sageman, B. B., Hollander, D. J., and Straeten Ver, C. A., 2000, Organic carbon burial and faunal dynamics in the Appalachian basin during the Devonian (Givetian-Famennian) greenhouse: An integrated paleoecological/biogeochemical approach, *in* Huber, B., MacLeod, K., and Wing, S., eds., Warm Climates in Earth History: Cambridge University Press, p. 351-385.
- NATCARB, 2014, Carbon Storage Atlas – Fifth Edition/Database, Sponsored by United States Department of Energy, National Energy Technology Laboratory, www.natcarb.org (accessed March 22, 2016).
- Noger, M. C., Meglan, J. F., Humphreys, M. and Baranoski, M. T., 1996, Upper Silurian Lockport Dolomite-Keefer ("Big Six") Sandstone, *in* J.B. Roen, and B. J. Walker, eds., The atlas of major Appalachian gas plays: West Virginia Geological and Economic Survey Publication V-25, p. 145-150.

- Nuttall, B. C., Drahovzal, J. A., Eble, C. F., and Bustin, R. M., 2006, Analysis of the Devonian black shale in Kentucky for potential carbon dioxide sequestration and enhanced natural gas production, Final Report. 12th. http://www.uky.edu/KGS/emsweb/devsh/final_report.pdf (Accessed October 1, 2006).
- Nuttall, B. C., Drahovzal, J. A., Eble, C. F., and Bustin, R. M., 2009, Regional assessment of suitability of organic-rich gas shales for carbon sequestration: An example from the Devonian Shales of the Illinois and Appalachian Basins, Kentucky, *in* Grobe, M., Pashin, J., and Dodge, R. L., eds., Carbon dioxide sequestration in geological media – state of the science, v. 59: Tulsa, Oklahoma, American Association of Petroleum Geologists Studies in Geology 59, p. 173-190.
- Ober, E. G., and Eckert, Craig, 2014, Identification of future oil potential from Upper Devonian Venango sandstones in central Appalachians: AAPG Search and Discovery, Article 20237, [38]p., http://www.searchanddiscovery.com/pdfz/documents/2014/20237ober/ndx_ober.pdf.html. (Adapted from an oral presentation given at AAPG Annual Convention and Exhibition, Pittsburgh, Pennsylvania, May 19, 2013. Accessed February 6, 2019.)
- Obermajer, M., Fowler, M. G. and Snowdon, L. R., 1999, Depositional environment and oil generation in Ordovician source rocks from southwestern Ontario, Canada: Organic geochemical and petrological approach: American Association of Petroleum Geologists Bulletin, v. 83, no. 9, p. 1426-1453.
- Ohio Department of Natural Resources, 2019, Horizontal Utica-Point Pleasant Well Activity in Ohio: Columbus, scale 1:1,300,000, revised 5/4/2019.
- Oliver, W. A., De Witt, Wallace, et al., 1971, Isopach and lithofacies maps of the Devonian in the Appalachian Basin: Pennsylvania Geological Survey, 4th Series, Progress Report 182, 7 sheets.
- Opsitnick, Alexandra, 2015, Reservoir quality of the Marcellus Shale play in the Hill Unit 2H and 3H wells: determining mineralogical and lithological properties: Undergraduate Thesis, Allegheny College, Meadville, PA, 99 p.
- PA DCNR, 2009, Geologic Carbon Sequestration Opportunities in Pennsylvania, revision 1.1, August 14, 2009, 150 p.
- Passey, Q. R., Creaney, S., Kulla, J. B., Moretti, F. J., and Stroud, J. D., 1990, A practical model for organic richness from porosity and resistivity logs: American Association of Petroleum Geologists Bulletin, v. 74, no. 12, p. 1777-1794.
- Patchen, D.G., 1996, Enhancement of the TORIS Database of Appalachian Basin Oil Fields: Final Report for Bartlesville Project Office and Morgantown Energy Technology Center, 23 p.
- Patchen, D. G., Hickman, J. B., Harris, D. C., Drahovzal, J. A., Lake, P. D., Smith, L. B., Nyahay, R., Schulze, R., Riley, R. A., Baranoski, M. T., Wickstrom, L. H., Laughrey, C. D., Kostlenik, J., Harper, J. A., Avary, K. L., Bocan, J., Hohn, M. E., and McDowell, R., 2006, A geologic play book for Trenton–Black River Appalachian Basin exploration: Morgantown, West Virginia, West Virginia University Research Corporation, 601 p.
- Patchen, D. G., and Carter, K. M., eds., 2015, A geologic play book for Utica Shale Appalachian Basin exploration, Final report of the Utica Shale Appalachian Basin exploration consortium, July 1, 2015, 205p.
- Pease, R. W. and Watts, R. J., 1979, Acquisition, classification and evaluation of engineering and geologic information and characteristics of West Virginia petroleum reservoirs amenable to enhanced oil recovery technology, particularly carbon dioxide injection: Final Report, U. S. Department of Energy, DOE/MC05602-6, 102 p.
- Petroleum Technology Transfer Council (PTTC), 2005, Tertiary Oil Recovery Information System (TORIS) database for the Appalachian Region.
- Popova, Olga, Small, M. J., McCoy, S. T., Thomas, A. C., Rose, Stephen, and Karimi, Bobak, 2013, Spatial stochastic modeling of sedimentary formations to assess CO₂ storage potential: A case study

- for the Pennsylvania part of the Appalachian Basin: AAPG Search and Discovery, Article 90163, [1]p. <http://www.searchanddiscovery.com/abstracts/html/2013/90163ace/abstracts/pop.htm?q=%2BtextStrip%3Apopova>. (AAPG Annual Convention and Exhibition, Pittsburgh, Pennsylvania, May 19, 2013. Accessed May 6, 2019.)
- Reed, J. D., Illich, H. A., and Horsfield, B., 1986, Biochemical evolutionary significance of Ordovician oils and their sources: *Organic Geochemistry*, v. 10, p. 347-358.
- Remis A. E., 2018, Reservoir characterization of the Gantz and Gordon sandstones, Linden Field, North Strabane Township, Washington County, Pennsylvania: Undergraduate Thesis, Allegheny College, Meadville, PA, 47 p.
- Repetski, J. E., Ryder, R. T., Weary, D., Harris, A. G. and Trippi, M. H. 2008 Thermal maturity patterns (CAI and %Ro) in Upper Ordovician and Devonian rocks of the Appalachian Basin: A major revision of USGS Map I-917-E using new subsurface collections: U.S. Geological Survey Scientific Investigations Map 3006, one CD-ROM.
- Reznik, A. A., Singh, P. K., and Foley, W. L., 1984, An analysis of the effect of CO₂ injection on the recovery of in-situ methane from bituminous coal: An experimental simulation: *Society of Petroleum Engineers Journal*, v. 24, p. 521-528. (SPE Paper 10822).
- Riley, R. A., Harper, J. A., Baranoski, M. T., Laughrey, C. D. and Carlton, R. W., 1993, Measuring and predicting reservoir heterogeneity in complex deposystems: The Late Cambrian Rose Run Sandstone of eastern Ohio and western Pennsylvania, DOE Cooperative Agreement No. DE-AC22-90BC14657, Appalachian Oil and Natural Gas Research Consortium, National Research Center for Coal and Energy, 257 p.
- Riley, R. A., Harper, J. A., Harrison, W. B., et al., 2010, Evaluation of CO₂-enhanced oil recovery and sequestration opportunities in oil and gas fields in the MRCSP region, Phase II Topical Report, DOE Cooperative Agreement No. DE-FC26-05NT42589, OCDO Grant Agreement No. DC-05-13, 177 p.
- Riley, R. A., Wicks, J. L., and Perry, C. J., 2011, Silurian "Clinton" sandstone reservoir characterization for evaluation of CO₂-EOR potential in the East Canton oil field, Ohio, Ohio Department of Natural Resources, Division of Geological Survey, Open-File Report 2011-2, 31 p.
- Rodgers, M. R., and Anderson, T. H., 1984, Tyrone-Mt. Union cross-strike lineament of Pennsylvania: A major Paleozoic basement fracture and uplift boundary: *American Association of Petroleum Geologists*, v. 68, no. 1, p. 92-105.
- Roen, J. B., and Walker, B. J., eds., 1996, The atlas of major Appalachian gas plays: West Virginia Geological and Economic Survey, Publication V-25, 201 p.
- Roen, J. B., Wallace, L. G., and De Witt, W., Jr., 1978a, Preliminary stratigraphic cross section showing radioactive zones in the Devonian black shales in eastern Ohio and west-central Pennsylvania: U.S. Geological Survey, Oil and Gas Investigations, Chart OC-82.
- Roen, J. B., Wallace, L. G., and De Witt, W., Jr., 1978b, Preliminary stratigraphic cross section showing radioactive zones in the Devonian black shales in the central part of the Appalachian Basin: U.S. Geological Survey, Oil and Gas Investigations, Chart OC-82.
- Roen, J. B., and De Witt, W., Jr., 1984, Stratigraphic framework of the Devonian black shales of the Appalachian Basin: U.S. Geological Survey, Open-file report 84-111, 71 p.
- Ryder, R. T., 2008, Assessment of Appalachian Basin oil and gas resources: Utica-Lower Paleozoic Total Petroleum System: U.S. Geological Survey Open-File Report 2008-1287, 29 p.
- Ryder, R. T., Burruss, R. C., and Hatch, J. R., 1998, Black shale source rocks and oil generation in the Cambrian and Ordovician of the central Appalachian Basin, USA: *American Association of Petroleum Geologists Bulletin*, v. 82, no. 3, p. 412-441.

- Ryder, R. T., and Zagorski, W. A., 2003, Nature, origin and production characteristics of the Lower Silurian regional oil and gas accumulation, central Appalachian basin, United States: American Association of Petroleum Geologists Bulletin, v. 87, no. 5, p. 847-872.
- Saboda, S. R., and Lash, G. G., 2014, Inorganic Geochemistry of the Trenton Limestone-Utica Shale Contact Based on XRF Data: American Association of Petroleum Geologists, Search and Discovery Article No. 51038.
- Sageman, B. B., Murphy, A. E., Werne, J. P., Ver Straeten, C. A., Hollander, D. J., and Lyons, T. W., 2003, A tale of shales: The relative roles of production, decomposition, and dilution in the accumulation of organic-rich strata, Middle–Upper Devonian, Appalachian Basin: Chemical Geology, v. 195, p. 229-273.
- Sanguinito, S., Goodman, A., Tkach, M., et al., 2018, Quantifying dry supercritical CO₂-induced changes of the Utica Shale: Fuel, v. 226, p. 54-64.
- Schepers, K. C., Nuttall, B. C., Oudinot, A. Y., and Gonzalez, R., 2009, Reservoir modeling and simulation of the Devonian gas shale of eastern Kentucky for enhanced gas recovery and CO₂ Storage: Society of Petroleum Engineers, SPE 126620-PP, p. 20.
- Schmoker, J. W., 1979, Determination of organic content of Appalachian Devonian Shales from formation-density logs: American Association of Petroleum Geologists Bulletin, v. 63, no. 9, p. 1504-1537.
- Schmoker, J. W., 1981, Determination of organic-matter content of Appalachian Devonian shales from gamma-ray logs: American Association of Petroleum Geologists Bulletin, v. 65, no. 7, p. 1285-1298.
- Schmoker, J. W., 1993, Use of formation-density logs to determine organic-carbon content in Devonian shales of the western Appalachian Basin and an additional example based on the Bakken Formation of the Williston Basin, *in* Roen, J. B., and R. C. Kepferle, eds., Petroleum geology of the Devonian and Mississippian black shale of eastern North America: U.S. Geological Survey Bulletin 1909, p. J1-J14.
- Slatt, R. M., and Rodriguez, N. D., 2012, Comparative sequence stratigraphy and organic geochemistry of gas shales: Commonality or coincidence?: Journal of Natural Gas Science and Engineering, v. 8, p. 68-84.
- Sminchak, J. R., Larsen, G. and Hicks, J.E., 2016, Subsurface geomechanics, fracture breakdown pressure, and 'fracture tunnels' in the Midwest United States: AAPG Search and Discovery, Article 80570, [2] p.
http://www.searchanddiscovery.com/pdfz/documents/2016/80570sminchak/ndx_sminchak.pdf.html
(Adapted from a poster presentation given at AAPG Eastern Section Meeting, Lexington, Kentucky, September 25-27, 2016. Accessed July 17, 2019.)
- Smith, L. B., 2013, Shallow transgressive onlap model for Ordovician and Devonian organic-rich shales, New York State: Society of Exploration Geophysicists, American Association of Petroleum Geologists, and Society of Petroleum Engineers, Unconventional Resources Technology Conference, Denver, Colorado, p. 524-533.
- Smosna, R. A., Bruner, Kathy, Riley, R. A., 2005, Paleokarst and reservoir porosity in the Ordovician Beekmantown Dolomite of the central Appalachian Basin: Carbonates and Evaporites, v. 20, no. 1, p. 50-63.
- Smosna, Richard, Conrad, J. M., and Maxwell, T., 1989, Stratigraphic traps in Silurian Lockport Dolomite of Kentucky: American Association of Petroleum Geologists Bulletin, v. 73, p. 874-886.
- Soeder, D. J., 2017, Unconventional: the development of natural gas from the Marcellus Shale: The Geological Society of America Special Paper 527, pp. 108-109.

- Solis, M. P. and Bloxson, J. M., 2019, Midwest Regional Carbon Sequestration Partnership - Structural Characterization of Potential Carbon Dioxide Reservoirs and Adjacent Strata Within the Llandovery Silurian to Middle Devonian Strata of Ohio, Midwest Regional Carbon Sequestration Partnership, DOE-NETL Cooperative Agreement DE-FC-05NT42589.
- Takacs, K. G., Nuttall, B. C., and Parris, T. M., 2011, Assessment of Kentucky fields for CO₂-Enhanced Oil Recovery: Chapter 2, Evaluation of Geologic CO₂ Sequestration Potential and CO₂ Enhanced Oil Recovery in Kentucky, Report of Investigations 21, Series XXII.
- The Energy Consulting Group, Marcellus 3D Thickness, http://energycg.com/USA/Marcellus/marcellus_3D_Thickness.htm (Accessed May 2019).
- Torry, Brad, Kegek, Jason, Nemati, M. H, and Keay, James, 2014, Geoscience integration: extracting value from seismic data observations – implications to Utica/Point Pleasant development, AAPG Utica/Pt. Pleasant Workshop, Pittsburgh, PA, June 17-19, 2014.
- Tracy, Keith, 2019, Section 45Q tax credits explained: Carbon Capture Journal, Issue 68, Mar/Apr 2019 p. 2-3.
- Tuite, M. L., and Macko, S. A., 2013, Basinward nitrogen limitation demonstrates role of terrestrial nitrogen and redox control of $\delta^{15}\text{N}$ in a Late Devonian black shale: *Geology*, v. 41, p. 1079-1082.
- U.S. Geological Survey (USGS) Geologic Names Committee (Orndorff, R.C., Chair and preparer), 2010, Divisions of geologic time—Major chronostratigraphic and geochronologic units: U.S. Geological Survey Fact Sheet 2010-3059, 2 p. IP-21451.
- Vargo, A. G. and Matchen, D. L., 1996, Lower Mississippian Big Injun Sandstones, *in* Roen, J. B., and Walker, B. J., eds., *The atlas of major Appalachian gas plays: West Virginia Geological and Economic Survey, Publication V-25*, p. 41-45.
- Verma, M. K., 2015, Fundamentals of carbon dioxide-enhanced oil recovery (CO₂-EOR)—a supporting document of the assessment methodology for hydrocarbon recovery using CO₂-EOR associated with carbon sequestration, U.S. Geological Survey, Open-File Report Wallace, L. G., and Roen, J. B., 1989, Petroleum source rock potential of the Upper Ordovician black shale sequence, northern Appalachian Basin: U.S. Geological Survey Open-File Report 89-488, 66 p.
- Wagner, W. R., 1976, Growth faults in Cambrian and Lower Ordovician rocks of western Pennsylvania: *American Association of Petroleum Geologists Bulletin*, v. 60, no. 3, p. 414-427.
- Wang, G., and Carr, T.R., 2013, Organic-rich Marcellus Shale lithofacies modeling and distribution pattern analysis in the Appalachian Basin: *American Association of Petroleum Geologists Bulletin*, v. 97, no. 12, p. 2173-2205.
- Wang, G., Shahkarami, A., and Bruno, J., 2016, TOC prediction analysis of Utica-Point Pleasant formations in the Appalachian Basin: *Search and Discovery #51283*. (searchanddiscovery.com/pdfz/documents/2016/51283shahkarami/ndx_shahkarami.pdf.html). 2015–1071, 24 p.
- Wegweiser, M. D., Wegweiser, A. E., Babcock, L. E., and Harper, J. A., 1998, Morphotectonic features associated with cross-strike structural discontinuities in upper Devonian rocks of northwestern Pennsylvania: 63rd Annual Field Conference of Pennsylvania Geologists, Erie, Pennsylvania, Guidebook, p. 15-17.
- Werne, J. P., Sageman, B. B., Lyons, T. W., and Hollander, D. J., 2002, An integrated assessment of a “type euxinic” deposit: evidence for multiple controls on black shale deposition in the Middle Devonian Oatka Creek Formation: *American Journal of Science*, v. 302, p. 110-143.
- WVGES ‘Pipeline Plus’. Online resource.
URL: <http://www.wvgs.wvnet.edu/pipe2/EfileViewer.aspx>.

- Whieldon, C. E., and Eckard, W. E., 1963, West Virginia oil fields discovered before 1940: U.S. Department of the Interior, Bureau of Mines, Washington, D.C., 187 p.
- Wickstrom, L.H., Venteris, E. R., Harper, J. A. and 26 others, 2005, Characterization of geologic sequestration opportunities in the MRCSP region, phase I task report: Period of performance—October 2003–September 2005: DOE Cooperative Agreement No. DE-PS26-05NT42255, 152 p.
- Wickstrom, L. H., Riley, R. A., Spane, F. A. and five others, 2011, Geologic assessment of the Ohio Geological Survey CO₂ No.1 well in Tuscarawas County and surrounding vicinity: Prepared for the Ohio Air Quality Development Authority, Ohio Coal Development Office and the US Department of Energy-National Energy Technology Laboratory: Ohio Department of Natural Resources, Division of Geological Survey, Open-File Report 2011-3, 82 p.
- Wickstrom, L. W., Perry, Chris, Riley, R. A. et al., 2012, Geology and activity update of the Ohio Utica-Point Pleasant play, (presented at Ohio Oil Gas Association meeting, March 16, 2012).
- Wilcox, R. R., 2010, Fundamentals of modern statistical methods, substantially improving power and accuracy: New York, Springer, 249 p.
- Wilson, M. J., Shaldybin, M. V. and Wilson, L., 2016, Clay mineralogy and unconventional hydrocarbon shale reservoirs in the USA. I. Occurrence and interpretation of mixed-layer R3 ordered illite/smectite: Earth-Science Reviews, v. 158, p. 31-50.
- Yost, A. B., II, Mazza, R. L., and Gehr, J. B., 1993, CO₂/sand fracturing in Devonian shales: Journal of Petroleum Technology, SPE 26925, p. 353-362.
- Zarghami, Shahin, Boukadi, Fathi, and Al-Wahaibi, Yahya, 2017, Diffusion of carbon dioxide in formation water as a result of CO₂ enhanced oil recovery and CO₂ sequestration: Journal of Petroleum Exploration and Production Technology, v. 7, no. 1, p. 161-168.
- Zhong, Zhi, and Carr, T. R., 2016, Constructing a geological model to estimate the capacity of commercial scale injection, utilization and storage of CO₂ in the Jacksonburg-Stringtown Field, West Virginia, USA, AAPG Search and Discovery, Article 20237, [5]p.
http://www.searchanddiscovery.com/documents/2016/80518zhi/ndx_zhi.pdf.html. [Adapted from a poster presentation given at AAPG Annual Convention and Exhibition, Denver, Colorado, May 31-June 3, 2015. Accessed 6/12/2019].

BATTELLE

It can be done